

McGRAW-HILL SERIES IN THE  
**GEOLOGICAL  
SCIENCES**







Digitized by the Internet Archive  
in 2022 with funding from  
Kahle/Austin Foundation

<https://archive.org/details/earthitsgravityf0000heis>

McGraw-Hill Series in the Geological Sciences

ROBERT R. SHROCK, *Consulting Editor*

---

**THE EARTH AND ITS GRAVITY FIELD**

 McGraw-Hill Series in the Geological Sciences

ROBERT R. SHROCK, *Consulting Editor*

---

DE SITTER · Structural Geology

EWING, JARDETZKY, AND PRESS · Elastic Waves in Layered Media

GRIM · Clay Mineralogy

HEINRICH · Microscopic Petrography

HEISKANEN AND VENING MEINESZ · The Earth and Its Gravity Field

SHROCK AND TWENHOFEL · Principles of Invertebrate Paleontology

# The Earth and Its Gravity Field

**W. A. HEISKANEN**

*Director, Institute of Geodesy,  
Photogrammetry, and Cartography  
The Ohio State University  
Finnish Geodetic Institute, Helsinki*

**F. A. VENING MEINESZ**

*Professor, Institute of Mineralogy,  
Geology, and Geophysics  
University of Utrecht*

McGRAW-HILL BOOK COMPANY, INC.

New York      Toronto      London

1958

## THE EARTH AND ITS GRAVITY FIELD

Copyright © 1958 by the McGraw-Hill Book Company, Inc. Printed in the United States of America. All rights reserved. This book, or parts thereof, may not be reproduced in any form without permission of the publishers.

*Library of Congress Catalog Card Number 57-9439*

Univ. of Arizona Library

## PREFACE

Knowledge of the gravity field of the earth is important in the study of our globe. If we know the gravity anomalies, as we now do in many places, not only can we investigate their causes and the phenomena connected with them, but also we can determine the figure of the earth and the shape of the geoid. If the earth were in equilibrium, its figure would be close to an ellipsoid of revolution, and the gravity field around it would be regular. There are, however, deviations from equilibrium and, consequently, irregularities in the shape of the geoid and gravity anomalies. The latter can be measured, and if we know them over a sufficiently large part of the globe, we can, by means of Stokes' theorem, derive the deviations between geoid and ellipsoid over a corresponding though smaller part. These deviations are relatively small, probably not exceeding 50 meters.

The gravity survey over a great part of the earth's surface thus makes possible a new and important branch of geodesy, which we may call physical geodesy. Besides the deviation of geoid from ellipsoid, we can also derive the deflection of the vertical from the gravity anomalies; this fact has consequences of vast importance in geodesy as it allows us to unify the geodetic nets over the earth, regardless of their separation by oceans, into one world geodetic system.

The great number of gravity data already available allow us, in addition, to make important conclusions about the way the earth tends toward equilibrium and about the character and size of the deviation from it. Gravity data are thus of great value in many geophysical problems. Needless to say, these problems are often intimately related to geological data and interpretations and to the results of seismology, geomagnetism, and geomorphology.

In recent years only short papers have been published on the earth's gravity field, the possibilities provided by the large number of gravity data, and the conclusions which can be drawn from them. The authors therefore feel that a book dealing with these problems and giving the most important lines of advance and results may be useful. Although concerned principally with the earth's gravity field and related subjects, the book also touches on the results of other branches of geodesy and geophysics, e.g., mathe-

matical and astronomical geodesy and the inner constitution of the earth as indicated by seismology and geomagnetism.

With a few minor exceptions, Chaps. 4 to 9 have been written by Heiskanen and Chaps. 1 to 3 and 10 to 12 by Vening Meinesz. The authors agree entirely on the content of their respective contributions but, preferring to preserve their personal styles, have not attempted to harmonize the details.

The authors wish to express their gratitude to Dr. J. Allen Hynek for his great assistance in checking the final version of the manuscript for accurate English idiom.

W. A. HEISKANEN  
F. A. VENING MEINESZ

## CONTENTS

<b>Preface</b>	v
<b>Chapter 1. Introduction and Summary</b>	1
<b>Chapter 2. Internal Constitution of the Earth</b>	6
2-1. The Crust	6
2-2. The Mantle	9
2-3. Definition of the Rigid Crust; Boundary between It and the Plastic Mantle	12
2-4. Stress and Strain Characteristics in the Earth	13
2-5. The Core	25
<b>Chapter 3. Gravity Field and Gravity Potential of the Earth. Equilibrium Figure. Earth Ellipsoid</b>	33
3-1. Gravity Field and Gravity Potential	33
3-2. Spherical Harmonics	36
3-3. Exterior Gravity Potential of the Spheroidal Earth	42
3-4. Equipotential Surfaces of the Spheroidal Earth	45
3-5. Exterior Gravity Field of the Spheroidal Earth	47
3-6. Basic Formulas for the Ellipsoidal Earth	51
3-7. Equilibrium Figure of a Fluid Earth and Its Gravity	55
3-8. Potential Caused by the Deviation Masses of the Earth; Distance $N$ between Geoid and Earth Spheroid; Gravity Anomaly	59
3-9. Stokes' Theorem	63
3-10. Formula Expressing Deflection of the Vertical in Gravity Anomalies	66
3-11. Exterior Equipotential Surfaces and Gravity	70
3-12. Basic Hypothesis of Geodesy; Stokes' Theorem and Related Equations; Applicability When Gravity Is Still Unknown over Large Parts of the Earth	72
3-13. Gravity Formulas	74
A. International Gravity Formula	74
B. Computation of the Gravity Formula	76
<b>Chapter 4. Gravity Measurements</b>	84
4-1. Pendulum Observations	84
A. Theory of Pendulum Observations	87
B. Physical Pendulum	90
C. Corrections of Pendulum Observations	94
D. Modern Pendulum Apparatus	98
4-2. Gravimeters	101
A. Dynamic Gravimeters	101

B.	Gas-pressure Gravimeters . . . . .	103
C.	Balance Gravimeters . . . . .	104
D.	Underwater Gravimeters . . . . .	113
E.	Vening Meinesz Pendulum Apparatus . . . . .	115
F.	Tidal Effect . . . . .	118
4-3.	Base Stations and Calibration Lines . . . . .	120
<b>Chapter 5. Historical Development of the Idea of Isostasy . . . . .</b>		<b>124</b>
5-1.	Definition . . . . .	124
5-2.	Early History of Isostasy . . . . .	125
A.	First Ideas concerning Isostatic Equilibrium . . . . .	125
B.	Isostatic Assumptions of Pratt and Airy . . . . .	126
C.	Some Isostatic Studies at the Turn of the Century . . . . .	129
5-3.	Main Isostatic Systems . . . . .	131
A.	Pratt-Hayford Isostatic System . . . . .	131
B.	Airy-Heiskanen Isostatic System . . . . .	135
C.	Vening Meinesz Regional Isostatic System . . . . .	137
5-4.	Some Other Isostatic Assumptions . . . . .	142
<b>Chapter 6. Reduction of the Gravity Measurements . . . . .</b>		<b>147</b>
6-1.	Nonisostatic Reductions . . . . .	147
A.	Free-air Reduction . . . . .	148
B.	Bouguer Reduction . . . . .	150
C.	Terrain Correction . . . . .	154
D.	Condensation and Inversion Reduction Methods . . . . .	156
E.	Reduction of Gravity Measurements at Sea . . . . .	158
6-2.	Isostatic Reductions . . . . .	159
A.	Pratt-Hayford Reduction . . . . .	159
B.	Airy-Heiskanen Reduction . . . . .	166
C.	Vening Meinesz Reduction . . . . .	168
D.	Geological and Isostatic Geological Corrections . . . . .	170
E.	Indirect Isostatic Reduction . . . . .	172
6-3.	Recent Methods for Isostatic Reduction . . . . .	175
A.	Cartographic Method . . . . .	176
B.	Mass-line Method . . . . .	181
<b>Chapter 7. Gravity Anomalies; Achievements of Isostasy . . . . .</b>		<b>187</b>
7-1.	Statistics of Gravity Anomalies . . . . .	187
A.	Gravity Anomalies in the United States and Canada . . . . .	187
B.	Gravity Anomalies in India . . . . .	190
C.	Gravity Anomalies in East Africa . . . . .	191
D.	Gravity Anomalies in the Alps . . . . .	192
E.	Gravity Anomalies at Sea . . . . .	198
7-2.	Achievements of Isostasy . . . . .	198
A.	Limitations of the Bouguer Gravity Anomalies . . . . .	198
B.	Normal Thickness of the Earth's Crust . . . . .	201
C.	One of Nature's Great Isostatic "Experiments" . . . . .	212
D.	Degree of Regionality of Isostatic Compensation over Volcanic Islands and Continental Margins . . . . .	215

<b>Chapter 8. Physical Geodesy</b>	222
8-1. Existing Geodetic Systems	222
A. Meaning of Geodetic Systems	223
B. Historical Development of Geodesy	224
C. Most Important Dimensions of Reference Ellipsoids	228
D. Significance of the Initial Point of Geodetic Systems	232
8-2. Physical Geodesy	235
A. Principles of Physical Geodesy	236
B. Gravity Material Necessary and Currently Available	240
C. Reduction Method to Be Used	243
8-3. Deflections of the Vertical	250
A. Astronomic-Geodetic Deflections of the Vertical	250
B. Topographic and Isostatic Reduction of Astronomic-Geodetic Deflections of the Vertical	252
C. Gravimetric Deflections of the Vertical	257
D. Dimensions of the Reference Ellipsoid	277
8-4. Shape of the Geoid	279
A. Practical Procedure	279
B. Hirvonen's Geoid and Tanni's Geoid	282
C. Some Other Geoids	289
<b>Chapter 9. World Geodetic System</b>	299
9-1. Conversion of Existing Geodetic Systems to the World Geodetic System	299
9-2. Supercontrol Points	304
9-3. Control of Small-scale Maps	306
9-4. Other Applications	308
9-5. Conclusions	309
<b>Chapter 10. Deviations from Isostatic Equilibrium</b>	311
<b>PART 10A. GENERAL CONSIDERATIONS. FORMULAS FOR ELASTIC, PLASTIC, AND SHEAR DEFORMATIONS OF THE CRUST. DEVELOPMENT OF GEOSYNCLINES</b>	
10A-1. Introduction and Summary	311
10A-2. Horizontal Compression in the Crust below the Elastic Limit	314
10A-3. Elastic Deformation of the Crust by Vertical Loading and Horizontal Compression	316
10A-4. Plastic Deformation of the Crust by Horizontal Compression	326
10A-5. Later History of Geosyncline Belts; Subcrustal Flow of Crustal Matter; <i>Mittelgebirge</i> ; Thickness of Continents	343
10A-6. Further Discussion of Crustal Deformation; Gravity Anomalies	346
10A-7. Preferred Starting Direction of Plastic Deformation by Uniaxial Compression	349
10A-8. Faulting and Shear Phenomena in the Crust	352
<b>PART 10B. POSTGLACIAL READJUSTMENT OF CRUSTAL EQUILIBRIUM. ISOSTATIC READJUSTMENT</b>	
10B-1. General Considerations; Readjustment Determined by Subcrustal Phenomena	357
10B-2. Subcrustal Reaction to Loading or Unloading of the Crust	359
10B-3. Evidence in Fennoscandia; Approximate Conclusions about $\eta$	365
10B-4. Conclusions about the Rate of Readjustment of Isostatic Equilibrium	368

**PART 10C. ISLAND-ARC AREAS**

10C-1. Introduction . . . . .	371
10C-2. The Downbuckled Belts . . . . .	373
10C-3. The Wrench-faulting Parts of the Belts . . . . .	377
10C-4. The Volcanic Arc . . . . .	382
10C-5. General Discussion of Island Arcs; Caribbean Arc . . . . .	385

**PART 10D. STRESS RELEASE IN THE CRUST. TILTED FAULT PLANES. GRABEN FORMATION**

10D-1. Introduction . . . . .	389
10D-2. Faulting and Graben Development as a Consequence of Uniaxial Stress Release in the Crust . . . . .	390
10D-3. Bullard's Gravity Results in Graben Areas; Later Development in Graben Areas . . . . .	394

**Chapter 11. Convection Currents in the Earth. Origin of Continents and Oceans. Great Geosyncline Belts . . . . .**

11-1. Introduction and Summary . . . . .	397
11-2. The Density-transition Layer from 200 to 900 km Depth . . . . .	397
11-3. Thermal Convection in a Plane Layer . . . . .	403
11-4. Thermal Convection in a Spherical Shell . . . . .	408
11-5. Thermal Convection in the Entire Globe . . . . .	412
11-6. Topography of the Earth Developed in Spherical Harmonics; Convection Currents as the Cause of Its Distribution . . . . .	421
11-7. First-order Term of the Topography; Origin of the Core and of an Ur Continent . . . . .	423
11-8. Waves of 2nd- to 7th-, 8th- to 11th-, and 12th- to 16th-order Terms of the Topography; Origin of Continents and Oceans . . . . .	430
11-9. Early History of the Earth; Large Geosynclines; Crustal Shear Pattern . . . . .	432
11-10. Deep Basins in Island-arc Areas; Deep and Intermediate Earthquakes . . . . .	435

**Chapter 12. Polar Migrations. Shear Pattern of the Earth's Crust . . . . .**

12-1. Introduction; Formulas for Elastic Deformation of a Crustal Shell with Change in Axis of Flattening . . . . .	443
12-2. Crustal Pattern Caused by Polar Migration . . . . .	447
12-3. The Pattern Present in the Earth's Crust; Polar-flight Forces Too Small to Have Been the Cause . . . . .	450

**Name Index . . . . .**

Name Index . . . . .	455
----------------------	-----

**Subject Index . . . . .**

Subject Index . . . . .	459
-------------------------	-----

# CHAPTER 1

## INTRODUCTION AND SUMMARY

This introductory chapter explains how the purpose of the book, broadly outlined in the preface, is carried out in the ensuing chapters, and thus it also serves as a summary of the contents.

Before dealing with the main subject, the earth's gravity field and the geodetic and geophysical implications and conclusions which can be drawn from it, we give a summary of the significant data relating to the earth provided by seismology, geomagnetism, and other geophysical means. Chapter 2 treats of the three major discontinuities, or interfaces, dividing the earth into four parts. Above the Mohorovičić, or M, interface is the M crust, so called to distinguish it from the rigid crust. It normally reacts elastically to stresses, and only tectonic forces are strong enough to cause plastic deformation in it. Between the M interface and the boundary of the core, at a depth of 2900 km, is the mantle. Since the mantle can be expected to react plastically to stresses, it can further be supposed that currents are possible there, though only slow ones of a few centimeters per year velocity. Between the interfaces at 2900 and about 5100 km depth is the outer, liquid core, in which currents of 200,000 to 1,000,000 times greater velocity can be assumed, i.e., of 5 to 25 km/year. Their presence seems to be indicated by geomagnetic data and by the irregularities astronomers have found in the earth's rotation, both of which are briefly dealt with in Sec. 2-5. Below the interface, at a depth of about 5100 km, is the inner core, about which little is known. The supposition has been made that it consists of the same matter as the outer core, i.e., of iron and nickel, but that it reacts more or less as a solid.

In Chap. 3 we deal with the foundation, by means of potential theory, of the treatment of the earth's gravity field and its relations to the geoid and to other equipotential surfaces outside the earth, and for this purpose spherical harmonics are introduced. In the course of our deductions we imagine the earth's mass to be divided into two parts: (1) a regular group of masses which together equal the total earth mass, have axial symmetry around the earth's axis, and are symmetric with respect to the equator plane and (2) the remainder of the earth's masses, of positive as well as negative sign, of which the total mass is zero.

We first derive the geoid and the gravity field of the regular group of masses. The geoid is a spheroid which we adopt as a reference surface for all geodetic measurements; the gravity on this surface represents our formula for normal gravity. By the proper choice of constants we can make the reference spheroid coincide with an ellipsoid of revolution or with the equilibrium figure of a fluid earth of the same total mass, the same total volume, and the same internal density distribution as the real earth. It is fortunate that both cases can be brought to practical coincidence and that therefore the appropriate ellipsoid of revolution and the gravity field belonging to it can be considered so nearly representing equilibrium of the earth that the difference can be neglected.

As a consequence, the gravity anomalies of the real earth, with respect to the formula for normal gravity corresponding to the ellipsoid of revolution, can be considered as representing deviations from equilibrium actually present in the earth, while the deviations of the real geoid from the equilibrium ellipsoid showing the warping and tilting of the geoid, and the deflections of the vertical correspond to these deviations from equilibrium. We can derive the geoid deviations and deflections of the vertical as functions of the gravity anomalies, and we thus arrive at the theorem first stated by Stokes in the middle of the nineteenth century.

Stokes' theorem is valid only if all the irregular masses of the second group mentioned above, which cause the anomalies, are inside the geoid. In discussing this point we shall come to the conclusion that this problem —like all other problems connected with the application of Stokes' theorem and of the formulas derived from it, which express the deflections of the vertical in the gravity anomalies—can best be solved by applying the appropriate topographic and isostatic reductions to the observed gravity anomalies. This means, however, that we shall have to correct the geoid and the deflections of the vertical derived from the reduced gravity anomalies to bring them back to the real geoid of the earth as it was before these masses were taken away.

Chapter 4, "Gravity Measurements," deals with the theory of the mathematical and physical pendulum, the pendulum gravity observations on continents and at sea, the most important types of ordinary and underwater gravimeters and their accuracy.

Chapter 5, on isostasy, contains the following sections: Definition, First Ideas concerning Isostatic Equilibrium, Isostatic Assumptions of Pratt and Airy, Some Isostatic Studies at the Turn of the Century, Pratt-Hayford Isostatic System, Airy-Heiskanen Isostatic System, Vening Meinesz Regional Isostatic System, and Some Other Isostatic Assumptions.

Chapter 6, "Reduction of Gravity Measurements," explains the theory and practice of the free-air reduction, Bouguer reduction, Helmert's condensation reductions, Rudski's inversion reduction, isostatic reductions

according to the Pratt-Hayford, Airy-Heiskanen, and Vening Meinesz systems, the indirect effect, or Bowie reduction, geological corrections, and the cartographic and mass-line methods for isostatic reduction.

Chapter 7 deals with the different types of gravity anomalies from the point of view of isostatic equilibrium. It shows by tables, diagrams, and maps that the Bouguer gravity anomalies are strongly negative in the mountains and still more strongly positive at sea—evidence that isostatic equilibrium exists. It likewise shows why and to what extent the Bouguer anomalies can be misleading in geophysical interpretations of the gravity anomalies. Further considered are the manner in which isostatic anomalies depend on the type of isostatic system in regard to the mode of isostatic equilibrium, the depths of compensation (Pratt-Hayford theory), normal thickness  $T$  of the earth's crust, and the density difference  $\Delta\rho$  of the substratum and earth's crust (floating theories). Finally, it is proved by several examples that the isostatic gravity anomalies according to different  $T$  values yield good values for the normal thickness of the earth's crust and for the thickness of the mountain roots and of the ocean antiroot. The "magical" figure of 30 km for  $T$  is shown to result from many studies carried out on the basis of material from different parts of the world.

For mathematical reasons we have used only one discontinuity in the isostatic studies. We thus get  $T$  values which correspond very closely, physically as well as numerically, to the discontinuity given by seismology. The assumption that  $T = 30$  km and  $\Delta\rho = 0.6$  agrees closely with the results of seismologists when they use two discontinuities and with the evidence of recent seismological surveys of the oceans.

From the gravity results found in areas where the topography appears to be regionally compensated, e.g., volcanic islands, we can also derive an approximate figure for the thickness of the rigid crust. It checks well with the depth in the continents of the M discontinuity.

Chapter 8, "Physical Geodesy," contains, among others, the following sections: Meaning of Geodetic Systems, Historical Development of Geodesy, Most Important Dimensions of Reference Ellipsoids, Significance of the Initial Point of Geodetic Systems, Principles of Physical Geodesy, Gravity Material Necessary and Currently Available, Reduction Method to Be Used, Deflections of the Vertical, Dimensions of the Reference Ellipsoid, and Shape of the Geoid.

Chapter 9, "World Geodetic System," shows in what way and with what accuracy the geodetic system can be converted to the world geodetic system and explains the significance of astronomic-gravimetric supercontrol points, the control of small-scale maps without triangulation, and several other applications of the gravimetric method.

Chapters 8 and 9 contain the essential portions of the main problems of modern geodesy, those which can be solved solely by the gravimetric

method and those in which the gravimetric method leads to simpler yet more accurate solutions than are possible by other existing methods.

Chapter 10 discusses the geophysical meaning of isostasy and of different types of deviations from isostatic equilibrium. In Part 10A, formulas for elastic, plastic, and shear deformations of the crust are developed, and the manner in which geosynclines are formed is dealt with. Geosynclines are probably a consequence of horizontal compression causing plastic thickening and downbulging of the crust.

In Part 10B the way in which the isostatic equilibrium of the crust is readjusted is dealt with by discussing the readjustment phenomena in Fennoscandia and elsewhere, where at the end of the glacial period the relatively quick removal of the ice load left a disturbance of equilibrium. We shall find that this phenomenon is mainly a function of plastic flow in the substratum.

In Part 10C we use the conclusions reached in Part 10A to discuss the geophysical phenomena in the Indonesian Archipelago and other island-arc areas, especially the belts of strong negative gravity anomalies found there. The phenomena may be interpreted as being the result of great crustal blocks' moving with respect to each other and thus causing, in the zones between them, crustal downbulging and geosyncline development. On the sides of the arcs, crustal shear is predominant, and the shapes of the island arcs can thus be explained.

Part 10D discusses the effects of stress release in the crust and the resulting development of grabens. Such crustal deformations, caused mainly by the formation of tilted fault planes, lead to gravity anomalies, although the system as a whole is in isostatic equilibrium.

Chapter 11 deals with the hypothesis of convection currents in the mantle. Section 11-1 contains a short summary of the chapter and gives the arguments for adopting this hypothesis, one of the most important of which is that the relative block movement in the Indonesian Archipelago, dealt with in Chap. 10A, points, over a great area, to uniaxial horizontal stress in the crust; such a stress can best be explained by the drag exerted by undercurrents.

Section 11-2 treats of the density-transition layer between 200 and 900 km depth, which, in this connection, we interpret as a layer where two modifications of the mantle material (probably olivine) are coexistent. The following sections develop formulas for convection in a plane layer, in a spherical shell, and in a sphere.

Section 11-6 begins the discussion of Prey's development, in spherical harmonics, of the earth's topography, which shows that its main lines, the distribution of continents and oceans, present regular features pointing to their connection with current systems in the mantle. These current systems have probably been preceded by a current system in the whole earth.

This conclusion leads to a theory of the origin, at the beginning of the earth's history, of the core of the earth and of an "ur" continent at the surface, both caused by a current system in the whole earth, which was probably followed by a current system in the mantle that drew the ur continent apart into the continents now existing. The elaboration of this hypothesis brings us further to the assumption of subsequent current systems in the mantle caused by the earth's cooling and repeating themselves during the whole of the earth's history. To these systems of convection currents we may attribute not only the relative movement of crustal blocks, and between them the development of geosynclines with accompanying orogeny, but also the subsidence in the latter zones of deep basins, e.g., the Banda Sea and Celebes Sea in the Indonesian Archipelago, the Gulf of Mexico and the Caribbean Sea in the West Indies, the Mediterranean basins, and the West Pacific basins.

The further probability that these episodic current systems brought about movements of the entire crust of the earth over the mantle explains the wanderings of the poles with respect to the crust, to which geomagnetic evidence seems to point.

In conclusion Chap. 12 investigates the shear pattern in the crust to which the stresses caused by crustal migrations over a flattened earth must have led.

## CHAPTER 2

### INTERNAL CONSTITUTION OF THE EARTH

Seismology has made major contributions to the study of the earth's interior. It has revealed three principal discontinuities within the earth, viz., the boundaries between the crust and the mantle, the mantle and the core, and inside the core. In addition, seismic-wave velocities have provided data for the densities of the different layers.

#### 2-1. The Crust

We shall call the first of the discontinuities the M interface and the crust above it the M crust, after Mohorovičić, who first mentioned this discontinuity in a paper<sup>46\*</sup> published in 1909, in which he assumed a single crustal layer 60 km thick to explain the two phases found in the Kulpa Valley earthquake. The reason for giving a special name to the crust above the M interface is to distinguish it from the rigid crust, which is based on a different definition related to its physical reaction to stress.

Since the publication of Mohorovičić's paper many investigations have been made of possible interfaces between surface layers of the earth in the continents. Discontinuities have been found between sedimental layers and the granite layer below them and between the granite layer and the lowest layer of the M crust, which is usually called the intermediate layer, but no clear picture has been obtained. Seismic velocities in the intermediate layer seem to indicate that it is basaltic, but its thickness and the thickness of the granite layer appear to vary considerably over the earth's surface. Jeffreys's results<sup>34</sup> (1926) calling for 12 km of granite and 25 km of basalt have been contradicted by other figures derived elsewhere. Lee<sup>42</sup> obtained for Northern Europe a sedimentary layer of 1 km, a granitic layer of 14 km, and a basaltic layer of 15 km. In 1937 Jeffreys<sup>35</sup> critically examined all the European data then available and, finding much inconsistency, assumed 17 km of granite and 9 km of basalt as fitting best. For southern California Gutenberg<sup>30</sup> found evidence for four layers of 14, 11, 6, and 8 km thickness, respectively, and for northern California Byerly and Wilson<sup>16</sup> obtained three layers of 13, 12, and 6 km, respectively. Leet<sup>43</sup> found, in 1933, a surface layer 23 km thick for New England; Robertson's

\* These numbers refer to references at the end of each chapter.

results<sup>50</sup> for Missouri showed two layers of 16 and 13 km, respectively. The great diversity of these figures is apparent; Macelwane<sup>44\*</sup> appears justified in pointing out "the futility of trying to determine these quantities by combining heterogeneous groups of observations of inadequate accuracy from many earthquakes."

We shall not discuss the matter further here, and henceforth we shall suppose a mean constitution of the continental crust of 17.5 km of granite of density 2.67 and of 17.5 km of basalt of density 3.00. We must keep in mind, however, while using these figures, the uncertainties resulting from the variability of constitution.

For the crust under the oceans present data are much fewer than for the continents, but they agree well. Seismic work at sea was started by Ewing<sup>24, 25</sup> and Bullard<sup>9</sup> and continued by their collaborators and by Hill<sup>32</sup> and Raitt.<sup>48</sup> The results indicate that the crust below the oceans consists of a thin layer of usually less than 1 km of unconsolidated sediments (small P-wave velocity  $V_P$ ), of 1 to 4 km of sediments ( $V_P = 4.5$  to  $5.3$  km/sec), of a layer probably basaltic ( $V_P = 6.5$  to  $7.0$  km/sec) possibly also containing old or dolomitized sediments, and lastly ultrabasic rocks (according to Raitt:  $V_P = 8.0$  to  $8.6$  km/sec). So, as far as our present knowledge goes, we are probably near the truth if we assume that the rigid oceanic crust consists on the average of 0.8 km of unconsolidated sediments of density 2.0, of 2.5 km of sediments of density 2.7, of 5 km of basalt of density 3.0, and below that of ultrabasic rocks of density 3.27. These views are also consistent with Kuenen's<sup>39</sup> estimate of about 3 km of sediments for the whole geological past, and (see Chap. 11) with petrographic ideas. For a more detailed picture we may have to change the thickness of the sediments and perhaps also of the basalt. Raitt<sup>48</sup> stresses the variability of these thicknesses.

Since it must be assumed that the M discontinuity is the interface between the basalt and the ultrabasic rock, the M crust would be only 8.3 km thick. Thus there can hardly be any doubt that, as far as the oceans are concerned, there is a great difference between the two crustal conceptions, the M crust and the rigid crust; in Chap. 7 we find evidence that the thickness of the rigid crust must be from 30 to 40 km.

We find the weights  $P$  of the continental and oceanic columns of unit cross section to be in equilibrium if the sea has a depth of 5100 m, which seems an acceptable figure for the mean depth of the deeper ocean basins. Figure 2-1 represents these columns, and Table 2-1 shows the balance.

The schematic picture used in this book for the application of the Airy hypothesis of isostasy assumes a homogeneous crust in continents and oceans of density 2.67, floating on a subcrustal plastic layer of density 3.27.

\* Page 248 of his contribution to Gutenberg's "The internal constitution of the earth," 2nd ed., from which all the above data have been taken.

		$5.1 \times 1.028$
0.8	$\times$	2.0
		$2.5 \times 2.7$
$17.5 \times 2.67$		
		$5.0 \times 3.0$
<hr/>		
		$21.6 \times 3.27$
$17.5 \times 3.00$		

FIG. 2-1. Continental and oceanic crust.

TABLE 2-1

<i>Thickness</i>	<i>Density</i>	$P_c$	<i>Thickness</i>	<i>Density</i>	$P_o$
17.5 km	$\times$ 2.67	= 46.73	5.1 km	$\times$ 1.028	= 5.24
17.5 km	$\times$ 3.00	= 52.50	0.8 km	$\times$ 2.0	= 1.60
			2.5 km	$\times$ 2.7	= 6.75
			5.0 km	$\times$ 3.00	= 15.00
			21.6 km	$\times$ 3.27	= 70.63
35 km		99.23	35 km		99.22

For its thickness  $T$ , in case of zero topography, values of 20, 30, 40, and 60 km have been introduced, and tables for isostatic reduction of gravity have been based on them. From the 37 observed gravity profiles over continental margins, reduced according to these tables, the value of  $T$  in those areas seems to be between 20 and 30 km. It is interesting to see that for the mean of these two values the crust is just in equilibrium with the crustal columns mentioned above. Figure 2-2 represents this case, and Table 2-2 gives the

TABLE 2-2

$25 \times 2.67$	<i>Thickness</i>	<i>Density</i>	$P_c$
	25 km	$\times$ 2.67	= 66.75
	10 km	$\times$ 3.27	= 32.7
			99.45

FIG. 2-2. Schematic crust, used for isostatic reductions.

weight  $P_c$  of the corresponding crustal column. It nearly approaches the previous figures  $P_c$  and  $P_o$ , and so the gravity results check well with the picture obtained seismically.

We may ask how great the sea depth would be if there were no sediments covering the basaltic layer. Comparing the continental column with the column corresponding to this condition, we find that a depth of 6200 m would result in equilibrium. The weight  $P_o$  of a column of unit cross section would be

$$\begin{aligned} P_o &= 6.2 \times 1.028 + 5 \times 3.00 + 23.8 \times 3.27 \\ &= 6.37 + 15.00 + 77.83 = 99.20 \end{aligned}$$

and this checks with the value of  $P_c$  of Table 2-1. If we assume that the basalt is also absent and that the ocean floor is therefore formed by ultrabasic matter of density 3.27, we find an ocean depth of 6800 m. The column weight would then be

$$P = 6.8 \times 1.028 + 28.2 \times 3.27 = 6.99 + 92.21 = 99.20$$

Since seismology shows that, when the effect of increasing pressure and temperature is neglected, the density of 3.27 probably continues for far over 100 km, we come to the interesting conclusion that the depth obtained would be about the maximum depth for an ocean floor in isostatic equilibrium. This result seems to be in fair agreement with the depth values of broad ocean basins, which seldom are much greater than 6500 m.

The last two discussions have already involved problems of isostasy. We shall deal with this subject in Chaps. 6 to 8, where it is discussed in detail.

## 2-2. The Mantle

The greater part of the earth, between the M interface and the discontinuity at 2900 km depth, is the mantle of the earth. There is no evidence of a discontinuity in the mantle itself, but that does not mean its density is constant. The density curve (Fig. 2-4) and Table 2-3 were derived by Bullen,<sup>12,13</sup> using certain assumptions, from Jeffreys's<sup>36</sup> velocity curve for seismic waves (Fig. 2-3) combined with figures of Lambert and Darling.<sup>41</sup>

Birch<sup>6</sup> has derived the density curve after reducing each value to surface temperature and pressure conditions, with highly interesting results. He finds an upper layer of the mantle, below the crust, reaching to a depth of 200 km, which probably has a constant density of about 3.3. Then there follows a layer from 200 to 900 km depth, where a gradual transition of density from 3.3 to 4.0 occurs, and finally a layer from 900 to 2900 km depth with a constant density of about 4.0 throughout (Fig. 2-5). The fact that the major part of the mantle, reaching from 900 to 2900 km depth, seems to be homogeneous points to the existence of current systems to keep it that way. The upper layer of the mantle, of 200 km, also appears to be

TABLE 2-3. DENSITY (AFTER BULLEN), GRAVITY, AND PRESSURE IN THE EARTH<sup>41</sup>

Depth, km	Radius $r$ , km	Density $\rho$ , g/cm <sup>3</sup>	Gravity $g$ , cm/sec <sup>2</sup>	Pressure $p$ bars * $\times 10^6$
0	6371	2.76	980	0.000
33	6338	2.82	983	0.009
33	6338	3.32	983	0.009
80	6291	3.36	984	0.025
80	6291	3.87	984	0.025
200	6171	3.94	983	0.071
400	5971	4.06	981	0.149
600	5771	4.18	979	0.230
800	5571	4.30	977	0.313
1000	5371	4.41	975	0.398
1200	5171	4.52	974	0.485
1400	4971	4.63	975	0.574
1600	4771	4.74	977	0.666
1800	4571	4.84	980	0.759
2000	4371	4.94	987	0.855
2200	4171	5.03	996	0.954
2400	3971	5.13	1010	1.056
2600	3771	5.22	1028	1.161
2700	3671	5.27	1041	1.216
2900	3471	5.57	1068	1.330
2900	3471	9.74	1068	1.33
3000	3371	9.90	1048	1.41
3200	3171	10.20	1005	1.62
3400	2971	10.47	960	1.82
3600	2771	10.72	913	2.02
3800	2571	10.95	865	2.21
4000	2371	11.16	816	2.40
4200	2171	11.36	767	2.58
4400	1971	11.54	717	2.75
4600	1771	11.71	670	2.91
4800	1571	11.87	632	3.06
4982	1389	12.00	598	3.19
5121	1250	15.01	564	3.30
5400 †	971	16.16	457	3.53
5700 †	671	17.07	326	3.72
6000 †	371	17.65	184	3.85
6371	0	17.9	0	3.92

\* The bar is the meteorologist's bar of  $10^6$  dynes/cm<sup>2</sup>, which is equal to 0.987 atm. The pressure at the center is thus  $3.92 \times 10^{12}$  cgs units.

† The figures for  $d = 5400$ , 5700, and 6000 km have been interpolated into Bullen's scheme.

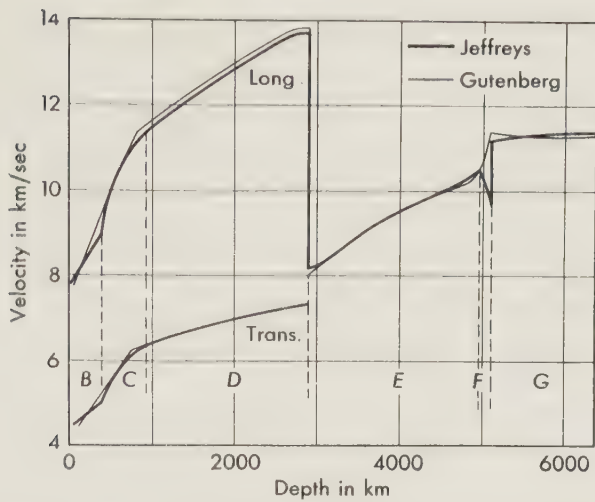


FIG. 2-3. Seismic velocities in the earth. (From Walter M. Elsasser, The earth's interior and geomagnetism, Rev. Modern Phys., vol. 22, no. 1, pp. 1-35, 1950.)

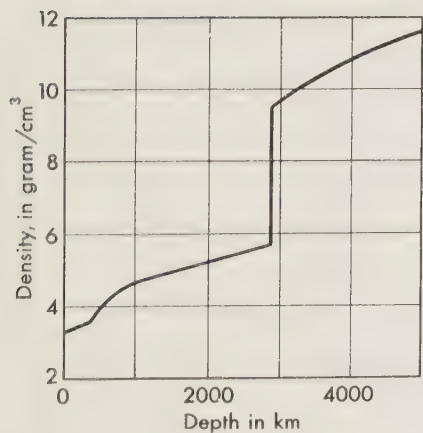


FIG. 2-4. Density in the earth (after Bullen); curve stops at boundary of central body. (From Walter M. Elsasser, The earth's interior and geomagnetism, Rev. Modern Phys., vol. 22, no. 1, pp. 1-35, 1950.)

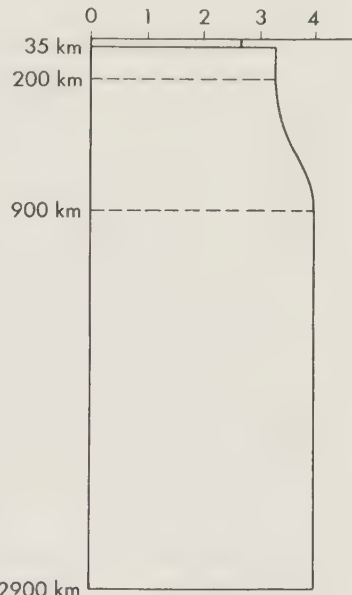


FIG. 2-5. Density in the mantle, reduced to surface temperature and pressure (after Birch).

homogeneous, but over the 700 km between these two layers there is a slow transition in density.

Putting the evidence together, the author (V.M.) is inclined to believe that convection currents exist over the whole thickness of the mantle below the rigid crust. Acceptance of this hypothesis requires the assumption of chemical homogeneity over the entire depth, which without doubt implies two different crystalline modifications, represented by the upper layer (from 35 to 200 km depth) and the lower layer (from 900 to 2900 km depth), and a transition in the intermediate 700 km. This picture could, under some special conditions, involve convection currents' breaking through the layer of transition. In Chap. 11 we return to this hypothesis and to the conditions required.

In his important paper "The Earth's Interior and Geomagnetism"<sup>22</sup> (p. 11) Elsasser mentions the high value of seismic velocities in the mantle and comes to the conclusion that laboratory experiments at high pressures equaling those in the upper part of the mantle show that only a few silicates fulfill the necessary condition, viz., olivine and pyroxenes, some garnets, and jadeite. The opinion of many geophysicists, e.g., Jeffreys and Adams,<sup>1</sup> tends toward the assumption that the mantle consists largely of olivine; in 1939 Birch<sup>5</sup> stated his opinion that the experiments do not permit a choice between olivine and the pyroxenes. It can be concluded that indications favor a mantle consisting of ferromagnesium silicates.

### 2-3. Definition of the Rigid Crust; Boundary between It and the Plastic Mantle

An important subject still to be dealt with, the definition of the rigid crust and its boundary with the plastic mantle, leads to the difficult problem of stress-strain relations. We shall define the rigid crust as that part of the earth which reacts elastically to all stresses—or, better, all stress differences—below a rather high elastic limit, i.e., probably more than 1000 kg/cm<sup>2</sup>. Although the stress differences exceed the limit in tectonic deformations, including the development of geosynclines and crustal fault planes, it is probably safe to assume that at all other times they do not.

For continents the lower boundary of the rigid crust thus defined probably coincides with the M discontinuity. It will be seen (Chap. 8) that the degree of regionality of isostatic compensation in the continents, as derived from gravity anomalies, corresponds to a thickness for the rigid crust of about 30 km and is therefore in the neighborhood of the value for the thickness of the M crust. Since the change in chemical composition can be expected to cause a certain discontinuity in physical behavior, there is some probability that the lower boundary of the rigid crust coincides with the M interface.

For oceans there can be no doubt that the lower boundary of rigidity occurs in the ultrabasic upper layer of the mantle, which probably can be considered homogeneous. So the change from the rigid to the plastic state must here be a function of temperature and pressure. Therefore, the decrease of the limit of elasticity with increasing depth, and likewise increasing temperature, is probably gradual, though the change may be fairly rapid, especially when the melting temperature is approached.

So in the oceans the lower boundary can be expected to vary with depth, according to temperature conditions in the upper layers of the earth. The same may be true in the continents, where the lower boundary may well deviate from the depth of the M interface, which itself may be variable. Consequently, differences between the depth of the rigidity boundary below the oceans and that below the continents can be expected.

In this connection it is appropriate to summarize the results for stress and strain characteristics of the materials of which the earth consists; stress-strain behavior plays a part in many of the geophysical problems dealt with in this book.

#### 2-4. Stress and Strain Characteristics in the Earth

This summary of stress-strain behavior is restricted to data and concepts believed to be applicable to the materials of the earth and valid for slowly varying strains. These data have been obtained from laboratory experiments on rock materials by Griggs,<sup>29</sup> Bridgman,<sup>7</sup> Goguel,<sup>26</sup> and many others; from extensive research on plastics, textiles, rubber, and metals; and from the results and conclusions drawn from geological and geophysical observations. Use will be made of the excellent summaries and views on these subjects given by Gutenberg and Benioff,<sup>31b</sup> Jeffreys,<sup>37</sup> and Goguel.<sup>27</sup>

In dealing with problems of strain we shall distinguish between the general compression caused by hydrostatic compressive stress  $\sigma$  (henceforth called "pressure"), which always has an elastic character, and the deformation caused by the stress deviator, which is given by the direction and size of the three principal stresses diminished by their mean value  $\sigma$ , i.e., by  $\sigma_1 - \sigma$ ,  $\sigma_2 - \sigma$ , and  $\sigma_3 - \sigma$  ( $\sigma = \frac{1}{3}\sigma_1 + \frac{1}{3}\sigma_2 + \frac{1}{3}\sigma_3$ ); (the positive sign given here to compressive normal stress will be used throughout the book, except where otherwise noted). The deformation depends not only on the stress deviator but also on the pressure  $\sigma$  and the temperature.

The compression by the hydrostatic stress  $\sigma$  causes a change of volume  $e$  per unit of volume given by the simple formula

$$e = \frac{\sigma}{k} \quad (2-1)$$

in which  $k$  is the bulk modulus.  $k$  slowly increases with depth below the

earth's surface. Gutenberg<sup>31a</sup> (p. 377) gives a curve for the values of  $k$  in the earth's interior derived from the velocities of longitudinal seismic waves. The curve (Fig. 2-6) starts from a value for  $k$  of  $5 \times 10^{11}$  dynes/cm<sup>2</sup> for the "granite" layer of the crust.\*

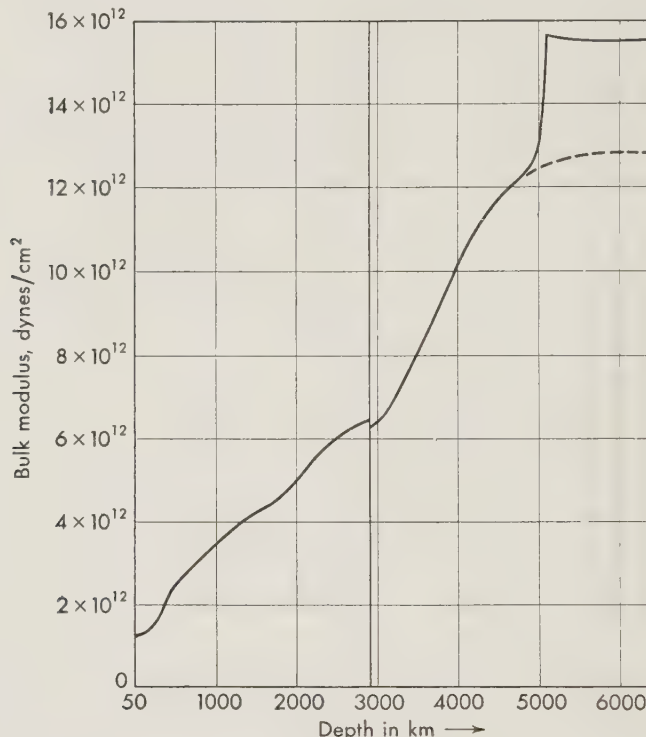


FIG. 2-6. Bulk modulus  $k$  in the earth (after Gutenberg). (From Beno Gutenberg (ed.), Internal constitution of the earth, 2nd ed., Dover, New York, 1951.)

Before taking up the more complicated subject of the strain behavior caused by the stress deviator, we shall review briefly some of the concepts of vector analysis essential to our discussion.†

If we consider an element of a body subjected to deformation and compare the position of an arbitrary point of it before and after application of

\* We have neglected here the fact that there may be a small part of the change of volume  $e$  which is not necessarily restored when the compression vanishes, and which, therefore, has a more or less permanent character. We refer to the possibility that strong compression may result in a closer approach to ideal crystallization of the rock. It does not seem likely that this small effect plays any great part in geophysical phenomena.

† For a more detailed treatment see F. A. Vening Meinesz, Elasticity and plasticity, Appl. Sci. Research, sec. A, vol. 6, pp. 205-225, 1956.

the field of stress by determining the components  $\Delta x$ ,  $\Delta y$ ,  $\Delta z$  of its translation with respect to a system of  $xyz$  coordinates of which the origin remains coincident with another point of the element, we obtain the following relations: we suppose an element small enough for the deformation to be homogeneous throughout.

$$\begin{aligned}\Delta x &= \epsilon_{11}x + \epsilon_{12}y + \epsilon_{13}z \\ \Delta y &= \epsilon_{21}x + \epsilon_{22}y + \epsilon_{23}z \\ \Delta z &= \epsilon_{31}x + \epsilon_{32}y + \epsilon_{33}z\end{aligned}\quad (2-2)$$

We can suppose the nine quantities  $\epsilon_{ik}$  to be so small that, with respect to unity, their squares and products can be neglected.

Indicating vectors by a bar above the letter and affinors, tensors, and deviators by capital letters, we can write Eqs. (2-2) in the form

$$\overline{\Delta r} = D\bar{r} \quad (2-2a)$$

where  $\bar{r}$  is the position vector (components  $x$ ,  $y$ ,  $z$ ) and  $\overline{\Delta r}$  the displacement vector (components  $\Delta x$ ,  $\Delta y$ ,  $\Delta z$ ). The affinor  $D$ , which characterizes the phenomenon, is given by

$$D = \begin{pmatrix} \epsilon_{11} & \epsilon_{12} & \epsilon_{13} \\ \epsilon_{21} & \epsilon_{22} & \epsilon_{23} \\ \epsilon_{31} & \epsilon_{32} & \epsilon_{33} \end{pmatrix} \quad (2-2b)$$

We can divide the affinor into three parts representing a general compression, a rotation, and a deformation without change of volume. The first part is determined by one quantity  $\epsilon$ , given by

$$\epsilon = \frac{1}{3}(\epsilon_{11} + \epsilon_{22} + \epsilon_{33}) \quad (2-3a)$$

It is related to the volume compression  $e$  by

$$\epsilon = \frac{1}{3}e \quad (2-3b)$$

The second part is determined by three quantities  $\epsilon''_{12}$ ,  $\epsilon''_{13}$ ,  $\epsilon''_{23}$ , given by

$$\begin{aligned}\epsilon''_{12} &= \frac{1}{2}(\epsilon_{12} - \epsilon_{21}) \\ \epsilon''_{13} &= \frac{1}{2}(\epsilon_{13} - \epsilon_{31}) \\ \epsilon''_{23} &= \frac{1}{2}(\epsilon_{23} - \epsilon_{32})\end{aligned}\quad (2-4)$$

It is called a rotor and can be represented by a vector in the direction of the axis of rotation, the length of the vector giving the angle of rotation.\*

The third part is determined by five quantities represented by the six constituents  $\epsilon'_{11}$ ,  $\epsilon'_{22}$ ,  $\epsilon'_{33}$ ,  $\epsilon'_{12}$ ,  $\epsilon'_{13}$ ,  $\epsilon'_{23}$ , the first three of which fulfill the

\* The  $x$ ,  $y$ ,  $z$  components of the vector are  $\epsilon''_{23}$ ,  $\epsilon''_{13}$ ,  $\epsilon''_{12}$ .

condition

$$\epsilon'_{11} + \epsilon'_{22} + \epsilon'_{33} = 0 \quad (2-5a)$$

They are given by

$$\begin{aligned}\epsilon'_{11} &= \epsilon_{11} - \epsilon \\ \epsilon'_{22} &= \epsilon_{22} - \epsilon \\ \epsilon'_{33} &= \epsilon_{33} - \epsilon\end{aligned} \quad (2-5b)$$

The other three are given by

$$\begin{aligned}\epsilon'_{12} &= \frac{1}{2}(\epsilon_{12} + \epsilon_{21}) \\ \epsilon'_{13} &= \frac{1}{2}(\epsilon_{13} + \epsilon_{31}) \\ \epsilon'_{23} &= \frac{1}{2}(\epsilon_{23} + \epsilon_{32})\end{aligned} \quad (2-5c)$$

This part of the affinor is called a deviator; it characterizes the deformation of the element without volume change.

The affinor  $D$  thus consists of the following three parts:

$$D_s = \begin{pmatrix} \epsilon & 0 & 0 \\ 0 & \epsilon & 0 \\ 0 & 0 & \epsilon \end{pmatrix} \quad (2-5d)$$

$$D_r = \begin{pmatrix} 0 & \epsilon''_{12} & \epsilon''_{13} \\ -\epsilon''_{12} & 0 & \epsilon''_{23} \\ -\epsilon''_{13} & -\epsilon''_{23} & 0 \end{pmatrix} \quad (2-5e)$$

$$D_d = \begin{pmatrix} \epsilon'_{11} & \epsilon'_{12} & \epsilon'_{13} \\ \epsilon'_{12} & \epsilon'_{22} & \epsilon'_{23} \\ \epsilon'_{13} & \epsilon'_{23} & \epsilon'_{33} \end{pmatrix} = -\epsilon'_{11} - \epsilon'_{22} \quad (2-5f)$$

which, multiplied by the position vector  $\bar{r}$ , give the compression, the rotation, and the deformation without change of volume of the element considered. The sum of the first and third parts is called a tensor; it gives the total deformation of the element including the change of volume.

In a manner analogous to that used for a vector and a scalar, an affinor, a deviator, and a tensor can be handled without going back to their constituent quantities. Further details of these operations can be found in treatises on vector analysis.

The six components of a stress field form a tensor  $S$

$$S = \begin{pmatrix} \sigma_x & \tau_z & \tau_y \\ \tau_z & \sigma_y & \tau_x \\ \tau_y & \tau_x & \sigma_z \end{pmatrix} \quad (2-6a)$$

of which each line gives the three components of the stress working on one of the coordinate planes; the  $\sigma$ 's represent the normal-stress components and the  $\tau$ 's the shear-stress components.

The mean value  $\sigma$  of the three normal-stress components of the principal diagonal causes the change of volume by general compression; such an all-sided stress is usually called a "hydrostatic stress" or "pressure" because it is the only stress present in water if the very slight inner friction is neglected.

The stress deviator  $S_d$  is given by

$$S_d = \begin{pmatrix} \sigma'_x & \tau'_z & \tau'_y \\ \tau'_z & \sigma'_y & \tau'_x \\ \tau'_y & \tau'_x & \sigma'_z \end{pmatrix} \quad (2-6b)$$

where

$$\begin{aligned} \sigma'_x &= \sigma_x - \sigma & \tau'_x &= \tau_x \\ \sigma'_y &= \sigma_y - \sigma & \tau'_y &= \tau_y \\ \sigma'_z &= \sigma_z - \sigma & \tau'_z &= \tau_z \end{aligned} \quad (2-6c)$$

The stress deviator causes the strain deviator mentioned above (2-5f), which determines the deformation without change of volume. The usually adopted theory of elasticity follows Hooke's law and assumes that the deformation is proportional to the stress, an assumption that is also made, using the same ratio, for each constituent of the strain and stress deviators. The ratio is  $2\mu$ , where  $\mu$  is the modulus of shear,\* and so

$$S_d = 2\mu D_d \quad (2-7)$$

As compression and deformation without change of volume must mean a different molecular phenomenon, the moduli  $2\mu$  and  $3k$  † cannot be expected to have the same value. It appears likely that the resistance to deformation is smaller than that to compression and that therefore, in general,  $2\mu < 3k$ . We shall denote the ratio  $2\mu/3k$  by  $\alpha$ , and so

$$\frac{2\mu}{3k} = \alpha \quad (2-8a)$$

$$\alpha < 1 \quad (2-8b)$$

This is confirmed by the reaction to compression in one direction. Although apparently a simple stress field, in reality it is somewhat more complicated; it combines the two basic phenomena discussed here, and the re-

\* Since Formula (2-5c) shows  $\epsilon'_{12}$ ,  $\epsilon'_{13}$ , and  $\epsilon'_{23}$  to be half of the sums  $\epsilon_{12} + \epsilon_{21}$ ,  $\epsilon_{13} + \epsilon_{31}$ , and  $\epsilon_{23} + \epsilon_{32}$ , which determine the angles of shear caused by  $\tau_x$ ,  $\tau_y$ , and  $\tau_z$ , the ratio is  $2\mu$  and not  $\mu$ .

† As  $k$  is related to  $e$ , the modulus of  $\sigma$  with respect to  $\epsilon$  [Formula (2-3b)] is  $3k$ .

sult is not only a compression in the stress direction but also a dilatation in the directions at right angles to it. The compression is given by Young's modulus  $E$  and the ratio compression/dilatation by Poisson's constant  $m$ . In some publications the inverse ratio,  $1/m$ , is used; it is usually indicated by  $\sigma$  and called Poisson's ratio.

We find for Poisson's constant

$$m = \frac{2 + \alpha}{1 - \alpha} \quad (2-8c)$$

and so  $\alpha = 1$  (or  $2\mu = 3k$ ) would mean no lateral dilatation and  $\alpha > 1$  (or  $2\mu > 3k$ ) a lateral compression. Such an unlikely lateral reaction has not been observed for any material, and so it can be concluded that  $2\mu$  can never be greater than  $3k$ .

The other constants used in describing elastic behavior according to Hooke's law can also be expressed in terms of  $\alpha$  and  $k$  or  $\alpha$  and  $\mu$ ; we obtain Young's modulus

$$E = \frac{9\alpha}{2 + \alpha} k = \frac{6}{2 + \alpha} \mu \quad (2-8d)$$

and Lamé's constant

$$\lambda = (1 - \alpha)k = \frac{2(1 - \alpha)}{3\alpha} \mu \quad (2-8e)$$

It is obvious that the behavior of the materials of the earth under the effect of stress fields is often more complicated than the elastic deformation according to Hooke's law. The hypothesis of plastic deformation is in many cases a better approximation. This refers to the deviator part of the strain; the hydrostatic-compression part probably remains elastic. We shall define the plastic behavior here as (1) an elastic reaction to stresses below a certain limit, which we shall call "elastic limit" or "strength," and (2) permanent strain, possibly some kind of flow, for greater stresses. The term "elastic" is used here to mean that when the stresses vanish, the deformation entirely disappears, while "permanent strain" indicates that it does not.

For the upper part of the crust the elastic limit of uniaxial stress can be assumed to be considerable, probably more than  $10^9$  dynes/cm<sup>2</sup>. Under the effect of higher temperatures farther down, the strength is likely to diminish, falling below  $1$  to  $2 \times 10^7$  dynes/cm<sup>2</sup> in the subcrustal layer and probably remaining of that order of magnitude in the whole mantle.

The presence of an elastic limit below which stresses bring about purely elastic deformation has been advocated, e.g., by Goguel.<sup>27,28</sup> One of his strongest arguments is based on the study of mixed rocks in which frag-

ments having different physical properties are present. He mentions that in "la Vanoise" (French Alps) alternating layers of limestone and dolomite occur that have been subjected to strong deformation. The limestone layers show flow, while the dolomite fragments are sharply angular. It must be concluded that the flow of the limestone prevented the stresses from reaching the elastic limit of the dolomite.

The authors believe that there are also strong geophysical indications that the materials of the crust have a certain strength. In many cases the crust reacts elastically to long-period stresses, e.g., where regional isostatic compensation is present, but for tectonic phenomena a plastic behavior prevails; this fact evidently implies an elastic limit. There are also geophysical arguments for an elastic limit in the mantle, though it must be much smaller; it can hardly be much more than 1 to  $2 \times 10^7$  dynes/cm<sup>2</sup>, for otherwise isostasy could not be approached so closely. We shall return to this problem, especially in Chap. 11.

Before discussing how the elastic limit has to be defined for different types of stress fields, we first examine how viscous flow in a Newtonian fluid can be dealt with. For an element as represented by Fig. 2-7 the elastic deformation  $\gamma$  is proportional to the shear stress  $\tau$ , and viscous flow in a Newtonian fluid would imply that  $\tau$  is proportional to  $\partial\gamma/\partial t$ . The equations for both cases have the same form, but the strain of the elastic case is replaced by the derivative with respect to time of the strain and the shear modulus  $\mu$  by the viscosity modulus  $\eta$ . So for the latter case, the constituents of the stress deviator are proportional to the time derivatives, or "fluxions," of the constituents of the strain deviator (2-5f). We can write this as

$$S_d = 2\eta \dot{D}_d \quad (2-9a)$$

For the compressional part of the stress field a similar flow phenomenon is evidently impossible; the compression must remain elastic, though for high stresses perhaps part of it may result in permanent strain. So the modulus of compression  $k$  for the compressional fluxion must be infinite. Thus, according to (2-8a) and (2-8c) we find that for flow  $\alpha = 0$  and Poisson's constant is

$$m = 2 \quad (2-9b)$$

For plastic flow we shall again start from the simple case of shear represented by Fig. 2-7. A possible supposition in connection with an elastic limit  $\tau_l$  is that the total strain is given by an elastic part proportional to

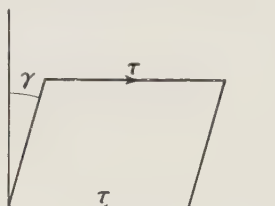


FIG. 2-7. Shear diagram.

the total stress  $\tau$  and a flow part of which the velocity is proportional to  $\tau - \tau_l$

$$\gamma = \frac{\tau}{\mu} + \int_0^t \frac{\tau - \tau_l}{\eta} dt \quad (2-10)$$

For more complicated stress fields two suggestions have been made for the introduction of an elastic limit, both of which are in harmony with (2-10). According to the first, the criterion for the limit is the maximum shear  $\tau$ —which can also be defined as half of the difference of the largest and smallest principal stress—and the second is the Huber-Hencky, or von Mises, criterion, according to which stress fields are equivalent if they have the same sum of the squares of the constituents of the stress deviator (2-6b),

$$F = \sigma_x'^2 + \sigma_y'^2 + \sigma_z'^2 + 2\tau_x'^2 + 2\tau_y'^2 + 2\tau_z'^2 = \frac{2}{3}\sigma_v^2 \quad (2-11)$$

in which  $\sigma_v$  is the equivalent uniaxial stress (Hencky). The criterion can also be stated as follows: stress fields are equivalent if they have the same energy connected with the deviator part of the strain. This elastic energy is given by  $F/4\mu$ . It can be shown (see e.g., Jeffreys,<sup>37</sup> p. 13) that this criterion for the stress limit can never differ more than 8 per cent from the first.

From a considerable amount of experimental research it seems to follow that, when pressure prevails—as is generally the case in the earth—the Huber-Hencky-von Mises criterion is in better harmony with the facts than the maximum-shear criterion. This conclusion can be derived from the stress limits found in different stress conditions (e.g., Jeffreys,<sup>37</sup> p. 13), but, as Bijlaard<sup>17-19</sup> has shown, still stronger evidence is given by the directions of belts of flow, forming in thin plates of great horizontal extent. In Sec. 10A-7, where we apply these results to the earth's rigid crust, we shall find good agreement. In all these cases we must assume that the material gives way by plastic flow. Fracturing and faulting of the crust (see Sec. 10A-8) appear to be governed by other conditions.

Since isotropy is assumed, the stress limit for each constituent of the stress deviator is proportional to the constituent. We denote by  $\psi$  the ratio  $\sigma_l/\sigma_v$  of the uniaxial elastic limit  $\sigma_l$  to the equivalent uniaxial stress  $\sigma_v$ . We may divide our strain deviator into an elastic part,  $D_{de}$ , and a pseudo-viscous part,

$$D_d = D_{de} + \int_0^t \dot{D}_d dt \quad (2-12)$$

where the constituents of the last deviator are the time derivatives of the constituents of the strain deviator of the left member.

The first term of the right member is proportional to the stress deviator

and the second to the excess of this deviator over the elastic-limit stress deviator, and so

$$D_d = \frac{1}{2\mu} S_d + \int_0^t \frac{1 - \psi}{2\eta} S_d dt \quad (2-13)$$

For simple shear, represented in Fig. 2-7, all the constituents of the stress deviator are zero except two, which are equal to  $\tau$ . So

$$F = 2\tau^2 \quad (2-14)$$

Our knowledge of the values, in the earth, of the shear modulus  $\mu$ , often called "rigidity," e.g., by Gutenberg and Jeffreys, of Poisson's constant  $m$ ,

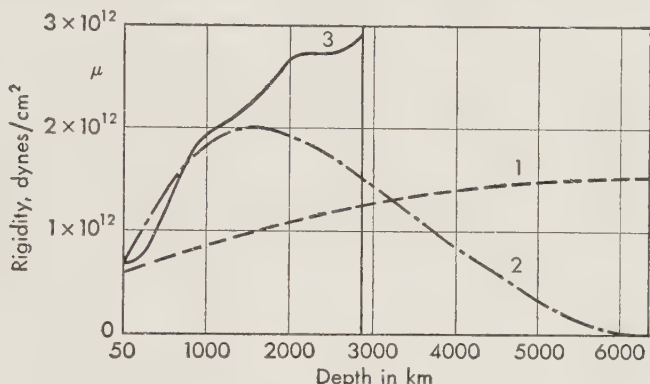


FIG. 2-8. Shear modulus  $\mu$  in the earth (after Gutenberg); curves 1 and 2 are based on observations of body tides and polar movements, curve 3 on the velocity of transverse earthquake waves and the density. (From Beno Gutenberg (ed.), Internal constitution of the earth, 2nd ed., Dover, New York, 1951.)

and of the pseudo-viscosity modulus  $\eta$  is still fragmentary. Discussing the shear modulus  $\mu$ , Gutenberg<sup>31a</sup> (pp. 366–379) gives a curve for its value in the crust and the mantle derived from the velocity of transverse seismic waves and the density; the latter is rather uncertain (see Fig. 2-8, curve 1). In his summary he comes to the conclusion shown in Table 2-4. These figures have been used for drawing curve 2 of Fig. 2-8.

TABLE 2-4. CONSTANT  $\mu$

	$\mu$ , dynes/cm <sup>2</sup>
Recent sediments.....	$\pm 1 \times 10^{10}$
Granitic layers.....	$\pm 3 \times 10^{11}$
At a depth of 100 km.....	$\pm 6\frac{1}{2} \times 10^{11}$
At a depth of a few hundred km.....	$\pm 1 \times 10^{12}$
At a depth of 1000–1500 km.....	$\pm 2 \times 10^{12}$
Near the boundary of the core.....	$\pm 4 \times 10^{12}$

We do not know the value of  $\mu$  in the core of the earth. The fact that transverse seismic waves do not seem to be transmitted by the core—perhaps we can conclude only that the transmitted waves are too weak to be discovered—points to  $\mu$  being small or negligible. The second possibility does not seem contradictory to the earth's behavior with respect to the body tides (Takeuti<sup>51</sup>), nor does it appear to lead to gravitational instability (Meissner,<sup>45</sup> Jeffreys<sup>53</sup>), as has been suggested.

Poisson's constant  $m$  in the earth's interior can be derived from the ratio of the velocities of longitudinal and transverse seismic waves. Data from laboratory experiments are also available. Gutenberg's<sup>31a</sup> conclusion (p. 378) is shown in Table 2-5. The last value follows from the fluid char-

TABLE 2-5. POISSON'S CONSTANT  $m$ 

Granitic layer.....	Slightly more than 4 *
Deeper layers of the crust.....	$m = \pm 4$ ( $\alpha = \pm 0.40$ )
Deeper parts of the mantle.....	$m = \pm 3.3$ ( $\alpha = \pm 0.31$ )
Outer part of the core.....	$m = \pm 2$ ( $\alpha = 0$ )

\* Birch and Bancroft<sup>4</sup> find 4.3 for granite, viz.,  $\alpha = 0.44$ . This low value is probably attributable to the quartz content. Voigt's<sup>54</sup> measurements on the elasticity of quartz point to a value of  $m$  for a pure quartz aggregate as high as 14 (Gutenberg,<sup>31a</sup> p. 69).

acter of the outer part of the core, which can be assumed because of the absence of transverse-wave transmission just mentioned.

According to these values of  $m$  and  $\alpha$ , the ratio of the value of Young's elasticity modulus  $E$  to  $\mu$  is that shown in Table 2-6. With the exception

TABLE 2-6. RATIO  $E/\mu$ 

Granitic layer.....	2.46
Deeper layers of the crust.....	2.50
Deeper parts of the mantle.....	2.60
Outer part of the core.....	3.00

of the last value in the table, which has little importance because we do not know  $\mu$  in the core, we see that in general we can put

$$E = 2.50\mu \quad (2-15)$$

For the modulus of pseudo viscosity  $\eta$  (often called simply the "viscosity") we have only one clear figure, which has been derived from the way the isostatic equilibrium of the rigid crust in Fennoscandia is readjusting itself after the disappearance of the ice. In Part B of Chap. 10, where we deal with this problem in detail, we obtain a value for  $\eta$  of  $1 \times 10^{22}$  poises. This value applies to the upper half of the mantle. For  $\eta$  in the deeper half we have no direct indications; nor do we have them for  $\eta$  in the core, except that the fluid character points to very much lower values.

For the crust,  $\eta$  is probably higher than for the mantle. In Parts A and C of Chap. 10 we shall find indications that values of at least  $10^{23}$  poises, perhaps even of  $10^{24}$  poises or more, are likely.

The elastic and plastic hypothesis discussed in this section will, in general, be followed for the problems dealt with in this book. Since practically always in the earth compression is normal and tension exceptional, we give a positive sign to compressive stress and strain. In Chap. 11, however, where we deal with convection currents and where the velocities are more important than the stresses, we shall keep to the usual system of giving a positive sign to tension; the sign of shear stresses is then also reversed.

We must keep in mind that our assumptions about plasticity are no more than approximations; the plastic behavior which really occurs in the earth is probably more complicated. The laboratory experiments of Griggs,<sup>29</sup> Bridgman,<sup>7</sup> Goguel,<sup>26</sup> and others show a more complex reaction of rocks to stress.

In the first place, a purely elastic reaction to a suddenly applied stress is only partly instantaneous; the second part of the strain takes place gradually with diminishing velocity. Gutenberg has called this behavior "elastic creep." Griggs gives the following formula for the two parts of the forward creep

$$\epsilon = a + b \log t \quad (2-16a)$$

and for the recovery, after the stress is suddenly taken away,

$$\epsilon = a - b \log t \quad (2-16b)$$

In these formulas  $a$  and  $b$  are empirical constants. Figure 2-9b represents this behavior.

Besides this elastic response there may also be pseudo-viscous flow, called "shear creep" by Gutenberg and Benioff (see Fig. 2-9c). The strain  $GH$  represents the permanent strain, which does not vanish after the stress disappears. For the part  $AF$  of the curve, Griggs gives the formula

$$\epsilon = a + b \log t + ct \quad (2-17a)$$

in which, under conditions favoring recrystallization, the velocity  $c$  can be represented by

$$c = a' \sinh b' (\sigma - \sigma_0) \quad (2-17b)$$

$a'$  and  $b'$  again being empirical constants. In this formula Griggs attributes the flow to the excess of stress above the elastic limit  $\sigma_0$ , as we have done in this section.

To the right of  $E$  the velocity of flow increases. Griggs believes that this can be approximately represented by

$$\epsilon = a + b \sinh \alpha (t - t_0) \quad (2-17c)$$

where  $\alpha$  is again an empirical constant. Griggs tentatively attributes this increase to a beginning rupture of the inner coherence of the rock specimen. For higher temperature the pseudo-viscous flow, including the increase of velocity to the right of  $E$ , takes place with greater velocity, and so the horizontal time axis of the curve is shortened.

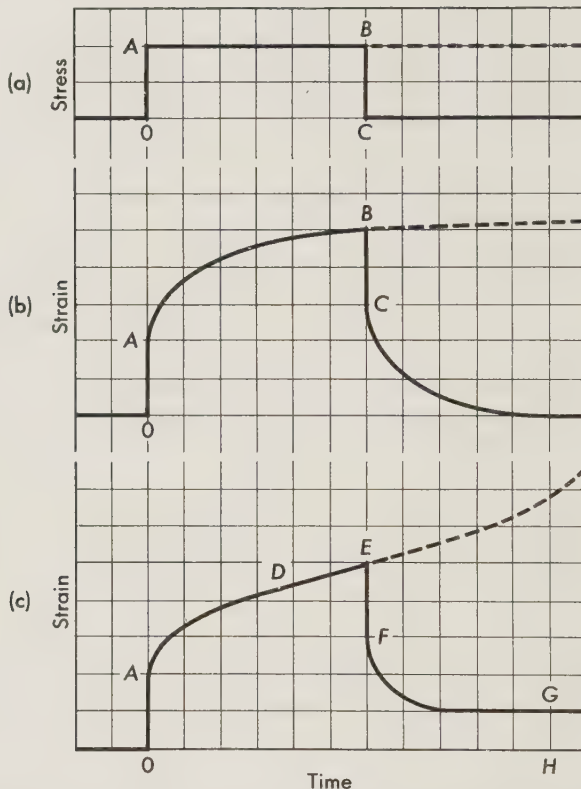


FIG. 2-9. Strain in response to constant stress. (a) The assumed stress as a function of time, (b) strain of a substance having "elastic creep" characteristics, (c) strain of a substance having "elastic flow creep"; characteristics after Gutenberg. (From Beno Gutenberg (Ed.), Internal constitution of the earth, 2nd ed., Dover, New York, 1951.)

We shall not go into a detailed discussion of these important results or of facts found by other investigators. It seems too early to draw final conclusions about the behavior of the earth's materials in deep layers. It does not seem likely, however, that elastic creep will play a great part in long-period stresses and similar phenomena. The deviation from Newtonian flow shown by the flow creep, viz., the increase of flow velocity with time, may have a greater effect, but it is not certain whether this will also occur under the high pressures occurring at great depths.

## 2-5. The Core

The outer part of the core is fluid enough to prevent the transmission of transverse seismic waves. This behavior as a fluid has been demonstrated by Jeffreys<sup>33</sup> along another line by showing that the amplitude of the lunar bodily tide is compatible with the shear modulus of the mantle, as follows from the seismic-velocity data, only if we assume the shear modulus of the core to be negligible. According to the velocity data on longitudinal waves, the density at the interface between mantle and core shows a sudden increase of about 5, and this fact has been an argument for returning to the opinion, e.g., Eucken<sup>28</sup> (1944) and Elsasser<sup>22</sup> (1950), that the core consists of iron and nickel. This great density difference can hardly be explained by a change of phase of ultrabasic matter, e.g., ferromagnesium silicates, in the way Ramsey<sup>49</sup> advocated in 1948, or of undifferentiated solar matter rich in hydrogen, as proposed in 1941 by Kuhn and Rittmann.<sup>40</sup> Neither does it seem possible by the modification of that hypothesis made in 1946 by Kronig, de Boer, and Korringa<sup>38</sup> when they assumed that in the core the hydrogen occurs not in molecular but in atomic form.

Inside the core, at about 5000 km depth, another discontinuity exists, which probably occurs in a narrow zone of transition from about 4980 to 5120 km depth. Table 2-3 shows an increase here of density from about 12.0 to 15.0, and Fig. 2-3 gives the manner of seismic-velocity transition proposed by Gutenberg and Jeffreys. The part of the core inside this zone is usually called the "inner core" or "central body." Its nature is still unknown. In 1946 Bullen<sup>14</sup> expressed the opinion that the greater seismic velocity here could be explained by supposing the inner core to consist of the same mixture of iron and nickel as the outer part of the core but in the solid state. In 1952 Bullen<sup>15</sup> (p. 398) gave some arguments for its being heterogenous and for its containing a fair quantity of material denser than nickel and iron.

Great light has recently been shed on the nature of the core of the earth by new theories about the secular terms of geomagnetism in connection with the irregularities of the earth's rotation, first discovered by Newcomb and since investigated by several astronomers. Both phenomena have a similar variability with time, showing changes at intervals of a few decades. As neither the rigid crust nor the mantle has sufficient mobility to explain these phenomena, and as the mass changes caused by atmospheric or oceanic currents are entirely insufficient for this purpose, the idea has arisen that perhaps movements in the core may be responsible. In harmony with these views is the fact that the world maps of geomagnetic secular change, of which we reproduce those of Vestine<sup>62</sup> for the vertical intensity at the epochs 1912.5 and 1942.5 (see Figs. 2-10 and 2-11), show a limited number of areas of variation having a size and a character that allow us to suppose

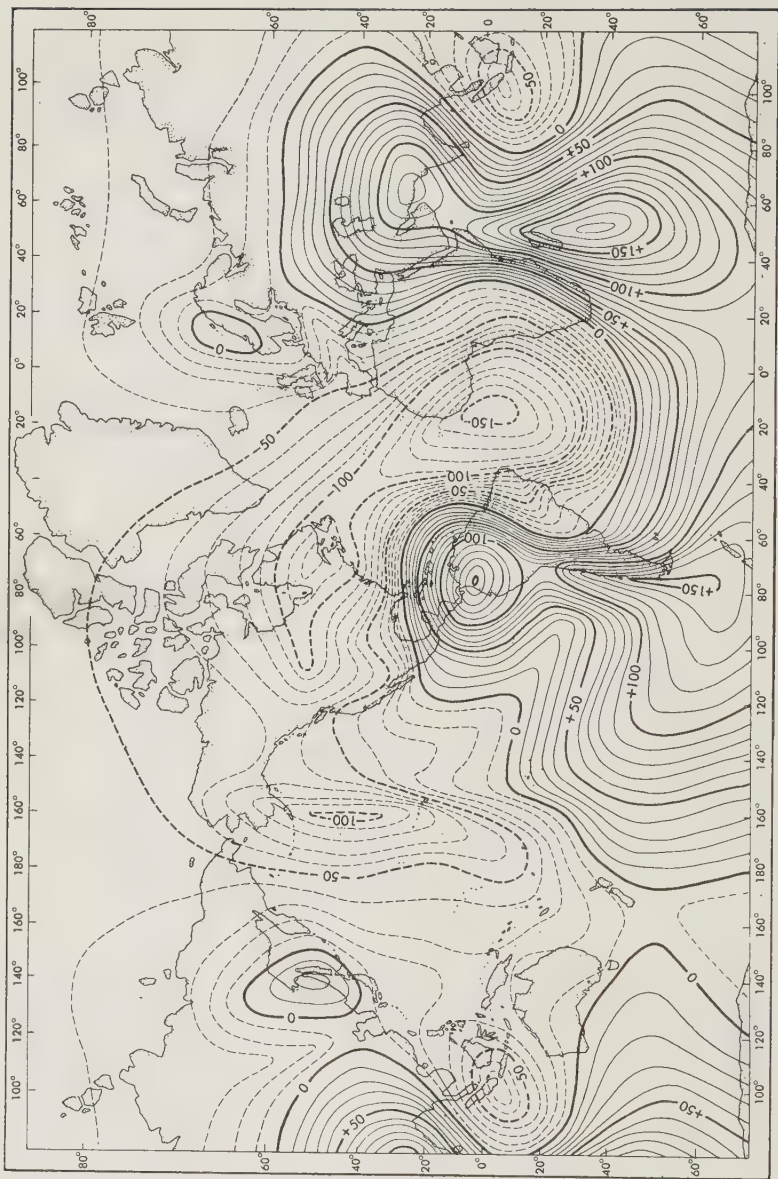


FIG. 2-10. Geomagnetic secular change in gammas per year, vertical intensity, epoch 1912.5 (after Vesteine). (From Walter M. Elsasser, The earth's interior and geomagnetism, Rev. Modern Phys., vol. 22, no. 1, pp. 1-35, 1950.)

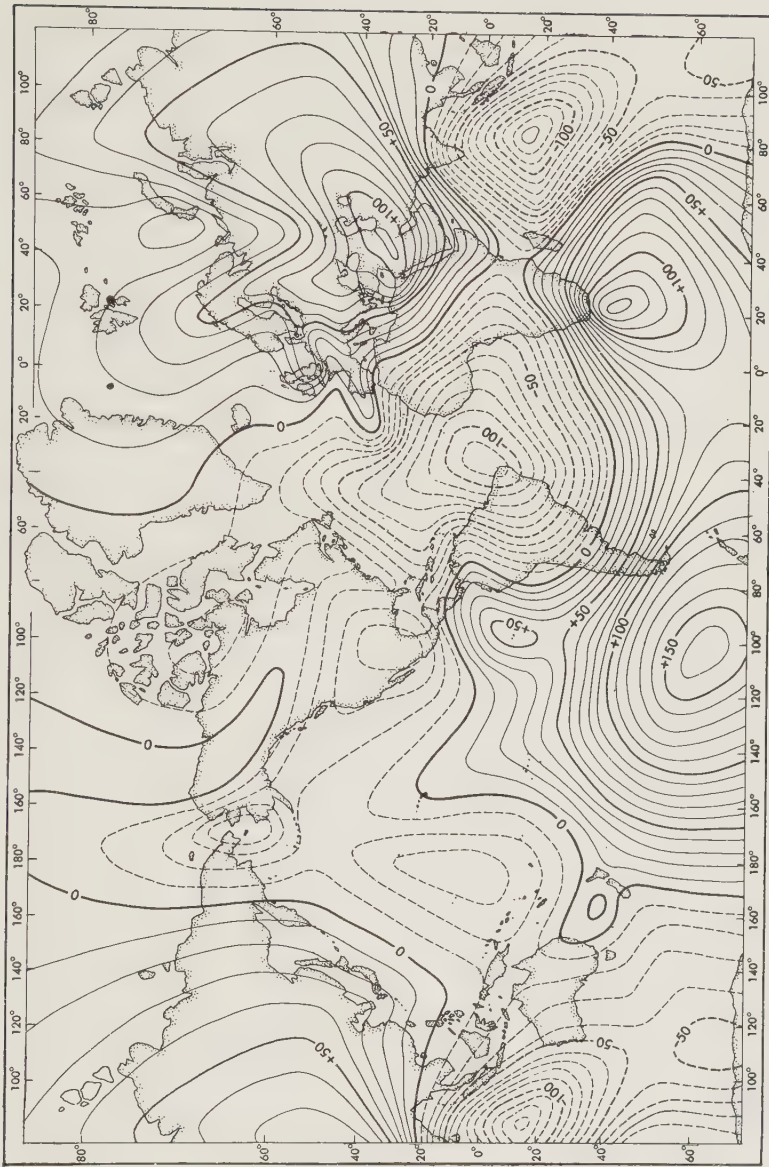


FIG. 2-11. Geomagnetic secular change in gammas per year, vertical intensity, epoch 1942.5 (after Vesteine). (From Walter M. Elsasser, The earth's interior and geomagnetism, Rev. Modern Phys., vol. 22, no. 1, pp. 1-35, 1950.)

that the cause is situated at 3000 km depth. The same is true for Vestine's investigation,<sup>52</sup> by means of spherical harmonics, of the depth at which a spherical sheet of electric currents could be assumed to produce the non-dipole part of the secular geomagnetic field. He finds that the depth could be as great as 3000 km but that it could not be much deeper, for then the series expressing the physical situation diverges.

Figures 2-10 and 2-11 show clearly that the areas of secular disturbance have a tendency to migrate westward; north-south components of movement seem to have a more random character. This westward tendency was noted by Bauer,<sup>2</sup> in 1895, and by Carlheim-Gyllensköld,<sup>20</sup> in 1906. Older references usually go back to van Bemmelen's<sup>3</sup> compilation from records of navigators from 1540 to 1680 of the lines of zero magnetic declination, which, combined with more modern data, give a systematic westward velocity of  $0^{\circ}22/\text{year}$ . This checks well with the result of Bullard;<sup>11</sup> applying the least-squares method to Vestine's maps, he derived a mean figure of the nondipole field of  $0^{\circ}180 \pm 0^{\circ}015/\text{year}$  and of  $0^{\circ}320 \pm 0^{\circ}067/\text{year}$  for the secular variation.

These results \* and considerations have been the basis of Bullard's<sup>10</sup> and Elsasser's<sup>22</sup> hypothesis that the secular part of terrestrial magnetism is caused by currents in the core, probably of a thermal-convection type, which are accompanied by electric currents. The thermal cause is still not quite clear; it may possibly be connected with the presence of radioactive matter in the inner core or with cooling at the upper boundary of the core by slow convection currents in the mantle. As we shall see later (Chap. 11), it is likely that this last type of convection is taking place in the present period and that it has velocities of 1 to 10 cm/year, while the supposed core-current velocity must be at least of the order of 10 km/year.

The electric currents and the corresponding magnetic fields must be assumed to consist of two parts, the "magnetic mode" and the "electric mode." Part of the magnetic field of the magnetic mode extends to the outside of the core, while the electric currents remain inside; the magnetic field of the electric mode remains entirely inside the core and therefore cannot be observed outside it, while part of the electric current probably passes through the mantle. Although we shall not go into details of these phenomena, we should mention that the terrestrial magnetism observed at the surface of the earth must be only part of the total magnetic field and perhaps not even the main part.

The existence of convection currents in the core is important for the other problem mentioned, the irregularity of the earth's rotation. The evidence that at some critical times, viz., about 1860, 1900, and 1920, rather sudden changes occurred in the rotation was difficult to explain

\* In connection with these investigations the names of Chapman, Runcorn, McNish, and several others also ought to be mentioned.

since no great events in the earth's history were known that could account for such changes. A recent study by Brouwer<sup>47</sup> has shed great light on this problem by proving that the observed time curve is one that might be caused by random disturbances of the earth's rotation lasting over several years or even decades.

In 1952 Munk and Revelle<sup>47</sup> reviewed a number of possible causes of these phenomena and concluded that by far the most probable cause, at least for the main part of the disturbances, is provided by the hypothesis of currents in the core. Frictional reaction seems insufficient for transferring the necessary energy from the core to the mantle, but electromagnetic coupling appears capable of effecting the transfer and of accelerating or retarding the rotation of the mantle and crust by the amounts observed astronomically if the velocity of the westward current inside the core varies. The fact that the changes in the length of the day, according to Brouwer's curve, appear to show a correlation with the variations of the westward drift of the secular disturbances of terrestrial magnetism is a strong argument for Bullard's or Elsasser's hypothesis about the earth's magnetism and at the same time for Munk and Revelle's explanation of the irregularities in the earth's rotation. Between 1890 and 1910 the length of the day increased by 3.6 msec, and between 1910 and 1930 it diminished by a similar amount. During the same time intervals the westward drift respectively decreased and increased. These results were confirmed in 1953 in an important paper by Vestine,<sup>53</sup> who concludes that the time fluctuations in the rate of westward drift of the geomagnetic field during the period from 1885 to 1945 correspond reasonably well to the fluctuations in the earth's rate of rotation as given by Brouwer and accord with the requirements of the law of conservation of angular momentum (for details see the papers by Munk and Revelle and by Vestine).

We may also refer to the papers by Bullard and Elsasser and to Vestine's other papers for a more thorough treatment of the important new hypothesis about geomagnetism mentioned in this short summary. The number of data and other considerations that harmonize with it is noteworthy, and the explanation it gives of the irregularity of the earth's rotation is fairly convincing. We shall return to it in Chap. 11, where we discuss the hypothesis of convection in the mantle; it appears likely that the reaction of the mantle on the core previously mentioned is one of the causes of the convection currents in the core.

## REFERENCES

1. Adams, L. H.: Some unsolved problems of geophysics, *Trans. Am. Geophys. Union*, vol. 28, pp. 673–679, 1947.
2. Bauer, L. A.: *Am. J. Sci.*, vol. 50, pp. 109, 189, 314, 1895.
3. Bemmelen, R. W. van: De isogenen in de 16 en 17de eeuw, Doctoral thesis, University of Utrecht, 1893.
4. Birch, Francis, and D. Bancroft: The effect of pressure on the rigidity of rocks, *J. Geol.*, vol. 46, pp. 59, 113, 1938.
5. ———: *Bull. Seis. Soc. Amer.*, vol. 29, p. 463, 1939.
6. ———: Remarks on the structure of the mantle, and its bearing upon the possibility of convection-currents, *Trans. Am. Geophys. Union*, vol. 32, pp. 533–534, 1951.
7. Bridgman, P. W.: *Phys. Rev.*, vol. 17, no. 3, 1945; *Rev. Modern Phys.*, vol. 18, no. 1, 1946; *Proc. Am. Acad. Arts Sci.*, vol. 76, no. 1, 1945; no. 3, 1948.
8. Brouwer, D.: A new discussion of the changes in the earth's rate of rotation, *Proc. Natl. Acad. Sci. U.S.*, vol. 38, pp. 1–12, 1952.
9. Bullard, E. C., and T. F. Gaskell: Submarine seismic investigations, *Proc. Roy. Soc. (London)*, ser. A, vol. 177, no. 971, 1941.
10. ———: The magnetic field within the earth, *Proc. Roy. Soc. (London)*, ser. A, vol. 197, pp. 433–453, 1949; also *Monthly Notices Roy. Astron. Soc., Geophys. Suppl.*, vol. 5, pp. 248–257, 1948.
11. ———, Cynthia Freedman, H. Gellman, and J. Nixon: The westward drift of the earth's magnetic field, *Trans. Roy. Soc. (London)*, ser. A, vol. 243, no. 859, pp. 67–92, 1950.
12. Bullen, K. E.: *Bull. Seis. Soc. Amer.*, vol. 30, p. 235, 1940.
13. ———: *Ibid.*, vol. 32, p. 19, 1942.
14. ———: *Nature*, vol. 157, p. 405, 1946.
15. ———: On density and compressibility at pressures to thirty million atmospheres, *Monthly Notices Roy. Astron. Soc., Geophys. Suppl.*, vol. 6, pp. 383–401, 1952.
16. Byerly, P., and J. T. Wilson: The central California earthquakes of May 16, 1933, and June 7, 1934, *Bull. Seis. Soc. Amer.*, vol. 25, pp. 223–246, 1934.
17. Bijlaard, P. P.: Weerstand van een verzwakte scheeve doorsnede van een getrokken plaat, berekend volgens de hypothese van Huber-Hencky, *Ing. Ned. Indië*, vol. 18, no. 37, 1931.
18. ———: Théorie des déformations plastiques et locales par rapport aux anomalies négatives de la grav., aux fosses océaniques, aux géosynclinaux, etc., *Rapp. cong. Edimbourg UGGI*, 1936.
19. ———: A theory of plastic buckling with its application to geophysics, *Proc. Koninkl. Ned. Akad. Wetenschap.*, ser. B, vol. 41, pp. 468–480, 1938.
20. Carlheim-Gyllensköld, V.: *Arkiv Mat. Astron. Fysik*, vol. 3, no. 7, 1906.
21. Elsasser, W. M.: *Phys. Rev.*, vol. 69, pp. 106–116, 1946; vol. 70, pp. 202–212, 1946; vol. 72, pp. 821–833, 1947.
22. ———: The earth's interior and geomagnetism, *Rev. Modern Phys.*, vol. 22, pp. 1–35, 1950.
23. Eucken, A.: *Naturwissenschaften*, vol. 32, p. 112, 1944.
24. Ewing, Maurice, E. P. Crary, H. N. Rutherford, and B. L. Miller: Geophysical investigations in the emerged and submerged Atlantic coastal plain, *Bull. Geol. Soc. Amer.*, vol. 48, 1937.
25. ———, G. P. Woollard, and A. C. Vine: *Bull. Geol. Soc. Amer.*, vol. 51, 1940.
26. Goguel, J.: Introduction à l'étude mécanique des déformations de l'écorce terrestre, *Mém. carte géol. détaillée France*, 2nd ed., Imprimerie Nationale, Paris, 1948.

27. Goguel, J.: Application de la mécanique à l'étude des plissements, *Geol. en Mijnbouw*, vol. 13, pp. 333–339, 1951.
28. ———: Les conditions de déformation mécanique des roches, *Ann. soc. géol. Belg. Bull.*, vol. 76, pp. B181–B185, 1953.
29. Griggs, D.: Creep of rocks, *J. Geol.*, vol. 47, pp. 225–251, 1939; see also vol. 44, pp. 541–577, 1936; *Bull. Geol. Soc. Amer.*, vol. 51, pp. 1001–1022, 1940.
30. Gutenberg, B.: Travel-time curves at small distances and wave velocities in southern California, *Gerlands Beitr. Geophys.*, vol. 35, pp. 6–45, 1932.
- 31a. ———: Internal constitution of the earth, 2nd ed., Dover, New York, 1951.
- 31b. ——— and H. Benioff: Strain characteristics of the earth's interior, in B. Gutenberg (ed.), Internal constitution of the earth, 2nd ed., pp. 382–407, Dover, New York, 1951.
32. Hill, M. N., and A. S. Laughton: Seismic observations in the eastern Atlantic, 1952, *Proc. Roy. Soc. (London)*, ser. A, vol. 222, pp. 348–356, 1954.
33. Jeffreys, H.: The rigidity of the earth's central core, *Monthly Notices Roy. Astron. Soc., Geophys. Suppl.*, vol. 1, p. 371, 1926.
34. ———: On near earthquakes, *ibid.*, pp. 385–402.
35. ———: The structure of the earth down to the 20° discontinuity, *ibid.*, vol. 3, pp. 401–422, 1936; 4, pp. 13–39, 1937.
36. ———: *Ibid.*, vol. 4, pp. 498, 537, 548, 594, 1939.
37. ———: The earth, 3rd ed., Cambridge, London, 1952.
38. Kronig, R., J. de Boer, and J. Korringa: On the internal constitution of the earth, *Physica*, vol. 12, p. 245, 1946.
39. Kuenen, Ph. H.: Marine geology, Wiley, New York, 1950.
40. Kuhn, W., and A. Rittmann: Ueber den Zustand des Erdinnern und seine Entstehung aus einem homogenen Urzustand, *Geol. Rundschau*, vol. 32, pp. 215–256, 1941.
41. Lambert, W. D., and F. W. Darling: Density, gravity, pressure and ellipticity in the interior of the earth, in B. Gutenberg (ed.), Internal constitution of the earth, 2nd ed., p. 359, Dover, New York, 1951.
42. Lee, A. W.: The North Sea earthquake of 1927, *Monthly Notices Roy. Astron. Soc., Geophys. Suppl.*, vol. 3, pp. 21–30, 1932.
43. Leet, L. D.: Velocity of elastic waves in granite and norite, *Physics*, vol. 4, pp. 375–385, 1933.
44. Macelwane, J. B.: Evidence on the interior of the earth derived from seismic sources, in B. Gutenberg (ed.), Internal constitution of the earth, 2nd ed., p. 248, Dover, New York, 1951.
45. Meissner, E. F. S.: On the stability of the earth, *Monthly Notices Roy. Astron. Soc., Geophys. Suppl.*, vol. 1, pp. 63–69, 1923.
46. Mohorovičić, A.: Das Beben vom 8 Oct. 1909, *Jahrb. Meteorol. Obs. Zagreb* 1909, Bd. 9, T. 4, Abh. 1, Zagreb, 1910.
47. Munk, Walter, and Roger Revelle: On the geophysical interpretation of irregularities in the rotation of the earth, *Monthly Notices Roy. Astron. Soc., Geophys. Suppl.*, vol. 6, pp. 331–347, 1952.
48. Raitt, Russell: Crustal structure of the equatorial Pacific Ocean from seismic refraction observations, *Compt. rend. 10<sup>e</sup> Conf. assoc. intern. séis. phys. interieur terre*, Rome, 1954, p. 145, Müh-Le Roux, Strasbourg, 1955; see also Roger Revelle, in *ibid.*, p. 42.
49. Ramsey, W. H.: Monthly Notices Roy. Astron. Soc., vol. 108, pp. 406–413, 1948.
50. Robertson, Florence: Evidences from deep focus earthquakes for the crustal structure of Missouri, *Bull. Seis. Soc. Amer.*, vol. 27, pp. 241–244, 1937.

51. Takeuti, H.: On the earth tide in the compressible earth of varying density and elasticity, *Trans. Am. Geophys. Union*, vol. 31, pp. 651–689, 1950.
52. Vestine, E. H., L. Laporte, C. Cooper, J. Lange and W. C. Hendrix: Carnegie Inst. Wash. Publ., no. 578, 1947.
53. ———: On variations of the geomagnetic field, fluid motions and the rate of the earth's rotation, *J. Geophys. Research*, vol. 58, pp. 127–145, 1953.
54. Voigt, W.: Bestimmung der Elastizitätskonstanten von Beryll und Bergkrystall, *Ann. Physik*, vol. 31, pp. 471, 701, 1887.

## CHAPTER 3

# GRAVITY FIELD AND GRAVITY POTENTIAL OF THE EARTH. EQUILIBRIUM FIGURE. EARTH ELLIPSOID

### 3-1. Gravity Field and Gravity Potential

The gravity field of the earth consists of two parts, the principal one caused by the attraction according to Newton's law, the second one caused by the earth's rotation. At the equator the second part is about  $\frac{1}{3}$  per cent of the first; elsewhere it is less.

As both parts are forces or combinations of forces acting in the radial direction to a fixed point and in size dependent only on the distance to the point, they have a potential. We can define the principal part, that caused by the attraction, at a point  $P$  as the work done by gravity when a unit of mass is brought from infinity to  $P$ . This definition implies that the work is independent of the path.

For an attraction directed toward a point this fact can be simply demonstrated by realizing that each path can be projected along spheres around the point on a straight line through the point, and since the work done by the attraction during the transportation along these spheres is zero, each path can be replaced by the same straight line as far as the work along that path is concerned.

For the potential caused by the earth's rotation we can give a similar definition, with the difference, however, that the unit mass has to be transported from a point on the rotation axis of the earth, for which we choose the center of gravity of the earth. As we shall use only differences and differential quotients of the potential, we can add the rotation potential to the attraction potential without taking into account the difference of the attraction potential between the center of gravity and infinity.

From the definition of the gravity potential we may conclude that gravity is everywhere perpendicular to equipotential surfaces. If this were not the case, gravity would do work when transporting a mass unit along the equipotential surface, but that is excluded by the definition of the equipotential surface as the surface on which the potential is constant. We can define the geoid as the equipotential surface at mean sea level.

We introduce an orthogonal coordinate system  $x, y, z$  with the  $Z$  axis coinciding with the rotation axis of the earth and the origin at its center of gravity. We see that the definition of the potential implies

$$\begin{aligned} g_x &= \frac{\partial W}{\partial x} \\ g_y &= \frac{\partial W}{\partial y} \\ g_z &= \frac{\partial W}{\partial z} \end{aligned} \quad (3-1)$$

where  $W$  is the total gravity potential. This follows from the fact that  $g_x dx$  is the work done by gravity when a mass unit is conveyed in a direction parallel to the  $X$  axis from the equipotential surface  $W$  to the equipotential surface  $W + dW$ , and the same reasoning holds for the other coordinate directions.

If a point  $P'$  is given by the coordinates  $x', y', z'$  and an element of mass of the earth  $dm$  by  $x, y, z$ , we have

$$W = k^2 \int_0^M \frac{dm}{\rho} + \frac{1}{2}(x'^2 + y'^2)\omega^2 \quad (3-2a)$$

$$\text{with } \rho^2 = (x' - x)^2 + (y' - y)^2 + (z' - z)^2 \quad (3-2b)$$

In (3-2a)  $M$  is the total mass of the earth,  $\omega$  its rotational angular velocity, and  $k^2$  Newton's constant, which has a value

$$k^2 = 6.673 \times 10^{-8} \text{ cm}^3 \text{ g}^{-1} \text{ sec}^{-2} \quad (3-2c)$$

This formula for  $W$  checks with the values for the three components of gravity, which obviously are given by

$$g_x = -k^2 \int_0^M \frac{x' - x}{\rho^3} dm + \omega^2 x' \quad (3-3a)$$

$$g_y = -k^2 \int_0^M \frac{y' - y}{\rho^3} dm + \omega^2 y' \quad (3-3b)$$

$$g_z = -k^2 \int_0^M \frac{z' - z}{\rho^3} dm \quad (3-3c)$$

If we introduce the geocentric coordinates for latitude  $\varphi$  (positive north) and for longitude  $\lambda$  (positive west), the radius vector  $\rho$  of  $dm$  and the

density  $\rho'$  of  $dm$ , we see that  $dm$  can be represented by

$$dm = \rho' \rho^2 \cos\varphi d\rho d\varphi d\lambda \quad (3-4)$$

Introducing this into Formulas (3-2a) and (3-3a) to (3-3c), we see that we can allow the value  $\rho = 0$  without having the integrals become indeterminate. Thus we find that the gravity potential, as well as gravity itself, is determinate, finite, and unique both inside and outside the earth and, therefore, that the equipotential surfaces do not show intersections or singular points where the normal changes discontinuously.

These conclusions are no longer valid for the 2nd-order differential quotients of  $W$  inside the earth. The following formulas can be applied only to points  $P$  outside the earth.

$$\begin{aligned} \frac{\partial^2 W}{\partial x'^2} &= 3k^2 \int_0^M \frac{(x' - x)^2}{\rho^5} dm - k^2 \int_0^M \frac{dm}{\rho^3} + \omega^2 \\ \frac{\partial^2 W}{\partial y'^2} &= 3k^2 \int_0^M \frac{(y' - y)^2}{\rho^5} dm - k^2 \int_0^M \frac{dm}{\rho^3} + \omega^2 \\ \frac{\partial^2 W}{\partial z'^2} &= 3k^2 \int_0^M \frac{(z' - z)^2}{\rho^5} dm - k^2 \int_0^M \frac{dm}{\rho^3} \end{aligned} \quad (3-5a)$$

Adding them together, we obtain Laplace's equation

$$\nabla^2 W = \frac{\partial^2 W}{\partial x'^2} + \frac{\partial^2 W}{\partial y'^2} + \frac{\partial^2 W}{\partial z'^2} = 2\omega^2 \quad (3-5b)$$

which for a nonrotating body would be zero. We can also write the left member as a function of  $g$ , for which we can use vector-analysis notation:

$$\operatorname{div} g = \nabla g = \frac{\partial g_x}{\partial x'} + \frac{\partial g_y}{\partial y'} + \frac{\partial g_z}{\partial z'} = 2\omega^2 \quad (3-5c)$$

This formula provides a short way of determining the form the equation takes inside the earth. If we derive the Gaussian surface integral of the flux of  $g$  through a sphere surrounding a concentrated mass  $dm$ , we find it to be equal to  $-4\pi k^2 dm$ , and so we can conclude that, as far as the attraction part of  $g$  is concerned,

$$\operatorname{div} g = \nabla g = -4\pi k^2 \rho' \quad (3-6a)$$

For the total gravity we thus obtain Poisson's theorem

$$\nabla^2 W = \nabla g = -4\pi k^2 \rho' + 2\omega^2 \quad (3-6b)$$

which shows that the 2nd-order differential quotients of  $W$  have discontinuities where the density changes abruptly. If the discontinuity

surface is parallel to the  $XY$  plane, the change of  $\nabla^2 W$  is entirely located in  $\partial^2 W / \partial z^2$ . Thus, in general, we can conclude that, if the normal to this surface makes angles  $\alpha, \beta, \gamma$  with the  $X, Y, Z$  directions, the discontinuities (which we shall indicate by the symbol  $\delta$ ) are given by

$$\begin{aligned}\delta \frac{\partial^2 W}{\partial x'^2} &= -4\pi k^2 \cos^2 \alpha \delta \rho' \\ \delta \frac{\partial^2 W}{\partial y'^2} &= -4\pi k^2 \cos^2 \beta \delta \rho' \\ \delta \frac{\partial^2 W}{\partial z'^2} &= -4\pi k^2 \cos^2 \gamma \delta \rho'\end{aligned}\quad (3-7)$$

From these formulas we can derive the discontinuities in curvature of the equipotential surfaces of gravity, to which the geoid also belongs. Since, as is well known, the curvature depends on these 2nd-order differential quotients, it must show discontinuities at the intersections of the equipotential surfaces and the discontinuity surfaces of density.

To deal with the problems of gravity, gravity potential, the geoid, and other equipotential surfaces of gravity we shall make use of spherical harmonics; a short introduction to these functions follows.

### 3-2. Spherical Harmonics

In a manner similar to that in which a nonanalytical function on a circle can be represented by a one-dimensional Fourier series, a non-analytical function on a sphere can be represented by a series of spherical harmonics. In both cases the zero-order term gives the mean value of the function over the circle and the sphere, respectively, and each further term gives a deviation of harmonic character from this mean value; the higher the order of the term, the smaller the horizontal dimensions. The mean value of each of these terms over the circle and sphere, respectively, is zero. If the development is pursued to higher orders, the original function is represented in more detail.

For the development of spherical harmonic functions we start from functions  $f$  obeying two conditions necessary and sufficient for defining them. For the order  $n$  these conditions are:

1.  $f$  is a harmonic function, i.e., it fulfills the Laplace equation

$$\nabla^2 f_n = 0 \quad (3-8)$$

2.  $f$  is a homogeneous function in  $x, y, z$  of degree  $n$ , i.e.,

$$f_n(kx, ky, kz) = k^n f_n(x, y, z) \quad (3-9)$$

We can easily show that these equations have  $2n + 1$  particular solutions,

which, when multiplied by arbitrary coefficients and added together, give the general solution. As (3-9) contains  $\frac{1}{2}(n+1)(n+2)$  terms which are each multiplied by a coefficient, and as (3-8) implies  $\frac{1}{2}(n-1)n$  conditions for these coefficients, there remain  $\frac{1}{2}(n+1)(n+2) - \frac{1}{2}(n-1)n = 2n+1$  coefficients which can be freely chosen.

We shall introduce the polar coordinates  $r, \vartheta, \lambda$ , which would have the meaning of radius, polar distance, and longitude for our system of  $xyz$  coordinates on the earth, but which here are intended to be more general.

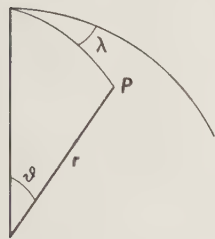


FIG. 3-1.

We thus obtain

$$f_n = r^n Y_n \quad (3-11)$$

where  $Y_n$  is a function of  $\vartheta$  and  $\lambda$ .

Writing the Laplace equation (3-8) in polar coordinates, we get a differential equation of the 2nd order in  $\vartheta$  and  $\lambda$ , of which  $Y_n$ , which is homogeneous in  $\sin \vartheta \cos \lambda, \sin \vartheta \sin \lambda, \cos \vartheta$ , is the solution. Putting

$$\cos \vartheta = t \quad (3-12a)$$

we obtain the following solution (see, for example, Hopfner,<sup>12</sup> pp. 30ff.).

$$Y_n = a_n P_n + a_{n1} P_n^1 \cos \lambda + \cdots + a_{np} P_n^p \cos p\lambda + \cdots + a_{nn} P_n^n \cos n\lambda \\ + b_{n1} P_n^1 \sin \lambda + \cdots + b_{np} P_n^p \sin p\lambda + \cdots + b_{nn} P_n^n \sin n\lambda \quad (3-12b)$$

where the quantities  $a$  and  $b$  are coefficients which can be chosen in such a way that the series represents a certain function over the sphere, while the quantities  $P$  are functions of  $\vartheta$  only. In the first term of the right member, for the sake of simplicity we have omitted the second index  $o$ , which some authors add. As the index  $p$  is a whole number and varies from 1 to  $n$ , the total number of terms checks with the value  $2n+1$  previously derived.

The first quantity  $P$ , which we have denoted by  $P_n$ , is called the "Legendre," "simple," or "zonal," spherical harmonic. It is given by the formula

$$P_n = \frac{1}{2^n n!} \frac{d^n(t^2 - 1)^n}{dt^n} \quad (3-12c)$$

As it is independent of  $\lambda$ , it is constant along "parallels." The equation  $P_n = 0$ , of degree  $n$ , determines  $n$  parallels on which  $P_n$  is zero; they separate positive and negative zones.

The other terms of (3-12b) are usually named "Associated Legendre functions," but they are often also called "tesseral" spherical harmonics, with the exception of the last term of both lines; the latter, for which  $p = n$ , are named "sectorial." The functions  $P$  of the tesseral and sectorial spherical harmonics are given by the formula \*

$$P_n^p = (t^2 - 1)^{p/2} \frac{d^p P_n}{dt^p} \quad (3-12d)$$

or, introducing (3-12c), by

$$P_n^p = \frac{1}{2^n n!} (t^2 - 1)^{p/2} \frac{d^{n+p} (t^2 - 1)^n}{dt^{n+p}} \quad (3-12e)$$

The pair of sectorial spherical harmonic terms is zero along  $n$  meridians separating sectors that are alternatingly positive and negative from pole to pole. The  $n - 1$  pairs of tesseral terms are zero along  $p$  meridians and  $n - p$  parallels which divide the sphere, like a chessboard, into fields.

Formulas (3-12c) to (3-12e) lead to the following results for the zonal, tesseral, and sectorial functions  $P_n$ ,  $P_n^p$ , and  $P_n^n$  for the orders up to the 5th. Since the factors  $i$  and  $-1$  in  $P_n^p$  and  $P_n^n$  follow from the first factor of the right member of (3-12d), they have been omitted. With this restriction, the tesseral and sectorial functions  $P_n^{n-2}$ ,  $P_n^{n-1}$ , and  $P_n^n$  are given by the formulas

$$P_n^{n-2} = \frac{1}{2}(2n-1)(2n-3) \cdots 3 \sin^{n-2} \vartheta \left( \cos^2 \vartheta - \frac{1}{2n-1} \right) \quad (3-12f)$$

$$P_n^{n-1} = (2n-1)(2n-3) \cdots 3 \sin^{n-1} \vartheta \cos \vartheta \quad (3-12g)$$

$$P_n^n = (2n-1)(2n-3) \cdots 3 \sin^n \vartheta \quad (3-12h)$$

They are shown in Table 3-1.

We can easily prove that the integral of an arbitrary spherical harmonic  $Y_n$  [see Formula (3-12b)] over the sphere is zero, and the same is obviously true for each of its terms, viz., for all the functions  $P_n$  and  $P_n^p$ . Equation (3-8) states that  $\text{div } (\nabla f)$  is zero, and so the Gaussian integral of the flux of  $\nabla f$  through a sphere of radius  $r$  over the sphere must also be zero. According to (3-11), this fact is expressed by the following equation, where

\* Some authors add to Formulas (3-12d) and (3-12e) a factor  $1/(n+1)(n+2) \cdots (n+p)$ .

TABLE 3-1. SPHERICAL HARMONIC FUNCTIONS  $P_n$ ,  $P_n^p$ , AND  $P_n^n$ 

Order $n$	Zonal $P_n$	$p$	Tesseral $P_n^p$	Sectorial $P_n^n$
0	1			
1	$\cos \vartheta$	..	.....	$\sin \vartheta$
2	$\frac{3}{2} (\cos^2 \vartheta - \frac{1}{3})$	1	$3 \sin \vartheta \cos \vartheta$	$3 \sin^2 \vartheta$
3	$\frac{5}{2} (\cos^3 \vartheta - \frac{3}{5} \cos \vartheta)$	1	$\frac{15}{2} \sin \vartheta (\cos^2 \vartheta - \frac{1}{5})$	$15 \sin^3 \vartheta$
3	.....	2	$15 \sin^2 \vartheta \cos \vartheta$	
4	$\frac{35}{8} (\cos^4 \vartheta - \frac{6}{7} \cos^2 \vartheta + \frac{3}{35})$	1	$\frac{35}{2} \sin \vartheta (\cos^3 \vartheta - \frac{3}{7} \cos \vartheta)$	$105 \sin^4 \vartheta$
4	.....	2	$\frac{105}{2} \sin^2 \vartheta (\cos^2 \vartheta - \frac{1}{7})$	
4	.....	3	$105 \sin^3 \vartheta \cos \vartheta$	
5	$\frac{63}{8} (\cos^5 \vartheta - \frac{10}{9} \cos^3 \vartheta + \frac{5}{21} \cos \vartheta)$	1	$\frac{315}{8} \sin \vartheta (\cos^4 \vartheta - \frac{2}{3} \cos^2 \vartheta + \frac{1}{21})$	$945 \sin^5 \vartheta$
5	.....	2	$\frac{315}{2} \sin^2 \vartheta (\cos^3 \vartheta - \frac{1}{3} \cos \vartheta)$	
5	.....	3	$\frac{945}{2} \sin^3 \vartheta (\cos^2 \vartheta - \frac{1}{9})$	
5	.....	4	$945 \sin^4 \vartheta \cos \vartheta$	

$S$  represents the surface of the sphere,

$$nr^{n-1} \int_0^S Y_n dS = 0$$

which is valid for all values of  $n > 0$ . So we obtain the required result

$$\int_0^S Y_n dS = 0 \quad . \quad (3-13)$$

which we had to prove. The only exception is found for  $Y_0$ , which is a constant.

It is also possible to show that the integral over the sphere of the product of two spherical harmonics of different order is zero.

$$\int_0^S Y_n Y_{n'} dS = 0 \quad . \quad (3-14)$$

This is also true for the product of two associated Legendre harmonics of the same order but of different  $p$

$$\int_0^S P_n^p P_{n'}^{p'} \cos p\lambda \cos p'\lambda dS = 0 \quad . \quad (3-15)$$

and remains true if one or both of the cosines is replaced by a sine.

The integral over the sphere of squares of  $P_n$  and  $P_n^p$  is not zero. It is given by

$$\int_0^S (P_n)^2 dS = \frac{S}{2n+1} \quad (3-16a)$$

and

$$\int_0^S (P_n^p)^2 \cos^2 p\lambda dS = \int_0^S (P_n^p)^2 \sin^2 p\lambda dS$$

$$= \frac{(n+p)!}{2(2n+1)(n-p)!} S \quad (3-16b)$$

The derivation of these different results and formulas can be found in handbooks, e.g., Whittaker-Watson.<sup>23</sup>

Another way of finding the spherical harmonic functions is by series development of the function  $1/\rho$ , where  $\rho$  is the distance between two points  $P$  and  $P'$  with radii vectors  $r$  and  $r'$  enclosing an angle  $\psi$ . If  $r'/r \geq 1$ , and if we put

$$\cos \psi = t \quad (3-17a)$$

we obtain

$$\frac{1}{\rho} = \frac{1}{r'} \left[ 1 - 2t \frac{r}{r'} - \left( \frac{r}{r'} \right)^2 \right]^{-\frac{1}{2}} \quad (3-17b)$$

Developing in series with respect to the ratio  $r/r'$ , we get

$$\frac{1}{\rho} = \frac{1}{r'} \sum_{n=0}^{\infty} \left( \frac{r}{r'} \right)^n P_n \quad (3-17c)$$

where  $P_1, P_2, \dots, P_n, \dots$  are Legendre spherical harmonics in the angle  $\psi$ .

If  $r'/r < 1$ , we can obviously write the development as follows

$$\frac{1}{\rho} = \frac{1}{r} \sum_{n=0}^{\infty} \left( \frac{r'}{r} \right)^n P_n \quad (3-17d)$$

Callandreau<sup>5</sup> has shown that both series are convergent, even when  $r'/r = 1$ .

We can use these formulas to develop the potential of bodies attracting according to Newton's law. We shall first apply this potential to derive means of developing a function on a sphere in a series of spherical harmonics.

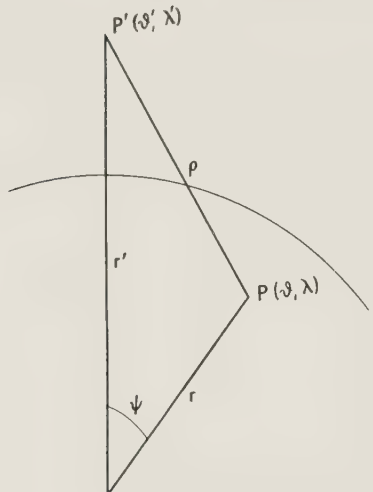


FIG. 3-2.

Let us assume a mass layer on the sphere given by the function to be developed,  $f(\vartheta, \lambda)$ , per surface unit. If the radius of the sphere is  $r$  and its surface element  $r^2 d\sigma$ , where  $d\sigma$  is the surface element of a sphere with unit radius, we find for the outside and inside potential at a point  $P'$  with the coordinates  $r', \vartheta', \lambda'$

$$P' \text{ outside} \quad v = k^2 r \sum_{n=0}^{n=\infty} \left( \frac{r}{r'} \right)^{n+1} \int_0^{\sigma=4\pi} P_n f(\vartheta, \lambda) d\sigma \quad (3-18a)$$

$$P' \text{ inside} \quad v = k^2 r \sum_{n=0}^{n=\infty} \left( \frac{r'}{r} \right)^n \int_0^{\sigma=4\pi} P_n f(\vartheta, \lambda) d\sigma \quad (3-18b)$$

For the radial components of the attraction at  $P'$  we thus obtain

$$P' \text{ outside} \quad \frac{dv}{dr'} = -k^2 \sum_{n=0}^{n=\infty} (n+1) \left( \frac{r}{r'} \right)^{n+2} \int_0^{\sigma=4\pi} P_n f(\vartheta, \lambda) d\sigma \quad (3-19a)$$

$$P' \text{ inside} \quad \frac{dv}{dr'} = k^2 \sum_{n=0}^{n=\infty} n \left( \frac{r'}{r} \right)^{n-1} \int_0^{\sigma=4\pi} P_n f(\vartheta, \lambda) d\sigma \quad (3-19b)$$

If we put  $r' = r$  in both Formulas (3-19) and thus let the two points  $P'$  approach the surface of the sphere, we find at that surface a discontinuity of  $dv/dr'$  given by (3-20a). Like the relation given by (3-6a), this quantity must equal the product of  $-4\pi k^2$  and the mass per surface unit of the layer on the sphere, which, at the radius of  $P'$  (coordinates  $\vartheta', \lambda'$ ), has the value  $f(\vartheta', \lambda')$ . We thus obtain

$$-\sum_{n=0}^{n=\infty} (2n+1) k^2 \int_0^{\sigma=4\pi} P_n f(\vartheta, \lambda) d\sigma = -4\pi k^2 f(\vartheta', \lambda') \quad (3-20a)$$

and this gives us our final formula

$$f(\vartheta', \lambda') = \sum_{n=0}^{n=\infty} \frac{2n+1}{4\pi} \int_0^{\sigma} P_n f(\vartheta, \lambda) d\sigma \quad d\sigma = \sin \vartheta d\vartheta d\lambda \quad (3-20b)$$

In this formula  $P_n$  is a Legendre spherical harmonic which, according to Formula (3-12c), is a function of  $t = \cos \psi$ ,  $\psi$  being the angle between the radius vector of  $P'$  (coordinates  $\vartheta', \lambda'$ ) and of the surface element  $d\sigma$  (coordinates  $\vartheta, \lambda$ ). To carry out the integration we can express  $P_n$  in terms of the coordinates  $\vartheta, \lambda$  and introduce the result into (3-12c):

$$t = \cos \psi = \cos \vartheta \cos \vartheta' + \sin \vartheta \sin \vartheta' \cos \lambda \cos \lambda' + \sin \vartheta \sin \vartheta' \sin \lambda \sin \lambda' \quad (3-20c)$$

We thus obtain  $P_n$  as a symmetrical function in the two coordinate systems  $\vartheta, \lambda$  and  $\vartheta', \lambda'$ . In the integration,  $\vartheta, \lambda$  disappear, and thus we get

$f$  expressed in terms of  $\vartheta'$ ,  $\lambda'$ . The integration thus provides us with the constants  $a_n$ ,  $a_{np}$ , and  $b_{np}$  of the development of  $f(\vartheta', \lambda')$  in a series of general spherical harmonics of the shape  $Y_n$  as given by (3-12b) which we were seeking.

### 3-3. Exterior Gravity Potential of the Spheroidal Earth

To deal with the problems connected with the earth's gravity field and its potential we shall divide the earth's masses into a regular part, in which the masses are axially symmetric around the rotation axis and also symmetric with regard to the equator plane, and a mass-deviation part, which is obtained by removing the regular part from the earth; Helmert<sup>10</sup> (p. 68) has shown that the gravitational attraction by the atmosphere can be neglected. In the mass-deviation part we shall also admit masses of negative density; we shall, in fact, suppose the sum of these masses to be zero, or, in other words, we shall assume the regular part to have the same mass  $M$  as the complete earth. We shall also suppose that its center of gravity  $O$  coincides with that of the earth and that the equipotential surface which forms its outer surface is a spheroid of revolution of regular shape and of the same volume and flattening  $\alpha$  as the geoid. We shall call this surface the earth spheroid, and we shall adopt it as the reference surface for all geodetic observations and deductions. When we later define the earth spheroid as an ellipsoid, we call it the earth ellipsoid.

Finally, when developing the potential of the spheroidal earth in spherical harmonics, we shall suppose the term of the 4th order to be of the order of  $\alpha^2$  and terms of higher order to be negligible.

In this section we deal with the potential of the spheroidal earth, which we call  $U$  to distinguish it from the potential  $W$  of the complete earth, and with its development in series. Restricting ourselves to the outside potential, we use Formula (3-17c) for this purpose. We introduce both an  $xyz$  coordinate system with the  $Z$  axis coinciding with the rotation axis and a geocentric system around the center of gravity of the earth  $O$ , with a radius  $r$ , a geocentric latitude  $\varphi = 90^\circ - \vartheta$ , positive to the north, and a longitude  $\lambda$ , positive to the west; we then find for a point  $P'$  (coordinates  $x'$ ,  $y'$ ,  $z'$  and  $r'$ ,  $\varphi'$ ,  $\lambda'$ , respectively)

$$U = \frac{k^2}{r'} \sum_{n=0}^{n=\infty} \int_0^M P_n \left( \frac{r}{r'} \right)^n dm + \frac{1}{2}(x'^2 + y'^2)\omega^2$$

$$\text{or } U = \frac{k^2}{r'} \left( M + \frac{1}{r'} \int_0^M P_1 r dm + \frac{1}{r'^2} \int_0^M P_2 r^2 dm + \frac{\omega^2 r'^3}{2k^2} \cos^2 \varphi' \right. \\ \left. + \frac{1}{r'^3} \int_0^M P_3 r^3 dm + \frac{1}{r'^4} \int_0^M P_4 r^4 dm + \dots \right) \quad (3-21a)$$

in which the Legendre functions  $P$  can be expressed in  $\varphi, \lambda, \varphi', \lambda'$  by means of (3-12c) and

$$t = \cos \psi = \sin \varphi \sin \varphi' + \cos \varphi \cos \varphi' \cos \lambda \cos \lambda' + \cos \varphi \cos \varphi' \sin \lambda \sin \lambda' \quad (3-21b)$$

We thus can obtain the potential  $U$  developed in a series of spherical harmonics of the form given by (3-12b), with the axis coinciding with the rotation axis, the origin at the center of gravity of the earth, and  $\cos \vartheta'$  replaced by  $\sin \varphi'$ .

The first term within the parentheses, which is the zero-order term of this development, is evidently the principal one. It would represent the attraction of the earth if it did not rotate and if it were spherically symmetrical; in that case the outside attraction would be identical with what it would be if the earth's mass were concentrated in the center.

The second term, i.e., the 1st-order spherical harmonic, is zero. By introducing  $P_1 = t$  and by replacing  $t$  by the right member of (3-21b), we may conclude that in the integration the contribution made by the terms  $r \cos \varphi \cos \lambda dm$  and  $r \cos \varphi \sin \lambda dm$  must vanish, as otherwise the result for the potential would contain terms multiplied by  $\cos \lambda'$  and  $\sin \lambda'$ , which is not compatible with the supposition that our spheroidal earth is axially symmetric. But the integral of  $r \sin \varphi dm$  must also vanish, because otherwise there would be a term containing  $r \sin \varphi' = z'$ , which would not fulfill the condition of symmetry with respect to the equatorial plane.

We can apply this same reasoning to the 3rd-order spherical harmonic term of the potential; the integral of the fifth term within the parentheses must be zero. It cannot give terms different from zero for the tesseral and sectorial parts as they depend on  $\lambda'$ , and the zonal part contains only first and third powers of  $r \cos \vartheta' = r \sin \varphi' = z'$ , which are not compatible with the symmetry with respect to the equator plane. For the 5th- and higher-odd-order spherical harmonic terms the same reasoning obviously also holds.

For the 1st-order term we can extend our conclusion to the development of the potential of the whole earth, although it has no properties of symmetry; we can prove that this term is zero because the center of gravity coincides with the origin  $O$  of the coordinates. When we introduce an orthogonal system of coordinates with the  $\zeta$  axis through  $O$  and  $P'$ , the integral of the 1st-order term becomes

$$\int_0^M P_1 r dm = \int_0^M r \cos \psi dm = \int_0^M \zeta dm \quad (3-22a)$$

and this integral is zero for all coordinate systems  $\zeta$  with their origin at

the center of gravity. So for the earth as a whole we likewise have

$$\int_0^M P_1 r \, dm = 0 \quad (3-22b)$$

Returning to Formula (3-21a) for the potential  $U$  of the spheroidal earth, we now take up the discussion of the 2nd-order spherical harmonic, i.e., the third term within the parentheses. We can again conclude that the tesseral and sectorial terms are zero, and so we need retain only the zonal term (see Table 3-1).

$$\begin{aligned} \int_0^M P_2 r^2 \, dm &= (\frac{3}{2} \sin^2 \varphi' - \frac{1}{2}) \int_0^M (\frac{3}{2} \sin^2 \varphi - \frac{1}{2}) r^2 \, dm \\ &= (\frac{3}{2} \sin^2 \varphi' - \frac{1}{2}) \int_0^M (z^2 - \frac{1}{2}x^2 - \frac{1}{2}y^2) \, dm \end{aligned}$$

and if we introduce the moments of inertia  $A$  around an arbitrary axis in the equatorial plane and  $C$  around the rotation axis

$$A = \int_0^M (x^2 + z^2) \, dm = \int_0^M (y^2 + z^2) \, dm \quad (3-23a)$$

$$C = \int_0^M (x^2 + y^2) \, dm \quad (3-23b)$$

we obtain

$$\int_0^M P_2 r^2 \, dm = -(\frac{3}{2} \sin^2 \varphi' - \frac{1}{2})(C - A) \quad (3-24a)$$

Introducing the quantity

$$H = \frac{C - A}{C} \quad (3-24b)$$

which is often called the "mechanical ellipticity," we get

$$\int_0^M P_2 r^2 \, dm = -(\frac{3}{2} \sin^2 \varphi' - \frac{1}{2})HC \quad (3-24c)$$

For the 4th-order spherical harmonic term we again can omit the tesseral and sectorial terms, and we find (see Table 3-1)

$$\begin{aligned} \int_0^M P_4 r^4 \, dm &= (\sin^4 \varphi' - \frac{6}{7} \sin^2 \varphi' + \frac{3}{35}) \\ &\times \int_0^M \frac{1}{6} \frac{2}{4} \frac{2}{5} r^4 (\sin^4 \varphi - \frac{6}{7} \sin^2 \varphi + \frac{3}{35}) \, dm \quad (3-25) \end{aligned}$$

Thus our formula for the outside potential of the spheroidal earth finally becomes

$$U = k^2 \frac{M}{r} \left[ 1 - \frac{C}{Mr^2} H \left( \frac{3}{2} \sin^2 \varphi - \frac{1}{2} \right) + \frac{\omega^2 r^3}{2k^2 M} \cos^2 \varphi + \frac{D}{r^4} (\sin^4 \varphi - \frac{6}{7} \sin^2 \varphi + \frac{3}{35}) \dots \right] \quad (3-26a)$$

with  $D = \frac{1}{M} \int_0^M \frac{1}{6} \frac{2}{3} \frac{5}{4} r^4 (\sin^4 \varphi - \frac{6}{7} \sin^2 \varphi + \frac{3}{35}) dm \quad (3-26b)$

In (3-26a) we have omitted the primes on the coordinates  $\varphi$  and  $r$  of the point to which the potential refers.

### 3-4. Equipotential Surfaces of the Spheroidal Earth

It is evident that the equipotential surfaces of the spheroidal earth are all axially symmetric. The equation of the equipotential surface which is assumed to be the earth's outer surface and to have the same volume as the geoid (we have called it the earth spheroid) is given by

$$U = W_0 \quad (3-27)$$

in which  $W_0$  is a constant indicating the potential of the geoid. When we introduce Formula (3-26) for  $U$ , Eq. (3-27) becomes an equation for the spheroid in the coordinates  $r, \varphi$ . We shall solve it by assuming the solution to be of the form

$$r = a [1 - (\alpha + \alpha_4) \sin^2 \varphi + \alpha_4 \sin^4 \varphi] \quad (3-28)$$

in which  $\alpha$  is the flattening of the earth spheroid, which we take to be the same as that of the geoid. Introducing (3-28) into (3-27), we obtain three conditions for making this equation an identity in  $r$  and  $\varphi$ ; they allow us to derive the three coefficients  $a, \alpha$ , and  $\alpha_4$ .

We introduce a constant  $c'$  giving the ratio of the centrifugal acceleration at the equator to  $k^2 M/a^2$ , which, to an accuracy of 2 per cent, represents gravity at the equator:

$$c' = \frac{\omega^2 a^3}{k^2 M} \quad (3-29)$$

Neglecting quantities of the 6th order, i.e., of the order of  $\alpha^3$ , we then find

$$\frac{W_0}{M} = \frac{k^2}{a} \left( 1 + \frac{1}{3} \alpha + \frac{1}{3} c' - \frac{1}{3} \alpha^2 + \frac{1}{3} \alpha c' + \frac{2}{15} \frac{D}{a^4} \right) \quad (3-30a)$$

$$P = 3 \frac{C}{Ma^2} H = 2\alpha - c' - 2\alpha^2 + 2\alpha c' + \frac{2}{7} \frac{D}{a^4} \quad (3-30b)$$

$$\alpha_4 = \alpha(\frac{5}{2}c' - 2\alpha) + \frac{D}{a^4} \quad (3-30c)$$

The quantity  $P$  introduced in (3-30b) does not appear to differ more than 1 per cent from the mechanical ellipticity  $H$ ;  $P$ ,  $H$ , and  $c'$  are all close to the flattening  $\alpha$ . By means of these formulas we can express the radius vector  $r$  of the earth spheroid in  $a$ ,  $\alpha$ , and  $c'$ ; Eq. (3-30a) gives the relation of  $W_0/M$  to these quantities. We obtain

$$r = a \left\{ 1 - \left[ \alpha(1 + \frac{5}{2}c' - 2\alpha) + \frac{D}{a^4} \right] \sin^2 \varphi + \left[ \alpha(\frac{5}{2}c' - 2\alpha) + \frac{D}{a^4} \right] \sin^4 \varphi \right\} \quad (3-31)$$

We see that the solution adopted in (3-28) is appropriate; the coefficient of  $\sin^2 \varphi$  is of the order of the flattening  $\alpha$ , and that of  $\sin^4 \varphi$  of the order of  $\alpha^2$ .

We shall now determine the figure of equipotential surfaces exterior to the spheroidal earth, which obviously are also spheroids of revolution. We shall denote the radius vector of such a surface by  $\rho$ , its potential by  $W_\rho$ , the radius of its equator by  $a_\rho$ , and its flattening by  $\alpha_\rho$ . Its equation is given by

$$U = W_\rho \quad (3-32a)$$

When we introduce the following constants and coefficients:

$$\frac{a_\rho}{a} = \nu \quad (3-32b)$$

$$P_\rho = 3 \frac{C}{Ma^2} H \nu^{-2} = P \nu^{-2} \quad (3-32c)$$

$$c'_\rho = \frac{\omega^2 a_\rho^3}{k^2 M} = c' \nu^3 \quad (3-32d)$$

the equation of the equipotential surface becomes

$$W_\rho = k^2 \frac{M}{\rho} \left[ 1 - \frac{1}{2} P_\rho \frac{a_\rho^2}{\rho^2} (\sin^2 \varphi - \frac{1}{3}) + \frac{1}{2} c'_\rho \frac{\rho^3}{a_\rho^3} (1 - \sin^2 \varphi) + \frac{D}{\rho^4} (\sin^4 \varphi - \frac{6}{7} \sin^2 \varphi + \frac{3}{35}) \dots \right] \quad (3-33)$$

from which we can derive  $\rho$  as function of  $\varphi$ . Again assuming this solution to have the form

$$\rho = a_\rho [1 - (\alpha_\rho + \alpha_{\rho 4}) \sin^2 \varphi + \alpha_{\rho 4} \sin^4 \varphi] \quad (3-34)$$

and introducing this value of  $\rho$  in (3-33), we must make this equation an identity in  $\rho$  and  $\varphi$ . Thus we again obtain three conditions from which we can derive  $\alpha_\rho$ ,  $\alpha_{\rho 4}$ , and the value of  $W_\rho$ , corresponding to a certain value

of  $a_\rho$ . The third relation is given by

$$W_\rho = \frac{k^2 M}{a_o} \left( 1 + \frac{1}{6} P_\rho + \frac{1}{2} c'_\rho + \frac{3}{35} \frac{D}{a_o^4} \right) \quad (3-35)$$

in which  $P_\rho$  and  $c'_\rho$  are functions of  $a_\rho$  in the way given by (3-32b) to (3-32d). When this relation is used, the two other conditions provide us with the following formulas for the flattening  $\alpha_\rho$  of the spheroid and for the coefficient  $\alpha_{\rho 4}$  of the last term of (3-34):

$$\alpha_\rho = (\alpha - \frac{1}{2} c') \nu^{-2} + \frac{1}{2} c' \nu^3 + \left( -\alpha^2 + \alpha c' + \frac{1}{7} \frac{D}{a^4} \right) \nu^{-2} (1 - \nu^{-2}) - \frac{1}{4} c'^2 \nu^6 (1 - \nu^{-10}) \quad (3-36a)$$

$$\alpha_{\rho 4} = \left[ -2(\alpha - \frac{1}{2} c')^2 + \frac{D}{a^4} \right] \nu^{-4} + \frac{1}{2} c' (\alpha - \frac{1}{2} c') \nu + \frac{3}{4} c'^2 \nu^6 \quad (3-36b)$$

Unless  $\nu$  is very large, we again find that  $\alpha_\rho$  is of the order of the flattening  $\alpha$  of the earth spheroid and  $\alpha_{\rho 4}$  of the order of  $\alpha^2$ . For very large values of  $\nu$ , the 6th- and higher-order terms clearly are no longer negligible, and the development in series becomes questionable. This is because of the centrifugal acceleration, which increases proportionally to the distance from the rotation axis and does not apply to the attraction potential alone. We shall not study the case of outside points not partaking in the rotation, the formulas for which can simply be derived from those given above by putting  $c' = 0$  and  $c'_\rho = 0$  everywhere.

For moderate distances from the earth's surface the expressions (3-36) may be simplified. If the elevation is not more than about 500 km, it is useful to replace  $\nu$  by  $1 + \delta$  in the 4th-order terms; as  $\delta < 0.078$ , in those terms we can neglect all powers of  $\delta$  higher than the first. If we are satisfied with an accuracy of 1:100,000, we find that we can even neglect the 1st-power terms, and so in the 4th-order terms we can omit the factors containing powers of  $\nu$ , causing them to vanish. We thus obtain

$$\alpha_\rho = (\alpha - \frac{1}{2} c') \nu^{-2} + \frac{1}{2} c' \nu^3 \quad (3-37a)$$

$$\alpha_{\rho 4} = 2\alpha(\frac{5}{4}c' - \alpha) + \frac{D}{a^4} \quad (3-37b)$$

At the end of Sec. 3-6, where we study the ellipsoidal earth and its gravity field, we discuss these results and examine the way the flattening changes with altitude.

### 3-5. Exterior Gravity Field of the Spheroidal Earth

Since the formula for the exterior potential of the earth is known (3-26), it is simple to derive the outside gravity field. By differentiating  $U$  with

respect to  $r$  and  $\varphi$  we obtain the component of gravity  $g_r$  in the direction of the radius vector  $r$  and  $g_N$  in the north direction on the sphere with radius  $r$ . The ratio of the second to the first is obviously of the order of the flattening  $\alpha$ , and so we can find the resultant  $g$  by means of the following formula, in which quantities of the order of the 4th and higher powers of  $\alpha$  are neglected:

$$g = g_r \left[ 1 + \frac{1}{2} \left( \frac{g_N}{g_r} \right)^2 \right] \quad (3-38a)$$

where

$$g_r = - \frac{\partial U}{\partial r} \quad (3-38b)$$

$$g_N = \frac{\partial U}{r \partial \varphi} \quad (3-38c)$$

Applied to (3-26a) it gives

$$\begin{aligned} g = k^2 \frac{M}{r^2} & \left[ 1 - \frac{1}{2} P \frac{a^2}{r^2} (3 \sin^2 \varphi - 1) - c' \frac{r^3}{a^3} \cos^2 \varphi \right. \\ & + 5 \frac{D}{r^4} (\sin^4 \varphi - \frac{6}{7} \sin^2 \varphi + \frac{3}{35}) \\ & \left. + \frac{1}{2} \left( P \frac{a^2}{r^2} + c' \frac{r^3}{a^3} \right)^2 \sin^2 \varphi \cos^2 \varphi + \dots \right] \quad (3-39) \end{aligned}$$

This formula provides us with the value of gravity outside the spheroidal earth. As we have already mentioned, Callandreau<sup>5</sup> has shown that it is valid down to the surface, the earth spheroid. Introducing the value of the radius vector  $r$  of this surface as given by (3-31), we obtain the value of gravity on the earth spheroid. We shall call this the formula of normal gravity and shall indicate it by  $\gamma_0$ ; its value at the equator is denoted by  $\gamma_e$ .

Applying (3-39) with (3-30b) and putting  $r = a$  and  $\varphi = 0$ , we find for  $\gamma_e$

$$\gamma_e = k^2 \frac{M}{a^2} \left( 1 + \alpha - \frac{3}{2} c' - \alpha^2 + \alpha c' + \frac{4}{7} \frac{D}{a^4} \right) \quad (3-40a)$$

This formula allows us to replace  $c'$ , defined by (3-29a), by the customary constant  $c$ , defined by the ratio at the equator of the centrifugal acceleration to the gravity,

$$c = \frac{\omega^2 a}{\gamma_e} \quad (3-41a)$$

which differs only from  $c'$  by the 4th-order terms. Applying (3-29a) and

(3-40a) and neglecting 6th- and higher-order terms, we have

$$c' = c(1 + \alpha - \frac{3}{2}c \dots) \quad (3-41b)$$

This gives

$$\gamma_e = k^2 \frac{M}{a^2} \left( 1 + \alpha - \frac{3}{2}c - \alpha^2 - \frac{1}{2}\alpha c + \frac{9}{4}c^2 + \frac{4}{7} \frac{D}{a^4} \right) \quad (3-40b)$$

Carrying out the above-mentioned introduction of the radius vector  $r$ , (3-31), in the formula for  $g$ , (3-39), and changing from  $c'$  to  $c$ , in the formula for  $r$  as well, we obtain the two basic complementary formulas for the radius vector and the normal gravity of the earth spheroid

$$r = a \left\{ 1 - \left[ \alpha(1 + \frac{5}{2}c - 2\alpha) + \frac{D}{a^4} \right] \sin^2 \varphi + \left[ \alpha(\frac{5}{2}c - 2\alpha) + \frac{D}{a^4} \right] \sin^4 \varphi \right\} \quad (3-42a)$$

$$\begin{aligned} \gamma_0 = \gamma_e & \left[ 1 + \left( \frac{5}{2}c - \alpha + 6\alpha^2 - \frac{1}{2}\alpha c - \frac{19}{7} \frac{D}{a^4} \right) \sin^2 \varphi \right. \\ & \left. + \left( -7\alpha^2 + 3 \frac{D}{a^4} \right) \sin^4 \varphi \right] \quad (3-42b) \end{aligned}$$

These formulas are usually transformed into somewhat different forms in two ways. First, by substituting

$$\sin^4 \varphi = \sin^2 \varphi - \frac{1}{4} \sin^2 2\varphi \quad (3-43)$$

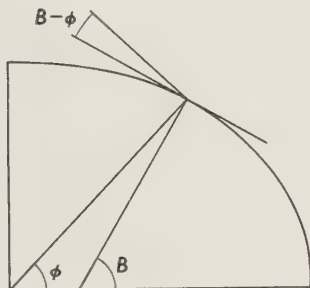


FIG. 3-3.

we can write the last term within the brackets in the form  $\sin^2 2\varphi$ , with the advantage that the coefficient of the middle term thus directly represents the flattening. Second, the geocentric latitude  $\varphi$  is usually replaced by the geographical latitude, which we shall here denote by  $B$ . From Fig. 3-3 we easily derive

$$B - \varphi = - \frac{dr}{r d\varphi} = 2\alpha \sin \varphi \cos \varphi = \alpha \sin 2\varphi$$

and, as up to 4th-order terms

$$\sin^2 B = \sin^2 \varphi + 2 \sin \varphi \cos \varphi (B - \varphi)$$

we obtain

$$\sin^2 \varphi = \sin^2 B - \alpha \sin^2 2\varphi \quad (3-44)$$

which allows the transformation of  $\varphi$  into  $B$  in the middle term. Since replacing  $\varphi$  by  $B$  in the 4th-order term involves only a difference of the 6th order, no further changes in the formula are needed.

The two transformations change our basic equations into the form in which they are usually given:

$$r = a \left[ 1 - \alpha \sin^2 B + \left( \frac{3}{2} \alpha^2 - \frac{5}{8} \alpha c - \frac{1}{4} \frac{D}{a^4} \right) \sin^2 2B + \dots \right] \quad (3-45a)$$

$$\gamma_0 = \gamma_e \left[ 1 + \beta \sin^2 B + \left( \frac{11}{4} \alpha^2 - \frac{5}{2} \alpha c - \frac{3}{4} \frac{D}{a^4} \right) \sin^2 2B + \dots \right] \quad (3-45b)$$

where  $\beta = \frac{5}{2}c - \alpha - \alpha^2 - \frac{1}{2}\alpha c + \frac{2}{7} \frac{D}{a^4}$  (3-45c)

The 2nd-order term of the last formula, which can be written

$$\alpha = \frac{5}{2}c - \beta + \dots \quad (3-45d)$$

is well known as the theorem of Clairaut. According to (3-45b), we can define the quantity  $\beta$  by the equation

$$\beta = \frac{\gamma_p - \gamma_e}{\gamma_e} \quad (3-45e)$$

where  $\gamma_p$  is the spheroidal gravity at the pole. So the meaning of  $\beta$  for the normal gravity is similar to that of the flattening  $\alpha$  for the radius vector  $r$ .

These basic formulas define a reference surface for all geodetic observations and deductions and the corresponding normal value of gravity. In these formulas we can still choose the two quantities  $\alpha$  and  $D$ . We can make  $\alpha$  as close as we wish to the flattening of the geoid, depending upon what definition we wish to give of this concept. In this book we shall define it to mean that the 2nd-order zonal spherical harmonic of the radius vector of the geoid is equal to that of the earth spheroid. This definition implies, however, that we can approach the true value of  $\alpha$  only as we gradually get more observational data for the geoid in the course of time. For many purposes we can, no doubt, keep to the value of 1/297.000 of the international ellipsoid, which is probably a good approximation; it seems likely that  $\alpha^{-1}$  does not differ by more than 0.5 from the value of 297.0.

We can choose the value of the 4th-order term  $D$ , provided, however, that we keep to the previously made supposition that it is of the order of  $\alpha^2$ . In the following sections we shall examine in turn two important possibilities, viz., we can make the spheroid coincide with an ellipsoid of revolution, which seems the simplest shape for the geodetic reference surface as far as mathematical treatment is concerned, or we can make it represent the equilibrium surface of an entirely fluid earth of the same general density distribution as the real earth. We shall see that the two

possibilities fortunately are so close together that the differences are of the order of present-day observational errors. So, with that limitation, the deviations of the geoid from a well-chosen ellipsoid can be considered deviations from equilibrium.

Before taking up these problems we shall extend our gravity deductions to the entire field exterior to the earth. For this purpose we shall go back to our geocentric-latitude coordinate  $\varphi$ . As we have done previously (at the end of Sec. 3-4) for the radius vector of the geoid, we can apply our formulas for gravity on the geoid to an arbitrary exterior equipotential surface. We again denote its radius vector by  $\rho$ , and we add a subindex  $\rho$  to the quantities  $a$ ,  $\alpha$ ,  $c'$ ,  $\gamma_e$ ; for  $\gamma_0$  we write  $\gamma_\rho$ . Instead of changing over to  $c$  [Formula (3-41b)], we shall keep to  $c'$ , and so we again use the formula

$$c'_\rho = c' \nu^3 \quad (3-32d)$$

where again

$$\nu = \frac{a_\rho}{a} \quad (3-32b)$$

From (3-40a) we conclude that

$$\gamma_{\rho e} = k^2 \frac{M}{a_\rho^2} \left( 1 + \alpha_\rho - \frac{3}{2} c'_\rho - \alpha_\rho^2 + \alpha_\rho c' + \frac{4}{7} \frac{D}{a_\rho^4} \right) \quad (3-46a)$$

and (3-42b) combined with (3-41b) and (3-43) provides us with

$$\gamma_\rho = \gamma_{\rho e} \left[ 1 + \beta_\rho \sin^2 \varphi + \left( \frac{7}{4} \alpha_\rho^2 - \frac{3}{4} \frac{D}{a_\rho^4} \right) \sin^2 2\varphi \dots \right] \quad (3-46b)$$

$$\text{where } \beta_\rho = \frac{5}{2} c'_\rho - \alpha_\rho - \alpha_\rho^2 - 3\alpha_\rho c'_\rho + \frac{15}{4} c'^2_\rho + \frac{2}{7} \frac{D}{a_\rho^4} \quad (3-46c)$$

These formulas give us the gravity  $\gamma_\rho$  on the exterior equipotential surface of potential  $W_\rho$ , which is expressed in  $a_\rho$  by (3-35). In the formulas we have to substitute the value of the flattening  $\alpha_\rho$  as it is given by (3-36a) or, for less than 500 km elevation and an accuracy of 1:100,000, by (3-37a), in which case the formula for  $\beta_\rho$  simplifies to

$$\beta_\rho = -(\alpha - \frac{1}{2} c') \nu^{-2} + 2c' \nu^3 - \alpha^2 - 3\alpha c' + \frac{15}{4} c'^2 + \frac{2}{7} \frac{D}{a^4} \quad (3-47)$$

As expected, the 2nd-order terms of  $\alpha_\rho$  (3-37a) and  $\beta_\rho$  added together give  $\frac{5}{2} c'_\rho$  and thus fulfill Clairaut's theorem.

### 3-6. Basic Formulas for the Ellipsoidal Earth

The equation of a meridian ellipse of half axes  $a$  and  $b$  is given by

$$\frac{x^2}{a^2} + \frac{y^2}{b^2} = 1 \quad (3-48)$$

Introducing our geocentric polar coordinates  $r$  and  $\varphi$  and the flattening  $\alpha = (a - b)/a$ , we obtain an expression for  $r$  in  $\varphi$ ,  $a$ , and  $\alpha$  which we can develop in a series with respect to  $\alpha$  and write

$$\begin{aligned} r &= a \left\{ 1 + \left[ \frac{1}{(1-\alpha)^2} - 1 \right] \sin^2 \varphi \right\}^{-\frac{1}{2}} \\ &= a [1 - (\alpha + \frac{3}{2}\alpha^2) \sin^2 \varphi + \frac{3}{2}\alpha^2 \sin^4 \varphi \dots] \end{aligned} \quad (3-49)$$

Terms of the order of the 3rd and higher powers of  $\alpha$  have again been omitted.

We see that we can make (3-49) coincide with the formulas (3-31) and (3-42a) for the radius vector  $r$  of the earth spheroid by choosing an appropriate value for the 4th-order term  $D$ . Neglecting 6th-order terms, we find the same formula when expressed in  $c$  or in  $c'$ :

$$\frac{D}{a^4} = \alpha(\frac{7}{2}\alpha - \frac{5}{2}c') = \alpha(\frac{7}{2}\alpha - \frac{5}{2}c) \quad (3-50)$$

We thus obtain the following formulas for the radius vector of the ellipsoidal earth and its gravity:

$$r = a(1 - \alpha \sin^2 B + \frac{5}{8}\alpha^2 \sin^2 2B + \dots) \quad (3-51a)$$

$$\gamma_e = \gamma_e [1 + \beta \sin^2 B - \alpha(\frac{5}{8}c - \frac{1}{8}\alpha) \sin^2 2B + \dots] \quad (3-51b)$$

$$\text{where } \beta = \frac{5}{2}c - \alpha - \frac{1}{4}\alpha c \quad (3-51c)$$

This formula is the well-known theorem of Clairaut extended by the last term to the 2nd order of  $\alpha$  and  $c$ .

Geodetic and astronomical data have led to the following figures for the ellipsoid, adopted by the assembly of the International Geodetic Association at Madrid in 1924 as defining the international ellipsoid; the figures were derived by Hayford from geodetic data in the United States. In the assembly at Stockholm in 1930 a corresponding formula for normal gravity, proposed by Cassinis, was internationally adopted (see Sec. 3-13, where Heiskanen deals with the different formulas for normal gravity derived from gravity data). We add also the corresponding values of  $c = \omega^2 a / \gamma_e$  and of  $c' = c(1 + \alpha - \frac{3}{2}\alpha c)$

$$\begin{aligned} a &= 6,378,388 \text{ meters} & \alpha &= \frac{1}{297.00} = 0.0033670 \\ \gamma_e &= 978,049 & c &= \frac{1}{288.36} = 0.0034678 \quad (3-52) \\ c' &= \frac{1}{288.90} = 0.0034614 \end{aligned}$$

and find the formulas for the radius vector of the international ellipsoid

$$r = 6,378,388(1 - 0.0033670 \sin^2 B + 0.0000071 \sin^2 2B) \quad (3-53a)$$

and for "normal gravity"

$$\gamma_0 = 978.049(1 + 0.0052884 \sin^2 B - 0.0000059 \sin^2 2B) \quad (3-53b)$$

which, because we have neglected terms of the order of  $\alpha^3$ , are accurate to about 1 m and 0.2 mgal, respectively, as far as the dependence on latitude is concerned. The values of  $a$  and  $\gamma_e$  are far less accurate; considering the observational errors and those caused in the arc measurements by deflections of the vertical and in the gravity values by anomalies, errors of more than 50 m in  $a$  and 5 mgal in  $\gamma_e$  are possible.

For the reduction of gravity to sea level, the value of  $\partial g/\partial r$  on the ellipsoid is important. We can easily determine it by differentiating Formula (3-39) for gravity exterior to the earth. For our purpose we can restrict ourselves to an accuracy comprising the 2nd-order terms but neglecting the 4th order. We find

$$\frac{\partial g}{\partial r} = -2k^2 \frac{M}{r^3} \left[ 1 - P \frac{a^2}{r^2} (3 \sin^2 \varphi - 1) + \frac{1}{2} c' \frac{r^3}{a^3} \cos^2 \varphi + \dots \right] \quad (3-54)$$

and, introducing the value of the radius vector of the earth spheroid given by (3-31) combined with (3-30b), we obtain

$$\frac{\partial g}{\partial r} = -2k^2 \frac{M}{a^3} (1 + 2\alpha - \frac{1}{2}c') [1 - (3\alpha - 2\frac{1}{2}c') \sin^2 \varphi + \dots] \quad (3-55a)$$

and applying (3-40a) for  $\gamma_e$

$$\frac{\partial g}{\partial r} = -2 \frac{\gamma_e}{a} (1 + \alpha + c') [1 - (3\alpha - 2\frac{1}{2}c') \sin^2 \varphi + \dots] \quad (3-55b)$$

As we neglect the 4th-order terms, we can replace  $\varphi$  by the geographical latitude  $B$  in these formulas.

For great elevations above the geoid we cannot entirely neglect the slight decrease of  $\partial g/\partial r$  with altitude. To derive this small correction we determine  $\partial^2 g/\partial r^2$ , but for this purpose we can neglect even the 2nd-order terms, and so the differentiation of (3-54) can be restricted to the following term:

$$\frac{\partial^2 g}{\partial r^2} = -\frac{3}{r} \frac{\partial g}{\partial r} + \dots = 6 \frac{\gamma_e}{a^2} + \dots \quad (3-56)$$

The corresponding correction for gravity is obviously half of this value multiplied by the square of the elevation  $h$ .

Introducing the values for the international ellipsoid, we find for the free-air reduction  $\Delta g$  of gravity, which must be added to gravity to reduce it to sea level,

$$\Delta g = (0.30877 - 0.00044 \sin^2 B)h_m - 0.073h_{km}^2 \text{ mgal} \quad (3-57)$$

where  $h_m$  is the elevation in meters and  $h_{km}$  in kilometers. This formula is practically the same as Lambert's formulas 9 and 11 derived in a different way<sup>13</sup> (p. 130).

We shall now apply the values of the international ellipsoid to the exterior field. Restricting ourselves to an elevation of not more than 500 km and an accuracy of about 1:100,000, we can apply Formulas (3-37) and (3-47) combined with (3-50), thus obtaining

$$\alpha_\rho = 0.0016363\nu^{-2} + 0.0017307\nu^3 \quad (3-58a)$$

$$\beta_\rho = -0.0016363\nu^{-2} + 0.0069228\nu^3 + 0.00000017 \quad (3-58b)$$

Applying these formulas to elevations of 100, 200, ..., 500 km, we get the results given in Table 3-2. From this table we see that over the dis-

TABLE 3-2. FLATTENING  $\alpha_\rho$  AND  $\alpha_\rho^{-1}$ , DIFFERENCE HALF AXIS  $a_\rho - b_\rho$ , AND  
 $\gamma_{\rho p} - \gamma_{pe}/\gamma_{pe} = \beta_\rho$

Elevation above sea level at equator, km	$\alpha_\rho$	$\alpha_\rho^{-1}$	$a_\rho - b_\rho$ , m	$\beta_\rho$
0	0.0033670	297.00	21,476	0.0052884
100	0.0033995	294.16	22,023	0.0056693
200	0.0034369	290.96	22,610	0.0060582
300	0.0034791	287.43	23,237	0.0064555
400	0.0035260	283.61	23,903	0.0068616
500	0.0035775	279.52	24,608	0.0072767

tance of 500 km the flattening  $\alpha_\rho$  changes much less than the corresponding quantity for the gravity  $\beta_\rho$ . The differences  $a_\rho - b_\rho$  change by 3132 m; we can also express this result by stating that the height of the outside potential surface above the ellipsoid, which at the equator has an altitude of 500 km, is 3132 m less at the poles, i.e., 496,868 km. The exterior potential surfaces are spheroids but not ellipsoids; if we examine Eq. (3-50), we see that, for increasing elevation, the quantity  $D/a_\rho^4$  changes in a different way from that of the right member of this equation and hence does not remain valid for the exterior equipotential surfaces. According to this equation and (3-45a), the distance of the spheroid from an ellipsoid

coinciding with it at equator and poles is given by

$$d = -a_p \left( \frac{1}{4} \frac{D}{a_p^4} - \frac{7}{8} \alpha_p^2 + \frac{5}{8} \alpha_p c'_p \right) \sin^2 2B = d_p \sin^2 2B \quad (3-59a)$$

(positive when the spheroid is outside the ellipsoid). In this equation  $d_p$  represents the maximum depression at  $45^\circ$  latitude. Introducing (3-50) with (3-32b), (3-32d), and (3-37a), we find

$$\begin{aligned} d_p = & -\frac{7}{8} \alpha^2 (1 - \nu^{-4}) + \frac{7}{8} \alpha c' \nu (1 - \nu^{-5}) - \frac{5}{8} (\nu - 1) \\ & + \frac{1}{32} c'^2 (\nu^3 - \nu^{-2}) (3\nu^3 + 7\nu^{-2}) \end{aligned} \quad (3-59b)$$

For the elevations of Table 3-2 we obtain

Elevation, km	0	100	200	300	400	500	
$d_p$ , m	0	-1.4	-2.9	-4.3	-5.8	-7.3	(3-59c)

Thus we find that the spheroid has a slight depression with respect to the ellipsoid; it is maximum at  $45^\circ$  latitude and increases with altitude.

### 3-7. Equilibrium Figure of a Fluid Earth and Its Gravity

For geodesy as well as for geophysics it is of fundamental importance to investigate the figure and the gravity of a fluid earth of the same general density distribution as the real earth. We may surmise that, with the exception of the rigid crust, the earth has closely approached such an equilibrium; its flattened spheroidal shape suggests this tendency, and the phenomenon of isostasy, which is generally interpreted as a floating equilibrium of the crust, shows that the tendency toward equilibrium is present even in the rigid and irregular thin outer layer. We can expect the same tendency in the main part of the earth, which has a higher temperature, and all observations point to the truth of this supposition.

In this section we shall assume that the rigid crust is replaced by a fluid layer constituted of about the same matter; thus we can expect it to adopt the shape of a regular thin shell.

The condition to be fulfilled is that all equipotential surfaces of the fluid earth be at the same time surfaces of equal density. Assuming this earth to rotate around a fixed axis—the slight migration of the poles of the order of not more than a few meters per year can be neglected here—we conclude that such equipotential surfaces must be rotation spheroids. Further, they must be symmetric with respect to the equator plane, and so the odd-order terms in the spherical harmonic series of their radii vectores  $r$  are zero. Finally we can assume that their 4th-order terms

are of the order of  $\alpha^2$ , i.e., of the square of their flattening, and their 6th- and higher-order terms negligible.

The elaboration of this problem is fairly complicated, but it has been solved. For a homogeneous body of constant density the solution is simple: the figure is an ellipsoid (e.g., Helmert,<sup>10</sup> pp. 130ff.). For the rotational velocity of the earth, it is an ellipsoid of revolution; at that speed triaxial ellipsoids do not represent equilibrium (Clausen<sup>6</sup>) unless the two equator axes have a ratio of more than 50, which is obviously not true for the earth.

For densities increasing toward the center, as is true of the earth, Clairaut has given the equation up to terms of the order of the flattening, and its solution for a few density distributions was given long ago (e.g., Tisserand<sup>20</sup>). Shortly afterwards, in 1899, Darwin<sup>7,8</sup> derived the equations up to the 2nd order of the flattening, and in 1924 de Sitter<sup>17</sup> further extended this solution to fulfill present-day requirements. In 1938 Brouwer<sup>1</sup> edited later notes by de Sitter and completed them. In those days, however, the inner constitution of the earth was imperfectly known, and so no definite result could be obtained. In 1946 Bullard<sup>2</sup> took up the subject again and gave a numerical solution based on Darwin's and de Sitter's equations, using Bullen's<sup>3,4</sup> recent figures for the density distribution in the earth; consequently his results seem the best presently obtainable. We shall give a short summary of them.

Bullard puts the radii vectores of the surfaces of equal potential and density in the following form (equations throughout the book are written in our own notation):

$$\rho = a_\rho \left[ 1 - \alpha_\rho \sin^2 B + \left( \frac{5}{8} \alpha_\rho^2 + \frac{d_\rho}{a_\rho} \right) \sin^2 2B \right] \quad (3-60)$$

where  $d_\rho$  again denotes the distance, at  $45^\circ$  latitude, of the spheroid outside an ellipsoid which coincides with it at equator and poles; for the surface we shall indicate the distance by  $d_0$ .

Bullard follows de Sitter's method of deriving the flattening  $\alpha$  at the surface from the value of the mechanical ellipticity  $H = (C - A)/C$ , which can be accurately deduced from the values of precession and nutation. Since the method is only slightly dependent on the density distribution inside the earth, it can give a good result even though the density distribution is not yet known with great precision.

To derive  $H$ , Bullard uses Spencer-Jones's<sup>16</sup> value for the mass of the moon  $\mu$  ( $\mu^{-1} = 81.271 \pm 0.021$ ) and thus deduces from the precessional constant,  $5493''.156 \pm 0''.175$ , a value for  $H$

$$H = 0.00327237 \pm 0.00000059 \quad (3-61)$$

To find  $\alpha$  from this value of  $H$  we determine the ratio  $P/H$ , which, ac-

cording to (3-30b), is given by

$$\frac{P}{H} = \frac{3C}{Ma^2} \quad (3-62)$$

In his work de Sitter introduced the ratio  $q$ , which is half of the ratio here given. From the right member of (3-62) it is clear that  $P/H$  depends on the density distribution in the earth; de Sitter showed that  $q$  differs only slightly from 0.5, and so  $P/H$  is close to unity. The effect of the density distribution on  $P/H$  turns out to be exceedingly small; it is involved only through the small quantity  $\lambda_1$ , which can be found by a fairly complicated system of integration. Using Bullen's density data, Bullard has carried the integration out and has found that

$$\lambda_1 = 0.00016 \quad (3-63)$$

When  $P/H$  has been derived, we can obtain  $P$ , and then Formula (3-30b) combined with (3-59a) gives

$$P = 2\alpha - c' - \alpha^2 + \frac{9}{7}\alpha c' - \frac{8}{7}\frac{d_0}{a} \quad (3-64)$$

by which, provided the small 4th-order quantity  $d_0/a$  is known, we can compute  $\alpha$ .

By applying Darwin's equations Bullard derived  $d_0/a$  and found

$$\frac{d_0}{a} = -68 \times 10^{-8} \quad (3-65a)$$

from which it follows that

$$d_0 = -4.3 \text{ meters} \quad (3-65b)$$

The surface spheroid—which we again shall call the earth spheroid—of an equilibrium earth thus turns out to show only a small depression with respect to an ellipsoid coinciding with it at equator and poles. Its maximum value is only 4.3 m at  $45^\circ$  latitude.

Let us return to the problem of determining the flattening  $\alpha$  from the mechanical ellipticity. Bullard has applied the formula given by de Sitter in its ultimate form as published by Brouwer; it expresses  $\alpha^{-1}$  as a function of the deviations from approximate numerical values upon which  $\alpha^{-1}$  depends. This formula and the formula for  $2q = P/H$  are

$$\frac{P}{H} = 1.00086[1 - 0.6640(u - v) + 0.6661w + 1.6581\psi] \quad (3-66a)$$

$$\alpha^{-1} = 296.753[1 - 0.1874(u - v) - 0.8138w + 0.1696\chi - 0.8098\psi] \quad (3-66b)$$

in which the quantities  $u$ ,  $v$ ,  $w$ ,  $\chi$ , and  $\psi$  are given by

$$r_1 = 6,371,260(1 + u) \text{ meters} \quad (3-66c)$$

$$g_1 = 979.770(1 + v) \text{ cm/sec}^2 \quad (3-66d)$$

$$H = 0.003279423(1 + w) \quad (3-66e)$$

$$-\frac{d_0}{a} = 0.00000050 + 10^{-3}\chi \quad (3-66f)$$

$$\lambda_1 = 0.00040 + \psi \quad (3-66g)$$

The quantities  $r_1$  and  $g_1$  are the mean values of  $r$  and  $\gamma_0$  at the surface, i.e., for the earth spheroid, for which Brouwer takes the values at a latitude  $\varphi = \arcsin \sqrt{\frac{1}{3}}$ . For  $r_1$  and  $g_1$  Bullard introduces Spencer-Jones's<sup>16</sup> values and thus obtains

$$\alpha^{-1} = 297.338 \pm 0.050 \quad (3-67a)$$

and so

$$\alpha = 0.00336317 \pm 0.00000057 \quad (3-67b)$$

Introducing  $\alpha$  and  $d_0/a$ , he gets the formula for the radius vector  $r$

$$r = a(1 - 0.00336317 \sin^2 B + 0.00000639 \sin^2 2B \dots) \quad (3-68a)$$

and for the corresponding gravity

$$\gamma_0 = \gamma_e(1 - 0.00529317 \sin^2 B - 0.00000787 \sin^2 2B \dots) \quad (3-68b)$$

The value thus obtained for the flattening of the earth agrees satisfactorily with that given by the astronomic-geodetic and gravity methods. Since the results of both those methods are affected by local or regional deviations caused by disturbing masses, the value obtained here may be considered the most accurate. It is gratifying that the differences are so small.

The main uncertainty about the figure found here results from a possible error in the mass of the moon; Bullard estimates the corresponding uncertainty of  $\alpha^{-1}$  at  $\Delta\alpha^{-1} = 0.042$ . For the effect of errors in  $\alpha^{-1}$  caused by uncertainties about the internal density distribution of the earth, Bullard gives  $\Delta\alpha^{-1} = 0.027$ , and for the combination of both sources of error,  $\Delta\alpha^{-1} = 0.050$ . This is a remarkably small figure; it gives an idea of the power of this method of determining the flattening.

If we compare Formulas (3-68a) and (3-68b) for the equilibrium earth with Formulas (3-51a) and (3-51b) for the ellipsoidal earth of the same volume, mass, and flattening, we obtain the differences  $\Delta r$  of the radius vector and  $\Delta\gamma_0$  of the gravity, given by corresponding zonal spherical harmonics of the 2nd and 4th order combined in such a way that in  $\Delta r$

the term with  $\sin^2 B$  vanishes. We thus obtain

$$\Delta r = 2.31 - 4.33 \sin^2 2B \text{ meters} \quad (3-69a)$$

$$\Delta \gamma_0 = 0.81 + 0.76 \sin^2 B - 2.00 \sin^2 2B \text{ mgal} \quad (3-69b)$$

Examining these differences, we see how small they are. For the radius vector we find a maximum increase at the poles and the equator of 2.3 m and a maximum decrease at a latitude of  $45^\circ$  of 2 m, and so we can say that, at the present level of accuracy of geodetic measurements, the differences between equilibrium figure and ellipsoid are negligible. For gravity we find a maximum increase at the poles of 1.6 mgal and at the equator of 0.8 mgal and a maximum decrease at  $45^\circ$  latitude of 0.8 mgal. Here also the differences are hardly more than the mean error of the observations, but the development of modern gravimetry is so rapid that perhaps in the future this statement will no longer be justified.

At present we can say that the ellipsoid is so close to the equilibrium figure of the earth that we can consider the deviations between the geoid and the appropriate ellipsoid, as well as the gravity anomalies with respect to the formula for normal gravity corresponding to that ellipsoid, as deviations from equilibrium. Both types of deviation are caused by the deviation masses mentioned in the beginning of this chapter; their effects on the geoid and on gravity are studied in the following sections. Topography, isostatic compensation, and geological mass deviations with their isostatic compensation form part of these deviation masses. As they are located in the rigid crust, they need not constitute deviations from equilibrium.

### 3-8. Potential Caused by the Deviation Masses of the Earth; Distance $N$ between Geoid and Earth Spheroid; Gravity Anomaly

As explained at the beginning of Sec. 3-3, we have divided the earth into a regular part bounded by the earth spheroid and a deviation part; in this section we study especially the effect of the latter.

We have supposed the regular part to have the same mass as the earth as a whole and the earth spheroid, i.e., the earth-ellipsoid,\* to have the same volume and flattening as the geoid. For that concept, viz., the equality of the flattening of the geoid and the earth spheroid, we have given the definition that, in a development in a series of spherical harmonics of the radii vectores of both surfaces, the 2nd-order zonal terms have the same value.

\* We shall continue to use the terms spheroid and spheroidal to keep our terminology more general and use ellipsoid and ellipsoidal only when we make use of the fact that an ellipsoid has been chosen for the earth spheroid.

To these conditions we have added that the earth spheroid must be the equilibrium figure of an entirely fluid earth. We must take into account the possibility that, although the international ellipsoid probably comes close to fulfilling these conditions, it may not quite do so. We shall return to this point in Sec. 3-12.

According to our concept, the deviation part of the earth comprises negative masses also, and so the total mass of the deviation part is zero. Thus, if we develop the outside potential field of these masses in spherical harmonics, the zero-order term must be zero. Since we have already shown that the 1st-order spherical harmonic of the potential of the whole earth is zero, and since the same is true for the potential of the spheroidal earth, it must also hold for the potential of the deviation masses. For the spherical-harmonic development of this potential, which we shall denote by  $V$ , we can therefore write (see Formula (3-26a) for  $U$ )

$$V = W - U = \frac{Y_2}{r^3} + \frac{Y_3}{r^4} + \frac{Y_4}{r^5} + \cdots + \frac{Y_n}{r^{n+1}} + \cdots \quad (3-70)$$

In this formula  $r$  is the radius vector of an exterior point or of a point on the geoid. In admitting this last possibility we assume that all deviation masses outside the geoid have been taken away, which implies reductions of gravity and equipotential surfaces. It is important to note in this connection that Helmert<sup>10</sup> (p. 68) has shown the effect of the atmosphere to be negligible; for elevations smaller than 3500 m its attraction is less than 1/3,000,000 part of gravity, and for greater elevations it is less than 1/1,000,000 part. We shall henceforth neglect it.

According to our assumption that the values of the zonal spherical harmonics of the 2nd order of  $W$  and  $U$  are equal,  $Y_2$  ought to have no zonal term. If shown to be present we have to correct our spheroid or we have at least to take it into account when deriving the flattening of the geoid from that of the spheroid.

From the definition of the potential of gravity given in the beginning of this chapter it follows that if  $N_\rho$  is the distance between some outside equipotential surface of the complete earth, which we shall distinguish by the subindex  $\rho$ , and the equipotential surface of the spheroidal earth having the same potential, we have

$$V_\rho = (W - U)_\rho = g_\rho N_\rho \quad (3-71a)$$

where  $g_\rho$  is the mean value of gravity over the distance  $N_\rho$ , which we know to be small—in fact, probably less than 50 m. As the right member is the work done by gravity if a mass unit is brought from the earth's equipotential surface to the spheroidal earth's equipotential surface, and as this latter surface must, in the gravity field of the complete earth, have

a potential which is  $V_\rho = (W - U)_\rho$  greater because it has the same potential in the spheroidal gravity field, Eq. (3-71a) is in harmony with the definition of the gravity potential.

The equation obviously also applies to the distance  $N_0$  from the geoid to the earth spheroid, i.e., the earth ellipsoid, in which case we use the subindex 0; so

$$V_0 = (W - U)_0 = g_0 N_0 \quad (3-71b)$$

where  $g_0$  indicates the value of gravity reduced to the geoid, which, because of the small value of  $N_0$ , is practically the same as the mean gravity over the distance  $N_0$ .

We need hardly add that neither the equipotential surfaces of  $W$  nor those of  $U$  coincide with the equipotential surfaces of  $V$ ; the latter must have a more irregular character. By giving the subindex  $\rho$  to  $V$  we indicate a value having reference to a point of the equipotential surface  $W_\rho$  of the complete earth.

The contribution to gravity of the deviation masses can be written

$$-\frac{\partial V}{\partial r} = 3 \frac{Y_2}{r^4} + 4 \frac{Y_3}{r^5} + 5 \frac{Y_4}{r^6} + \cdots + (n+1) \frac{Y_n}{r^{n+2}} + \cdots \quad (3-72)$$

This formula gives the component of their attraction in the direction of the radius vector from the center of gravity of the earth. Since the difference between this component and that in the direction of gravity itself must be of the order of the flattening, and since we assume these components to be of the order of the gravity anomalies, we shall neglect the difference. Because gravity anomalies seldom exceed 100 mgal, it seems justifiable to neglect the order of the flattening in these quantities.

We shall now proceed to express the gravity anomalies  $\delta g$  in the spherical harmonics  $Y$ . That they are not identical with  $-\partial V/\partial r$  although they are brought about by the deviation masses, of which  $V$  is the potential field, can be seen from the fact that, if we subtract from  $g_0$  the normal gravity  $\gamma_0$ , we compare gravity on the geoid to spheroidal gravity in the same vertical on the spheroid. Their difference, therefore, is brought about not only by the direct attraction of the deviation masses but also by the difference in the positions, which, in the direction of the vertical, deviate over a distance  $N_0$ .\* Assuming that this distance is entirely outside the attracting masses, the corresponding effect is given by  $\Delta g = 2gN_0/r$ . As  $N_0$  is small, we have used here the usual approximate for-

\* Usually it is not realized that the effect of the disturbing masses on both the attraction and the geoid, the anomaly being diminished by the last of the two effects, holds for all gravity interpretations. When masses are small, as is usually the case, the effect is too small to be appreciable; but for large masses this is no longer true, and if the effect of the shift of the geoid is neglected, the masses will be somewhat underestimated.

mula instead of the accurate one, (3-57);  $g$  and  $r$  here are mean values over the earth, which, if expressed in milligals and meters, make the ratio  $2g/r$  equal to 0.3086. The use of this formula implies, however, that the distance  $N_0$  must, under all circumstances, be situated outside the attracting masses, and so the reductions of the gravity and of the equipotential surfaces must remove all effects of masses outside the geoid as well as outside the spheroid.

Application of (3-71b) leads to the following equations and formulas:

$$\delta g = g_0 - \gamma_0 = -2 \frac{g}{r} N_0 - \left( \frac{\partial V}{\partial r} \right)_0 = -2 \frac{V_0}{r} - \left( \frac{\partial V}{\partial r} \right)_0$$

and, using (3-70) and (3-72),

$$\delta g = \frac{Y_2}{r^4} + 2 \frac{Y_3}{r^5} + 3 \frac{Y_4}{r^6} + \cdots + (n-1) \frac{Y_n}{r^{n+2}} + \cdots \quad (3-73a)$$

while for  $N_0$

$$N_0 = \frac{r}{g} \left( \frac{Y_2}{r^4} + \frac{Y_3}{r^5} + \frac{Y_4}{r^6} + \cdots + \frac{Y_n}{r^{n+2}} + \cdots \right) \quad (3-73b)$$

We can extend these considerations and formulas to the field outside the geoid. We define the gravity anomaly  $\delta g$  as the difference between the gravity on an exterior equipotential surface of the earth's field (again denoted by the subindex  $\rho$ , and its mean radius vector by  $\rho$ ) and the normal gravity, which we define as the gravity caused by the spheroidal earth on the spheroidal equipotential surface of the same potential; the two equipotential surfaces therefore have a common distance of  $N_\rho$ . In a manner similar to that in which we derived Formulas (3-73a) and (3-73b) we can obtain

$$\delta g_\rho = \frac{Y_2}{\rho^4} + 2 \frac{Y_3}{\rho^5} + 3 \frac{Y_4}{\rho^6} + \cdots + (n-1) \frac{Y_n}{\rho^{n+2}} + \cdots \quad (3-74a)$$

$$N_\rho = \frac{\rho}{g_\rho} \left( \frac{Y_2}{\rho^4} + \frac{Y_3}{\rho^5} + \frac{Y_4}{\rho^6} + \cdots + \frac{Y_n}{\rho^{n+2}} + \cdots \right) \quad (3-74b)$$

where  $\rho$  and  $g_\rho$  are mean values over the equipotential surface of the earth's field.

By means of (3-73a) and (3-73b) we can, in principle, solve the important problem of determining the geoid from gravity; if gravity were known over the whole earth, we would be able to develop the anomaly  $\delta g$  in spherical harmonics and thus find the coefficients of the functions  $Y_2$ ,

...,  $Y_n, \dots$ . Introducing these into (3-73b), we would obtain  $N_0$  and thus find the geoid. The method has a great advantage over the astronomic-geodetic method for determining the geoid in that (1) it is applicable to the oceanic parts of the earth's surface and (2) it provides us with the distance  $N_0$  from the geoid to the spheroid whose center coincides with the earth's center of gravity and whose position thus is known.

By introducing the functions  $Y_2, \dots, Y_n, \dots$  into (3-74a) and (3-74b) we can also obtain the exterior gravity anomalies and, thereby, the exterior gravity field of the earth; we can likewise determine the values of  $N_\rho$  and thus find the figure of the external equipotential surfaces of this field.

The method is, however, extremely laborious, and so it is of great importance that, as early as 1854, Stokes derived a quicker method, which has also the great advantage of giving more insight into the way in which gravity anomalies enter into the values of  $N_0$  over the earth. This is especially important in view of the fact that both methods have to cope with the difficulty of gravity's being still unknown over a greater part of the earth, as it will no doubt remain for some time. We shall return to this point, but first we develop Stokes' theorem and (Sec. 3-10) a formula expressing the absolute deflections of the vertical in terms of the gravity anomalies.

### 3-9. Stokes' Theorem

According to (3-20b), the development of  $\delta g$  in spherical harmonics is given by

$$\delta g = \sum_{n=2}^{n=\infty} \frac{2n+1}{4\pi} \int_0^\sigma P_n \delta g d\sigma \quad (3-75)$$

in which we shall leave  $P_n$  expressed as a zonal spherical harmonic in the angle  $\psi$ , between the radius vector of the external point at which we wish to determine  $N_\rho$  and the element of the geoid where the gravity anomaly is  $\delta g$ . The element  $d\sigma$  is the element of a sphere of unit radius with a radius vector coinciding with that of  $\delta g$ .

Interchanging the summation and the integration, we find, according to (3-73a) and (3-74b),

$$N_\rho = \frac{\rho}{4\pi g_\rho} \int_0^\sigma \sum_{n=2}^{n=\infty} \frac{2n+1}{n-1} P_n \left(\frac{r}{\rho}\right)^{n+2} \delta g d\sigma \quad (3-76a)$$

We can now introduce the function  $F$  given by

$$F_\rho = \sum_{n=2}^{n=\infty} \frac{2n+1}{n-1} P_n \left(\frac{r}{\rho}\right)^{n-1} \quad (3-76b)$$

which we can derive, and then we can write Formula (3-76a) in the form of a simple integral

$$N_\rho = \frac{r^3}{4\pi g_\rho \rho^2} \int_0^\sigma F_\rho \delta g \, d\sigma \quad (3-76c)$$

which we must extend over the whole sphere.

For the derivation of  $F_\rho$  we are able to use the following expression for  $\sum_{n=2}^{n=\infty} P_n \left(\frac{r}{\rho}\right)^n$ , which we shall call  $q$ . For the sake of simplicity, we here introduce  $u = r/\rho$ . From (3-17b) and (3-17c) we derive

$$\begin{aligned} q &= \sum_{n=2}^{n=\infty} P_n u^n = (1 - 2u \cos \psi + u^2)^{-\frac{1}{2}} - P_0 - P_1 u \\ &= (1 - 2u \cos \psi + u^2)^{-\frac{1}{2}} - 1 - u \cos \psi \end{aligned} \quad (3-77)$$

For  $F_\rho$  we successively get

$$\begin{aligned} F_\rho &= \sum_{n=2}^{n=\infty} \frac{2n+1}{n-1} P_n u^{n-1} = \sum_{n=2}^{n=\infty} \int_0^u (2n+1) P_n u^{n-2} \, du \\ &= 2 \int_0^u u^{-\frac{1}{2}} \frac{d}{du} \left( \sum_{n=2}^{n=\infty} P_n u^{n+\frac{1}{2}} \right) \, du \end{aligned}$$

and so we obtain

$$F_\rho = 2 \int_0^u u^{-\frac{1}{2}} \frac{d}{du} (u^{\frac{1}{2}} q) \, du \quad (3-78)$$

The summation of spherical harmonics has disappeared from this formula, and thus a great simplification has been achieved. By substituting Formula (3-77), for  $q$ , and by carrying out the differentiation and integration after we introduce a quantity  $v$  given by

$$v = (1 - 2u \cos \psi + u^2)^{\frac{1}{2}} \quad (3-79a)$$

we obtain the following result for  $F_\rho$ :

$$F_\rho = \frac{2}{uv} + \frac{1}{u} - 5 \cos \psi - 3 \frac{v}{u} - 3 \cos \psi \ln \frac{1}{2}(1 - u \cos \psi + v) \quad (3-79b)$$

By means of this formula it is simple to compute values of  $F_\rho$  for all values of  $\rho$  and  $\psi$ . From (3-76c) we then can derive  $N_\rho$  for all external potential surfaces.

As we have said, these considerations and formulas are valid down

to the geoid, and so we can apply them to that surface, obtaining

$$u = 1 \quad v = 2 \sin \frac{1}{2}\psi$$

$$F_0 = \csc \frac{1}{2}\psi + 1 - 5 \cos \psi - 6 \sin \frac{1}{2}\psi - 3 \cos \psi \ln [\sin \frac{1}{2}\psi(1 + \sin \frac{1}{2}\psi)] \quad (3-80a)$$

In Formula (3-76c) we replace the integration over the sphere with unit radius by an integration over a sphere  $S$  with the mean radius  $r$  of the geoid and get

$$N_0 = \frac{1}{4\pi gr} \int_0^S F_0 \delta g \, dS \quad (3-80b)$$

where  $r$  and  $g$  are mean values over the geoid.

We thus have obtained the *theorem of Stokes*, which is of fundamental importance for geodesy because it allows us to determine the geoid from gravity. Thus we can find the geoid even at sea, which is not possible by any other method.

Attention should be drawn to several features of the theorem. In the first place, because of the manner in which it has been derived, the theorem is valid only if no masses are present outside the geoid. Therefore reductions must be applied to gravity anomalies and to the geoid. The simplest kind of reduction is that suggested by Helmert, who suggests considering that the outside topographic masses are condensed in an infinitely thin layer just inside the geoid. This mass displacement is so small that its effect on the geoid can be neglected. In Sec. 3-12 we return to these problems in a further discussion of Stokes' theorem.

In the second place, Stokes' theorem provides us with the distance  $N_0$  from the geoid to an earth spheroid which has the same volume as the geoid and of which the center coincides with the center of gravity of the earth, and so  $N_0$  contains no zero- or 1st-order spherical harmonics. This fact implies that the theorem cannot be used to find a more correct figure for the equatorial radius  $a$  of the earth spheroid; i.e., we cannot determine the scale of our model of the geoid, nor can we get a figure for the equatorial value of normal gravity  $\gamma_e$ . For the flattening  $\alpha$ , on the other hand, we can get a new figure.

In the third place, although the applicability of Stokes' theorem seems to be impeded by the fact that the integral must be extended over the whole earth and that gravity is still unknown over great parts of it, actually, however, for great distances from the station where  $N_0$  is to be determined the function  $F_0$  is small, and so distant anomalies have only a slight effect.

Since  $F_0$  depends only on the angular distance  $\psi$  from the point  $N_0$ , it

may be of value to carry out the integration in Formula (3-80b) by first computing the mean values of the gravity anomaly  $\delta g_m$  over circular rings around the station. As the area of such a ring of a breadth of  $d\psi$  is  $2\pi r^2 \sin \psi d\psi$ , we can substitute for  $F_0$  a function given by

$$F'_0 = \frac{1}{2}F_0 \sin \psi \quad (3-81)$$

and, correspondingly, write (3-80b) as

$$N_0 = \frac{r}{g} \int_{0^\circ}^{180^\circ} F'_0 \delta g_m d\psi \quad (3-82)$$

Tables of the functions  $F_0$  and  $F'_0$  for different values of  $\psi$  between  $0^\circ$  and  $180^\circ$  have been derived by Lambert and Darling,<sup>14</sup> excerpts from which are given in the appendix to this chapter. The original tables give  $\frac{1}{2}F_0$ ,  $F'_0$ , and  $\int_0^\psi F'_0 d\psi$ ; in our table  $\frac{1}{2}F_0$  has been replaced by  $F_0$ .

From (3-80a) we may conclude that for small distances  $D$  from the point  $N_0$ , the first term of the right member is predominant; it shows that under those conditions the effect of the anomalies is approximately inversely proportional to  $D$ . In fact, we can write, as a rough approximation,

$$F_0 \cong \frac{2r}{D} \quad \text{and} \quad N_0 \cong \frac{1}{2\pi g} \int_0 \frac{\delta g}{D} dS \quad (3-83)$$

Formulas (3-81) and (3-82) thus become

$$F'_0 \cong 1 \quad \text{and} \quad N_0 \cong \frac{1}{g} \int_0 \delta g_m dD \quad (3-84)$$

This simple formula gives a reasonable though rough approximation for anomaly distances up to 2500 km; between 300 and 1300 km distance the effect of the anomalies is about 20 per cent larger.

Before taking up further discussion of the problems raised by the Stokes' theorem, we shall derive from it a formula expressing the deflection of the vertical in gravity anomalies, give a brief study of the external gravity field, and deduce the equipotential surfaces and the gravity anomalies at large elevations above the geoid.

### 3-10. Formula Expressing Deflection of the Vertical in Gravity Anomalies

The "absolute" deflection of the vertical at a station  $P$  on the geoid is the angle between the normals at  $P$  to the geoid and to the earth spheroid.

If the second normal is taken with respect to a reference spheroid of arbitrary location, the word "absolute" in the definition is omitted.

From Fig. 3-4 it follows that the north component of the deflection  $\xi$ , i.e., the component in a vertical plane through the horizontal in the

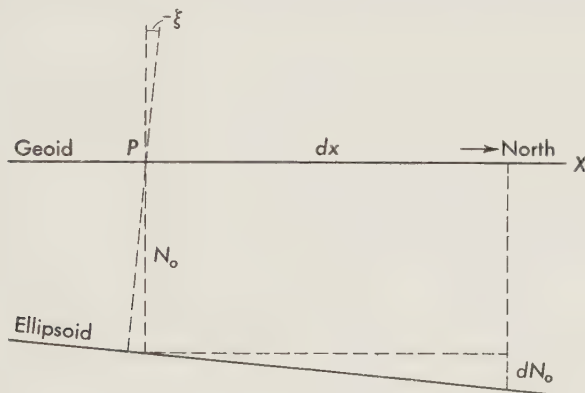


FIG. 3-4.

north direction at our station, which we shall take as the  $X$  axis, equals the differential quotient  $-\partial N_0 / \partial x$ :

$$\xi = -\frac{\partial N_0}{\partial x} \quad (3-85a)$$

We thus consider  $\xi$  as the difference geoidal minus ellipsoidal latitude. In the same way we have

$$\eta'' = -\frac{\partial N_0}{\partial y} \quad (3-85b)$$

where  $\eta$  is the deflection component in the plane of the prime vertical; we shall count  $\eta$  and  $y$  positive toward the east. As we give a positive sign to westward longitude, the deflection in longitude is given by

$$\lambda_a - \lambda_g = -\eta'' \sec B \quad (3-86)$$

where the subindexes  $a$  and  $g$  indicate astronomic and geodetic longitudes, respectively, and where  $B$  is the geographic latitude.

Equations (3-85a) and (3-85b) show that the astronomic-geodetic method of determining  $N_0$  from deflections of the vertical turns out to be an integration of these deflections. It is clear that we thus find  $N_0$  up to an arbitrary constant.

Since Stokes' theorem expresses  $N_0$  as an integral function of the gravity anomalies, by means of (3-85a) and (3-85b) we can find similar

formulas for the two components  $\xi''$  and  $\eta''$  of the deflection; we have to differentiate (3-80b) with respect to  $x$  and  $y$ , i.e., to the north and east directions. We introduce at  $P$  the azimuth  $\alpha$ , counted from north via east, of the great circle connecting  $P$  with an element  $dS$  of the geoid, which here we can treat as a sphere; the gravity anomaly in  $dS$  is again

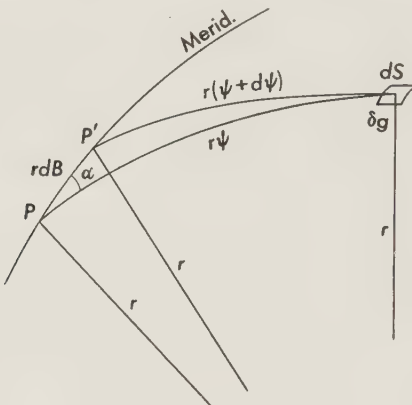


FIG. 3-5.

denoted by  $\delta g$ . In Fig. 3-5  $P'$  is a point on the meridian of  $P$  at an infinitely small distance  $dB$  from  $P$ . We note from this figure that

$$r d\psi = -r dB \cos \alpha = dx \cos \alpha$$

and so the differentiation of (3-80b) gives

$$\xi'' = -\frac{1}{4\pi gr^2 \sin 1''} \int_0^S \frac{dF_0}{d\psi} \cos \alpha \delta g dS \quad (3-87a)$$

$$\eta'' = -\frac{1}{4\pi gr^2 \sin 1''} \int_0^S \frac{dF_0}{d\psi} \sin \alpha \delta g dS \quad (3-87b)$$

Thus, because of (3-86), we have

$$\lambda_a - \lambda_g = \frac{\sec B}{4\pi gr^2 \sin 1''} \int_0^S \frac{dF_0}{d\psi} \sin \alpha \delta g dS \quad (3-87c)$$

If we wish to, we can express  $dS$  in terms of the differentials of the angles  $\psi$  and  $\alpha$  and introduce in these formulas

$$dS = \sin \psi d\psi d\alpha \quad (3-87d)$$

By differentiating the formula for  $F_0$ , (3-80a), we obtain the functions of  $\psi$  that follow the integral sign:

$$\begin{aligned} \frac{dF_0}{d\psi} = & -\frac{\cos \frac{1}{2}\psi}{2 \sin^2 \frac{1}{2}\psi} + 8 \sin \psi - 6 \cos \frac{1}{2}\psi - 3(1 - \sin \frac{1}{2}\psi) \csc \psi \\ & + 3 \sin \psi \ln [\sin \frac{1}{2}\psi(1 + \sin \frac{1}{2}\psi)] \quad (3-88a) \end{aligned}$$

$$\begin{aligned} \frac{dF_0}{d\psi} \sin \psi = & -\csc \frac{1}{2}\psi - 3 - 8 \sin \frac{1}{2}\psi + 12 \sin^3 \frac{1}{2}\psi + 8 \sin^2 \psi \\ & + 3 \sin^2 \psi \ln [\sin \frac{1}{2}\psi(1 + \sin \frac{1}{2}\psi)] \quad (3-88b) \end{aligned}$$

Formulas (3-87a) to (3-87d) combined with (3-88a) and (3-88b) give the complete solution. They allow us to derive the absolute deflection of the vertical from the gravity anomalies.

Detailed tables of the two functions (3-88a) and (3-88b) have been given by Sollins;<sup>18</sup> one set of them provides values of (3-88b) for different radii  $r$  from the station  $P$  from 10 to 5560 m, and a second set gives the values of (3-88a) for different angular distances  $\psi$  from  $P$ , ranging from 0°01 to 180°. An excerpt from the second set is contained in the appendix to this chapter. Both sets of Sollins's tables list half the values of the functions used here; the excerpt in the appendix gives the functions used here, obtained by doubling Sollins's values.

For small distances  $D$  from  $P$  the first term of (3-88a) predominates. Here it is approximately inversely proportional to the square of the distance  $D$ , and we may give the following rough approximation:

$$\frac{dF_0}{d\psi} \cong -\frac{2r^2}{D^2} \quad (3-89a)$$

$$\xi'' = \frac{1}{2\pi g \sin 1''} \int \frac{\delta g}{D^2} \cos \alpha dS \quad (3-89b)$$

$$\eta'' = \frac{1}{2\pi g \sin 1''} \int \frac{\delta g}{D^2} \sin \alpha dS \quad (3-89c)$$

These formulas show how strongly the effects diminish with distance. To find a formula for the effect of the central part of this near field, which includes the point  $D = 0$ , we shall represent the field by

$$\delta g = a + \beta x = a + \beta D \cos \alpha \quad (3-90a)$$

in which  $\beta$  is the gradient of gravity in the horizontal plane; it is here presumed to have a direction coinciding with the north, or  $X$ , direction.

We denote the outer boundary of this inner field by  $D_r$ , introduce it in (3-89b), and put  $dS = D d\alpha dD$ ; we then get

$$\begin{aligned}\xi'' &= \frac{\beta}{2\pi g \sin 1''} \int_0^{2\pi} \cos^2 \alpha d\alpha \int_0^{D_r} dD = \frac{D_r}{2g \sin 1''} \beta \\ \eta'' &= 0\end{aligned}\tag{3-90b}$$

We find that this central field has an effect proportional to the product of  $D_r$  and the gradient  $\beta$  and that its direction coincides with that of the gradient. We can obviously generalize this result to an arbitrary direction of the gradient. If we indicate the difference of the two values of gravity at both ends of the diameter of the central field in this direction by  $v_g$ , we can write

$$\theta'' = \frac{v_g}{4g \sin 1''} \tag{3-90c}$$

where  $\theta''$  represents the total deflection in so far as it is caused by the circular central field; its direction coincides with that of the gravity gradient. We can apply this formula over the area where the gradient is sufficiently constant, provided that the approximate formulas (3-89) can still be allowed; up to a radius of 30 km the error thus incurred is less than 1 per cent.

To derive the effect of the gravity anomalies for greater distances from  $P$  we can introduce templates marking circular zones divided into compartments in such a way that, according to Sollins's tables, the mean anomaly read from the anomaly map in each compartment has to be multiplied by the same factor as its contribution to the value of  $\xi$ . Taking the sum of the mean anomalies of all the compartments multiplied by this factor, and combining with the distribution by the central field, we obtain  $\xi$ . To find  $\eta$  we apply the same system of templates, after turning them  $90^\circ$ , and proceed in the same way. For systems of computation used up to the present see de Vos van Steenwijk<sup>22</sup> and Rice.<sup>15</sup>

The rapid falling off of the effect of gravity anomalies with distance implies that the principal part of the deflection of the vertical is provided by the gravity field in the neighborhood of the station; thus the formula can yield satisfactory accuracy even if the field is known only up to a moderate distance.

### 3-11. Exterior Equipotential Surfaces and Gravity

For equipotential surfaces exterior to the earth we have already developed Formulas (3-76c) and (3-79b). If we again replace  $r^2 d\sigma$  by  $dS$ , they become

$$N_\rho = \frac{r}{4\pi g_\rho \rho^2} \int_0^S F_\rho \delta g dS \quad (3-76c')$$

$$F_\rho = \frac{2}{uv} + \frac{1}{u} - 5 \cos \psi - 3 \frac{v}{u} - 3 \cos \psi \ln \frac{1}{2}(1 - u \cos \psi + v) \quad (3-79b)$$

with

$$u = \frac{r}{\rho}$$

and

$$v = (1 - 2u \cos \psi + u^2)^{\frac{1}{2}} \quad (3-79a)$$

For the gravity anomaly  $\delta g_\rho$  on this surface we found formula (3-74a); and, as (3-75) gives the value of the coefficients in the spherical harmonics  $Y_2, \dots, Y_n, \dots$ , we can follow a line similar to that followed in the development of (3-76c) and (3-79b), which led to Stokes' theorem. We obtain

$$\begin{aligned} \delta g_\rho &= \frac{1}{4\pi r^2} \int_0^S \sum_{n=2}^{n=\infty} (2n+1) P_n u^{n+2} \delta g dS \\ &= \frac{1}{4\pi r^2} \int_0^S f_\rho \delta g dS \end{aligned} \quad (3-91a)$$

with

$$\begin{aligned} f_\rho &= 2u^{\frac{1}{2}} \sum_{n=2}^{n=\infty} (n + \frac{1}{2}) P_n u^{n-\frac{1}{2}} \\ &= 2u^{\frac{1}{2}} \sum_{n=2}^{n=\infty} \frac{d}{du} (P_n u^{n+\frac{1}{2}}) \\ &= 2u^{\frac{1}{2}} \frac{d}{du} (u^{\frac{1}{2}} q) \end{aligned} \quad (3-91b)$$

where  $q$  has the meaning given by (3-77). Carrying out the differentiation, we find

$$f_\rho = \frac{1-u^2}{u^3} (1 - 2u \cos \psi + u^2)^{-\frac{1}{2}} - 1 - 3u \cos \psi \quad (3-91c)$$

Formulas (3-91a) and (3-91c) with (3-76c) and (3-79b), combined with Formulas (3-34), (3-36a), (3-36b), (3-46a), and (3-46b) for the external field of the spheroidal earth, give us the complete solution for the external gravity and the external equipotential surfaces of the earth. We shall not discuss them here in detail; for a short study of external gravity anomalies compared with the corresponding gravity anomalies on the geoid, see Vening Meinesz.<sup>21</sup>

### 3-12. Basic Hypothesis of Geodesy; Stokes' Theorem and Related Equations; Applicability When Gravity Is Still Unknown over Large Parts of the Earth

For centuries geodesy has been based on the hypothesis that the geoid is so close to being an ellipsoid of revolution that the latter can be substituted for the geoid. The basis of this hypothesis was the assumption that the ellipsoid of revolution represented the equilibrium figure of the rotating earth. This assumption was satisfactory as long as it corresponded to the accuracy of observations or, to put it more exactly, as long as the imperfections of the hypothesis did not give rise to contradictions exceeding the observational errors. The hypothesis was the basis for large extrapolations from the observations; from a few measurements of arc in a relatively small part of the earth's surface conclusions were drawn for the dimensions and the flattening of the ellipsoid.

This procedure was continued up to the present time, although it has long been known that the above condition was not fulfilled. The results of the different measurements of arc show discrepancies far surpassing the observational errors, and a quickly growing number of results for deflections of the vertical demonstrated the deviations of the geoid from the ellipsoid of revolution. A vague hope that the divergencies in the measurements of arc would somehow cancel out in finding the mean values for the dimensions and flattening of the ellipsoid took the place of the original confidence. We can be sure, however, that the basic hypothesis has outlived its usefulness and that it no longer provides a sound base for geodesy.

We therefore need a new concept which is in closer harmony with present-day observational results and at the same time adequate to work with. It seems possible to outline such a concept. We can assume that the earth is close to equilibrium and that the deviations from equilibrium are limited in size and extent. To define our concept more accurately we can express the deviations from equilibrium by the isostatically reduced gravity anomalies with respect to a value for normal gravity which is in harmony with the assumption of an entirely fluid earth in equilibrium. We can suppose, for example, that the anomalies thus defined show no areas of deviation where the mean anomaly multiplied by the area is more than a certain number of  $\text{mgalMm}^2$ , where  $Mm$  denotes a megameter ( $= 10^6 \text{ m}$ ) and  $Mm^2 = 10^{12} \text{ m}^2$ . For this number a figure of 30  $\text{mgalMm}^2$  appears to agree with the facts. In view of what we know, we may further suppose that in the part of the earth's surface where the value of gravity is still unknown there are no more than 10 such deviation areas.

On this basic hypothesis, which doubtless is a less bold extrapolation from the known into the unknown parts of the earth than the old one was, we can construct a satisfactory framework for geodetic investigation.

It allows us already to apply Stokes' theorem for determining  $N_0$  and the equation derived from it for computing the absolute deflections of the vertical, despite the fact that over great parts of the earth gravity measures have not yet been made. We shall examine this point shortly.

According to (3-83), a circular anomaly area which has a diameter of about  $10^\circ$  and a mean anomaly of about 30 mgal, and which thus corresponds to a total deviation of 30 mgal/M $\text{m}^2$ , gives a figure for the rise or fall of the geoid with respect to the ellipsoid of about 20 m in the center. From the values of  $F_0$  and  $dF_0/d\psi$  in the appendix to this chapter we can further conclude that over the earth, beyond a distance of 3000 km from the center,  $N_0$  varies from 0 to 1.18 m and that the range in the components of the deflection of the vertical is from  $0''$  to  $0''.22$ . For 10 such deviation areas distributed in the gravimetrically unsurveyed part of the earth and distant at least 3000 km from a station where we apply Stokes' theorem for obtaining  $N_0$  or the equations for deriving the deflection of the vertical we thus find at that station uncertainties  $\Delta N_0$ ,  $\Delta \xi$ , and  $\Delta \eta$ , respectively, of which the mean value can be estimated by

$$\Delta N_0 = \sqrt{10} \times \frac{1}{2}\sqrt{2} \times 1.18 \text{ m} = 2.6 \text{ m} \quad (3-92)$$

$$\Delta \xi = \Delta \eta = \sqrt{10} \times \frac{1}{2} \times 0''.22 = 0''.35$$

Since  $\Delta N_0$  is less than  $1/2,400,000$  part of the earth's radius, for stations at sufficient distances from unsurveyed areas, the application of Stokes' theorem gives a satisfactorily accurate result for  $N_0$ . The same is true for the two components of the deflection of the vertical.

Much deeper and more elaborate studies of possible applications of Stokes' theorem have been made by de Graaff Hunter,<sup>9</sup> Hirvonen,<sup>11</sup> and Tanni,<sup>19</sup> especially the latter two, and investigations of the deflection of the vertical have been made by de Vos van Steenwijk<sup>22</sup> and Rice,<sup>15</sup> their work will be discussed in Chaps. 8 and 9, where these important problems are studied more deeply and in greater detail.

It can be concluded from the foregoing discussion that the application of these formulas and Stokes' theorem, notwithstanding our present lack of gravity values over large parts of the earth, is warranted only if it is based on the above considerations regarding the degree of equilibrium attained by the earth; otherwise uncertainties would arise about possible systematic effects of neglecting gravity anomalies in the unsurveyed areas. It follows that the anomalies used must be isostatically reduced and that the change in both the geoid and the deflections of the vertical implied by these reductions must be taken into account. Therefore, after  $N_0$ ,  $\xi$ , and  $\eta$  are computed, they must be corrected to derive their values for the uncorrected earth.

Chapters 6 and 7 treat of these reductions and corrections. Chapters 8 and 9 deal with the way in which we can use the values of  $N_0$  and of the deflections of the vertical to place geodesy on a correct basis, thus enabling us to make geodetic computations on the ellipsoid even though the observations refer to the geoid.

### 3-13. Gravity Formulas

We need a gravity formula giving the normal gravity value at sea level for different latitudes and longitudes. All gravity formulas have been derived by the aid of the gravity values measured in various parts of the world. The accuracy of the derived gravity formula increases according to the number of gravity observations available, the breadth of their distribution at different latitudes, and the suitability of their reduction to sea level. Since many areas of the earth's surface are covered only by very few, if any, gravity stations, we must correct the gravity values so that every gravity station can, if necessary, represent a relatively large area. In other words, we must find a method which smoothes the effect of the local disturbing masses on the observed gravity as completely as possible. These prerequisites are best satisfied by the isostatic reductions.

#### A. International Gravity Formula

The best gravity formulas can be derived just from the isostatically reduced gravity values. One of these formulas is the international gravity formula, which was accepted in the General Assembly of the International Union of Geodesy and Geophysics at Stockholm in 1930.

The general gravity formula is

$$\gamma = \gamma_E(1 + \beta \sin^2 \varphi + \epsilon \sin^2 2\varphi) \quad (3-93)$$

where  $\gamma_E$  = gravity value at equator

$\varphi$  = latitude of station

$\beta$  = coefficient of principal latitude term

In addition there is another, smaller latitude term, the coefficient of which is  $\epsilon$ . Therefore, while the parameters  $\gamma_E$  and  $\beta$  must be obtained empirically from the gravity measurements, the constant  $\epsilon$  is derived theoretically.

The values of the three quantities of the international gravity formula are clear from the international gravity formula itself

$$\gamma = 978.0490(1 + 0.0052884 \sin^2 \varphi - 0.0000059 \sin^2 2\varphi) \text{ cm/sec}^2 \quad (3-94)$$

The first term was computed by Heiskanen <sup>29</sup> in 1928, using the  $\beta$  value 0.005289, on the basis of several thousand isostatically reduced gravity stations. The third constant, -0.0000059, was derived theoretically by Somigliana and Cassinis <sup>25</sup> in 1930. The  $\beta$  term has been computed on

the basis of Clairaut's formula from the flattening value  $\alpha = 1/297.0$  of the meridian. This value was derived by Hayford in 1910 and accepted as the flattening value of the international reference ellipsoid at the Madrid Assembly of the International Union of Geodesy and Geophysics in 1924.

That there was good reason to adopt the  $\beta$  value 0.0052884 is clear from earlier  $\beta$  values: Helmert<sup>32</sup> obtained from the gravity material in 1901 the  $\beta$  value 0.005302 and, in 1915,<sup>33</sup> 0.005285; in 1917 Bowie<sup>24</sup> found 0.005294; and in 1924 Heiskanen<sup>28</sup> found 0.005285—all of which agree well with the accepted value of  $\beta$ .

In this way both the international ellipsoid

$$a = 6,378,388 \text{ meters}$$

$$\alpha = \frac{1}{297.0} = 0.00336700$$

and the international gravity formula have been bound together. The gravity formula gives the normal gravity at the surface of the international ellipsoid. The values of  $\alpha$  and  $\beta$  are not independent. If, for instance, a change is made in the value of  $\beta$ , the value of  $\alpha$  also has to be changed. Such changes, however, are not expedient, since tables for both the international ellipsoid and the international gravity formula have been computed and are in general use. Most countries have adopted the international ellipsoid, and the majority of the gravity anomalies of the world have been computed on the basis of the international gravity formula. Changing the fundamental quantities  $\alpha$  and  $\beta$  would therefore cause some confusion; if any changes are to be made in  $\alpha$  and  $\beta$ , they should be definitive and should be proposed only after very careful consideration. Our present knowledge does not justify such changes.

In the General Assembly of the International Union of Geodesy and Geophysics in Toronto, Canada, in September, 1957, it was unanimously decided not to change the international gravity formula.

Quite a different question, though one connected with the gravity formula, is whether the whole gravity system, i.e., the basic gravity value at the world gravity base station at Potsdam, Germany, should be changed. We know that the Potsdam value  $g = 981.274 \text{ cm/sec}^2$  is more in error than previously supposed. According to Heyl's absolute-gravity measurements at Washington, D.C., the correction of the Potsdam value is  $-20 \text{ mgal}$ ; according to Bullard's at Teddington, the correction is  $-15 \text{ mgal}$ ; and according to Ivanoff's at Leningrad, it is  $-4 \text{ mgal}$ . In discussing the problem, Heyl gives the correction as  $-15 \text{ mgal}$ ; Bullard and Browne, as  $-16 \text{ mgal}$ ; Morelli, as  $-16 \text{ mgal}$ ; Jeffreys, as  $-13 \text{ mgal}$ ; Woppard, as  $-14$  to  $-18 \text{ mgal}$ ; and Berroth, as  $-13 \text{ mgal}$ .<sup>30</sup>

There appears to be no doubt that the Potsdam gravity value must be changed, approximately by  $-10$  to  $-15$  mgal, but since the exact correction is not yet known, the General Assembly of the International Union of Geodesy and Geophysics at Rome in 1954 and at Toronto in 1957 decided to await more information before adopting the change.

From the geodetic point of view it is, of course, about the same whatever Potsdam value we use, so long as we use the same value and the same gravity system everywhere. This system can be 20 or even 50 mgal in error, because we do not operate with the gravity values themselves but merely with their differences. If, for instance, we diminish the Potsdam value by 15 mgal and at the same time diminish the equator value of the gravity formula also by 15 mgal, the gravity anomalies will, practically speaking, not change at all. However, from a purely scientific point of view, it is best to have as correct a gravity system as possible.

### B. Computation of the Gravity Formula

If we intend to derive a new gravity formula, we must use some existing formula and compute corrections to the parameters of this formula. It can be done only on the basis of the gravity anomalies obtained from the observed gravity values  $g$  properly reduced to the sea level  $g_0$ . The gravity anomalies are  $\Delta g = g_0 - \gamma$ , where  $\gamma$  is the gravity value obtained, say, from the international gravity formula.

When we add the correction terms to the gravity formula used, we get the corrected gravity formula

$$\gamma' = \gamma + \Delta\gamma = 978.049(1 + 0.0052884 \sin^2 \varphi - 0.0000059 \sin^2 2\varphi) + \Delta\gamma \quad (3-95)$$

where the correction  $\Delta\gamma$  is

$$\Delta\gamma = x' + y' \sin^2 \varphi \quad (3-96)$$

We do not compute any correction to the  $\epsilon$  term. Here  $x'$  is the correction of the equatorial value,  $y'$  the correction of the  $\sin^2 \varphi$  term.

Before correction the anomalies are

$$\Delta g = g_0 - \gamma$$

After correction they are

$$v = \Delta g - \Delta\gamma \quad (3-97)$$

Therefore we get the error equation, changing the sign,

$$x' + y' \sin^2 \varphi - \Delta g = -v \quad (3-98)$$

We use the observed gravity anomalies  $\Delta g$  as if they were observational errors, which, of course, they are not. Then we determine the corrections

$x'$ ,  $y'$  according to the least-squares method, so that the square sum  $\Sigma v^2$  of the remaining anomalies  $v$  becomes a minimum

$$\Sigma v^2 = \min \quad (3-99)$$

Every gravity station used in the computation of the gravity formula will give an error equation of Formula (3-98). For instance, the error equation of the pendulum gravity station at Chicago, Illinois,  $\varphi = 41^\circ 47' 4''$ ,  $\lambda = 87^\circ 36' 1''$  would be

$$x' + 0.6664y' - 7 = v$$

where 7 mgal is the isostatic gravity anomaly according to the Airy system,  $T = 40$  km.

As an example, let us take the computation of the gravity formula carried out by Heiskanen<sup>31</sup> in 1938, as follows. Some regions, especially in Europe, the United States, and India, since they are covered with a thick gravity-station net, will be given too great a weight in the determination of the gravity formula as compared to regions where only a few gravity measurements have been made. As a consequence, in regions with a dense gravity-station net, the new gravity formula will agree well with observations, but in the other, much greater part of the earth, it will agree perhaps badly or not at all.

To avoid this difficulty one hypothetical station is used to represent a whole square degree, regardless of whether there actually are 1, 10, 50, or 200 gravity stations there, and the hypothetical station is assumed, for convenient computation, to be located in the center of the square. The gravity anomaly of the hypothetical gravity station is the mean of all the anomalies of the square, but the weight of all hypothetical stations is taken as one, regardless of the number of actual gravity stations in the square. Stations with a gravity anomaly of  $\pm 80$  mgal or more are omitted, because such great anomalies are usually the result of local phenomena and do not give a real representation of the regional gravity-anomaly field. Whole squares with a mean anomaly of  $\pm 80$  mgal or more are likewise omitted.

Thus there are the following numbers  $n$  of squares:

	<i>n</i>		<i>n</i>
United States.....	292	Europe.....	241
Canada.....	123	East Africa.....	71
Mexico.....	26	Vening Meinesz:	
West Indies.....	80	At sea.....	383
India.....	242	South Seas *.....	211
Siberia.....	94		
Caucasus.....	39	Total.....	1802

\* These anomalies were not reduced isostatically.

All isostatically reduced stations (in all, 1591 squares) give the following normal equations \*

$$\underline{1591x + 496.0y' - 676.7 = 0}$$

$$\underline{239.5y' - 1394.0 = 0}$$

which give the following values for  $x'$ ,  $y'$

$$x' = -3.92$$

$$y' = +13.94$$

When we further consider that the unit of the computed quantities is a milligal, the unit of the gravity formula being 1 cm/sec<sup>2</sup>, or 1000 mgal, we get the following corrected gravity formula

$$\gamma_0 = (978.049 + x)[1 + (0.0052884 + y) \sin^2 \varphi - 0.0000059 \sin^2 2\varphi]$$

where  $x = x' \times 10^{-3}$

$$y = y' (1 + 0.022) \times 10^{-6}$$

Thus we get

$$x = -0.0039$$

$$y = +0.0000142$$

and finally the gravity formula

$$\gamma_0 = 978.0451(1 + 0.0053026 \sin^2 \varphi - 0.0000059 \sin^2 2\varphi)$$

The corresponding flattening is  $\alpha = 1/298.2$ .

Similar computations have given the following gravity formulas, with corresponding flattening values:

Helmut <sup>32</sup> .....	1901	$978.030(1 + 0.005302 \sin^2 \varphi - 0.000007 \sin^2 2\varphi)$ $\alpha = 0.0033535 = 1/298.2$
Bowie <sup>24</sup> .....	1917	$978.039(1 + 0.005294 \sin^2 \varphi - 0.000007 \sin^2 2\varphi)$ $\alpha = 0.0033614 = 1/297.5$
Heiskanen <sup>29</sup> .....	1928	$978.049(1 + 0.005289 \sin^2 \varphi - 0.000007 \sin^2 2\varphi)$ $\alpha = 0.0033664 = 1/297.06$
Heiskanen, <sup>35</sup> Uotila <sup>37</sup> .....	1957	$978.0496(1 + 0.0052934 \sin^2 \varphi - 0.0000059 \sin^2 2\varphi)$ $\alpha = 0.0033622 = 1/297.4$
International.....	1930	$978.0490(1 + 0.0052884 \sin^2 \varphi - 0.0000059 \sin^2 2\varphi)$ $\alpha = 0.0033670 = 1/297.00$

\* The underlined quadratic coefficients 1591 and 239.5 indicate that the equations are normal equations.

From these values of  $\alpha$ , it seems that the flattening derived from gravity values, as far as they were then available, shows a tendency to be slightly smaller than the value of 1/297.00 adopted in Madrid in 1924.

During the last four decades, the question of the triaxiality of the earth has been raised in earnest, for the following reasons. The available gravity material was so distributed on the earth's surface that it gave quite strong evidence for triaxiality. The observed gravity anomalies were negative in large parts of North America; in India they were still more clearly negative; but in Europe, the eastern part of the Atlantic, and many regions of the Pacific Ocean they were systematically positive. As the longitude differences between North America, Europe, India, and the middle part of the Pacific are each about  $90^\circ$ , the derivation of the gravity formula led to the conclusion that the maximum gravity and the long axis are not very far from the longitude of Greenwich and the minimum gravity value and the short axis approximately  $90^\circ$  east and west of Greenwich.

The most important gravity formulas with longitude terms are:

Helmholtz <sup>33</sup> .....	1915	$978.052[1 + 0.005285 \sin^2 \varphi - 0.0000070 \sin^2 2\varphi + 0.000018 \cos^2 \varphi \cos^2(\lambda + 17^\circ)]$
Heiskanen <sup>28</sup> .....	1924	$978.052 * [1 + 0.005285 * \sin^2 \varphi - 0.0000070 \sin^2 2\varphi + 0.000027 \cos^2 \varphi \cos 2(\lambda - 18^\circ)]$
Heiskanen <sup>29</sup> .....	1928	$978.049[1 + 0.005293 \sin^2 \varphi - 0.0000070 \sin^2 2\varphi + 0.000019 \cos^2 \varphi \cos 2(\lambda - 0^\circ)]$
Niskanen <sup>34</sup> .....	1945	$978.0468[1 + 0.0052978 \sin^2 \varphi - 0.0000059 \sin^2 2\varphi + 0.0000230 \cos^2 \varphi \cos 2(\lambda + 4^\circ)]$
Uutila <sup>37</sup> .....	1957	$978.0516 [1 + 0.0052910 \sin^2 \varphi - 0.0000059 \sin^2 2\varphi + 0.0000106 \cos^2 \varphi \cos 2(\lambda + 6^\circ)]$

\* These two terms are by accident the same as in Helmert's formula.

The additional gravity material later obtained from the East Indies and several other parts of the world, however, has not fully proved the triaxiality of the earth. For instance, the large shelf area north of Sumatra is a region of strongly positive anomalies, although they ought to be negative if the earth is triaxial with the short axis close to longitude  $90^\circ$ .

As we now have sufficient gravity material to determine the undulations of the geoid around the world, we can easily determine whether the geoid fits an ellipsoid of revolution or a triaxial ellipsoid best. It appears that we had better forget the triaxial ellipsoid, particularly because since

the earth is in close isostatic equilibrium, it can hardly have the shape of a triaxial ellipsoid.

It may be worthwhile mentioning that the leading Russian geodesists are strong defenders of the triaxial ellipsoid, as Heiskanen was two decades ago. The parameters of the Russian triaxial ellipsoids are

$$a = 6,378,245 \text{ meters}$$

$$\alpha = \frac{1}{298.3}$$

$$\alpha' = \frac{1}{30,000}$$

$$\lambda_0 = +15^\circ$$

$$a_{\max} - a_{\min} = 212 \text{ meters}$$

where  $\alpha'$  = flattening of equator

$\lambda_0$  = longitude of long axis

## APPENDIX

TABLE OF STOKES' FUNCTIONS

$$F_0 = \csc \frac{1}{2}\psi + 1 - 5 \cos \psi - 6 \sin \frac{1}{2}\psi - 3 \cos \psi \ln [\sin \frac{1}{2}\psi(1 + \sin \frac{1}{2}\psi)] \quad (3-80a)$$

$$F'_0 = \frac{1}{2} F_0 \sin \psi \quad (3-81a)$$

$$\begin{aligned} \frac{dF_0}{d\psi} = & -\frac{\cos \frac{1}{2}\psi}{2 \sin^2 \frac{1}{2}\psi} + 8 \sin \psi - 6 \cos \frac{1}{2}\psi - 3(1 - \sin \frac{1}{2}\psi) \csc \psi \\ & + 3 \sin \psi \ln [\sin \frac{1}{2}\psi(1 + \sin \frac{1}{2}\psi)] \end{aligned} \quad (3-88a)$$

$\psi$	$F_0$	$F'_0$	$\frac{dF_0}{d\psi}$
0°	$\infty$	+1.0000	$\infty$
0.3	+395.78	+1.0362	-73,528.6
0.6	+202.70	+1.0613	-18,528.6
1.0	+124.74	+1.0885	-6,742.0
2	+65.28	+1.1392	-1,731.9
3	+44.88	+1.1746	-791.42
4	+34.40	+1.1996	-457.90
5	+27.92	+1.2165	-301.58
6	+23.48	+1.2267	-215.56
7	+20.20	+1.2309	-163.04
8	+17.676	+1.2300	-128.514
9	+15.654	+1.2244	-104.536
10	+13.988	+1.2146	-87.160
12	+11.384	+1.1834	-64.082
14	+9.414	+1.1388	-49.768
16	+7.856	+1.0826	-40.192
18	+6.576	+1.0162	-33.408
20	+5.502	+0.9410	-28.383
25	+3.418	+0.7224	-20.151
30	+1.894	+0.4736	-15.135
35	+0.732	+0.2100	-11.6801
40	-0.168	-0.0543	-9.0849
50	-1.402	-0.5371	-5.2771
60	-2.068	-0.8957	-2.4795
70	-2.302	-1.0820	-0.2927
80	-2.198	-1.0821	+1.4279
90	-1.828	-0.9142	+2.7363
100	-1.266	-0.6230	+3.6543
110	-0.576	-0.2700	+4.1958
120	+0.178	+0.0773	+4.3778
130	+0.934	+0.3577	+4.2251
140	+1.636	+0.5258	+3.7727
150	+2.236	+0.5590	+3.0659
160	+2.694	+0.4608	+2.1592
170	+2.980	+0.2588	+1.1147
180	+3.080	0.0000	0.0000

## REFERENCES

1. Brouwer, D.: On the system of astronomical constants, Bull. Astron. Inst. Netherlands, vol. 307, pp. 213–231, 1938.
2. Bullard, E. C.: The figure of the earth, Monthly Notices Roy. Astron. Soc., Geophys. Suppl., vol. 5, no. 6, 1948.
3. Bullen, K. E.: The problem of the earth's density variation, Bull. Seis. Soc. Amer., vol. 30, no. 3, 1940.
4. ———: The density variation of the earth's central core, *ibid.*, vol. 32, no. 1, 1942.
5. Callandreau, O.: Sur le développement en série du potentiel, J. polytech., 1889.
6. Clausen, Th.: Astron. Nachr., vol. 18, no. 418, p. 145, 1841.
7. Darwin, George H.: The theory of the figure of the earth, carried to the second order of small quantities, Monthly Notices Roy. Astron. Soc., vol. 60, pp. 82–124, 1899.
8. ———: Scientific papers, vol. 3, covering period 1907–1916, p. 78.
9. de Graaff Hunter, J.: The figure of the earth from gravity observations and the precision obtainable, Trans. Roy. Soc. (London), ser. A, vol. 234, no. 743, pp. 377–431, 1935.
10. Helmert, F. R.: Die mathematischen und physikalischen Theorien der höheren Geodäsie, vol. 2, Teubner, Leipzig, 1884.
11. Hirvonen, R. A.: On the precision obtainable for gravimetric determinations of the geoid, Ohio State Univ. Mapping and Charting Research Lab., Tech. Paper, no. 171, 1953.
12. Hopfner, F.: Physikalische Geodäsie, Akademische Verlagsgesellschaft, Leipzig, 1933.
13. Lambert, W. D.: The reduction of observed values of gravity to sea level, Bull. géod., no. 26, pp. 107–181, 1930.
14. ——— and F. W. Darling: Tables for determining the form of the geoid and its indirect effect on gravity, USCGS, Spec. Publ., no. 199, 1936.
15. Rice, D. A.: Deflections of the vertical from gravity anomalies, USCGS Rept., 1951.
16. Spencer-Jones, H.: Mem. Roy. Astron. Soc., vol. 66, p. 60, 1941.
17. Sitter, W. de: On the flattening and the constitution of the earth, Bull. Astron. Inst. Netherlands, vol. 55, pp. 97–108, 1924.
18. Sollins, A. D.: Tables for the computation of deflections of the vertical from gravity anomalies, Bull. Géod., N.S., no. 6, pp. 279–300, 1947.
19. Tanni, L.: On the continental undulations of the geoid as determined from the present gravity material, Publ. Isos. Inst. IAG (Helsinki), no. 18, 1948.
20. Tisserand, F.: Traité de mécanique céleste, vol. 2, chap. 15, Paris, 1891.
21. Vening Meinesz, F. A.: A formula expressing the deflection of the plumb-line in the gravity anomalies and some formulae for the gravity field and the gravity-potential outside the geoid, Proc. Koninkl. Ned. Akad. Wetenschap., vol. 31, no. 3, pp. 315–331, 1928.
22. Vos van Steenwijk, J. E., baron de: Plumbline deflections and geoid in Eastern Indonesia, Publ. Neth. Geod. Comm., Waltman, Delft, 1946.
23. Whittaker-Watson: A course of modern analysis, 5th ed., Cambridge, London, 1950.
24. Bowie, William: Investigations of gravity and isostasy, USCGS, Spec. Publ., no. 40, 1917.
25. Cassinis, G.: Sur l'adoption d'une formule internationale pour la pesanteur normale, Bull. géod., no. 26, 1930.
26. Hayford, J. F.: The figure of the earth and isostasy, from measurements in the United States, USCGS, 1909.

27. Hayford, J. F.: Supplementary investigation in 1909 of the figure of the earth and isostasy, USCGS, 1910.
28. Heiskanen, W. A.: Untersuchungen über Schwerkraft und Isostasie, Publ. Finn. Geod. Inst., no. 4, 1924.
29. ———: Ist die Erde ein dreiachsiges Ellipsoid?, Gerlands Beitr. Geophys., vol. 19, 1928.
30. ———: On the figure and structure of the earth, Publ. Isos. Inst. IAG (Helsinki), no. 8, 1941.
31. ———: Investigations on the gravity formula, Publ. Isos. Inst. IAG (Helsinki), no. 1, 1938.
32. Helmert, F. R.: Der normale Teil der Schwerkraft im Meeresniveau, Ber. Kgl. preuss. Akad. Wiss., vol. 14, p. 328, 1901.
33. ———: Neue Formeln für den Verlauf der Schwerkraft im Meeresniveau beim Festlande, *ibid.*, vol. 41, 1915.
34. Niskanen, Erkki: Gravity formulas derived by the aid of the level land stations, Publ. Isos. Inst. IAG (Helsinki), no. 16, 1945.
35. Heiskanen, W. A.: Achievements of the World-wide Gravity Program of the Mapping and Charting Research Laboratory of the Ohio State University, Report to the Toronto General Assembly of the IUGG in 1957.
36. ———: The Columbus Geoid, Trans. Am. Geophys. Union, no. 6, 1957.
37. Uotila, U. A.: Determination of the Shape of the Geoid; Symposium: Size and Shape of the Earth, held at the Ohio State University, Columbus, Ohio, Nov. 13–15, 1956, Publ. no. 7, Inst. of Geodesy, Photogrammetry and Cartography.

## CHAPTER 4

### GRAVITY MEASUREMENTS

#### 4-1. Pendulum Observations

The acceleration  $g$  of gravity can be measured either by "dynamic" or "static" apparatus. The most important dynamic gravity-measuring methods are (1) measurement of the velocity of a falling body (Atwood's machine, Galileo's tilted plane, and Volet's machine) and (2) measurement of the period of a swinging body under the attraction of gravity force (usual pendulum apparatus, inverted pendulum, and gravity variometer). To the static group belong (1) instruments using the spring-balance principle (usual gravimeters) and (2) gas-pressure gravimeters.

Gravity measurements are either "absolute" or "relative." In the first, the value of the gravity  $g_0$  itself is determined; in the second, the difference, or ratio, between the gravity  $g_0$  measured at the gravity base station and  $g$  at gravity field stations is determined. Relative gravity measurements are based on the following identities

$$g = g_0 \frac{g}{g_0} \quad \text{and} \quad g = g_0 + (g - g_0)$$

Absolute gravity measurements have been carried out at several stations, generally by the reversing-pendulum method. Table 4-1 gives some of these base stations and the corresponding measured gravity value.

Many nations have taken an interest in gravimetric measurements, as is shown by the large number of absolute-gravity base stations. The accuracy of many of the measurements, however, is rather low, and until recently it was seldom possible to obtain an accuracy higher than 3 mgal in absolute gravity measurements. When poor measurements are adjusted to the same system, there may remain an error of even 1 milligal. Since modern gravimeters and air transportation now make it possible for gravity base stations, even on different continents, to be tied in to the same system by relative measurements with an accuracy better than 1 mgal, it might well be advisable to have only one reference base station for the entire world. It would not matter whether this world base station were chosen at Pots-

TABLE 4-1. SOME ABSOLUTE GRAVITY MEASUREMENTS<sup>9,16</sup>

Station	Observed $g$ , cm/sec <sup>2</sup>	$g$ converted to Potsdam, cm/sec <sup>2</sup>
Rome.....	980.343	981.254 *
Vienna.....	.862	.283
Paris.....	.970	.300
Teddington.....	981.181	.256 *
Washington.....	980.080	.252 *
Ottawa.....	.616	.260 *
Potsdam.....	981.274	.274

\* Modern measurements.

dam, Paris, Teddington, Washington, Dehra Dun, Buenos Aires, or at any other acceptable location. At such an international base station absolute gravity measurements should be carried on for several years.

The national base stations both of different countries and of the ocean islands could then be tied in by the aid of relative measurements with respect to the international base station. Relative measurements could be carried out in part by sensitive pendulum apparatus and in part by gravimeters. Adjustment of these accurate ties between base stations would give a unique and a very accurate world gravimetric system.

Since, however, the dictates of national pride may preclude this ideal solution, we are faced with the serious problem of measuring the absolute gravity at various base stations so accurately that the errors of these respective "standard" values would not cause gravity systems in different parts of the world to differ significantly from each other. The progress of the absolute gravity measuring methods since 1953 seems in broad terms to guarantee this.

Regardless of how many absolute-gravity stations there are, in every country there should be at least one national gravity base station tied as accurately as possible by relative measurements to the base stations of other countries or to the international base. Relative measurements have connected most European national base stations, as well as Washington, Mexico City, Dehra Dun, etc., to the Potsdam system, and since the national base stations of South Africa, Australia, and Canada are based on the gravity value at Cambridge, England, which has also been connected to Potsdam, practically speaking, all gravity base stations are now on the Potsdam system. The gravity field measurements of different countries are, of course, based on the national gravity base station of the respective

TABLE 4-2. GRAVITY AT SOME NATIONAL GRAVITY BASE STATIONS<sup>10</sup>

Name	Latitude	Longitude	Height, m	Adjusted gravity, cm/sec <sup>2</sup>
Potsdam.....	52°22'9	13° 4'1	87.24	981.2740
Munich.....	48 8.7	11 36.6	525	980.7327
Binningen.....	47 32.5	7 35.1	314.4	.7637
Basel, Bern.....	47 33.6	7 34.8	277	.7775
Karlsruhe.....	49 0.7	8 24.7	114	.9558
de Bildt.....	52 6.2	5 10.7	2.1	981.2679
Paris.....	48 50.2	2 20.3	62	980.9435
Vienna, Observatory.....	48 13.9	16 20.4	236	.8528
M.G.I.....	48 12.7	16 21.5	183	.8595
Padua.....	45 24.0	11 52.3	18.9	.6561
Genoa.....	44 25.1	8 55.3	97.5	.5572
Rome.....	41 53.5	12 29.7	49.3	.3663
Budapest.....	47 28.8	19 3.2	106	.8533
Zurich.....	47 22.7	8 33.2	463	.664
Strasbourg.....	48 35.0	7 46.1	137	.897
Turin.....	45 4.1	7 41.8	233	.537
Madrid.....	40 24.5	-3 41.2	655	979.9807
Lisbon.....	38 42.5	-9 11.2	75	980.0876
Uccle.....	50 47.9	4 21.5	102	981.1322
Cambridge.....	52 12.9	0 5.8	25	.2685
Teddington.....	51 25.2	-0 20.4	9.3	.1963
Warsaw.....	52 14.4	21 0.2	111	.2398
Cracow.....	50 3.9	19 57.6	205	.0528
Poznań.....	52 24.7	16 55.7	57	.2635
Oslo.....	59 55.2	10 46.6	30.4	.9284
Copenhagen.....	55 44.3	12 30.1	44.7	.5575
Stockholm.....	59 19.5	18 2.7	8.6	.8470
Helsinki.....	60 10.6	24 57.5	20.5	.9158
Pulkovo.....	59 46.3	30 19.6	75.2	.8993
Tallinn.....	59 26.3	24 44.4	42.5	.8400
Riga.....	56 57.1	24 7.0	4.6	.6589
Kaunas.....	54 53.7	23 52.4	70.3	.4911
Danzig.....	54 22.1	18 37.0	21.4	.4487
Moscow.....	55 45.3	37 34.3	145	.5598
Kasan.....	55 47.4	49 7.3	75.6	.5587
Poltava.....	49 36	39 34	146	.0067
Leningrad, I.M.S.....	59 55.1	30 19.0	4	.9317
Observatory.....	59 56.5	30 17.7	3	.9324
A.I.....	59 56.2	30 20.9	4	.9339
Tiflis.....	41 43.1	44 47.8	406	980.1777
Tashkent.....	41 19.5	69 17.7	478	.081
Dehra Dun.....	30 19.4	78 3.2	683	979.063
Tokyo.....	35 42.6	139 46.0	18	.8010
Washington, D.C.....	38 53.6	-77 2.0	0.2	980.1191
Ottawa.....	45 23.6	-75 43.0	82	.6220
La Plata.....	-34 54.5	-57 55.9	10.6	979.748
Buenos Aires.....	-34 35	-58 29	18.9	.7078
Cape Town.....	-33 57.1	18 28.1	38.4	.6475
Melbourne.....	-37 47.2	144 53.5	43.9	.9776

countries. Gravity observations of the last few years have not changed these values essentially.<sup>28</sup>

### A. Theory of Pendulum Observations

To derive the formula for pendulum observations we use a fictitious "mathematical pendulum," which helps in the derivation of the expression for the period of oscillation of the actual pendulum. By definition, the mathematical pendulum is a dimensionless mass point hanging on a weightless thread.

Let  $O$  be the suspension point (Fig. 4-1) and  $l$  the length of a mathematical pendulum  $P$  which swings in the  $xz$  plane. The acceleration of gravity  $g$  attracting the pendulum mass can be divided into a radial component  $g \cos \varphi$  and a component  $g \sin \varphi$  perpendicular to it. The latter gives the pendulum an acceleration  $l(d^2\varphi/dt^2)$ , which satisfies the following equation:

$$g \sin \varphi = -l \frac{d^2\varphi}{dt^2}$$

where  $\varphi$  is the elongation angle of the pendulum. The differential equation of the free-swinging pendulum is therefore

$$\frac{d^2\varphi}{dt^2} + \frac{g}{l} \sin \varphi = 0 \quad (4-1)$$

or, because  $\varphi$  is so small that  $\sin \varphi$  can be replaced by  $\varphi$ ,

$$\frac{d^2\varphi}{dt^2} + \frac{g}{l} \varphi = 0 \quad (4-1a)$$

The solution of this equation is simple. If  $\varphi_0$  is the amplitude,  $\psi$  the phase angle, and  $T_0$  the period of the pendulum, we have

$$\varphi = \varphi_0 \sin \psi \quad (4-2)$$

$$\psi = \sqrt{\frac{l}{g}} t \quad (4-2a)$$

$$T_0 = \pi \sqrt{\frac{l}{g}} \quad (4-3)$$

and

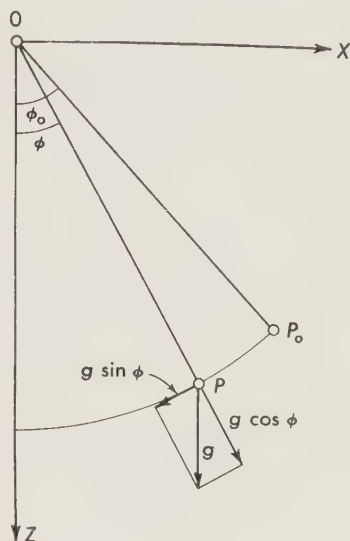


FIG. 4-1. Mathematical pendulum. The swinging time  $T$  of a pendulum is a measure of the gravity. When  $T$  is measured, the gravity  $g$  can be computed.

For larger values of  $\varphi$  we solve as follows. The velocity  $v$  of a mass point is  $v = ds/dt = -l(d\varphi/dt)$ , where  $ds$  is the distance traveled by the mass point in time  $dt$ . We get, therefore,

$$\frac{dv}{dt} = g \sin \varphi = -l \frac{d^2\varphi}{dt^2} \quad (4-4)$$

Multiplication by  $v = ds/dt$  gives

$$v \frac{dv}{dt} = g \sin \varphi \frac{ds}{dt} \quad \text{or} \quad v dv = g \sin \varphi ds$$

As  $ds \sin \varphi = dz$ , we get

$$v dv = g dz$$

By integration we obtain

$$\frac{1}{2}v^2 = gz + c \quad (4-5)$$

where  $c$  is the integration constant.

At the point  $P_0$  of the largest elongation we have  $z = z_0$  and  $v = 0$ , so that

$$c = -gz_0$$

As  $z = l \cos \varphi$  and  $z_0 = l \cos \varphi_0$ , we can write

$$v^2 = 2g(z - z_0) = 2gl(\cos \varphi - \cos \varphi_0) \quad (4-6)$$

$$\text{or} \quad v^2 = \left( \frac{ds}{dt} \right)^2 = 4gl \left( \sin^2 \frac{\varphi_0}{2} - \sin^2 \frac{\varphi}{2} \right) \quad (4-6a)$$

$$\text{As now} \quad ds = l d\varphi = \pm 2dt \sqrt{gl \left( \sin^2 \frac{\varphi_0}{2} - \sin^2 \frac{\varphi}{2} \right)} \quad (4-7)$$

we get finally

$$dt = \pm \frac{1}{2} \sqrt{\frac{l}{g}} \frac{d\varphi}{\sqrt{\sin^2 \frac{\varphi_0}{2} - \sin^2 \frac{\varphi}{2}}} \quad (4-8)$$

If  $T$  is the oscillation time of the pendulum, or the time the pendulum needs to swing from the phase  $+\varphi_0$  to  $-\varphi_0$ , we get

$$\frac{1}{2}T = \frac{1}{2} \sqrt{\frac{l}{g}} \int_0^{\varphi_0} \frac{d\varphi}{\sqrt{\sin^2 \frac{\varphi_0}{2} - \sin^2 \frac{\varphi}{2}}} \quad (4-9)$$

If we now put

$$\sin \frac{\varphi}{2} = \sin \frac{\varphi_0}{2} \sin \psi$$

we get

$$\frac{d\varphi}{\sqrt{\sin^2 \varphi_0/2 - \sin^2 \varphi/2}} = \frac{2d\psi}{\cos \varphi/2}$$

Since to the values  $\varphi = 0$  and  $\varphi = \varphi_0$  there correspond the values  $\psi = 0$  and  $\psi = \pi/2$ , we have

$$\frac{1}{2}T = \sqrt{\frac{l}{g}} \int_0^{\pi/2} \frac{d\psi}{\cos \varphi/2} = \sqrt{\frac{l}{g}} \int_0^{\pi/2} \frac{d\psi}{\sqrt{1 - \sin^2(\varphi_0/2) \sin^2 \psi}} \quad (4-10)$$

Denoting  $\sin \varphi_0/2$  by  $e$ , we finally get the elliptical integral

$$\frac{1}{2}T = \sqrt{\frac{l}{g}} \int_0^{\pi/2} \frac{d\psi}{\sqrt{1 - e^2 \sin^2 \psi}} \quad (4-11)$$

After expanding in power series and integrating we find

$$T = \pi \sqrt{\frac{l}{g}} \left( 1 + \frac{1}{4} \sin^2 \frac{\varphi_0}{2} + \frac{9}{64} \sin^4 \frac{\varphi_0}{2} + \dots \right) \quad (4-12)$$

As  $\varphi_0$  is small, of the order of minutes of arc, we can write

$$\sin^2 \frac{\varphi_0}{2} = \frac{\varphi_0^2}{4} - \frac{1}{48} \varphi_0^4 \quad \text{and} \quad \sin^4 \frac{\varphi_0}{2} = \frac{\varphi_0^4}{16}$$

Thus we get

$$T = \pi \sqrt{\frac{l}{g}} \left( 1 + \frac{\varphi_0^2}{16} + \frac{1}{3072} \varphi_0^4 + \dots \right) \quad (4-13)$$

We substitute now the oscillation period  $T_0$ , corresponding to the infinitely small amplitude  $\varphi_0$ , and obtain successively

$$\begin{aligned} T_0 &= \pi \sqrt{\frac{l}{g}} \\ T &= T_0 \left( 1 + \frac{\varphi_0^2}{16} + \frac{1}{3072} \varphi_0^4 \dots \right) \end{aligned} \quad (4-14)$$

If  $\varphi_0$  is so small that we can neglect the terms with  $\varphi_0^4$ , etc., we can derive oscillation period  $T_0$  from the observed period  $T$  using the formula

$$T_0 = T - \frac{\varphi_0^2}{16} T \quad (4-15)$$

The term  $-(\varphi_0^2/16)T$  is the arc reduction, which is small for the amplitudes used in practice.

The oscillation times  $T_1$  and  $T_2$  of two pendulums of length  $l_1$  and  $l_2$  at the same place and corrected for arc reduction satisfy the equations

$$T_1 = \pi \sqrt{\frac{l_1}{g}} \quad T_2 = \pi \sqrt{\frac{l_2}{g}} \quad (4-16)$$

$$l_1:l_2 = T_1^2:T_2^2 \quad (4-17)$$

or, in words, the lengths  $l_1$  and  $l_2$  of pendulums are proportional to the squares of the periods  $T_1$  and  $T_2$ .

If we use the same pendulum at a base station and at a field station and assume that the length  $l$  does not change between observations, the relation between the gravity values  $g_0$  and  $g_1$  and the swinging times  $T_0$  and  $T_1$  after the arc reduction is

$$g_1:g_0 = T_0^2:T_1^2 \quad (4-18)$$

Formula (4-18) is the fundamental law of the relative gravity measurements made by pendulum.

### B. Physical Pendulum

An actual physical pendulum is the sum of an infinite number of mathematical pendulums of different lengths. We now consider a solid body swinging in the  $xz$  plane around a horizontal axis through the point  $O$ , with the angular velocity  $\omega$  (Fig. 4-2). The linear velocity  $v$  of a mass element  $dm$  at the distance  $r$  from the axis is

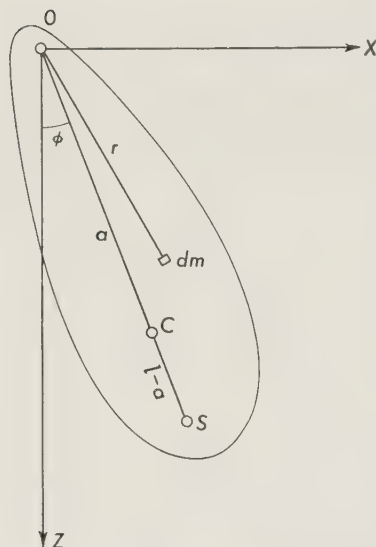
$$v = \frac{ds}{dt} = r\omega$$

FIG. 4-2. The swinging time  $T$  of the real (physical) pendulum is equal to the swinging time of the mathematical pendulum of length  $OS$ .  $T$  is the same regardless of whether the suspension point is on  $O$  or in  $S$  (principle of the reversing pendulum).

and the velocity components  $dx/dt$  and  $dz/dt$  are

$$\frac{dx}{dt} = +\omega r \cos \varphi = +z\omega$$

$$\frac{dz}{dt} = -\omega r \sin \varphi = -x\omega$$



When we multiply the first equation by  $z$  and the second by  $-x$ , we get

$$z \frac{dx}{dt} - x \frac{dz}{dt} = \omega(z^2 + x^2) = \omega r^2$$

and by differentiation

$$\begin{aligned} -x \frac{d^2z}{dt^2} - \frac{dx}{dt} \frac{dz}{dt} + \frac{dz}{dt} \frac{dx}{dt} + z \frac{d^2x}{dt^2} &= r^2 \frac{d\omega}{dt} \\ \text{or} \quad -x \frac{d^2z}{dt^2} + z \frac{d^2x}{dt^2} &= r^2 \frac{d\omega}{dt} \end{aligned} \quad (4-19)$$

As the quantities  $d^2z/dt^2$  and  $d^2x/dt^2$  are the acceleration components of gravity along the  $z$  and  $x$  axes, they are, respectively,  $g$  and zero, and we get

$$-gx = r^2 \frac{d\omega}{dt}$$

The integration of this equation over the pendulum mass gives

$$\frac{d\omega}{dt} \int r^2 dm = -g \int x dm$$

If  $M$  is the mass and  $C$  the center of gravity of the pendulum,  $x_C$  and  $z_C$  the coordinates of  $C$ , and  $a$  its distance from the swinging axis, we have, by definition of the gravity center,

$$\int x dm = x_C M$$

and as  $x_C = a \sin \varphi$ , we get

$$\frac{d\omega}{dt} \int r^2 dm = -g Ma \sin \varphi$$

Since  $\int r^2 dm = K$  is the moment of inertia of the pendulum about its axis, and since

$$\omega = \frac{d\varphi}{dt} \quad \text{and} \quad \frac{d\omega}{dt} = \frac{d^2\varphi}{dt^2}$$

we get

$$\frac{d^2\varphi}{dt^2} + \frac{Ma}{K} g \sin \varphi = 0 \quad (4-20)$$

If we substitute  $K/Ma$  by  $l$  and  $\sin \varphi$  by  $\varphi$ , we get

$$\frac{d^2\varphi}{dt^2} + \frac{g}{l}\varphi = 0 \quad (4-21)$$

which is simply the equation for the mathematical pendulum of length  $l$ . Or, in words, the physical pendulum swings as fast as the mathematical pendulum of the length  $l = K/Ma$ . The quantity  $l$  is called the “reduced length” of the physical pendulum. The point  $S$  on the continuation of line  $OC$ , at the distance  $l$  from  $O$ , is the “swinging center” of the pendulum.

Using the identity

$$r^2 = x^2 + y^2 \equiv [x_C + (x - x_C)]^2 + [z_C + (z - z_C)]^2$$

we get

$$r^2 = x_C^2 + z_C^2 + (x - x_C)^2 + (z - z_C)^2 + 2x_C(x - x_C) + 2z_C(z - z_C)$$

When  $x_C^2 + z_C^2 = a^2$ , if we denote  $(x - x_C)^2 + (z - z_C)^2$  by  $\rho^2$ , we get

$$r^2 = a^2 + \rho^2 + 2x_C(x - x_C) + 2z_C(z - z_C)$$

and

$$K = \int r^2 dm = a^2 M + \int \rho^2 dm + 2x_C \int (x - x_C) dm + 2z_C \int (z - z_C) dm \quad (4-22)$$

$$\text{But } \int (x - x_C) dm = \int (z - z_C) dm = 0$$

because the coordinates  $x - x_C$  and  $z - z_C$  refer to the center of gravity. Therefore there results

$$K = a^2 M + \int \rho^2 dm$$

where  $\int \rho^2 dm = k^2 M$  is the moment of inertia of the pendulum about the axis of the pendulum through the gravity center  $C$ . So we get, finally,

$$K = (a^2 + k^2) M \quad (4-23)$$

and

$$l = \frac{a^2 + k^2}{a} = a + \frac{k^2}{a} \quad (4-24)$$

The distance  $CS$  is  $l - a$ , and the length of the pendulum  $l'$  about the axis  $S$  is

$$l' = l - a + \frac{k^2}{l - a}$$

and since, because of (4-24),  $l - a = k^2/a$ , we get

$$l' = l \quad (4-25)$$

In every pendulum there are two axes separated by a distance  $l$ . Their distances from the gravity center are  $a$  and  $l - a$ , respectively, and the oscillation times around both axes are equal.

This is the principle used in the "reversing pendulum," which is well fitted for absolute gravity measurements and has, so far, given the best results. The difficulty is to keep the distance between the axes exactly equal to  $l$ . If the distances of the axes from the gravity center are  $a_1$  and  $a_2$ , the reduced lengths  $l_1, l_2$  around both axes are

$$l_1 = a_1 + \frac{k^2}{a_1}$$

$$l_2 = a_2 + \frac{k^2}{a_2}$$

and the corresponding swinging times are  $T_1$  and  $T_2$ .

On the other hand,  $l = a_1 + a_2$ , and the corresponding oscillation time is  $T$ , so that we get

$$\frac{a_1 + a_2}{l} = \frac{T^2}{T_1^2} \quad \text{and} \quad \frac{a_1 + a_2}{l_2} = \frac{T^2}{T_2^2}$$

Substituting the values of  $l_1$  and  $l_2$  gives

$$T^2 = \frac{a_1 T_1^2 - a_2 T_2^2}{a_1 - a_2} \quad (4-26)$$

as it is easy to prove, or

$$T^2 = \frac{T_1^2 + T_2^2}{4} + \frac{T_1^2 - T_2^2}{4} + \frac{T_1^2 - T_2^2}{2} \frac{a_1 + a_2}{a_1 - a_2}$$

As  $T_1^2 - T_2^2$  is very small, we can neglect it and obtain easily the final value of  $T$ , expressed in  $T_1, T_2, a_1$ , and  $a_2$

$$T = \frac{T_1 + T_2}{2} - \frac{T_1 - T_2}{2} \frac{a_1 + a_2}{a_1 - a_2} \quad (4-27)$$

As the second term decreases with  $T_1 - T_2$  and increases with  $a_1 - a_2$ , we must take care to see that the former is very small and the latter as large as possible. This means that the center of gravity of the pendulum

must be as far off center as possible, or, what amounts to the same thing, one end of the pendulum heavy and the other light.

The reversing pendulum generally has been used for absolute gravity measurements. Of other methods<sup>16</sup> invented and put into practice recently, the most interesting is the method of the freely falling body, used first by C. Volet at the International Bureau of Weights and Measures at Breteuil, France, and with considerable success by R. H. Field at the National Research Laboratories in Ottawa, Canada, and also by E. Rieckmann at the Physikalisch-Technische Bundesanstalt in Brunswick, Germany. The method, as practiced in Canada, is as follows.

A 2-m metal rule has several transparent scales spaced so that, when the rule falls, the scales pass the axis of a camera in synchrony with a spark light source flashing 10 times per second. The rule can be released in a vacuum chamber from its topmost position and arrested by means of springs and an oil-dashpot mechanism at the bottom. A motor-driven carriage raises the bar to its position before the drop without breaking the vacuum seals.

The scale intervals are calibrated against the international meter, and the time intervals between the flashes are obtained by photographing oscilloscope traces controlled by a standard-frequency signal, which, in turn, is compared with the standards of Dominion Observatory at Ottawa. A pressure of  $0.05 \mu \text{ Hg}$  is used. The scales of the rule are mounted on a channel-section bar of nonmagnetic stainless steel.

The mean value of 12 provisional repetitions at about  $0.05 \mu \text{ Hg}$  was  $g = 980,616 \text{ mgal}$  at Ottawa, corresponding to a correction less than  $-10 \text{ mgal}$  in the Potsdam value. As several connections between different base stations have shown that the Potsdam system needs a correction of  $-10$  to  $-15 \text{ mgal}$ , the tentative gravity value obtained by this new method seems to be not very far from the truth.

In the German experiments the accuracy of the measurement of length, temperature, and time, as well as the perturbations due to the microseism and vibrations caused by the fall of the rule, have been studied carefully.

### C. Corrections of Pendulum Observations

In pendulum observations—absolute and relative alike—the following corrections must be taken into account:

1. Barometric correction, or reduction to vacuum
2. Effect of the flexure of the stand
3. Temperature correction
4. Clock rate
5. Arc correction

The air pressure affects the measurements in three ways.<sup>9</sup> (1) It decreases the weight of the pendulum according to Archimedes' principle and

causes a slight increase of pendulum length  $l$ . (2) The pendulum carries a small amount of air with it, so that the pendulum mass increases as well as its length. (3) The friction between the pendulum and air slows down the swinging. Since this damping effect will diminish the arc of swinging, it must be measured in the beginning and at the end of the observations. Either these disturbing effects on  $T$  can be corrected for, or they can be eliminated by swinging in as high vacuum as possible. The oscillation time  $T$  can thus be reduced to the absolute vacuum.

The effect of the flexure of the stand is much larger than one might imagine. Even the heaviest stand, only 20 to 30 cm high, will sway slightly with the pendulum. Moreover, the sway generally will not be constant and therefore represents a more dangerously deceptive factor in the observations. A good method of determining how much a stand sways is to let one pendulum swing and the other be initially motionless. After a while the flexure of the stand causes the second pendulum to swing, and from the measured arcs of both pendulums the effect of flexure can be computed.

Because of flexure, the swinging of the pendulum is no longer free. The principal formula (4-1) cannot be used but must be replaced by the formula for forced swinging

$$\frac{d^2\varphi}{dt^2} + \frac{g}{l}\varphi + \frac{1}{l}\frac{d^2f}{dt^2} = 0 \quad (4-28)$$

where  $d^2f/dt^2$  is the horizontal acceleration of the pendulum's suspension point. Because of flexure, the reduced length  $l$  and the period  $T$  of the pendulum will increase, so that  $T$  needs a negative correction. The effect of flexure, according to Pesonen,<sup>18</sup> amounts to about  $30 \times 10^{-7}$  sec when a conventional pendulum apparatus is used on a strong gravel ground; on swampy ground it can be as much as twenty times greater. The best way to eliminate the effect of flexure is to use two synchronized pendulums of the same length swinging on the same apparatus in the same plane and with the same amplitudes but in opposite phases; it is clear that then the flexure is zero.

By applying Formula (4-28) for two pendulums with lengths  $l_1$  and  $l_2$  swinging on the same apparatus and in the same plane we can obtain a more general result which allows the elimination of all horizontal acceleration in this plane

$$\frac{d^2\varphi_1}{dt^2} + \frac{g}{l_1}\varphi_1 + \frac{1}{l_1}\frac{d^2f}{dt^2} = 0 \quad (4-29)$$

$$\frac{d^2\varphi_2}{dt^2} + \frac{g}{l_2}\varphi_2 + \frac{1}{l_2}\frac{d^2f}{dt^2} = 0$$

If now  $l_1 = l_2 = l$ , we get, subtracting the first equation (4-29) from the second,

$$\frac{d^2(\varphi_2 - \varphi_1)}{dt^2} + \frac{g}{l} (\varphi_2 - \varphi_1) = 0 \quad (4-30)$$

We thus can introduce a fictitious pendulum of elongation angle  $\varphi_2 - \varphi_1$  and of length  $l$  which is synchronous with the original pendulums and free from the effect of flexure or any other disturbing horizontal accelerations. This is the principle of the Vening Meinesz pendulum apparatus for gravity measurements at sea, which directly records the angle  $\varphi_2 - \varphi_1$ . Because this method can be successful only if the ship's accelerations are small, measurements are usually made in a submerged submarine. The method is discussed more fully later in this chapter.

As the flexure correction was generally neglected in the past, many observations have very little significance, and the errors of 10 to 25 mgal in the older gravity observations<sup>19</sup> may be the result of this neglect.

The need for temperature correction is, of course, caused by the fact that the length of the pendulum changes with variations in temperature. For brass pendulums the temperature correction is large, but it must be considered also when Invar pendulums are used.

The effect of the temperature is  $-k_t(t - t_0)$  where  $t$  is the observation temperature,  $t_0$  the normal temperature, and  $k$  the temperature constant determined empirically for each pendulum. The constant  $k_t$  of the Finnish brass pendulums<sup>18</sup> is  $k_t = (48.25 \pm 0.27) \times 10^{-7}$  sec and of the Invar pendulums  $k_t = (1.82 \pm 0.02) \times 10^{-7}$  sec, or only about 4 per cent of the temperature constant of the brass pendulum.

Also to be considered is the dynamic-temperature correction  $k_\Delta \Delta t$ , where  $k_\Delta$  is the dynamic-temperature constant and  $\Delta t$  the temperature change of pendulum per hour. This correction is necessitated by the fact that changes in temperature do not affect the pendulum and the thermometer in the same way. When the temperature rises, the pendulum usually has a lower temperature than the thermometer, and vice versa. The dynamic-temperature constant of the Finnish brass pendulums is  $+40 \times 10^{-7}$  sec.

Pendulum observations take a long time because the effect of clock rate must be carefully considered. Even so small an hourly rate as 0.0007 sec causes a change of  $10^{-7}$  sec in the period. The only modern method for determining the clock rate is to use time signals, which now fortunately will be sent so frequently that even the irregular, short, periodic rate variations can be controlled by the measurements of some hours. Some years ago it was necessary to let the pendulums swing for 24 hr to be able to eliminate completely the effect of clock rate. The crystal clocks improve the accuracy in this respect.

If  $\gamma$  is the diurnal clock rate, the observed period  $T$  will be reduced by

$$\Delta T = + \frac{\gamma}{86,400} T = + 115.7 \times 10^{-7} \gamma T \quad (4-31)$$

We have already derived the formula (4-15) needed for the arc corrections. If we neglect the error introduced by changing the pendulum length, differentiation of Formula (4-16) will give the relation between the accuracy  $dT$  of the period and  $dg$  of the gravity, as follows

$$T^2 = \pi^2 \frac{l}{g}$$

$$2T dT = - \frac{\pi^2 l}{g^2} dg = - T^2 \frac{dg}{g} \quad (4-32)$$

or

$$\frac{dg}{g} = -2 \frac{dT}{T} \quad (4-32a)$$

To get the accuracy  $dg = 1$  mgal, or  $dg/g = 10^{-6}$ , we must know the period of the  $\frac{1}{2}$ -sec pendulum ( $T = \frac{1}{2}$  sec) with an accuracy of

$$dT = 2.5 \times 10^{-7} \text{ sec}$$

The large discrepancies between different gravity observations at Dehra Dun, the national base station of India, provide an excellent example of

TABLE 4-3. BASE VALUES AT DEHRA DUN <sup>5</sup>

Year	Author	Reference station	Apparatus	Gravity, cm/sec <sup>2</sup>
1904	Lenox Conyngham	Kew	Potsdam pendulums	979.063
1905	Hecker	Potsdam via Jalpaiguri	Potsdam pendulums	.065
1906	Alessio	Potsdam via Colaba	Potsdam pendulums	.059
1913	Alessio	Genoa	Italian pendulums	.079
1924	Cowie	Kew	Potsdam pendulums	.054
1927	Glennie	Cambridge	Cambridge apparatus	.072
1929	Glennie and Cowie	Kew	Potsdam pendulums	.068
1929	Spoletto	Genoa	Italian pendulums	.069
1929	Vening Meinesz	de Bilt via Colombo	.....	.075
1932	Lejay	Potsdam via Colombo	.....	.085
1939	Brown and Glennie	Cambridge	Cambridge apparatus	.056
1948	Woppard and Gulatee	Washington via Delhi	Worden and Frost gravimeters	.063

how difficult it is to get reliable gravity observations even at national gravity base stations. The total spread of these observations is 31 mgal. It is interesting to note that the first measurement, in 1904, gives exactly the same value as the measurement of 1948.

#### D. Modern Pendulum Apparatus

The type of pendulum apparatus constructed in 1887 by Sterneck for relative gravity measurements has been used, with proper corrections, in most pendulum measurements. Figure 4-3 shows this apparatus, in which

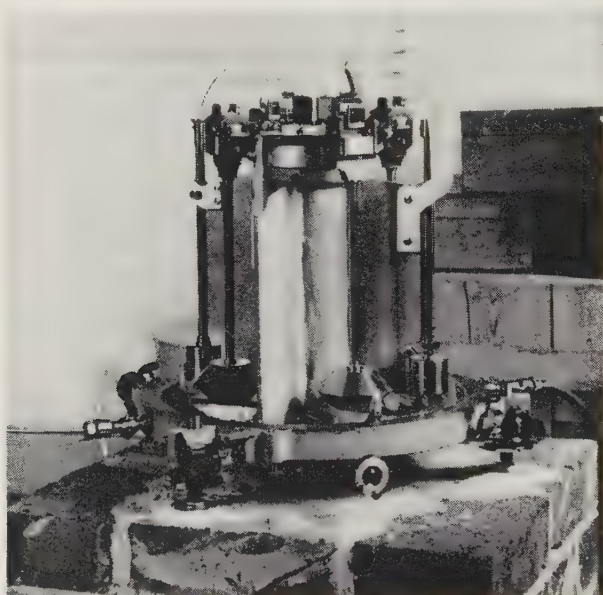


FIG. 4-3. Sterneck's four-pendulum apparatus. One pendulum of each pendulum pair is shown. In operation the apparatus is placed in a high-vacuum flask. Two pendulums swing in the same plane to eliminate the effect of flexure of the stand.

a  $\frac{1}{2}$ -sec pendulum is used so that the size of the instrument can be kept as small as possible. It is called the " $\frac{1}{2}$ -sec pendulum" or "four-pendulum apparatus."

Theoretically speaking, two pendulums would be sufficient. If they are allowed to swing in same plane at a phase difference of  $180^\circ$ , the effect of the flexure can be almost entirely eliminated; however, since the change in pendulum length, which influences the accuracy of the measurement, cannot be controlled, it is better to use four pendulums and let them swing in two pairs, the pendulums of each pair in the same plane. If the length of the pendulums changes between the field observations and the control observations at the base station, it is not likely that all four pendulums will

change by the same amount and in the same direction. By using four pendulums it is relatively easy to prove which of the pendulums has changed.

The observations are made by the "coincidence apparatus." All four pendulums are adjusted so that the mirrors of the pendulums reflect the scales into the observation telescope. The swinging of the clock pendulum is compared with the swinging of the gravity pendulum. The moments when both pendulums have exactly the same phase are observed, e.g., the zero position. These moments are the coincidences. In the coincidence apparatus a light flashes every second. The light beams are directed from the coincidence apparatus to the pendulum mirror, where they are reflected to the observing telescope. The telescope is installed in such a way that the flash reaches the horizontal thread when the pendulum of the apparatus is in zero position. With the swinging of the gravity pendulum the light flash moves slowly back and forth in the vertical direction, because the period of the gravity pendulum is slightly different from 1 or  $\frac{1}{2}$  sec, and so the position of the mirror changes between flashes. The light flash is visible on the thread only when the gravity pendulum has made one swing more or less than the clock pendulum; i.e., the moments when the flash is on the thread are "coincidence times." If the clock pendulum has made  $c$  swings between two coincidences, the gravity pendulum has made  $(c \pm 1)$ . The oscillation time  $T$  for the gravity pendulum will therefore be

$$T = \frac{c}{c \pm 1} = 1 \mp \frac{1}{c \pm 1} \quad (4-33)$$

Since only  $\frac{1}{2}$ -sec pendulums are used in gravity measurements, the gravity pendulum will make in  $c$  seconds  $2c \pm 1$  oscillations, so the formula becomes instead

$$T = \frac{c}{2c \pm 1} = \frac{1}{2} \mp \frac{1}{4c \pm 2} \quad (4-34)$$

In making the observations we observe first, say, 20 coincidences and then the coincidences 101 to 120 but not the coincidences 21 to 100. In this way we get values for the 100 coincidence times. If the coincidence time is 35 to 40 sec, such an observation series will last 70 to 80 min. The observations with the different pendulums are distributed throughout the day to eliminate the variation of the clock rate as completely as possible.

By this method the period  $T$  of the gravity pendulum can be observed with an accuracy of  $2.2 \times 10^{-7}$  sec, which corresponds to an accuracy of 0.8 mgal in gravity. To obtain such accuracy observations over a 2-day period are usually necessary. If a photographic recording box is used to register the swing of the pendulums as well as the time signals, as now in general is the case, the same accuracy can be obtained in 2.5 hr.

Because of the Eötvös effect, gravity observations at sea cannot attain an accuracy greater than 3 or 4 mgal. This effect—first noted by von Eötvös—is caused by the change in the centrifugal part of gravity by the east-west component of the ship's velocity. At the equator an error of 1 km/hr in the velocity introduces an error of 4 mgal in  $g$ , and the fact that the ocean current is difficult to estimate when a submarine is submerged causes considerable uncertainty.

Because of this source of error there is no use in trying to push the observations to an extreme degree of accuracy. An observation of about  $\frac{1}{2}$  hr

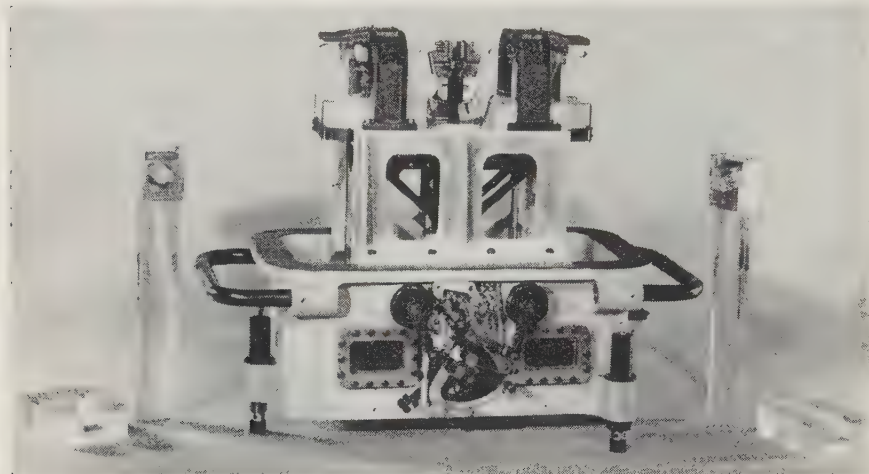


FIG. 4-4. Gulf minimum-pendulum apparatus with the top case removed. An extra pair of fused-quartz pendulums and pyrex knife-edge flats illustrate the design of the minimum pendulums, which are barely visible in the apparatus. (Courtesy of the Gulf Research and Development Co.)

is usually sufficient to reduce the uncertainty in the corrected period of the pendulums—including that which follows from the vertical component of the ship's acceleration—to a value corresponding to an error in  $g$  of about 2 mgal, and greater accuracy seems superfluous. (For further details and for second-order corrections, see Vening Meinesz<sup>20-22</sup> and Browne.<sup>23</sup>)

*Minimum pendulum.* The accuracy of pendulum apparatus can be fundamentally improved by applying the principle of the "minimum pendulum." In pendulums of this type the point of suspension is so located with respect to the center of gravity of the pendulum that the pendulum has a minimum period. Any change of the length of the pendulum, in either direction, increases the period. Most important, however, is the fact that the period of this type of pendulum is far less sensitive than that of any other type to small changes in the length of the pendulum, caused by thermal expansion or wear of the knife-edge.

Perhaps the best known of this type is the Gulf pendulum, which was used two decades ago even for gravimetric prospecting, and which in recent years has been used to measure gravimetric calibration lines. The pendulum apparatus (Fig. 4-4) consists of two fused-quartz pendulum arms of equal length, swinging in the same vertical plane but in opposite phase to eliminate the sway.

Fused quartz is used because its thermal expansion coefficient is only  $0.25 \times 10^{-6}$  per degree centigrade as compared with  $1 \times 10^{-6}$  for Invar and  $18 \times 10^{-6}$  for brass. In addition, it is insensitive to magnetic effects, as Invar is not. For instance, in the Cambridge, England, apparatus, in which an Invar pendulum is used, it is necessary to add a Helmholtz coil to eliminate magnetic effects.

#### 4-2. Gravimeters

There are three basic types of gravimeter: dynamic, gas-pressure, and static.

##### A. Dynamic Gravimeters

Most dynamic gravimeters use the Holweck-Lejay "inverted pendulum." The pendulum rod, which is upside down, consists of a quartz cylinder 6 cm long and 4 mm wide suspended by an elastic Elinvar spring 0.02 to 0.03 mm thick. The swing of the pendulum is caused by the combined effect of gravity and the elastic force of the pendulum mass. The accuracy of the pendulum depends on the constancy of the elastic properties of the spring and on the value chosen for the ratio of gravity over the elastic force.

Figure 4-5 shows the pendulum mass and its gravity center  $M$ , the spring  $OA$ , and the elongation angle  $\phi$  of the pendulum. The equation for this type of pendulum is

$$F = \frac{3\pi r^4}{4l^2} E \quad (4-35)$$

where  $l$  = length of pendulum

$M$  = mass of quartz rod

$r$  = radius of rod

$E$  = Young's coefficient of spring

$F$  = elastic force acting on mass  $M$

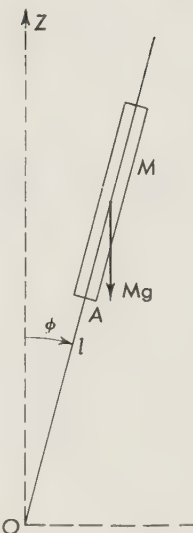


FIG. 4-5. The principle of the Holweck-Lejay inverted pendulum. The swinging of pendulum  $OM$  is caused by the difference  $k - g$  of the acceleration  $k$  of the elastic force and the acceleration  $g$  of the gravity. As  $k$  and  $g$  can be made nearly equal, the swinging time is much larger than that of the usual pendulum and need not be measured so accurately.

If we put  $F = kM$ , we get the differential equation for this type of pendulum

$$l \frac{d^2\varphi}{dt^2} + k\varphi - g\varphi = 0 \quad (4-36)$$

and for the period  $T$  the expression

$$T = \pi \sqrt{\frac{l}{k-g}} \left[ 1 + \frac{g}{16(k-g)} \varphi_0^2 + \dots \right] \quad (4-37)$$

The period  $T_0$ , corresponding to the infinitely small arc, is

$$T_0 = \pi \sqrt{\frac{l}{k-g}} \quad (4-37a)$$

This formula is similar to our basic formula (4-14) of the pendulum apparatus. The only difference is that we have, instead of  $g$ , the difference  $k - g$ . Differentiation of this formula gives

$$\frac{dT}{T} = \frac{dg}{2(k-g)} - \frac{dk}{2(k-g)} \quad (4-38)$$

If  $k$  and  $g$  are nearly equal, the period of the pendulum is very sensitive to the variations of  $g$  and  $k$ , since  $dg$  and  $dk$  are then multiplied by a large factor,  $1/(k-g)$ . The accuracy of this gravimeter depends on how accurately we can keep  $dk$  equal to 0. If the equality is maintained, the error  $dg$  is given by the formula

$$dg = 2(k-g) \frac{dT}{T} \quad (4-39)$$

Since the ratio  $dT/T$  will be multiplied by the small factor  $k-g$ , the period of the pendulum need not be measured so accurately as that of other pendulums; observations lasting  $\frac{1}{2}$  hr will suffice. In practice, the factor  $k-g$  is as small as  $0.005g$ . If  $l$  is 3 cm, the period is about 2 sec. Even when the error in  $dT$  is 800 times larger than in ordinary pendulums, the same accuracy for  $g$  can still be achieved.

Lejay<sup>13-15</sup> has used the Holweck-Lejay gravimeter with success in Europe, Africa, the Near East, Indochina, China, and the Philippines. The instrument weighs only a few kilograms. If the stations are close to each other, five to six stations can be covered in one day. Of course, like most gravimeters, this pendulum must be carefully calibrated. Although this interesting apparatus has been used for geodetic purposes, it has seldom been used

for geophysical prospecting because the modern and more convenient spring-balance gravimeters have replaced it.

### B. Gas-pressure Gravimeters

In the gas-pressure gravimeter devised by Haalek, who followed up the old experiments of Hecker,<sup>7</sup> the pressure of the closed gas mass is used instead of a spring or torsion as the counterforce of gravity. Figure 4-6 shows the principle of the instrument. The height variations of the barometer levels  $z$  and  $z'$  are measured, and the gravity variations are measured by the height  $h$  of the mercury column, which is kept in equilibrium by the pressure  $p$  of a closed gas mass. The equation is, of course,  $p = h\sigma g$ , where  $\sigma$  is the density of the mercury. Logarithmic differentiation of this equation gives

$$\frac{dp}{p} = -\frac{dv}{v} + \alpha dt = \frac{dh}{h} + \frac{d\sigma}{\sigma} + \frac{dg}{g} \quad (4-40)$$

where  $\alpha$  is the expansion coefficient of gas and  $dt$  the temperature variation.

To get an accuracy of 1 mgal  $dh/h$  must be measured with an accuracy of 1 part in  $10^{-6}$ , and the temperature must be measured to  $0.0003^{\circ}\text{C}$  or kept thermostatically controlled to the same accuracy. To achieve the required accuracy in measuring  $dh$  the ends of the barometer columns have been enlarged so that the mercury surfaces are relatively large. Above these surfaces is a capillary tube filled with some light liquid. For every minute change in the large mercury surface there is a corresponding but considerably larger change in the narrow capillary tube. The reading accuracy of  $h$ , of course, increases in the ratio of the areas of the mercury and the capillary tubes. If the capillary tubes are tilted, the accuracy is still higher.

Regardless of how carefully such gravimeters are constructed, their accuracy is not sufficient—hardly better than 3 mgal. Their advantage lies in their ability to measure gravity at sea with an accuracy of about 10 mgal, but so far as the author (H.) knows, these instruments have seen very little use.

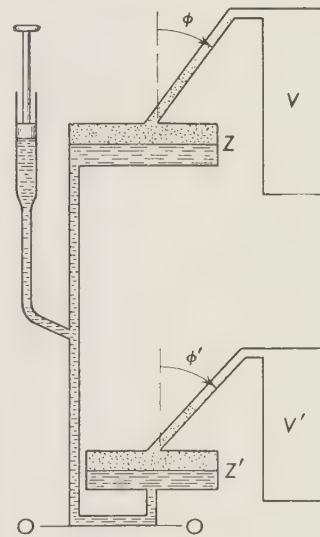


FIG. 4-6. Principle of Haalek's gas-pressure gravimeter. The variations of  $g$  are measured by the height  $h$  of the mercury column kept in equilibrium by the pressure  $p$  of a closed gas mass. If the temperature can be controlled, the change in  $h$  is caused only by the variation of  $g$ . To increase the measuring accuracy of  $h$ , the ends of the barometer columns are large compared with the surface of the capillary tubes where the readings are made. As these tubes are tilted, the accuracy is still higher.

### C. Balance Gravimeters

The usual type of gravimeter is based either on the spring-balance principle (stable system) or on the astatic-balance principle (unstable system).

*Stable gravimeters.* The principle of the stable system can be described as follows. When a weight hangs from a spring, the length of the spring will change with the variations of the gravity  $g$ . The greater the gravity, the longer the spring. Provided that other conditions, particularly the

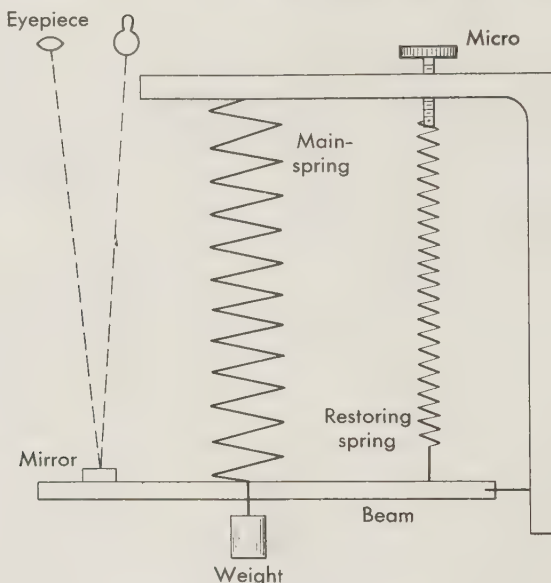


FIG. 4-7. Principle of the balance gravimeter (Hartley gravimeter).

elastic properties of the spring, remain unchanged, relative values of  $g$  can be obtained by measuring the length of the spring at the observation points.

Although this type of gravimeter is simple in principle, the practical difficulties are great. The total elongation  $S$  of a spring supporting a weight  $mg$  is  $S = mg/c$ , where  $c$  is the spring constant. Since the accuracy demanded of gravimeters at present is at least 0.1 mgal, or  $1 \times 10^{-7}g$ , the change  $dS$  of  $S$  must be measured with the relative accuracy  $1 \times 10^{-7}$ . When  $S = 10$  cm, this implies an accuracy of  $1 \times 10^{-6}$  cm, or one-fiftieth the wavelength of light. To overcome this obstacle the displacement  $dS$  must be greatly magnified by optical, mechanical, or electric means. Because of these practical difficulties it was many years before reliable, stable gravimeters were designed and constructed.

In principle, the Hartley gravimeter is perhaps the simplest.<sup>3</sup> Although it has never been used extensively, many of its details have been used in more modern stable gravimeters. Figure 4-7 shows its parts: beam, hinge,

mainspring supporting the weight, adjusting spring with micrometer screw, light source, eyepiece, mirror, and scale. With the variation of gravity the elongation  $S$  of the mainspring changes. When the mainspring is returned to its fixed, original position by tightening or loosening the adjusting spring,

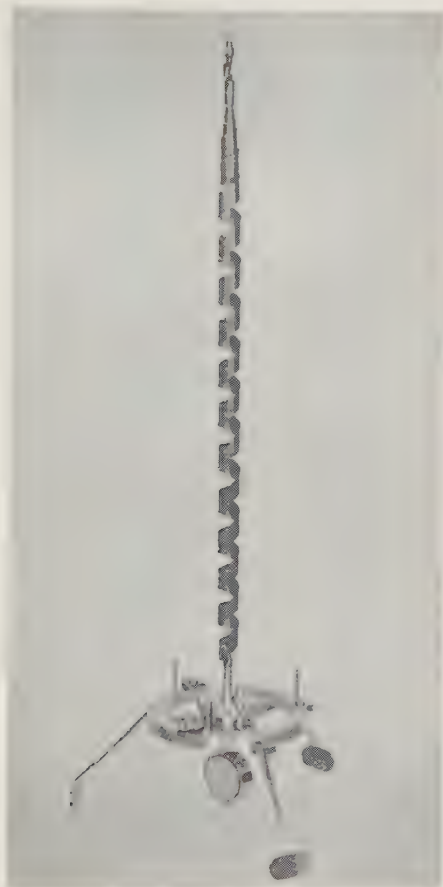


FIG. 4-8. The Gulf (Hoyt) gravimeter helical spring. (Courtesy of the Gulf Research and Development Co.)

the dial of the micrometer screw is read, and the difference between the readings at the reference station and the field station gives the gravity difference of these stations. By placing the adjusting spring close to the hinge and the mirror at the end of the beam and by using a long optical path it is possible to get a large magnification of  $dS$  and to obtain an accuracy of 1 mgal.

The Gulf gravimeter, designed by Hoyt, is interesting because its springs have the form of a "helix" (Fig. 4-8).<sup>6</sup> Any change in gravity will cause the

spring to elongate and rotate, and it is easy to see that the rotation is much greater than the elongation and therefore easier to measure with the required accuracy. In fact, the rotation of the spring under total gravity is  $2880^\circ$ , or eight revolutions. Therefore, for a relative accuracy of  $10^{-7}g$ , or

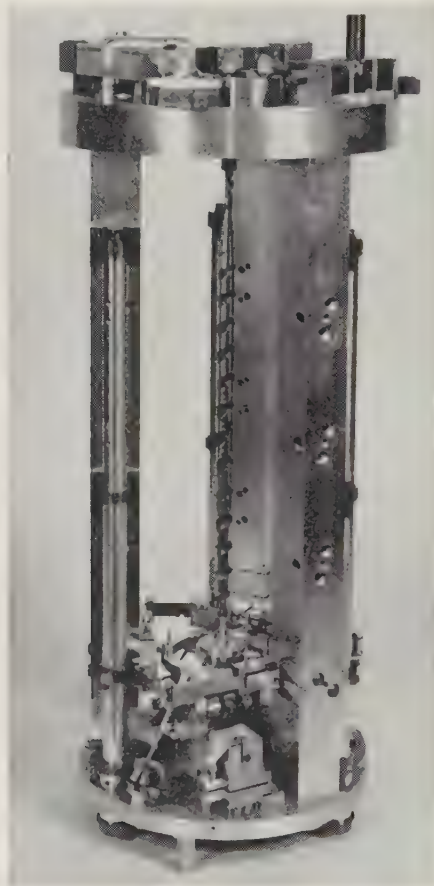


FIG. 4-8a. Inside view of Gulf (Hoyt) gravimeter. (Courtesy of the Gulf Research and Development Co.)

0.1 mgal, the rotation must be read with an accuracy of  $1''$  (second of arc). The rotation is measured by a multiple-reflection system of aluminized suspended mirrors, which lengthens the optical path.

The spring material is nickel-chrome-iron alloy, aged at elevated temperatures. A drift of about 0.3 mgal per 24 hr is typical for new instruments and generally decreases with aging of the instrument.

Gravity measurements made with this gravimeter by the Gulf Oil Company at about 100,000 field points indicate a standard error for a single

observation of 0.03 to 0.07 mgal. The accuracy of the Gulf gravimeter is 0.02 mgal; the new model weighs only 25 lb. One drawback of this interesting instrument is its low range, only 25 to 30 mgal. To measure larger gravity differences the instrument has to be readjusted. Figure 4-8a gives an idea about this gravimeter.

The Nørgaard gravimeter is also of the stable type. The weight and mirror are supported at the end of a small horizontal quartz beam by the torsion of the quartz thread fastened in a quartz frame (Fig. 4-9). With changing gravity the weight will rise and fall, thus tilting the mirror. In

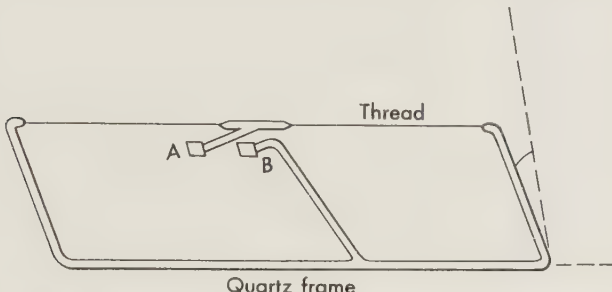


FIG. 4-9. Nørgaard gravimeter. A mirror  $A$  is supported at the end of a small horizontal quartz beam;  $B$  is a fixed mirror. The effect of gravity will be counteracted by the torsion of the thread. The tilting angle  $i$  of the beam (and the mirror  $A$ ), caused by the changing gravity, can be measured by comparing the direction of the rays reflected from the mirrors  $A$  and  $B$  and it indicates the difference of gravity between the base station and the field stations. The frame with thread and mirrors is put in a special liquid to maintain the temperature and protect the instrument against shocks during transportation.

addition, there is a fixed mirror in a quartz frame. From the light source, one light beam is reflected to the observation telescope from the weighted mirror, the other from the fixed mirror. To get them to coincide the whole frame must be tilted. There are two positions of the frame in which the picture from the weighted mirror coincides with that from the fixed mirror. In the first position the frame is tilted at an angle  $i$  upward and in the second, downward. The difference  $v$  of these two directions, which can be read from the micrometer, gives the tilting  $i$  of the frame from the horizontal direction because  $i = v/2$ . Measuring the tilting angle  $i_0$  at the base stations (gravity  $g_0$ ) and the angles  $i_1, i_2, \dots$  at the field stations (gravity  $g_1, g_2, \dots$ ) gives the basic equation for this gravimeter:

$$g_0 \cos i_0 = g_1 \cos i_1 = g_2 \cos i_2 = \dots = c \quad (4-41)$$

Therefore 
$$g_1 = \frac{c}{\cos i_1} \quad g_2 = \frac{c}{\cos i_2}$$

where the constant  $c = g_0 \cos i_0$ .

The difficulty of eliminating changes in the quartz with changes in temperature has been solved by using a special kind of liquid, in which the whole frame, thread, and mirrors are immersed. This liquid also protects the instrument against shock during transportation. No thermostat is

needed. The accuracy is of the order 0.1 mgal, and the total weight does not exceed 10 kg. The Nørgaard gravimeter has been used in different countries, and particularly in Northern Europe.

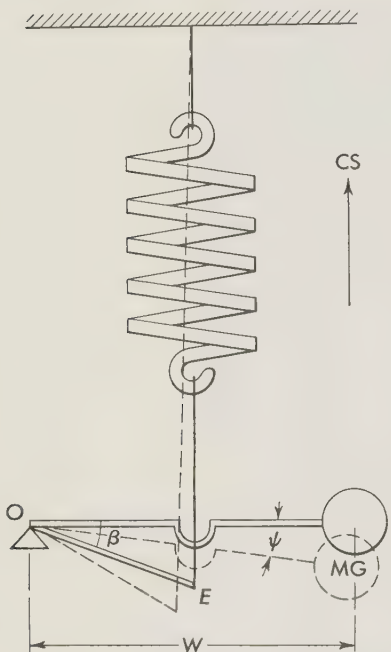


FIG. 4-10. Principle of the astatic balance gravimeter. A mass  $M$  at the end of a beam with length  $W$  is pivoted at  $O$ . The moment of its weight  $MGW \sin \psi$  is balanced by the balancing couple, also a function of  $\psi$ .

arm which is hinged at one end and carries the weight  $MG$  at the other. If the spring were attached to the weight arm, the system would be similar to the stable system. In fact, however, the spring is attached to a lever arm  $E$  at an angle  $\beta$  with respect to the weight arm  $W$ . If the angle  $\beta$  is large, the spring-restoring-torque curve becomes nonlinear. In adjusting the system it is possible to change the angle  $\beta$  so that the restoring-torque curve (Fig. 4-11) intersects the gravitational-deflecting torque at different angles  $\xi_1, \xi_2$ , etc. The smaller the angle  $\xi$ , the greater the sensitivity of the instrument. When the instrument works close to the instability point  $\xi = 0$ , its sensitivity is very high.

The instability principle is used in a great number of gravimeters, some operating in the same way as the type of seismograph devised by LaCoste.

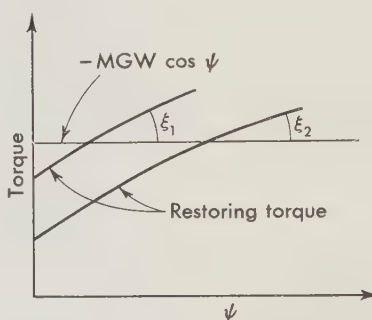


FIG. 4-11. Restoring torque.

*Unstable gravimeters.* The principle of unstable gravimeters is illustrated in Figs. 4-10 and 4-11. The force of gravity is kept in unstable equilibrium with the restoring force by a third force which enlarges the effect of any change in gravity from its equilibrium value. The moving system has an

Since the gravimeter and the seismograph both are devices sensitive to acceleration and have the same sensitivity criterion—the long period—these two important instruments, though used for quite different purposes, are essentially similar. The LaCoste seismograph can, in fact, be converted with relative ease into a sensitive gravimeter. The LaCoste-Romberg, Frost, Magnolia, and North American gravimeters are modifications of the LaCoste seismograph.

The “zero-length” spring of the LaCoste gravimeter is new and interesting. Only in this type of gravimeter is the elongation of the spring, caused by change in gravity, proportional to the change itself.

*Worden gravimeter.* In designing gravimeters it has been difficult to combine the required high *accuracy* of 0.1 mgal with sufficient *range*. Several types of gravimeter give the needed accuracy, but their range is only 50 to 200 mgal or so. It is true that this range is sufficient for most local-prospecting purposes, but it is much too small for geodetic measurements. Therefore, it is of basic significance for the geodetic application of the gravimetric method that the Nørgaard instrument (stable system) and the Worden instrument (unstable system) combine high accuracy and wide range. They are in this respect superior to other gravimetric types.

As the Worden gravimeter has been used more than any other for geodetic purposes, particularly for connecting the gravity base stations of different continents and ocean islands, it is shown in detail in Figs. 4-12 to

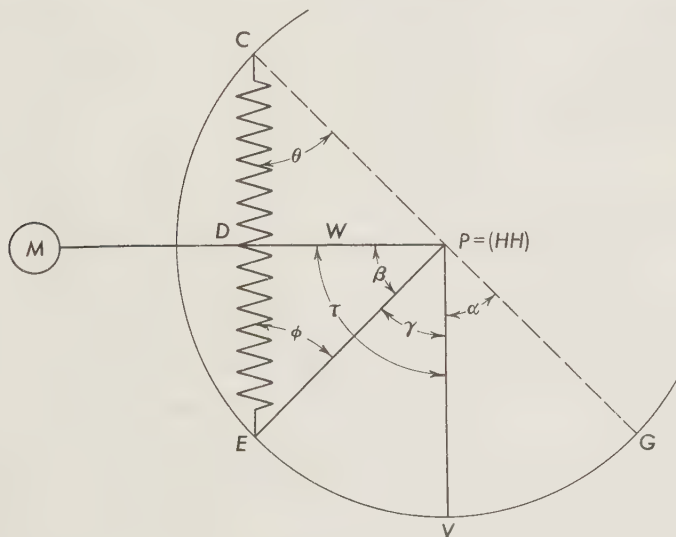


FIG. 4-12. Principle of the Worden gravimeter. The torque  $T_t$  of the instrument counteracting the gravity is  $T_t = (k \times PC^2 - MW) \sin \tau$ . If  $T_t$  is zero, the period of instrument is infinite. The period can be adjusted by using torques of slightly different values. (Courtesy of the Houston Technical Laboratories.)

4-14. It is an unstable instrument and employs the zero-length spring. The quartz element has a zero-length spring balanced against the mass very near the point of instability ( $\xi = 0$ ) so that it will elongate or contract even with a very small change in gravity. The gravity differences are determined by returning the spring to its original position by means of a calibrated dial, from which the reading is taken. A special device for temperature compensation is used.

The proof of the infinite period of the system using a zero-length spring (see Fig. 4-12) is as follows. The weight  $M$  is attached to the weight arm  $W$ , which is pivoted along the hinge line  $HH$ . The spring  $CE$  is attached to the frame at  $C$  and to the arm  $PE$  at  $E$ , which is equivalent to being attached to the weight arm  $W$ , since  $PE$  and  $W$  are rigidly attached along the hinge line  $HH$ .  $\tau$  is the angle between the weight arm and the vertical, and  $\tau = 90^\circ - \psi$ ;  $PE = PC = a$ .

The torque produced by  $M$  is  $T_m = -MW \sin \tau$ . The sign of this torque is taken as negative since it opposes the action of the spring. The torque exerted by the zero-length spring is  $T_s = k \times CE \times PD$ , where  $PD$  is the moment arm and  $k$  the spring constant. Since  $\phi = \theta$ ,  $PD = a \sin \theta$ , and  $CE = 2a \cos \theta$ , we have  $T_s = ka^2 \sin 2\theta$ .

As  $C$ ,  $E$ , and  $G$  are on the arc of a circle

$$\theta = \frac{1}{2}(\alpha + \gamma)$$

and as  $\beta = \alpha$ ,

$$\theta = \frac{1}{2}(\beta + \gamma) = \frac{1}{2}\tau$$

and therefore

$$T_s = ka^2 \sin \tau \quad (4-42)$$

The total torque is

$$T_t = T_s + T_m = (ka^2 - MW) \sin \tau$$

If  $MW = ka^2$ , the total torque is zero and the period is infinite. Since the period is dependent upon the total torque, it can be adjusted by having torques of slightly different values.

The temperature compensation of the gravimeter is adjusted in both amplitude and linearity of action for equal correction at all temperatures. It is also designed to change amplitude of action with changes in gravity so that the compensation will not vary appreciably with latitude. In addition, the temperature of all parts of the compensator and spring must change in the same way, making their adjustment somewhat complicated.

As seen in Fig. 4-13, the temperature-compensation structure consists of a pair of arms, 29 and 36b, joined at their extending ends and connected by a spacing arm 37 at the other end. These arms are made of suitable materials having different coefficients of thermal expansion. It is apparent that a change in temperature will cause the relative lengths of the arms to

change, thus creating a force tending to bend or move one or both of the arms 29 and 36b and thereby moving the extending ends of the arms generally in an arc about the extending ends of arms 29 and 36b; the movement of the compensating structure moves the end or the spring 30 to which it is connected so as to compensate for the effect of temperature variations on the system.

The system gives accurately compensating movement through only a very limited temperature range, a difficulty overcome by the addition of a short nonlinear spring 36 to an arm of the temperature-compensation structure. Spring 36 yields nonlinearly to the force produced by the dif-

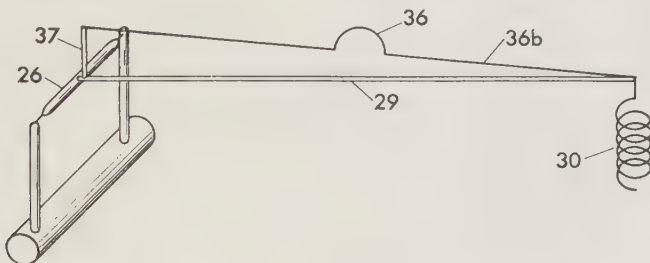


FIG. 4-13. Temperature compensation. Arms 29 and 36b having different temperature coefficients are joined at one end and connected by a spacing arm 37 at the other end. Change in temperature will change the relative lengths of the arms and move the extending ends of the arms. (Courtesy of the Houston Technical Laboratories.)

ferential expansion in the connected arms 29 and 36b, resulting in a controlled compensating movement of the extending end over a large temperature range.

The elastic system of the Worden gravimeter is made of fused quartz, which makes it quite resistant to shock and fatigue and completely free from all magnetic effect. The basic mass of the quartz used is only 5 mg. and the entire system is sealed in a partial vacuum. The low mass, combined with the almost perfectly elastic qualities of quartz, eliminates the necessity of clamping the system to prevent breakage during transportation.

The quartz elastic system is so constructed that its response to gravity is proportional to the cosine of the angle of tilt, thus affording a convenient, accurate, and basic means of *calibration*. Tilt-table calibration is used to give consistent calibration from one meter to another. Recent field calibration runs against University of Wisconsin pendulum stations, Dominion Observatory pendulum bases, and bases set by the U.S. Coast and Geodetic Survey between Fairbanks, Alaska, and Mexico City indicate that tilt calibrations of the Worden gravimeter give absolute gravity differences to an accuracy of  $\frac{1}{2000}$ . The small dial is adjusted until it is linear to  $\frac{1}{1000}$  over its entire scale.

Figure 4-13a gives a clear idea about the spring system of the Worden gravimeter.

The Worden gravimeter (Fig. 4-14) is 12 cm in diameter and 29 cm high. The meter itself weighs only about 2.3 kg and in the carrying case with

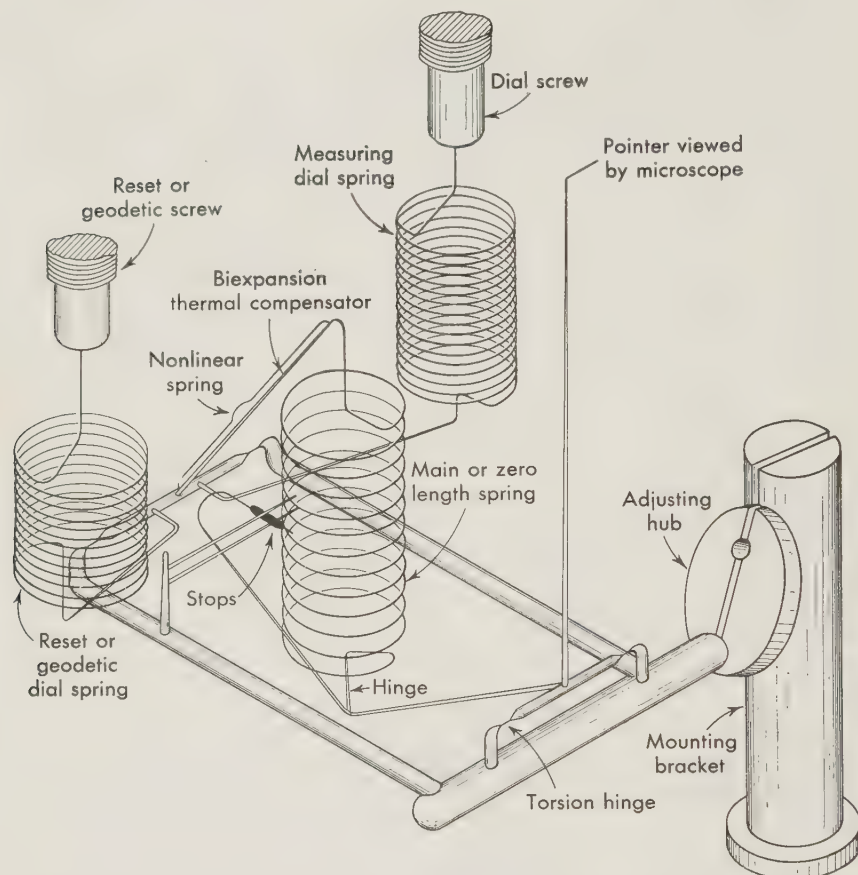


FIG. 4-13a. Spring system of Worden gravimeter. Enlarged about five times. (Courtesy of the Houston Technical Laboratories.)

base plate attached only 5.4 kg. This is approximately one-fourth to one-fifth the weight of other gravimeters on the market today. The size of this gravimeter and the elimination of an external power source for thermostat control make it readily portable.

*Can gravimeters be used on surface boats or in aircraft?* Since gravimeters give very accurate gravity values in a few minutes, there has been much discussion of the possibility of using direct-reading gravimeters on such unstable supports as ships and aircraft. Several scientists have tried to

solve this important problem. It must be remembered that gravimeters devised for use of this kind would have to contain an integrating device so that the periodical vertical acceleration of the support could be averaged over a sufficiently long interval to ensure that no residual one-sign accelerations are hidden in the readings.

For instance, to get an accuracy of  $10^{-7}g$  from a flying aircraft, it must be possible both to keep the total change in elevation of the aircraft within 20 ft/hr and to determine the elevation with an accuracy of 1 ft. This example is probably sufficient to demonstrate that the use of high-precision gravimeters in aircraft, and perhaps in surface boats, is unlikely.

#### *D. Underwater Gravimeters*

Special underwater gravimeters for gravimetric survey of shallow waters out to depths of approximately 200 m are very important because the shallow shelf areas, where submarines cannot be used, underlie about 7 per cent of the ocean surface.

To be effective these gravimeters must be designed to operate on the bottom of the shelf. Such instruments consist of (1) a bell (or housing) containing the instrument and operator, or (2) an underwater unit containing only the instrument, or (3) a pressure housing in which the instrument is leveled directly by gravity, or (4) a pressure housing in which the instrument can be leveled by remote control by the use of level indicators.

The Gulf underwater gravimeter, described by Pepper,<sup>17</sup> is, so far as the author (H.) knows, the earliest instrument of this type; it was devised and used two decades ago. It is of the remote-control type and quite complicated because of the leveling-control system, which must guarantee a leveling accuracy of 10".

A durable combination of a level vial and photovoltaic cells with no

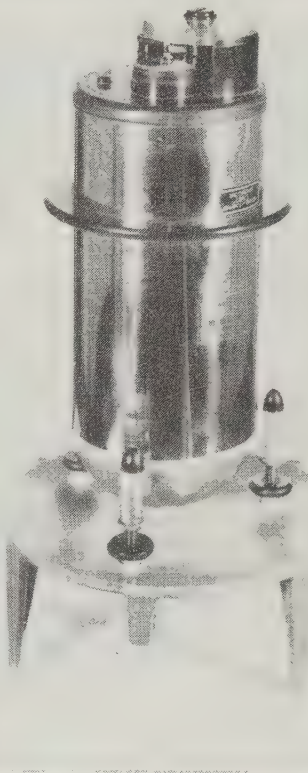


FIG. 4-14. Exterior view of Worden gravimeter. Diameter 12 cm, height 29 cm, weight 2.3 kg, with the carrying case and base plate 5.4 kg.

amplification has been devised. One cell is used on each end of the vial to compensate for light-source voltage fluctuations. The cells are connected in parallel but in such a manner that they apparently short each other, i.e., positive to negative, and leads are run from the junctions to a 25-0-25 microammeter. Illumination for both ends of the vial comes from a common source. When the meter indicates zero, the instrument is level. At

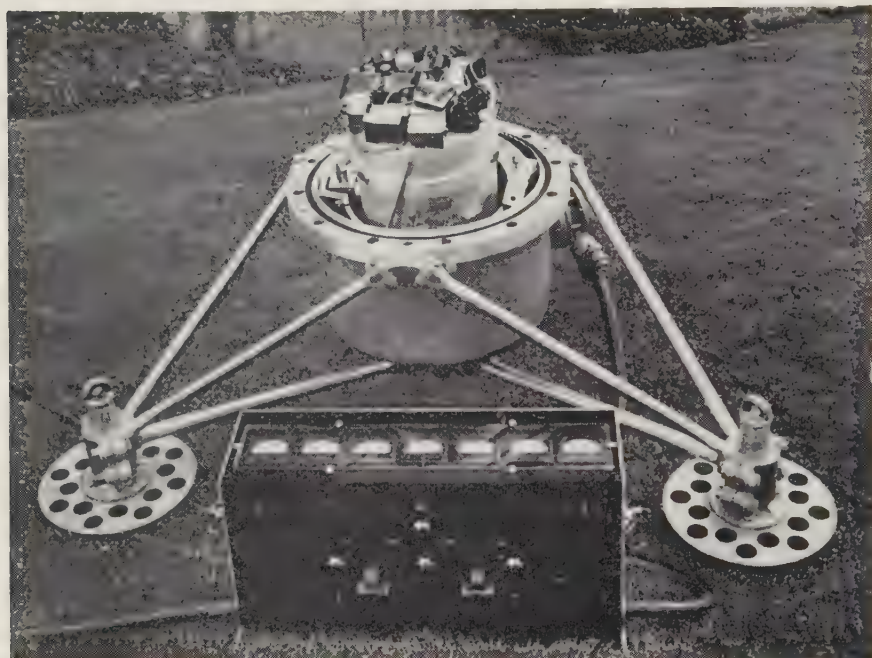


FIG. 4-15 The Gulf underwater gravimeter and remote control. Watertight housing cover removed. (Courtesy of the Gulf Research and Development Co.)

the zero position on the microammeter no appreciable change is noted when the light-source voltage is varied from zero to any voltage the lamp is able to withstand.

Leveling is accomplished by a motor-driven gimbal arrangement in which the two components of leveling motion are sufficiently independent to permit leveling in both directions simultaneously. The maximum available leveling motion is  $15^\circ$  in any direction from center. To tilt from one extreme position to another, or  $30^\circ$ , requires less than 3 min, including time for all minor adjustments.

To handle all the controls and safety devices, several electric cables connect the control cabinet to the gravimeter. Four of the conductors are used for a common ground but provide one or more spare conductors in

case of damage to other wires; the remaining conductors are 4 motors (3 of which are reversible), 3 separate light-source circuits, thermostatic heat control,  $15^{\circ}$ -limit control, water alarm, clamped signal, and 2 photocell circuits, which do not use the common ground.

Recording is accomplished photographically. The film runs continuously and provides a complete record of the instrument deflections during the time the moving system is open. Accuracy of recording, in spite of possible film shrinkage, is maintained by using fiducial lines photographed simultaneously with the images used for recording gravity. The records are later read by a special micrometer comparator, much in the same way as the gravimeter is read directly by a micrometer eyepiece. Under good conditions the accuracy of the reading is 0.02 mgal, and the standard error of gravity measurements will not exceed 0.3 mgal.

A maximum of about 20 stations per day has been taken, the average being 6 stations per day. The principal causes of delay are unfavorable weather conditions and the slow speed of the boat. The standard Gulf gravimeter is used as the underwater gravimeter. To convert it to a land-measuring unit takes less than  $\frac{1}{2}$  hr. The equipment (Fig. 4-15) is constructed mostly of aluminum, weighs about 300 lb out of water and 25 to 30 lb under water. An additional weight of 350 lb of lead can be used to provide the needed stability under water and can be quickly removed when the instrument is to be carried to a land base station.

Several other types of underwater gravimeter exist; altogether about 30 underwater gravimeters have been constructed thus far.

#### *E. Vening Meinesz Pendulum Apparatus*

For the determination of gravity at sea Vening Meinesz<sup>20</sup> constructed an apparatus with three pendulums (Fig. 4-16) which are as nearly synchronous as possible. They are of the Sterneck type (Fig. 4-3), with an oscillation period of slightly over  $\frac{1}{2}$  sec, and at the top they are provided with mirrors for recording. Since they are made of brass, they are practically

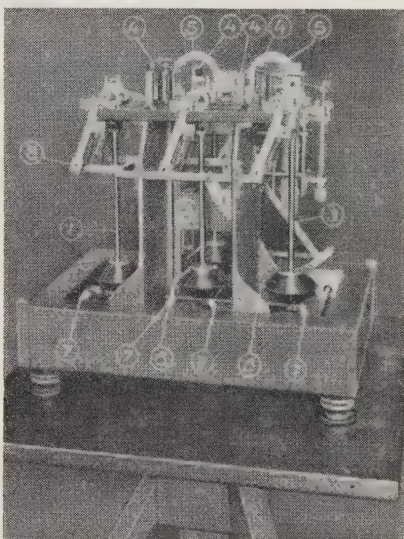


FIG. 4-16. The three pendulums of the Vening Meinesz apparatus swing in the same plane and are combined in two pairs; in this way the effect of the horizontal acceleration of the support can be eliminated. (Ref. 20, Fig. 2.)

nonmagnetic. The pendulums swing in the same plane and are combined in two pairs; an apparatus records the differences of the angles of elongation  $\varphi_1 - \varphi_2$  and  $\varphi_3 - \varphi_2$ . As shown by Formula (4-30), these two angles can be considered as the angles of elongation of two fictitious pendulums which are independent of the greatest disturbance caused by the ship's movement, viz., that by the horizontal component in the direction of the swinging plane.

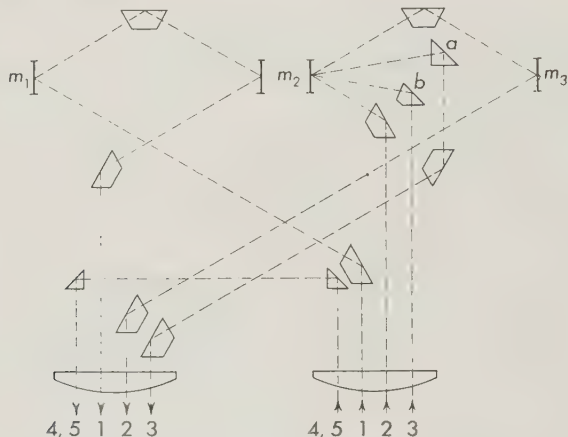


FIG. 4-17. The light rays 1, 2, 3, 4, and 5 give the differences of the elongation  $\varphi_1 - \varphi_2$ ,  $\varphi_3 - \varphi_2$ ,  $\varphi_2$ , air temperature, and the tilt of the swinging plane.

Figure 4-17 shows how these differences are recorded by light rays made parallel by a lens, shown at the right; they are afterward concentrated on the photographic paper by the lens shown at the left. Ray 1 registers the elongation  $\varphi_1 - \varphi_2$ , ray 2 the elongation  $\varphi_3 - \varphi_2$ , and ray 3 the elongation  $\varphi_2$  of pendulum 2 in respect to a damped pendulum swinging parallel to the swinging plane of the main pendulums. The prisms *a* and *b* are fixed to the damped pendulum. Ray 4 registers the air temperature and ray 5 registers, with the aid of another help pendulum which can swing in a plane perpendicular to the swinging plane of the main pendulums, the deviation of the swinging plane of the main pendulums from the vertical.

In connection with the two further second-order corrections to which Browne<sup>2</sup> drew attention, the addition was made of an auxiliary instrument with two very slow damped free-hanging pendulums with periods large with respect to those of the waves (see Vening Meinesz<sup>21,22</sup>). Two light rays make records of the auxiliary pendulums on the same photographic paper strip on which the others are recorded. This auxiliary device gives the horizontal components of the ship's acceleration and thus allows the derivation of the tilt of apparent gravity.

The periods of the two fictitious pendulums can be determined from the interruptions of the records caused by the interception of the light rays by

the timepiece, e.g., a quartz clock. When possible, it is better to make records of continuous time signals, as is now done by Worzel and other collaborators of Ewing's.

The whole apparatus hangs in gimbals, as shown by Fig. 4-18. The accuracy obtainable for a gravity determination during  $\frac{1}{2}$  hr is of the

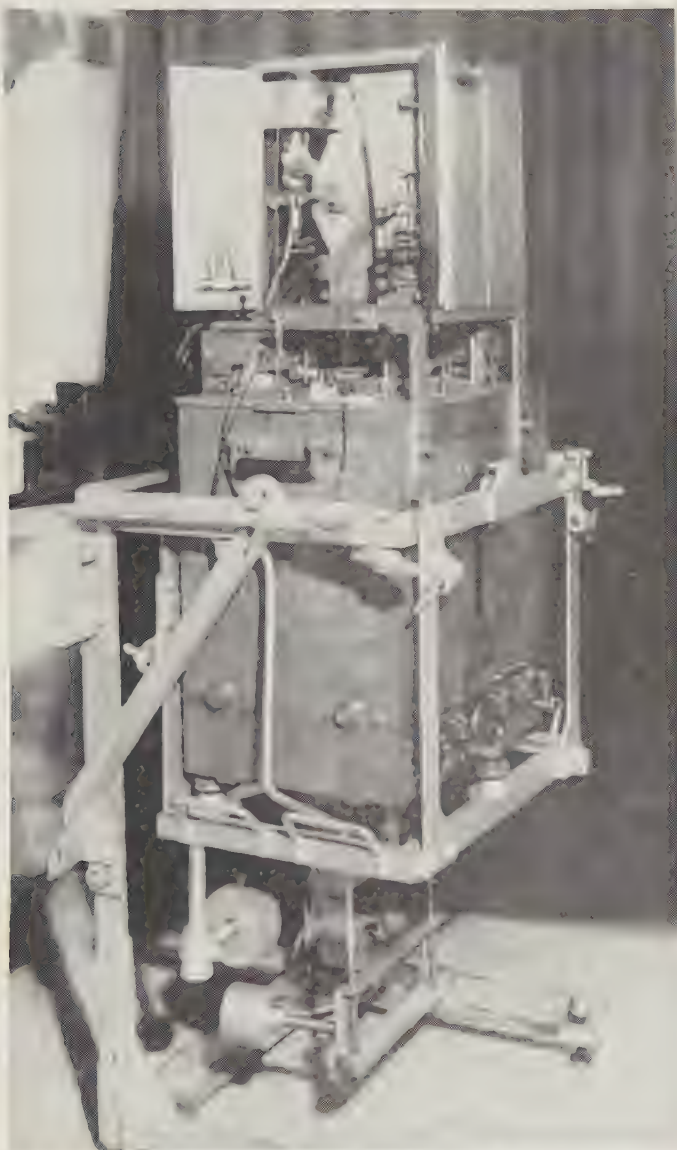


FIG. 4-18. The Ewing-Messé apparatus must be hung in gimbals to reduce the effect of horizontal acceleration.

order of 2 mgal, but the Eötvös correction, mentioned before, raises the mean error to 3 to 5 mgal. For further details about gravity observations at sea according to the method of Vening Meinesz, see Vening Meinesz.<sup>20</sup>

### F. Tidal Effect

In addition to the attraction of the earth's mass we have also to consider the attraction of the moon's and sun's mass when we need to measure gravity with very high accuracy. The effect of the moon's and sun's

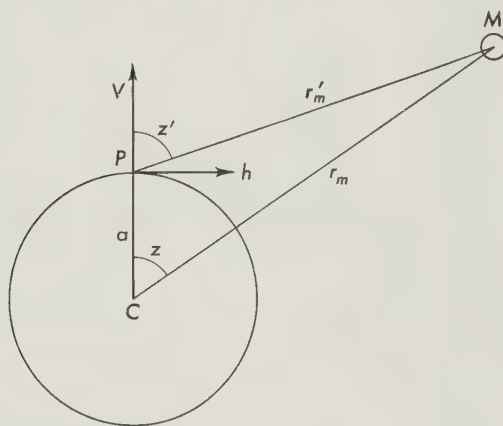


FIG. 4-19. Derivation of the tidal effect.

attraction is called the tidal effect, because it is also in connection with the tides. The formulas for computation of the effect of the moon and sun on the tides and the effect on the observed gravity are essentially the same. Figure 4-19 illustrates this effect.

Because of the attraction of the moon and sun, the gravity of the earth—as well as the direction of the plumb line—has periodical deviations from its normal value. This periodical attraction, the *tidal force*, can be obtained at any point of the earth's surface by subtracting the attraction of the celestial body—in our case, the moon and sun—at the computation point  $P$  from the attraction of the same bodies at the earth's center  $C$ . This difference is the tidal force. It consists of a horizontal and vertical component and is easy to understand.

The moon  $M$  is—in our case—closer to the computation point  $P$  than to the earth's center. Consequently, the attraction of the moon is larger at point  $P$  than it is at  $C$ .

The horizontal and vertical components  $h_m$  and  $v_m$  of the tidal force at the point  $P$  are obviously

$$h_m = km_m \left( \frac{\sin z'_m}{r'^2_m} - \frac{\sin z_m}{r^2_m} \right) \quad (4-43)$$

$$v_m = km_m \left( \frac{\cos z'_m}{r'^2_m} - \frac{\cos z_m}{r^2_m} \right) \quad (4-44)$$

where  $k$  is the Newtonian gravitation constant,  $m_m$  the mass of moon,  $z'_m$  the zenith distance of moon at point  $P$ ,  $z_m$  the angle  $PCM$ ,  $r'_m$  and  $r_m$  the distances  $PM$  and  $C.M.$ . When we eliminate  $r'_m$ ,  $z'_m$ , and  $k$  we get the components of the tidal force in this form:

$$h = \frac{3}{2} km_m \frac{a}{r_m^3} \sin 2z_m = \frac{3}{2} g \frac{m_m}{M} \frac{a}{r_m^3} R^2 \sin 2z_m \quad (4-45)$$

$$v = 3km \frac{a}{r^3} \left( \cos^2 z_m - \frac{1}{3} \right) = 3g \frac{m_m}{M} \frac{a}{r_m^3} R^2 \left( \cos^2 z_m - \frac{1}{3} \right) \quad (4-46)$$

where  $R$  is the average radius of the earth,  $a$  the earth's radius in  $P$ ,  $M$  the mass of the earth, and  $g$  the gravity.

The formulas for the tidal effect of the sun are similar. We have, in fact, only to replace the moon's mass  $m_m$ , distance  $r_m$ , and angle  $z_m$  with the sun's mass  $m_s$ , distance  $r_s$ , and angle  $z_s$ .

The combined effect of the attraction of the moon and sun depends on the direction of these bodies. If they both are, as seen from the earth, at the same direction (conjunction) or at the opposite direction (opposition) the effect of both bodies works in the same direction and the tidal force is at maximum; we have the *spring tide*. If moon and sun are  $90^\circ$  from the tidal force, it is at minimum; we have the *neap tide*.

Using the values  $m_m/M = 1/81$ ,  $m_s/M = 333,400$ ,  $a/r_m = 1/60$  and  $a/r_s = 1/23,500$ , the maximum horizontal and vertical acceleration of the moon and sun are:

$$h_m = \frac{1}{11,800,000} g \quad v_m = \frac{1}{8,800,000} g \quad (4-47)$$

$$h_s = \frac{1}{25,600,000} g \quad v_s = \frac{1}{19,200,000} g \quad (4-48)$$

The maximum effect in the deflection of the vertical is respectively  $\xi_m = \rho'' \frac{h_m}{g}$  and  $\xi_s = \rho'' \frac{h_s}{g}$ ;  $0.^{\prime\prime}0175$  for the moon and  $0.^{\prime\prime}008$  for the sun. The

maximum effect to the gravity is  $\Delta g = \frac{v}{g}$  and is for the moon  $0.11$  mgal

and for the sun 0.05 mgal. During the maximum tides the combined effect is 0."0255 for the deflection of the vertical and 0.16 mgal for the gravity.

The periodical attraction of moon and sun also produces tide phenomena in the solid earth. The amount of this tide is a good measure of the rigidity of the earth's interior. Because of this fact, the tide phenomenon has been studied carefully and will be a part of the program of the International Geophysical Year.

Earlier it was possible to measure the tide effect only by the aid of horizontal pendulums and variometers. The same type of instruments also will be used now on a small scale. However, now we can get the results faster by using the very accurate gravimeters which yield an accuracy about a hundred times higher than the tidal effect to be measured.

The most accurate tidal gravimeter has been devised by LaCoste.<sup>24</sup> He has with his coworkers developed a photoelectric optical system which is free from the drift associated with most reading systems of gravimeters. He has also produced an improved servo system with a compensation network. Comparison of two tidal gravimeters at Austin, Texas, has indicated that accuracy of better than 1 microgal can be obtained. In fact, of 97 comparisons, the differences between the readings of these two gravimeters were in 2 cases 1; in 18 cases 2; in 22 cases 3; in 26 cases 4; in 18 cases 5; in 11 cases 6 microgals. Since 1 gal = 1,000 mgal = 1,000,000 microgal this accuracy means that the variation of the gravity can be measured with an error of 1 billionth ( $10^{-9}$ ) part of the gravity itself. This superaccurate gravimeter type will be used extensively in different parts of the world during the International Geophysical Year 1957-1958.

#### 4-3. Base Stations and Calibration Lines

All relative gravity observations need gravity base stations, which must be used before and after the field observations. Since the error of the base-station gravity value is, of course, transferred to all field observations, it is of the utmost importance to measure the gravity at the base stations as accurately as possible.

The Assembly of the International Union of Geodesy and Geophysics at Rome in 1954 accepted the following gravity stations as world base stations of first order:

In Europe: Helsinki, Potsdam-Harzburg, Teddington, Paris, Milan, Lisbon-Madrid

In America: Fairbanks, Vancouver, Ottawa, Washington, D.C., Mexico City, Quito, Rio de Janeiro, Buenos Aires

In Asia: Kyoto, New Delhi, Singapore, Beirut

In Africa: Algiers, M'Bour, Khartoum, Leopoldville, Johannesburg

In Australia and in the ocean areas: Melbourne, Christchurch, Honolulu, Reykjavik, Azores.

These stations will be connected with each other in several ways. In all, more than 1500 gravity base stations exist in different parts of the world. The connection between them has been carried out chiefly by gravimeters, particularly by Woppard and his group.<sup>31, 32</sup> The accuracy of the Sterneck pendulum apparatus and similar types is of the order of 1 mgal. Since there now are gravimeters which can give more than 20 times higher accuracy, but which must be calibrated by pendulum methods, higher accuracy in pendulum apparatus is needed. The Cambridge pendulum and the Gulf pendulum yield at best an accuracy of 0.2 to 0.5 mgal. To keep the observational errors of the pendulum measurements from interfering too much in gravimeter calibration it is best to locate pendulum base stations only at large gravity differences, e.g., 500 mgal. If this is done, the error of 0.2 to 0.5 mgal of the best pendulum observations introduces a relative error of only  $\frac{1}{2500}$  to  $\frac{1}{1000}$  in the gravimeter calibration. Between the pendulum base stations other base stations having smaller gravity intervals of 50 to 100 mgal are measured by gravimeter. As the accuracy of well-calibrated gravimeters is of the order of 0.05 mgal, the relative accuracy of these other base stations will be (regardless of the small gravity interval) of the same order as when pendulum base stations are used. Thus an accuracy of 0.05 mgal can be guaranteed for the calibration of gravimeters to be used in local surveys.

The most accurate tie between the gravity base stations can be obtained in measuring, by gravimeters using air transportation, the gravity differences of stations which are close at the same parallel so that their gravity difference is very small. In this case the effect of calibration error is almost zero. Such connections have been done by Morelli<sup>30</sup> and Rice between Rome and New York; by Innes, Morelli,<sup>29</sup> and Rice between Paris and Ottawa; and by Honkasalo and Kukkamäki between Helsinki and Oslo. We call these connections "ghost flights," because only the gravimeters fly several times back and forth—for instance, across the Atlantic—and the European geodesist reads the dials of the gravimeter on the European side, the American scientist on the American side. The obtained accuracy<sup>30</sup> of the gravity difference between Europe and America was better than 0.1 mgal. Similar ghost flights can be arranged, for instance, between Potsdam, Harzburg, Amsterdam, and Cambridge as well as between Lenin-grad, Helsinki, and Oslo.

#### REFERENCES

1. Bomford, G.: Geodesy, Oxford, London, 1952.
2. Browne, B. C.: Second order corrections to pendulum observations at sea, Monthly Notices Roy. Astron. Soc., Geophys. Suppl., September, 1937.
3. Dobrin, Milton B.: Introduction to geophysical prospecting, McGraw-Hill, New York, 1952.

4. Gay, Malcolm W.: Relative gravity measurements using precision pendulum equipment, *Geophysics*, vol. 5, pp. 176-191, 1940.
5. Gulatee, B. L.: Geol. Survey India, Tech. Rept. 1948-1949, part 3, Geodetic work, chap. 3, Gravity.
6. Encyclopaedia Britannica, vol. 10, Gravitation, pp. 663-668, 1955.
7. Hecker, O.: Bestimmung der Schwerkraft auf dem Atlantischen Ozean sowie in Rio de Janeiro, Lissabon und Madrid, Veröffentl. preuss. geod. Inst. (Berlin), N.F., no. 11, 1903.
8. ———: Bestimmung der Schwerkraft auf dem Indischen and Grossen Ozean und deren Küsten, *ibid.*, no. 16, 1908.
9. Heiskanen, W. A.: Beobachtung der Schwerkraft, Die Lotabweichungen, Das Problem der Isostasie, in B. Gutenberg (ed.), *Handbuch der Geophysik*, Abschn. 10, Bd. 1, Lief. 4, Borntraeger, Berlin, 1936.
10. Hirvonen, R. A.: On the establishment of the values of gravity for the national reference stations, *Publ. Isos. Inst. IAG* (Helsinki), no. 19, 1948.
11. Houston Technical Laboratories: Information and pictures.
12. International Association of Geodesy, Rome Assembly, 1954.
13. Lejay, R. P. Pierre: Developpements modernes de la gravimétrie, pp. 26-32, Gauthier-Villars, Paris, 1947.
14. ———: Exploration gravimétrique des états du levant sous mandat français, Comité national français de géodésie et géophysique, Paris, 1938.
15. ———: Étude gravimétrique des îles philippines, Imprimerie Tōu-sè-wè, Shanghai, 1939.
16. Morelli, Carlo: Rept. Study Comm. 10, Rome Assembly IUGG, 1954.
17. Pepper, T. B.: The Gulf underwater gravimeter, *Geophysics*, vol. 6, no. 1, January, 1941.
18. Pesonen, U.: Relative Bestimmungen der Schwerkraft in Finnland in den Jahren 1926-1929, *Publ. Finn. Geod. Inst.*, no. 13, 1930.
19. Tanni, L.: On the isostatic structure of the earth's crust in the Carpathian countries and the related phenomena, *Publ. Isos. Inst. IAG* (Helsinki), no. 11, 1942.
20. Vening Meinesz, F. A.: Theory and practice of pendulum observations at sea, *Publ. Neth. Geod. Comm.*, Waltman, Delft, 1929.
21. ———: Theory and practice of pendulum observations at sea, part II, *Publ. Neth. Geod. Comm.*, Waltman, Delft, 1941.
22. ———: The second order corrections for pendulum observations at sea, *Koninkl. Ned. Akad. Wetenschap. Proc.*, ser. B, vol. 56, no. 3, 1953.
23. Woppard, George P., N. C. Harding, and J. C. Rose: The problem of calibrating high-range geodetic-type gravimeters, *Trans. Am. Geophys. Union*, vol. 36, pp. 12-23, 1955.
24. Clarkson, H. N., and L. J. B. LaCoste: Improvements in tidal gravity meters and their simultaneous comparison, *Trans. Am. Geophys. Union*, vol. 38, no. 1, 1957.
25. Honkasalo, Tauno: Gravity survey of the Baltic Sea: Symposium, Size and shape of the earth, *Publ. Inst. Geod., Photogram. Cartog.*, Ohio State Univ., no. 7, pp. 67-69, 1957.
26. Innes, M. J. S.: Gravity Measurements in Canada for Geodetic Purposes, Symposium, Size and Shape of the Earth, *Publ. Inst. Geod., Photogram. Cartog.*, Ohio State Univ., no. 7, pp. 70-73, 1957.
27. ———, C. Morelli, and D. A. Rice: Gravimetric ties Europe-America II (unpublished).
28. Lejay, Pierre: Rapport sur l'activité du Bureau Gravimétrique International, *Publ. Bureau Gravimétrique International*, 1957.

29. Morelli, Carlo: Special Study Group No. 5, Report for Eleventh General Assembly, Toronto, 1957.
30. ———, and D. A. Rice: Gravimetric ties Europe-America, Bull. Geod., no. 38, 1955.
31. Woppard, G. P.: World gravity connections: Symposium, Size and shape of the earth, Publ. Inst. Geod., Photogram. Cartog., Ohio State Univ., no. 7, pp. 73-75, 1957.
32. ———, J. C. Rose, and W. E. Bonini: The establishment of an international gravity standard, Trans. Am. Geophys. Union, vol. 37, no. 2, 1956.

## CHAPTER 5

### HISTORICAL DEVELOPMENT OF THE IDEA OF ISOSTASY

#### 5-1. Definition

We have previously mentioned the fact that in many places gravity anomalies (after considering the effect of such visible irregularities as mountains, valleys, oceans, and ocean islands) are much greater than can be accounted for by errors of measurement. We know that the Bouguer gravity anomalies are generally strongly negative in mountain areas and still more strongly positive at sea. These facts can be explained objectively only if we assume that the average mass density is smaller under mountains and larger under the oceans than it is under lowlands. In this way, the effect of the mountains and oceans on the gravity anomalies will be at least partly compensated by the invisible-mass distribution of the earth's crust. This evidence from gravity anomalies, as well as the similar evidence from the astronomic-geodetic deflections of the vertical, leads to the hypothesis of isostatic equilibrium.

Isostatic equilibrium means that crustal elements which are at a depth not too far below sea level are under the same pressure regardless of whether the surface units are under mountains, lowlands, or oceans. The depth at which isostatic equilibrium prevails is called the "depth of compensation." It can vary from place to place.

If all the topographic masses are compensated, isostatic equilibrium is said to be complete. If only a part is compensated, there is said to be undercompensation. On the other hand, it is possible that the compensating masses in some areas are even larger than the topographic masses, and such areas are overcompensated. If all topographic features, however small they may be, are compensated by the internal-mass distribution, the compensation is said to be "local." If compensation occurs only in larger blocks of, say, 50 to 100 km diameter, in which the compensating mass of the topography is distributed in a horizontal direction over large areas, the compensation is said to be "regional."

Different features of topography are compensated in different ways. For instance, it is likely that mountain chains are compensated locally but that

areas of sedimentation and postglacial uplift are compensated regionally. On the other hand, the strength of the earth's crust is so great that complete isostatic equilibrium is hardly possible. When, despite this fact, the local compensation is used in computations, it is only to make the mathematical computations easier.

The purpose of isostatic studies of gravity anomalies is to find out in what way and to what extent different parts of the world are compensated and to investigate the reasons for deviations from isostatic equilibrium.

There are two basically different conceptions of isostasy. If we picture mountains as having been uplifted like fermenting dough, the density of which becomes smaller as it rises higher, isostatic equilibrium is caused by the density differences. The alternative is to assume that the earth's crust under mountains has sunk into the subcrustal layer (the higher the mountain, the deeper the sinkage) just as icebergs and timber float in water. In a similar way, we can believe that the heavier subcrustal material under oceans is higher than under lowlands. In this assumption, mountains have root formations of light crustal material, ocean basins have "antiroots" of heavier subcrustal material, and isostatic equilibrium is caused by these root formations and antiroots. We must try to determine, by studying gravity anomalies, which of these two assumptions is the more likely.

For the first assumption, we must determine the depths of compensation at which isostatic equilibrium prevails; for the second, we must compute the thickness of the earth's crust, which, of course, is larger under mountains and smaller under oceans than under continental lowlands.

## 5-2. Early History of Isostasy

Before explaining the details of isostatic equilibrium, it seems worthwhile to give a short historical survey of isostasy.

### A. First Ideas concerning Isostatic Equilibrium

The proverb "There is nothing new under the sun" seems to be valid in isostasy. Leonardo da Vinci, that versatile man of genius of the Renaissance, was of the opinion, although rather dimly, that the visible masses of the earth's surface are in equilibrium. In 1940 Delaney found the following quotation in da Vinci's notebook:<sup>10</sup>

That part of the surface of any heavy body will become more distant from the centre of its gravity which becomes of greater lightness. The earth, therefore, the element of which the rivers carry away the slopes of mountains and bear them to the sea, is the place from which such gravity is removed; it will make itself lighter and in consequence more remote from the centre of gravity of the universe which is always concentric with the centre of gravity of the earth. . . . The summits of the mountains in course of time rise continually. . . .

Delaney comments on this:

We see that the famous author of the sixteenth century, of course, is still a supporter of the old geocentric world system. But he also says clearly that the density of the mountains is smaller than that of the level lands, or exactly as Pratt supposes.

We can claim therefore that Leonardo da Vinci was an isostasist—obviously the first one in the history of geodesy. If we like, we can regard him as the first defender of Pratt's "dough hypothesis."

We have to jump about two and a half centuries, to 1749, before we find anything concerning the equilibrium of the earth's crust. In that year Bouguer,<sup>4</sup> a member of the French geodetic expedition sent to Peru to measure the meridian arc, wrote "La figure de la terre," in which he expressed the conviction that the attraction of the huge mass of the Andes "is much smaller than expected from the mass of matter represented in such mountains."

A little later, Boscovich<sup>5</sup> gave an explanation of the phenomenon noted by Bouguer. He said:

The mountains, I think, are to be explained chiefly as due to the thermal expansion of material in depth, whereby the rocky layers near the surface are lifted up. This uplifting does not mean the inflow or addition of material at depth; the void ("vide") within the mountain compensates ("compense") for the overlying mass.

This quotation is noteworthy because here the word "compensate" is used for the first time and because Boscovich closely approaches Pratt's later hypothesis of isostasy.

#### *B. Isostatic Assumptions of Pratt and Airy*

After a wait of another century the existence of isostatic equilibrium was attested to by geodetic measurements. The arc measuring of India advanced so far that it was possible to measure the latitude differences between some Indian triangulation points both with the aid of astronomical observations and along the triangulation chains. When the famous geodesist Everest had computed the latitude difference between the Indian stations Kaliana and 375 miles to the south, Kalianpur, he realized that the latitude difference computed along the triangulation chain was 5".24 greater than that obtained from the astronomical observations, which meant that the relative deflection of the vertical between these points was 5".24.

An English archdeacon at Calcutta, J. H. Pratt, studied the difference and came to the correct conclusion that it could not have been caused by the geodetic measurements. He stated that the attraction of the superficial topographic matter was the real reason for the phenomenon, and he

realized that the mass of the Himalayas attracts in such a direction that the discrepancy can be explained qualitatively at least.

When Pratt computed the deflections of the vertical caused by the topographic masses, he found that the topographic deflection at Kaliana was  $27^{\circ}85$  but at Kalianpur only  $11^{\circ}97$ . The difference is  $15^{\circ}88$ , instead of the  $5^{\circ}24$  computed from the geodetic and astronomical observations. This result was something new and showed that two-thirds of the horizontal attraction of the Himalayas on these stations must be compensated by mass deficiencies located in or under the mountain mass.

Pratt's paper of 1854 contained the first numerical computation of how large the effect of the mountains and underlying compensating masses on the deflections of the vertical can be.<sup>24</sup> Four years later, in 1859, when Pratt studied the problem in greater detail, he stated that when the earth was completely fluid, no mountains, valleys, or ocean basins were possible but when the earth's crust began to form and grow gradually thicker, contractions and expansions may have occurred at different places, thus depressing and elevating the corresponding areas of the surface.

If these changes took place chiefly in a vertical direction, then at any epoch a vertical line drawn down to a sufficient depth from any place in the surface will pass through a mass of matter which has remained the same in amount all through the changes. By the process of expansion the mountains have been forced up, and the mass thus raised above the level has produced a corresponding attenuation of matter below. This attenuation is most likely very trifling, as it probably exists through a great depth. Whether this cause will produce a sufficient amount of compensation can be determined only by submitting it to calculation, which I proceed to do.

According to Pratt, thermal attenuation best explains the deflections of the vertical. He realized that if the attenuation under the Himalayas extends uniformly through a depth of about 100 miles, the meridian deflection of the plumb line at the northern stations of India would be reduced to zero.

Pratt believed that the Himalayan mountain range had risen from its base like fermenting dough, the density of which decreases the more it rises. Thus the density underneath the Himalayas would be less than under the Indian lowland.

Quite frequently two scientists working independently discover an important phenomenon or perfect a significant invention simultaneously. It is well known that the English astronomer Adams, in October, 1845, and the French astronomer Leverrier, in the summer of 1846, independently computed the orbital elements of Neptune. Unfortunately for Adams, the new planet was discovered September 23, 1846, on the basis of Leverrier's computations. A similar thing happened in 1868, when the English astronomer

Lockyer and the French astronomer Janssen without knowing each other's results invented a method for observing the prominences of the sun, which previously could be studied only during total solar eclipses. In 1892 both the American astronomer Hale and the French astronomer Deslandres invented the spectroheliograph, an important tool in the hands of astronomers. Einstein delivered a paper on his general theory of relativity on November 11, 1915, to the Academy of Sciences in Berlin, and on November 20 of the same year Hilbert gave at the Scientific Association of Göttingen the results of his investigation of a similar theory.

In the same way it happened that on January 25, 1855, the British astronomer G. B. Airy sent to the Royal Society his paper on the same

equilibrium problem Pratt had discussed before the same society on December 7, 1854. Airy also realized that the attraction of the mountain masses were much larger than shown by the observations, but he maintained that, instead of being a surprise, such results were to be anticipated; i.e., instead of expecting a large mountain mass to have a positive attraction effect a considerable distance away, we should expect no effect whatever or, in some cases, a small negative effect.

Airy came to the conclusion that such high mountains as the Himalayas are, in a sense, impossible. The weight of such a huge mass would break the earth's crust through its whole depth from the top of the tableland to the surface of the lava, so that the whole mountain, or at least a small part of it, would sink into the lava. Because such high mountains do exist, they must be supported from below.

Airy therefore proposed his "mountain-root theory," which is clearly explained by his illustration<sup>1</sup> (Fig. 5-1) and the following quotation.

I conceive that there can be no other support than that arising from the downward projection of a portion of the earth's light crust into the dense lava; the horizontal extent of that projection corresponding rudely with the horizontal extent of the table-land, and the depth of its projection downwards being such that the increased power of floatation thus gained is roughly equal to the increase of weight above from the prominence of the table-land. It appears to me that the state of the earth's crust lying upon the lava may be compared with perfect correctness to the state of a raft of timber floating upon the water; in which, if we remark one log whose upper surface floats much higher than the upper surfaces of the others we are certain that its lower surface lies deeper in the water than the lower surface of the others.

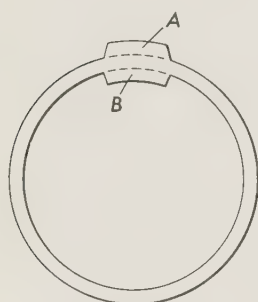


FIG. 5-1. Airy's original isostatic assumption. The downward prominence (root) compensates the mass of high plateau.

small part of it, would sink into the lava. Because such high mountains do exist, they must be supported from below.

Concerning the double effect of the elevated tableland and its downward projection, he says

It will be remarked that the disturbance depends on two actions; the positive attraction produced by the elevated table-land; and the diminution of attraction, or negative attraction, produced by the substitution of a certain volume of light crust (in the lower projection) for heavy lava.

The diminution of attractive matter below, produced by the substitution of light crust for heavy lava, will be sensibly equal to the increase of attractive matter above.

The essential meaning of the isostatic-floating theory could hardly be explained more clearly. Airy goes into even greater detail in discussing the mechanism of the floating hypothesis. He emphasizes that the compensation cannot be quite local, i.e., that very small mountains cannot have root formations sufficient for equilibrium.

The theories of Pratt and Airy are as contradictory as they can possibly be. According to Pratt, the Himalayas have uplifted in such a way that the higher the mountain, the smaller its mean density. According to Airy, the Himalayas have sunk into the underlying layer as timber floats in a lake. In one important and essential respect, however, the theories are similar, for according to both, the gravitational effect of mountain masses will be compensated, either because of the smaller density of the matter in the mountain and underneath it (Pratt), or by the aid of the downward prominences, or root formations, which support the mountain (Airy). Each hypothesis has its defenders.

### *C. Some Isostatic Studies at the Turn of the Century*

The existence of isostatic compensation was established in India on the basis of deviations of the plumb line and of gravity anomalies. Later other geodesists, e.g., Schiøtz, Burrard, Bonsdorff, Putnam, Helmert, and Hayford, investigated gravity anomalies or plumb-line deviations and established that the visible-mass anomalies cannot explain the observed gravity anomalies or plumb-line deviations but that compensating subterranean mass defects or mass excesses are needed.

By 1884 Helmert was already convinced of the existence of such compensation. In his "Höhere Geodäsie" he claims that the continental masses are not absolute mass surpluses but that their effect is more or less compensated by a diminution in density of the earth's crust underneath the continental masses. Thus, from a certain depth below sea level up to the physical surface of the earth, prisms of the same cross section have approximately the same mass wherever the prisms are assumed to be. The success of Helmert's condensation method is, in fact, due to the existing isostatic compensation.

During Nansen's polar expedition, Schiøtz<sup>27</sup> carried out measurements on the ice of the Arctic Sea, investigated the course of gravity anomalies from the continent to the sea, and reached the conclusion that isostatic equilibrium prevails.

Bonsdorff<sup>2</sup> computed the influence of visible-mass anomalies on the plumb-line deviation in Spitsbergen, and Hayford conducted extensive computations to determine the effect of the visible masses on the plumb-line deviation of the United States; both reached the conclusion that isostatic equilibrium prevails.

Later on, Bonsdorff also made isostatic reductions in the plumb-line deviations and the gravity anomalies in Spitsbergen. The mean value of the remaining plumb-line deviations (11 points) is 2".7 according to the topographic reduction but only 1".7 according to the topographic-isostatic reduction (depth of compensation  $T = 120$  km). The mean value of the Bouguer anomalies  $\Delta_B g$  is 23 mgal, and that of isostatic gravity anomalies  $\Delta_i g$  only 12 mgal. Bonsdorff developed the Bouguer and isostatic anomalies as a function of the height  $h$  of the gravity station and got the following result ( $h$  in kilometers):

$$\Delta_B g = 29.8 - 72h \text{ mgal}$$

$$\Delta_i g = 6.3 - 7h \text{ mgal}$$

While the isostatic gravity anomalies in Spitsbergen hardly seem to depend on the height of the gravity station, for the Bouguer gravity anomalies this dependence is very clear. We later give other examples which show this phenomenon still more clearly.

Geologists have been greatly interested in the isostatic structure of the earth's crust. Some of them, e.g., Hall and Jamieson, came near to the concept of isostatic equilibrium, but the geologist who contributed the most in this respect before the end of the last century was C. E. Dutton,<sup>11</sup> an American. In 1889 he published his famous article "On Some of the Greater Problems of Physical Geology." Since this article used the word "isostasy" for the first time, and since it was important from the isostatic point of view, one quotation is worth repeating despite its frequent appearance in textbooks.

If the earth were composed of homogeneous matter its normal figure of equilibrium without strain would be a true spheroid of revolution; but if heterogeneous, if some parts were denser or lighter than others, its normal figure would no longer be spheroidal. Where the lighter matter was accumulated there would be a tendency to bulge, and where the denser matter existed there would be a tendency to flatten or depress the surface. For this condition of equilibrium of figure, to which gravitation tends to reduce a planetary body, irrespective of whether it

be homogeneous or not. I propose the name isostasy (from the Greek *isostasios*, meaning "in equipoise with"; compare *isos*, equal and *statikos*, stable). I would have preferred the word isobary, but it is preoccupied. We may also use the corresponding adjective, *isostatic*. An isostatic earth, composed of homogeneous matter and without rotation, would be truly spherical. If slowly rotating, it would be a spheroid of two axes. If rotating rapidly within a certain limit, it might be a spheroid of three axes.

But if the earth be not homogeneous—if some portions near the surface are lighter than others—then the isostatic figure is no longer a sphere or spheroid of revolution, but a deformed figure, bulged where the matter is light and depressed where it is heavy. The question which I propose is: How nearly does the earth's figure approach to isostasy?

### 5-3. Main Isostatic Systems

There are several isostatic systems, and they differ from each other in their assumptions about the way in which mass compensation is achieved. Only three—the Pratt-Hayford, Airy-Heiskanen, and Vening Meinesz systems—have been applied to geophysical and geodetic studies.

#### A. Pratt-Hayford Isostatic System

A new phase in the study of isostasy began in 1909 and 1910, when Hayford in America and Helmert in Germany published their important studies on isostatic equilibrium. Both of them used Pratt's ideas in more precise form. Helmert applied a generalized mathematical method and tried to determine the depths of compensation on the basis of the gravity anomalies obtained at steep seacoasts. As his mathematical method can be used only in those rare instances when the topographic masses have, in broad terms, the shape of a regular mathematical body, it has not been used since. Hayford and Bowie, of the U.S. Coast and Geodetic Survey, chose a method which, though more laborious, can be applied universally.

The Pratt-Hayford isostatic system can be summarized as follows:

1. Isostatic compensation is uniform, i.e., density underneath mountains is uniformly smaller than underneath level land.
2. The compensating layer is located directly underneath the mountains and reaches to the depth of compensation  $D$ , where equilibrium prevails.
3. The density  $\rho'$  of the compensation, corresponding to a topographic elevation  $h$ , and the density  $\rho$  of the topography satisfy the equation

$$\rho' = - \frac{h}{D} \rho \quad (5-1)$$

4. The depth of compensation is everywhere equal when measured from the physical surface of the earth and not from sea level.

Pratt's original assumption is explained<sup>19</sup> by figures in Fig. 5-2. The higher the mountain, the smaller the density of the earth's crust; the deeper the ocean, the higher the density. For instance, to an elevation of 6 km there corresponds a density of 2.52, to a depth of 5 km below the ocean, a density of 2.76 if we assume that the normal density corresponding to the zero elevation is 2.67 and the depth of compensation 100 km.

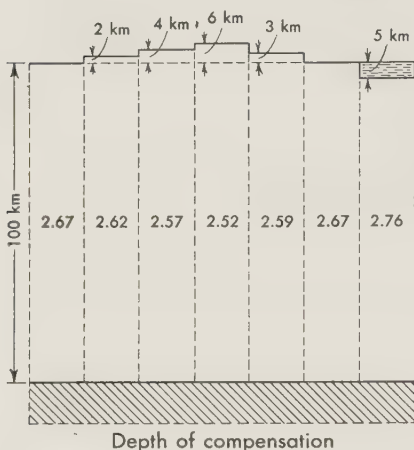


FIG. 5-2. Idea of Pratt's original isostatic hypothesis. Smaller density of the mountain columns and greater density of the ocean columns compensate the mass surplus of the mountains and mass deficiency of the oceans.

deep (Fig. 5-4). This assumption has also been used by Bowie and other geodesists of the U.S. Coast and Geodetic Survey and in Europe by Inglada Ors, Niethammer, Cassinis, and the author (H.).

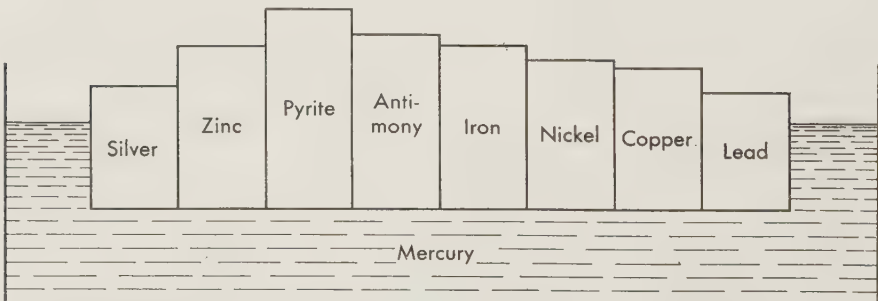


FIG. 5-3. Bowie's interpretation of the Pratt-Hayford assumption. The lower the density of each block, the higher it rises above the surface to achieve isostatic equilibrium.

There are two essentially different ways of regarding isostatic equilibrium: in terms of equal pressure or in terms of equal mass.

In Fig. 5-3 the meaning of the Pratt assumption is clearly illustrated. If columns of different metals float on mercury in such a way that their undersurfaces are at the same depth  $D$ , then the smaller their density, the higher they must rise to achieve isostatic equilibrium.

To simplify the computation formulas Hayford<sup>12</sup> measures the depth of compensation from the physical surface of the earth; e.g., the depth of compensation under a mountain 3 km high lies 8 km higher than underneath an ocean<sup>5,6</sup> 5 km

Isostasy means, by definition, that at a depth of compensation  $D$  hydrostatic equilibrium prevails, so that every area unit at the depth  $D$  is under the same pressure regardless of whether the unit is under mountain, lowland, or ocean. This condition (equality of pressure) can be given for a unit column by the equation

$$\int_{-D}^h \rho g dz = C \quad (5-2)$$

For the frequently used assumption of equality of mass, on the other hand, the equation is

$$\int_{-D}^h \rho \left(1 + \frac{z}{R}\right)^2 dz = C \quad (5-3)$$

In these equations  $\rho$  denotes the density,  $R$  the earth's radius, and  $z$  the vertical coordinate, positive outward and measured from the equilibrium level. The second equation corresponds to equality of mass in all truncated pyramids of the same cross section reaching from the depth of compensation  $D$  to the earth's surface  $h$ . The lateral sides of these pyramids coincide with the direction of gravity and therefore converge towards the earth's center.

The observations on which isostasy is based are not sufficiently accurate for us to decide empirically which equation best corresponds to the facts. As the value of  $D$ , according to present opinion, averages only 30 km and never exceeds 60 km, the difference of the two integrals is of the order of only 1 per cent.

The Pratt-Hayford assumption, as a consequence of the basic equation (5-1), is in harmony neither with the hypothesis of equality of pressure nor with the hypothesis of equality of mass. It is, however, much closer to the former because it neglects only the small change of  $g$  over the depth  $D$ . In fact, if  $\rho_t$  is the density of the topography, it corresponds to the equation

$$\int_{-D}^h \rho dz = \rho_t D \quad (5-4)$$

If  $l$  is the vertical distance between the gravity centers of the topography and the compensation level and  $r$  the earth's radius, the difference of grav-

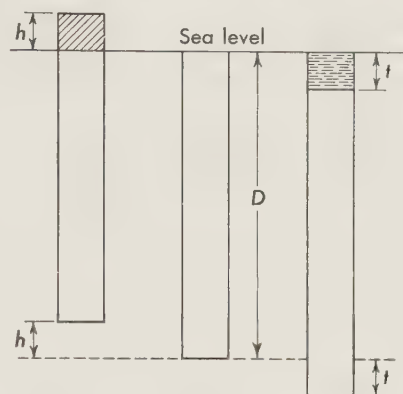


FIG. 5-4. Pratt-Hayford isostatic system. To simplify the isostatic reductions Hayford computed the depth of compensation from the physical surface of the earth instead of from sea level. Consequently, the surface of equal pressure is higher under the mountains and lower under the oceans than under lowlands.

ity  $g_c - g$  at these two points is

$$g_c - g = 2 \frac{g}{R} l - 3 \frac{\rho}{\rho_m} \frac{g}{R} l \quad (5-5)$$

where  $\rho$  = mean density over distance  $l$

$\rho_m$  = mean density of earth.

The first term is the free-air reduction, the second term the *double* Bouguer reduction of the attraction of the mass layer between the two gravity centers. The latter reduction increases the gravity at the higher point and decreases it at the lower point. If we put the ratio  $\rho/\rho_m = 0.5$ , we get

$$g_c - g = \frac{1}{2} \frac{g}{R} l \quad (5-6)$$

and so

$$\frac{g_c - g}{g} = \frac{1}{2} \frac{l}{R}$$

It follows from this formula that if  $h$  is the elevation of topography of the column in question, the difference of mass between the compensation according to Formulas (5-4), Pratt-Hayford, and (5-2), equal-pressure, is

$$m_4 - m_2 = \frac{1}{2} \rho \frac{lh}{R}$$

In a similar way the difference of mass between the compensation according to Formulas (5-4), Pratt-Hayford, and (5-3), equal-mass, is

$$m_4 - m_3 = -2\rho \frac{lh}{R}$$

Therefore the Hayford compensation lies between the compensations given by the equal-pressure and equal-mass hypotheses but is four times closer to the first.

If we indicate the mass of topography as  $m_t$  and of the compensating layer as  $m_c$ , we have

$$\text{Equal-mass} \qquad \qquad \qquad m_t - m_c = 0$$

$$\text{Equal-pressure} \qquad \qquad \qquad m_t - m_c = 2.5 \frac{lh}{R} \quad (5-7)$$

$$\text{Hayford's compensation} \qquad \qquad \qquad m_t - m_c = 2.0 \frac{lh}{R}$$

Computation tables for the Pratt-Hayford system are discussed in Chap. 6.

### B. Airy-Heiskanen Isostatic System

Airy's hypothesis can be illustrated, as we have said, by picturing the earth's crust as floating in a magma-like layer that is denser than the crust, just as icebergs float in the ocean. And just as the invisible part of an iceberg is much larger than the visible part, so also the root formations of the mountains are much thicker than the mountains themselves. The analogy, however, is not complete; there are two essential differences between floating icebergs and "floating" mountains: (1) the root of an iceberg begins at sea level, while the root of a mountain begins only at a considerable depth, 30 km or so; (2) since the underlayer will not flow so easily as water, floating of mountains cannot be so complete as that of icebergs, as Airy emphatically stated.

Because of the root formations of the mountains, the earth's crust is thicker under mountains than under lowlands. The relatively light root material compensates the effect of the mass surplus of the mountain. If it is also assumed that the mass deficiency of ocean basins is compensated isostatically, the further assumption that antiroots of the heavy underlayer exist under ocean basins must also be made.

In the years 1924, 1931, and 1938 the author (H.)<sup>15-17</sup> made the Airy assumption more precise and computed the necessary tables for isostatic reduction. The assumptions of the Airy-Heiskanen system are as follows:

1. Isostatic compensation is complete.
2. The compensation is local, i.e., the compensating layers are directly under the topography.
3. The density of the earth's crust is everywhere constant, 2.67.
4. The density of the underlayer is also constant everywhere and greater by 0.6 than the density of the earth's crust. (The system is illustrated schematically in Fig. 5-5.)

If the normal thickness of the earth's crust is assumed to be 30 km, it follows that under a mountain 3 km high the crust is 46.4 km thick and that under an ocean 5 km deep it is 11.2 km thick.

The author's assumption in 1924 and 1931 was in one respect similar to Hayford's, viz., the density  $\rho$ , the elevation  $h$  of the topographic masses,

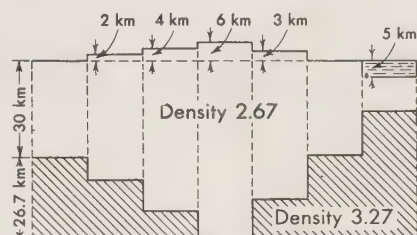


FIG. 5-5. Airy-Heiskanen isostatic system. The mountains float in the denser substratum like icebergs in the ocean. The light roots of the continents and the heavy antiroots of the oceans compensate the topographic masses.

the compensating density  $\Delta\rho$ , and the thickness  $t$  of the root formation satisfy the equation

$$\rho h = \Delta\rho t \quad \text{or} \quad t = \lambda h \quad (5-8)$$

where  $\lambda = \rho/\Delta\rho$ . In other words, the increase of the gravity  $g$  and the convergence of the earth's radii were neglected. As Formulas (5-7) show, this assumption is close to the isostatic compensation in terms of equal pressure.

In a similar way the thickness  $t'$  of the antiroot of the oceans is

$$t' = \mu h' \quad (5-8a)$$

where  $\mu = (\rho - 1.027)/\Delta g$ , in which 1.027 is the density, and  $h'$  is the depth of the ocean.

When the author prepared his final tables in 1938, he acceded to the request of many geodesists and made the compensating and topographic masses equal, so that the total mass of the earth would not be changed by the reduction. Instead of Formula (5-8), we get now for  $t$  from Formula (5-3), neglecting the terms of order  $(l/R)^2$ , the formula

$$t = h \left( 1 + 2 \frac{l}{R} \right) = \lambda h \left( 1 + \frac{2T + h + t}{R} \right) \quad (5-9)$$

where  $T$  is the normal thickness of the earth's crust. So we get

$$t = \lambda h \left[ 1 + 2 \frac{T}{R} + (\lambda + 1) \frac{h}{R} \right] \quad (5-10)$$

The thickness of the antiroot under the oceans would be

$$t' = \mu h \left[ 1 + \frac{2T - (\mu + 1)h'}{R} \right] \quad (5-11)$$

The elementary derivation of Formulas (5-10) and (5-11), with the terms of the order  $(l/R)^2$ , is as follows.<sup>31</sup> The mass of a topographic cap of height  $h$  and angular radius  $\omega$  is, as we easily see,

$$\frac{4}{3}\pi \sin^2 \frac{\omega}{2} \rho [(r + h)^3 - r^3]$$

The mass of the compensating column at the depths  $T$  to  $T + t$  is similarly

$$\frac{4}{3}\pi \sin^2 \frac{\omega}{2} \Delta\rho \{(r - T)^3 - [r - (T + t)]^3\}$$

Equating these two masses and omitting the factor  $\frac{4}{3}\pi \sin^2 \omega/2$ , we get

$$\rho[(r + h)^3 - r^3] = \Delta\rho \{(r - T)^3 - [r - (T + t)]^3\} \quad (5-12)$$

Expanding this formula, developing in series, and considering the terms of first and second order, we get

$$t = \lambda h \left\{ 1 + \frac{2T + (\lambda + 1)h}{R} + \frac{(2T + \lambda h)[2T + (\lambda + 1)h]}{R^2} - \frac{T(T + \lambda h)}{R^2} - \frac{(\lambda^2 - 1)h^2}{3R^2} \right\} \quad (5-13)$$

which is the end formula for a land zone or compartment;  $\lambda$  is, of course, given by  $\lambda = \rho/\Delta\rho$ . For  $\rho = 2.67$  and  $\Delta\rho = 0.6$  we get  $\lambda = 4.45$ .

For an ocean zone or compartment we get a similar formula

$$t' = \mu h' \left\{ 1 + \frac{2T - (\mu + 1)h}{R} + \frac{(2T - \mu h)[2T - (\mu + 1)h]}{R^2} - \frac{T(T - \mu h)}{R^2} - \frac{(\mu^2 - 1)h^2}{3R^2} \right\} \quad (5-14)$$

When we neglect the second-order terms, we get Formulas (5-10) and (5-11).

According to these formulas and the author's 1938 tables, the new value is for  $t$  a little larger than in his earlier tables; e.g., if  $T = 30$  km,  $t$  is 0.94 per cent larger under lowlands, 1.20 per cent larger under a mountain 3 km high, and 0.66 per cent larger under an ocean 5 km deep.

When the Airy-Heiskanen system is used in terms of equal pressure, corresponding small corrections must be added to the 1938 tables.

The total thickness  $T_c$  of the earth's crust under mountains is

$$T_c = T + t + h \quad (5-15)$$

and under the ocean is

$$T_o = T - t' - h' \quad (5-16)$$

The smaller the density difference between the underlayer and the earth's crust, the greater the thickness of the mountain root and the ocean antiroot; e.g., for the differences 0.6 and 0.3, the mountain root  $t$  is 4.45 and 8.90 km, respectively, per kilometer of mountain elevation, and, correspondingly, the ocean antiroot  $t'$  is 2.73 and 5.46 km per kilometer of the ocean depth (the tables will be dealt with in Chap. 6).

### C. Vening Meinesz Regional Isostatic System

Isostatic compensation, in many cases, cannot be entirely local. Small topographic masses cannot be isostatically compensated, and we do not know how large topographic features must be before complete compensation can take place. Several studies on the subject have been carried out. According to Bowie,<sup>5</sup> features whose horizontal extension is of the order of

10,000 km<sup>2</sup> are compensated; according to a study by Lehner,<sup>22</sup> the Alp blocks of 1000 km<sup>2</sup> are large enough to be compensated; but Niskanen's mathematical study,<sup>23</sup> on the other hand, shows that small areas like the Harz Mountains in Germany or the Hawaiian Islands are still too small to be in complete isostatic equilibrium. Actually it is very unlikely that any feature will be in complete equilibrium; the strength of the earth's crust will prevent it.

Taking all these facts into account, in 1931 Vening Meinesz<sup>24</sup> modified the Airy floating theory and established his own system of regional isostatic compensation. In 1939 and 1941 he published<sup>25</sup> the theoretical basis

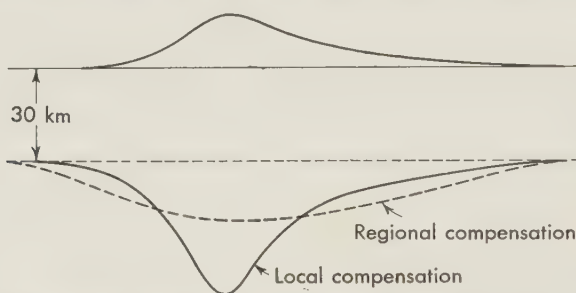


FIG. 5-6. Difference between the Airy-Heiskanen local and the Vening Meinesz regional isostatic-floating theories. In the regional theory the compensating masses of the mountain are distributed broadly in the horizontal direction.

and rigorous fundamental tables for the isostatic reduction of gravity values according to this regional system, and in 1941 there followed computation tables<sup>26</sup> for practical isostatic reduction work.

According to his modification, the topography is a "load" on an unbroken crust or, in ocean areas, a load taken away from the crust. The crust is assumed to behave like an elastic plate, strong enough to resist the shear stresses caused by the load floating on the denser substratum. The amount of downbending at each point is used to determine the effect of the isostatic compensation present at the computation point. The distance reached by the main part of the downbending caused by a concentrated load is called the regionality  $R$  of the isostatic compensation (Fig. 5-6). Like the previous systems of isostatic equilibrium, the regional assumption can be understood either in terms of mass or in terms of pressure.

Horizontal spreading of the compensation occurs in such a way that the compensating density diminishes from the center of the area toward the periphery according to a curve derived from the shape of the bending of the crust when the latter is considered as an elastic plate floating on a liquid and loaded by the topography. The bending curve (Fig. 5-7) is derived from Hertz's formula for the bending of a plastic plate of infinite

dimensions loaded by a concentrated load and shows how the compensation density diminishes with the distance from the load center. The ordinate of this curve is the measure of the compensation density.

In fact, in addition to the bending curve, there are also concentric crustal waves of small amplitude which surround it, but the amplitude

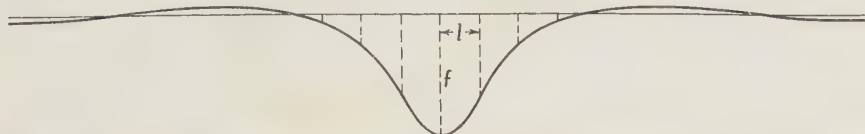


FIG. 5-7. Bending curve of the Vening Meinesz system. The load of the topographic mass causes the earth's crust to bend until equilibrium prevails.

of these waves is so small and diminishes so rapidly that they can be totally neglected.

The hydrostatic equilibrium given by the buoyancy principle provides, on the lower boundary, a pressure of

$$\sigma = \Delta \rho g z \quad (5-17)$$

where  $z$  is the vertical coordinate, positive downward. The cavity left by the sinking surface is assumed to be filled with sediments. To make the problem as simple as possible the density of the sediment layer has been put equal to the crustal density, 2.67. For a negative load accompanied by crustal upbending the crust is assumed to have been peneplained.

Introducing a length  $l$  given by the formula

$$l = \sqrt[4]{\frac{m^2}{m^2 - 1} \frac{ET^3}{12(\rho' - \rho)g}} \quad (5-18a)$$

where  $m$  is Poisson's constant and  $E$  the elastic modulus of the earth's crust, and assuming the concentrated load equal to the weight  $\rho g$  of the unit of volume, we find a curve of the type given in Fig. 5-7. The sinking in the center of the loaded plate is given by

$$f = \frac{\rho}{8(\rho' - \rho)l^2} \quad (5-18b)$$

The sinking  $z$  at distance  $x$  from the center is

$x$	$z$
0.000	1.000 $f$
1.000 $l$	0.646 $f$
2.000 $l$	0.258 $f$
3.000 $l$	0.066 $f$
3.887 $l$	0.000

For greater values of  $x$  we obtain waves of a rapidly diminishing amplitude and of a wavelength

$$\lambda = \pi\sqrt{2}l = 4.45l$$

The curve discussed above has been the basis of the method for regional isostatic reduction, but the outer waves have been neglected, and the border of the central sinking part has been slightly reduced in order to obtain equilibrium between the load and the integral of the upward pressure exerted by the substratum, according to Formula (5-17).

Keeping the values of  $z$  for  $x = 0$ ,  $x = l$ , and  $x = 2l$  and putting  $z = 0$  for  $x = 2.905l$ , we get a satisfactory curve (Fig. 5-7). Since we assume no more sinking or rising of the crust beyond  $x = 2.905l$ , this is also the border of the isostatic compensation; we shall call it the radius of regionality  $R$ . For the spreading of the isostatic compensation the adopted curve seems a reasonable one, even though we may not be entirely convinced about the crustal bending mechanism which is here used as a basis for computation.

As the physical constants of the crust are unknown, it is difficult to derive the values of  $l$  and  $R$  theoretically, and so tables have been made for a large number of values, i.e., for

$l$ , km	0	10	20	40	60	80	(5-19)
$R$ , km	0	29.05	58.1	116.2	174.3	232.4	

Thus it is possible to check all the degrees of regionality independent of any physical theory. To complete the picture, tables for local compensation have been added; for these tables we can put  $l = R = 0$ .

Starting from the local Airy-Heiskanen system, based on formulas (5-8) or (5-8a), Vening Meinesz distributed the compensation of each column in a horizontal sense, so that at each distance  $x$  from this column inside the radius  $R$ , the amount is made proportional to the ordinate  $z$  of the adopted curve. It is thus easy to see that for the central area of an extensive topographic feature of constant elevation or depth the compensation is independent of  $R$  and is identical with that of the local Airy-Heiskanen compensation. This result was considered more important than the fact that for a local topographic feature the compensation is not distributed in a way corresponding directly to the physical reality. For local topographic features the total compensation in each column is correct, but it is not vertically distributed in the correct way; however, it seems that no better system is possible as long as we want the compensation in each column to be integrable in a clear way. Moreover, the disadvantage of the wrong distribution of the compensation in a vertical sense

does not appear to be too serious; it causes only a small regionality  $R$  as best adapted to the gravity results.

Since both the final and the provisional tables are based on the regional spreading of an isostatic compensation determined by Formula (5-8), they correspond to Formulas (5-2) and (5-7) as well as to the Pratt-Hayford system, and to Heiskanen's 1931 tables. So the tables almost correspond to the equal-pressure hypothesis [Formula (5-2)]; they would do so exactly if the variability of gravity with depth had been taken into account. As a result of this omission there is an excess of mass after isostatic reduction, given by

$$m_d = \frac{\rho}{4R} \frac{h}{R} [2T + (\lambda + 1)] = 0.67 \frac{h}{R} (2T + 5.45h) \quad (5-20)$$

This mass causes a correction equal to 0.2 of the corresponding corrections of Heiskanen's 1938 tables. Although the correction would usually be negligible, only some tenths of a milligal for a precise application of Stokes' theorem for determination of the geoid it might be better to take it into account because being widespread, it may have a perceptible effect in this case.

The regional isostatic system is a modification of the Airy-Heiskanen floating theory. The Airy compensation is vertical, calling for the existence of local roots of light crust material below the mountains to support the load of the mountain masses. At the lower border, therefore, a hydrostatic equilibrium prevails, as it does when an iceberg floats in the sea. According to the regional theory, the compensation occurs in wide areas; regional roots exist because the earth's crust is bent by the load of the mountains.

Now it can be asked whether the strength of the earth's crust (or of the denser substratum below it) is strong enough to undergo this bending without breaking or whether it will give way. In that case we may have local compensation according to the Airy-Heiskanen system or we may have a mixed crustal reaction.

Altogether there are three main isostatic systems: the Pratt-Hayford "dough" hypothesis, the Airy-Heiskanen local-floating theory, and the Vening Meinesz regional-floating theory. A great number of reduction tables based on each of these systems exists, so that every scientist has ample opportunity to use those which, in his opinion, fit best. He can also make use of all three systems, as, in fact, many geodesists have done. On the basis of the different types of gravity anomalies, he can try to determine which system corresponds most closely to the behavior of the earth's crust in the area concerned. These types of studies for some areas, however, may be difficult, viz., if we can choose one set of Pratt-Hayford anomalies, one set of Airy-Heiskanen anomalies, and another set of Vening Meinesz

anomalies, which gravimetrically give nearly the same results. In order to decide among these systems in that case, other independent evidence must be found.

We already know that generally the floating hypothesis, either in the local or the regional sense, is closer to the real state of the earth than the Pratt-Hayford system. As we shall see a little later, there is a great deal of seismological evidence in favor of the floating theory. On the other hand, the huge strips of negative gravity anomalies discovered in the East Indies, the West Indies, and east of Japan can hardly be explained without root formations. Also, the behavior of postglacial-uplift areas favors the root-formation theory.

According to Vening Meinesz and several other scientists, isostatic compensation occurs in various parts of the earth in different ways, so it is impossible to find a system which would correspond everywhere to the actual conditions. The Pratt-Hayford system, used in the U.S. Coast and Geodetic Survey, is in harmony with the progress of mountain formations by vertical expansion of the earth's crust caused by decreasing density due to chemical action or rise of temperature. The Airy-Heiskanen system, which assumes local compensation but concentrates it chiefly or entirely in downward prominences of the earth's crust at its lower boundary, fits more or less closely the root-formation theory in the case of folded mountain chains and continental coasts. The regional-bending system of Vening Meinesz seems to be in harmony with topography brought about by erosion, sedimentation, volcanism, or folding of the upper crust layers.

#### 5-4. Some Other Isostatic Assumptions

If local compensation is used to compute gravity anomalies, even though the compensation is actually regional, the resulting isostatic reductions are too large for mountaintop stations and too small for valley stations. Therefore positive gravity anomalies at mountaintop stations and negative gravity anomalies at the valley stations are to be expected. Such, in fact, is the case, as Hayford and later Bowie<sup>5</sup> have shown.

It was for this reason that Putnam,<sup>25</sup> as early as the turn of the century, suggested a kind of regional isostatic reduction or compensation corresponding to the average elevation of the larger area. He computed the mean elevation of the surroundings of the station to a distance of 166.7 km from the station, i.e., to the outer border of Hayford zone O, and used it to compute the isostatic reduction.

In several publications Putnam emphasized the significance of this modified reduction and pointed out that good results cannot be obtained from the use of the Pratt-Hayford local isostatic system. For instance, he noted that because the mountaintop stations give systematically positive gravity anomalies and the valley stations systematically negative gravity anom-

lies, one cannot compute correct values for the depth of compensation by the Pratt-Hayford method.

Putnam's method has rarely been used except by its originator, although it is correct in many respects. Its significance is now lessened by the development of the theoretically better Vening Meinesz regional system.

In 1932, the author<sup>18</sup> (H.) presented one intermediate hypothesis which incorporates the mountain-root theory but in which it is considered that a part, 37 per cent, of the compensation occurs in the crust above the root formation. He accepted the seismological evidence for the existence of density discontinuities in the earth's crust and also used Washington's findings that the higher the elevation, the smaller the density of the earth's crust. The author's assumptions were (1) the higher the elevation, the more the surface density of the sial layer decreases with the height of the topography; (2) the surface density corresponding to the elevations 0, 1, 2, and 3 km is, respectively, 2.76, 2.74, 2.72, and 2.70; (3) the density of the sial increases with depth by 0.04 for every 10 km; (4) the density of the sima layer increases more slowly, being 3.06 at the depth of 10 km below the Pacific Ocean and 40 km deeper 3.14; (5) the compensation is local and vertical under the topography. Figure 5-8 explains the essential meaning of this hypothesis.

Since it has been very difficult to decide whether this intermediate assumption is closer to the actual conditions of the earth's crust, it has been little used.

It was mentioned earlier that, according to the floating system, root formations exist under the mountains and antiroots of denser material under the oceans. The roots of light material compensate for the effect of the topography in continents, and the heavy antiroots compensate for the effect of the mass deficiency of the sea water.

In 1941 Daly<sup>9</sup> published his isostatic hypothesis of antiroots under the continents and root formations under the oceans. Essential to this hypothesis is the assumption that the crystalline sima layer goes deeper under the oceans than under the continents, where, below the relatively light sial layer, there exists only a thin crystalline sima layer; the thinner the layer, the higher the continental mountain. Beneath the sima layer lies the vitreous substratum, density about 2.8 (smaller than that of the crystalline

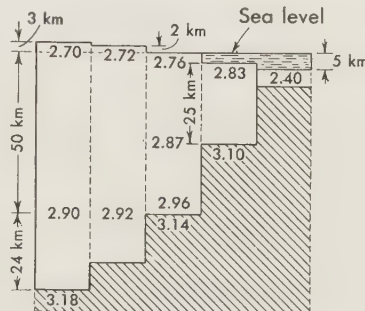


FIG. 5-8. Heiskanen's intermediate assumption. Approximately two-thirds of the topography will be compensated by the root formations and antiroots and one-third by the earth's crust above the boundary between the crust and substratum (M discontinuity).

sima layer), which forms the antiroots under mountains while the crystalline sima layer, of density 3.06, forms the roots of oceans. The figure presented by Daly himself shows how the heavy root of oceans compensates the mass deficiencies of oceans and the light antiroot of mountains compensates the mass surplus of mountains.

It is naturally very easy to compute the density differences and the thickness of the ocean roots and mountain antiroots so that isostatic equilibrium prevails. The Daly hypothesis, however, does not seem likely, especially because seismological findings show that there are roots under the mountains, as the general isostatic-floating hypothesis supposes, and no antiroots.

In this connection it may be worthwhile to mention an attempt by de Cizancourt<sup>8</sup> to explain the behavior of areas like the Hawaiian Islands, the Mid-Atlantic Ridge, and the Western Mediterranean Basin, where considerable isostatic anomalies exist. According to him, the anomalies are caused by a plastic deformation, reaching the relatively great depth of 300 km. The deformations are brought about by stresses which can cause a great many gliding surfaces to form two systems of orthogonal planes, about 45° from the horizontal main stresses. These gliding-mass systems produce deep undulations, or "undations," as de Cizancourt calls them, negative downward undations of light material, and positive upward undations of heavier material, the former explaining areas of negative Bouguer anomalies, the latter areas of positive Bouguer anomalies.

Assuming that the undations reach to infinity, de Cizancourt tries to compute, by an approximate method, the width and depth of the undations, which he believes explain the regional phenomena. His results are that the width and depth of the negative Hawaiian undation are 230 and 138 km, respectively; of the negative Mid-Atlantic undation, 350 to 400 and 280 to 300 km; and of the positive Western Mediterranean undation, 200 and 100 km. The more or less quadrangular basins and massifs he tries to explain by the aid of deep domes and basins, the dimensions of which ought to be of the order of 400 km.

This method obviously does not succeed in explaining the details of the behavior of the earth's crust; for one thing, it makes use of the Bouguer anomalies, which when used alone can be misleading in geophysical studies. The classical isostatic computations are needed, and de Cizancourt himself states,<sup>8</sup> "Isostatic anomalies are not, however, devoid of any meaning. The classical methods yield concordant results in the continental areas where the crust is practically in equilibrium." But this quotation gives only one-half or one-third of the truth because the oceans, with few exceptions, are in isostatic equilibrium, which is why the Bouguer anomalies are strongly positive on the oceans, +250 to +380 mgal, depending on the depth of the ocean, whereas the isostatic anomalies are close to zero.

## REFERENCES

1. Airy, G. B.: On the computations of the effect of the attraction of the mountain masses as disturbing the apparent astronomical latitude of stations in geodetic surveys, *Trans. Roy. Soc. (London)*, ser. B, vol. 145, 1855.
2. Bonsdorff, I.: *Détermination d'attractions locales sur les points astronomiques du réseau russe au Spitzberg, Mesure d'un arc de méridien au Spitzberg*, vol. 1, sec. 4B, 1905.
3. Boscovich, R. J.: *De litteraria expeditione per pontificiam ditionem*, p. 475, 1750.
4. Bouguer, Pierre: *La figure de la terre*, p. 364, Paris, 1749.
5. Bowie, William: Investigations of gravity and isostasy, USCGS, Spec. Publ., no. 40, 1917.
6. ———: Isostatic investigations and data since 1915, USCGS, Spec. Publ., no. 99, 1924.
7. ———: *Isostasy*, Dutton, New York, 1927.
8. Cizancourt, H. de: Deep tectonics and isostasy, *Am. J. Geol.*, vol. 59, no. 1, 1951.
9. Daly, Reginald A.: Strength and structure of the earth, Prentice-Hall, Englewood Cliffs, N.J., 1940.
10. Delaney, John P.: Leonardo da Vinci on isostasy, *Science*, vol. 91, p. 546, 1940.
11. Dutton, C. E.: On some of the greater problems of physical geology, *Bull. Wash. Phil. Soc.*, ser. B, vol. 11, pp. 51–64, 1889.
12. Hayford, J. F.: The figure of the earth and isostasy, from measurements in the United States, USCGS, 1909.
13. ———: Supplementary investigation in 1909 of the figure of the earth and isostasy, USCGS, 1910.
14. ——— and William Bowie: The effect of topography and isostatic compensation upon the intensity of gravity, USCGS, Spec. Publ., no. 10, 1912.
15. Heiskanen, W. A.: Untersuchungen über Schwerkraft und Isostasie, *Publ. Finn. Geod. Inst.*, no. 4, 1924, or *Investigations regarding gravity and isostasy*, *Geol. Survey India*, for department use, 1928.
16. ———: Tables isostatiques pour la réduction dans l'hypothèse de Airy des intensités de la pesanteur observées, *Bull. géod.*, no. 30, 1931.
17. ———: Investigations on the gravity formula, *Publ. Isos. Inst. IAG (Helsinki)*, no. 1, 1938.
18. ———: Die Erdkrustendicke und die Schwereanomalien in den Vereinigten Staaten, *Ann. Acad. Sci. Fenniae*, ser. A, no. 35, 1932.
19. ———: Das Problem der Isostasie, chap. 45 in B. Gutenberg (ed.), *Handbuch der geophysik*, Absch. 12, Bd. 1, Lief. 4, Borntraeger, Berlin, 1936.
20. Helmert, F. R.: Die Tiefe der Ausgleichsfläche bei der Prattschen Hypothese für das Gleichgewicht der Erdkruste und der Verlauf der Schwerestörung vom Innern der Kontinente und Ozeane nach den Küsten, *Sitzber. Kgl. preuss. Akad. Wiss.*, no. 48, p. 1192, 1909.
21. ———: Die Schwerkraft und die Massenverteilung der Erde, *Enzyklopädie der mathematischen Wissenschaften*, vol. 6, fig. 1.7, 1910.
22. Lehner, Mariette: Beiträge zur Untersuchung der isostatischen Kompensation der schweizerischen Gebirgsmassen, *Verhandl. schweiz. naturforsch. Ges.*, 1930.
23. Niskanen, Erkki: On the deformation of the earth's crust under the weight of a glacial ice-load and related phenomena, *Publ. Isos. Inst. IAG (Helsinki)*, no. 12, 1945.
24. Pratt, J. H.: On the attraction of the Himalaya Mountains and of the elevated regions beyond upon the plumb-line in India, *Trans. Roy. Soc. (London)*, ser. B,

- vol. 145, 1855; other studies of Pratt's are printed in *Trans. Roy. Soc. (London)*, ser. B, vol. 149, pp. 745, 779, 1859; vol. 161, p. 335, 1871.
25. Putnam, G. R.: Relative determinations of gravity with half-second pendulums and other gravity investigations with notes on geologic formations by G. K. Gilbert, USCGS, Rept., 1894, appendix 1.
26. ———: Results of transcontinental series of gravity measurements, *Bull. Wash. Phil. Soc.*, vol. 13, no. 61, 1895.
27. Schiøtz, O. E.: Results of the pendulum observations and some remarks on the constitution of the earth's crust, in Fridjof Nansen, *The Norwegian North Polar Expedition 1893–1896*, vol. 8, London, 1900; *Die Schwerkraft auf dem Meere längs dem Abfall der Kontinente gegen die Tiefe*, Christiania, 1907.
28. Vening Meinesz, F. A.: Une nouvelle méthode pour la réduction isostatique régionale de l'intensité de la pesanteur, *Bull. géod.*, no. 29, 1931.
29. ———: Tables fondamentales pour la réduction isostatique régionale, *Bull. géod.*, no. 63, 1939.
30. ✓——: Tables for regional and local isostatic reduction (Airy system) for gravity values, *Publ. Neth. Geod. Comm.*, Waltman, Delft, 1941.
31. Lambert, W. D., and F. W. Darling: Tables for determining the form of the geoid and its indirect effect on gravity, USCGS, Spec. Publ., no. 199, 1936.

## CHAPTER 6

### REDUCTION OF THE GRAVITY MEASUREMENTS

#### 6-1. Nonisostatic Reductions

Gravity surveys give as good gravity values as can be obtained by the methods used at present. The pendulum method yields an accuracy of 1 to 2 mgal on the continents and 3 to 4 mgal at sea. Most modern gravimeters have an accuracy of about 0.1 mgal, and in local surveys it is still higher.

Since gravity measurements are carried out at different points—some of them in low, level lands, others in mountains, and some at sea—they are



FIG. 6-1. Since the acceleration of gravity has been measured at mountain (elevation  $h$ ), lowland, and ocean stations in different conditions, the gravity values  $g_1$ ,  $g_0$ ,  $g_2$  cannot be compared with each other until they have been reduced to sea level.

not comparable. For example, on a mountaintop (Fig. 6-1) the gravity  $g_1$  must be smaller than  $g_0$  in the level lands at the same latitude because mountain stations are farther from the earth's center of gravity than the lowland stations are. At sea the gravity  $g_2$  is—or at least ought to be—smaller than on the continents, for the density of sea water is less than that of the earth's crust.

Before we use the observed gravity values for practical purposes or for theoretical studies, we must reduce them in a proper way to the same level, usually to sea level or geoid. Depending upon how accurately and in what manner we consider the attraction effect of the visible-mass anomalies and the other smaller effects, we have the following different reductions:

- Free-air reduction
- Bouguer reduction with terrain correction
- Helmholtz condensation reductions
- Rudzki inversion reduction

Isostatic reductions:

1. Pratt-Hayford reduction
2. Airy-Heiskanen reductions
3. Vening Meinesz reductions

Geological and isostatic geological corrections

Indirect effect, or Bowie reduction

#### A. Free-air Reduction

Free-air reduction is so named because it takes account only of the elevation of the station and not the mass between the station and sea level (Fig. 6-2); the result is the same as if the pendulum or gravimeter were in free air  $h$  m above sea level.

If we consider only the main term of gravity  $g$ , we obtain the following value for gravity at sea level

$$g_0 = k \frac{M}{R^2} \quad (6-1)$$

where  $M$  = mass of earth

$R$  = radius of curvature of earth

$k$  = gravitational constant

The gravity  $g$  at point  $P$ ,  $h$  m above point  $P_0$ , is equal to

$$g = k \frac{M}{(R+h)^2} = k \frac{M}{R^2} \left(1 - 2 \frac{h}{R} + 3 \frac{h^2}{R^2} - \dots\right) \quad (6-2)$$

$$\text{or} \quad g = g_0 \left(1 - 2 \frac{h}{R} + 3 \frac{h^2}{R^2} - \dots\right) \quad (6-2)$$

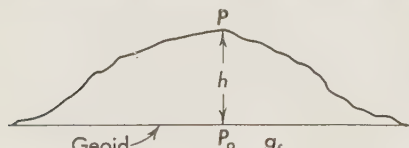
Thus, the free-air reduction  $g_0 - g$ , or  $g_f$ , is

$$g_f = g_0 - g = 2 \frac{g_m}{R_0} h \left(1 - \frac{3}{2} \frac{h}{R_0} + \dots\right) \quad (6-3)$$

In general, we mean by  $g_m$  the average gravity value and by  $R_0$  the average

radius of curvature of the earth, so that the factor  $2g_m/R_0$  is constant, but in practice instead of these average values we must use the actual values  $g_0$  and  $R$  at the gravity station. The combined effect of the change of  $g_0$  and  $R$  with the latitude, however, is small, according to Lambert,<sup>33</sup> only 0.07 per cent of the main term.

FIG. 6-2. Free-air reduction. In this reduction only the elevation  $h$  of the observation point  $P$  has been considered. This reduction is positive because the gravity at  $P_0$  of the geoid is larger than at  $P$ .



The second term of the expression for  $g_f$  can be neglected, except in altitudes of over 2000 m. For instance, for  $h = 5000$  m, the influence of the second term is 1.7 mgal, but for  $h = 2000$  m, 0.3 mgal, and for  $h = 1000$  m, only 0.07 mgal. So we can safely use, except in high mountains, the following numerical values for the free-air reduction  $g_f$ :

$$g_f = +0.3086h \text{ mgal} \quad h \text{ in meters}$$

$$= 0.09406h \text{ mgal} \quad h \text{ in feet}$$

Table 6-1 gives the free-air reduction  $g_f$  in milligals as a function of the gravity-station height  $h$  in meters.

TABLE 6-1. SOME VALUES OF THE FREE-AIR REDUCTION

$h, m$	$g_f, \text{mgal}$	$h, m$	$g_f, \text{mgal}$	$h, m$	$g_f, \text{mgal}$
10	3.1	500	154.3	3000	925.8
50	15.4	1000	308.6	4000	1234.4
100	30.9	2000	617.2	5000	1543.0

Although the latitude effects of  $g$  and  $R$  nearly cancel each other, there may be *local* disturbing masses causing the actual curvature  $1/R$ , which should be used, to differ considerably from the mean radius of curvature  $1/R_0$ . To consider this effect we must, of course, be able to estimate the actual curvature  $R$ , which can be computed when we know the relative deflections of the vertical  $\xi$ .

If, for instance,  $\xi = 10''$  at two points  $A$  and  $B$  31 km apart and in opposite directions, and if we assume the geoid fraction  $AB$  (Fig. 6-3) to be a circle arc, we get the actual radius of curvature  $R$  as follows. If  $R_0$  is the mean radius of curvature,  $v_0$  the mean and  $v$  the actual angle, and  $l$  the arc  $AB$ , we easily get

$$R_0 = \frac{l}{v_0} \quad \text{and} \quad R = \frac{l}{v_0 + 2\xi} \quad (6-4)$$

Therefore, the approximate value of  $R$  is

$$R = \frac{l}{v_0(1 + 2\xi/v_0)} \quad \text{or} \quad R = R_0 \left(1 - \frac{2\xi}{v_0}\right) \quad (6-5)$$

As  $l = 31$  km corresponds to the value  $v_0 = 1000''$ , we have  $2\xi/v_0 = 0.02$ . In this event, as often happens in high mountains,  $R$  would be 2 per cent shorter than  $R_0$ .

One method for determining the relative deflections of the vertical might

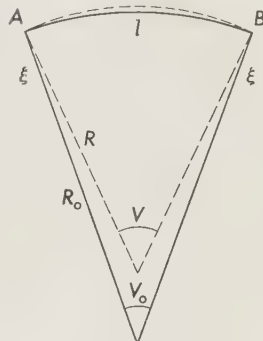


FIG. 6-3. If in the mountain  $AB$  or under it there is material that is too heavy, which causes deviation of the geoid and deflections of the vertical, the radius of curvature is too small and the free-air reduction too large.

be to measure the reciprocal vertical angle observed at pairs of observation points. Kobold's measurements<sup>31</sup> in 1951 on Alpine mountaintops show that such measurements take a long time and can be used only for high mountaintops between which the light trace goes far out from the earth's surface. Since the gravity stations to be reduced are seldom on high mountaintops, generally being along highways, the method is not suitable for this purpose.

The actual curvature can also be derived from local gravity measurements if a sufficiently good local gravity-station net exists, which seldom is true in rugged mountains. Torsion-balance measurements can hardly be used because the effect of the rough topography around most stations is too great and cannot be considered with sufficient accuracy for analysis of the variometer measurements. Nor can the actual curvature obtained be extrapolated very far from the point where it has been estimated, because it changes rapidly in the mountains, as shown by the rapid change in the deflections of the vertical from point to point. On high plateaus, e.g., those in Arizona, it would be possible to compute the actual curvature because there it is not too difficult to carry out a local gravity survey. On plateaus, however, the actual curvature generally does not differ very much from the average curvature at the corresponding latitude.

Because of all these difficulties in estimating the actual curvature, and because the difference between actual and mean curvature is, in most cases, only very slight, it seems best, in free-air reduction, to use the same coefficient, 0.3086, everywhere in order to avoid confusion.<sup>26</sup> Where observational material permits, small corrections between the average and the actual curvature can be added at the gravimetric analyzing institutes.

In general, however, this effect can be neglected, because either the elevation  $h$  of station or the difference between  $R$  and  $R_0$  or both are small. Occasionally, however, the effect is considerable. If the curvature used is 3 per cent too small or too large (values which de Graaff Hunter<sup>14</sup> believes possible), the reduction of gravity from a station 3000 m high would be not less than 28 mgal wrong.

The free-air reduction is often called Faye's reduction after the man who called attention to it. The correction is positive on the continents, with exception of areas like the Caspian and Dead Sea regions and Death Valley, which are of negative height. This kind of reduction was frequently used in the eighteenth century and at the beginning of the nineteenth; important work of Stokes and Faye was based on it. It must always be applied to obtain the gravity at sea level, generally called  $g_0$ .

### B. Bouguer Reduction

Besides the attraction of the earth mass below the geoid surface—assuming it to be concentrated at the earth's center is a close enough approxima-

tion because the shape of the earth is so close to being a sphere—the mass between the geoid and the observation point exerts an influence on the observed gravity. Therefore the attraction of this additional mass must be subtracted from the observed gravity values. Imagine a horizontal plane through the point  $P$ , so that there is a plate between the point  $P$  and the geoid. The attraction  $dK$  of the mass element  $dm$  on  $P$  can be obtained easily when the cylindrical coordinates  $r$ ,  $A$ , and  $z$  are used. It is

$$dK = k \frac{dm}{d^2}$$

where  $d$  is the distance of  $dm$  from point  $P$ .

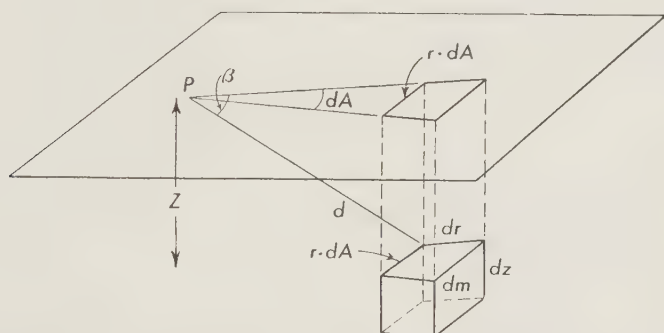


FIG. 6-4. Derivation of the Bouguer reduction. The vertical attraction of the mass element is computed at  $P$ .

The mass element is obviously (Fig. 6-4)  $dm = \rho r dr dA dz$ , where  $\rho$  is the density of the mass element.

We get for  $dK$  the expression

$$dK = k\rho \frac{r dr dA dz}{d^2} \quad (6-6)$$

The vertical component  $dZ$  of this attraction is

$$dZ = dK \cos \beta = k\rho \frac{dA z dz r dr}{d^3}$$

$$\text{or } dZ = k\rho \frac{dA z dz r dr}{(r^2 + z^2)^{\frac{3}{2}}} \quad (6-7)$$

because  $d^2 = r^2 + z^2$

If we integrate this expression between the limits  $0 < A < 2\pi$ ,  $r_1 < r < r_2$ , and  $h_1 < z < h$ , we get the vertical attraction  $Z$  of a cylindrical ring with

the radii  $r_1$  and  $r_2$  and the height  $h - h_1$  at the point  $P$  (Fig. 6-5) when  $P$  lies  $h_1$  m above the upper surface of the cylinder. Therefore,

$$Z = k\rho \int_0^{2\pi} dA \int_{h_1}^h z dz \int_{r_1}^{r_2} \frac{r dr}{(z^2 + r^2)^{\frac{3}{2}}}$$

Integration results in

$$Z = 2\pi k\rho \int_{h_1}^h z dz \left( \frac{1}{\sqrt{z^2 + r_1^2}} - \frac{1}{\sqrt{z^2 + r_2^2}} \right) \quad (6-8)$$

If this equation is integrated between the boundaries  $h$  and  $h_1$ , we obtain

$$Z = 2\pi k\rho (\sqrt{r_1^2 + h^2} - \sqrt{r_1^2 + h_1^2} - \sqrt{r_2^2 + h^2} + \sqrt{r_2^2 + h_1^2}) \quad (6-9)$$

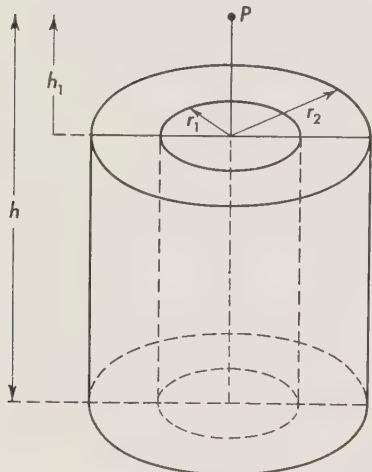


FIG. 6-5. To determine the Bouguer reduction the topography around the gravity station is distributed in circular cylinders, and the effect of these cylindrical rings is computed.

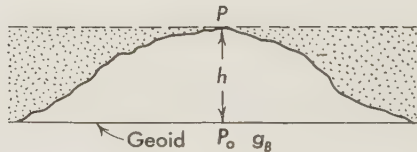


FIG. 6-6. Terrain correction at a mountaintop station. As the Bouguer plate also subtracts the nonexistent mass of the hatched area, a positive correction is needed.

If, instead, we substitute  $r_1 = 0$ ,  $r_2 = \infty$ , and  $h_1 = 0$  in Eq. (6-8), we get for the vertical attraction  $Z'$  of the infinite horizontal rock layer of thickness  $h$  (Fig. 6-6) the expression

$$Z' = 2\pi k\rho \int_0^h \frac{z dz}{z} = 2\pi k\rho h \quad (6-10)$$

We still have to eliminate from Eqs. (6-8) and (6-10) the gravitational con-

stant  $k$ , using the gravity  $g$ , which is approximately

$$g = k \frac{M}{R^2} = \frac{4}{3}\pi k \rho_m R \quad (6-11)$$

where  $M$  = mass of the earth

$R$  = its radius

$\rho_m$  = its mean density

Thus we get

$$Z' = \frac{3}{2} \frac{\rho}{\rho_m} \frac{g}{R} h \quad (6-12)$$

The expressions  $Z'$  and  $Z$  must be subtracted from the observed gravity value. If we combine  $-Z'$  with the free-air reduction, we get for the sum of the free-air reduction  $g_f$  and the simplified Bouguer reduction  $g'_B$  the expression

$$g_f + g'_B = 2 \frac{g}{R} h - \frac{3}{2} \frac{\rho}{\rho_m} \frac{g}{R} h$$

$$\text{or } g_f + g'_B = 2 \frac{g}{R} h \left(1 - \frac{3}{4} \frac{\rho}{\rho_m}\right) = \left(1 - \frac{3}{4} \frac{\rho}{\rho_m}\right) g_f \quad (6-13)$$

We get different numerical values for this reduction according to the values used for  $\rho$  and  $\rho_m$ ; e.g., for  $\rho = 2.67$  and  $\rho_m = 5.576$ , the values Hayford used, we get

$$g_f + g'_B = (0.3086 - 0.1108)h \text{ mgal} = 0.1978h \text{ mgal} \quad h \text{ in meters} \quad (6-14)$$

The values  $\rho = 2.80$  and  $\rho_m = 5.52$  give

$$g_f + g'_B = (0.3086 - 0.1174)h \text{ mgal} = +0.1912h \text{ mgal} \quad h \text{ in meters}$$

and the values  $\rho = 2.67$  and  $\rho_m = 5.53$  give

$$g_f + g'_B = (0.3086 - 0.1118)h \text{ mgal} = +0.1968h \text{ mgal} \quad h \text{ in meters} \quad (6-15)$$

The effect of the Bouguer's plate diminishes the effect of the free-air reduction by about one-third.

This reduction was originated by Bouguer,<sup>2</sup> who derived the formula in his work "La figure de la terre" in 1749. He used this reduction to compare the gravity values observed on the plateau of Quito and the neighboring seacoast of Peru. First mention of the general reduction problem was made in 1819 by Thomas Young<sup>37</sup> in a letter to Captain Kater. He gave, for an extensive tableland, a reduction formula which is about the same as the Bouguer formula. Poisson<sup>44</sup> also arrived at this formula in 1833.

### C. Terrain Correction

Since the Bouguer reduction assumes level surroundings of the station, topographic irregularities around the station still have to be considered. In other words, a "terrain correction" (in German, *Geländereduktion*) has to be computed; it is necessary because of gravity variations, e.g., that between a mountaintop and the surface of an equally high plateau. Since the surrounding crust does not rise to the height of a mountaintop station (Fig. 6-6), a positive correction has to be made.

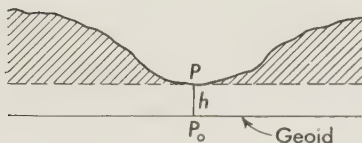


FIG. 6-7. Terrain correction at a valley station. As the mass (hatched area) above the gravity station diminishes the gravity, terrain correction is also positive at valley stations.

sections, estimating the height of the terrain from maps, and calculating the attraction of each part with the help of formulas.

Table 6-2, giving the terrain correction at several stations, shows that,

TABLE 6-2. TERRAIN CORRECTION  $g' - g$  AT SELECTED STATIONS  
( $g' - g$  always positive)

Station	$h$ , m	$g' - g$ , mgal	Station	$h$ , m	$g' - g$ , mgal
Mont Blanc.....	4807	123	Pikes Peak.....	4293	48
Chamonix.....	1050	46	Mauna Kea, Hawaii.....	3981	36
Fuji-no-Yama....	3792	119	Säntis, Switz....	2500	64
Etna, Italy.....	2943	52	Rigi, Switz.....	1784	40
Sonnblick, Germ.	3099	52			

although the terrain correction can be ignored in level lands, it can reach considerable values on cone-shaped mountaintops, on oceanic islands, and in mountain chains and therefore must be considered.

Although the terrain correction farther from the station is small, it too cannot be neglected, and ideally it should be reckoned out to the Hayford zone O (166.7 km from the station).

To avoid confusion about the Bouguer reduction, all gravimetric publications should state how far from the station the effect of the topographic masses and the terrain correction have been computed.

When all three corrections are considered, viz., the effect of the Bouguer plate, the terrain correction, and the effect of the earth's curvature, the result is the "expanded Bouguer reduction"

$$g_B = -\frac{3}{2} \frac{\rho}{\rho_m} \frac{g}{R} h + (g' - g) + b \quad (6-16)$$

To get the Bouguer anomalies the free-air reduction  $g_f$  must be added.

Although the Bouguer reduction records both the effect of station elevation and the attraction of the visible masses, Bouguer gravity anomalies are close to zero only at lowland stations. In mountains they are generally strongly negative and on the oceans still more positive. This apparent contradiction results from the fact that the attraction of the isostatically compensating masses has not been considered.

The Bouguer gravity anomaly  $\Delta_B g$ , or  $g''_0 - \gamma$ , is

$$\Delta_B g = g + g_f + g_B - \gamma$$

where  $g$  and  $\gamma$  are the observed and theoretical gravity, respectively.

*Gravitational constant k and the mean density  $\rho_m$  of the earth.* Since the gravitational constant  $k$  and the mean density  $\rho_m$  of the earth appear frequently in the equations of mechanics, physics, geodesy, and astronomy (they occur frequently in the formulas of this chapter), there have been many attempts to measure these important constants as accurately as possible.<sup>10</sup> The results are listed in Table 6-3. The determinations of

TABLE 6-3. OBSERVED VALUES OF  $k$  AND  $\rho_m$

Author	Year	$k \times 10^{-8}$ , cgs units	$\rho_m$
Von Jolly.....	1878-1881	6.465	5.692
Richarz and Krigar-Menzel..	1898	6.685	5.505
Poynting.....	1891	6.698	5.493
Cavendish.....	1798	6.754	5.448
Reich.....	1838	.....	5.49
	1852	.....	5.58
Baily.....	1841-1842	.....	5.6747
Boys.....	1895	6.6576	5.5270
Braun.....	1896	6.6579	5.5275
Burgess.....	1901	6.64	5.55
Eötvös.....	1896	6.65	5.53
Heyl.....	1930	6.670	
Heyl and Chrzanowski.....	1942	6.673	
Zahradnicek.....	1933	6.659	

Boys, Braun, Heyl, Zahradnicek, and Heyl and Chrzanowski are considered the most significant. The value of  $k$  obtained by Heyl and Chrzanowski

$$k = 6.673 \pm 0.003 \times 10^{-8} \text{ cm}^3 \text{ g}^{-1} \text{ sec}^{-2}$$

might be most reliable.

The relative accuracy of the gravitation constant  $k$  is therefore only 1:2000, which is quite poor. Fortunately, the other quantities concerning the gravity field of the earth, like gravity itself, can be measured with a much higher accuracy. A measuring accuracy of 0.1 mgal of gravity differences corresponds to the relative accuracy of  $10^{-7}$  in measuring  $g$ . Unfortunately, the accuracy of absolute gravity measurements is much lower, only of the order 3 mgal, and the accuracy of the equatorial gravity value, obtained from the gravity formula, is of the same order, which means that the relative accuracy of the gravity is  $3 \times 10^{-6}$ . As the technique of absolute gravity measurements improves, even an accuracy of 1:1,000,000 can soon be obtained.

#### D. Condensation and Inversion Reduction Methods

The most important geodetic application of gravity anomalies is the determination of the shape of the geoid. According to Green's theorem the potential of the earth along the geoid surface can be determined, and, consequently, the form of geoid can be determined from the gravity anomalies

measured at this surface if all masses exterior to the geoid are thought of as being transferred either to infinity or to within the geoid. From the practical point of view, the mass must be transferred so that the shape of the geoid is changed as little as possible.

Since the Bouguer reduction causes large changes in the geoid (in some places as much as 500 m), the shape of the geoid will be illusory if Bouguer anomalies are applied. To avoid this drawback Stokes, and later Helmert, introduced the con-

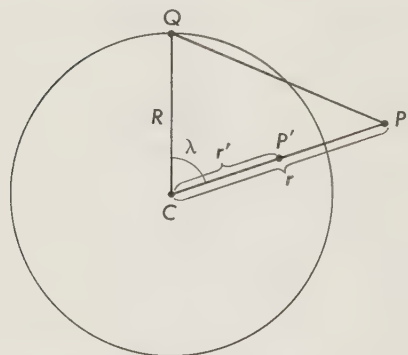


FIG. 6-8. Principle of Rudzki's inversion reduction method.

densation reduction. In this reduction the masses above the geoid are transferred inside the geoid and as close to it as possible, the best method being to transfer the masses to the actual geoid surface in the form of a coating, or "Ideelle störende Schicht," as Helmert<sup>28</sup> calls it. After this transformation we get an "ideal geoid," which differs from the actual geoid by only a few meters (never more than 3 m). The series of the po-

tential function also converges despite Helmert's original doubts about the success of his method. The condensation method will be used now in this form.

It is easy to see that the condensation reduction actually corresponds to isostatic reduction with zero depth of compensation: the success of the method depends on this very fact. Condensation reduction has not been widely used, however, because the usual isostatic reductions come closer to the real distribution of the masses in the earth's crust and those under it.

In the inversion method, which was developed by the Polish scientist Rudzki<sup>41</sup> in 1905, and which is similar to the condensation method, the masses are manipulated so that the geoid surface does not change at all. The procedure is as follows (Fig. 6-8). A mass element  $dm$  at a point  $P$  outside the geoid is replaced by the mass element  $dm'$  at a point  $P'$  inside the geoid and in the line  $PC$ . The potential  $V$  of the mass  $dm$  at the point  $Q$  of the geoid is

$$V = \frac{k dm}{\sqrt{r^2 + R^2 - 2rR \cos \lambda}}$$

and the potential  $V'$  of the transferred mass element  $dm'$  at  $Q$  is

$$V' = \frac{k dm'}{\sqrt{R^2 + r'^2 - 2r'R \cos \lambda}}$$

where  $r = CP$

$r' = CP'$

$R = CQ$

$\lambda = \text{angle } QCP$

Since it is required that the potential remain unchanged,  $V$  must be equal to  $V'$ , and thus

$$\frac{dm}{r} \frac{1}{\sqrt{1 - 2(R/r) \cos \lambda + R^2/r^2}} = \frac{dm'}{R} \frac{1}{\sqrt{1 - 2(r'/R) \cos \lambda + r'^2/R^2}} \quad (6-17)$$

By changing the form in which this equation is written it can be shown that Formula (6-17) is satisfied when, simultaneously,

$$dm' = \frac{R}{r} dm \quad \text{and} \quad r' = \frac{R^2}{r} \quad (6-18)$$

The advantage of this reduction, viz., that the geoid remains unchanged, is offset by the fact that, since the mass element  $dm'$  is a little smaller than the mass element  $dm$ , there remains a small part of the topographic mass which is not transferred inside the geoid surface.

Kladivo,<sup>30</sup> Lambert, and Gromov<sup>15</sup> have suggested the use of this method in geoid computation, but since the isostatic reductions, although more time-consuming, lead to a better result, the inversion method has not been widely used.

### E. Reduction of Gravity Measurements at Sea

As most gravity measurements at sea have been made in submarines some tens of meters below sea level, their reduction differs in several respects from the reduction of land observations.

First to be considered is the Eötvös effect, caused by the centrifugal force increasing and the gravity-diminishing influence of the west-east velocity of the submarine. If  $\omega = 2\pi/T = 0.00007292 \text{ sec}^{-1}$ , where  $T$  is the sidereal day, and  $\omega$  is the angular velocity of the earth, the centrifugal acceleration  $c$  is

$$c = \omega^2 r \quad \text{and} \quad dc = 2\omega r d\omega \quad (6-19)$$

where  $r$  is the radius of the latitude circle of the observation point at latitude  $\varphi$ . The corresponding change of gravity is

$$dg = -dc \cos \varphi = -2\omega \cos \varphi r d\omega$$

If the linear west-east velocity component of the submarine is  $v$ ,  $v = r d\omega$ , the change in the acceleration of gravity will be

$$dg = -2\omega \cos \varphi v \quad (6-20)$$

For  $v = 8 \text{ km/hr}$ , the Eötvös correction is  $dg = -32 \cos \varphi \text{ mgal}$ . To get an accuracy of 1 mgal the hourly west-east velocity of the submarine must be known to an accuracy of  $250/\cos \varphi \text{ m/hr}$ . Since, because of the more or less unknown ocean currents, such accuracy is hardly possible, the Eötvös effect may be the largest error source in gravity measurements at sea. The only way to avoid this error is to use underwater gravimeters, but their use is restricted to shallow waters.

Next to be considered are (1) the reduction to sea level which includes the normal free-air reduction, and which equals  $-0.3086d$ , where  $d$  is the observation depth, and (2) the Bouguer reduction, which considers the effect of the water layer above the submarine; it is equal to the attraction of this mass and must be taken with opposite signs. Together these reductions give the correction

$$-0.3086 \left( 1 - \frac{3}{4} \frac{1.027}{\rho_m} \right) d$$

If we wish to apply the Bouguer reduction, i.e., to adjust for the fact that the density of water (1.027 for sea water and 1.00 for fresh) is smaller than

the density of the earth's crust, we have to take into account the attraction of the layer of thickness  $d$  and density  $\rho = 1.027$ . When we add this reduction and the Eötvös effect, the whole reduction of gravity measurements at sea is<sup>24</sup>

$$-0.3086 \left( 1 - \frac{3}{4} \frac{1.027}{\rho_m} \right) d + 0.3086 \frac{3}{4} \frac{\rho - 1.027}{\rho_m} t' + 2\omega \cos \varphi v \quad (6-21)$$

where  $\rho_m$  is the mean density of the earth and  $t'$  the depth of the ocean.

Applying all these reductions, we get the Bouguer gravity anomalies at sea, which are comparable with the Bouguer anomalies on the continents.

If the ocean bottom in the neighborhood of the gravity point is very rugged, we still have to add the terrain correction, but it can generally be neglected except at the seacoast and close to islands where it can be as much as 30 mgal.

## 6-2. Isostatic Reductions

Since the topographic masses seem to be in isostatic equilibrium, as we have seen, application of isostatic reduction methods to the observed gravity anomalies is also of basic importance. Although several isostatic assumptions have been formulated, only the three that have been extensively used in gravimetric studies, viz., the Pratt-Hayford, Airy-Heiskanen, and Vening Meinesz isostatic systems, will be handled in detail.

### A. Pratt-Hayford Reduction

On the basis of the Pratt-Hayford isostatic system, Hayford,<sup>20</sup> Bowie,<sup>3a</sup> and others have derived the required reduction formulas and computed the associated reduction tables.

If  $\rho$  is the density of the mountain,  $h$  its height and  $D^*$  the depth of compensation, then the negative density of the corresponding mass defect equals

$$\Delta\rho = -\frac{h}{D} \rho \quad (5-1)$$

To compute the effect on the gravity station of the topography and the corresponding compensation over the whole earth Hayford introduced a system of circular zones with the radii given in Table 6-4. For each zone he computed the vertical attraction exerted by the topography and the isostatic compensation. Starting with the formulas for the zones near the station, if the radii of the cylinder are  $r_1$  and  $r_2$  and the computation point is at the axis of the cylinder  $h_1$  m above the upper and  $h$  m above the lower

\* Hayford's  $T$  has been replaced by  $D$  (depth) to reserve  $T$  for the thickness of the earth's crust.

surface of the cylinder, Formula (6-9) gives the formulas for the determination of the influences  $Z_t$  of the topographic mass and  $Z_c$  of the compensating mass deficiency within the circular cylinder

$$Z_t = 2\pi k\rho(\sqrt{r_1^2 + h^2} - \sqrt{r_1^2 + h_1^2} - \sqrt{r_2^2 + h^2} + \sqrt{r_2^2 + h_1^2}) \quad (6-22)$$

$$Z_c = -2\pi k \frac{h}{D} \rho(\sqrt{r_1^2 + D^2} - \sqrt{r_1^2 + h_1^2} - \sqrt{r_2^2 + D^2} + \sqrt{r_2^2 + h_1^2}) \quad (6-23)$$

Since the compensating effect is assumed to begin from the earth's physical surface, and since  $h_1$ , in the vicinity of the station, is generally small compared with  $r_2$ , we can put  $h_1 = 0$  without committing a serious error. Then we get

$$Z_t = 2\pi k\rho(\sqrt{r_1^2 + h^2} - \sqrt{r_2^2 + h^2} - r_1 + r_2) \quad (6-24)$$

$$Z_c = -2\pi k\rho \frac{h}{D} (\sqrt{r_1^2 + D^2} - \sqrt{r_2^2 + D^2} - r_1 + r_2) \quad (6-25)$$

The small effect of the omissions of  $h_1$  is considered in special correction tables.

For determining the topographic elevation each zone is divided into sectors, or compartments, and the height of each compartment is estimated. If a zone is divided, say, into 10 compartments and the attraction effect of each compartment is computed, the factor  $\pi k\rho/5$  has to be used in Formulas (6-24) and (6-25) instead of  $2\pi k\rho$ .

Hayford<sup>20</sup> computed tables wherein the effects of topography and isostatic compensation of each compartment are given as functions of the height of the compartment. Table 6-4 gives the outer radii and number of compartments in each Hayford zone. As a great many stations have already been reduced by Hayford's method, the circular-ring division is still used, but in general the division into compartments has not been maintained.

For an ocean with depth  $h'$  the negative influence of the mass deficiency of the ocean water and the positive influence of the compensating mass excess underneath the ocean must be considered. Since Hayford used the value 2.67 for  $\rho$ , and since the density of the ocean water is 1.027, the density of the mass deficiency of the ocean is  $\rho' = -(2.67 - 1.027) = -1.643$ , and the density  $\Delta\rho'$  of the compensating mass excess underneath the ocean level equals  $+1.643(h'/D)$ , where  $D$  again stands for the depth of compensation. Therefore  $\Delta\rho' = 0.615\Delta\rho$ .

TABLE 6-4. HAYFORD ZONES AND COMPARTMENTS

Zone	Outer radius, m	Number of compartments	Zone	Outer radius	Number of compartments
A	2	1	18	1°41'13"	1
B	68	4	17	1 54 52	1
C	230	4	16	2 11 53	1
D	590	6	15	2 33 46	1
E	1,280	8	14	3 03 05	1
F	2,290	10	13	4 19 13	16
G	3,520	12	12	5 46 34	10
H	5,240	16	11	7 51 30	8
I	8,440	20	10	10 44	6
J	12,400	16	9	14 09	4
K	18,800	20	8	20 41	4
L	28,800	24	7	26 41	2
M	58,800	14	6	35 58	18
N	99,000	16	5	51 04	16
O	166,700 (1°29'58")	28	4	72 13	12
			3	105 48	10
			2	150 56	6
			1	180 00	1

The effect of topography is, of course, dominant close to the station and decreases (relative to the effect of compensation) with the distance from the station. Depending on the depth of compensation  $D$ , the effects are equal at different distances; e.g., for  $D = 113.7$  they are equal in zone K, radii 12.4 and 18.8 km. Farther from the station the effect of the topography becomes small compared with the effect of the compensation, and very far from the station both effects are again approximately equal. As they have different signs, they eliminate each other almost but not completely, so that the topographic-isostatic reduction must be extended all over the world.

The effect of the zones out to L can be computed from the plane formulas (6-24) and (6-25).

Zones M, N, and O, farther from the station, are, because of the earth's curvature, on the average 500, 1600, and 4500 ft below the horizontal plane through the station. In order to use the plane formula in these zones, Hayford computed a table for the small correction that has to be applied. Outside zone O, i.e., in the numbered zones 18 to 1, spherical formulas must be employed.

Putting  $\alpha$  = angular distance between station  $A$  and compensating mass element  $dm$  at  $B$

$a$  = chord corresponding to angle  $\alpha$

$h$  = depth of compensating mass element

$d$  = chord  $AB$

$R$  = earth's radius (Fig. 6-9)

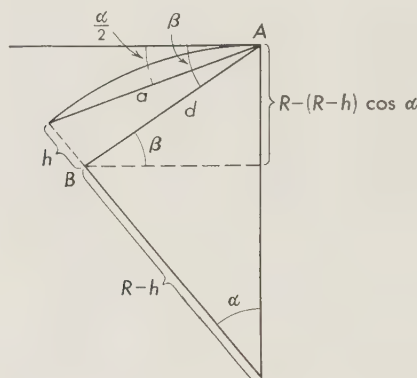


FIG. 6-9. The earth's curvature must be considered in isostatic reduction of Hayford zones 18 to 1.

we easily get for the vertical attraction  $dZ$  of the mass element  $B$  at  $A$

$$dZ = k \frac{\sin \beta}{d^2} dm$$

where

$$d^2 = a^2 + h^2 - 2ah \sin \frac{\alpha}{2}$$

and

$$\sin \beta = \frac{R - (R - h) \cos \alpha}{d}$$

But as

$$R - (R - h) \cos \alpha = R - R \cos \alpha + h \cos \alpha = \frac{a^2}{2R} + h \cos \alpha$$

it is

$$\sin \beta = \frac{a^2}{2R} + h \cos \alpha$$

Then we get

$$dZ = k \frac{a^2/2R + h \cos \alpha}{(a^2 + h^2 - 2ah \sin \alpha/2)^{3/2}} dm = k dm E_C \quad (6-26)$$

where

$$E_C = \frac{a^2/2R + h \cos \alpha}{(a^2 + h^2 - 2ah \sin \alpha/2)^{3/2}}$$

To obtain the attraction  $Z$  which corresponds to the circular-cylinder ring, the above expression would have to be integrated for  $dZ$  with respect to  $\alpha$  and  $h$  (Rainesalo<sup>40</sup>), but the integration is unnecessary because without it we can obtain usable approximate values for  $E$  in each zone.

If  $h$  is the height of the mass element above the *niveau* plane through a station, instead of the depth of the compensating mass element, we have

$$dZ = k \frac{a^2/2R - h \cos \alpha}{(a^2 + h^2 + 2ah \sin \alpha/2)^{\frac{3}{2}}} dm = k dm E_T \quad (6-27)$$

where

$$E_T = \frac{a^2/2R - h \cos \alpha}{(a^2 + h^2 + 2ah \sin \alpha/2)^{\frac{3}{2}}}$$

As the topographic and compensating masses are equal, the sum of the topographic and isostatic reductions in a cylindrical ring will be

$$2\pi k\rho(E_T - E_C) = 2\pi k\rho E_R$$

Hayford computed tables for the quantities  $E_T$ ,  $E_C$ , and  $E_R$  as functions of the angular distance  $\alpha$  from the computation point. Table 6-5 shows part of Hayford's table. For the lettered zones A to O the effects of topography and compensation are given separately, whereas in the outer zones 18 to 1

TABLE 6-5.  $E_T$ ,  $E_C$ , AND  $E_R$  AS FUNCTIONS OF  $\alpha$ <sup>20</sup>

$\alpha$	$E_T \times 10^{20}$	$E_C \times 10^{20}$	$E_R \times 10^{20}$
1.5	+4,674	-96,711	-92,037
2.0	+3,516	-47,164	-43,648
3.0	+2,350	-16,567	-14,217
4.0	+1,764	-7,986	-6,222
5.0	+1,412	-4,658	-3,246
7.5	+941.8	-1,925.9	-984.1
10.0	+706.8	-1,125.8	-419.0
15.0	+472.0	-598.7	-126.7
20.0	+354.79	-409.32	-54.53
30.0	+238.04	-255.10	-17.06
40.0	+180.138	-187.877	-7.739
50.0	+145.784	-150.115	-4.331
60.0	+123.222	-125.994	-2.772
70.0	+107.416	-109.368	-1.952
80.0	+95.8500	-97.326	-1.476
90.0	+87.1314	-88.3089	-1.1775
100.0	+80.4277	-81.4071	-0.9794
140.0	+65.5654	-66.1943	-0.6289
180.0	+61.6112	-62.1664	-0.5552

only the sum is considered. Of course, the farther the zone is from the gravity station, the smaller the value.

Hayford's reduction tables are complete—in fact, too complete in a way. His inclusion of the effect of compartments in different zones but not the effect of the whole zone can cause errors of several milligals even. For instance, his tables of zone G show for the compartment having 500 ft elevation a zero effect but for the 600-ft elevation a 0.1-mgal effect. When zone G has 12 compartments, the tables give, in the first case, the value zero for the effect of the whole zone; in the second case they give 1.2 mgal, which, of course, cannot be right. If Hayford's tables are used, this source of error has to be considered.

Another disadvantage of his tables is the fact that, in the topographic reduction, Hayford computed the elevation of the zones from sea level and not from station level. To find the total effect of the topography in the lettered zones A to O, 199 different quantities, most of them very small, have to be added; besides, their accuracy generally is not high. This drawback can be avoided by first computing the effect, over zones A to O, of the spherical cap having the thickness of the station elevation and then adding to it the terrain correction, which usually is zero, but which can range up to more than 50 mgal in rough mountains (Table 6-2).

This improvement on Hayford's tables was made by Bullard<sup>5</sup> in 1936 and has been used since that time. Bullard's formula is

$$g_B = -1.118h + b + c$$

where the unit of  $g_B$  is 0.1 mgal and that of  $h$  is 1 m. The factor 1.118 corresponds to the values  $\rho = 2.67$ ,  $\rho_m = 5.53$ . It will vary, of course, depending on the values of  $\rho$  and  $\rho_m$  used.

The first term of this formula represents the effect of the Bouguer mass plate. Term  $b$  (Table 6-6) removes the effect of the part of the plate which

TABLE 6-6. CORRECTION  $b$

( $h$  = elevation of station)

$h$ , m	100	200	300	400	500	600	700	800	1000	1500
$b$ , 0.1 mgal	-1	-3	-4	-6	-7	-8	-9	-10	-12	-15

is outside zone O and adds the correction caused by the curvature of the earth. Correction  $c$  is the terrain correction, which usually is small and which can be tabulated for every zone as a function of the difference  $h_z - h_s$ , where  $h_z$  is the average elevation of the zone and  $h_s$  the elevation of the station (Cassini,<sup>8</sup> Bullard,<sup>5</sup> Tanni<sup>43</sup>).

Since the effect of the isostatic compensation is small in the nearest zones, in the tables of Heiskanen<sup>21, 21a</sup> (1931, 1938) and Vening Meinesz<sup>46</sup> (1940),

zones A to I or even A to K have been combined into one zone. For the zones lying farther out, i.e., L to O out, the mean elevation of each zone has been used. The same procedure is used in the numbered zones, for which the combined effect of topography and elevation can be obtained from Hayford's tables.

In Hayford's topographic-isostatic reduction the effects of the topographic-mass anomalies and the compensating invisible-mass anomalies are considered from zone to zone. Therefore this reduction already contains both the Bouguer reduction and the terrain correction, and need be supplemented only by the free-air reduction to obtain the complete reduction. The following reduction formula results:

$$g_i = g + 2 \frac{g}{R} h - \Delta g_t + \Delta g_i \quad (6-28)$$

where  $g$  = observed gravity

$g_i$  = isostatically reduced gravity

$2(g/R)h$  = free-air reduction

$-\Delta g_t$  = topographic reduction

$\Delta g_i$  = isostatic reduction

Of these reductions,  $2(g/R)h$  is positive on the continents,  $-\Delta g_t$  usually negative, and  $\Delta g_i$  generally positive; at sea the relations are, as a rule, reversed.

The isostatic gravity anomalies  $\Delta g$  are, of course,  $g_i - \gamma$ , where  $\gamma$  is the normal gravity derived from the gravity formula used.\*

According to Eq. (6-23), the depth of compensation  $D$  enters into the reduction formula so that we obtain different tables for each value of  $D$ . If we want to determine the corresponding gravity anomalies for different values  $D$  of the depths of compensation, we must compute tables for all of these values of  $D$ . This work was undertaken by Bowie <sup>3a</sup> in 1917. He computed the factors  $F_c = (C_D - C_0)/C_0$  and  $F_R = (R_D - R_0)/R_0$ , which yield, respectively, the compensation  $C_D$  and  $R_D$  for the values  $D = 42.6, 56.9, 85.3, 127.9, 156.2, 184.6$  km if  $C_0$  and  $R_0$  are known. His table shows that the effect of isostatic compensation in the nearest zones and out to zone M is greater for the smaller values of  $D$  than for the larger ones but that the reverse is true from zone M on.

For the depth of compensation  $D$ , Hayford <sup>18</sup> obtained 113.7 km, and

\* Hayford <sup>20</sup> and other Americans add all reductions to  $\gamma$  to obtain the calculated "theoretical" gravity  $g_c$  at the *observation point*, which then gives the gravity anomalies  $g - g_c$ . In other words, they reduce  $\gamma$  to the observation point instead of reducing  $g$  to sea level. Whenever this is done, of course, all corrections of Formula (6-28) are to be used with reversed signs. Naturally, the gravity anomalies will be the same in both cases.

later,<sup>19</sup> 122 km; Helmert,<sup>20</sup> using his mathematical method, obtained 118 km; Bowie,<sup>3a</sup> 96 km; and others, from 80 to 120 km—values that agree fairly well with each other.

This problem, however, will not be discussed further because the common opinion today is that isostatic compensation seldom occurs according to the Pratt-Hayford assumption.

### B. Airy-Heiskanen Reduction

In manner similar to that used in the Pratt-Hayford system, in the Airy-Heiskanen system the effect of compensation of zones A to O is also computed from the plane formula (6-23). The compensating layer under the continental zones begins at depth  $T$  and ends at depth  $T + t$ ; under the ocean zones it begins at depth  $T - t'$  and ends at depth  $T$ ;  $t$  is the thickness of the root of the continental zone,  $t'$  of the antiroot of the ocean zone. For the values  $\rho = 2.67$  and  $\Delta\rho = 0.6$ ,  $t$  is  $4.45h$ , and  $t'$  is  $2.73h'$ , where  $h$  is the elevation of the continental zone and  $h'$  the depth of the ocean zone. If the isostatic assumption is used in terms of the equality of mass,  $t$  and  $t'$  are slightly larger than the basic formulas (5-13) and (5-14) show.

The final formulas for computing the effect of the isostatic compensation of continental zones  $Z_1$  and ocean zones  $Z_2$  are

$$Z_1 = -2\pi k \Delta\rho [\sqrt{r_1^2 + (T+t)^2} - \sqrt{r_1^2 + T^2} + \sqrt{r_2^2 + T^2} - \sqrt{r_2^2 + (T+t)^2}] \quad (6-29)$$

$$Z_2 = +2\pi k \Delta\rho [\sqrt{r_1^2 + T^2} - \sqrt{r_1^2 + (T-t')^2} + \sqrt{r_2^2 + (T-t')^2} - \sqrt{r_2^2 + T^2}] \quad (6-30)$$

where  $r_1$  and  $r_2$  are the inner and outer radii of the cylindrical ring.

For the numbered zones the curvature of the earth's surface has to be considered, as it was in the Pratt-Hayford system, and consequently, the quantities  $E_c$ , and  $E_T$ , and  $E_R$ , obtained from Formulas (6-26) and (6-27) are used; the procedure has already been explained.

On the basis of Formulas (5-8), (5-13), (5-14), (6-29), and (6-30) the author<sup>21</sup> (H.) in 1931 computed topographic-isostatic reduction tables for the thickness  $T$  of the earth's crust, corresponding to zero elevation, for  $T = 40, 60, 80$ , and  $100$  km. Since subsequent isostatic studies showed that the normal thickness  $T$  is between 20 and 40 km, rather than between 60 and 80 km, he computed new reduction tables<sup>21a</sup> in 1938 for the normal thickness  $T = 20, 30$ , and  $40$  km and for 60 km.

The computation was not too difficult because in 1937 Cassinis<sup>8</sup> and his

collaborators, at the request of the International Association of Geodesy, computed fundamental tables adapted for all kinds of isostatic systems. Their tables are based on the Hayford zones (as are all other isostatic computation tables prepared to date) and give (at sea level for unit density) the vertical attraction in 0.01 mgal at the center of the mass rings corresponding to each Hayford zone. The tables extend, at intervals of 1 km, from an elevation of 10 km to a depth of 125 km; furthermore, they give the attraction for depths of 150, 175, and 200 km. Consequently the tables are valid for computations of topographic and isostatic reductions. Since, however, the effect of topography had already been computed by Hayford, and since it is, of course, the same regardless of which isostatic reduction is made, only the tables for the effect of compensation had to be compiled, except in the numbered zones 18 to 10.

To compute tables adapted for practical reduction work we took from Cassinis' tables for different zones the effect of compensation corresponding to unit density and multiplied it by the compensation density 0.6. In the numbered zones 18 to 11 we computed, as usual, the sum of the effect of topography and compensation. Therefore for these zones it was necessary to take the values corresponding to the topography from Cassinis' tables and multiply them by 2.67 and 1.64 for land and ocean compartments, respectively. In addition, we had to take Cassinis' values corresponding to the depth of the upper and lower end of the compensating column, multiply them by 0.6, and find the difference between them.

For zones 10 to 1, the Hayford reduction corresponding to the depth of compensation  $2D$  (in our tables  $T$  is used instead of  $D$ ) is almost identical with the Airy-Heiskanen reduction corresponding to an *average* depth of compensation  $D$ . So there is no need to compute new tables, because the reduction figures can be obtained from the tables of Hayford and Bowie. If  $T$  is the normal thickness of the earth's crust, the average depth of the compensation is  $T + \frac{1}{2}t$ , where  $t$  is the length of the compensating columns, and the depth of compensation corresponding to Hayford's hypothesis is  $2(T + \frac{1}{2}t)$ .

Since, in 1938 and 1952, the Isostatic Institute published isostatic reduction maps<sup>23,39</sup> which give the whole topographic-isostatic reduction of zones 10 to 1, the correction tables for these zones are no longer necessary.

Heiskanen's tables give the isostatic compensation for zones A to G, H, I, J, K, L, M, N, O<sub>1</sub>, and O<sub>2</sub> and the sum of the effect of topography and compensation for zones 18 to 10 for the elevations 0 to 6000 and for the depths 0 to 8000 m. The table interval is 100, 200, or 500 m, depending on the size of the reduction. Hayford's zone O has been divided, as usual, into zones O<sub>1</sub> and O<sub>2</sub>, the outer radii being 132.85 and 166.70 km, respectively. These reduction tables give the effect for zero station elevation; auxiliary tables supply the rather small correction to be added to the zero-

elevation compensation to get the effect of station elevation for elevations of 1000, 2000, 3000, and 4000 m.

*Example.* Land compartment; zone 15;  $h = 1000$  m;  $T = +40$  km. The effect of topography originates in the visible mass between the heights 1 and 0 km, and the compensation occurs at the depth between 40 and 44.510 km, the corresponding  $t$  being 4.510 km. Cassinis' number for zone 15 corresponding to +1 km is -12, which, multiplied by 2.67, makes -32.0. Cassinis' number corresponding to -40 km is +2439, and the one corresponding to -44.510 km is +2943; the difference is +504, which, multiplied by 0.6, makes +302.4. The difference of 302.4 and 32.0 is 270.4, or +2.70 mgal, which is the sum of the effect of topography and compensation for zone 15 when  $h = 1000$  m and  $T = 40$  km.

When the Airy-Heiskanen system in terms of equality of pressure is used, the small corrections mentioned in Chap. 5 must be added.

### C. Vening Meinesz Reduction

On the basis of the formulas derived in Chap. 5, Vening Meinesz computed the necessary tables for practical reduction, which fall into three groups. In the first group are the "Tables fondamentales pour la réduction isostatique régionale,"<sup>45</sup> which make it possible to derive all kinds of reductions and tables for regional isostatic reductions based on some specific assumptions for the manner in which the compensation occurs in a vertical sense. For comparison, the values for local reduction, which are identical with those of Cassinis, Dore, and Ballarin, have been added in the first column.

This group of tables gives the attraction of a cylindrical mass (or, to be more accurate, a truncated conical mass of which the cone's top coincides with the earth's center) reaching from sea level to a depth  $H$  at 1-km intervals from 0 to 60 km. For the first column ( $l = R = 0$ ) the density is assumed to equal unity; for the following columns it is spread according to the curve of Fig. 5-7, up to a distance of the radius of regionality  $R = 2.905l$ . The six columns of the tables thus correspond to the adopted values

$l$ , km	0	10	20	40	60	80
$R$ , km	0	29.05	58.1	116.2	174.3	232.4

The tables give the values up to 0.01 mgal; their internal accuracy corresponds to  $\frac{1}{1000}$  of the value of each figure and generally also of their differences. The somewhat complicated system used in computing these tables and the necessary formulas are dealt with in Vening Meinesz.<sup>46</sup>

The second group of tables corresponds to the general assumptions of the first Airy-Heiskanen tables (1931) for local isostatic reduction, viz., a ho-

mogeneous crust of density 2.67 floating on a substratum of density 3.27. The first column gives the local isostatic reduction for roots below the topography, corresponding to Formulas (6-29, 6-30) and the next five columns give the regional reduction for the values of  $l$  and  $R$ . The tables give values for three crustal thicknesses  $T$  (corresponding to zero elevation), viz.,  $T = 20, 30$ , and  $40$  km.

The sign of the tables is the same as that of Hayford's tables; they give the attraction by the isostatic compensation, which has to be subtracted from the gravity anomaly. The depth for ocean compartments had to be multiplied by  $(2.67 - 1.027)/2.67 = 0.615$  before being entered in the tables as a negative value of  $h$ . The accuracy of the tables is 0.1 mgal.

As in reduction tables of all systems, these tables give only the attraction of the compensation for the zones A to  $O_2$ ; for the numbered zones 18 to 1 they provide the combined effect of the topography and the compensation, and zones A to G have been combined into one, as in Heiskanen's tables. To each table is appended a small table for calculating the effect of the elevation of the station above sea level; for zones 11 to 1 this effect is negligible. For each of zones 10, 9, 8 and the group 7 to 1 the tables provide the combined effect of topography and compensation, not for values of  $h$  but for values of the combined effect  $L$  of the Hayford reduction, which we can read in Heiskanen and Nuotio's maps.<sup>23</sup>

As was true of Heiskanen's tables for local Airy compensation, the effect of the compensation is not proportional to the elevation, and so, in general, the mean elevation of a zone could not be entered in the tables. The simplest way is to follow Heiskanen's method of entering the mean elevation of the land area and of the sea area and combining the two results after each has been multiplied by the ratio, respectively, of the land and sea areas to the total area of the zone. This procedure is certainly allowable for the regional reduction if it is valid for the local reduction.

The purpose of the third group of tables is to facilitate the study of isostasy for two-dimensional topographic features,<sup>48</sup> e.g., the schematized picture of continental coasts and folded mountain ranges. In view of this purpose and in view of the fact that the effect could not be pursued to distances greater than a few hundred kilometers without being too strongly altered by the earth's curvature, the accuracy was not developed further than 1 mgal. As the tables were intended only for isostatic investigations, there was no need to choose small dimensions for the central zones. The system of zones shown in Table 6-7, extending to 350 km on both sides of the station, was used. The tables have been calculated for  $T = 30$  km and for  $R = 0, 20, 40, 60$ , and  $80$  km.

A table for computing the bending of the crust by the topographic load is appended to the main tables. As the bending is proportional to the elevation  $h$  of the topography, only figures for  $h = 1000$  m are given. Unlike

TABLE 6-7

<i>Zone</i>	<i>Boundaries,</i> km	<i>Zone</i>	<i>Boundaries,</i> km	<i>Zone</i>	<i>Boundaries,</i> km
	0		40		150
a	5	g	50	m	170
b	10	h	70	n	190
c	15	i	90	o	230
d	20	j	110	p	270
e	30	k	130	q	310
f	40	l	150	r	350

the tables for regional reduction of gravity, this table gives the complete bending curve, including the outer waves.

#### D. Geological and Isostatic Geological Corrections

The three methods of isostatic reductions we have discussed are the principal ones in use. The values of the thickness  $D$  of the layer of compensation of Hayford's system and of the thickness  $T$  of the homogeneous crust assumed by the Airy-Heiskanen system and by the regional Vening Meinesz system have been adapted to the observed gravity results.

The value of 3.27 usually adopted for the density of the substratum appears acceptable if the substratum is assumed to consist of ultrabasic matter. This assumption is borne out by seismology, and so it seems reasonably safe. The values given for the densities of ultrabasic rocks vary somewhat, but 3.27 is well within the range, although we must consider it to have an uncertainty of a few per cent.

A value of 2.67 is generally adopted for the density of the topography; it may be considered as the mean density of granite, which, according to Birch, Daly, and Douglas, respectively, is 2.667, 2.656, and 2.630.<sup>1</sup>

If, to keep our system of reduction from being complicated, we wish to introduce only one figure for the topography, the adopted one appears not too badly chosen; for part of the topography the density will be less, as is generally true for sediments, but part of it may have greater density, e.g., basalt and gabbro. There is, however, no doubt that in many areas considerable deviations must occur, e.g., where we find thick layers of sediments and especially if the sediments are not consolidated, which may occur on continental shelves and in troughs, as shown by Ewing's recent findings below the Puerto Rico Trough. Such large deviations require a gravity

correction, which, since the necessary data are provided by geology, has been called the "geological correction."

The geological reduction has to comprise all deviations of mass caused by densities different from 2.67, not only for the topographic masses but also below sea level. These mass deviations can be considered in the same light as the topography itself, viz., as mass irregularities in the earth's surface layer. Taking away their attraction has, therefore, the nature of a perfection of the topographic reduction. Attraction graphs or tables are usually needed for application of the geological reduction.

Indications are that these masses can be assumed to be isostatically compensated in the same way as the topography itself and that a corresponding reduction, called the isostatic geological correction, can be applied. The simplest way of applying it is to replace the masses in the same vertical by topographic masses of equal size, to be added to the existing topography. The resulting increase of topographic elevation is obviously given by

$$\Delta_h = \frac{\Delta\rho}{2.67} h_g \quad (6-31)$$

where  $\Delta_h$  is the excess density of the geological mass and  $h_g$  its height in the vertical considered; it is clear that  $\Delta_h$  can be negative as well as positive. The resulting isostatic reduction according to one of the three systems is now easy to derive.

We can make the corrections in one of two ways. Either we can compute, on the basis of the known disturbing layers, the correction for the gravity anomalies caused by the disturbing masses, or we can try, using probable values for the density of the disturbing masses, to construct such forms and dimensions for the masses that the residual gravity anomalies can be explained. In the first alternative we generally find the thickness, density, and locality of the disturbing layers by seismological methods or by drilling.

Both methods have been used; the first, for example, by Woppard<sup>50</sup> in 1939. As the over-all title "Gravity Anomalies and Geologic Structure" of his five short papers shows, he tries to interpret the observed American gravity anomalies geologically. He states that there are four possible causes of gravity anomalies: variation in near-surface densities; "structure," or configuration, of the surface of the crystalline basement; structural configuration of deep-seated, dense subbasement strata; and the existing degree of isostatic equilibrium.

In India and Burma Evans<sup>12</sup> in 1946 used the density and thickness of the light sediment layers, taken from the geological survey, to compute the geological correction of the gravity anomalies due to these layers. According to Evans, in very large areas this correction is more than -50 mgal and in some regions even more than -75 mgal. The accuracy of the cor-

rection can hardly be high, because it is rather difficult to estimate the density and the thickness of the sediment layers. His anomaly maps show that the correction can diminish the isostatic anomalies, which, as is well known, are rather large in India, but it cannot explain them totally, so that in the earth's crust there must be disturbing masses, of unknown locality and dimensions, which cause residual gravity anomalies. We may add that there might also be disturbances of isostatic equilibrium caused by forces in the crust, as discussed in Part A of Chap. 10.

The second method, i.e., estimation of the disturbing masses by the aid of residual anomalies, was used by Erola <sup>41</sup> in 1941, when he tried to explain the remaining strongly negative isostatic anomalies of the Ferghana Basin in Central Asia, and by Tanni <sup>43</sup> in 1942, when he computed, with the aid of strongly negative isostatic anomalies of Galicia and of remarkably positive anomalies of Hungary, the form and dimension of the disturbing masses. The thicknesses of this layer or of these layers are different, depending upon whether or not they are considered to be compensated.

In the Ferghana Basin the isostatic anomalies are about -150 mgal. Erola explains -50 mgal with the aid of an additional root of light material and believes that the other -100 mgal is caused by a sediment layer. Assuming the density of the underlayer to be 3.27 and that of the sediment layer to be 2.07 instead of 2.67, he comes to the conclusion that the thickness of the additional root varies between 2 and 10 km and that the thickness of the sediment layer is about 4 km. After the correction caused by these disturbing layers the remaining anomalies are small.

In a similar way, Tanni <sup>43</sup> constructed the disturbing masses that account for the negative anomalies in Galicia and the large positive anomalies in Hungary, as well as the enormously strong gradient of the gravity values along the profile Tarnopol-Tuchla-Munkacs-Debrecen. Taking into the account the known light superficial layers (tuff) of Hungary and assuming the density of the disturbing layers in the regions of negative anomalies to be 0.6 smaller than the usual density of 2.67, Tanni concludes that the positive disturbing layer in Hungary and in Bohemia varies between 0 and 2.2 km and that in Galicia the thickness of the negative disturbing layer varies between 0 and 7.6 km.

In determining the disturbing masses the Bouguer anomalies also can be used as a basis; Salonen <sup>42</sup> used them in 1932, when he computed the thickness of the crust in the region of the Alps, and Bullard <sup>7</sup> and Cooper used them in more detail when, in 1948, they computed tables for the distribution of mass at a given depth which will produce a specific Bouguer anomaly.

#### *E. Indirect Isostatic Reduction*

The problem of determining the equilibrium figure of the earth, i.e., the shape the geoid would have if no disturbing effects were present, consists of

two parts: (1) What shape would the geoid adopt if the whole earth, including the outer layer, were fluid? (2) What changes are caused by the presence of the rigid crust with its topography and covering of sea water over two-thirds of it?

Since the second question arises by virtue of the masses transferred by topographic and isostatic reductions, the changes in the geoid are identical to the shift accompanying these reductions. In this section we deal especially with this problem.

The first question, the shape of the geoid of an entirely fluid earth, has been treated by many scientists of great renown, e.g., Clairaut, Poincaré, Véronnet, Wavre, Darwin, and de Sitter. The last two carried out the deductions to terms of the second order.

It has been found (see Chap. 3) that the geoid would assume the shape of a spheroid that deviates only slightly from an ellipsoid of revolution. When compared with an ellipsoid of the same volume and flattening, the geoid is found to be outside the ellipsoid at poles and equator and inside at 45° latitude. The value of the deviations depends on the density distribution in the earth. According to recent data, the deviation  $D$  is given by

$$D = 2.31 - 4.33 \sin^2 2\varphi \text{ meters}$$

and so it is everywhere less than 2.4 m.

The resulting deviation  $\Delta g$  of gravity on the geoid from that on the ellipsoid is

$$\Delta g = 0.81 + 0.76 \sin^2 \varphi - 2.00 \sin^2 2\varphi \text{ mgal} \quad (6-32)$$

The slight gravity deviation given by the formula has to be taken into account when gravity anomalies for the unsurveyed areas of the earth's surface are introduced into Stokes' theorem. If equilibrium is assumed in these areas, Formula (6-32) gives the theoretical anomaly with respect to the value of normal gravity based on the ellipsoid.

Turning now to our main problem—the shift of the geoid caused by the presence of the topography, the sea water, and the isostatic compensation—we can state that the shift results from the change of the earth's potential caused by these masses. Since this change, however, also affects the inner potential surfaces, all interface surfaces inside the earth, which separate different layers, will likewise be altered. All these changes, including that of the geoid, mean changes in the mass distribution, which again affects the potential. The resulting problem has been solved by Vening Meinesz<sup>47</sup> by the introduction of spherical harmonics; a series of linear equations is found, the solution of which depends on the order of the spherical harmonic. Solutions have been found for isostatic compensation according to both Formula (5-3), i.e., equal mass, and Formula (5-4), i.e., nearly equal pressure; the latter corresponds to the Hayford-Bowie and the

regional Airy systems of reduction. The solution for isostatic compensation according to Formula (5-2), i.e., exactly equal pressure, can be derived from these two systems by extrapolation. Although we shall not enter into details of these solutions, a few points are worth mentioning.

In the first place, the changes of mass caused by the shift of the equipotential surfaces must affect the gravity, and the shift also gives rise to a free-air reduction corresponding to the shift at the gravity station. As our aim is to derive the value of gravity that would be found if the masses were taken away from the earth, both effects on gravity must be subtracted from the anomaly. This procedure also removes a difficulty which would otherwise arise if we intend to apply the Stokes' theorem, when we must take away all the masses outside the geoid, for part of the masses dealt with here satisfy this condition.

In this respect it may be mentioned that the need for the free-air reduction corresponding to the shift of the geoid is generally recognized. Tables for it have been derived, e.g., by Lambert<sup>34</sup> and Darling, by Vening Meinesz,<sup>47</sup> and by Lejay.<sup>35</sup> On the other hand, the effect of the gravity attraction by the mass changes caused by the shift of the geoid and of the interfaces inside the earth has usually been neglected. Since, because of the equilibrium prevailing in the earth, these new masses were believed to be isostatically compensated in the same way as the topography, and since these masses are widespread and regular, it has usually been assumed that the effect of the compensation must practically neutralize the attraction by the masses themselves. It appears quite certain, however, that these masses are not isostatically compensated. They are caused by the shift of the geoid or of an interface between different densities, and so they are kept in their places by the change of the potential field of the earth and not as a consequence of hydrostatic balance of a floating mass on an equipotential surface. The change of the potential field gives rise solely to the masses themselves and not to masses of opposite sign somewhere below them.

It seems certain, therefore, that the attraction of these masses must be taken into account fully and that it thus has to be added to the free-air reduction over the shift of the geoid. Together they may be called the "indirect isostatic reduction." The derivation of its amount can be found in Vening Meinesz.<sup>46</sup>

It may be added that the complication of a floating crust, as it is dealt with here, is also present in the simple case of a smaller body floating on water, although there it is imperceptibly small. The presence of the body causes a slight alteration of the equipotential surface coinciding originally with the water surface, and so the position of the floating body is subjected to a correspondingly small disturbance with respect to the position given by Archimedes' law.

A shift of the geoid as a consequence of the removal of the topographic and isostatic masses obviously is also present for the first-order spherical harmonic of the topography, which shows a land hemisphere and a sea hemisphere or, more accurately, the topography given by a physical earth surface obtained by displacing the geoid over a certain distance. It is clear that removal of this topography and its isostatic compensation must shift the center of gravity of the earth. This fact has often puzzled geodesists and geophysicists because it is evidently impossible for such a shift to be the result of phenomena taking place in the earth itself, and on the other hand it seems extremely unlikely that outside effects could be responsible for this kind of topography. Still, there is a strong term present of this type; it is well known that one hemisphere contains much more continent than the other. The first-order term of the earth's topography has a value of 1204 m; the maximum elevation of this amount occurs at a spot somewhat east of Constantza (Romania), viz., at  $43^{\circ}57'N$  and  $31^{\circ}4'E$ , and the maximum depression of the same amount at a spot in the South Pacific some 3000 km east of the South Island of New Zealand.

The solution of this problem is given by the shift of the geoid accompanying the removal of the topography and the isostatic compensation as dealt with in this section. For this first-order term the shift has exactly the same value, but with opposite sign, as the shift of the center of gravity directly caused by the removal of the topographic and compensation masses, and so the two shifts neutralize each other.

One more point merits mention, viz., the problem of the zero-order term of the shift of the geoid. This term is a constant, equal to the mean value of the shift over the whole surface of the earth. Since it turns out that the term can be arbitrarily chosen, it seems practical to choose it in such a way that it also neutralizes the zero-order term of the direct effect of the removal of the topographic and isostatic masses. So the mean value over the earth of the distance between the geoid before and after the topographic and isostatic reductions is made zero. This can also be expressed by saying that the volume of the geoid does not change because of the reductions. It follows that this result, which will be especially appreciated by geodesists, can be obtained independently of the masses of the isostatic compensation, being chosen equal to those of the topography [Formula (5-3)].

### 6-3. Recent Methods for Isostatic Reduction

In isostatic reductions the circular-zone method developed by Hayford and his colleagues at the U.S. Coast and Geodetic Survey and outlined in Sec. 6-2A has been used so far. In this method the mean elevations or depths of the consecutive zones around the station to the antipode are estimated by the aid of topographic and hydrographic maps, and the effect of each zone is computed on the basis of suitable reduction tables. All this

takes a great deal of time; particularly because the estimation of the mean elevations or depths of the many circular zones has to be made separately for every, or at least almost every, gravity station or computation point. Hardly more than one rough-mountain station a day can be reduced by one computer.

Realizing the basic significance of the isostatic gravity anomalies for geodesy and geophysics, the U.S. Coast and Geodetic Survey, the Netherlands Geodetic Commission, the International Gravity Center at Paris and particularly the International Isostatic Institute at Helsinki, as well as some other institutions, have to the present time isostatically reduced altogether more than 15,000 individual gravity stations. This is a considerable number, and many important geophysical studies have been carried out on the basis of these isostatically reduced gravity anomalies.

#### A. Cartographic Method

Since, however, in geodetic applications the *same* geodetic system has to be used everywhere in the world, and since different institutions have used different isostatic systems, only a small part of the isostatic gravity values can be used for geodetic purposes. On the other hand, because an enormous number of gravity observations exist, we face a serious problem. How will it be possible to handle this vast material isostatically in a way that will not consume too much time? The station-by-station method can hardly be considered, at least not without great institutes with large staffs.

Fortunately there is a shorter method, i.e., the cartographic method, started by the author<sup>23, 24</sup> (H.) in 1938. This method gives sufficient accuracy for all world-wide studies. The free-air reduction, like the simplified Bouguer reduction, requires no topographic maps. If the terrain correction, the effect of which is, practically speaking, negligible except in rugged mountains, has also been computed for the country where the gravity station concerned is situated (as has been continuously suggested in the assemblies of the International Association of Geodesy), all that has to be added is the isostatic reduction obtained in some way. On the other hand, the isostatic reduction of the nearest zones is fairly small; e.g., when zones A to H, with the outer radius 5.24 km, have a mean elevation of 2000 km, the correction is only 2.6 mgal for  $T = 30$  km and 0.7 mgal for  $T = 60$  km. Consequently, the isostatic reduction changes slowly from point to point and can therefore be presented in the form of suitable maps.

It is even easier to use the cartographic method for the numbered Hayford zones, where the combined effect of topography and compensation is still smaller and changes still less from point to point. This is particularly true in the outermost zones, 10 to 1. Although the effect is small, its computation is very laborious, especially in zones 7 to 1, because the mean elevation or depth of these wide zones must be estimated for many sta-

tions. Furthermore, in most of the charts and maps which figure in these estimations, the boundaries between the zones are not circles but more or less complicated curves; because of the map projection used, drawing these curves is also time-consuming. The estimation of the mean elevation or depth of the zones is the most thankless part of the isostatic reduction of gravity anomalies, as everyone who has carried out these computations knows.

To avoid this tedious work the author<sup>23</sup> proposed that the work be done once and for all at the International Isostatic Institute, in other words, that the effect of zones 10 to 1 over the whole earth surface be estimated and computed. The method used is simple. A globe was covered by transparent paper on which the curves of equal elevations and depths were drafted. Contour curves corresponding to the elevations 200, 500, 1000, 2000, 3000, 4000, and 5000 m and to the depths 200, 1000, 2000, 3000, 4000, 4500, 5000, 5500, 6000, 6500, and 7000 m were used.

These isobathymetric lines were drafted on the basis of the Monacan bathymetric charts (scale 1:10,000,000) and completed by information obtained from British Admiralty charts and United States hydrographic charts (scales of about 1:2,000,000 to 1:3,000,000). From the curves drafted on the globe, estimation of the mean elevations or depths of the compartments of zones 10 to 1 was made possible. As the combined effect of topography and compensation varies very slowly, the mean elevation or depth of the zones was estimated and the effect was computed at intervals of 20° in zones 7 to 1, 10° in zones 8 to 9, and 10° to 5° or, in some places, 2.5° in zone 10.

The results have been published in tables giving the combined effect of topography and compensation of the zones 1 to 2, 3, 4, 5, 6, 7, 8, 9, 10 and in four reduction maps giving the effect for zones 7 to 1, 8, 9, and 10 in units of 1 mgal. The accuracy of the reduction maps, of course, depends on the accuracy of the topographic and hydrographic charts used in the study. It is likely that the accuracy of the combined effect of zones 10 to 1 is higher than 1 mgal in lowland areas. In regions of high mountains and deep ocean coasts, the accuracy is naturally smaller. The error, however, probably seldom exceeds 2 mgal.

Because the reduction maps, which were computed in 1938, give only the effect of topography and compensation according to the Pratt-Hayford system for  $D = 113.7$  km, and because they are now out of print, in 1951 the Isostatic Institute computed new maps giving the combined effect of zones 10 to 1 for both the Airy-Heiskanen system, thickness of earth's crust  $T = 20, 30, 40$ , and 60 km, and the Pratt-Hayford system, depth of compensation  $D = 113.7$  km.<sup>39</sup>

In addition, in 1939, the Isostatic Institute computed the total effect of the topography and isostasy of zones 11 to 13 for Europe, India, the East

Indies and the eastern Atlantic.<sup>24</sup> Later the Institute undertook the full-scale project of computing and drafting reduction maps which contain the isoanomaly curves of the entire isostatic reduction, i.e., the effect of the isostatic compensation for zones A to O and the combined effect of topography and compensation in zones 18 to 1. The complete isostatic reduction maps are now available for the whole of Europe and its neighboring areas.

The Bataafsche Petroleum Co. has made similar maps which cover a wide zone from Portugal to the East Indies,<sup>4</sup> giving the whole isostatic reduction according to different assumptions.

In connection with the world-wide Gravity Project we have computed in Columbus six isostatic reduction maps for the United States. These maps will give the isostatic correction for the Hayford zones A to L, M, N, O, and the sum of the topographic and isostatic correction for the zones 18 to 14 and 13 to 11. There is one map for the whole isostatic correction in the zones A to O and the sum of the topographic and isostatic correction in zones 18 to 1.

In addition, the International Gravity Centre at Paris has prepared reduction maps for the isostatic reduction of France and its neighborhood which give the isostatic reduction in the various Hayford zones or zone groups according to the Pratt-Hayford system ( $D = 113.7$  km), the Airy-Heiskanen system ( $T = 30$  km), and the Vening Meinesz system ( $T = 30$  km and regionality  $R = 29$  km).<sup>9</sup> Similar maps for Sweden were prepared in 1954 by the Swedish Cartographic Institute (Wideland<sup>49</sup>), in 1951 for North Italy by Morelli,<sup>38</sup> and in 1950 for the Union of South Africa by Hales and Gough.<sup>17</sup>

These maps can be used for topographic isostatic reduction of individual gravity stations and have been so used. They markedly help in the isostatic reduction of areas covered by the maps. It is necessary only to add the isostatic reduction taken from the maps to the combined free-air and Bouguer reduction expanded to 166.7 km from the station.

There has been some criticism of the Isostatic Institute's complete isostatic reduction maps. In particular, it has been pointed out that the isostatic reduction varies so rapidly, at least in mountainous regions, that such maps are hardly able to give sufficient accuracy for scientific study. For that reason, Tanni,<sup>24</sup> of the Isostatic Institute, experimented by taking for 45 American mountainous gravity stations the whole isostatic reduction from the Institute's map and comparing it with the corresponding values taken from the original American tables of gravity data ("Principal Facts"). The results are given in Table 6-8, which gives the number of the station, its elevation  $h$ , the rigorous isostatic correction of "Principal Facts," I, the isostatic correction II taken from the Institute's map, II, and their difference. The differences are small, although the areas studied are

TABLE 6-8. SOME COMPARISONS BETWEEN THE ISOSTATIC CORRECTIONS FROM THE ORIGINAL AMERICAN TABLES ("PRINCIPAL FACTS . . ."), I, AND FROM THE ISOSTATIC INSTITUTE MAP, II

Station no.	<i>h</i>	I	II	Difference	Station no.	<i>h</i>	I	II	Difference
Appalachian Area					321	7	-2	-2	0
19	166	+15	+17	+2	322	155	+4	+3	-1
20	770	+42	+42	0	323	12	-1	-1	0
21	14	-2	-2	0	324	26	-15	-14	+1
101	422	+33	+33	0	325	30	-14	-14	0
102	1890	+56	+54	-2	326	135	+4	+4	0
103	994	+54	+54	0	327	588	+27	+26	-1
104	184	+29	+32	+3	328	486	+36	+34	-2
152	228	+51	+52	+1	329	1065	+49	+44	-5
153	263	+26	+28	+2	330	1149	+54	+53	-1
154	284	+21	+22	+1	331	638	+49	+49	0
155	280	+32	+35	+3	333	789	+34	+37	+3
156	514	+46	+48	+2	334	967	+40	+38	-2
171	300	+22	+22	0	335	280	+22	+21	-1
172	325	+39	+41	+2	336	291	+11	+10	-1
175	324	+31	+31	0	337	0	-2	-2	0
176	193	+26	+29	+3	338	88	0	0	0
					339	151	+19	+21	+2
Vicinity of Meridian 100°W									
260	306	+36	+36	0	9	129	+17	+19	+2
261	421	+41	+44	+3	40	469	+55	+55	0
262	790	+42	+44	+2	61	655	+65	+66	+1
263	751	+44	+45	+1	83	932	+99	+100	+1
264	493	+40	+38	-2	108	366	+37	+39	+2
					118	454	+62	+63	+1

in mountains. Zero error occurs 15 times, 1-mgal error 12 times, 2-mgal error 12 times, 3-mgal error 5 times, 4-mgal error never, and 5-mgal error only once. The mean quadratic error of the Institute's correction, supposing the values of "Principal Facts" to be absolutely rigorous, which can hardly be the case, is only  $\pm 1.7$  mgal.

It should be added, however, that the same 45 stations were considered in preparing the Institute's map, but since they are too numerous, only the mean value of many stations was used. Thus Table 6-8 can hardly give too misleading a picture of the maps' accuracy.

To get quite independent comparisons between the isostatic reductions obtained by the rigorous point-by-point method (I) and the cartographic method, in Columbus we have used seven isostatic reduction maps, which give the isostatic corrections for the Hayford zones A to L, M, N, O, 18 to 14, 13 to 11, and 10 to 1 (II), and one isostatic reduction map, which gives the sum of these seven corrections (III), and computed the isostatic corrections for five random points in the mountainous areas of the United States. The results are given in Tables 6-8a and 6-8b. Table 6-8a shows that the

TABLE 6-8a. COMPARISON BETWEEN THE ISOSTATIC CORRECTIONS FOR  $T = 30$  KM,  
OBTAINED BY POINTWISE REDUCTION, I; FROM THE REDUCTION MAPS FOR  
ZONES A-L, M, N, O, 18-14, 13-11, 10-1, II; AND FROM THE  
REDUCTION MAP FOR WHOLE WORLD, III; UNIT, 1 MGAL

Number	$\varphi$	$\lambda$	$h, m$	I	II	III	I-II	I-III
1	42°00'N	76°00'W	460	38.0	39.6	37.0	-1.6	+1.0
2	37°00'	79°30'	235	27.7	28.1	27.5	-0.4	+0.2
3	43°00'	105°00'	1520	166.4	164.5	166.0	+1.9	+0.4
4	39°00'	104°00'	1850	186.1	189.1	185.0	-3.0	+1.1
5	35°30'	108°00'	2400	225.8	222.2	220.0	+3.6	+5.8

TABLE 6-8b. COMPARISON BETWEEN THE ISOSTATIC CORRECTIONS FOR  $T = 30$  KM,  
EXCLUDING ZONES A-L, OBTAINED BY POINTWISE REDUCTION, I,  
AND FROM REDUCTION MAPS, II; UNIT, 1 MGAL

Point	I	II	I-II
1	26.3	26.9	-0.6
2	20.2	19.2	+1.0
3	125.2	125.5	-0.3
4	138.2	139.6	-1.4
5	167.0	165.2	+1.2
6	41.5	41.3	+0.2
7	176.0	175.5	+0.5

differences between I and II and between I and III are rather small, indicating that the error brought about by using the reduction maps is rather small even if only one reduction map has been used. In fact, the largest I-II error is 3.6 mgal and I-III 5.8 mgal.

Table 6-8b gives the reduction results I and II, and the differences between I and II for the same five points and, in addition, two other points

of very rugged topography. In this case the effect of the nearest zones, A to L, have been excluded. The differences between I and II show that in this case the difference between the rigorous computation and the cartographic method is nearly negligible; in fact, the mean deviation is  $\pm .07$  mgal.

The scientists who apply these reductions can best judge when it is necessary to compute the effect of the isostatic compensation of zones A to L separately, a work of half an hour. Tables 6-8a and 6-8b together will, I hope, convince everybody that the cartographic method will be sufficiently accurate also, with some few exceptions, in rugged topography. The amount of work saved by this method is enormous.

Computation of the terrain correction for mountain stations takes much more time.

To avoid misunderstandings it may be mentioned further that the accuracy of the reduction maps is *not* sufficient for any detailed study of the isostatic equilibrium of a mountainous area if the gravity measurements have been made with high accuracy; but for world-wide studies, e.g., study of the geoid, such maps are indispensable. If one wanted to undertake an investigation of the isostatic structure of the earth's crust in a small, interesting area, a good approach would be to reduce the gravity stations with the aid of the topographic maps, but the cartographic method would be better. Six reduction maps would be sufficient; one to give the effect of zones A to L, the second, third, and fourth of M, N, and O, the fifth of 18 to 14, and the sixth of 13 to 11. The effect of zones 10 to 1 can be taken from the maps.<sup>39</sup>

#### B. Mass-line Method

Isostatic reduction maps, if they exist, help a great deal in the reduction of the gravity anomaly. Unfortunately, only a small part of the world has as yet been covered by such maps. Bearing this fact in mind, and realizing the significance of the isostatic gravity anomalies in geophysical and geodetic applications of gravity measurements, the author<sup>27</sup> (H.) introduced at the Mapping and Charting Research Laboratory of The Ohio State University a new mass-line method which offers possibilities of use in high-speed computing machines.

In this method, Hayford zones are replaced by squares (more correctly, spherical trapezoids) 5' by 5', 10' by 10', 0°.5 by 0°.5, 1° by 1°, 2° by 2°, and so on. The mean elevations or depths of the squares have been estimated and used from the computation point over Hayford zones A through 11. The topographic-isostatic reduction of zones 10 to 1 can be taken from existing reduction maps.<sup>39</sup> Needless to say, this method can be expanded even to the antipode of the computation point if desired.

The estimation of the mean elevations or depths takes rather a long

time but needs to be done only once. When maps giving these elevations or depths are completed, they can be used for any isostatic reduction, as well as for other purposes. Similar square maps have been used: in smaller scale, by Bonsdorff in 1916 and the author in 1926; in different scales, by

Glennie<sup>13</sup> for all India and vicinity and by Lejay in his isostatic reduction of French gravity stations.

In the mass-line method it is necessary, in computing the vertical attraction, to use compensating-mass prisms whose square sections are spherical trapezoids. Because of the convergence of the earth's radius, the lower surface of such a prism is smaller than the upper. As the integration of the vertical attraction of such mass prisms at the computation point is difficult, if not impossible, the author uses a mass line to represent the spherical prism (Fig. 6-10). In other words, he computes the vertical attraction of the compensating column as if it were condensed to the axis of the column.

It is possible to consider the correction

FIG. 6-10. Mass-line method for isostatic reduction. Compensating prism  $dx dy(z_2 - z_1)$  is replaced by mass line EF.

due to the fact that the attraction of this mass line is not quite equivalent to the attraction of the compensating column. The computation of the height of the compensating column can be carried out in terms either of equal mass or of equal pressure.

If the effect of the convergence of the earth's radius is disregarded (as was done by Hayford), the formula for the effect  $F$  of the compensating-mass line for land areas is

$$F = k \Delta\rho dx dy \{ (r^2 + T^2)^{-\frac{1}{2}} - [r^2 + (T + t)^2]^{-\frac{1}{2}} \} \quad (6-33)$$

and for the effect  $F'$  for ocean areas it is

$$F' = k \Delta\rho dx dy \{ [r^2 + (T - t)^2]^{-\frac{1}{2}} - (r^2 + T^2)^{-\frac{1}{2}} \} \quad (6-34)$$

where  $k = 6.673 \times 10^{-8}$  (Newtonian gravitational constant)

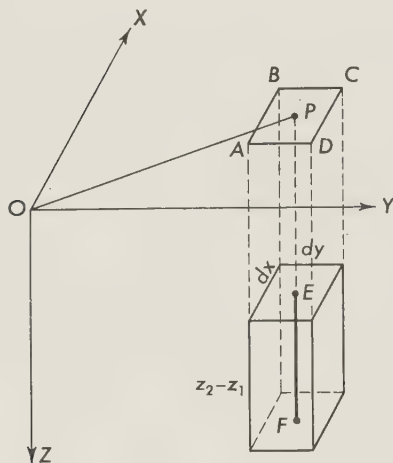
$\Delta\rho$  = density of compensating mass (generally 0.6)

$dx, dy$  = dimensions of spherical trapezoid

$r$  = horizontal distance of mass line from computation point

$T$  = normal thickness of earth's crust

$t$  = thickness of compensating layer (root or antiroot)



Farther from the computation point the curvature of the earth's surface must be considered, for instance, in the way used by Hayford and Bowie [Formulas (6-26) and (6-27) and Table 6-5]. Angular distance  $\alpha$  can be computed from the spherical formula

$$\cos \alpha = \sin \varphi \sin \varphi_0 + \cos \varphi \cos \varphi_0 \cos (\lambda - \lambda_0) \quad (6-35)$$

where  $\varphi$  and  $\lambda$  are the coordinates of the gravity center  $P$  of the spherical

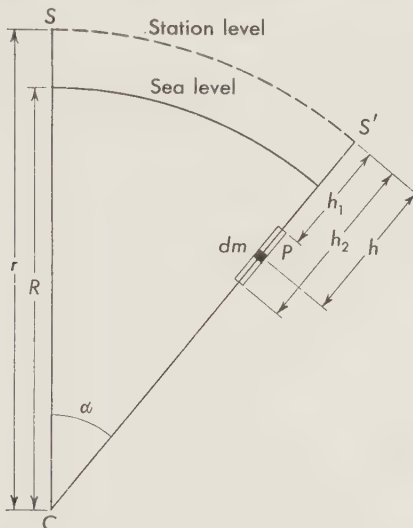


FIG. 6-11. Computation of formulas suitable for the isostatic reduction in electronic computers.

trapezoid  $ABCD$  (Fig. 6-10) and  $\varphi_0$  and  $\lambda_0$  are the coordinates of the computation point (see Chap. 8).

As Formulas (6-33) and (6-34) are approximate, although in most cases sufficient, Kukkamäki<sup>32</sup> studied this problem further to find a rigorous formula for isostatic reduction of the mass-line method for use in electronic computers. Starting from Cassini's fundamental tables, he derived the following formula for the computation of the vertical attraction of the compensating mass line  $AB$  at the gravity station  $S$  (Fig. 6-11):

$$F = k\rho d\alpha r \left\{ [(1 - 16x^2 + 24x^4)(1 - i) \right.$$

$$+ (3 - 20x^2 + 24x^4)(1 - ij)y_2 + (-1 + 2x^2)(1 - ij^2)y_2^2] \frac{1}{\sqrt{T_2}} \right.$$

$$\left. - 2(1 - 6x^2 + 6x^4) \ln \frac{\sqrt{T_2} + y_2 + 2x^2}{\sqrt{T_1} + y_1 + 2x^2} \right\} \quad (6-36)$$

where  $k$  = Newtonian gravitational constant

$\rho$  = density of column

$\alpha$  = angular distance  $SS'$

$r$  = distance  $SC$

$R$  = earth's radius

$h_1$  = depth of oversurface of compensating-mass line  $AB$

$h_2$  = distance of undersurface of  $AB$

$h$  = distance of mass element  $dm$  (Fig. 6-12)

Furthermore

$$x = \sin \frac{\alpha}{2} \quad y = \frac{h}{r} \quad y_1 = \frac{h_1}{r} \quad y_2 = \frac{h_2}{r}$$

$$T = 4x^2 + 4x^2y + y^2 \quad i = \frac{\sqrt{T_2}}{\sqrt{T_1}} \quad \text{and} \quad j = \frac{y_1}{y_2}$$

If  $y_1$  and  $y_2$  are negative and  $x = 0$ , the quotient

$$\frac{\sqrt{T_2} + y_2 + 2x^2}{\sqrt{T_1} + y_1 + 2x^2}$$

is indefinite. After two differentiations of the numerator and the denominator its limit is found to be  $y_1/y_2$ .

If column  $AB$  is far from the computation point, a relatively large number of significant figures is lost by computing the value of  $F$  from Formula (6-36). Herget therefore suggested numerical integration of the attraction of some mass point at suitable positions in the column followed by computation of the average value of the whole compartment by Simpson's rule.

For the attraction  $dF$  of the mass element  $dm$  the expression is

$$dF = k\rho d\alpha \frac{(1+y)^2[2x^2(1+y) - y]}{[4x^2(1+y) + y^2]^{\frac{3}{2}}} dy \quad (6-37)$$

The result will be essentially the same if we use Formulas (6-33) and (6-34).

#### REFERENCES

1. Birch, Francis, J. F. Schairer, and H. Cecil Spicer: Geol. Soc. Amer., Spec. Paper, no. 36, pp. 14, 16, 1942.
2. Bouguer, Pierre: *La figure de la terre*, Paris, 1749.
3. Bowie, William: Isostatic investigations and data for gravity stations in the United States, USGS, no. 99, 1924.
- 3a. ———: Investigations of gravity and isostasy, *ibid.*, no. 40, 1917.
4. de Bruyn, J. W.: Isostatic isocorrection line maps, Council, European Association of Exploration Geophysicists, The Hague, 1951.

5. Bullard, E. C.: Gravity measurements in East Africa, *Trans. Roy. Soc. (London)*, ser. A, vol. 235, 1936.
6. ———: The figure of the earth, *Monthly Notices Roy. Astron. Soc., Geophys. Suppl.*, vol. 5, no. 6, pp. 186–192, 1948.
7. ——— and R. I. B. Cooper: The determination of the masses necessary to produce a given gravitational field, *Proc. Roy. Astron. Soc.*, ser. A, vol. 194, 1948.
8. Cassinis, G., P. Dore and S. Ballarin: Fundamental tables for reducing gravity observed values, *Reale comm. geod. ital. publ. N.S.*, no. 13, 1937.
9. Coron, Suzanne: Contribution a l'étude du champ gravimétrique en France, *Dissertation, Sorbonne*, 1954.
10. Encyclopaedia Britannica, Gravitation, vol. 10, p. 663–667N, 1955.
11. Erola, V.: On the structure of the earth's crust in the neighbourhood of the Ferghana Basin, *Publ. Isos. Inst. IAG (Helsinki)*, no. 10, 1941.
12. Evans, P., and W. Crompton: Geological factors in gravity interpretation illustrated by evidence from India and Burma, *Quart. J. Geol. Soc. London*, vol. 102, pp. 211–249, 1946.
13. Glennie, E. A.: Gravity and deviation of the vertical, *Geol. Survey India, Geod. Rept.*, vol. 4, 1929; vol. 5, 1930.
14. de Graaff Hunter, J.: The geodetic uses of gravity measurements and their appropriate reduction, *Proc. Roy. Soc. (London)*, ser. A, vol. 206, 1951; Earth curvature and refraction, *ibid.*, vol. 207, 1951.
15. Gromov, S. V.: The inversion method of Rudzki considered and extensively developed, *Trudy Astron. Observatorii Leningrad. Univ.*, vol. 16, 1952; The inversion of the deflection of the vertical, *ibid.*
16. Gutenberg, B.: Internal constitution of the earth, 2nd ed., p. 42, Dover, New York, 1951.
17. Hales, A. L., and D. J. Gough: Measurements of gravity in Southern Africa, *The Government Printer, Pretoria*, 1950.
18. Hayford, J. F.: The figure of the earth and isostasy, from measurements in the United States, USCGS, 1909.
19. ———: Supplementary investigation in 1909 of the figure of the earth and isostasy, USCGS, 1910.
20. ——— and William Bowie: The effect of topography and isostatic compensation upon the intensity of gravity, USCGS, no. 10, 1912.
21. Heiskanen, W. A.: Tables isostatiques pour la réduction dans l'hypothèse de Airy des intensités de la pesanteur observées, *Bull. géod.*, no. 30, 1931.
- 21a. ———: New isostatic tables for the reduction of the gravity values calculated on the basis of Airy's hypothesis, *Publ. Isos. Inst. IAG (Helsinki)*, no. 2, 1938.
22. ———: Investigations on the gravity formula, *Publ. Isos. Inst. IAG (Helsinki)*, no. 1, 1938.
23. ——— and U. Nuotio: Topographic-isostatic world maps of the effect of the Hayford zones 10, 9, 8 and 7 to 1, *Publ. Isos. Inst. IAG (Helsinki)*, no. 3, 1938.
24. ———: On the isostatic structure of the earth's crust, *Publ. Isos. Inst. IAG (Helsinki)*, no. 24, 1950.
25. ———: World gravity needs for geodetic purposes, Ohio State Univ. Mapping and Charting Research Lab., Tech. Paper, no. 118, 1950; The geodetic significance of world wide gravity studies, *ibid.*, no. 124, 1950.
26. ———: Rept. isostasy, Brussels Assembly IUGG, *Trav. assoc. géod. (Paris)*, 1951.
27. ———: Isostatic reductions of the gravity anomalies by the aid of high-speed computing machines, *Publ. Isos. Inst. IAG (Helsinki)*, no. 28, 1953.
28. Helmert, F. R.: Die mathematischen und physikalischen Theorien der höheren Geodäsie, vol. 2, p. 155, 1884.

29. Helmert, F. R.: Die Tiefe der Ausgleichsfläche bei der Prattschen Hypothese für das Gleichgewicht der Erdkruste und der Verlauf der Schwerestörung vom Innern der Kontinente und Ozeane nach den Küsten, *Sitzber. kgl. preuss. Akad. Wiss.* no. 48, p. 1192, 1909.
30. Kladivo, B.: Reduction de la pesanteur d'après Rudzki, Brno, 1940.
31. Kobold, F.: Die Bestimmung der Lotabweichungen im Meridian des St. Gotthard aus Hohenwinkelmessungen, *Commission Géodesique Suisse*, Neuchatal, March, 1951.
32. Kukkamäki, T. J.: Gravimetric reductions with electronic computers, *Publ. Isos. Inst. IAG* (Helsinki), no. 30, 1955.
33. Lambert, W. D.: The reduction of observed values of gravity to sea level, *Bull. géod.*, no. 26, pp. 128–130, 1930.
34. ——— and F. W. Darling: Tables for determining the form of the geoid and its indirect effect on gravity, *USCGS Spec. Publ.*, no. 199, 1936.
35. Lejay, R. P. Pierre: Tables pour le calcul de l'effet indirect et la déformation du géoïde, *Bull. géod.*, N.S., no. 8, 1948.
36. ———: A l'effet indirect et l'interprétation des anomalies gravimétriques, *Ann. géophys.*, vol. 7, fasc. 3, 1951.
37. Trans. Roy. Soc. (London), 1819, p. 93.
38. Morelli, Carlo: Rilievo gravimetrico e riduzione isostatica nell'Italia Nord-Orientale, *Osserv. geofis.* (Trieste), N.S., no. 20, 1951.
39. Niskanen, Erkki, and L. Kivioja: Topographic-isostatic world maps of the effect of the Hayford zones 10 to 1 for the Airy-Heiskanen and Pratt-Hayford systems, *Publ. Isos. Inst. IAG* (Helsinki), no. 27, 1951.
40. Rainesalo, A.: Ein Integral in der Theorie der isostatischen Reduktion der Schwerkraft, *Ann. Acad. Sci. Fenniae*, ser. A, Bd. 13, no. 9, 1920.
41. Rudzki, M. P.: Sur la détermination de la figure de la terre d'après les mesures de la gravité, *Bull. astron.*, ser. B, vol. 22, 1905; *Physik der Erde*, Leipzig, 1911.
42. Salonen, E.: Über die Erdkrustendicke und die isostatische Kompensation in den Schweizer Alpen, *Ann. Acad. Sci. Fenniae*, ser. A, vol. 37, no. 3, 1932.
43. Tanni, L.: On the isostatic structure of the earth's crust in the Carpathian countries and the related phenomena, *Publ. Isos. Inst. IAG* (Helsinki), no. 11, 1942.
44. Poisson, D.: *Traité de mécanique*, 2nd ed., vol. I, pp. 492–496.
45. Vening Meinesz, F. A.: Tables fondamentales pour la réduction isostatique régionale, *Bull. géod.*, no. 63, 1939.
46. ———: Fundamental tables for regional isostatic reduction of gravity values, *Verhandel. Koninkl. Ned. Akad. Wetenschap. Afdel. Natuurk.*, Sec. 1, vol. 17, no. 3, 1940.
47. ———: The indirect isostatic or Bowie reduction and the equilibrium figure of the earth, *Bull. géod.*, N.S., no. 1, 1946.
48. ———: Tables bi-dimensionnelles pour la réduction isostatique selon l'hypothèse de Airy avec  $T = 30$  km, *ibid.*, no. 2, 1946.
49. Wideland, Bror: Topographic-isostatic reduction of the Swedish gravity stations, *Rikets allm. kartverk*, Publ. no. 23, Stockholm, 1954.
50. Woppard, George P.: Gravity anomalies and geologic structure, *Trans. Am. Geophys. Union*, vol. 20, 1939.

## CHAPTER 7

# GRAVITY ANOMALIES; ACHIEVEMENTS OF ISOSTASY

### 7-1. Statistics of Gravity Anomalies

It has already been mentioned (Chap. 6) that the Bouguer gravity anomalies are small in the lowlands, strongly negative in the high mountains, and more strongly positive on the oceans. This is true even after the effect of station height and the mass surplus of the mountains and deficiency of the oceans have been carefully taken into account. Therefore there must be something to account for this strange situation. This "something" is the prevailing isostatic equilibrium.

The review of the gravity-anomaly situation in several parts of the world that follows discusses this important problem in detail on the basis of gravity-anomaly lists of mountains and their surroundings and of oceans. The lowland stations in tectonically stable areas are not interesting in this connection because the anomalies there are generally small. When considerable anomalies do exist in such areas, they can be attributed to mass-anomaly areas close to the gravity stations. Mass anomalies need not have any connection with the topography but are to be interpreted on the basis of geological features.

In the gravity-anomaly tables that follow the stations have been taken at random; shown in successive columns are the name of the station; its latitude, longitude, and elevation,  $h$ ; the free-air, Bouguer, and isostatic anomaly, according to either the Hayford system ( $D = 113.7$  km) or Airy-Heiskanen system (generally for  $T = 30$  km but also for  $T = 20$ , 40, or 60 km), or both. The material is not quite homogeneous because the same isostatic systems have not been used in all the regions studied.

#### *A. Gravity Anomalies in the United States and Canada*

Table 7-1 is divided into two parts, showing mountain stations below and above the surrounding terrain. The free-air anomalies, except in half a dozen cases, are seen to be partly positive and partly negative but not large. The strongest negative free-air anomalies are found at the low valley stations. Thus, for instance, at the Clifton Forge, Boise, and Grand Canyon stations, at the respective elevations of 325, 821 and

TABLE 7-1. GRAVITY ANOMALIES IN THE UNITED STATES<sup>2, 10</sup>

Station	$\varphi$	$\lambda$	$h, m$	Anomalies, mgal			
				Free-air	Bouguer	Isostatic	
						Hayford, 113.7 km	Airy- Heiskanen, 40 km

## 1. Mountain Stations below the Surrounding Terrain

Gallup.....	35°32'	108°44'	1990	+17	-203	-5	-2
State College.....	40 48	77 52	358	+5	-30	-13	-8
Goldfield.....	37 42	177 15	1716	+30	-158	-5	+2
Harrisburg.....	40 19	76 53	104	-11	-23	-21	-6
Clifton Forge.....	37 49	79 50	325	-21	-57	-26	-20
Prestonsburg.....	37 41	82 46	193	-12	-34	-16	-14
Knoxville.....	35 58	83 55	280	-6	-37	-13	-9
El Paso.....	31 46	106 29	1146	+24	-103	+15	+29
Heppner.....	45 21	119 33	598	-18	-85	-19	-17
Olympia.....	47 03	122 53	19	+37	-36	+41	+43
Boulder.....	46 13	112 7	1493	-6	-173	-7	-6
Guernsey.....	42 16	102 44	1322	+36	-105	+44	+47
Sheridan.....	44 48	106 59	1150	+17	-108	+40	+46
Gunnison.....	38 33	106 56	2340	+35	-221	+28	+34
Colorado Springs	38 51	104 49	1841	+2	-180	+1	+8
Salt Lake City..	40 26	111 54	1322	-15	-138	+18	+26
Boise.....	43 37	116 12	821	-48	-109	+16	+16
Grand Canyon..	36 05	112 07	849	-90	-165	-2	+5
Green River....	38 59	110 10	1243	-48	-172	-3	-4
Mean.....	.....	.....	.....	-4	-112	+4	+9

## 2. Mountain Stations above the Surrounding Terrain

Las Vegas.....	35°36'	105°12'	1960	+36	-181	+11	+8
Helenwood.....	36 26	84 31	422	+71	+23	+48	+51
Norris Geyser Basin.....	44 44	110 42	2276	+68	-169	+29	+34
Asheville.....	35 36	82 33	670	+37	-37	+3	-1
Grand Canyon..	44 43	110 30	2386	+52	-200	+6	0
Nogales.....	31 21	110 57	1181	+4	-124	-42	-44
Lake Placid.....	44 18	73 59	571	+38	-9	+14	+16
Lead.....	44 21	103 46	1590	+112	-64	+60	+58
Truckee.....	39 20	120 11	1805	+45	-154	-20	-4
Mount Hamilton	37 20	121 39	1282	+133	+11	+5	+9
Pikes Peak.....	38 50	105 02	4293	+224	-196	+29	+19
Mean.....	.....	.....	.....	+75	-100	+15	+13

849 m, the corresponding anomalies are -21, -48, and -90 mgal, while at Goldfield, El Paso, and Gunnison, at the respective elevations of 1716, 1146, and 2340 m, the anomalies are +30, +24, and +35 mgal. Similar correlations are often found in other mountainous regions. At the mountain stations above the surrounding terrain all free-air anomalies are positive; at Pikes Peak, elevation 4293 m, it is as high as +224 mgal. The deviation of the free-air anomalies from the average value is rather large.

Except at two stations, Helenwood and Mount Hamilton, the Bouguer anomalies are negative, and in general the higher the elevation, the more negative they are.

The isostatic anomalies are given according to the Hayford system,  $D = 113.7$  km, and the Airy-Heiskanen system,  $T = 40$  km. The difference between these two sets of anomalies is small, as can readily be understood because these two assumptions are nearly equivalent as far as the gravity effect of isostatic compensation is concerned. Both sets of these anomalies are rather small. The deviation of individual anomalies from the average value is much smaller than according to the free-air or Bouguer anomaly. No one who glances at this list can deny the existence of isostatic equilibrium in the mountains of the United States.

TABLE 7-2. GRAVITY ANOMALIES IN CANADA<sup>18</sup>

Station	$\varphi$	$\lambda$	$h$ , m	Anomalies, mgal			
				Free-air	Bouguer	Isostatic	
						Hayford, 113.7 km	Airy- Heiskanen, 40 km
Kinderley.....	51°28'3	109°09'0	1288	+3	-74	-1	+1
Calgary.....	51 02.7	114 03.8	1046	-23	-140	-17	-15
Kinuso.....	55 19.9	115 25.9	586	-9	-75	+1	+3
Banff.....	51 10.9	115 34.5	1380	-2	-157	+31	+36
Jasper.....	52 52.6	118 04.7	1059	-73	-192	-16	-8
Paradise Mine..	50 28.4	116 19.8	2277	+54	-201	-12	-11
Phoenix.....	49 05.8	118 36.3	1380	+52	-100	+24	+27
Barkerville....	53 03.8	121 29.8	1288	-1	-145	-8	-6
Mean.....	.....	.....	.....	0	-135	0	+3

The extreme values of the free-air anomalies are +224 and -90 mgal, of the Bouguer anomalies +23 and -221 mgal, but of the Hayford anomalies only -42 and +60 mgal, and of the Airy-Heiskanen anomalies -44 and +58 mgal. The variations of the Bouguer and free-air anomalies, 244 and 314 mgal, are much larger than the variation of both sets of isostatic anomalies, 102 mgal.

Table 7-2, giving eight Canadian gravity anomalies of mountain areas, confirms the results obtained from the gravity anomalies of the United States. In Canada the deviation of the moderate free-air anomalies is also large, while the Bouguer anomalies are systematically negative, the average value being -135 mgal. Both the Hayford and the Airy-Heiskanen isostatic anomalies are small, the largest being +31 and +36 mgal. The average values, 0 and +3 mgal, show that the Canadian mountains, at least between the latitudes  $49^{\circ}$  and  $53^{\circ}$  and longitudes  $109^{\circ}$  and  $121^{\circ}$ , are in isostatic equilibrium. In fact, most other Canadian mountains are almost compensated isostatically.

### B. Gravity Anomalies in India

It has been claimed<sup>5</sup> that India, the birthplace of the theory of isostasy, is not in isostatic equilibrium. From examination of Table 7-3 of Indian gravity anomalies it must be admitted that the isostatic equilibrium is not so complete as in America, but it is hardly possible to interpret the gravity material of India as evidence of the absence of isostatic equilibrium. If it were absent, the average Bouguer anomalies would be close to zero and the isostatic Hayford anomalies,  $D = 113.7$  km, strongly positive, which is not the case. The average of 22 Bouguer anomalies chosen at random between the latitudes  $10^{\circ}$  and  $34^{\circ}$  and the longitudes  $68^{\circ}$  and  $96^{\circ}$  is -115 mgal, and the average of the free-air anomalies is +45 mgal; but the average of the Hayford anomalies is only -5 mgal. Evans's efforts to explain the remaining Bouguer anomalies on the basis of geological corrections have not been successful. On the contrary, the geologically corrected Bouguer anomalies are much larger than the geologically corrected Hayford isostatic anomalies; e.g., in the northern part of India the average values of the corrected Bouguer anomalies, according to Evans, are, on the average, -159 mgal, while the corrected Hayford isostatic anomalies are, on the average, only -59 mgal. If in the isostatic reduction, the Airy-Heiskanen system,  $T = 30$  km, had been used instead of the Pratt-Hayford system, the residual isostatic anomalies probably would have been still smaller.

Consequently the study of Indian gravity anomalies leads to the conclusion that in India too the major part of the mountain masses is isostatically compensated.

TABLE 7-3. GRAVITY ANOMALIES IN INDIA

Station	$\varphi$	$\lambda$	$h, m$	Anomalies, mgal		
				Free-air	Bouguer	Hayford, $D = 113.7$
Dehra Dun (base station).....	30°19'29"	78°03'22"	683	-89	-160	-9
Mussoorie (Camel's Back).....	30 27 35	78 04 32	2110	+68	-139	+37
Darjeeling.....	27 02 47	88 16 08	2123	+38	-171	+15
Sandakphu.....	27 06 06	88 00 15	3586	+172	-172	+31
Mach.....	29 52 25	67 18 20	1073	-38	-150	-20
Rajpur.....	30 24 02	78 05 47	1012	-57	-160	+9
Yercand.....	11 46 56	78 12 29	1369	+64	-76	-52
Kodaikānal.....	10 13 50	77 27 56	2336	+148	-98	-51
Badnur.....	21 54 10	77 54 10	642	+38	-33	+20
Maymyo.....	22 01 13	96 28 24	1065	+43	-74	0
Abu.....	24 35 40	72 43 00	1169	+97	-25	+12
Murree.....	33 54 07	73 23 15	2098	+16	-200	-41
Korag.....	33 48 32	74 33 19	3338	+133	-221	+18
Pachmarhi.....	22 28 23	78 25 42	1066	+22	-94	-39
Pottangi.....	18 33 56	82 58 03	932	+89	-10	+20
Ranikhet.....	29 37 38	79 26 08	1812	+15	-176	+4
Mercara.....	12 25 44	75 43 50	1135	+42	-82	-44
Pirmed.....	9 34 34	76 58 20	1013	+7	-98	-91
Ziārat.....	30 22 57	67 43 15	2454	+117	-148	+28
Landi Kotal.....	34 30 58	71 53 50	472	-155	-205	-59
Shillong.....	25 33 55	91 53 42	1530	+152	-13	+73
Ajal.....	23 43 00	93 43 22	1148	+77	-37	+24
Mean.....	.....	.....	.....	+45	-115	-5

### C. Gravity Anomalies in East Africa

Table 7-4 gives the free-air, Bouguer, Hayford, and Airy-Heiskanen anomalies for  $T = 40$  km and  $T = 60$  km at 18 gravity stations of East Africa. As before, the free-air anomalies are not too large on the average, but the deviation from the mean is great. The Bouguer anomalies are still more clearly negative than in the previous cases, and the isostatic anomalies are again small.

The free-air, Bouguer, Hayford, and Airy-Heiskanen anomalies average +13, -146, -20, -16, and -24 mgal, respectively. Consequently the

TABLE 7-4. GRAVITY ANOMALIES IN EAST AFRICA<sup>3</sup>

Station	$\varphi$	$\lambda$	$h, m$	Anomalies, mgal				
				Free-air	Bouguer	Isostatic		
						Hayford, 113.7 km	40 km	60 km
Lira.....	+2°15'	32°55'	1128	+11	-117	-8	-6	-9
Soroti.....	+1 43	33 36	1125	-25	-153	-37	-34	-37
Kasenyi.....	+1 23	30 26	638	-122	-193	-87	-83	-83
Kabwoya.....	+1 15	31 05	1197	-2	-137	-24	-23	-25
Kitale.....	+1 01	35 01	1894	+24	-189	-28	-21	-38
Butembo.....	+0 10	29 22	1758	+83	-115	+19	+18	+9
Nakuru.....	-0 17	36 04	1848	+6	-202	-17	-7	-25
Lwasamaire.....	-0 50	30 08	1573	+30	-147	+1	+5	-3
Ssurae.....	-2 04	35 40	2197	+75	-171	-13	-13	-23
Voi.....	-3 24	38 34	557	+17	-45	+10	+15	+8
Benne.....	-3 56	37 09	1146	+9	-119	-21	-16	-23
Sela.....	-4 41.6	35 48.5	1807	+37	-163	-33	-28	-37
Kazuramimba.....	-4 58.7	30 00.7	1097	-27	-151	-46	-48	-48
Itigi.....	-5 42.6	34 29.5	1305	-16	-164	-39	-35	-42
Kitunda.....	-6 46.4	33 15.2	1248	+2	-139	-11	-6	-14
Iringa.....	-7 49.3	35 41.8	1634	+48	-137	-11	-7	-21
Nyamapara.....	-8 24	31 58	1601	+65	-115	+8	+21	+13
Itewe.....	-8 57.2	33 24.6	1730	+23	-171	-28	-24	-37
Mean.....	.....	.....	....	+13	-146	-20	-16	-24

area in question, located between the latitudes +2° and -9° and longitudes +29° and +39° in East Africa, is, practically speaking, in isostatic equilibrium.

#### D. Gravity Anomalies in the Alps

The free-air, Bouguer, and isostatic Airy-Heiskanen anomalies for  $T = 20, 30$ , and 40 km are given in Table 7-5. As the Alps are much rougher than the American mountains, the free-air anomalies have a much larger deviation from the mean, varying from +143 mgal at Sonnblick, elevation 3099 m, to -127 mgal in Innsbruck, elevation 584 m. The higher the elevation, the more positive the free-air anomalies, as will be seen

TABLE 7-5. GRAVITY ANOMALIES IN THE ALPS<sup>15</sup>

Station	$\varphi$	$\lambda$	$h, m$	Anomalies, mgal				
				Free-air	Bouguer	Isostatic, Airy-Heiskanen		
						20 km	30 km	40 km
Campiglio.....	46°13'9	10°51'4	1530	+58	-103	+26	+16	+8
Ober-Drauburg 1....	46 44.9	12 58	618	-38	-91	+42	+33	+24
Greifenburg 2.....	46 45.1	13 11	632	-36	-93	+29	+21	+13
Sandbüchel.....	46 45.3	11 01.8	2967	+116	-193	-30	-44	-56
S. Leonardo.....	46 48.7	11 16.4	655	-107	-152	+9	-4	-17
Lienz 1.....	46 50.0	12 46	674	-51	-112	+28	+16	+6
Möllbrücken.....	46 50.3	13 22	556	-42	-83	+38	+28	+22
Hochstradenkogl....	46 50.8	15 56	607	+69	+1	+37	+38	+40
Iselsberg.....	46 51.4	12 52	1198	+19	-107	+35	+22	+11
Sterzing.....	46 53.9	11 26	950	-75	-164	-4	-17	-28
Weissenbachscharte.	47 01.4	10	2196	+71	-156	-16	-30	-41
Sonnblick.....	47 03.4	12 58	3099	+143	-153	-10	-24	-35
Steinach.....	47 05.4	11 28.4	1050	-76	-177	-19	-31	-42
Bucheben.....	47 09.5	12 58	1062	-68	-162	-20	-33	-44
Innsbruck 1.....	47 15.7	11 24.3	584	-127	-183	-33	-44	-52
Mixnitz.....	47 19.8	15 22	445	-46	-83	-4	-8	-12
Bruck an der Mur...	47 24.6	15 15	487	-19	-70	+14	+8	+4
Wörgl.....	47 29.5	12 03.9	508	-108	-161	-41	-45	-49
Semmering.....	47 38.0	15 50	986	+70	-37	+32	+26	+21
Benediktbeuern.....	47 42.5	11 24.1	618	-37	-106	-20	-20	-21
Hohenpeissenberg...	47 48.1	11 00.9	996	+4	-102	-17	-18	-19
Wiener Neustadt 1..	47 48.5	16 15	270	-13	-43	+1	+1	+1
Kaufbeuren.....	47 52.8	10 38	680	-16	-93	-16	-17	-17
Mean.....	.....	.....	.....	-14	-115	+2	-7	-13

particularly from the anomalies +116 and -107 mgal at the two stations Sandbüchel (elevation 2967 m) and S. Leonardo (elevation 655) only 18 km apart. They indicate that the free-air anomalies are very sensitive to gravity-station elevation and can hardly be used in the general interpretation of the gravity anomalies.

The Bouguer anomalies, on the other hand, are more representative; e.g., at the two stations mentioned they are -193 and -152 mgal, or a difference of only 41 mgal as compared with the 223-mgal difference of

the free-air anomalies. The Bouguer anomalies here also show the same dependence upon station height as previously.

The isostatic anomalies depend on the value given the thickness  $T$  of the earth's crust. The smaller  $T$  is, the larger the positive and the smaller the negative isostatic anomalies are. All three sets of isostatic anomalies are not very far from zero. The maximum deviations are 83 mgal for  $T = 20$

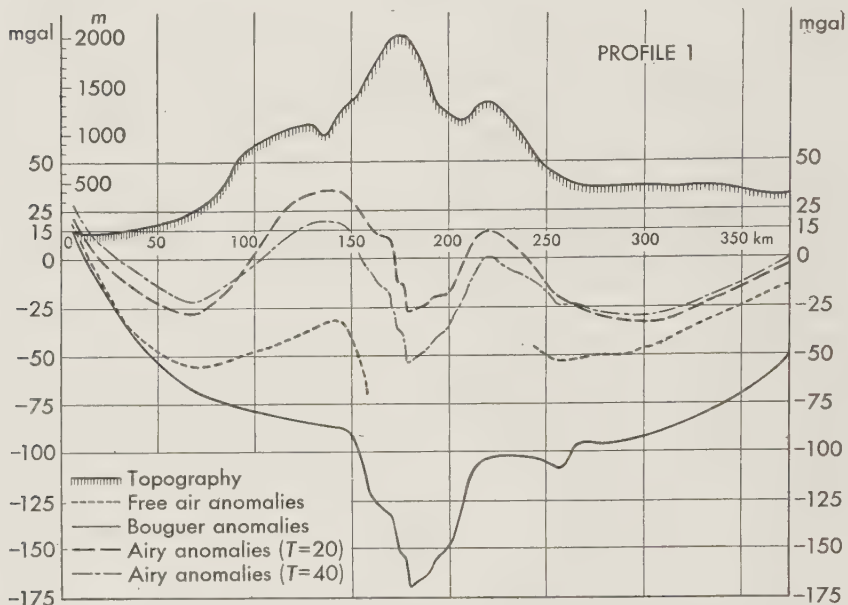


FIG. 7-1. The profile Pirano-Landau across the Alps shows that the Bouguer anomalies are an exaggerated mirror picture of topography. The isostatic anomalies are much smaller and nearly independent of the elevation of the mountain. [From Paavo E. Holopainen, On the gravity field and the isostatic structure of the earth's crust in the East Alps, Publ. Isos. Inst. IAG (Helsinki), no. 16, 1947.]

20 km, 83 mgal for  $T = 30$  km, and 96 mgal for  $T = 40$  km. The five average anomalies are free-air, -14 mgal; Bouguer, -115 mgal; isostatic,  $T = 20$  km, +2 mgal;  $T = 30$  km, -7 mgal; and  $T = 40$  km, -13 mgal.

Figure 7-1, showing the dependence of the free-air, Bouguer, and Airy ( $T = 20$  and 40 km) anomalies on the topography along the profile, indicates quite clearly that the curve of the Bouguer anomalies is like an exaggerated mirror picture of the topography. The higher the mountain, the more negative the anomalies. Also the free-air anomalies, jumping as they do rather rapidly from one point to another, are more dependent on the topography than the isostatic anomalies are. The better the correspondence of  $T$  value to the behavior of the earth's crust, the smaller the dependence of the isostatic anomalies on the topography.

Similar profiles in other parts of the Alps and in other mountains as well, published in different investigations, show the same phenomenon relative to the dependence of anomalies of different types on the elevation of the mountains.

The map of the East Alps (Fig. 7-2) best shows the correlation between the Bouguer anomalies and the topography. It can be seen that these

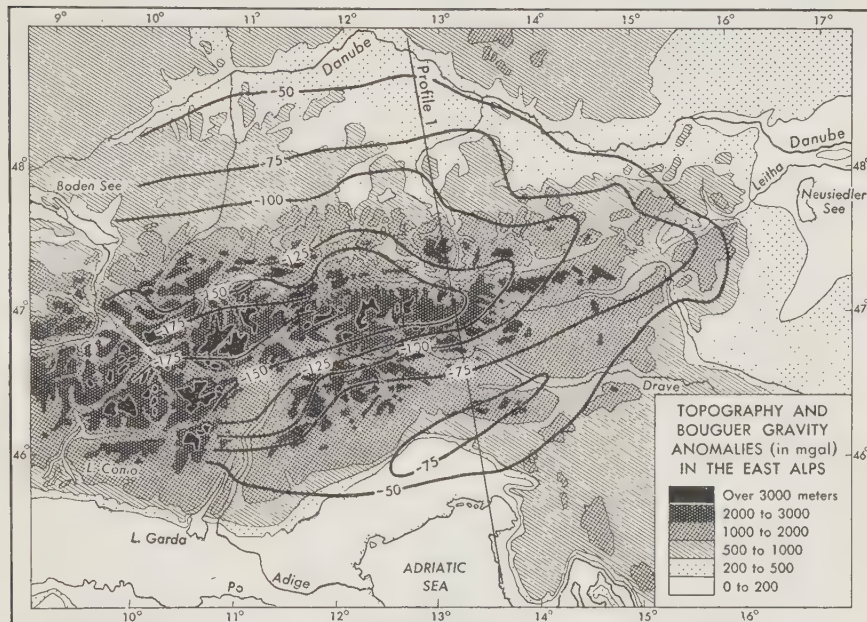


FIG. 7-2. The Bouguer gravity anomalies of the Alps bear a close relation to the topography. The higher the mountain, the more negative the Bouguer anomaly. The isoanomaly line  $-150$  mgal encircles the mountains higher than 3000 m.

anomalies are negative in the whole East Alps and in the surrounding areas. The  $-50$ -mgal isoanomaly line crosses the Po Valley, continues to Vienna, and surrounds the Alps along the Danube Valley, while the  $-75$ -mgal isoanomaly line is closer to the mountain itself. The  $-125$ - and  $-150$ -mgal lines are still closer to the highest area of the Alps. The contour line of 3000 m elevation is almost completely inside the  $-150$ -mgal anomaly line.

It is not correct to claim that the elevation of north Italy and of the Danube Valley is too low to correspond to the negative Bouguer anomalies from  $-50$  to  $-75$  mgal since these excessively large negative gravity anomalies are actually anticipated because of the "horizontal effect" of the light root formation of the Alps (see Sec. 7-2). Therefore, the essential part of the anomalies found can be explained by isostatic equilibrium,

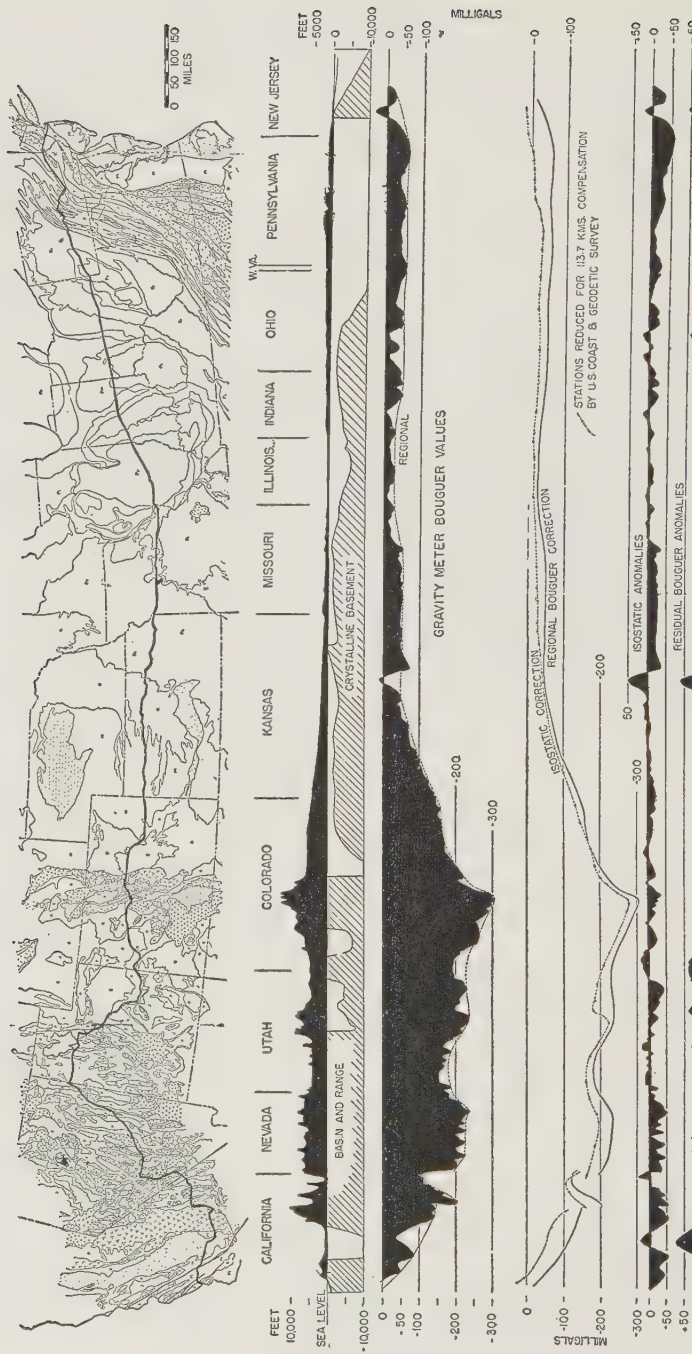


FIG. 7-3. Woollard's map of topography, topography profile in feet, Bouguer anomalies in milligals, and isostatic anomalies (Hayford system  $D = 113.7$  km) in milligals, resulting from his transcontinental measuring trip from New York to Los Angeles. The Bouguer anomalies are large and mirror the topography, whereas the isostatic anomalies are small. (From Bull. Geol. Soc. Am., vol. 54.)

except in the steep anomaly hollow of the Po Valley, which is caused in part by the light sediment layers of this area.

Among the evidence for isostatic equilibrium is the transcontinental gravity-anomaly profile measured by Woollard across the United States from New York to Los Angeles (Fig. 7-3). It can be seen that the Bouguer anomalies reach as high as  $-300$  mgal and are a true mirror picture of the topography, in striking contrast to the isostatic anomalies, which in general are smaller than  $\pm 25$  mgal and only rarely exceed  $\pm 50$  mgal. If the Airy-Heiskanen system,  $T = 30$  km, had been used, the isostatic anomalies might have been still less.

TABLE 7-6. GRAVITY ANOMALIES AT SEA<sup>17</sup>

Station no.	Location	$\varphi$	$\lambda$	Depth, m	Anomalies, mgal			
					Free-air	Bouguer	Isostatic, Airy-Heiskanen	
							20 km	30 km
Northern Hemisphere								
1	Mediterranean Sea .....	64°58'N	16°47'E	2200	-1	+149	+5	+8
2	Red Sea.....	20 42 N	38 28 E	1260	-8	+78	+17	+28
3	Indian Ocean.....	10 02 N	55 25 E	4210	-19	+267	-11	+3
4		7 53 N	65 58 E	4390	-33	+266	-34	-30
5		5 44 N	87 07 E	4020	-27	+247	-29	-24
6	Atlantic Ocean.....	36 23 N	26 43 W	3610	+26	+272	+31	+36
7		23 21 N	47 05 W	3550	+21	+263	+10	+5
8		21 35 N	63 22 W	5690	-6	+381	-7	-6
9	Pacific Ocean.....	10 21 N	88 30 W	3470	+29	+265	+27	+31
10		15 35 N	98 20 W	4730	-97	+225	-59	-18
11		29 13 N	117 06 W	3320	-49	+177	-36	-27
12		33 12 N	134 01 W	4930	-6	+329	-2	+5
13		15 32 N	168 27 E	5600	-6	+375	+1	+8
14		9 52 N	132 46 E	6050	+12	+424	+23	+33
Southern Hemisphere								
15	Atlantic Ocean.....	52°27'S	26°50'W	5600	-24	+357	-23	-20
16		15 02 S	37 03 W	4200	-40	+246	-37	-26
17		34 47 S	23 27 W	3700	+28	+280	+26	+26
18		31 56 S	1 58 E	1455	+93	+192	+50	+20
19		32 09 S	11 14 E	4690	+5	+324	+15	+30
20	Indian Ocean.....	29 30 S	36 50 E	4040	-12	+263	-6	+5
21		29 49 S	67 27 E	4570	+30	+341	+31	+36
22		31 55 S	110 19 E	5130	-13	+336	-8	-3
23		19 21 S	111 39 E	2390	-38	+125	-48	-46
Mean.....				....	-6	+269	-1	+3

*E. Gravity Anomalies at Sea*

Table 7-6 shows some gravity anomalies at sea collected by Vening Meinesz. The gravity stations have been taken at random. The striking phenomenon is again the small free-air and isostatic anomalies as compared with the strongly positive Bouguer anomalies, which are dependent on the depth of the ocean at the observation point. Thus we find, for instance, the following correlations. At stations 2, 4, 11, 14, 18, and 22 with the respective depths of 1260, 4390, 3320, 6050, 1455, and 5130 m, the corresponding Bouguer anomalies are +78, +266, +177, +424, +192, +336 mgal. The average depth of these six stations is 3767 m, and the average Bouguer anomaly is +249 mgal. If the oceans are in complete isostatic equilibrium, the Bouguer anomaly of an ocean 3767 m deep ought to be  $+0.06867 \times 3767 = +259$  mgal as compared with our figure of 249 mgal. These two figures indicate that isostatic equilibrium prevails at sea. This fact can be seen still better from the average free-air anomaly -6 mgal and the average isostatic anomaly -1 mgal for  $T = 20$  km and +3 mgal for  $T = 30$  km.

**7-2. Achievements of Isostasy**

We have taken so many examples—perhaps too many—from the gravity-anomaly fields of different continents and oceans to show that the mountains and the oceans are very close to being in complete isostatic equilibrium, in other words, that isostasy is a proved global phenomenon. We have done this deliberately, for there still are scientists of the opinion that isostatic equilibrium does not exist. If our tables and maps were to convince them that isostatic equilibrium prevails, the authors would be satisfied. All scientists interested in the structure of the earth's crust could then proceed on the same sound basis, and we could all, with our different methods and different materials, better advance this science. When isostatic equilibrium is accepted as a proved fact, it will be possible to investigate the thickness of the earth's crust, the magnitude of the deviation of the earth's crust from complete isostatic equilibrium in the different parts of the world, and the causes of such deviations. These interesting problems are handled in Chap. 10.

*A. Limitations of the Bouguer Gravity Anomalies*

The Bouguer anomalies have been widely used, not only in explorations for oil fields and mineral deposits, but in general geophysical studies as well. These anomalies have, in fact, advanced the science a great deal. The Bouguer anomalies are, of course, different depending on the density value used in computing them. In exploration geophysics it is just this fact that is utilized. A series of Bouguer-anomaly profiles using different

density values, ranging from 2.00 to 2.67, is computed. These "density profiles" also depend on the elevation variation along the profile. The density value which makes the elevation term of the gravity anomalies disappear is presumed to approach the actual density most closely.

In general geophysical studies of the earth's interior, too, the Bouguer anomalies have value. They are, in fact, qualitative evidence of isostatic equilibrium. In geophysical studies of lowlands and ocean basins, as well as of other regions where the topography is not too rugged, these anomalies even give reliable quantitative hints concerning the degree of isostatic equilibrium. If, however, one studies the behavior of the earth's crust close to mountain chains (*Randseken*), along the coastlines of deep oceans, or on ocean islands and in their vicinity on the basis of Bouguer anomalies, one can easily be misled.

For instance, in the northern *Randseken* of the Alps the Bouguer gravity anomalies at nine stations were studied by the author (H.) and were

TABLE 7-7. GRAVITY ANOMALIES IN THE RANDSENKEN OF THE ALPS<sup>11,15</sup>

Station	$\varphi$	$\lambda$	$h$ , m	Anomalies, mgal		
				Free-air	Bouguer	Airy-Heiskanen, 40 km
Vienna.....	48°13'	16°22'	183	0	-19	+21
Wels.....	48 10	14 02	317	-18	-50	+27
Traunstein.....	47 52	12 39	593	-35	-92	-5
Munich.....	48 09	11 37	525	-15	-62	+6
Hohenpeissenberg.....	47 48	11 01	996	+7	-102	-19
Augsburg.....	48 22	10 54	496	-2	-47	+10
Konstanz.....	47 40	09 10	401	-28	-70	+14
Ludwigshafen.....	47 49	09 04	401	-12	-53	+24
Waldshut.....	47 37	08 13	336	+9	-24	+46
Mean.....	.....	.....	....	-10	-58	+14

found to be, on the average, -58 mgal. Interpreting this fact as evidence that the root of the *Randseken* is too deep and the root of the Alps themselves too low, so that the *Randseken* helps to carry the mass of the Alps, as, for instance, Kossmat<sup>16</sup> claims, leads to a false conclusion. Negative Bouguer anomalies near mountain chains are caused by the effect of the light root formation of the mountain itself, even when the mountain is in complete isostatic equilibrium. This "horizontal effect" of the com-

pensation is considerable, and the deeper the root or antiroot formations are, the farther it reaches horizontally. This influence is felt particularly at island stations of isostatically compensated deep oceans; e.g., the horizontal effect of an ocean 5 km deep in the Hayford zones N and O, from 59 to 167 km, is no less than 100 mgal according to the Airy-Heiskanen system,  $T = 40$  km.

In the *Randsenken* of the Alps the isostatic anomalies,  $T = 40$  km, are on the average +14 mgal and indicate that the mountains themselves are overcompensated (roots too deep) rather than undercompensated, regardless of the fact that the Bouguer anomalies are strongly negative.

Consequently the Bouguer anomalies can hardly be used to decide whether or not the *Randsenken*, valleys, or rugged mountains are in complete isostatic equilibrium. It is quite different if other evidence, e.g., seismological findings or geological conclusions, leads to the result that, say, the *Randsenken* have sunk deeper than they should have according to isostatic equilibrium. In that case it must be accepted as a proved fact, but it cannot be claimed that the *Randsenken* have sunk too deep simply because the Bouguer anomalies are systematically negative there.

Since the Bouguer anomalies in the Hawaiian area (Table 7-8) are about

TABLE 7-8. GRAVITY ANOMALIES IN THE HAWAIIAN AREA

Station no.	$\varphi$	$\lambda$	Depth, m	Anomalies, mgal			
				Free-air	Bouguer	Airy-Heiskanen	
						20 km	30 km
110	22°13'N	155°24'W	4510	+3	+312	-7	-8
111	21 45	156 13	5430	-96	+271	-82	-65
112	21 09	157 28	510	+165	+195	+116	+86
113	21 18.4	157 52.0	Honolulu	+213	+217	+139	+103
114	20 48	158 36	4290	-18	+270	-17	-5
115	20 29	160 30	4590	-14	+324	+9	+13
116	19 58	164 56	4960	+10	+352	+8	+10

+200 mgal but on the surrounding sea are about +300 mgal, this area is, in a sense, a region of negative residual Bouguer anomalies. The isostatic or free-air anomalies, about +100 and +190 mgal in the Hawaiian area and -30 and +100 mgal on the surrounding sea show, however, that the Hawaiian area is a region of positive residual gravity anomalies.

Some geologists have claimed that isostasy is difficult to understand be-

cause the Hawaiian Islands are isostatically a positive-anomaly area but on the basis of Bouguer anomalies a negative-anomaly area. In fact, however, this is the way it must be, because isostatic equilibrium prevails under the adjacent ocean. On the basis of Bouguer anomalies every ocean is, up to +250 to +370 mgal, a positive-anomaly area, nearly every mountain a negative-anomaly area, and the lowlands almost a zero-anomaly area. In ocean islands the positive Bouguer anomalies must be much smaller than in open ocean.

The Bouguer anomalies behave this way for the following reason. In the Bouguer reduction on the continents and at sea we assume, in fact, that the mountains represent an absolute-mass-surplus area and the oceans an absolute-mass-deficiency area of the earth's crust. Consequently, in the Bouguer reduction we suppose that the topographic masses of the mountains have to be removed completely and that masses from outside the earth would have to be added to the ocean basins to fill them with a mass of the normal density, 2.67, of the earth's crust. But since the mountains are not mass additions or the oceans mass deficiencies, this reduction cannot give correct anomalies. The mean density of the earth's crust is smaller under the mountains and greater under the oceans than under the lowlands.

Because of this the mountain masses, instead of being removed, should only be transferred to the root formation of the mountains or, in the Hayford reductions, to the earth's crust between the geoid and the surface of compensation, where the mean density is too small. In a similar way, instead of further masses being added to the ocean basins, the mass surplus already existing under the ocean bottom in the antiroot of the ocean should be transferred to the ocean. No masses are to be discarded, nor are any new masses to be brought in; all that is needed is to transfer the existing mass anomalies from the mountains to the root formation and from the antiroots to the ocean basins. This is the meaning of topographic-isostatic reductions.

If we try to discover the mass anomalies of the earth's interior on the basis of the Bouguer anomalies, we now and then "bark up the wrong tree"; i.e., we try to find the mass anomalies near the earth's surface when they may actually be deep-seated. In such cases the observed gravity anomalies are caused, to a considerable extent, by the existing light root formations of the mountains or heavy antiroots of the oceans. Therefore, either only small disturbing masses under the gravity stations are needed or none at all.

#### *B. Normal Thickness of the Earth's Crust*

Before going into this question, it is well to keep in mind that in lowlands all kinds of gravity anomalies are relatively small. There are no

remarkable differences between the free-air, Bouguer, and isostatic anomalies. This fact is easily understood because in lowlands there are no mountains, valleys, or islands requiring isostatic compensation. Therefore existing anomalies are caused by local, irregular mass anomalies, which will be mirrored in the gravity anomalies regardless of how they have been reduced.

Because of this characteristic of the lowlands, it has been claimed that isostatic reduction has only small significance, since in most parts of the world the free-air anomalies are as small as the isostatic ones; but it is misleading to consider the lowlands when studying isostasy. Any meteorologist who interpreted the average temperature of the tropics on the basis of the temperature of the whole earth's surface would be bound to come to faulty conclusions. A gravimetrist will also reach the wrong conclusion if he studies isostatic equilibrium on the basis of lowland gravity anomalies and claims that only a small percentage of the topography of the continents is compensated isostatically because the mean Bouguer anomalies of the continents are not much greater than the isostatic anomalies. In fact, the average Bouguer anomalies of the continents are relatively small only because the gravimetrically surveyed mountains cover only a small part of the surveyed continents. In studying isostatic equilibrium in detail, it is essential to use the areas with variable topography, i.e., high mountains, ocean coasts and deeps, and ocean islands.

It is impossible, as we have seen, to study the details of isostatic equilibrium, particularly the mode and degree of the compensation, on the basis of Bouguer anomalies; these questions can be adequately solved only on the basis of isostatic anomalies. Since we cannot guess beforehand what isostatic system will be best or what the thickness of the earth's crust in the area to be studied will be, we have to make several assumptions, e.g., to compute the gravity anomalies using the values 20, 30, 40, and 60 km for the normal thickness  $T$  of the earth's crust. By analyzing the gravity-anomaly sets according to different  $T$  values we can then conclude what thickness corresponds to the behavior of the earth's crust.

We must bear in mind that the Bouguer reduction corresponds, in a way, to an isostatic reduction with infinite thickness and that the free-air reduction corresponds to an isostatic reduction with zero thickness of the earth's crust. As the Bouguer anomalies are negative and free-air anomalies positive in mountains, we can presume that there must be some particular thickness of the earth's crust for which gravity anomalies are zero on the average.

This fact makes it possible to determine the most probable thickness of the earth's crust, which is fairly easy, especially if the isostatic compensation is complete and local, as we have supposed, and thereby to choose the best isostatic system. It is likely that the best isostatic system

TABLE 7-9. GRAVITY ANOMALIES  $\Delta g$  AS FUNCTIONS OF THE OBSERVATION HEIGHT  $h$   
 $(\Delta g$  according to free-air,  $T = 0$  km, Bouguer,  $T = \infty$  km, and isostatic Airy-Heiskanen reductions;  $g$  in milligals,  $h$  in thousands of meters;  $T$  denotes normal thickness of earth's crust, corresponding to zero elevation)

Norway <sup>12</sup>		Ferghana Basin (Central Asia) <sup>4</sup>	
$T = 0$ km; = 40 km; = 60 km; = 80 km; = 100 km; = $\infty$ km;	$\Delta g = -6 + 38h$ $\Delta g = +20 - 8h$ $\Delta g = +21 - 20h$ $\Delta g = +18 - 18h$ $\Delta g = +14 - 35h$ $\Delta g = -3 - 80h$	$T = 0$ km; = 20 km; = 30 km; = 40 km; = 60 km; = 80 km; = 100 km; = $\infty$ km;	$\Delta g = -138 + 16h$ $\Delta g = -71 + 14h$ $\Delta g = -59 + 7h$ $\Delta g = -51 - 1h$ $\Delta g = -38 - 12h$ $\Delta g = -31 - 20h$ $\Delta g = -26 - 27h$ $\Delta g = -138 - 87h$
Central Alps <sup>15</sup>		West Carpathians <sup>20</sup>	
$T = 0$ km; = 20 km; = 30 km; = 40 km; = 60 km; = $\infty$ km;	$\Delta g = -137 + 60h$ $\Delta g = -1 - 2h$ $\Delta g = +1 - 11h$ $\Delta g = 0 - 17h$ $\Delta g = -6 - 23h$ $\Delta g = -85 - 39h$	$T = 0$ km; = 30 km; = 60 km; = $\infty$ km;	$\Delta g = +13 + 14h$ $\Delta g = +28 + 0h$ $\Delta g = +34 - 23h$ $\Delta g = +8 - 53h$
Northeast Italy <sup>19</sup>		South Africa <sup>9</sup>	
$T = 0$ km; = 20 km; = 30 km; = 40 km; = 60 km; = $\infty$ km;	$\Delta g = -58 + 39h$ $\Delta g = +38 + 9h$ $\Delta g = +40 - 1h$ $\Delta g = +40 - 8h$ $\Delta g = +37 - 18h$ $\Delta g = -36 - 43h$	$T = 0$ km = 20 = 30 = 40 = 60 = $\infty$	$r = +0.275$ $= +0.049$ $= -0.002$ $= -0.026$ $= -0.063$ $= -0.900$
Sweden <sup>22</sup>			
$T$ values	South of $58^\circ$ latitude	Between $58^\circ$ and $61^\circ$ latitude	North of $61^\circ$ latitude
$T = 0$ km $T = 20$ km $T = 30$ km $T = 40$ km $T = 60$ km $T = \infty$ km	$\Delta g = +11 + 49h$ $\Delta g = +13 + 4h$ $\Delta g = +13 - 7h$ $\Delta g = +12 - 15h$ $\Delta g = +12 - 31h$ $\Delta g = +12 - 63h$	$\Delta g = -10 + 19h$ $\Delta g = -7 + 12h$ $\Delta g = -6 + 3h$ $\Delta g = -7 - 2h$ $\Delta g = -7 - 11h$ $\Delta g = -10 - 91h$	$\Delta g = -7 + 37h$ $\Delta g = +1 + 25h$ $\Delta g = +3 + 15h$ $\Delta g = +3 + 9h$ $\Delta g = +4 - 7h$ $\Delta g = -7 - 74h$

will not be the same in all parts of the world. That system is best which gives the same mean gravity anomaly for mountainous regions as for neighboring plains and which eliminates the dependence of residual anomalies on the elevation of the station. Therefore, we express the gravity anomalies  $g$  as a function of the elevation  $h$  of the gravity station, as Bonsdorff<sup>1a</sup> first did when reducing the gravity anomalies in Spitsbergen in 1916. In this way we get the sets of values shown in Table 7-9.

In all seven of these places the dependence of the different gravity anomalies on the station height is similar. According to the free-air reduction the elevation term is clearly positive; according to the Bouguer reduction, very strongly negative. In South Africa, instead of the elevation term, the correlation factor  $r$  has been used

$$r = \frac{\sum h \Delta g}{\sum |h \Delta g|}$$

where  $|h \Delta g|$  is always positive but  $h \Delta g$  has the sign of  $\Delta g$ . The smaller  $r$  is, the better the  $T$  value fits.

When choosing the  $T$  values, according to which the elevation term is zero, we find the most probable normal thickness of the earth's crust to be 38 km in Norway and in the Ferghana Basin, 20 km in the East Alps, 30 km in the West Carpathians, 29 km in northeast Italy, 30 km in South Africa, 23 km in south Sweden, 36 km in central Sweden, and 56 km in north Sweden. It seems that the gravity anomalies yield values close to 30 km for the thickness of the earth's crust; in the Alps, however, the thickness appears smaller and in Norway, Sweden, and Ferghana distinctly larger.

The actual crust of the earth is, of course, thinner or thicker depending on the elevation of the area. For the density difference 0.6 between the substratum and the earth's crust, the thickness of the earth's crust can be taken from

$$T_c = T + 5.45h \text{ km} = T + 4.45h + h$$

$$T_s = T - 3.73t \text{ km} = T - (2.73t + t)$$

where  $T$  = normal thickness of earth's crust

$T_c$  = its thickness under continents

$T_s$  = its thickness under oceans

$h$  = elevation of area in question

$t$  = ocean depth

If, for instance, we use the values  $T = 30$  km,  $h = 3000$  m, and  $t = 5000$  m, we get  $T_c = 46$  km and  $T_s = 11$  km; here the thickness of the root would be 13 km and that of the antirroot below the ocean 14 km. If we use the value of 0.3 for the density difference instead of 0.6, we must multiply the

elevation of the continent by 8.9 to get the thickness of the root and multiply the depth of the ocean by 5.5 to get the thickness of the antiroot.

If we assume the following elevations: Norwegian mountains, 1 km; Sweden, 0.5 km; Ferghana, 2.5 km; East Alps, 2 km; West Carpathians, 0.5 km; northeast Italy, 1.5 km; and South Africa, 1 km, we obtain the following values for the real thickness of the earth's crust in these seven places: 43 km (Norway), 41 km (Sweden), 52 km (Ferghana), 31 km (East Alps), 33 km (West Carpathians), 36 km (northeast Italy), and 37 km (South Africa).

We can compare these gravimetric values for the thickness of the earth's crust with seismological results, which show one very clear discontinuity, called the Mohorovičić or M discontinuity, as well as one or two less clearly defined discontinuities. If we hold that the depth of the M discontinuity is equal to the thickness of the earth's crust, we shall not be very far from the truth. As late as about a decade ago seismologists were generally of the opinion that the M discontinuity lay at a depth of 40 to 60 km, except in California, New Zealand, and New England, where it was considered to be at a depth of 30 to 36 km.<sup>7</sup> Under the oceans it was, of course, closer to the earth's surface. Above this discontinuity there were two layers, the granitic and the intermediate. The resulting discrepancy between the seismological thickness (40 to 60 km) and the gravimetric thickness (about 30 km) was resolved when Tuve and Tatel<sup>21</sup> showed that different seismographs located only 25 m from each other can show considerably different records of the same explosion. Interpretation of seismograph records is therefore difficult, and for that reason it is possible that more discontinuities have been found than really exist in the earth's interior. According to several geophysicists, the existence of the granitic layer is questionable, and some seismologists are of the opinion that only the M discontinuity can be clearly discovered. Its depth in the continents is 30 to 45 km, depending on the elevation of the ground.

To make isostatic reduction as simple as possible, in their computations gravimetrists have used only two layers and, consequently, one discontinuity, which differs only slightly from the M discontinuity. Above the M level is the earth's crust, with the density 2.67; below it is the under-layer, the density of which is assumed to be 0.6 greater than that of the earth's crust.

Some seismologists have claimed that this assumption is incorrect because 0.5 would be a better density difference and because there are two or, if the thin sediment layer is also considered, even three discontinuities. The recent studies of Hess, Ewing, and Worzel have in fact shown that no granitic layer exists under the ocean and that the simatic layer, of density 2.9 to 3.0, is only 4 to 6 km thick. According to Gutenberg,<sup>8</sup> under the lowlands of continents there is a sediment layer of density 2.50 and

thickness 1 km, then a granitic layer of density 2.67 and thickness 19 km, and, finally, an intermediate layer of density 2.98 and thickness 10 km. For the column of a mountain 3 km high the granitic layer would be 27 km thick and the intermediate layer 25 km. An ocean 6 km deep has first a 6-km water layer, density 1.03, under it a 1-km sediment layer, density 2.50, and then a 5-km intermediate layer, density 2.98. The M discontinuity, under the intermediate layer, is 50 km deep under high mountains, 30 km deep under lowlands, and 12 km deep under oceans. The thickness of the antiroot of the ocean, density 3.3, would therefore be  $30 - 12 = 18$  km, as can be seen from the following equations (the sediment layer is omitted because its effect is the same in both cases):

$$1.03 \times 6 + 2.98 \times 5 + 3.3x = 2.67 \times 19 + 2.98 \times 10$$

$$x = 18.0 \text{ km}$$

If we compute the thickness of the antiroot as the isostasists do, using densities of 1.03 for the ocean (depth 6 km), 2.67 for the earth's crust, and 3.27 for the underlayer, we get the value 16.4 km, or a difference of only 1.6 km.

It is also evident that two discontinuities bring isostatically almost the same end result as one discontinuity, as Fig. 7-4 clearly demonstrates. To take another example, one half of the compensation occurring at a depth of 20 km and the other half at a depth of 40 km is isostatically nearly equivalent to one discontinuity at a depth of 32 km. Since isostasists use only one discontinuity, even though according to seismologists another discontinuity exists above it, the thickness  $T$  of the earth's crust computed gravimetrically ought to be slightly smaller than the depth  $M$  of the M discontinuity. Systematic differences between  $M$  and  $T$ —if the other discontinuity in fact exists—may be about 5 km.

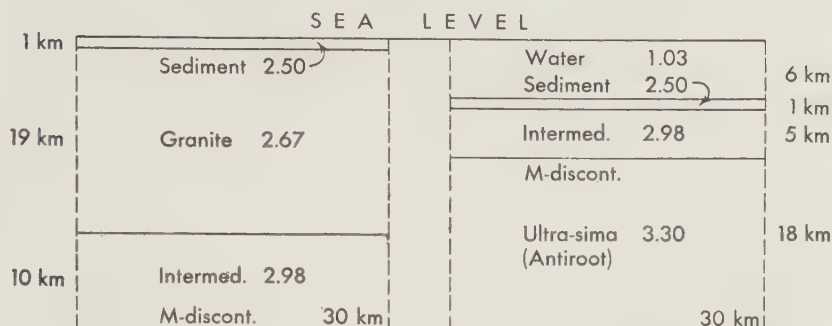
Since it is difficult, perhaps quite impossible, to determine the existence of two discontinuities gravimetrically, seismology must give reliable evidence concerning the density difference and the depth of the secondary discontinuity above the M discontinuity before two discontinuities can be used in the practical computation of isostatic reduction tables.

Recent work by Worzel in the West Indies has confirmed the finding that the thickness of the intermediate layer in the ocean area is only about 4 to 5 km and that the granitic layer is completely lacking there. In isostatic reduction it has always been assumed that, under the oceans, the thickness of the earth's crust—or the depth of the M discontinuity below the sea floor, to use the language of the seismologists—must be small. In our example it is 6.6 km, and generally it is hardly more than 10 km. If the density difference between the underlayer and the crust

## ISOSTATIC EQUILIBRIUM (Seismologists)

## Lowland profile

## Ocean profile



## ISOSTATIC EQUILIBRIUM (Isostasists)

## Lowland profile

## Ocean profile

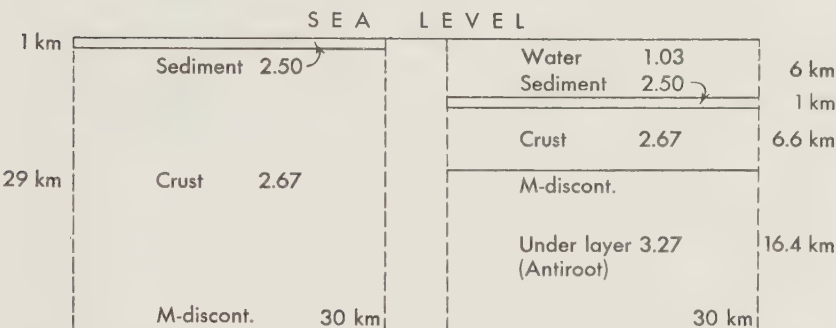


FIG. 7-4. From the gravimetric point of view there is no great difference between using one or two density discontinuities in the computations.

were 0.5 instead of 0.6, we should get 4.3 km instead of 6.6 km. So seismological evidence of recent years has proved the isostatic-floating theory to be true, as has the fact that the dependence of the thickness of the earth's crust upon the elevation of mountains and depth of oceans is practically the same according to both methods.

The above discussion does not mean, however, that the values  $T$  of the thickness of the earth's crust obtained gravimetrically are without error. On the contrary, it is very likely that the more new seismological evidence, particularly from the oceans, becomes available, the more the derived  $T$  values will vary from area to area. Nor is it necessary that isostatic compensation occur everywhere according to the concept of the floating theory, although it seems to be the general rule. In some places the Pratt-Hayford assumption might correspond to the reality better.

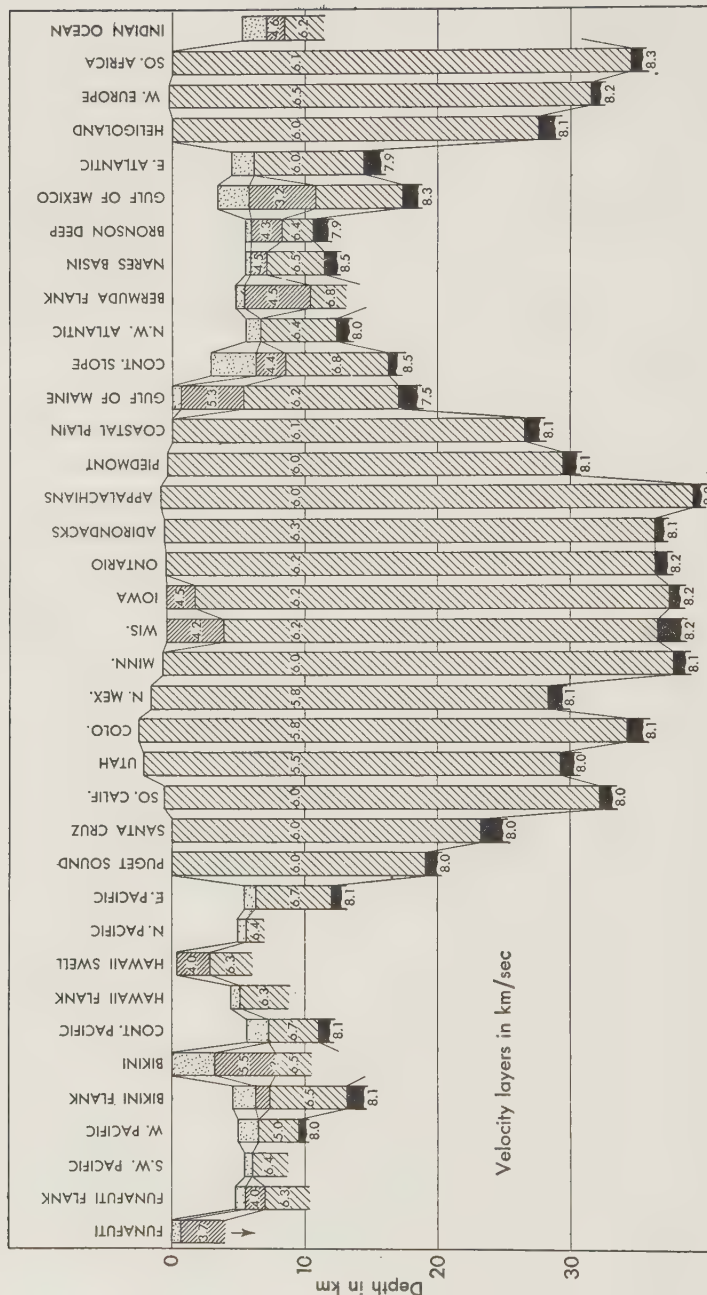


Fig. 7-5. Striking evidence for the Airy-Heiskanen theory. According to the material analyzed by Woppard, the earth's crust under both the Old World and the New World is much thicker and under the oceans much thinner than under the lowlands. Isostatic equilibrium will be caused by the roots of the mountains and the antiroots of the oceans. Average thickness is close to 30 km. (Courtesy of the Transactions of American Geophysical Union.)

It is, however, quite wrong to claim, as occasionally has happened, that neither the Pratt nor the Airy assumption can explain the gravimetric and seismological evidence. Also wrong is to use the small free-air anomalies as evidence against the isostatic theory. On the contrary, the small free-air anomalies prove the existence of isostatic equilibrium because free-air reduction is essentially a type of isostatic reduction, corresponding to the case when topographic masses are considered to be compensated at zero depth. The free-air anomalies, on the other hand, increase with the elevation of topography because the compensation actually occurs at a depth of 30 to 45 km and not at 0 km.

Tables 7-10 and 7-11 and Fig. 7-5 show clearly the existence of isostatic equilibrium and prove, in broad lines, the Airy assumption that the higher the topography, the thicker the earth's crust; the deeper the ocean, the thinner the earth's crust.

In the preceding discussion we have assumed the isostatic compensation to be local. We know, however, that there are areas, e.g., the ocean islands, where the compensation is regional. This aspect of isostasy will be handled later in this chapter.

Until now, sea level has been used as the reference surface from which not only the elevation of the continents or depths of the oceans but also the normal depth of the underboundary of the earth's crust have been computed. Below this normal depth exist the relatively light root formations under the mountains and above it the antiroots of the heavy ultrasimatic layer under the oceans. A different approach has been taken by Hess.<sup>14</sup> Seismological studies have shown, as mentioned before, that the M discontinuity is only 4 to 6 km below the ocean floor. Hess believes that, because the crust under oceans, which comprise 70 per cent of the earth's surface, is much simpler than under continents, it may be best to use the M discontinuity as the reference surface. His point of view is interesting. He simply claims that the M discontinuity exists at 35 km below the continents and that it can be neither higher nor deeper. If it were deeper, the continents, unless their density changed, would stand higher. If they stood higher, erosion would plane them off. If, on the other hand, the M discontinuity were higher, the continents would have been below sea level, emerging later, after epochs of diastrophism had compressed them laterally and thickened them. Obviously therefore, according to Hess, there is a direct connection between the sea level and the depth of the M discontinuity under continents.

The isostatic-floating theory postulates that under the mountains there are root formations of light crustal material and under the oceans antiroots of heavy subcrustal material. If the thickness of the root or antirroot is sufficient, isostatic compensation is complete. If the root and antirroot

TABLE 7-10. SEISMOLOGICAL DETERMINATION OF THE DEPTH OF THE M DISCONTINUITY IN AMERICA<sup>23</sup>

Area	Elevation, m	Depth of M discontinuity, km	Observer
Coastal Plain:			
Maryland, Virginia . . . . .	30	26-29	Tuve, Tatel
Appalachian Mountains:			
Virginia, Tennessee . . . . .	750	39	Tuve, Tatel
Pennsylvania . . . . .	220	33	Katz
Canadian Shield:			
Minnesota . . . . .	420	37	Tuve, Tatel
Central Adirondacks . . . . .	360	36	Katz
East Adirondacks . . . . .	330		Katz
Ontario . . . . .	300	36	Hodgson
Michigan, Wisconsin . . . . .	440	36	Slichter
Wisconsin . . . . .	190	36	Slichter
Coast ranges:			
California (Corona) . . . . .	450	23-32	Tuve, Tatel
Washington . . . . .	360	30	Tuve, Tatel
Southern California . . . . .	450	32	Shor
Pacific Coast:			
Puget Sound . . . . .	210	19	Tuve, Tatel
California (Santa Cruz) . . . . .	40	23	Tuve, Tatel
British Columbia . . . . .	0	33	Milne
Colorado Plateau:			
South boundary-north . . . . .	2100	34*	Tuve, Tatel
South boundary-south . . . . .	1350	28*	Tuve, Tatel
Basin and range:			
East boundary-east . . . . .	1950	29	Tuve, Tatel
New England Highlands . . . . .	60	36	Leet
Connecticut . . . . .	20	25	Slichter
Interior lowlands:			
Iowa, Wisconsin . . . . .	160	37	Slichter
Allegheny Plateau:			
New York . . . . .	20	38	Slichter

\* About 45 km, as corrected by Ewing and Press.

are too thin, the topography is undercompensated, and if they are too thick, it is overcompensated.

There are also places where root formations exist without any mountains above them, e.g., in the belts of negative gravity anomalies in the East Indies, in the West Indies, and east of Japan. On the other hand, there are isolated mountains and islands, like the Harz Mountains in Germany

TABLE 7-11. SEISMOLOGICAL DETERMINATION OF THE DEPTH OF THE M DISCONTINUITY AT SEA<sup>23</sup>

Area	Elevation, km	Depth of M discontinuity, km	Observer
Northwest Atlantic.....	-5.20	12.0	Ewing
Nares Basin.....	-5.34	11.1	Officer, Ewing
Northwest Atlantic.....	-4.8	9.5	Ewing
Gulf of Mexico.....	-3.7	17.5	Ewing
Caribbean.....	-2.1	13.5	Ewing
Bronson Deep.....	-5.3	10.4	Hersey, Officer
Continental Slope.....	-2.87	15.9	Officer, Ewing
Gulf of Maine.....	-0.02	16.5	Katz
East Pacific.....	-5.5	12.0	Raitt
Bikini Flank.....	-4.6	13.0	Raitt
Central Pacific.....	-5.5	10.8	Raitt
Marianas area.....	-4.9	9.4	Gaskell, Swallow

and several volcanic ocean islands, where only a thin root formation or none exists.

These facts bring us to the general "root-formation theory," which is concerned with formations of three types: mountains with normal roots, where isostatic equilibrium prevails and gravity anomalies are small; mountains without corresponding roots, where gravity anomalies are positive; and roots without any mountains over them, where the gravity anomalies are negative. The second type occurs when the mass load of

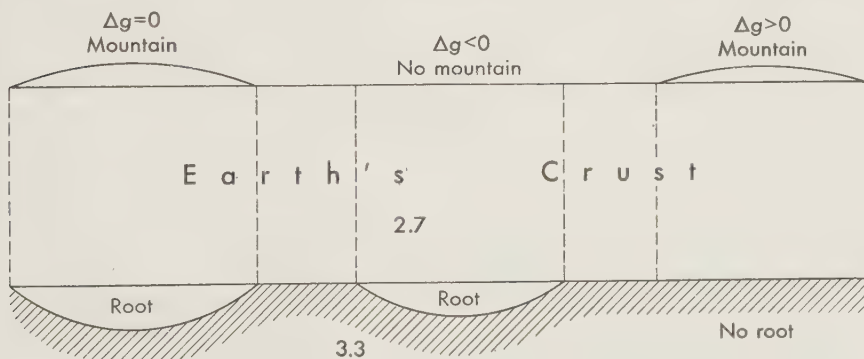


FIG. 7-6. General root theory.<sup>13</sup> When the mountains have normal roots, isostatic equilibrium prevails. When there are root formations without any mountains or mountains without any roots, there is no isostatic compensation, and gravity anomalies  $\Delta g$  are negative and positive, respectively.

the mountain is too small to force the earth's crust to sink into equilibrium. The third type appears in areas where the mountain chains are in *statu nascendi*, and where the earth's crust rises until isostatic equilibrium prevails (Fig. 7-6). These problems are handled in detail in Chap. 10.

### C. One of Nature's Great Isostatic "Experiments"

The postglacial uplift of land in Fennoscandia, one of the most interesting of geophysical phenomena, has been studied thoroughly, particularly by Finnish, Norwegian, and Swedish geologists, and during the last few decades by geodesists also. By measuring the elevation of the ancient shorelines of different parts of Fennoscandia, it has been possible to determine the amount, and to a certain extent the rate, of land uplift. The general opinion of Quaternary geologists is that the earth's surface in this area rose about 250 m during the last period of glacial time and about 270 m since the end of glacial time.

The geodetic method for measuring the rate of the uplift is the most accurate. When two precise levelings of the land-uplift area are made at intervals of, say, 40 to 50 years (as has been done in Finland—one from 1892 to 1910, the other from 1937 to 1953), the relative uplift of the ground is easy to find. These two levelings have yielded the land uplift<sup>16a, b</sup> shown in Fig. 7-7.

The uplift in the middle part of the Gulf of Bothnia amounts to 90 cm per 100 years; on the Swedish side it might even be 100 cm per 100 years. This value gradually diminishes toward the southeast and is zero in the vicinity of Leningrad.

Beyond the zero line of land uplift the land is sinking, although rather slowly. The mathematics of this interesting problem are outside of the scope of this chapter (they are dealt with thoroughly in Chap. 10); however, this phenomenon should be noted because it is such good evidence of the trend toward isostatic equilibrium of the earth's crust. It is even more interesting because it is an "experiment" which nature itself is making before our very eyes.

During the glacial period, when an icecap about 2000 to 2500 m thick covered Fennoscandia, the earth's crust sank under the load of the extra weight, perhaps so deep that an approximate equilibrium prevailed.

The subcrustal layers at that time moved only in a horizontal direction toward the unloaded areas and forced the land to rise a little along the periphery. After the icecap melted, the land began to rise in the central region and consequently to sink slightly near the periphery. This uplift of the central area and subsidence beyond the zero elevation still continue, as shown both by the map in Fig. 7-7 and the drowned forests near the periphery. Of course, other phenomena also take part, particularly the vari-

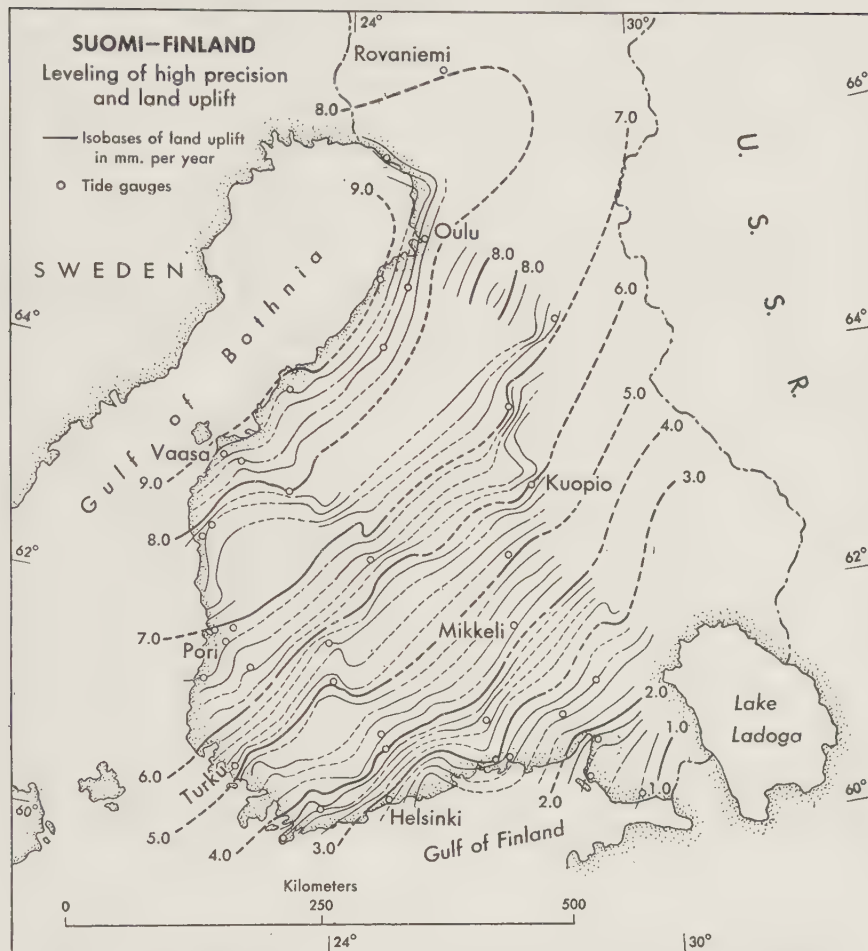


FIG. 7-7. Land uplift in Finland according to E. Kääriäinen.<sup>16b</sup> (From an article of T. J. Kukkamäki; courtesy of Bulletin géodésique of the IAG.)

able uplift or sinking of the sea level itself. The movement of the earth's crust itself, however, is the main phenomenon.

At the present time the flow of the subcrustal material should be directed toward the center. Since all the mass that flowed outward during the glacial period has not had time to move back, there is too little mass under the uplift, and the gravity anomalies are therefore negative, being as high as  $-50$  mgal at the center of the area. The existence of negative gravity anomalies (Fig. 7-8) in the uplift area is of great significance. If the subcrustal masses had moved only vertically downward during the glacial period and upward later on, the mass under the glacial areas would



FIG. 7-8. Correlation between the land uplift and gravity anomalies (according to Daly). The larger the land uplift, the more negative the gravity anomalies. (Courtesy of the Isostatic Institute of the IAG and Prentice-Hall, Inc.)

not have changed, so that there would be no reason for the systematically negative gravity anomalies. The existence of the negative gravity field in this area is evidence of the horizontal movement of the suberustal masses. It should be understood, however, that other effects, e.g., the local density differences close to the earth's surface, make the gravity field rather complicated and that the gravity anomalies, therefore, are due not only to the uplift of the land but also to some local causes as well.

On the basis of the gravity-anomaly field of the land-uplift area of Fennoscandia, Niskanen came to the conclusion, as the map (Fig. 7-9)

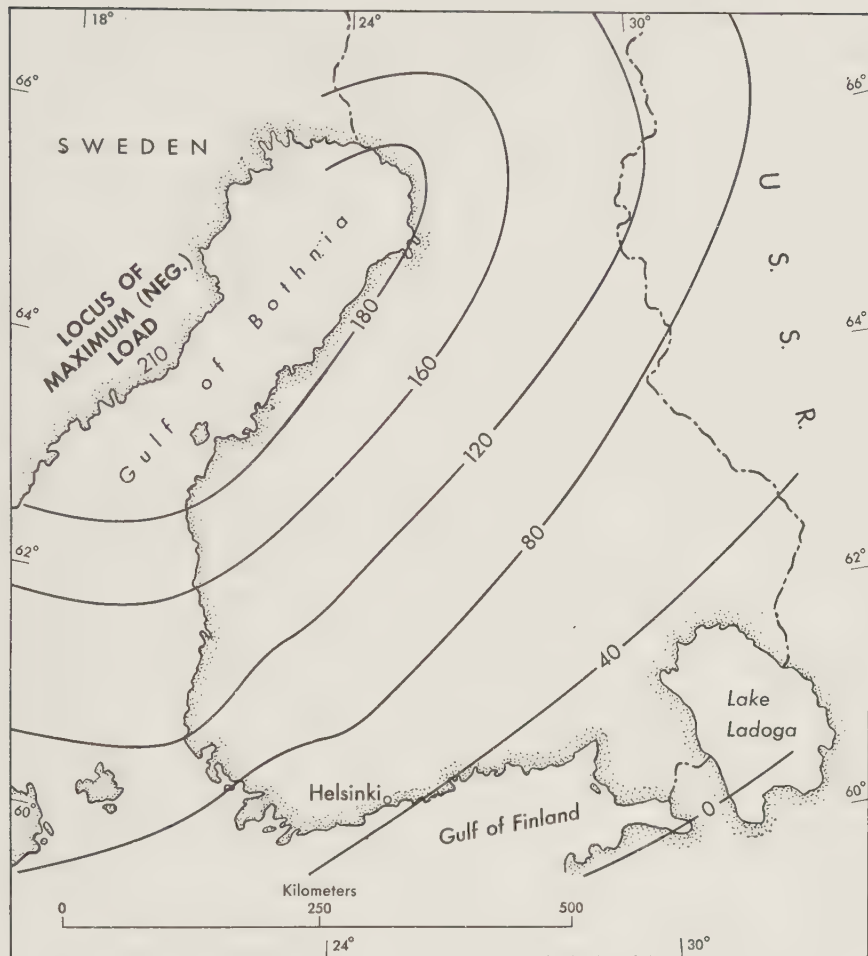


FIG. 7-9. According to Niskanen, the land still has to rise about 200 m before isostatic equilibrium is complete. The rigidity of the earth's crust is, however, so great that complete isostatic equilibrium will hardly be reached. (Courtesy of the Isostatic Institute of the IAG.)

from his valuable publication<sup>16c</sup> shows, that the land still has to rise about 200 m before complete isostatic equilibrium prevails. Since, however, the area is too small to reach complete equilibrium, the total remaining land uplift in the central area of Fennoscandia may not be so high as 200 m.

#### *D. Degree of Regionality of Isostatic Compensation over Volcanic Islands and Continental Margins*

In several volcanic-island areas gravity has been measured both on land and over the adjacent seas. The anomalies on the islands usually show

large positive values. We shall see that they can be explained by the combination of two effects: the high density of the volcanic lava constituting these islands and the regional compensation of this topography.

It is clear that the eruption did not leave any empty chambers directly below the islands because in that case the corresponding deficiencies of mass would to some extent provide a locally concentrated mass compensation, which would make itself apparent in the gravity anomalies. The gravity measurements also indicate that the rigid crust is strong enough to carry the loads represented by the volcanoes and hence to readjust the isostatic equilibrium by bending. From the radius of this bending, which is dependent on the degree of regionality of the compensation, the thickness  $T_r$  of the rigid crust can be derived. This crustal thickness is different from that of the M crust, i.e., the depth of the M interface, which borders the chemical crust.

The computations leading to the results contained in Table 7-12 have been carried out for two values of the density of the island masses, viz.,  $\rho = 2.937$  and  $\rho = 3.07$ , between which, in most cases, the true value must lie. The table gives the anomalies after isostatic reduction according to  $T = 30$  km and for five values of the radius  $R$  of regionality from 0 to 232.4 km; it shows the mean anomaly of the number of stations listed in the last column. The deep-sea value following each island group gives mean anomaly at sea in the neighborhood.

It is clear that, with the exception of the Azores, regional isostatic reduction can bring the results for the island stations into fair harmony with those for the deep sea around them; smaller local anomalies, of course, remain present. If a value of 2.67 had been used for the density  $\rho$  of the topography, this result could not have been fully attained. For Madeira the best-fitting radius  $R$  is about 174.3 km, but for the other islands it is 232.4 km or perhaps somewhat larger.

Applying Formulas (5-18a) and (5-19) for  $l$  and  $R$  and introducing  $m = 4.1$ ,  $E = 10^{12}$  dynes/cm<sup>2</sup>,  $\rho_s = 3.27$ , and putting for  $\rho_0$  a value of 2.4, corresponding to the filling of the downbending by sediments, we obtain for  $l = 60$  km and  $R = 174.3$  km a value for the thickness  $T_r$  of the rigid crust of 24.3 km and for  $l = 80$  km and  $R = 232.4$  km a value for  $T_r$  of 35.6 km.

We can conclude that for most of the islands investigated the thickness of the rigid crust is about 35 km or slightly more. Though this refers to the oceanic crust, it seems to correspond remarkably well to the mean thickness of the M crust in the continents. An explanation of this coincidence may perhaps be given by assuming that below this depth, because of the higher temperature, the rocks under continents and oceans are plastic and that, therefore, sialic matter below the continents, reaching

TABLE 7-12. MEAN ISOSTATIC GRAVITY ANOMALIES IN MILLIGALS FOR  $T = 30$  km  
IN VOLCANIC-ISLAND AREAS

Radius $R$ :	0 km		58.1 km		116.2 km		174.3 km		232.4 km		Number of stations
	2.937	3.07	2.937	3.07	2.937	3.07	2.937	3.07	2.937	3.07	
Density:											
Hawaii.....	+188	+174	+163	+148	+108	+91	+52	+32	+10	-13	6
Oahu.....	+106	+98	+86	+77	+47	+36	+16	+3	-4	-17	6
Deep sea.....	-16	-16	-9	-9	+1	+2	+11	+12	+15	+16	4
Madeira.....	+107	+96	+81	+69	+43	+28	+15	-1	-5	-24	3
Deep sea.....	+14	+14	+16	+17	+16	+16	+14	+14	+12	+11	10
São Vicente, Cape Verde Island.....	+128	+120	+107	+98	+70	+58	+53	+40	+28	+12	4
Deep sea.....	+5	+4	+8	+8	+10	+10	+7	+7	+4	+2	4
Hamilton, Bermuda.....	+149	+139	+120	+109	+75	+61	+45	+30	+24	+7	1
Deep sea.....	-11	-11	-8	-8	-6	-6	-7	-7	-10	-10	4
Las Palmas, Grand Canary.....	+72	+68	+64	+61	+46	+40	+33	+26	+22	+13	2
Deep sea.....	-8	-8	-4	-4	+1	+1	+4	+4	+5	+4	8
Port Louis, Mauritius.....	+140	+133	+119	+111	+85	+75	+59	+47	+37	+23	1
Deep sea.....	+18	+18	+23	+24	+22	+22	+20	+20	+17	+16	4
Fayal.....	+24	+19	+17	+12	+12	+2	-3	-10	-18	-29	3
Ponta Delgada, São Miguel.....	+43	+37	+29	+17	+9	+0	-8	-18	-27	-40	1
Sea, depth 1000– 2500 m.....	+39	+37	+39	+37	+34	+31	+26	+23	+14	+8	14
depth > 2500 m.	+37	+35	+38	+38	+42	+42	+47	+46	+47	+45	8

to greater depths, is carried away by convection currents in the mantle. Chapter 11 deals with the problem of the existence of such currents.

The results for the Azores, which present a different and rather complicated picture, can perhaps be explained by the presence of great fault planes breaking up the crust in blocks and thus effecting a more or less local adjustment of the isostatic balance; such fault planes are probable because of the distribution of the volcanoes and the topography.

Further details of gravity results in the area of volcanic islands can be found in Vening Meinesz.<sup>17</sup> The gravity results he found over continental margins are dealt with in Chapter 4 of the same publication. We shall summarize his conclusions here. Table 7-13 gives the differences of two stations in each gravity profile, one on the ocean side of the shelf and one on the continental side. As the stations were chosen more or less arbi-

TABLE 7-13. DIFFERENCES OF GRAVITY IN MILLIGALS OF OCEAN MINUS CONTINENTAL STATION

trarily, the differences are only roughly representative of the profiles. The figures for depth given in the last two columns refer to the same stations.

For most of the coasts the data indicate local or nearly local isostatic compensation, a result that might have been expected. The great difference in elevation of the crust in the continents and the oceans can be attributed to a sudden thinning near the coast of the sialic layer; hence, the compensation can be expected to be nearly local.

Disturbances occur for three reasons. (1) The coasts are especially liable to sedimentation, and so in many places parts of the continental shelves must consist of light sediments with densities considerably lower than the value of 2.67 adopted for the topographic reductions. (2) Isostatic equilibrium means that a continental shield consisting of a layer of density 2.67 in its upper half and a layer of density 3.00 in its lower half is nearly 87 per cent submerged in the olivine of the mantle, which has a density of 3.27. We can expect a continental block to have an edge which bulges out farthest at a level of half its height, which implies a hidden bulge of lighter continental matter under the edge of the ocean floor. (3) Coasts are often marked by tectonic belts, and if they are active in the present period, mass deviations can be expected along such coasts.

Hence it is not surprising that the gravity profiles show deviations from the picture adopted for the isostatic reductions and that complicated isostatic anomalies are therefore found in continental margins. This is true of several of the profiles given in the table. A more detailed study in the original publication<sup>17</sup> led to the following conclusion, which is in fair agreement with the results given by Table 7-13:

With the exception of only two coasts we have found everywhere evidence of local isostatic compensation of the Airy type and in most cases this evidence was clear and decisive. The conclusion about the best value of  $T$  for the different coasts was somewhat less sure but in most cases a value of  $T$  of 30 km seems to fit best. In a few cases as e.g., the west-coast of Africa near the Canary Islands, the northwest cape of Australia and Socotra a value of 20 km seemed preferable, but in none of these cases the evidence was complete enough for a decision.

We may make mention here of the important seismic evidence for coastal shelves recently collected by Ewing, Worzel, and their collaborators.

The seismic and gravimetric data they gathered for several profiles on the east coast of the United States give an almost complete solution of the important problem of crustal constitution near continental coasts. In general, they confirm the provisional conclusions given above.

## REFERENCES

1. Bonsdorff, I.: Détermination d'attractions locales sur les points astronomiques du réseau russe au Spitzberg, Mesure d'un arc de méridien au Spitzberg, vol. 1, sec. 4B, 1905.
- 1a. ———: Réductions isostatiques de la direction de la verticale et de l'intensité de la pesanteur; *Ibid.*, sec. 4B1, 1916.
2. Bowie, William: Investigations of gravity and isostasy, USCGS, Spec. Publ., no. 40, 1917.
3. Bullard, E. C.: Gravity measurements in East Africa, Trans. Roy. Soc. (London), ser. A, vol. 235, 1936.
4. Erola, V.: On the structure of the earth's crust in the neighbourhood of the Ferghana Basin, Publ. Isos. Inst. IAG (Helsinki), no. 10, 1941.
5. Evans, P., and W. Crompton: Geological factors in gravity interpretation illustrated by evidence from India and Burma, Quart. J. Geol. Soc. London, vol. 102, pp. 211–249, 1946.
6. Ewing, Maurice, and J. Lamar Worzel: Gravity anomalies and structure of the West Indies, Bull. Geol. Soc. Amer., vol. 65, pp. 165–173, 195–199, 1955.
7. Gutenberg, B.: Crustal layers of the continents and oceans, Bull. Geol. Soc. Amer., vol. 62, pp. 427–440, 1951.
8. ———: Geophysical data implied in isostatic calculations, unpublished study.
9. Hales, A. L., and D. J. Gough: Measurements of gravity in Southern Africa, The Government Printer, Pretoria, 1950.
10. Heiskanen, W. A.: Beobachtung der Schwerkraft, Die Lotabweichungen, Das Problem der Isostasie, in B. Gutenberg (ed.), Handbuch der geophysik, Abschn. 12, Bd. 1, Lief. 4, Borntraeger, Berlin, 1936.
11. ———: *Ibid.*, p. 903.
12. ———: Schwerkraft und isostatische Kompensation in Norwegen, Publ. Finn. Geod. Inst., no. 5, 1926.
13. ———: Rept. isostasy, Brussels Assembly IUGG, 1951.
14. Hess, Harry: Changes in the earth's crust with time, Bull. géod., no. 31, 1954.
15. Holopainen, Paavo E.: On the gravity field and the isostatic structure of the earth's crust in the East Alps, Publ. Isos. Inst. IAG (Helsinki), no. 16, 1947.
16. Kossmat, F.: Die Entstehung der mediterranen Kettengebirge in ihrer Beziehung zum Gleichgewichtszustande der Erdrinde, Abhandl. math.-physik. Kl. sächs. Akad. Wiss. (Leipzig), vol. 38, no. 2, 1921.
- 16a. Kukkamäki, T. J.: Über zwei dem Präzisionsnivelllement sich anschliessende Fragen, Publ. Finn. Geod. Inst., no. 26, pp. 119–125, 1939.
- 16b. Kääriäinen, E.: On the recent uplift of the earth's crust in Finland, Publ. Finn. Geod. Inst., no. 42, 1953.
- 16c. Niskanen, E.: On the upheaval of land in Fennoscandia, Publ. Isos. Inst. IAG (Helsinki), no. 6, 1939.
17. Vening Meinesz, F. A.: Gravity expeditions at sea 1923–1938, vol. 4, Publ. Neth. Geod. Comm., Delftsche Uitgevers Mij, Delft, 1948.
18. Miller, A. H., and W. G. Hughson: Gravity and isostasy in Canada, Publs. of Dominion Observatory, Ottawa, vol. 11, no. 3, 1936.
19. Morelli, Carlo: Rilievo gravimetrico e riduzione isostatica nell'Italia Nord-Orientale, Osserv. geofis. (Trieste), N.S., no. 20, 1951.
20. Tanni, L.: On the isostatic structure of the earth's crust in the Carpathian countries and the related phenomena, Publ. Isos. Inst. IAG (Helsinki), no. 11, 1942.

21. Tuve, M. A., H. E. Tatel, and L. H. Adams: Coherent explosion wave patterns at 100 kilometers, 1951.
22. Wideland, Bror: Topographic-isostatic reduction of the Swedish gravity stations, Rikets allm. kartverk, Publ. no. 23, Stockholm, 1954.
23. Woollard, George P.: Report of the special committee on the geophysical and geological study of the continents, 1952-1954, Trans. Am. Geophys. Union, vol. 36, pp. 695-708, 1955.
24. Worzel, J. Lamar, and G. L. Shurbet: Crustal density based on gravity and seismic data, Symposium, New era of geodesy, Bull. géod., no. 36, 1955.

## CHAPTER 8

### PHYSICAL GEODESY

#### 8-1. Existing Geodetic Systems

Geodesy is both theoretical and practical. Its theoretical function is to determine the size and shape of the earth and, in conjunction with other earth sciences, to study the structure of the earth's crust and of the immediately underlying layers. Its practical function is to perform the measurements and computations that will give the coordinates of selected control points on the earth's surface, i.e., to fix their positions on the earth's surface.

A good and reliable control-point system is a prerequisite for good maps. It is like a skeleton which has to be covered with flesh and blood, i.e., by the measurements of details. Without a good control-point system it is impossible to prepare accurate maps, however careful the measurement of detail and the drafting of the maps may be. The arrangement of a good control-point system by means of very accurate measurements, long formulas, and time-consuming computations is the most difficult and important part of geodesy.

By control points are meant points on the ground whose geographic latitude and longitude (often also elevation computed from sea level) are very accurately given. In mapping work, however, it is simpler to use rectangular plane coordinates  $x$  and  $y$  instead of latitude and longitude. These, of course, can be computed, for different map projections, from the geographic coordinates.

Depending on the accuracy required and the purpose for which the geodetic computations are intended, either a plane, sphere, ellipsoid of revolution, triaxial ellipsoid, or geoid can be used to represent the earth's true surface. The plane, of course, does not require any parameter. The sphere requires one, the radius  $R$ . The ellipsoid of revolution requires two, the earth's equatorial radius  $a$  and the flattening  $\alpha$  of the meridian. The triaxial ellipsoid requires four,  $a$  and  $\alpha$ , as above, the flattening of the equator  $\alpha'$ , and the longitude  $\lambda_0$  of the major axis of the equator. Since the geoid is not a mathematical surface but depends upon the irregular distribution of visible and invisible masses near the earth's surface,<sup>26,27</sup> it must be determined point by point.

### A. Meaning of Geodetic Systems

If only a small region is to be mapped, a plane is sufficient. In computing the control point of larger areas, the curvature of the earth becomes appreciable, and a sphere or an ellipsoid of revolution must be used. The triaxial ellipsoid is used more rarely in geodesy, but the need for it, if it truly exists, has great geophysical significance. The geoid plays a basic part in modern geodesy.

Control-point systems can be divided into three groups, local systems, nationwide systems, and the world geodetic system. There is also another division into horizontal and vertical control systems. The last mentioned is, however, not discussed in this book.

If we have a *local* mapping project, e.g., a city survey, we can usually neglect the curvature of the earth and assume the measurements to be made on a plane. If the curvature is needed, a sphere will represent the earth sufficiently well. For local mapping, we make a local triangulation or traverse polygon which includes the essential part of the area to be mapped. Either one gives the control points of the first order, which control the traverses measured along the streets and highways. Of course, we have to carry out adjustments of the local triangulations and traverses in order to get undisputed local systems.

We could compute the coordinates of local systems without any state control points or astronomic observations. We have only to take one point as origin of the coordinates and give it any arbitrary coordinates. In the same way we could choose any direction not very far from north as the starting direction from which to compute the grid azimuths and coordinates.

This method, however, is not very acceptable. It is much better to join the local survey to the triangulation system of the country or to make astronomic observations of the latitude, longitude, and azimuth at the initial point of the local system—as is usually done. In the first case we have the geodetic coordinates and azimuth (referred to the reference ellipsoid); in the second case, the astronomic coordinates and azimuth of the point of origin (referred to the geoid).

When we have to make a control survey of an entire *country* or a large part of it, the above requirements are not sufficient. Besides triangulation and traverses of different order, we need a reference surface which approaches the real earth as closely as possible and which can be used in computing the coordinates of the control points.<sup>26, 27, 29</sup>

To define this *national* geodetic control system completely we need five quantities, the latitude  $\varphi_0$  and longitude  $\lambda_0$  of the initial point of the geodetic datum, the azimuth  $A$  from this point to a control point, and the equatorial radius  $a$  and flattening  $\alpha$  of the reference ellipsoid employed.

In other words, we need a point *from* which to compute, a direction *in* which to compute, and a surface *along* which to compute. Even if only one of these fundamental quantities changes, the whole geodetic system in question will change too.

We establish a national geodetic system by choosing one triangulation point as the initial point of the geodetic datum. At this initial point we measure astronomically the latitude  $\varphi'_0$ , longitude  $\lambda'_0$ , and azimuth  $A'_0$  as accurately as possible. Beginning with the initial point, we then compute the coordinates of the triangulation points along the adopted reference ellipsoid. If for some reason we know or believe that at the initial point there exists a considerable deflection of the vertical, we subtract its effects from  $\varphi'_0$ ,  $\lambda'_0$ , and  $A'_0$ ; until recently, however, this has seldom been done.

If the country in question is not very large, we can use any reasonable reference ellipsoid because, in any case, its effect will be so small that it will do no harm in practical mapping. The reliability of the astronomic, triangulation, and traverse data depends on the accuracy of the measurements. It is true that we can improve the triangulation and traverses, in a way, by the aid of adjustment computations. No adjustment, however, can give good control points from poor measurements. The significance of the adjustment computation lies mainly in the elimination of the *inner discrepancies* of the geodetic system in question. Only in this way can we get the same coordinates for the control points regardless of *along* which line of control points we compute them. Accurate measurements, however, are the prerequisite of a good control-point system.

The adjustment of the triangulation must be made with great care. If we have to adjust the triangulation of a large area, we must be sure that the quality of the triangulation does not differ significantly in different parts of the area, that the astronomic observations are reliable, and that the same scale is used for all base lines. If we fail to observe these precautions, or if we adjust heterogeneous material into one system, using the same weight everywhere regardless of the diversity of the observations, we can do the triangulation more harm than good.

The conversion of national systems to a world geodetic system is explained in Chap. 9.

### B. Historical Development of Geodesy

To determine the dimensions of the earth ellipsoid two problems must be solved, one geodetic and the other astronomic. The geodetic problem consists in measuring in some direction the length of arc  $l$  along the earth's surface. In the past the arcs were generally measured at the meridian direction or close to it. Now it makes no difference which direction the arcs are measured in because the geographic longitude can now be deter-

mined almost as accurately as the latitude. The astronomic problem consists in measuring the corresponding center  $v$ . By the aid of  $l$  and  $v$ , the earth's radius  $r$  can be obtained from the formula

$$r = \frac{l}{v} \quad (8-1)$$

where  $v$  is given in radians (see Fig. 8-1).

In Homer (ca. 900–800 B.C.) the earth was described as a plate surrounded by the stream Oceanus.<sup>43</sup> According to other wise Greeks of that time, the earth was supported by four elephants standing on a big turtle, but what supported the turtle they could not say. Pythagoras (born ca. 582 B.C.) believed the earth to be a sphere, and that great figure of antiquity Aristotle (384–322 B.C.) came to the same conclusion; however, the title "the father of geodesy" can be awarded to Eratosthenes (ca. 276–194 B.C.), who was the first man to determine the size of the earth. He, of course, supposed that the earth was a sphere. His method was very simple, and its principle is still used today.

He measured the length of the meridian arc between Alexandria and Syene, in Egypt, by the aid of camel caravans. The corresponding central angle was measured by the aid of a well. He noted that, at the summer solstice at noon, the sun shone vertically down a well at Syene. He mea-

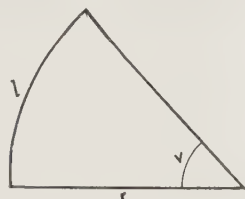


FIG. 8-1. Principle of the arc-measuring method. The arc  $l$  measured by triangulation and the corresponding central angle  $v$  obtained astronomically yield the radius  $r$  of the earth.

asured the direction of the sunbeams at the same time of year, at noon, in Alexandria and realized that they made an angle  $360^\circ/50$ , or  $7^\circ 12'$ , with the vertical. Therefore, he concluded that the central angle between Syene and Alexandria was  $7^\circ 12'$  (Fig. 8-2). The caravan could, according to Eratosthenes, travel from Alexandria to Syene in 50 days, assuming that the fairly constant speed of the camels was 100 stadia. The whole meridian

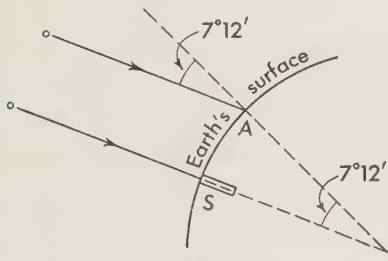


FIG. 8-2. Arc-measuring method of Eratosthenes 2200 years ago.

circle is, of course, 50 times longer. He obtained for this whole circle, therefore, the value 250,000 stadia, or 46,250,000 m, assuming the length of a stadion to be 185 m. His value is only 16 per cent too large; by definition the length of the meridian is 40,000,000 m, and its actual length is very close to this.

Obviously Eratosthenes had good luck, or his result would have been more in error than it was. In fact, Alexandria and Syene are not at the same meridian, as he assumed. Furthermore, the sun 2200 years ago could not have shone directly down into the well at Syene at noon at the summer solstice. And using camels to measure the length of the arc was surely not too accurate either! On the other hand, we must give to Eratosthenes full credit. His method was right in principle; we call it now the "arc-measuring method." Now geodesists carry out the astronomic part of their calculations with fine observation instruments instead of wells and measure the length of the arcs not by camels but by triangula-

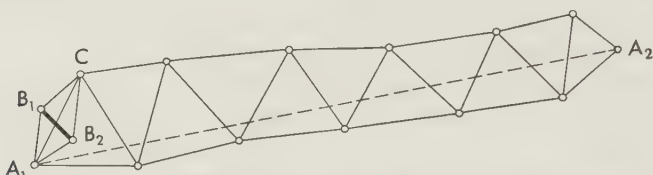


FIG. 8-3. Principle of triangulation. When the distance  $B_1B_2$  (base line) and the angles of all triangles are measured, it is possible to compute not only all sides of the triangle but also the distance  $A_1A_2$ .

tion. One of the most important methods of geodesy, triangulation was introduced by the Dutch scientist Snellius in 1615.

There is a jump of some 18 centuries between the time of Eratosthenes and the beginning of geodesy as a modern science. Without the telescope the development of scientific geodesy would hardly have been possible. The more accurate the geodesist's instruments, the better his observations. The development of geodetic instruments, therefore, is intimately connected with the progress of geodesy itself.

Seventeenth-century contributions to geodesy were the telescope, logarithmic tables, and the method of triangulation (Fig. 8-3). Eighteenth-century contributions were estimates of the earth's size close to the values now used and discovery of the flattened shape of our planet, an important and interesting phase of geodesy.

In 1669 and 1670 the Frenchman Picard<sup>65</sup> carried out an arc measurement that is modern in some respects. He measured a real base line by the aid of wooden rods; he used a telescope in his angle measurements and logarithms in his computations. His chain consisted of 13 triangles. The significance of Picard's measurement is enhanced by the fact that when Newton derived his famous gravitational law, he used Picard's values for the dimensions of the earth.

Cassini later continued Picard's arc northward to Dunkirk and southward to the Spanish boundary. The measurement was already so accurate that it was possible to try to determine not only the size of the earth

but the shape of the meridian as well. Cassini divided the measured arc into two parts, one northward from Paris, another southward. When he computed the length of a meridian degree from both chains, he came to the unexpected result that the length of the degree in the northern part of the chain was 111,017 m, or 267 m shorter than in the southern part (111,284 m), a finding that could have resulted only from the earth's being egg-shaped or from observational errors.

Cassini's result started an intense controversy between French and English scientists. The English claimed that the earth must be flattened, as Newton and Huygens had shown theoretically; Frenchmen, particularly Cassini, defended their own measurement and were inclined to keep the earth egg-shaped.

The controversy had to be decided once and for all; so in 1735 the French Academy of Sciences sent a geodetic expedition, under the leadership of Bouguer<sup>4</sup> and la Condamine, to Peru to measure the length of a meridian degree close to the equator and, in 1736, another expedition, under the leadership of Maupertuis, to Lapland to make a similar measurement near the arctic circle<sup>58</sup> (Fig. 8-4). The measurements of these expeditions showed that the meridian degree in Lapland was 900 m greater than in France and that the corresponding flattening of the meridian was 1/310 (the value computed by Maupertuis was 1/216.8). So

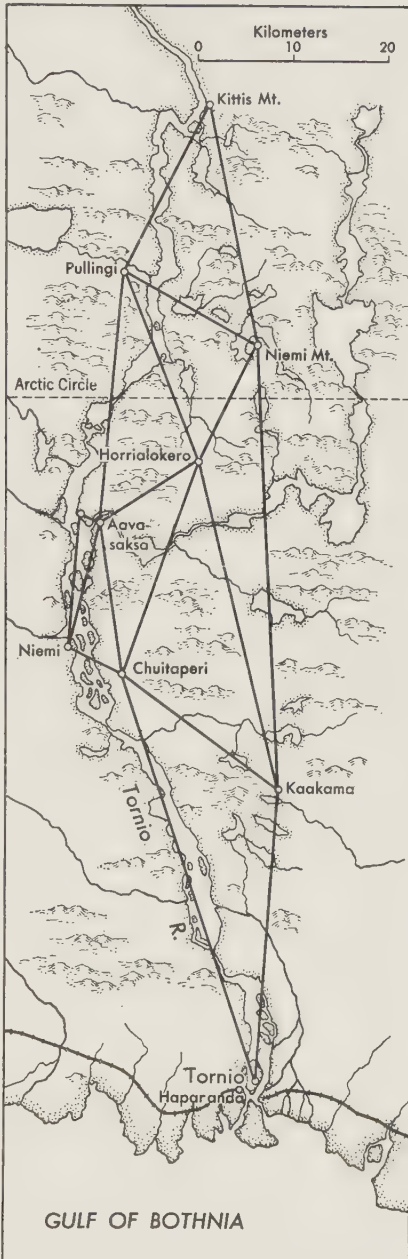


FIG. 8-4. Arc measurement in Lapland 1736-1737 according to Outhier's map, September 2, 1736.

the earth was proved to be flattened, as Newton had forecast it would be.

At the turn of the nineteenth century geodesy was advanced, by the genius of the eighteen-year-old Gauss, by the important method of adjustment computation and, through the work of French scientists, by the definition and preliminary length of the meter. By definition the meter is 1/10,000,000 part of the distance from the pole to the equator along the Paris meridian. Actually it is a little shorter. In fact, the length of the Paris meridian is, if the international ellipsoid is used, not 10,000,000 but 10,002,286 m.

The nineteenth century saw the introduction of the methodical and fundamental triangulation works of Gauss and Bessel, the mathematical basis (Stokes' formula)<sup>75</sup> of physical geodesy, and, as we shall soon see, international cooperation in geodesy.

Finally, the twentieth century opened a new era for geodesy. In reviewing the history of geodesy three eras can be distinguished, the "spherical," the "ellipsoidal," and the "geoidal." During the spherical era, which lasted from the time of Eratosthenes to the eighteenth century, the earth was assumed to be a sphere, and so the objective of geodesy was simply to measure the radius of the sphere. The ellipsoidal era began with the theoretical studies of Newton and Huygens on the flattening of the earth. Measurements by Bouguer and Maupertuis and many other scientists as well proved that there was flattening and led to the computation of relatively accurate values for it. The new era opening in this century is the geoidal era because the approximate reference ellipsoid is no longer sufficient; it has become necessary to learn not only accurate values for the dimensions of the reference ellipsoid but also the detailed shape of the geoid. Only the new methods can master this difficult task.

### C. Most Important Dimensions of Reference Ellipsoids

For more than two hundred years geodesists have been seeking the most accurate values for the equatorial radius  $a$  and the flattening  $\alpha$  of the meridian of the reference ellipsoid. The results, however, have not been entirely satisfactory. The measured arcs used in deriving the dimensions of the earth were too short and frequently not connected with each other. Geodesists realized, too, that geodesy is an international science, more so than any other science. Only cooperation between different countries can give sufficiently long measured arcs and the necessary astronomic observations for determining the dimensions of the earth.

Several internationale organizations were established. The Mitteleuropäische Gradmessung, established by Baeyer, a German, in 1862 and enlarged in 1886 to the Internationale Erdmessung, had its last general assembly in 1912 in Hamburg.<sup>50</sup> After the First World War, in 1922, a

new cooperative venture, the International Union of Geodesy and Geophysics, was organized. As a result of the work of individual scientists, of national geodetic institutes in different countries, and of international organizations, there now are a great many values for  $a$  and  $\alpha$ , the most important of which are shown in Table 8-1.

The equatorial radius  $a$  of the ellipsoid has generally been computed from the measured arcs; the flattening of the meridian  $\alpha$  has been computed both from the measured arcs and by gravimetric and astronomic observations. The most accurate  $\alpha$  values, obtained gravimetrically and astronomically, have frequently been used in the computation of  $a$  from the arc measurements.

From a historical point of view it is not hard to understand why Germany and several other Continental countries have used Bessel's ellipsoid since 1841 or why England has used Clarke's 1880 ellipsoid. Ideological differences may also explain why the U.S.S.R. has used its own ellipsoid, Krassowski's, since 1938. The United States is in the process of changing from Clarke's 1866 ellipsoid to the international ellipsoid computed by the American geodesist Hayford in 1910.

Although these five reference ellipsoids are the basis on which most geodetic computations of the earth have been carried out, several scientists in different countries have tried to derive additional ellipsoids but often from too scanty material. If such reference ellipsoids are computed on the basis of a small area, they will agree rather well with the geoid of that area, but this has no real significance because there are often great discrepancies between local ellipsoids and ellipsoids computed from adequate material.

It is impossible to derive the dimensions of a reference ellipsoid that fits the geoid at all parts of the earth's surface. The reason is, of course, the considerable irregularities of the geoid. It is possible, however, to find an average reference ellipsoid, the dimensions of which are too small in some areas and too large in others. In other words, the average ellipsoid is partly below and partly above the geoid but never very far from it.

What ellipsoid is the best average ellipsoid to be used everywhere in the world?

Supporting the equatorial-radius value of 6,378,388 m, adopted for the international ellipsoid, are the fact that the Russo-Scandinavian chain gives  $a = 6,378,444$  m, the Indian measurements,  $a = 6,378,358$  m, the South African measurements,  $a = 6,378,307$  m<sup>20</sup> and that in 1926 the author<sup>20</sup> (H.) obtained  $a = 6,378,397$  m from the European arc measurements.

Despite these facts, Jeffreys<sup>41</sup> claims that the equator value of the international ellipsoid is about 300 m too large. He obtained the value  $a = 6,378,099$  m by deliberately not using the isostatically reduced de-

TABLE 8-1. DIMENSIONS OF THE EARTH ELLIPSOID

Author	Year	$a$	$1/\alpha$
A. From Arc Measurements			
Bouguer, Maupertuis.....	1738	6,397,300	216.8
Delambre.....	1800	6,375,653	334.0
Walbeck.....	1819	6,896	302.8
Everest.....	1830	7,276	300.8
Airy.....	1830	6,542	299.3
Bessel.....	1841	7,397	299.15
Clarke.....	1857	8,345	294.26
Pratt.....	1863	8,245	295.3
Clarke.....	1866	8,206	295.0
Clarke.....	1880	8,249	293.5
Bonsdorff, A.....	1888	8,444	298.6
Hayford.....	1906	8,283	297.8
Helmholtz.....	1907	8,200	298.3
Hayford <sup>16</sup> .....	1910	8,388	297.0
Heiskanen <sup>20</sup> .....	1926	8,397	(297.0)
Krassowski <sup>44</sup> .....	1938	8,245	298.3
Jeffreys <sup>41</sup> .....	1948	8,099	297.1
Ledersteger <sup>52</sup> .....	1951	8,298	(297.0)
U.S. Army Map Service (Hough) <sup>8</sup> .....	1956	8,260	(297.0)
B. By Other Methods			
Helmert.....	1884	.....	299.25 †
Ivanov.....	1889	.....	297.2 †
Helmert <sup>34</sup> .....	1901	.....	298.2 †
Bowie <sup>6</sup> .....	1917	.....	297.4 †
Berroth.....	1916	.....	297.4 †
Helmert <sup>35</sup> .....	1915	.....	296.7 †
Heiskanen <sup>18</sup> .....	1924	.....	297.4 †
Heiskanen <sup>21</sup> .....	1928	.....	297.0 †
Heiskanen <sup>22</sup> .....	1938	.....	298.2 †
Niskanen <sup>63</sup> .....	1945	.....	297.8 †
Heiskanen, <sup>97</sup> Uotila.....	1957	.....	297.4 †
de Sitter.....	.....	.....	296.96 ‡
de Sitter.....	.....	.....	296.75 ‡
Spencer-Jones.....	1941	.....	296.78 ‡
Bullard <sup>7</sup> .....	1948	.....	297.34 ‡
Jeffreys <sup>41</sup> .....	1948	.....	297.34 ‡

† Gravimetrically.

‡ Astronomically.

flections of the vertical, as Hayford and the author did. This neglect appears to be the weak point in Jeffreys's argument. The local deflections of the vertical and the local undulations of the geoid have too great an influence on his  $a$  value. His statement that the West European chain gives the value  $a = 6,377,950$  while the European chain along the parallel  $52^\circ$  only  $a = 6,377,317$  is just as we have anticipated: in northern Scotland we get a value for the latitude  $\varphi_2$  that is too large, and in southeastern Spain a value  $\varphi_1$  that is too small, because the mountains in these places are on the southern and northern sides, respectively, of the vertical-deflection station. The latitude difference  $\varphi_2 - \varphi_1$  is therefore too great, and consequently the  $a$  value is too small, since the resulting  $a$  is inversely proportional to  $\varphi_2 - \varphi_1$ . In fact, the effect of the topographic-isostatic reduction averages  $1.^7$  at two northern stations of the West European chain<sup>28</sup> and  $4.^1$  at four southern stations (Chinchilla, Mola de Formentera, Tetica, Roldan), for a total of  $5.^8$ , which corresponds to a correction of 180 m for the length of this  $24^\circ$ -long chain and, consequently, to a positive correction in the  $a$  value of about 380 m.

The European chain along parallel  $52^\circ$  must give too small a value for  $a$  because Europe is nearly at the end of the long axis of the parallel circles; and the chain along parallel  $47.5^\circ$ , which crosses the Central European mountains, cannot be used without topographic-isostatic reduction to determine the dimensions of the earth or it gives too small a value for  $a$ .

It was Jeffreys's use of these three chains that caused his  $a$  value to be too small; the author believes that Hayford's value,  $a = 6,378,388$  m, is much nearer to the truth than Jeffreys' value,  $a = 6,378,099$  m.

Ledersteger<sup>51</sup> has developed an interesting method of partial systems for determining the dimensions of the reference ellipsoid, which is based on the fact that the gravity center of the astronomic-geodetic points is invariable with respect to any change from one ellipsoid to another. As a result, the elements of the displacement and twist of a net are invariable when a system of the least-squares deviations of the plumb line and of the discrepancies of the Laplace equation is computed. On the other hand, the corrections of a partial system  $A$  at the gravity center of another partial system  $B$  are functions of the dimensions of the accepted ellipsoid, and, correspondingly, the corrections of the partial system  $B$  at the gravity center of system  $A$  give a solution for the corresponding best-fitting ellipsoid. If  $n$  is the number of the partial systems, there are  $n(n - 1)$  observation equations for correcting  $da$  and  $d\alpha$ .

The fact that Ledersteger's computations, despite the excellence of his method, gave a value for  $a$  which is about 500 m smaller than that of the international ellipsoid was caused largely by the fact that he computed the best-fitting ellipsoid for Europe and not an average ellipsoid for the whole world. Another cause was his failure to make topographic-isostatic

reductions in the observed vertical-deflection components. When we realize that in the Yugoslavian system, for example, these components swing from  $+3.^{\circ}34$  to  $-21.^{\circ}39$ , in the Swiss system from  $+16.^{\circ}94$  to  $-25.^{\circ}11$ , in the Italian system from  $+15.^{\circ}03$  to  $-25.^{\circ}17$ , and in the Austrian system from  $+18.^{\circ}88$  to  $-14.^{\circ}55$ , it is clear that we can get very different values for  $a$  depending on what astronomic-geodetic points happen to be at our disposal.

Ledersteger<sup>52</sup> later checked the dimensions of the reference ellipsoid by comparing the European gravimetric and astronomic-geodetic deflections of the vertical with each other and obtained the value  $a = 6,378,315$  m, which is only 73 m smaller than the  $a$  value of the international ellipsoid.

If we further note that the  $a$  value of Krassowski's ellipsoid is only 143 m smaller, Ölander's<sup>54</sup>  $a$  value, obtained from Baltic measurements, 322 m larger, and Wideland's,<sup>56</sup> computed from the Swedish and Finnish deflections of the vertical, 689 m larger than the  $a$  value of the international ellipsoid, it seems likely that Jeffreys's  $a$  value is too small.

The recent computations of the U.S. Army Map Service<sup>8</sup> in 1956 on the basis of superlong measured arcs now available have given a value of 6,378,260 m for the equatorial radius  $a$ .

#### *D. Significance of the Initial Point of Geodetic Systems*

As the latitude, longitude, and azimuth of the initial point of the geodetic datum are the uncorrected astronomic values—let us denote them by  $\phi'_0$ ,  $\lambda'_0$ , and  $A'_0$ —they are referred to the geoid and not to the reference ellipsoid along which the geodetic computation is made. This fact becomes clearer when we note that the spirit level used in the astronomical observations is, at least practically, parallel to the geoid surface. To convert the coordinates  $\phi'_0$ ,  $\lambda'_0$ ,  $A'_0$  from geoid to ellipsoid the vertical-deflection components  $\xi_0$  and  $\eta_0$  at the initial point should be known, but they seldom are known. The irregularity of the geoid surface therefore results in quite different geodetic systems, depending on what point has been selected as the initial point. This is true even when the same reference ellipsoid is used.

Most countries now have their own national geodetic systems. One point, either a triangulation point or an astronomical observatory (usually the base of a telescope pier), has been used as the initial point. Since initial points, even of neighboring stations, have not been connected to the same system, it is generally not known how much the various geodetic systems differ from each other. Computations carried out between Sweden, Denmark, Norway, and Germany and between England and France show, according to Nares,<sup>61</sup> Director of the International Hydrographic Bureau of Monaco, the discrepancies given in Table 8-2.

TABLE 8-2. DIFFERENCES BETWEEN SOME EUROPEAN GEODETIC SYSTEMS<sup>61</sup>

Location	In latitude	In longitude	In meters
In the Kattegat and the Baltic:			
Denmark — Sweden.....	+0"4	-5"5	95
Denmark — Germany.....	-6"3	+8"9	251
Denmark — Norway.....	-5"5	-1"0	171
Between England and France:			
Mont Saint Lambert (British values — French values).....	+5"43	-4"03	190

We can readily understand that we must eliminate the confusion caused by different geodetic systems, and in most places it is already possible. For example, now that the Baltic Geodetic Commission has accurately computed and executed the Baltic geodetic ring encircling the Baltic Sea, all Baltic countries are joined to the same geodetic system.<sup>94</sup> Still more has been done. After the U.S. Coast and Geodetic Survey, under a contract with the U.S. Army Map Service and using high-speed computing machines, completed the adjustment of the European triangulations,<sup>85</sup> it was possible for Bomford to join the European countries to the one and same system. Because he did not use the gravimetric undulation of the geoid or vertical-deflection components, a correction still has to be made.

Why was this connection of the European systems to one system not made earlier? Because it was both difficult and unnecessary. France, for instance, saw no reason why Germany should not have a different geodetic system from her own; the same was true of Germany and Poland. Now the situation is quite different. Long-range measuring methods, like Decca, Shoran, and Hiran extend from one country to another. A common geodetic system is a necessity, particularly for hydrographic work along the coasts and in coastal seas. For example, in the North Sea and in the Baltic Sea the hydrographic-survey ships use Decca stations in different countries. Needless to say, all these stations must be in the same system.

Not only the European countries but several other great areas are connected to the same geodetic system. Canada, Alaska, Mexico, and the West Indies have been joined to the American datum. Argentina and several other countries of South America have their own systems, which, in the near future, will be connected with the North American system. When this has been done, the entire New World will belong to the same system.

In the Old World the situation is similar. The U.S. Army Map Service<sup>1</sup> has connected the European and African triangulation chains across the Mediterranean and filled the gap of the African arc measurement from Cairo to Cape Town. Thus the South African, North African and European geodetic systems are molded into one.

In Asiatic triangulations, the Russian arc measurements have been connected to the European system. The long arc between Ireland and Singapore unfortunately has at least one gap still to be filled before the Indian and European systems can be connected. Australia can also be joined to the southeastern geodetic system of Asia.

The initial points and the coordinates of the most-used geodetic systems are as follows:<sup>27</sup>

1. The initial point of the North American datum of 1927, on Clarke's ellipsoid of 1866, is Meades Ranch, Kansas. Its astronomic latitude and longitude are  $\varphi'_0 = 39^{\circ}13'25\overset{''}{.}67$  and  $\lambda'_0 = 98^{\circ}32'28\overset{''}{.}20$ . The vertical-deflection components are  $\xi_0 = -1\overset{''}{.}3$  and  $\eta_0 = 0\overset{''}{.}3$ , according to Rice, who obtained these tentative values gravimetrically.

2. The initial point of the European system, which has now been converted to the international ellipsoid, is Helmert Tower in Potsdam, with astronomic latitude and longitude  $\varphi'_0 = 52^{\circ}22'54\overset{''}{.}8$  and  $\lambda'_0 = 13^{\circ}04'01\overset{''}{.}7$ . The vertical-deflection components  $\xi_0$  and  $\eta_0$  have been computed by different authors, and they vary:  $\xi_0$  from  $+3''$  to  $+6''$  and  $\eta_0$  from  $+1\overset{''}{.}2$  to  $+4\overset{''}{.}0$ . Bomford used the values  $\xi_0 = +3\overset{''}{.}36$ ,  $\eta_0 = +1\overset{''}{.}78$  in his tentative computation of the European geoid.

3. The Russian system is computed on Krassowski's ellipsoid. Its initial point is Pulkovo, either of the center of the Observatory building or at a triangulation point called "Pulkovo A." The astronomic coordinates of the Pulkovo Observatory center are latitude  $\varphi'_0 = 59^{\circ}46'18\overset{''}{.}72$  and longitude  $\lambda'_0 = 30^{\circ}19'38\overset{''}{.}55$ , the latitude and longitude of Pulkovo A being  $3\overset{''}{.}19$  and  $13\overset{''}{.}77$  smaller, respectively. The vertical-deflection components are  $\xi_0 = -0\overset{''}{.}16$  and  $\eta_0 = 3\overset{''}{.}54 \cos \varphi$  (Molodenskij, 1945).

4. The Indian system, with its initial point at Kalianpur has changed several times according to Gulathee.<sup>14</sup> The following astronomic coordinates and azimuth for Kalianpur have now been accepted:  $\varphi'_0 = 24^{\circ}7'10\overset{''}{.}97$ ,  $\lambda_0 = 77^{\circ}39'17\overset{''}{.}57E$ , and azimuth  $A'$  to triangulation point Surantal,  $A' = 190^{\circ}27'6\overset{''}{.}39$ , with the vertical-deflection components as referred to the international ellipsoid  $\xi_0 = +2\overset{''}{.}42$  and  $\eta_0 = +3\overset{''}{.}17$ .

All published geodetic latitudes and longitudes in India are in terms of the Everest ellipsoid— $a = 6,377,276$  m,  $\alpha = 1/300.8$ . The deflections of the vertical in India are also given for the international ellipsoid.

Arc measurements vary in accuracy according to when and where they have been carried out. Ölander<sup>94</sup> states that the Baltic geodetic ring, approximately 2500 km long, is perhaps the most accurate so far, with

a closure error of only 1:1,000,000. On the other hand, as Whitten<sup>85</sup> points out, the relative accuracy of triangulation loops is often only about 1:100,000. The relative accuracy of very long-range arc measurements might be still less. This is true particularly of arcs running along rough mountain chains, e.g., the American triangulation chain from Alaska to Panama. The systematic error of the measured angles caused by lateral refraction and by the deflections of the vertical at the triangulation points can even exceed 1".

In addition, the geoid to which the observations have been reduced is irregular; e.g., in Europe it is about 40 m above, in India about 30 m below, and in the western part of the United States about 30 m above the reference ellipsoid along which the geodetic computations are carried out.<sup>97</sup> Therefore, the triangulation base lines measured in Europe need a negative correction of about 1:150,000, the base lines of India a positive correction of about 1:200,000, and the base lines of the western United States a negative correction of 1:200,000 before they can be used in the adjustment of the long-range triangulation. Similar corrections are needed in other parts of the world. Since the reduction from geoid to ellipsoid of the base lines has not been considered—for the very good reason that the undulations  $N$  of the geoid have been known only approximately or not at all—a considerable source of systematic errors is hidden in the adjustments.

On the oceans, which cover 70 per cent of the earth's surface, triangulation cannot be applied at all. Nor can the arc-measuring method be used to determine the deflections of the vertical on ocean islands. These drawbacks to the classic method demonstrate how important it is to have a method which can furnish the corrections for the dimensions of the reference ellipsoid, join the different parts of the world to the same system even across the oceans, however broad they may be, and determine the undulations of the geoid and the deflections of the vertical at any given point. This universal method is the gravimetric method.<sup>26, 27</sup>

Connecting the continents to one geodetic system also seems to be possible by electronic mensuration methods, particularly Shoran and Hiran, and by celestial methods, which include the solar-eclipse method (Kukkamäki<sup>47</sup>), occultation methods (O'Keefe<sup>64</sup>), and the moon-camera method (Markowitz<sup>57</sup>); however, very little is known about the results obtained by these methods. At best they fail when the question is one of determining the detailed shape of the geoid or the components of the absolute deflection of the vertical at the required points on different continents and on the ocean islands.

## 8-2. Physical Geodesy

Two branches of geodesy can be distinguished:<sup>29</sup> geometrical geodesy, which uses triangulation with astronomical observations, i.e., the arc-

measurement method, and physical geodesy, which uses the gravimetric method. Geometrical geodesy does not deal with the structure of the earth's interior. Solely astronomical observations on the earth's surface and triangulation, in either the classic or the modern modified sense, along the earth's surface give the size and general shape of the earth, even when nothing is known about the structure of the earth. As we have seen, geometrical geodesy has had considerable success. It has provided the necessary reference ellipsoids, which are not very far from the best possible.

Regardless of all efforts, only a small portion of the continents has been adequately covered by arc measurements, and the method fails completely at sea. We must therefore make the astronomically observed quantities  $\varphi'$ ,  $\lambda'$ , and  $A'$  as representative as possible; in other words, we must consider the effect of the topography and of the isostatically compensating masses. In the topographic-isostatic reduction of  $\xi$  and  $\eta$  we must also consider the internal structure of the earth's crust and of the layers under, and close to, it. In this way physical geodesy also enters into the usual arc-measuring method if we choose to take full advantage of the triangulation carried out in different parts of the world. The fact that Hayford's ellipsoid, although computed solely on basis of the American vertical-deflection material, was sufficiently good to be adopted as the international ellipsoid, is due to his use of the physical method. A similar example is the derivation of the equator value for the international gravity formula by the author (H.).

#### *A. Principles of Physical Geodesy*

When we speak of physical geodesy, we generally imply the gravimetric method, which is its chief characteristic. The only tools of the gravimetric method are the gravity anomalies  $\Delta g$ , i.e., the differences between the observed gravity value properly reduced to sea level,  $g_0$ , and the theoretical gravity  $\gamma$  obtained from the gravity formula;  $\Delta g = g_0 - \gamma$ . If the gravity formula being used fits well, the only phenomena causing gravity anomalies are the disturbing-mass anomalies  $\Delta m$ , visible or invisible, topographic or subcrustal.

Figure 8-5 shows how the mass surplus of the mountains and the mass deficiency of the oceans cause the deflections of the vertical  $\xi$  and the undulations  $N$  of the geoid. At point  $A$  the mountain mass pulls the vertical, or plumb line (full line), from the normal of the ellipsoid (dashed line); in a similar way the mass deficiency of the ocean "pushes" the plumb line. These effects of the mass anomalies cause the deflection of the vertical  $\xi$ . As the geoid is always perpendicular to the plumb line, it must rise above the ellipsoid under mountains and fall below it under oceans. In Fig. 8-5 it is assumed that the ellipsoid and geoid cross each other

at point *A*, but this is not essential. The shape of the geoid in the area shown is the same regardless of the value of *N* at point *A*.

Figure 8-6 indicates that similar  $\xi$  and *N* values are the result of the invisible subcrustal disturbing masses  $\Delta m$ . Excessive mass pulls and

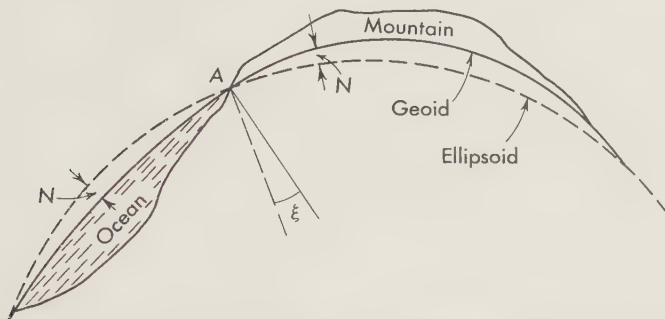


FIG. 8-5. Mass surplus of the mountains and mass deficiency of the oceans cause the undulations *N* of the geoid and the deflections of the vertical  $\xi$ .

deficient mass pushes the plumb line causing  $\xi$  and *N*, which depend solely on the disturbing-mass anomalies.

The same mass anomalies also cause the gravity anomalies  $\Delta g$ . In the area of mass surplus the  $\Delta g$ 's are generally positive; in the area of mass deficiency they are negative.

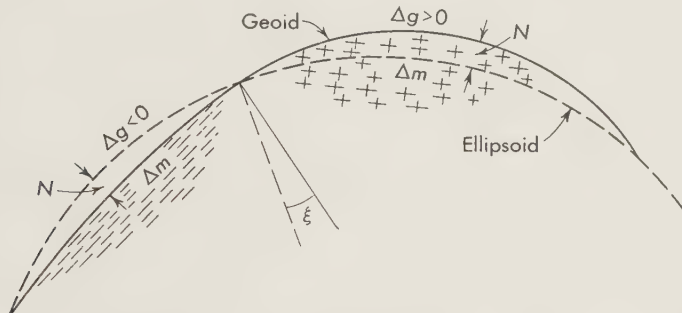


FIG. 8-6. The mass anomalies  $\Delta m$ , visible or invisible, positive (+) or negative (-), cause the gravity anomalies  $\Delta g$ , the undulations *N* of the geoid, and the deflections of the vertical  $\xi$ .  $\Delta g$  can be measured; *N* and  $\xi$  can be computed. This fact is the basic concept of the world-wide gravity program at The Ohio State University.

The physical basis of physical geodesy lies in the fact that the quantities  $\xi$ ,  $\eta$ , *N*, and  $\Delta g$  all result from the same cause, the disturbing masses  $\Delta m$ . Of these quantities, the  $\Delta g$ 's can be measured, and from them the important quantities  $\xi$ ,  $\eta$ , and *N* can be computed.<sup>26,27</sup>

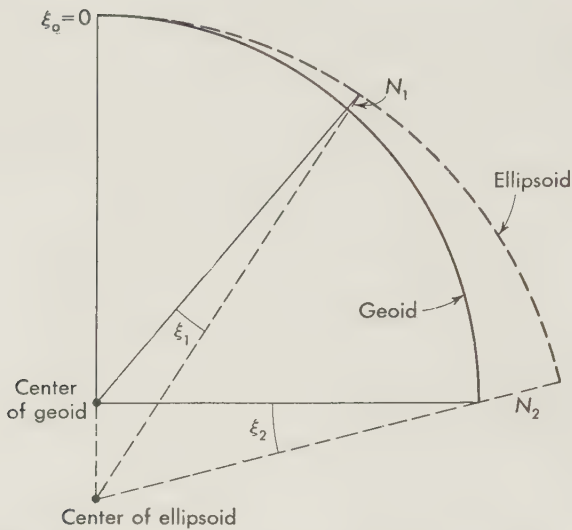


FIG. 8-7. Limitations of the arc-measuring method. An incorrect reference ellipsoid—in this case one that is too large—causes systematical but unreal undulations  $N_1$  and  $N_2$  and deflections  $\xi_1$  and  $\xi_2$ .

Physical geodesy has obvious advantages and is to be preferred to geometrical geodesy. As Figs. 8-7 and 8-8 clearly indicate, the values of  $\xi$  and  $N$  computed by geometrical geodesy depend on the dimensions of the reference ellipsoid used and on the vertical-deflection components  $\xi_0$  and  $\eta_0$  assumed to exist at the initial point. Therefore, the computed

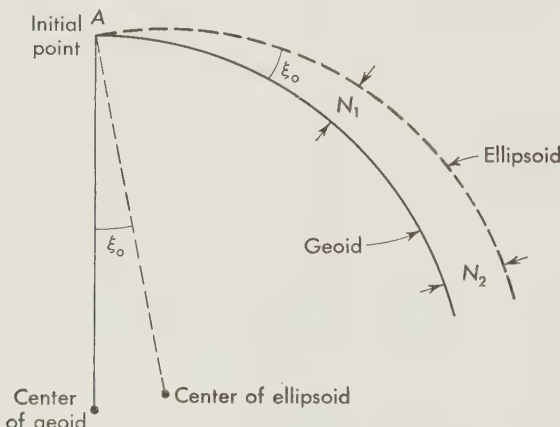


FIG. 8-8. Limitations of the arc-measuring method. Unknown deflections of the vertical  $\xi_0$  at the initial point  $A$  of the geodetic system cause systematical quantities  $N_1$  and  $N_2$  which in fact do not exist.

$\xi$ ,  $\eta$ , and  $N$  values are only relative. The well-known vertical-deflection equations

$$\begin{aligned}\xi &= \varphi' - \varphi \\ \eta &= (\lambda' - \lambda) \cos \varphi \\ \eta &= (A' - A) \cot \varphi\end{aligned}\quad (8-2)$$

show this still more clearly. Here  $\varphi'$ ,  $\lambda'$ , and  $A'$  denote the astronomic,

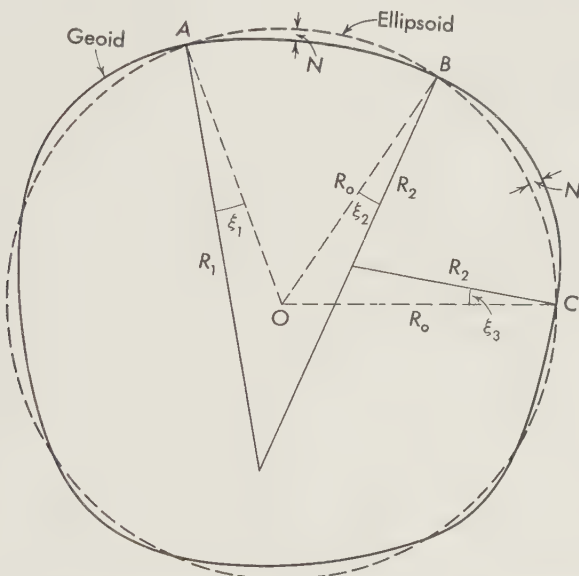


FIG. 8-9. The undulations  $N$  and deflections of the vertical  $\xi_1$ ,  $\xi_2$ , and  $\xi_3$  cause incorrect dimensions for the reference ellipsoid. Arc  $AB$  gives too large a radius  $R_1$ ; arc  $BC$  gives too small a radius  $R_2$ . The correct radius  $R_0$  can be obtained only if  $\xi_1$ ,  $\xi_2$ , and  $\xi_3$  are computed gravimetrically and their effect is considered in the computations.

and  $\varphi$ ,  $\lambda$ , and  $A$  the geodetic, latitude, longitude, and azimuth of the astronomic-geodetic points, respectively.

The gravimetrically computed quantities  $N$ ,  $\xi_g$ , and  $\eta_g$  are independent of the dimensions of the reference ellipsoid. They depend only on the gravity formula employed because the derived gravity anomalies are of course dependent on the gravity formula.

Now it is easy to understand why geodesists have obtained different values for the earth's dimensions (Fig. 8-9). Since the geoid is below the ellipsoid between points  $A$  and  $B$  and above it between points  $B$  and  $C$ , the measured arc  $AB$  gives too large a value  $R_1$  for the earth's radius, while the arc  $BC$  gives too small a value  $R_2$ ; the correct value is  $R_0$ . In

Fig. 8-9 the undulations  $N$  of the geoid and the deflections of the vertical  $\xi_1$ ,  $\xi_2$ , and  $\xi_3$  have been exaggerated nearly a million times. For better results the undulations  $N$  have to be "smoothed out." Isostatic reduction, used by Hayford nearly half a century ago and later by Bowie, Vening Meinesz, Lejay, the author, and others, accomplishes this, but it cannot eliminate the whole effect of the undulations  $N$ . This can be done only by the gravimetric method, which yields the absolute deflections of the vertical. When the absolute deflections of the vertical  $\xi_1$ ,  $\xi_2$ , and  $\xi_3$  at the points  $A$ ,  $B$ , and  $C$  are taken into account, the two arcs  $AB$  and  $BC$  give the correct radius of curvature  $R_0$ .

Astronomic-geodetic deflections of the vertical depend on the dimensions of the reference ellipsoid, but those found gravimetrically do not. Using this fact, when deflection has been measured by both methods at the same points, to check the dimensions of the reference ellipsoid being used is but one of the many important applications of physical geodesy (see Chap. 9).

The mathematical basis of modern physical geodesy (see Chap. 3) is Stokes' formula<sup>75</sup> for the gravimetric computation of the warping  $N$  of the geoid, published in 1849, and the related formulas, developed in 1928 by Vening Meinesz,<sup>76</sup> for computing the vertical-deflection components  $\xi_g$  and  $\eta_g$ . All that is needed in addition to these formulas is knowledge of the distribution of the earth's gravity anomalies rather accurate in the neighborhood of the computation point and in broad lines over the rest of the world.

Although Stokes' formula has been known for a century, it could not be used for these purposes because the gravity material was too scarce. Only during the last few decades has enough gravity material been available to permit application of Stokes' formula and the Vening Meinesz formulas. They are now used not only for the local purposes but on a world-wide scale as well.

### *B. Gravity Material Necessary and Currently Available*

Stokes' formula for the gravimetric computation of the undulations  $N$  of the geoid and the Vening Meinesz formula for the determination of the vertical-deflection components  $\xi_g$  and  $\eta_g$  require:

1. A general gravity field, i.e., gravity maps giving the isoanomaly curves and the average gravity-anomaly value of squares of suitable size. Squares of  $10'$  by  $10'$ ,  $0^{\circ}5$  by  $0^{\circ}5$ , or  $1^{\circ}$  by  $1^{\circ}$ , depending on the interval of the gravity stations, seem to be best.

2. A detailed gravity survey in the neighborhood of the point  $A$  at which the quantities  $N$ ,  $\xi_g$ , and  $\eta_g$ , or some of them, are to be computed. For this purpose about 100 gravity stations inside the circle of  $0^{\circ}5$  will generally be sufficient. The computation of  $N$  does not require so many

local gravity stations. When, in addition, a general gravity survey at point intervals of 20 to 30 km exists for the region beyond this boundary to about 1000 km from  $A$  and at least some gravity anomalies for the rest of the world are available, an accuracy of  $0.^{\circ}5$  to  $1.^{\circ}0$  for  $\xi_g$  and  $\eta_g$  can be attained.

3. A very detailed gravity-anomaly field in the immediate neighborhood of the initial points of the different geodetic data. Several initial points, particularly Meades Ranch, in America, and Potsdam, already fulfill these conditions. If an adequate gravity-station net does not exist in the vicinity of the initial point, any other astronomic-geodetic point of the system can be used instead of the initial point for orienting the system.

4. When a general gravity field is very far from the computation points, it is possible, in an emergency, to let one gravity station, properly reduced to sea level, represent an area up to  $3^{\circ}$  by  $3^{\circ}$ . The probable error of the gravity anomalies of this square would then be  $\pm 13$  mgal, according to Hirvonen.<sup>40</sup> To represent larger "gravimetrically empty" areas it is best to use a zero isostatic gravity anomaly or a properly computed weighted mean of zero and observed anomaly.

To what extent these prerequisites are currently available is a very serious question. The answer will decide whether or not the gravimetric method can be used on a world-wide scale for computing the quantities  $N$ ,  $\xi_g$ , and  $\eta_g$ . The geoid computations published by Hirvonen<sup>38</sup> in 1934 and by Tanni<sup>77</sup> in 1948 gave rather promising results. Despite the fact that, because of the war, Tanni had at his disposal only prewar gravity material, he was able, even at that time, to compute  $N$  with relatively high accuracy; e.g., the errors in his  $N$  values for Europe rarely exceed 10 m. The computation of  $\xi_g$  and  $\eta_g$  was not yet possible because gravimeter measurements had not become available.

What has happened on the gravimetric frontier since 1939? Additions to the material available then can be summarized as follows:

1. Very detailed local gravity surveys have been made by oil companies in the United States, Canada, Venezuela, Great Britain, France, Germany, Netherlands, Arabia, Egypt, North Africa, Mozambique, Madagascar, Australia, and several ocean islands.

2. Regional gravity surveys at intervals of 10 to 20 km are available for the greater part of Europe and the British Isles and for parts of French Africa, the Union of South Africa, India, Japan, New Zealand, Australia, the United States, Canada, Argentina, Mexico, and Iceland.

3. Thanks to the activity in measuring gravity at sea of Great Britain, France, Italy, Spain, and particularly the United States (that of Ewing and Worzel, of Columbia University, and their collaborators), there are now over 4000 ocean gravity stations as compared with the number available to Tanni, i.e., the 840 gravity stations first measured by Vening

Meinesz. The North Atlantic has been surveyed relatively well by Vening Meinesz<sup>79</sup> and by Worzel.<sup>93</sup> The east coast of the United States, the Caribbean Sea, and the West Indies area have almost been adequately surveyed. Along the west coast of America are a gravity-survey line and several profiles perpendicular to the coastline. More than 10 gravimetric cruises across the Pacific and adjacent areas have been carried out.

4. National institutes and many universities now take such a lively interest in the gravimetric survey that every month brings essential additions to the existing gravity material.

5. The gravity survey of shallow waters by means of underwater gravimeters, perfected in 1940 by the Gulf Research and Development Co., has been extended from year to year; about 30 underwater gravimeters are now available. When it is realized that the use of gravimeters makes it possible to measure the gravity to a depth of 200 m and that such shelf areas cover about 7 per cent of the oceans, the great potentialities of this method can readily be understood. The shallow-shelf area of the East Indies alone is about  $10^{\circ}$  by  $20^{\circ}$  in area.

During the last few years underwater gravimeters have been used by Morelli for the gravity survey of the waters around Italy, by Collette<sup>103</sup> for the North Sea, and by Honkasalo<sup>101</sup> for measuring the Gulf of Bothnia, the Gulf of Finland, and the Baltic Sea. The accuracy of these measurements is about 0.1 mgal. The drift, at least of the Gulf Oil Company's gravimeter, is so constant that calibrations at the interval of three to four days seem to be sufficient.

It is hoped that during the International Geophysical Year it will also be possible to survey gravimetrically some other shallow areas.

This almost incredibly rapid advancement of the gravimetric method would not have been possible without the four following developments:

1. The invention in 1923 of the Vening Meinesz pendulum apparatus for gravity surveying at sea and the construction of the underwater gravimeter for gravity surveying in shallow waters.

2. The invention of rapid and accurate land gravimeters, which in a few minutes allow measurements fifty times more accurate than were previously possible even in two days.

3. The increasing interest in gravity measurements on the part of government and private institutions in many countries and the numerous local gravity surveys made by both oil and exploration companies.

4. The gravity measurements for tying the existing gravity base stations in with each other, which have been carried out on a smaller scale by French, British, Italian, and German scientists and on a world-wide scale at Wisconsin University by Woppard's group, alone have united about 3000 gravity base stations in the same world gravimetric system with an error seldom exceeding 1 mgal. These measurements constitute

one of the most important prerequisites for geodetic applications of the gravimetric method.

Now that geodesists have the excellent gravity material described above and know what promise the gravimetric method holds for solving the basic geodetic problems, several institutions have used this method during the last few years, especially the U.S. Coast and Geodetic Survey and The Ohio State University in its world-wide gravity project supported by the Air Force Cambridge Research Center.

### C. Reduction Method to Be Used

During the last two decades much has been written on the question of what reduction of the gravity anomalies best suits geodetic purposes. Men like de Graaff Hunter,<sup>11</sup> Hirvonen,<sup>37</sup> and Jeffreys<sup>42</sup> prefer the free-air reduction, either alone or together with the condensation correction; others, like Kladivo,<sup>46</sup> Lambert,<sup>49</sup> Michailov,<sup>59</sup> and Gromov,<sup>13</sup> believe the inversion reduction to be best; while still others, like Vening Meinesz,<sup>80</sup> Lejay,<sup>55</sup> Tanni,<sup>77</sup> and the author,<sup>28</sup> defend the isostatic reduction.

In deciding this question, it must be kept in mind that the method used to reduce gravity anomalies to sea level has to:

1. Transfer the masses from the outside to the inside of the geoid
2. Make the gravity anomalies as representative as possible
3. Offer the possibility of getting reliable gravity anomalies for areas with no gravity observations
4. Change the geoid surface as little as possible
5. Be not too laborious

Only three of the methods previously discussed can come under consideration: the free-air reduction with condensation, the inversion method, and the isostatic reduction; the Bouguer reduction is ruled out because it changes the geoid itself too markedly.

The free-air reduction is the simplest. At sea no reduction is necessary —except for a small correction due to the fact that the submarine is below sea level during the measurement. Most parts of the continents have such smooth topography that only the simple correction  $+0.3086h$  mgal, where  $h$  is the elevation of the station, is necessary. Only in rugged mountains do the topographic masses have to be condensed to sea level. The condensation reduction can be made either in a local sense, as Helmert did, or in a regional sense, as de Graaff Hunter has suggested.

Since the free-air anomalies are not sufficiently representative without any correction, de Graaff Hunter<sup>96</sup> has suggested using a "model earth" the topography of which is defined by  $H$ , the weighted area average of the real elevation  $h$  taken over a circular area of a certain radius (for instance, 100 miles). The gravity anomaly  $\Delta g_E$  of the model earth will equal  $\Delta g + (g' - g) + A(H - h)$  or will equal the Bouguer anomalies  $\Delta g_B + AH$ ,

where  $\Delta g$  is the free-air anomaly and  $(g' - g)$  is the terrain correction. According to him the obtained gravity anomalies  $\Delta g_E$  are as representative of the mean anomalies as the isostatic anomalies themselves, and it is not necessary to consider the indirect effect brought about by the isostatic reduction; the term  $+AH$  is a substitute of the isostatic reduction.

This method also has drawbacks, however. It is quite arbitrary without any geophysical correspondence because it neglects the real isostatic equilibrium. In addition, it will not be much faster than the usual topographic-isostatic reduction, because in the "model-earth reduction" also we have to consider the terrain correction in the neighborhood of the station, a task that takes more time than the whole isostatic reduction, which, by the way, has already been computed for the larger part of the world.

de Graaff Hunter has also suggested computing the differences  $N'$  between the geopotential surface (geop) and the spheropotential surface (spherop) at the physical earth surface, instead of the geoid undulations  $N$  at sea level. This suggestion is theoretically interesting because we, in fact, do not need the  $N$  values at the geoid surface under the continents. In practice it seems, in my opinion, better to use the geoid and reduce the gravity observations to sea level, because the oceans (two-thirds of the earth's surface) are part of the geoid itself and the undulations  $N$  and  $N'$  obviously are in lowlands, with elevation less than 500 m (more than half of the continents), practically speaking the same. In addition, the suggested procedure will obviously make the geoid computation more complicated. It will be interesting to see how large is the difference  $(N - N')$  in high mountains such as those in the Rocky Mountains and in the highlands of Asia;  $(N - N')$  hardly exceeds 1 to 3 m. When we have more gravity observations, properly analyzed, from the mountainous regions, the suggestion of de Graaff Hunter may have practical significance and not only academic interest. For the time being we are glad to have the  $N$  values in the highlands of Asia with an accuracy of 15 m.

The free-air reduction also has drawbacks. In some places, particularly on the ocean islands and close to them and along the coastlines of deep oceans, it gives an erroneous picture of the surrounding gravity field. This is likewise true in the vicinity of rugged mountains. For instance, on the ocean islands the free-air anomalies are usually strongly positive (Chap. 7). Also values along seacoasts are, for the same reason, systematically different from values farther inland on continents or at sea. In other words, the free-air anomalies often are not sufficiently representative.

If most of the earth's surface were sufficiently well covered by gravity-station nets, this limitation would not be too serious, but since many stations still must represent large areas of the earth's surface, use of the free-air reduction leads to difficulties.

The inversion reduction is in many respects similar to the free-air reduction with the condensation correction. Its advantage is that it will not change the geoid surface at all, as compared with a change of 1 to 3 m by the free-air reduction. On the other hand, the mirror image of the topography features requires a new correction, the size and sign of which are more dependent on the topography than in the condensation method. Besides, this method does not lead to more representative gravity anomalies than the free-air reduction method.

To save the free-air reduction, de Graaff Hunter has tried to smooth the point value of the gravity anomalies in order to make them more representative and has suggested a regional condensation instead of the local one. The radius of regionality can be different in different cases; values of 50 to 100 km would be suitable. After very careful studies of the gravity material of India he has come to the conclusion that his method does not give larger or more irregular gravity anomalies in the area studied than the Pratt-Hayford isostatic reduction does.

The different isostatic reductions remain to be discussed. One of them is Putnam's reduction,<sup>69</sup> modified from the usual Hayford reduction in such a manner that a kind of regional isostatic compensation will result. For geoid studies it is considerably better than the usual method of condensation, because when Putnam's reduction is applied, the gravity anomalies are small and relatively independent of the local features of topography. The method, however, is time-consuming, though not so much so as the complete isostatic reduction. It has not been used.

Some scientists, e.g., the staff of the U.S. Coast and Geodetic Survey and Lejay,<sup>56</sup> have preferred the classic Pratt-Hayford reduction, with the depth of compensation 113.7 km, while others, e.g., Vening Meinesz,<sup>80</sup> Tanni,<sup>77</sup> Morelli,<sup>60</sup> Hales,<sup>15</sup> the author,<sup>28</sup> and recently Lejay, prefer the Airy-Heiskanen system. As shown in Chap. 7, the gravimetric, seismological, and other geophysical investigations carried out in different parts of the world have shown that the isostatic-floating theory corresponds best to the real behavior of the earth's crust and substratum. For the normal thickness of the earth's crust the value of 30 km seems to suit the gravimetric and seismological evidence best. Gravimetric studies on the basis of gravity material obtained from the Alps, Pyrenees, Fennoscandia, Carpathian countries, France, and South Africa, and at sea, as well as seismological studies of the Alps, Appalachian Mountains, California, New England, and New Zealand yield values very close to 30 km for the normal thickness  $T$  of the earth's crust.

Because of this strong evidence, the Airy-Heiskanen system, with  $T = 30$  km and the density difference 0.6 between the density of the substratum and the earth's crust, seems to be best for geodetic purposes. This system was suggested at the gravimetric conference in London in

June, 1952, and at the geodetic-geophysical symposium in Columbus, Ohio, in November, 1953. The International Association of Geodesy, at the suggestion of the study commission for geophysical studies of the gravity anomalies, announced preference for this system at the Rome Assembly in September, 1954, and at the Toronto Assembly in September, 1957.

Table 8-3, taken from Tanni<sup>77</sup> (p. 22), shows that isostatic compensa-

TABLE 8-3. EFFECT OF DIFFERENT REDUCTION METHODS ON GRAVITY ANOMALIES IN MOUNTAINOUS REGIONS, LEVEL LAND, AND AT SEA<sup>77</sup>

Typical station	Eleva-tion, m	Anomalies, mgal				
		Free-air	After conden-sation	Bouguer	Isostatic	
					Putnam	Airy- Heiskanen, 30 km
<b>Mountain:</b>						
Hochköning, East Alps.....	2938	+157	+225	-102	+37	+7
Sonnblick, East Alps.....	3099	+143	+190	-153	+15	-24
Pikes Peak, Colo., U.S.A.....	4293	+206	+265	-215	+43	+8
<b>Valley:</b>						
Lana, East Alps.....	266	-131	-111	-142	+51	-3
S. Leonardo, East Alps.....	655	-107	-78	-152	+38	-4
Grand Canyon, Ariz., U.S.A.....	847	-109	-87	-183	+30	-5
<b>Lowland:</b>						
Kaunas, Lithuania.....	71	+8	+8	0	+8	+8
Szeged, Hungary.....	84	+25	+25	+15	+23	+29
Landau, a.I., Germany.....	360	-17	-17	-57	-10	-6
At sea, westward from Portugal over the Madeira area, Vening Meinesz no.:						
480	-5360	-7	-7 *	+349	0	+18
481	-890	+123	+123	+211	+40	+20
482	-5060	-65	-65	+276	-38	-34
468	-3250	+80	+80	+304	+88	+76
469	-5	+231	+231	+254	+118	+104
470	-4070	-6	-6	+255	+21	+20

\* No condensation correction needed.

tion prevails in broad lines and also how closely the gravity anomalies, after free-air reduction with or without the condensation reduction, depend on the elevation of the station. Even at the same mountain the difference between the mountaintop and valley stations may exceed 250 mgal. A similar phenomenon also occurs at sea, although in a more moderate form. Table 8-3 is clear evidence for the superiority of the isostatic gravity anomalies over the free-air reduction and even the condensation reduction.

It must be remembered, however, that the best method usually is also the most complicated and time-consuming. The isostatic reduction is no exception to that rule. To begin with, it takes a considerable length of time to carry out the isostatic reductions for all the areas of the world for which gravity observations have been made, and this remains true despite the fact that considerable areas have already been isostatically reduced. To fill the gaps between the isostatically reduced areas requires a great deal of time even when the cartographic method or the mass-line method is used in conjunction with high-speed computing machines. The next step is to consider the indirect effect, or Bowie reduction, caused by the isostatic reduction, which must be done twice: once to correct the gravity anomalies and once to convert the co-geoid obtained to the actual geoid. Misunderstandings have arisen concerning the best method to be used in computing the indirect effect; the question is dealt with in Chap. 6.

If, in addition, the isostatic anomalies are used in the computations of the gravimetric deflections of the vertical, topographic-isostatic reductions of the geodetic-astronomic deflections of the vertical must be made, and this is also tedious work. Because of these facts, free-air anomalies have been used at Columbus, Ohio, for the tentative computations of the shape of the geoid of the world.<sup>31</sup>

The free-air anomalies must be corrected if they are to be as representative as possible. The corrections are not very large, because the free-air reduction is also an isostatic reduction—corresponding to zero thickness of the earth's crust; but since isostatic compensation will, in fact, happen not at sea level but at a depth of 20 to 50 km below it, the free-air anomalies must be related to the topography around the station (Chap. 7). We therefore develop the anomalies  $\Delta g$  as a function of the elevation  $h$  of the station in the form  $\Delta g = a + bh$ .

Hirvonen and Uotila have done this graphically at the Mapping and Charting Research Laboratory of The Ohio State University for more than 1000 squares  $1^\circ$  by  $1^\circ$  of hilly and mountainous regions; in areas of relatively smooth topography, of course, no elevation term is needed. In nearly all the squares studied the coefficient  $b$  is positive, as shown in Fig. 8-10, in which the straight line represents the dependence of anomalies  $\Delta g$  on the elevation  $h$  in the square in question. The value of  $\Delta g$  corresponding to the mean elevation taken from the topographic maps best represents the mean free-air anomaly of the square in question. A similar correction term must be added to the free-air anomalies of steep seacoasts, as Helmert pointed out in 1910.

This correction method is, of course, only approximate and cannot replace the isostatic method. It is, however, a useful device for making free-air anomalies as representative as possible.

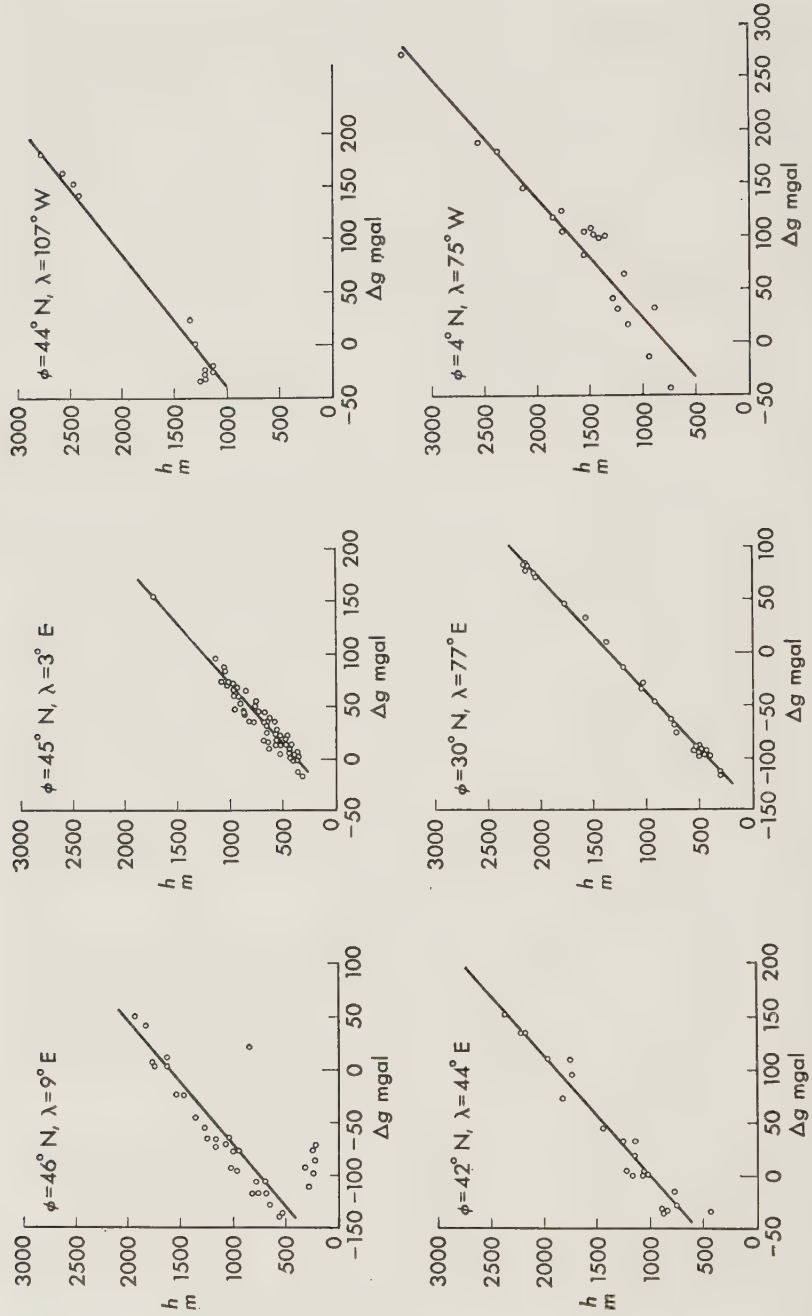


FIG. 8-10. Correlation between the elevation of the station and free-air anomalies. The higher the station, the more positive the free-air anomalies.

What free-air gravity anomalies should be used in the unsurveyed areas? Hirvonen applied to his  $5^{\circ}$  by  $5^{\circ}$  squares the mean free-air anomalies taken from Prey's anomaly maps<sup>67</sup> obtained from the development of the topography into spherical harmonics to the sixteenth order.

After 1934, when Hirvonen's geoid studies were published, 816 theretofore gravimetrically empty  $5^{\circ}$  by  $5^{\circ}$  squares were surveyed, in the Northern Hemisphere and 182 in the Southern. Comparison of the observed mean anomalies  $O$  with Hirvonen's mean anomalies  $H$  taken from the spherical harmonics indicated that the quadratic mean of the observed mean anomalies  $O$  was  $\pm 17.4$  mgal but that the standard error of the difference  $O - H$  was  $\pm 18.4$  mgal. Zero free-air anomaly is therefore shown to be slightly more representative of the observed mean free-air anomaly  $O$  than is the mean free-air anomaly  $H$  obtained from the spherical harmonics. It was for this reason that the author (H.) decided to use zero anomaly in his world-wide computation of the  $N$ ,  $\xi_g$ , and  $\eta_g$  values.

Hirvonen's work also shows that reliable gravity anomalies for unsurveyed areas cannot be found by means of spherical harmonics, although the method has been suggested from time to time.

In the final computations, however, the real isostatic anomalies must be used. Because the earth's crust is, broadly speaking, in isostatic equilibrium, the isostatic anomalies are more representative. In areas where there are no gravity observations there is every reason for using zero isostatic anomaly, which corresponds to complete isostatic equilibrium. These "zero areas" also make the computation of the geoid rather simple. When gravity observations become available for areas now gravimetrically empty, the observed isostatic gravity anomalies will of course be used. Corrections in the computed values of  $N$ ,  $\xi_g$ , and  $\eta_g$  caused by new observations are easy to make.

Since the isostatic reduction causes the geoid to shift downward under the continents, the indirect effect, or Bowie reduction of the gravity anomalies, is positive. It amounts, in general, to 2 to 3 mgal except in high mountains, where it can be as much as 10 mgal. At sea the sign of the indirect effect is, of course, negative, because the isostatic reduction causes the geoid to shift upward.

When we consider the indirect effect, we obtain the gravity anomalies referred to the changed geoid, which de Graaff Hunter calls the "co-geoid," an abbreviation of the words "computed geoid" or "compensated geoid." Applying Stokes' formula to the corrected gravity anomalies gives, of course, the co-geoid. To obtain the actual geoid we must find the distance between them.

Tables computed by Lambert, Lejay, Vening Meinesz, Niskanen, and the author give values of the indirect effect for the areas where gravity observations exist; the Vening Meinesz tables are the most rigorous. The

elevations of the Hayford zones do not need to be so accurate for this purpose as for computation of tables for the direct isostatic reduction.

### 8-3. Deflections of the Vertical

The difference between the normal of the geoid, or the plumb line, and the normal of the reference ellipsoid is called the deflection of the vertical  $\theta$ . Its components  $\xi$  and  $\eta$  can be computed both by astronomic-geodetic and gravimetric methods. Astronomic-geodetic deflections of the vertical are relative because they depend not only on the mass anomalies of the earth but also on the dimensions of the reference ellipsoid being used and on the  $\xi_0$  and  $\eta_0$  values of the initial point of the geodetic datum. Gravimetric deflections of the vertical, on the other hand, are nearly absolute because they depend only on the disturbing masses of the earth and on the gravity formula being used and not on the size of the earth or on  $\xi_0$  and  $\eta_0$ .

#### A. Astronomic-Geodetic Deflections of the Vertical

Since the astronomic latitude  $\phi'$ , longitude  $\lambda'$ , and azimuth  $A'$  are referred to the geoid and the corresponding geodetic quantities  $\phi$ ,  $\lambda$ , and  $A$  are computed along the reference ellipsoid (Sec. 8-1), the differences be-

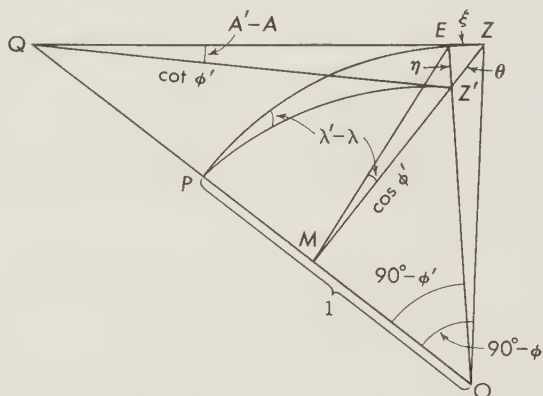


FIG. 8-11. Explanation of the vertical-deflection equations. Because of the deflection of the vertical  $\theta$  the astronomic and geodetic zenith points  $Z'$  and  $Z$  are different.  $\theta$  causes the deflections in latitude  $\phi' - \phi$ , longitude  $\lambda' - \lambda$ , and azimuth  $A' - A$ ; these deflections can be observed and yield  $\xi$  and  $\eta$ .

tween the two sets of coordinates must give the angle between the normal of the reference ellipsoid and of the geoid, i.e., the deflection of the vertical  $\theta$ . We cannot, however, measure  $\theta$  itself directly but only its meridian component  $\xi$ , and its east-west component  $\eta$ .

The differences  $\phi' - \phi$ ,  $\lambda' - \lambda$ , and  $A' - A$  are called the deflections of the vertical in latitude, longitude, and azimuth. The relationship be-

tween them and  $\xi$  and  $\eta$  is indicated in Fig. 8-11, where  $P$  is the pole of the unit sphere,  $Z$  and  $Z'$  the zenith of the ellipsoid and geoid, respectively, at point  $O$ .

We easily see that  $\xi = (90^\circ - \varphi) - (90^\circ - \varphi') = \varphi' - \varphi$ , and we can compute  $\eta$  from the triangle  $Z'ME$ , where angle  $Z'ME = \lambda' - \lambda$  and  $Z'E = \eta$  is perpendicular to  $ZE$ . As  $MZ' = \cos \varphi'$ , we get  $\eta = (\lambda' - \lambda) \cos \varphi'$ . We can also compute  $\eta$  from the triangle  $Z'QE$ , where  $Z'Q = \cot \varphi'$ , angle  $Z'QE = A' - A$ , and  $\eta = (A' - A) \cot \varphi$  when we replace  $\varphi'$  by  $\varphi$ . We therefore get the vertical-deflection equations

$$\begin{aligned}\xi &= \varphi' - \varphi \\ \eta &= (\lambda' - \lambda) \cos \varphi \\ \eta &= (A' - A) \cot \varphi\end{aligned}\tag{8-3}$$

or, in another form,

$$\begin{aligned}\lambda' - \lambda &= \eta \sec \varphi \\ A' - A &= \eta \tan \varphi\end{aligned}\tag{8-4}$$

As  $\eta$  can be obtained from  $\lambda' - \lambda$  as well as from  $A' - A$ , their relationship is given by the Laplace equation

$$A' - A = (\lambda' - \lambda) \sin \varphi\tag{8-5}$$

or, in another form,

$$(A' - A) - (\lambda' - \lambda) \sin \varphi = 0\tag{8-5a}$$

The  $\xi$  component is obviously known at all triangulation points where the astronomic latitude has been obtained. If either the astronomic longitude or azimuth has been observed, the  $\eta$  component can be computed as well, and if both have been observed, two values for  $\eta$ , related by the aforementioned Laplace equation, are found. Triangulation points with astronomic longitude and azimuth observations are therefore called "Laplace points."

The Laplace equation has nothing to do with the real deflections of the vertical: it gives only a measure of the accuracy of the differences  $A' - A$  and  $\lambda' - \lambda$ . The closure error  $w$  of the equation

$$(A' - A) - (\lambda' - \lambda) \sin \varphi = w\tag{8-5b}$$

is consequently caused not by any deflections of the vertical but solely by errors in the astronomically observed and geodetically computed longitude and azimuth.

It has already been mentioned (see Figs. 8-7 and 8-8) that the astronomic-geodetic  $\xi$  and  $\eta$  of the triangulation points are dependent not only on the deflections of the vertical  $\xi_0$  and  $\eta_0$  at the initial points and the dimensions of the reference ellipsoid being used but also on the observation errors of

the astronomic and geodetic quantities. From this fact follow Helmert's equations<sup>43</sup> for the deflection of the vertical—improved by Vening Meinesz<sup>81</sup> so that the effect of  $N_0$  is also considered:

$$\begin{aligned}\xi_\nu &= -p_1\xi_0 - p_2\eta_0 + p_3N_0 + p_5 \frac{da}{a} + p_6 d\alpha + (\varphi' - \varphi) \\ \eta_\nu &= -q_1\xi_0 - q_2\eta_0 + q_3N_0 + q_5 \frac{da}{a} + q_6 d\alpha + (\lambda' - \lambda) \\ \eta_\nu &= -r_1\xi_0 - r_2\eta_0 + r_3N_0 + r_5 \frac{da}{a} + r_6 d\alpha + (A' - A) \\ N_\nu &= -s_1\xi_0 - s_2\eta_0 + s_3N_0 + s_5 \frac{da}{a} + s_6 d\alpha + (N' - N)\end{aligned}\tag{8-6}$$

The last terms are the observed deflections of the vertical in latitude, longitude, azimuth, and geoid distance  $N$ ;  $p_\nu$ ,  $q_\nu$ ,  $r_\nu$ , and  $s_\nu$  are coefficients which are dependent on the position of the triangulation points and which can be computed;  $\xi_0$  and  $\eta_0$  are the vertical-deflection components at the initial point,  $N_0$  the geoid distance at this point, and  $da$  and  $d\alpha$  the corrections to the parameters  $a$  and  $\alpha$ . On the basis of equations of this kind  $\xi$ ,  $\eta$ , and  $N$  can be computed at any astronomic points of the triangulation.

As shown by Fig. 8-6,  $\xi_g$  and  $\eta_g$  can also be computed gravimetrically, because they, as well as the gravity anomalies  $\Delta g$ , are dependent on the visible- and invisible-mass anomalies of the earth. Since  $\Delta g$  can be observed,  $\xi_g$  and  $\eta_g$  can be computed. These gravimetric deflections of the vertical depend not at all on the dimensions of the reference ellipsoid but only on its flattening value  $\alpha$ .

### B. Topographic and Isostatic Reduction of Astronomic-Geodetic Deflections of the Vertical

As already mentioned, the astronomic-geodetic  $\xi$  and  $\eta$  are subject to systematic error, caused in part by the errors  $da/a$  and  $d\alpha$  of the reference ellipsoid being used and in part by those in the vertical-deflection components  $\xi_0$ ,  $\eta_0$  at the initial points, and to accidental error caused by the visible- and invisible-mass anomalies. The effect of the mass anomalies can be estimated as follows.

The attraction  $dK$  of a mass element  $dm$  (Figs. 6-3 and 6-4) at the origin is

$$dK = k\rho \frac{r dr dA dz}{r^2 + z^2}\tag{6-6}$$

where  $r dr dA dz =$  volume of  $dm$

$\rho$  = density of  $dm$

$k$  = Newtonian gravitational constant

$r, z$  = cylindrical coordinates of  $dm$

The horizontal component  $dH$  of  $dF$  is

$$dH = \frac{r}{\sqrt{r^2 + z^2}} dF = k\rho \frac{r^2 dr dA dz}{(r^2 + z^2)^{\frac{3}{2}}} \quad (8-7)$$

The division of  $dH$  into a north-south component  $dX$  and an east-west component  $dY$  is given by

$$dX = dH \cos A = k\rho \frac{r^2}{(r^2 + z^2)^{\frac{3}{2}}} dr \cos A dA dz \quad (8-8)$$

and similarly for  $dY$ .  $A$  is the azimuth of the mass element  $dm$ . The integration of (8-8) to  $A$ ,  $r$ , and  $z$  between the boundaries  $A_1$  and  $A_2$ ,  $r_1$  and  $r_2$ , and  $0$  and  $h$  gives the effect of the compartment  $(A_1, A_2; r_1, r_2; 0, h)$ . Two integrations yield

$$X = k\rho(\sin A_2 - \sin A_1)h \int_{r_1}^{r_2} \frac{dr}{r\sqrt{1 + h^2/r^2}} \quad (8-9)$$

and a third one gives

$$X = k\rho h(\sin A_2 - \sin A_1) \ln \frac{r_2 + \sqrt{h^2 + r_2^2}}{r_1 + \sqrt{h^2 + r_1^2}} \quad (8-10)$$

As  $h$ , in general, is small compared with  $r_1$  and  $r_2$ , we get, without committing any practical error, the equation for  $X$

$$X = k\rho h(\sin A_2 - \sin A_1) \ln \frac{r_2}{r_1} \quad (8-11)$$

A similar equation for  $Y$  is obtained by substituting  $\sin \alpha_2 - \sin \alpha_1$  for  $\cos \alpha_1 - \cos \alpha_2$ :

$$Y = k\rho h(\cos A_1 - \cos A_2) \ln \frac{r_2}{r_1} \quad (8-12)$$

The vertical attraction of the earth is  $g$ , and consequently the effects  $\Delta\xi_1$  and  $\Delta\eta_1$  of the whole compartment on the  $\xi$  and  $\eta$  components are

$$\Delta_1\xi = \frac{X}{g} \quad \Delta_1\eta = \frac{Y}{g} \quad (8-13)$$

When we denote the mean density of the earth by  $\rho_m$ , we get

$$g = \frac{4}{3}\pi k\rho_m R$$

where  $R$  is earth's radius. The end result will be

$$\Delta_1 \xi'' = \frac{3\rho''}{4\pi} \frac{\rho}{\rho_m} \frac{h}{R} (\sin A_2 - \sin A_1) \ln \frac{r_2}{r_1} \quad (8-14)$$

$$\Delta_1 \eta'' = \frac{3\rho''}{4\pi} \frac{\rho}{\rho_m} \frac{h}{R} (\cos A_1 - \cos A_2) \ln \frac{r_2}{r_1}$$

where  $\rho''$  is the analytical angle unit,  $\rho'' = 206,265''$ .

Hayford used the values  $\rho = 2.67$ ,  $\rho_m = 5.576$ ,  $\sin A_2 - \sin A_1 = 0.25$ , and  $r_2/r_1 = 1.420$  and got the simple computation formula

$$\Delta \xi'' = 0.0001h \text{ ft}$$

The outer radii of these zones are given in Table 8-4.

TABLE 8-4. HAYFORD ZONES

Zone	Outer radius, km	Zone	Outer radius, km	Zone	Outer radius, km	Zone	Outer radius, m
1	4126	11	113.730	21	3.272	31	94.1
2	2828	12	79.760	22	2.295	32	66.0
3	1962	13	55.920	23	1.609	33	46.3
4	1369	14	39.220	24	1.129	34	32.5
5	958	15	27.500	25	0.791	35	22.8
6	670.8	16	19.290	26	0.555	36	16.0
7	470.3	17	13.530	27	0.389	37	11.2
8	329.8	18	9.487	28	0.273	38	7.9
9	231.3	19	6.653	29	0.192		
10	162.3	20	4.665	30	0.134		

The effect of the isostatic compensation according to the Pratt-Hayford system is rather easy to take into account because there is the fundamental equation

$$\Delta \rho = - \frac{h}{D} \rho \quad (5-1)$$

where  $\Delta \rho$  is the compensation density and  $D$  the depth of compensation. So we must replace  $\rho$  by  $\Delta \rho$  and  $h$  by  $D$  in Formula (8-14) to get the equation for the effect  $\Delta_2 \xi''$  of the compensation

$$\Delta_2 \xi'' = - \frac{3\rho''}{4\pi} \frac{\Delta \rho}{\rho_m} \frac{D}{R} (\sin A_2 - \sin A_1) \ln \frac{r_2 + \sqrt{D^2 + r_2^2}}{r_1 + \sqrt{D^2 + r_1^2}} \quad (8-15)$$

The whole topographic-isostatic reduction  $\Delta_0 \xi''$  is, of course,

$$\Delta_0 \xi'' = \Delta_1 \xi'' + \Delta_2 \xi'' = \Delta_1 \xi'' \left( 1 + \frac{\Delta_2 \xi''}{\Delta_1 \xi''} \right) \quad (8-16)$$

or, on the basis of Formulas (8-15) and (8-16)

$$\Delta_0\xi'' = F \times \Delta_1\xi'' \quad F = 1 - \frac{\log [(r_2 + \sqrt{D^2 + r_2})/(r_1 + \sqrt{D^2 + r_1^2})]}{\log r_2/r_1} \quad (8-17)$$

The formula for  $\Delta_0\eta''$  is naturally similar.

Hence the topographic-isostatic reduction  $\Delta_0\xi''$  can be computed simply by multiplying the topographic reduction  $\Delta_1\xi''$  from zone to zone by the factor  $F$ .

TABLE 8-5. FACTOR  $F^{17}$

Zone	$r_2$ , km	Depth of compensation $D$ , km				
		231.3	162.2	113.7	79.8	55.9
29	0.192	.....	.....	.....	.....	0.997
27	0.389	.....	.....	0.997	0.996	0.994
25	0.791	0.997	0.996	0.994	0.992	0.988
23	1.609	0.994	0.991	0.988	0.983	0.976
21	3.272	0.988	0.983	0.975	0.965	0.951
19	6.653	0.975	0.965	0.950	0.929	0.900
17	13.53	0.949	0.928	0.899	0.857	0.799
15	27.52	0.898	0.856	0.798	0.720	0.617
13	55.96	0.796	0.718	0.615	0.491	0.357
11	113.79	0.613	0.489	0.356	0.232	0.137
10	162.27	0.488	0.355	0.231	0.137	0.075
9	231.41	0.353	0.230	0.136	0.074	0.038
8	330.04	0.229	0.134	0.073	0.037	0.018
7	470.77	0.132	0.071	0.036	0.017	0.008
6	671.71	0.069	0.034	0.016	0.007	0.003
5	959.02	0.032	0.014	0.006	0.002	0.0003
4	1,370.92	0.012	0.004	0.0006	-0.0006	-0.001
3	1,964.86	0.001	-0.001	-0.002	-0.002	-0.002
2	2,831.70	-0.004	-0.004	-0.003	-0.003	-0.002
1	4,131.21	-0.007	-0.005	-0.004	-0.003	-0.002
A	6,212.69	-0.008	-0.006	-0.004	-0.003	-0.002
B	10,408.69	-0.009	-0.006	-0.004	-0.003	-0.002
C	15,011.79	-0.009	-0.006	-0.004	-0.003	-0.002
D	20,015.72	-0.009	-0.006	-0.004	-0.003	-0.002

Hayford's original table was not quite correct in the farther zones. Therefore, the abbreviated tables of Hayford, corrected by Darling,<sup>95</sup> are given in Table 8-5. The effect of the far zones is, in fact, negative and not

positive as Hayford had; that means that the effect of compensation is there larger than the effect of the topography because the compensating columns are closer to the computation point than the topography column. New zones A, B, C, and D have also been added.

*Reduction of the astronomic data.* To make the astronomic-geodetic and gravimetric deflections of the vertical comparable with each other some corrections must be added to the astronomic data. First of all, the reduction to sea level must be considered because the gravity anomalies used in computing the gravimetric deflections are also reduced to sea level. In other words, the slope between the geoid surface and the equipotential surface at the observation point must be determined.

The general part of this slope correction can be obtained from the latitude term of the gravity formula used. The correction consistent with the international gravity formula is

$$d\varphi = -0.^{\circ}000171h \sin 2\varphi \quad (8-18)$$

where  $h$  is the elevation of station in meters. No correction is needed for the longitude as the international gravity formula has no longitude term.

Since the horizontal attraction of the disturbing topographic and invisible crustal and subcrustal masses is not the same at sea level as at higher altitudes, the direction of the plumb line varies with the altitude. These differential vertical-deflection components  $d\xi$  and  $d\eta$  can be computed with high accuracy by means of the gravity anomalies of the vicinity of the astronomic point, properly reduced to sea level.

The effect of the horizontal gravity gradient on  $d\xi$  and  $d\eta$  at sea level, as will be shown in (8-47) is  $d\xi = 0.^{\circ}105(\partial\Delta g/\partial x)r_0$ ,  $d\eta = 0.^{\circ}105(\partial\Delta g/\partial y)r_0$ , where the factor  $0.^{\circ}105 = \rho/2G$ ,  $\rho = 206,265''$ , and  $G = 981,000$  mgal is the mean gravity at the sea level. When the elevation  $h$  of the astronomic point is also considered, these formulas read

$$\begin{aligned} d\xi &= 0.^{\circ}105 \frac{\partial\Delta g}{\partial x} (1 + 2h)r_0 \\ d\eta &= 0.^{\circ}105 \frac{\partial\Delta g}{\partial y} (1 + 2h)r_0 \end{aligned} \quad (8-19)$$

Thus the elevation correction of the astronomic latitude and longitude caused by the irregular gravity anomalies is

$$\begin{aligned} d\varphi &= 0.^{\circ}210 \frac{\partial\Delta g}{\partial x} h \\ d\lambda &= 0.^{\circ}210 \frac{\partial\Delta g}{\partial y} h \sec \varphi \end{aligned} \quad (8-20)$$

where the gravity gradients are given in milligals and  $h$  is in the same linear unit as  $x$  and  $y$ .

From the 16 American astronomic-geodetic points studied by Rice,<sup>71</sup> the correction of  $\varphi$  exceeds  $0.^{\circ}1$  at only three points, with maximum  $+0.^{\circ}14$ , and the correction of  $\lambda$  exceeds  $0.^{\circ}03$  only three times, with maximum  $-0.^{\circ}10$ .

Theoretically, a small additional correction is needed to take into account the difference in the horizontal attraction of the real topography on the computation point before and after the transfer of the topographic masses. In practice this correction

$$\begin{aligned} d\varphi &= 0.^{\circ}024 \frac{\partial h}{\partial x} h \\ d\lambda &= 0.^{\circ}024 \frac{\partial h}{\partial y} h \sec \varphi \end{aligned} \quad (8-21)$$

can be neglected, because the astronomic stations are generally located either on high points, where the ground falls away in all directions, or in lowlands, where both the slope of the topography and  $h$  are small.

The second correction to be considered, the correction for variation of pole, is very small. According to the International Latitude Service, which has been in operation for half a century, the pole of the earth wanders around its mean position along an irregular path inside a circle of 10 m, or  $0.^{\circ}3$ . As the astronomic observations have been made in different years, they must be reduced to the same epoch to eliminate the effect of pole variation.

The latitude correction for this effect can be obtained from the formula

$$d\varphi = -y \sin \lambda + x \cos \lambda \quad (8-22)$$

where  $\lambda$  is the longitude, positive eastward from Greenwich, and  $x$  and  $y$  are expressed in seconds of arc. The corresponding longitude correction is  
 $d(\lambda_2 - \lambda_1) = -(y \cos \lambda_2 + x \sin \lambda_2) \tan \varphi_2 + (y \cos \lambda_1 + x \sin \lambda_1) \tan \varphi_1$

$$(8-23)$$

where subindex 1 refers to the observatories giving the time signals and subindex 2 refers to the field astronomic point.

### C. Gravimetric Deflections of the Vertical

As shown in Chap. 3, we can compute the geoid distances  $N$  gravimetrically by using the Stokes' formula

$$N = \frac{1}{2\pi} \frac{R}{G} \int_0^{2\pi} dA \int_0^\pi f(\psi) \sin \psi \Delta g d\psi \quad (8-24)$$

or, as adopted by Helmert,

$$N = \frac{R}{G} \int_0^\pi F(\psi) \Delta g \, d\psi \quad (8-25)$$

where  $R$  = mean radius of earth

$G$  = mean gravity

$\psi$  = angular distance of circular zone

$\sin \psi \, d\psi \, d\alpha$  = surface element

$\Delta g$  = average value of gravity anomalies in circular ring between  $\psi$  and  $\psi + d\psi$

The functions  $S(\psi)$  and  $F(\psi)$  are

$$\begin{aligned} S(\psi) &= 2f(\psi) = \csc \frac{\psi}{2} + 1 - 6 \sin \frac{\psi}{2} - 5 \cos \psi - 3 \cos \psi \ln \left( \sin \frac{\psi}{2} + \sin^2 \frac{\psi}{2} \right) \\ F(\psi) &= f(\psi) \sin \psi \end{aligned} \quad (8-26)$$

where  $S(\psi)$  is the original Stokes' function.

When computing the vertical-deflection components  $\xi_g$  and  $\eta_g$  gravimetrically, we use the Vening Meinesz formulas<sup>78</sup> derived in 1928 and obtained by derivation of the Stokes' formula in respect to  $\psi$ .

Using the abbreviation  $f'(\psi) = \partial f(\psi)/\partial \psi$ , we get

$$\begin{aligned} d\xi'' &= - \frac{\partial N}{\partial x} = \frac{\rho''}{2\pi G} \int_q f'(\psi) \cos A \, \Delta g \, dq \\ d\eta'' &= - \frac{\partial N}{\partial y} = \frac{\rho''}{2\pi G} \int_q f'(\psi) \sin A \, \Delta g \, dq \end{aligned} \quad (8-27)$$

where  $G = 979.8$  cm/sec<sup>2</sup> is the mean gravity value,  $\rho'' = 206,265''$ ,  $A$  the azimuth,  $\Delta g$  the mean gravity anomaly of the surface element  $dq$ , and  $y$  is taken in an east-west direction,  $x$  in a north-south direction.

As  $\Delta g$  is generally given in milligals, the constant  $c$  before the integral is

$$c'' = \frac{\rho''}{2\pi G} = 0''.0335 \quad (8-27a)$$

The values of the functions  $f'(\psi)$  and  $f'(\psi) \sin \psi = \partial F(\psi)/\partial \psi$  will be given as a function of  $\psi$  in the following paragraph with the Stokes' functions  $f(\psi)$  and  $f(\psi) \sin \psi$ .

We can write Formulas (8-27) as

$$\begin{aligned} d\xi'' &= c'' \sum f'(\psi)_q \cos A_q \, \Delta g_q \, q \\ d\eta'' &= c'' \sum f'(\psi)_q \sin A_q \, \Delta g_q \, q \end{aligned} \quad (8-28)$$

where  $q$  is the square (more correctly, the spherical trapezoid)  $1^\circ$  by  $1^\circ$  or  $5^\circ$  by  $5^\circ$  and  $f'(\psi)_q$ ,  $\cos A_q$ ,  $\sin A_q$ , and  $\Delta g_q$  are the respective mean values of  $f'(\psi)$ ,  $\cos A$ ,  $\sin A$ , and  $\Delta g$  of the square in question. The summation must be extended over all the globe.

The best practical procedure is to divide the globe into  $10^\circ$ -broad azimuth zones having the computation point as the center, with the  $\psi$  circles in circular rings so that the function  $f'(\psi)$  can be kept constant inside every circle. The area  $q = nq_0 \cos \varphi$ , where  $n = 1$  between latitudes  $0^\circ$  and  $60^\circ$ , 2 between  $60^\circ$  and  $70^\circ$ , and 3 between  $70^\circ$  and  $80^\circ$ , 6 between  $80^\circ$  and  $85^\circ$ , and 18 between  $80^\circ$  and the pole;  $q_0$  is the area in radians of  $1^\circ$  by  $1^\circ$  or  $5^\circ$  by  $5^\circ$  squares at the equator of the unit sphere. The lines of equal azimuth—the  $A$  curves and the  $\psi$  circles—are the same at every point of the parallel circle but change, of course, with latitude. They must be computed at latitude intervals of  $5^\circ$ .

In drawing the gravity-anomaly maps it is best to use stereographic projection because in this projection (center point at pole) meridians are straight lines and parallel circles remain circles; furthermore, all templates with  $\psi$  circles and  $A$  curves are circles, regardless of the latitude of the computation point.

The fundamental formulas of the stereographic projections are

$$s = a \tan \left( 45^\circ - \frac{\varphi}{2} \right) = a \frac{1 - \sin \varphi}{\cos \varphi} \quad (8-29)$$

$$y = s \sin \Delta\lambda \quad x = s \cos \Delta\lambda \quad (8-30)$$

where  $a$  = arbitrary scale factor

$s$  = radius of parallel circle of latitude  $\varphi$

$\varphi$  = latitude of computation point  $P$

$\Delta\lambda$  = longitude difference between  $P$  and center point  $P'$  of square

$x, y$  = rectangular coordinates

The effect of  $\Delta\lambda$  has to be computed. From Eq. (8-29) we get easily

$$\cos \varphi = \frac{2as}{a^2 + s^2} \quad \sin \varphi = \frac{a^2 - s^2}{a^2 + s^2} \quad (8-31)$$

From spherical trigonometry we get the equations

$$\cos \psi = \sin \varphi' \sin \varphi + \cos \varphi' \cos \varphi \cos \Delta\lambda \quad (8-32)$$

$$\sin \psi \cos A = \cos \varphi' \sin \varphi - \sin \varphi' \cos \varphi \cos \Delta\lambda \quad (8-33)$$

$$\sin \psi \sin A = \cos \varphi \sin \Delta\lambda \quad (8-34)$$

where  $\varphi'$ ,  $\varphi$  = respective latitudes of computation point  $P'$  and center point  $P$  of  $1^\circ$  by  $1^\circ$  or  $5^\circ$  by  $5^\circ$  square

$\Delta\lambda$  = longitude difference of points  $P$  and  $P'$

$A$  = azimuth of  $P'P$

$\psi$  = angular distance  $P'P$

Substituting the values (8-31) into Eq. (8-32), we get

$$\cos \psi = \frac{(a^2 - s^2) \sin \varphi' + 2as \cos \varphi' \cos \Delta\lambda}{a^2 + s^2}$$

or, if we replace  $s$  by  $x$  and  $y$  [Eq. (8-30)],

$$(x^2 + y^2)(\cos \psi + \sin \varphi') - 2ax \cos \varphi' + a^2(\cos \psi - \sin \varphi') = 0 \quad (8-35)$$

This, as can easily be shown, is the equation of a circle with radius

$$r = \frac{a \sin \psi}{\cos \psi + \sin \varphi'} \quad (8-36)$$

and center at the point

$$y = 0 \quad x = \frac{a \cos \varphi'}{\cos \psi + \sin \varphi'} \quad (8-37)$$

In a similar way Eqs. (8-27) and (8-28) give

$$\cot A = \frac{(a^2 - s^2) \sin \varphi' - 2as \sin \varphi' \cos \Delta\lambda}{2as \sin \Delta\lambda} \quad (8-38)$$

$$\text{and } (x^2 + y^2 - a^2) \cos \varphi' + 2ax \sin \varphi' + 2ay \cot A = 0 \quad (8-39)$$

which also is the equation of a circle (the  $A$  circle) with radius

$$r_A = \frac{a}{\cos \varphi' \sin A} \quad (8-40)$$

and with the center at

$$y_A = -\frac{a \cot A}{\cos \varphi'} \quad x_A = -a \tan \varphi' \quad (8-41)$$

Using Eqs. (8-36) to (8-41), it is easy to draw the  $\psi$  and  $A$  circles, i.e., the circles of equal  $\psi$  and of equal  $A$ , for any latitude.

Although the "square" method described is a good one for finding the effect of the gravity anomalies not close to the computation point  $P$ , it cannot be used in the vicinity of  $P$  because  $f'(\psi)$  increases too fast with decreasing  $\psi$ .

When, instead, we use the "circle-ring" method, consequently substituting for the surface element  $dq$  the expression  $\sin \psi d\psi dA$ , we get<sup>78</sup>

$$d\xi'' = \frac{\rho''}{2\pi G} \int_{A_1}^{A_2} \cos A dA \int_{\psi}^{\psi+d\psi} f'(\psi) \sin \psi \Delta g_{\psi} d\psi \quad (8-42)$$

or  $d\xi'' = \frac{\rho''}{2\pi G} (\sin A_2 - \sin A_1) \int_{\psi}^{\psi+d\psi} f'(\psi) \sin \psi \Delta g_{\psi} d\psi \quad (8-42a)$

where<sup>72</sup>

$$\begin{aligned} 2f'(\psi) \sin \psi &= -\csc \frac{\psi}{2} - 3 - 8 \sin \frac{\psi}{2} + 32 \sin^2 \frac{\psi}{2} \\ &+ 12 \sin^3 \frac{\psi}{2} - 32 \sin^4 \frac{\psi}{2} + 3 \sin^2 \psi \ln \left( \sin \frac{\psi}{2} + \sin^2 \frac{\psi}{2} \right) \end{aligned} \quad (8-43)$$

The quantity  $d\xi''$ , in seconds of arc, is the effect of a circular-ring compartment with the boundaries  $\psi$  and  $\psi + d\psi$ ,  $A_1$  and  $A_2$ , and the gravity anomaly  $\Delta g_{\psi}$  on the vertical-deflection component  $\xi_g$ . We get a similar formula for  $d\eta''$  when we substitute  $\cos A_1 - \cos A_2$  for  $\sin A_2 - \sin A_1$ . The numerical values of the function  $f'(\psi) \sin \psi$  can be computed beforehand with  $\psi$  as argument.

Near the computation point, where  $\psi$  is small,  $\sin \psi/2$  can be neglected and  $\cos \psi/2$  taken to be 1. Thus we get

$$-2f'(\psi) \sin \psi = \csc \frac{\psi}{2} + 3 \quad (8-44)$$

Using the approximate formula

$$\csc \frac{\psi}{2} = \frac{2R}{r} + \frac{r}{12R} = \frac{2}{\psi} + \frac{\psi}{12} \quad (8-45)$$

we get

$$-2f'(\psi) \sin \psi = \frac{2R}{r} + 3 + \frac{r}{12R} \quad (8-46)$$

Quite close to the computation point, however, Formula (8-42a) cannot be used because  $\csc \psi/2$  approaches infinity. Instead, we have the following formulas, suitable inside a circle with a radius  $r_0$  of a few kilometers:

$$\Delta\xi'' = \frac{\rho''}{2\gamma} \frac{\Delta g}{\Delta x} r_0 = 0''.105 r_0 \frac{\Delta g^*}{\Delta x} \quad (8-47)$$

$$\Delta\eta'' = \frac{\rho''}{2\gamma} \frac{\Delta g}{\Delta y} r_0 = 0''.105 r_0 \frac{\Delta g}{\Delta y}$$

\*  $\Delta g = \Delta g_S - \Delta g_N$  for  $\xi$  and  $\Delta g = \Delta g_W - \Delta g_E$  for  $\eta$ .

where  $\Delta g/\Delta x$  and  $\Delta g/\Delta y$  are the average gradients, inside the circle  $r_0$ , of the gravity in milligals per kilometer in the direction of meridian and perpendicular to it, respectively;  $r_0 = \Delta x/2 = \Delta y/2$  is also given in kilometers.

How large a circle we use depends on the gravity material available. If we have a very good local gravity survey, with many stations, it is best to use a small radius  $r_0$ , 1 km or so. If, however, only few stations exist in the neighborhood of the computation point, we can use a larger radius

$r$  without losing too much real accuracy. Rice,<sup>71</sup> who had available the very good gravity-station net of the oil companies, used the value  $r = 4.32$  km but at some points a radius of only 0.28 km. Kasansky<sup>45</sup> used the value 5.0 km, and de Vos van Steenwijk<sup>74</sup> even used the value 30 km.

The amount of error caused by using too large a circle depends on how smooth the gravity field is. If the field remains nearly constant inside the particular circle, the contribution to quantities  $d\xi''$  and  $d\eta''$  is quite correct. The more irregular the gravity gradient, the larger the error. It is best to avoid, as far as possible, using computation points in whose neighborhood the gravity field is rough and to use, if possible, points where it changes almost linearly.

FIG. 8-12. Rice's three-gradient method for computing the effect of the immediate neighborhood of the station on  $\xi$  and  $\eta$ .

Rice<sup>71</sup> evaluated the gradient in three north-south and three east-west directions and took the weighted means of the results (Fig. 8-12). To accomplish this he established points on the circle at  $45^\circ$  intervals. To the central gradients he gave a weight of 1 and to each of the outer gradients a weight of 0.5. Honkasalo applied the same method when computing the contributions  $\Delta\xi''$  and  $\Delta\eta''$  on the basis of the Finnish gravity material.

Rice's results at seven computation points in the southern middle United States and Honkasalo's results at seven points in Finland are given in Table 8-6, which shows for each station the radius  $r_0$ ,  $\Delta_1\xi$  and  $\Delta_1\eta$  (one gradient),  $\Delta_3\xi$  and  $\Delta_3\eta$  (three gradients), and differences  $\Delta_1\xi - \Delta_3\xi$  for the  $\xi$  component and  $\Delta_1\eta - \Delta_3\eta$  for the  $\eta$  component. The table shows that the differences between the one-gradient and three-gradient methods are very small in the American material, on the average only  $0.^{\prime\prime}016$  in  $\Delta\xi$  and  $0.^{\prime\prime}025$  in  $\Delta\eta$ . The considerably larger differences in the Finnish material obviously are caused by the fact that in Finland the rock is on the earth's surface or close to it while there are sediment

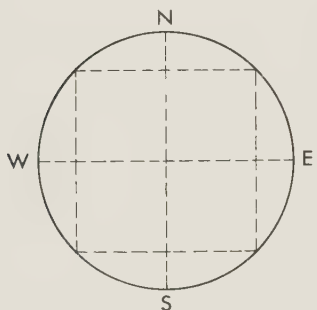


TABLE 8-6. DIFFERENCES BETWEEN ONE-GRADIENT-METHOD DEFLECTIONS  $\Delta_1\xi$ ,  $\Delta_{1\eta}$   
AND THREE-GRADIENT-METHOD DEFLECTIONS  $\Delta_3\xi$ ,  $\Delta_{3\eta}$  IN CIRCLES OF RADIUS  $r_0$

Place	$r_0$ , km	$\Delta_1\xi$	$\Delta_3\xi$	$\Delta_1\xi - \Delta_3\xi$	$\Delta_{1\eta}$	$\Delta_{3\eta}$	$\Delta_{1\eta} - \Delta_{3\eta}$
America:							
Bartley.....	4.32	+0".121	+0".112	+0".009	+0".178	+0".171	+0".007
Roby.....	4.32	-0.116	-0.102	-0.014	-0.058	-0.040	-0.018
Little Rock.	4.32	+0.010	-0.048	+0.058	+0.326	+0.375	-0.049
Legion.....	4.32	-0.173	-0.154	-0.019	+0.194	+0.216	-0.022
Sears.....	4.32	+0.536	+0.536	-0.002	+0.042	-0.026	+0.068
Brooks.....	4.32	-0.037	-0.046	+0.009	+0.026	+0.017	+0.009
Bogue.....	4.32	-0.152	-0.144	-0.008	-0.068	-0.054	-0.014
Finland:							
Vastinki....	6.8	-0.131	-0.123	-0.008	-0.110	-0.076	-0.034
	9.6	-0.168	-0.226	+0.058	-0.205	-0.153	-0.052
	18.9	-0.126	-0.114	-0.012	-0.158	-0.072	-0.086
Haavisto....	6.8	-0.400	-0.362	-0.038	+1.152	+0.846	+0.306
	9.6	-0.153	-0.157	+0.004	+0.684	+0.404	+0.280
	18.9	+0.410	+0.439	-0.029	-0.021	-0.182	+0.161
Erkylä.....	6.8	-0.163	-0.247	+0.084	+0.999	+1.085	-0.086
	9.6	-0.452	-0.269	-0.183	+0.989	+1.192	-0.203
	18.9	+0.068	-0.129	+0.197	+1.657	+1.468	+0.189
Kivesvaara..	6.8	+0.510	+0.471	+0.039	-0.410	-0.393	-0.017
	11.3	+0.295	+0.283	+0.012	-0.118	-0.161	+0.043
	22.4	+0.168	+0.299	-0.131	-0.305	-0.391	+0.086
Aulanko....	5.7	-0.363	-0.290	-0.073	+0.542	+0.305	+0.237
	9.6	-0.016	-0.133	+0.117	+0.668	+0.481	+0.187
	22.4	+0.663	+0.562	+0.101	+0.689	+0.372	+0.317
Pohjaslahti.	4.8	-0.531	-0.496	-0.035	-0.310	-0.237	-0.073
	13.4	-0.468	-0.238	-0.230	-0.605	-0.685	+0.080
	18.4	-0.663	-0.546	-0.117	-0.521	-0.645	+0.124
Mestilä.....	6.8	+0.316	+0.294	+0.022	+0.305	+0.385	-0.080
	9.6	+0.379	+0.383	-0.004	+0.463	+0.469	-0.006
	18.9	+0.568	+0.737	-0.169	+0.305	+0.269	+0.036

layers above the rock in the part of the United States Rice studied. In fact, at Haavisto, inside the 6.8-km circle, the difference in the  $\eta$  component is 0".306, and at Aulanko, where the circle is 5.7 km, it is 0".237; the difference in the  $\xi$  component at Erkylä, with a 9.6-km circle, is 0".183, and at Aulanko it is 0".117.

If, therefore, the gravity material allows detailed evaluation of  $\Delta\xi$  and  $\Delta\eta$  in the neighborhood of the computation point, it is safest to use the three-gradient method, which takes very little more time. If this is not possible, we read only the gravity anomalies  $g_N$ ,  $g_E$ ,  $g_S$ ,  $g_W$  at the north,

east, south, and west points of the circle  $r_0$  and neglect the outer gradients. Then we get simply

$$\Delta\xi'' = 0''.0525(g_s - g_N) \quad \Delta\eta'' = 0''.0525(g_w - g_E) \quad (8-48)$$

To find how large an error may result from using circles of different size Honkasalo computed for many Finnish points the effect of the circles on  $\Delta\xi$  and  $\Delta\eta$  when only the circles are used ( $\Delta_c\xi$ ,  $\Delta_c\eta$ ) and when several

TABLE 8-7. DIFFERENCES  $\Delta_c\xi - \Delta_r\xi$  AND  $\Delta_c\eta - \Delta_r\eta$  BETWEEN APPROXIMATE VALUES  $\Delta_c\xi$  AND  $\Delta_c\eta$  (CIRCLE METHOD) AND  $\Delta_r\xi$  AND  $\Delta_r\eta$  (CIRCLE-RING METHOD)

( $r_{\min}$  = smallest radius;  $r_0$  = other radii used)

Place	$r_0$	$r_{\min}$	$\Delta_c\xi$	$\Delta_r\xi$	$\Delta_c\xi - \Delta_r\xi$	$\Delta_c\eta$	$\Delta_r\eta$	$\Delta_c\eta - \Delta_r\eta$
Vastinki.....	6.8	6.8	-0''.123	-0''.123	.....	-0''.076	-0''.076	.....
	9.6	...	-0.226	-0.180	-0''.046	-0.153	-0.124	-0''.029
	13.4	...	-0.299	-0.269	-0.030	-0.189	-0.186	-0.003
	18.9	...	-0.114	-0.323	+0.209	-0.072	-0.229	+0.157
Haavisto.....	2.9	2.9	-0.323	-0.323	.....	+0.947	-0.947	.....
	6.8	...	-0.362	-0.630	+0.268	+0.846	+1.848	-1.002
	9.6	...	-0.157	-0.700	+0.543	+0.404	+2.088	-1.604
	13.4	...	+0.086	-0.713	+0.799	+0.026	+2.178	-2.152
Erkylä.....	18.9	...	+0.439	-0.657	+1.096	-0.182	+2.188	-2.370
	0.7	0.7	-0.054	-0.054	.....	+0.167	+0.167	.....
	2.1	...	+0.093	-0.065	+0.158	+0.389	+0.427	-0.038
	4.1	...	-0.102	-0.052	-0.050	+0.786	+0.803	-0.017
Saarimäki.....	6.8	...	-0.247	-0.172	-0.075	+1.085	+1.280	-0.195
	9.6	...	-0.269	-0.251	-0.018	+1.192	+1.691	-0.499
	13.4	...	-0.145	-0.326	+0.181	+1.439	+2.155	-0.716
	18.9	...	-0.129	-0.395	+0.266	+1.468	+2.714	-1.246
Kivesvaara.....	2.1	2.1	+0.055	+0.055	.....	-0.075	-0.075	.....
	4.1	...	+0.075	+0.069	+0.006	-0.193	-0.180	-0.013
	6.8	...	+0.153	+0.143	+0.010	-0.248	-0.305	+0.057
	9.6	...	+0.175	+0.207	-0.032	-0.224	-0.389	+0.165
Aulanko.....	2.9	2.9	+0.352	+0.352	.....	-0.262	-0.262	.....
	4.8	...	+0.438	+0.556	-0.118	-0.339	-0.400	+0.061
	6.8	...	+0.471	+0.720	-0.249	-0.393	-0.516	+0.123
	11.3	...	+0.283	+0.926	-0.643	-0.161	-0.653	+0.492
Pohjaslahti.....	16.0	...	+0.237	+1.019	-0.782	-0.279	-0.719	+0.440
	22.4	...	+0.299	+1.100	-0.801	-0.391	-0.817	+0.426
	2.9	2.9	-0.523	-0.523	.....	+0.193	+0.193	.....
	5.7	...	-0.290	-0.788	+0.498	+0.305	+0.355	-0.050
Mestilä.....	9.6	...	-0.133	-0.867	+0.734	+0.481	+0.514	-0.033
	16.0	...	+0.016	-0.824	+0.840	+0.546	+0.742	-0.196
	22.4	...	+0.562	-0.712	+1.274	+0.372	+0.876	-0.504
	31.5	...	+0.614	-0.552	+1.166	+0.276	+0.975	-0.699
Mestilä.....	2.9	2.9	-0.387	-0.387	.....	-0.161	-0.161	.....
	4.8	...	-0.496	-0.581	+0.085	-0.237	-0.315	+0.078
	8.1	...	-0.332	-0.779	+0.447	-0.326	-0.494	+0.168
	13.4	...	-0.238	-0.955	+0.717	-0.685	-0.728	+0.043
Mestilä.....	18.9	...	-0.546	-1.080	+0.534	-0.645	-0.969	+0.324
	26.6	...	-0.489	-1.273	+0.784	-0.779	-1.252	+0.473
	6.8	6.8	+0.294	+0.294	.....	+0.385	+0.385	.....
	9.6	...	+0.383	+0.398	-0.015	+0.469	+0.543	-0.074
Mestilä.....	13.4	...	+0.547	+0.543	+0.004	+0.513	+0.723	-0.210
	18.9	...	+0.737	+0.772	-0.035	+0.269	+0.897	-0.628

circular rings inside them are used ( $\Delta_r\xi$ ,  $\Delta_r\eta$ ). Results at seven computation points are given in Table 8-7. The differences  $\Delta_c\xi - \Delta_r\xi$  and  $\Delta_c\eta - \Delta_r\eta$  show that the circle method generally is not sufficiently accurate.

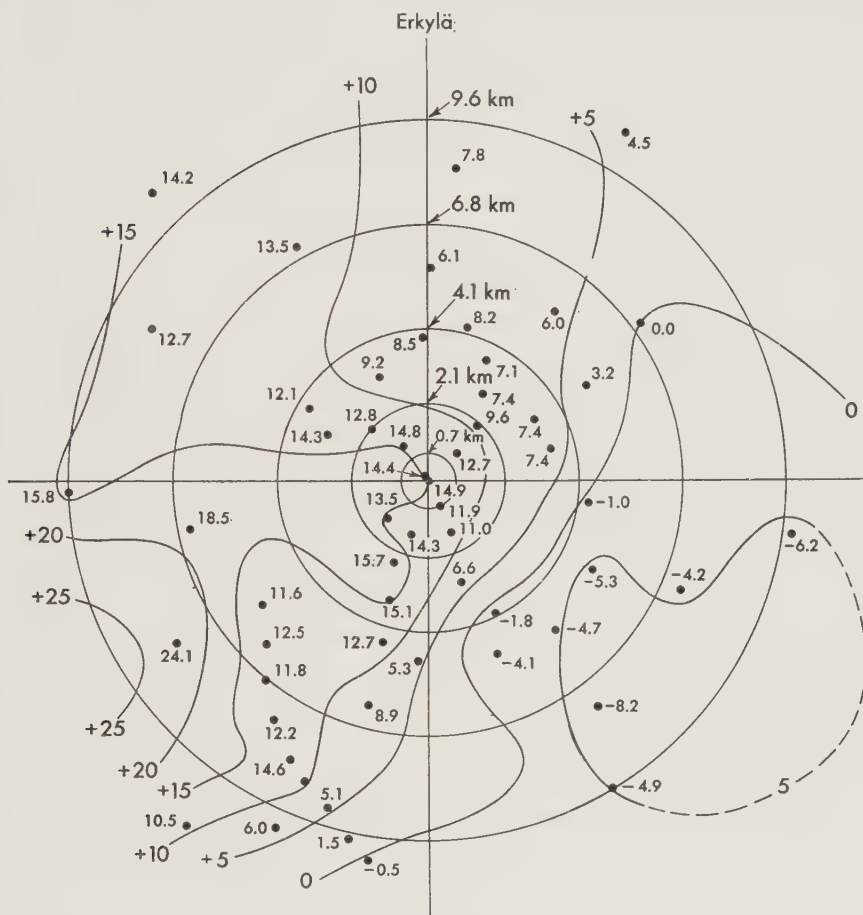


FIG. 8-13. Gravity-anomaly field in the vicinity of a lowland computation point Erkylä (Finland). The numbers 5.0, 4.5, etc., are gravity anomalies (in milligals); the numbers 0.7, 2.1, 4.1, 6.8, and 9.6 (in kilometers) are the radii of the circles used in the computations. (Courtesy of the Finnish Geodetic Institute.)

When a circle of 6.8 km radius is used, at Haavisto the discrepancy in  $\xi$  is already  $0.^{\circ}27$  and in  $\eta$  not less than  $1.^{\circ}00$ ; when only the circle of 9.6 km radius is used, the corresponding differences are  $0.^{\circ}54$  and  $1.^{\circ}60$ . At Aulanko the difference in  $\xi$  for 5.7 km radius is  $0.^{\circ}50$ .

Figures 8-13 and 8-14 for the neighborhood of the stations Erkylä and Saarimäki, where circles of 0.7, 2.1, 4.1, 6.8 and 9.6 km radius used

in the computations are given, show why the circle method cannot always give reliable results. In fact, the gravity-anomaly field is frequently so irregular that only the combination of a very small circle and circular rings around it can give a reliable result.

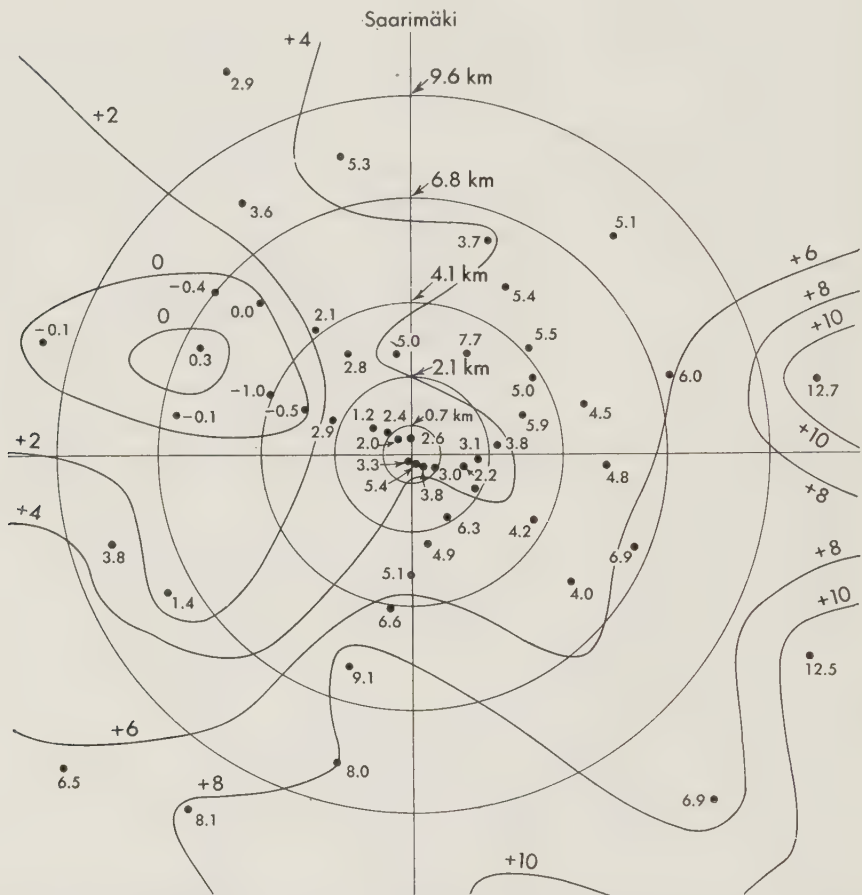


FIG. 8-14. Gravity-anomaly field of another lowland computation point, Saarimäki. (Courtesy of the Finnish Geodetic Institute.)

Consequently, a rather dense gravity-station net in the neighborhood of the computation point is a necessity. The more gravity stations we have and the smaller circle  $r_0$  we can use, the higher the accuracy. Before we choose the computation point, therefore, we must have a guarantee that a good local gravity survey exists or that one can be made, which generally takes only a few days.

It is difficult to say what distribution of gravity observations in the neighborhood of the computation points is sufficient and most economic.

In many cases four to eight points in a 5-km circle are sufficient, and it is better if they are mostly in north-south and east-west directions. Table 8-8 shows how many gravity stations Honkasalo had available for his computations.)

TABLE 8-8. NUMBER OF GRAVITY STATIONS IN THE CIRCLES OF RADIUS  $r_0$  AROUND SOME FINNISH COMPUTATION POINTS \*

Place	Radius $r_0$ , km				
	2.05	6.79	9.56	13.45	18.92
Vastinki.....	...	3	8	20	48
Virttaankangas.....	...	5	6	16	29
Haavisto.....	...	5	13	19	38
Erkylä.....	10	36	61	74	96
Kivesvaara.....	...	3	5	11	15
Aulanko.....	...	8	14	22	37
Pohjaslahti.....	...	8	13	24	40
Mestilä.....	...	2	11	16	33

\* Honkasalo, verbal communication.

Outside the circle  $r_0$  such a ratio of successive circles is employed and such compartments are used that the effect of each compartment is  $0.^{\circ}001$  per milligal. If the sine differences are  $1/8$  (32 compartments), the ratio of the radii is 1.270, and  $r_n = 1.270^n r_0$ ; this yields the  $0.^{\circ}001$ . Farther from the station the ratio, because of the curvature of the earth, will be slightly smaller than 1.270. Kasansky used this division, as shown in Table 8-9.

TABLE 8-9. KASANSKY'S CIRCLE RINGS

( $n$  = ring number;  $r$  = inner radius)

$n$	$r, \text{ km}$						
1	5.0	7	20.9	13	86.4	19	341
2	6.4	8	26.5	14	109.1	20	424
3	8.1	9	33.6	15	138	21	524
4	10.2	10	42.6	16	173	22	645
5	13.0	11	54.0	17	218	23	788
6	16.5	12	68.3	18	273	24	955

Rice divided the circle rings into 36 equal compartments of  $10^{\circ}$  angular aperture instead of 32 unequal compartments, as Kasansky<sup>45</sup> did. Of course, he had to multiply the effect of the compartments by the corresponding cosine and sine terms, but in return he had to estimate the

mean anomalies of the compartments only once. The multiplication by the cosine gave the effect on the  $\xi$  component, the multiplication by sine on the  $\eta$  component. The ratio of the radii is 1.1864. The circles used by Rice are given in Table 8-10.

TABLE 8-10. RICE'S CIRCLE RINGS

 $(n = \text{circle number}; r = \text{inner radius})$ 

$n$	$r, km$										
1	0.119	11	0.657	21	3.641	31	20.09	41	109.0	51	541.5
2	0.141	12	0.780	22	4.320	32	23.83	42	128.7	52	628.1
3	0.167	13	0.926	23	5.125	33	28.25	43	151.9	53	725.9
4	0.198	14	1.099	24	6.081	34	33.48	44	179.1	54	835.9
5	0.235	15	1.304	25	7.216	35	39.67	45	210.9	55	958.5
6	0.279	16	1.547	26	8.560	36	47.00	46	248.0	56	1094.3
7	0.331	17	1.836	27	10.15	37	55.66	47	291.2		
8	0.393	18	2.179	28	12.05	38	65.90	48	341.2		
9	0.467	19	2.586	29	14.29	39	77.97	49	399.0		
10	0.554	20	3.068	30	16.94	40	92.22	50	465.5		

Rice used only circles 1 to 51. In Columbus we have also used zones 52 to 56, to be able to compute by the circle-ring method the effect of the gravity-anomaly field inside the circle of  $10^\circ$  radius.

If the gravity material is poor, it is better to join two circles and two neighboring compartments into one, so that the compartments are larger; their effect is, of course,  $0.^{\circ}004$ . When computing  $\xi_g$  and  $\eta_g$  at 16 stations of the Middle West, including Meades Ranch, the initial point of the American datum, Rice had about 40,000 stations available to a distance of 600 km from the computation points. As he was able to compute  $\xi_g$  and  $\eta_g$  by the aid of an adequate gravity material only to 600 km and on an approximate basis only to 1400 km from the computation point, the values he obtained, though not far from the real value, are, of course, only relative.

It is possible, however, to study the accuracy of the difference of the resulting deflections when we compare the gravimetric values  $\xi_g$  and  $\eta_g$  with the astronomic-geodetic values  $\xi_a$  and  $\eta_a$  at neighboring stations not far from each other. The effect of the gravity field outside 600 km is approximately the same at neighboring stations—distance not exceeding 100 km—so that  $\xi_g - \xi_a$  and  $\eta_g - \eta_a$  are broadly similar at all stations and give a measure of the effect of the gravity field of the area omitted in the computation. When this more or less constant systematic part is subtracted, the remaining residuals  $(\xi_g - \xi_a)_r$  and  $(\eta_g - \eta_a)_r$  are rather small. Rice found that the systematic difference in  $\xi$  was  $-0.^{\circ}23$  and in  $\eta +0.^{\circ}38$ ; the average deviation from the mean in  $\xi$  was  $\pm 0.^{\circ}46$  and in  $\eta \pm 0.^{\circ}68$ ; and the maximum residuals in  $\xi$  were  $-0.^{\circ}98$  and in  $\eta +2.^{\circ}26$ .

\* Tsuboi <sup>109</sup> has ingeniously applied the Bessel Fourier series for computation of the effect of the neighborhood on  $\xi$  and  $\eta$ .

Rice<sup>71</sup> was even able to discover errors in the astronomic-geodetic deflections of the vertical. The triangulation points Roby and Sears are only 37 km apart, but the differences  $\eta_g - \eta_a$  at these stations show a discrepancy of 1".46, or much more than the error of the relative gravimetric deflection determination would lead one to expect. Consequently, new, very accurate longitude observations were carried out at these stations. When the new values were used, the discrepancy was reduced to 0".40. According to Rice, the relatively large residuals ( $\eta_g - \eta_a$ ) at Bynum (+1".88), Bartley (+2".26), and Arcadia (-1".24) are in large part due to uncertainty in the astronomic longitude.

These examples show that if astronomic-geodetic deflections are to be used to verify gravimetric deflections, they must be of the highest accuracy.

Rice tried to estimate the effect of the gravity field at a distance of 600 to 1400 km by the aid of gravity material available from the United States, Canada, Mexico, and the Gulf of Mexico. The accuracy of the computed effect of this area is, of course, rather small. The effect of the region from 1400 km to the antipode was computed from the data of Jeffreys, who estimated the free-air anomalies for 10° by 10°, considering the correlation of these anomalies with height. On the basis of these data the gravity field was expressed in spherical harmonics up to the third degree. The effect of both remote areas is small, as can be seen from Table 8-11, where

TABLE 8-11. EFFECT ON  $\xi_g$  AND  $\eta_g$  OF THE AREAS A, TO 600 km, B, TO 1400 km, AND C, TO ANTIPODE;  $P_w$ ,  $P_E$  FICTITIOUS POINTS

	$\xi_g$					$\eta_g$				
	A	B	B - A	C	C - B	A	B	B - A	C	C - B
Twin...	-0".73	-0".58	+0".15	-0".87	-0".29	-0".61	-0".60	+0".01	-0".14	+0".46
$P_w$ ....	-0.53	-0.76	-0.23	-1.58	-0.82	+0.68	-0.07	+0.75	+0.93	+1.00
$P_E$ ....	+0.37	-0.70	-1.07	-1.08	-0.38	+0.28	+0.05	-0.23	+0.22	+0.17

column A gives the effect of the gravity field out to 600 km from three stations, column B to the distance 1400 km, and column C the effect of the total gravity field. The effect of the area from 600 to 1400 km is rather small at the three computed points; on  $\xi_g$  only +0".15, -0".23, and -1".07 and on  $\eta_g$  +0".01, +0".75, and -0".23; the effect of the entire gravity field beyond 1400 km on  $\xi_g$  is -0".29, -0".82, and -0".38 and on  $\eta_g$  +0".46, +1".00, and +0".17. The whole area beyond 600 km will give only the following small corrections: in  $\xi_g$  -0".14, -1".05, and -1".45 and in  $\eta_g$  +0".47, +0".25, and +0".06. Unfortunately the situation is not so advantageous. When we were able in Columbus to compute the

gravimetric deflections of the vertical on the basis of the gravity material of the whole world, the vertical deflections of Rice got a correction of  $2''$  to  $3''$ . The case is similar in other parts of the world. Although at two-thirds of the computation points used by us, the effect of the zone  $3^\circ$  to  $20^\circ$  on  $\xi_g$  and  $\eta_g$  is less than  $1''$ , it is between  $1''$  and  $2''$  in one-third of the cases. The effect of the gravity anomalies beyond the boundary  $\psi = 20^\circ$  is of the same order. Therefore, if we try to get the absolute deflections of the vertical by considering only the gravity-anomaly field of the limited area, we can easily commit an error of  $2''$  to  $4''$ . Since this error of  $\xi_g$  and  $\eta_g$  can be positive as well as negative, the total error brought about by the neglected gravity field of the farther zones is considerable. Before one gets a good beef steak the whole animal must be killed. To compute reliable gravimetric deflections of the vertical one must know the gravity-anomaly field for the major portion of the world.

As the real gravity field changes rather rapidly from point to point, it is hardly possible to interpolate, and still less possible to extrapolate, gravity anomalies far from the observation points, as Jeffreys did. For instance, the isostatic gravity anomalies average +35 mgal in the western basin of the Mediterranean, +60 mgal in Cyprus, and about +30 mgal in the Holy Land. Interpolation between these values gives an average gravity value of +35 mgal for the eastern basin of the Mediterranean, while observations give the value -22 mgal. This fact and others similar to it diminish the significance of Jeffreys's procedure.

How dangerous it is to use the anomalies obtained from the expansion in spherical harmonics as representative of the gravity anomalies of un-surveyed areas can be seen from Zhongolovich's geoid. He expanded the gravity anomalies of the world in spherical harmonics to the eighth order on the basis of the anomalies of the surveyed areas. Applying his gravity-anomaly field, he computed the geoid distances  $N$  and obtained a triaxial ellipsoid with  $N$  values from -160 to +136 m; these values are more than twice as large as those of Tanni, who let the observed anomalies represent only relatively small areas, and three times larger than those obtained in Columbus.

The reason for the discrepancy between Zhongolovich's and Tanni's geoids was discovered in Columbus when Uotila compared the observed average gravity anomalies of the  $5^\circ$  by  $5^\circ$  squares with the anomalies Zhongolovich obtained from his spherical harmonics. Table 8-12 gives the differences between the observed *average* anomalies of the *whole* longitude zones (from pole to pole) and those obtained by Zhongolovich. More than 100 squares  $5^\circ$  by  $5^\circ$  need a correction exceeding 30 mgal.

Thus Zhongolovich's geoid is hardly based on reliable material. The gravity anomalies change so much from point to point that we must have many more gravity observations than we have now before it is possible to

TABLE 8-12. DIFFERENCES BETWEEN THE OBSERVED AND ZHONGOLOVICH AVERAGE ANOMALIES IN SOME LONGITUDE ZONES

Longitude	No. of $5^{\circ}$ by $5^{\circ}$ squares used	Correction, mgal
0°–30°E	96	18
60°–90°E	67	8
120°–150°E	79	13
150°–120°W	42	3
90°–60°W	100	2
30°–0°W	66	5

let the gravity anomalies obtained from spherical harmonics represent the unsurveyed areas. We are nearer the truth when we use zero isostatic anomaly for such regions.

Further confirmation is found in studies of the “error of representation,” which enters the picture when we determine how accurately a few gravity values can give the mean gravity anomaly of large areas.

If the individual values of the gravity anomaly of a square with the side  $s$  are  $\Delta g$ , if the arithmetical mean of them in a square of side  $s$  is  $\Delta g_s = \Sigma \Delta g / n$ , and if  $v$  is the difference  $\Delta g - \Delta g_s$ , then the standard error of representation  $E_s$  will be  $E_s = \sqrt{\Sigma v^2 / n}$ .  $E_s$  is therefore the standard mean deviation of one observed anomaly  $\Delta g$  from the average gravity anomaly  $\Delta g_s$  of the square. In other words, the standard error of the gravity anomaly of a square will be  $E_s$  if one gravity station has to represent the whole square.

This important problem was first handled by de Graaff Hunter<sup>12</sup> in 1935 on the basis of the gravity material of India. He came to the conclusion that the error of representation  $E_s$  of the squares with  $s = 2^{\circ}$ ,  $4^{\circ}$ ,  $8^{\circ}$  was 23.1, 36.4, and 43.3 mgal, respectively. As the material was small in quantity and rather one-sided, a new, thorough study of the problem on the basis of the dense gravity-station nets of Mozambique, Finland, Sweden, France, and the U.S.S.R. and on the basis of Tanni's material was undertaken in 1953 and 1955 by Hirvonen.<sup>37, 40</sup> He had to study the following questions:

1. What accuracy can be obtained using the present gravity material for computation of  $N$ ,  $\xi$ , and  $\eta$ ?
2. What is the minimum amount and the proper distribution of gravity points for a prescribed accuracy for  $N$ ,  $\xi$ , and  $\eta$ ?
3. How big an area can be represented by one gravity point?

To solve these problems we have to estimate empirically, on the basis of the existing gravity material, not only the function  $E_s$ , the error of representation, or standard mean deviation of one anomaly  $\Delta g$  from the mean anomaly  $\Delta g_s$ , but also the function  $G_s$ , or standard mean value of all anomalies of the square of side  $s$ . We easily obtain for  $G_s$  the equation

$$nG_s^2 = \Sigma \Delta g_s^2 \quad (8-49)$$

where  $n$  is the number of gravity points in the square. In a similar way we obtain from the formula  $E_s = \sqrt{\Sigma v^2/n}$

$$nE_s^2 = \Sigma (\Delta g - \Delta g_s)^2 \quad (8-50)$$

It is easy to see that  $G_s$  is largest for small  $s$  and decreases with  $s$  toward zero, which value it approximately reaches when the square covers a whole hemisphere. The function of  $E_s$  is zero, of course, in very small squares and increases with  $s$ .

Between  $E_s$  and  $G_s$  we obviously have the relation

$$E_s^2 = G_0^2 - G_s^2 \quad (8-51)$$

Table 8-13 gives the functions  $E_s$  and  $G_s$  according to Hirvonen's study

TABLE 8-13. ERROR OF REPRESENTATION  $E$ , MEAN GRAVITY ANOMALY  $G$ , AND  $(G_s/G_0)^2$  AS FUNCTIONS OF SQUARE SIDE  $s$ <sup>40</sup>

$s$	$E$	$G$	$(G_s/G_0)^2$
0°0	$\pm 0.0$	$\pm 28.0$	1.00
0.2	$\pm 5.4$	$\pm 27.5$	0.96
0.5	$\pm 6.0$	$\pm 26.5$	0.90
1.0	$\pm 12.7$	$\pm 25.0$	0.79
2.0	$\pm 17.6$	$\pm 21.8$	0.60
3.0	$\pm 20.8$	$\pm 18.7$	0.45
5.0	$\pm 23.1$	$\pm 15.8$	0.32
10.0	$\pm 24.9$	$\pm 12.8$	0.21
30.0	$\pm 26.6$	$\pm 8.7$	0.10

mentioned above. We see that  $E$  increases with  $s$  from 0 to  $\pm 26.6$  mgal for  $s = 30^\circ$  and that  $G$  decreases from  $\pm 28.0$  to  $\pm 8.7$  mgal for  $s = 30^\circ$ . The square  $s = 2^\circ 6$  (not shown in the table) is interesting, because there  $E = G = \pm 19.8$  or, rounded,  $\pm 20$  mgal. It means that for  $s$  smaller than  $2^\circ 6$ , one observed gravity anomaly represents the whole square better than zero gravity anomaly but for values larger than  $2^\circ 6$  a smaller error results if zero gravity anomaly is used instead of the observed anom-

aly. For instance, for  $s = 5^\circ$  the standard errors, resulting from the use of either zero anomaly or one observed anomaly, are  $\pm 15.8$  and  $\pm 23.1$  mgal, respectively, and the weight factor  $(G_s/G_0)^2$ , 0.32. Here  $G_s^2$  is the variance of the mean anomalies of squares of side length  $s$  and  $G_0^2$  is the variance of a point value. Values  $E$ ,  $G$ , and  $(G_s/G_0)^2$  are, of course, empirical, obtained by the gravity anomaly material available in Columbus in 1954.

Factors  $(G_s/G_0)^2$  show how a large portion of a one-point gravity anomaly is the best representative of a square of side length  $s$ . If we, for instance, use point value 50 mgal as representative of the squares,  $s = 0^\circ 5$ ,  $1^\circ 0$ ,  $2^\circ 0$ ,  $5^\circ 0$ ,  $10^\circ 0$ , and  $30^\circ 0$ , the best mean  $\Delta g$  values would be 45, 40, 30, 16, 10, and 5 mgal. Before electing the mean gravity anomalies we must, however, also consider carefully such geophysical factors as the mountains, valleys, coastal areas of oceans, ocean islands, etc. For instance, we can use the gravity anomalies of small ocean islands only as representative of the island itself and its shallow "apron," because the island anomalies are exceptionally positive, and the anomalies of the belts of negative anomalies represent only the belt itself.

If one is not sure what anomaly to use, it is good to keep in mind that isostatic anomaly zero is a rather good representative. It is also wise not to venture to use any anomaly except zero for large gravimetrically unsurveyed areas like the southern Pacific.

If we could get observations for this area at least at an average distance of  $10^\circ$ , it would solve the whole problem satisfactorily. Still better would be gravity profiles across the gaps at a distance of, say,  $5^\circ$  with a point distance of 50 miles along the profiles.

On the basis of American gravity material Kaula<sup>102</sup> has studied the accuracy of  $N_g$ ,  $\xi_g$ , and  $\eta_g$  when the gravity anomalies to a given radius have been used. He concludes that the standard error of  $N_g$  is 13 m when the computation has been carried out only to  $20^\circ$ ; the effect of the zone between  $30^\circ$  to  $60^\circ$  is very small. If we omit only an area of  $25^\circ$  radius around the antipode it will cause an uncertainty of about 5 m. The standard error of gravimetrically computed deflections of the vertical with perfect knowledge of gravity out to 500 km will be  $\pm 3'' 3$ ; to 1500 km,  $\pm 2'' 0$ ; and to 3000 km,  $\pm 1'' 3$ .

Practical computations in Columbus have revealed that the total effect of the area beyond  $3^\circ$  is seldom more than  $4''$ , of the area beyond  $20^\circ$  seldom more than  $2''$ .

An interesting gravimetric study of  $\xi_g$  and  $\eta_g$  has been carried out by Honkasalo<sup>100</sup> at 14 points of western Finland. At his disposal were both the good local gravity survey of Finland (over 5000 stations along the highways) at intervals of 5 km and the gravity material of Norway and the countries around the Baltic Sea. Like Rice, he used the free-air

anomalies at most stations without terrain correction, which, except in Norway, is small. He used the gravity field to 690 km from the computation points, which were rather close to each other. According to his study of the differences between the gravimetric and astronomic-geodetic deflections of the vertical, the systematic parts of  $\xi_g - \xi_a$  and  $\eta_g - \eta_a$  are  $+1.^{\circ}20$  and  $-2.^{\circ}85$ , respectively; from them we get the residual differences  $(\xi_g - \xi_a)_r$  and  $(\eta_g - \eta_a)_r$  given in Table 8-14.

TABLE 8-14. RESIDUAL DIFFERENCES BETWEEN GRAVIMETRIC AND ASTRONOMIC-GEODETIC DEFLECTIONS  $\xi_g - \xi_a$  AND  $\eta_g - \eta_a$  AT 14 FINNISH ASTRONOMIC-GEODETIC POINTS<sup>100</sup>

Point	$\varphi$	$\lambda$	$(\xi_g - \xi_a)_r$	$(\eta_g - \eta_a)_r$
Erkylä.....	60°42'	24°55'	-0°11	+0°51
Haavisto.....	60 57	24 0	-1.41	+2.02
Virttaankangas.....	60 59	22 36	+1.10	-0.55
Aulanko.....	61 1	24 28	+0.07	-1.38
Mestilä.....	61 4	22 4	+1.32	-0.49
Saarimäki.....	61 8	23 48	+0.09	-0.48
Vuores.....	61 26	23 46	-0.14	-0.09
Mutala.....	61 40	23 31	-0.28	-0.15
Vatula.....	61 43	22 56	-0.36	+0.26
Pohjaslahti.....	62 12	24 5	-0.33	+1.28
Alavus.....	62 35	23 35	+0.16	-0.45
Seinäjoki.....	62 42	22 53	-0.05	-0.33
Vastinki.....	62 57	24 58	+1.01	-0.10
Sopero.....	64 43	25 12	-1.12	-0.10
Standard error.....	.....	.....	±0.76	±0.84

It is seen that five residuals in  $\xi$  and three in  $\eta$  exceed 1°. The standard error of residuals  $(\xi_g - \xi_a)_r$  is  $\pm 0.76$  and of  $(\eta_g - \eta_a)_r$ ,  $\pm 0.84$ . These relatively high residuals are caused not only by the unknown gravity field at the Gulf of Bothnia but also by insufficient terrain correction, as indicated by the small residuals (only  $+0.09$  and  $+0.16$  in  $\xi$  and  $-0.48$  and  $-0.45$  in  $\eta$ ) at Saarimäki and Alavus, which are not hilltop triangulation points but chosen points of the lowland.

Similar computations were carried out by Wideland<sup>86</sup> at seven astronomic-geodetic points of the Swedish triangulation. Using the Swedish gravity survey and a part of the gravity survey of Norway and Finland, he measured a dense local gravity-station net of about 40 points inside the 5-km circle around the computation point and applied the isostatic gravity anomalies ( $T = 60$  km) out to 645 km from these points. Consequently,

topographic-isostatic reductions were also made in the astronomic-geodetic deflections  $\xi_a$  and  $\eta_a$ .<sup>86</sup>

Table 8-15 shows the systematic differences in  $\xi_g$  and  $\eta_g$  to be  $+1.^{\circ}35$

TABLE 8-15. RESIDUALS  $(\xi_g - \xi_a)_r$  AND  $(\eta_g - \eta_a)_r$  OF THE ASTRONOMIC-GEODETIC GRAVIMETRIC DEFLECTIONS OF THE VERTICAL

(System differences  $+1.^{\circ}35$  in  $\xi$  and  $-1.^{\circ}73$  in  $\eta$  have been considered)

Place	$\varphi$	$\lambda$	$(\xi_g - \xi_a)_r$	$(\eta_g - \eta_a)_r$
Tornberget.....	60°00'	16°26'	-0.25	-1.17
Östra Älvhöjden.....	60 00	14 48	+0.31	+0.23
Tomasboda.....	59 23	14 58	+0.41	-0.62
Tomtabacken.....	57 30	14 28	-0.54	+0.03
Mälensås.....	56 47	14 16	-0.02	+1.26
Råda.....	58 30	13 6	+0.03	+0.79
Bläbergskullen.....	59 50	12 52	+0.04	-0.57

and  $-1.^{\circ}73$ , respectively. When this systematic part is considered, the residual differences  $(\xi_g - \xi_a)_r$  and  $(\eta_g - \eta_a)_r$  are rather small (amounting to only  $\pm 0.^{\circ}23$  in  $\xi_g$  and  $\pm 0.^{\circ}69$  in  $\eta_g$ ), obviously because the vicinity of the computation points in Sweden was covered by many gravity stations and the terrain correction was also considered.

The work of Rice, Honkasalo, and Wideland indicates that the accuracy of the gravimetric deflections of the vertical is rather high. Whenever relatively large residuals appear, there is good reason to remeasure the astronomic latitude and longitude at the most important astronomic points. Only in this way is it possible to check the accuracy of the gravimetric deflections. It must not be forgotten, however, that the computed  $\xi_g$  and  $\eta_g$  are not absolute. To get the absolute values the gravity field must be known much further from the computation point. Computations of this kind are currently in progress in Columbus, Ohio.

Brief mention should be made here of the interesting computation of  $\xi_g$  and  $\eta_g$  at 25 points in Argentina by the Instituto de Geodesia de la Universidad de Buenos Aires under the leadership of Baglietto.<sup>2</sup> As the results have not yet been compared with the astronomic-geodetic deflections, the relative accuracy of these  $\xi_g$  and  $\eta_g$  values is not known. When the comparison has been made the value of this computation will be greatly increased.

Of another kind but important are the computations of Rice and Fischer, which were made on the basis of relatively poor gravity material. Consequently, the residuals  $(\xi_g - \xi_a)_r$  and  $(\eta_g - \eta_a)_r$  are considerably larger than those discussed above, having a probable error on the order of  $\pm 3.^{\circ}0$ .

For the U.S. Coast and Geodetic Survey Rice<sup>70</sup> studied a rectangular area of about 300 by 1800 km, the long axis extending from Cape Canaveral, Florida, to the southwest corner of Puerto Rico. Deflections of the vertical at sea level were computed for 441 regularly spaced points in the area by the Stokes' formula, using available gravity anomalies reduced according to the Pratt-Hayford hypothesis with compensation depth of 113.7 km. Deflections thus determined are slopes between the compensated geoid and the reference ellipsoid, requiring the additional computation of isostatic deflections according to the Hayford method. Combining these two steps gives, theoretically, the slope between the actual geoid and the reference ellipsoid. Observed deflections were available at 78 astronomic-geodetic stations in the area, providing an estimate of accuracy of the method employed and permitting an evaluation of the various broad systematic effects operating on the computed deflections. If the observed deflections at these control points are accepted as being free from error, the corresponding computed values have a standard error of about  $\pm 4.5''$  in each component. This degree of accuracy was substantially what had been expected from the gravimetric and bathymetric information at hand. The largest deflection component observed at any of the control points was  $42.8''$ , and the largest computed deflection for the regular stations was  $56.7''$ .

Fischer's study<sup>9</sup> for the U.S. Army Map Service consisted of the gravimetric computation of  $\xi_g$  and  $\eta_g$  for the western and central Mediterranean and vicinity; the values obtained at 23 stations were compared with the astronomic-geodetic deflections of the vertical  $\xi_a$  and  $\eta_a$ . Here too the isostatic (Hayford) gravity anomalies ( $T = 113.7$  km) were used because they are more representative than other anomalies. Since the isostatic anomalies were used, it was also necessary to make topographic-isostatic reductions in the astronomic-geodetic deflections so that both sets of deflections would refer to the co-geoid and be comparable with each other.

The available gravity material was poor in the vicinity of the astronomic-geodetic points and still poorer outside the circle of 450 km radius. Under these conditions we cannot expect high accuracy, particularly because the effect of the gravity field of the nearest neighborhood, say inside 50 km, can even exceed  $10''$ . We have seen (Tables 8-6 and 8-7) that the effect of this area can be adequately obtained only on the basis of a rather good local gravity survey, which in this case did not exist. We are therefore satisfied to find that the average discrepancy between the gravimetric and astronomic-geodetic deflections of the vertical is not more than  $3.1''$  in the  $\xi$  component and  $4.79''$  in  $\eta$  component.

Our lengthy discussion of the gravimetric deflections of the vertical can be summarized as follows. Very accurate values for  $\xi_g$  and  $\eta_g$  can be obtained at computation point  $P$  if its neighborhood has a rather

smooth gravity-anomaly field and is covered by a very dense gravity-station net—up to 30 stations in a circle of 20 km radius and up to 100 stations in a circle of 100 km radius. If, in addition, a good regional gravity survey exists out to 2000 km from  $P$ , as is true in Europe, North America, and some other areas, an accuracy  $\theta = \sqrt{\xi_g^2 + \eta_g^2}$  of  $0.^{\circ}8$  (Hirvonen) or of  $0.^{\circ}5$  (Vening Meinesz) can be obtained on the basis of present gravity material. The effect of the gravity anomalies beyond 2000 km is small, in Europe smaller than  $2.^{\circ}$ .

High accuracy of  $0.^{\circ}5$  is desirable at the initial points of the geodetic datum of different geodetic systems as well as at some other vertical-deflection stations of the first order. For the control points of 1:200,000 maps or smaller, an accuracy of  $\theta$  from  $2.^{\circ}$  to  $3.^{\circ}$  is sufficient. In fact,  $2.^{\circ}$  corresponds to 62 m on the ground and 0.3 mm on a 1:200,000 map, a value that is smaller than the drafting and reproduction accuracy.

#### *D. Dimensions of the Reference Ellipsoid*

We now turn to the problem of how physical geodesy can avoid the limitations of the classic astronomic-geodetic method for determining the dimensions of reference ellipsoid discussed in Sec. 8-2. The gravimetric method for determining the flattening  $\alpha$  of the reference ellipsoid was described in Chap. 3 and shown to be capable of rather high accuracy. In this method the most probable corrections for the equatorial value  $\gamma_E$  and for the  $\beta$  term of the gravity formula being used are computed on the basis of gravity anomalies obtained at different latitudes. The resulting  $\beta$  value gives, through Clairaut's formula, the most probable flattening value  $\alpha$ .

To check the equatorial value  $a$  of the reference ellipsoid we must solve two problems. First, we must measure the longest possible distances or arcs along the continents and, if possible, across the oceans as well. We already have a large number of such yardsticks on different continents, the accuracy of which may not be too poor. If we can use them effectively, a good value for  $a$  can be obtained.

The difficulties are caused chiefly by the second problem, that of localizing the measured arcs at the proper places on the reference ellipsoid; i.e., we must determine accurately the central angle corresponding to every measured arc. Astronomic observations alone are not sufficient, because they are referred to the geoid. To convert them to the ellipsoid we must know the components of the absolute deflection of the vertical  $\xi_g$ ,  $\eta_g$  at the end points of the measured arcs. Figure 8-9 shows clearly the difficulties we face when we do not know them. The isostatic reduction of the astronomic coordinates will help considerably, but the problem remains a source of error, which becomes greater as the length of the measured arcs decreases.

The gravimetric method which helps solve these difficulties is very simple. As already mentioned, we have only to make very accurate astronomic observations at the end points of the measured arc or in their neighborhood. A good local gravity survey around these points is essential. So long as we also have a general gravity survey to at least 1000 km from the end points and some knowledge of the gravity-anomaly field beyond this boundary, we are able to compute the components  $\xi_g$  and  $\eta_g$  gravimetrically.

If we have chosen some arbitrary value, say zero, for  $\xi_a$  and  $\eta_a$  at one end point of the arc, we can easily compute, along the measured arc, the astronomic-geodetic components  $\xi_a$  and  $\eta_a$  at the other triangulation end point of the arc. The quantities  $\xi_a$  and  $\eta_a$  are, of course, dependent on  $a$  and  $\alpha$  of the reference ellipsoid being used, while  $\xi_g$  and  $\eta_g$  are totally independent of  $a$ . If the differences  $\xi_g - \xi_a$  and  $\eta_g - \eta_a$  are nearly equal at both end points of the arc, the reference ellipsoid is good. If there is a difference, say, of  $10''$ , the  $a$  value of the reference ellipsoid has to be corrected to eliminate the difference.

In computing the astronomic-geodetic deflections  $\xi_a$  and  $\eta_a$  we use a reference ellipsoid whose flattening corresponds to the  $\beta$  term of the gravity formula being used. If we use the international ellipsoid, we must also use the international gravity formula, because the  $\beta$  value of the latter,  $\beta = 0.0052884$ , has been obtained from the  $\alpha$  value of the former,  $\alpha = 1/297.0$ .

Each measured arc at whose end points the astronomic observations and good local gravity survey have been carried out can be used for determining the  $a$  value. By the method of least squares the different measured arcs of this kind will give the best possible correction to the  $a$  value of the reference ellipsoid. This method<sup>32, 33</sup> may be the simplest, because it does not require any astronomic observations except at the end points of the measured arc or close to them. To increase the accuracy it is well to use more than one astronomic-geodetic point at each end of the measured arc. If astronomic observations also have been made between the end points, of course they must be used too.

Whenever possible we avoid astronomic-geodetic points of rough topography as computation points of  $\xi_g$  and  $\eta_g$  and take instead lowland points in the neighborhood of which a good local gravity survey exists or can be carried out and which can be easily connected to the triangulation chain. At this lowland point we carry out accurate astronomic measurements.

When, instead of measured arcs, there are large areas covered by astronomic-geodetic points, as in the United States, Europe, India, etc., it is best to compute the gravimetric  $\xi_g$  and  $\eta_g$  first at the initial point of the geodetic datum or at some other astronomic-geodetic point approximately in the middle of the surveyed area and then at several points in different directions from the first point and close to the boundary of the surveyed

area. Of course, the boundary points must be chosen so that the gravimetric  $\xi_g$  and  $\eta_g$  can be computed adequately, i.e., so that in the neighborhood of these points a relatively good gravity survey to at least 1000 km distance exists or can be carried out.

We again compare the differences between the gravimetric and the astronomic-geodetic deflections of the vertical. If the differences  $\xi_g - \xi_a$  and  $\eta_g - \eta_a$  are nearly equal at all computation points, the reference ellipsoid employed is good, but if systematic differences appear, the equator radius of the reference ellipsoid must be corrected so that they vanish.

When measured arcs and surveyed areas treated in the manner described are combined, the least-squares adjustment gives the best  $a$  values for the reference ellipsoid. The flattening  $\alpha$  cannot be corrected by this procedure, because changing it would also change the adopted gravity formula and consequently the gravity anomalies too. The gravity anomalies themselves will yield the needed correction for  $\alpha$ . The corrected ellipsoid will not fit best with the geoid in some particular areas, but it is—and this is the most important—a good average ellipsoid. It is always rather close to the geoid although it is above or below it in some countries and ocean areas (Fig. 8-9). When the corresponding undulations  $N$  of the geoid at the required points are added to the geocentric radii of this ellipsoid, the exact size and shape of the geoid are obtained.

#### 8-4. Shape of the Geoid

In Chap. 3 Stokes' formula, which makes gravimetric computation of the geoid distances  $N$  possible, was derived, and in Sec. 8-3 it was given both in the original form [Formula (8-24)] and as modified by Helmert [Formula (8-25)].

##### A. Practical Procedure

Figure 8-15 illustrates the functions  $S(\psi) = 2f(\psi)$  and  $F(\psi)$ , which are also given in Table 8-16 together with their derivatives  $f'(\psi) = \partial f / \partial \psi$  and  $f'(\psi) \sin \psi$ , with  $\psi$  as argument. The zero points of both  $f$  and  $F$  are at  $\psi_1 = 38^\circ 57' 44''$  and  $\psi_2 = 117^\circ 39' 42''$ ; the zero point of  $f'$  and  $f' \sin \psi$  is at the antipode,  $\psi = 180^\circ$ , as can readily be understood. (More extensive tables for  $f$  and  $F$  have been published by Lambert and Darling<sup>48</sup> and for  $f'$  by Sollins.<sup>72</sup>)

The formula for the computation of  $N$  can easily be divided into two parts

$$N = \sum c_\psi \Delta g_\psi \quad (8-52)$$

$$c_\psi = \frac{R}{G} F(\psi) d\psi$$

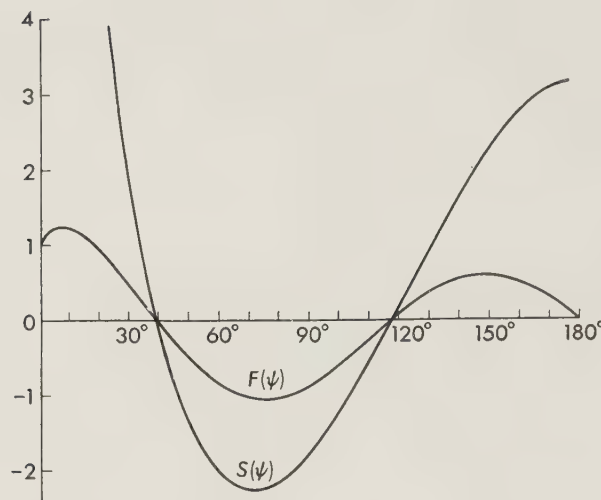


FIG. 8-15. Stokes' functions  $S(\psi)$  and  $F(\psi)$  as functions of the angular distance  $\psi$  from  $0^\circ$  to  $180^\circ$ .

TABLE 8-16. STOKES' FUNCTIONS AND VENING MEINESZ FUNCTIONS

$\psi$	$f(\psi)$	$F(\psi)$	$f'(\psi) = \frac{df(\psi)}{d\psi}$	$f'(\psi) \sin \psi$
$0^\circ$	$\infty$	1.000	$-\infty$	$-\infty$
0.1	582	1.015	-329,142	-574
0.2	294	1.026	-82,502	-288
0.5	121	1.054	-13,305	-116
1	62	1.088	-3,371	-59
2	32.6	1.14	-866	-30.2
5	14.0	1.22	-151	-13.1
10	7.0	1.21	-43.6	-7.6
20	2.75	0.94	-14.2	-4.9
30	0.95	0.47	-7.6	-3.8
40	-0.08	-0.05	-4.5	-2.9
50	-0.70	-0.54	-2.6	-2.0
70	-1.15	-1.08	-0.1	-0.1
90	-0.91	-0.91	+1.4	+1.4
120	+0.09	+0.08	2.2	1.9
150	1.12	0.56	1.5	0.8
180	1.54	0.00	0.0	0.0

where  $c_\psi$  is the Stokes' coefficient for the circular-ring division and depends only on the angular distance  $\psi$ . The undulations  $N$  can be obtained by estimating the average gravity anomalies of each circular ring, multiplying them by the corresponding Stokes' coefficient  $c_\psi$ , and summing up the products  $c_\psi \Delta g_\psi$  over all the earth's crust.

The chief advantage of this method lies in the fact that the function  $F(\psi)$  is also finite at the computation point, in contrast to the original Stokes' function  $f(\psi)$ , which, because of the factor  $\csc \frac{1}{2}\psi$ , is infinite at that point. Its drawback lies in the fact that the mean gravity anomaly of the circular rings must be evaluated *separately* for each computation point. In this respect the square division is better because a gravity-anomaly map giving the mean gravity anomalies of good-sized squares, e.g.,  $1^\circ$  by  $1^\circ$ , once prepared and drafted, can be used for all computation points. Another advantage of the square-division method is the ease with which corrections introduced by new measurements can be computed for the  $N$  values. Despite the infinite value of function  $f(\psi)$  at the computation point, the product  $c_\psi \Delta g_\psi$  is also finite close to the computation point.

When the square-division method is used, as it was by Tanni, for instance, the following two formulas result

$$\begin{aligned} N &= \Sigma c_q \Delta g_q \\ c_q &= \frac{1}{2\pi} \frac{R}{G} \int_q f(\psi) dq \end{aligned} \tag{8-53}$$

where  $R = 6371$  km = mean value for earth's radius

$G = 979.8$  gal = mean value of gravity

$dq$  = area of  $1^\circ$  by  $1^\circ$  or  $5^\circ$  by  $5^\circ$  square

$\psi$  = angular distance of center point of square from computation point

$\Delta g_q$  = average gravity anomaly of square

$c_q$  = corresponding Stokes' coefficient for square division

This coefficient is the same along the whole parallel but will change with latitude if the lengths of the square sides used are  $1^\circ$  or  $5^\circ$  of latitude and longitude, respectively. The undulations  $N$  are obtained by summing up the products  $c_q \Delta g_q$  over the earth's surface.

The error due to the derivation of the Stokes' formula without considering the flattening of the earth is rather small. Vening Meinesz<sup>78</sup> estimated that the effect of the omitted terms does not exceed 1 m. According to Zagrebin (1944), who derived the Stokes' formula for the ellipsoidal level surface, the maximum effect of the omitted terms is less than  $\alpha \Delta N$ , which amounts to only +35 cm if  $N$  is  $\pm 100$  m. Therefore these error sources can be neglected because the inaccuracy caused by the uncertainty of the gravity-anomaly field is much larger.

### B. Hirvonen's Geoid and Tanni's Geoid

At the suggestion of the author (H.), Hirvonen carried out, from 1932 to 1934, the practical computation of the geoid distances on the basis of the gravity material available at that time. This first computation of  $N$  on a world-wide scale is interesting in several respects.

Hirvonen<sup>38</sup> used the free-air gravity anomalies because at that time only relatively few gravity values were reduced isostatically. He prepared stereographic-projection maps giving the mean anomalies of squares  $5^\circ$  by  $5^\circ$ , except close to the poles, where the compartments were  $5^\circ$  by  $10^\circ$ ,  $5^\circ$  by  $20^\circ$ , and  $5^\circ$  by  $30^\circ$ . The pole cap, of radius  $5^\circ$ , made one compartment. The stereographic projection was chosen because the curves of equal  $\psi$  are always circles. He drafted the templates for the standard latitudes  $10^\circ$ ,  $20^\circ$ ,  $30^\circ$ ,  $40^\circ$ ,  $50^\circ$ , and  $60^\circ$ . The zones farther to the north and south did not need any maps because there were, practically speaking, no observations. Hirvonen divided the earth's gravity field into three parts: the regional part  $N_r$  from the computation point to the circle  $\psi = 10^\circ$ , the continental part  $N_c$  between the circles  $\psi = 10^\circ$  and  $\psi = 39^\circ$ , and the universal part  $N_u$  outside the circle  $\psi = 39^\circ$  where the Stokes' function is zero. The shares contributed by all these regions to the undulations  $N$  were computed. The total undulation  $N$  is, of course, the sum of these three parts,  $N_r$ ,  $N_c$ , and  $N_u$ .

In the areas without any gravity measurements the relatively small free-air anomalies corresponding to the isostatic equilibrium and computed from the spherical harmonic tables and Prey's maps<sup>67</sup> were used.

The undulation values  $N_r$ ,  $N_c$ ,  $N_u$ , and  $N$  were computed for 62 points distributed in an east-west band encircling the earth's surface. The largest positive  $N$  values, of about 70 to 80 m, are in the Pacific between the eastern longitudes  $130^\circ$  and  $190^\circ$  and in the eastern part of the Atlantic and in Europe between the longitudes  $30^\circ\text{W}$  and  $20^\circ\text{E}$ . The largest negative values are in India between the eastern longitudes  $60^\circ$  and  $90^\circ$ . The maximum positive and negative values are +85 m at longitude  $180^\circ$  and -115 m at longitude  $70^\circ\text{E}$ .

From 1941 to 1948 Tanni and the author (H.), at the International Isostatic Institute, computed another geoid, under the guidance of the author, using the much more extensive material available at that time.

Tanni used isostatic gravity anomalies because they are the most representative and because in the unsurveyed areas zero isostatic anomaly corresponds to isostatic equilibrium, which actually prevails to about 85 to 90 per cent. Since most of the gravity stations handled isostatically were reduced either according to the Pratt-Hayford system,  $D = 113.7$  km, or the nearly equivalent Airy-Heiskanen system,  $T = 60$  km, these isostatic anomalies were used. The basis of Tanni's study was maps

giving the mean gravity anomalies of  $1^\circ$  by  $1^\circ$  squares and at the higher latitudes, beginning at  $\varphi = 60^\circ$ , of  $1^\circ$  by  $2^\circ$ ,  $1^\circ$  by  $4^\circ$ , and  $1^\circ$  by  $6^\circ$  squares.

In the computation of the geoid, however, Tanni<sup>77</sup> used the mean anomalies of  $5^\circ$  by  $5^\circ$  squares and got the undulations  $N$  for 218 points. He later computed the correction for the geoid of Europe using  $1^\circ$  by  $1^\circ$  square maps instead of  $5^\circ$  by  $5^\circ$  squares close to the computation points.

The method of practical computation used is a convenient one. The square system is put on a meridional equidistant cylinder projection map. Transparent paper is used; the mean anomalies  $\Delta g$  are written on the lower part of a square (positive ones in black, negative ones in red), and the respective coefficients are written a little higher. The computer multiplies the products  $c_q \Delta g_q$  and dictates them to the recorder, who enters them on the calculating machine. Because the number of  $5^\circ$  by  $5^\circ$  squares over the whole globe is 2012, the method might appear impractical; however, owing to the lack of gravity observations, Tanni was able to determine the mean anomalies for only about one-third of the squares, and of these anomalies a considerable number were zero. Without losing any essential accuracy, he rounded the coefficients  $c_q$  to whole numbers, which, for the most part, were less than 10. In the same way he rounded the mean anomalies to end with 5 or 0, which was allowable because of the inaccuracy of the majority of the mean anomalies. So the multiplication was easy for a trained computer. The computation and control of one  $N$  value took an average of 1.5 hr.

In computing the coefficients  $c_q$  it is possible to use the value of  $\psi_m$  corresponding to the center of square for the whole square when the angle  $\psi_m$  is large compared with  $q$ . The areas  $q$  depend on the latitude but are on the average

$$q = \frac{4\pi}{2012} = 6.246 \times 10^{-3} \quad \text{for squares } 5^\circ \text{ by } 5^\circ$$

$$q = 0.2498 \times 10^{-3} \quad \text{for squares } 1^\circ \text{ by } 1^\circ$$

For the values  $R = 6371$  km and  $G = 979.8$  cm/sec $^2$  the corresponding coefficients are

$$c_q = 6.464f(\psi) \text{ mm/mgal} \quad \text{for squares } 5^\circ \text{ by } 5^\circ$$

$$c_q = 0.258f(\psi) \text{ mm/mgal} \quad \text{for squares } 1^\circ \text{ by } 1^\circ$$

The angular distance  $\psi_m$  is best derived from the accurate formula

$$\cos \psi_m = \cos \varphi_0 \cos \varphi_m \cos \lambda_m + \sin \varphi_0 \sin \varphi_m \quad (8-54)$$

where  $\varphi_0$  and  $\lambda_0 = 0$  are the latitude and longitude of the computation point,  $\varphi_m$  and  $\lambda_m$  for the center of the square. As the latitude  $\varphi_m$  is con-

stant for the whole parallel, the formula can be written in the following practical form:

$$\cos \psi_m = a \cos \lambda_m + b \quad (8-55)$$

The corresponding  $\cos \psi_m$  values for the southern hemisphere can be obtained by changing the sign; they are then in opposite order with respect to  $\lambda$ . The angular distances  $\psi_m$  can also be taken graphically from the  $\psi$  maps in stereographic projection.

For computing the coefficients  $c_q$  the tables of Lambert and Darling<sup>48</sup> were used. Diagrams with  $\cos \psi_m$  as argument, based on these tables, give the values for  $c_q$  directly. As the computed  $q$  values are valid only near the latitude  $\varphi = 35^\circ$ , the  $c_q$  values obtained from the diagrams must be multiplied by the factors  $1.22 \cos \varphi$  and by their multiples when  $\varphi > 60^\circ$ .

The error of the coefficients  $c_q$  is, for the squares  $5^\circ$  by  $5^\circ$ , smaller than 0.1 mm/mgal inside the circle  $\psi_m = 20^\circ$  and for the squares  $1^\circ$  by  $1^\circ$  inside the circle  $\psi_m = 2^\circ$ .

The coefficients  $c_q$  have to be computed, as mentioned above, for different latitudes at intervals of  $5^\circ$ . Figure 8-16 shows  $c_q$  for latitude  $\varphi = 40^\circ$ . The large table is valid for  $5^\circ$  by  $5^\circ$ , the small one for  $1^\circ$  by  $1^\circ$ . The former covers half the globe and the latter covers the compartment  $20^\circ$  by  $15^\circ$ . On the other side of the central meridian the coefficients are symmetrically equal.

The figures give the undulation  $N$ , in millimeters per milligal, caused by the different squares. The effect of the first northern  $5^\circ$  by  $5^\circ$  square is 155 mm/mgal; on the south side it is 163 mm/mgal. For values  $0^\circ < \psi \leq 39^\circ$  the coefficients  $c_q$  are positive; for values  $39^\circ < \psi \leq 117^\circ$  they are negative and for values  $117^\circ < \psi \leq 180^\circ$  again positive.

Since isostatic anomalies were used, it was necessary to compute the indirect effect  $\Delta_{ig}$  of the anomalies caused by the isostatic reduction. This correction, which is rather small (generally of the order 2 to 5 mgal), gives gravity anomalies valid on the co-geoid. Use of the corrected anomalies gives the  $N_c$  values of the co-geoid. To get the  $N$  values of the actual geoid the distance between the co-geoid and actual geoid must be considered. It is usually less than 10 m but in the Himalayas is as high as 30 m. The indirect effect  $\Delta_{ig}$  is generally positive on the continents and generally negative at sea because the actual geoid is respectively above and below the co-geoid.

Tanni computed the undulations of the geoid at 218 corner points of the squares  $5^\circ$  by  $5^\circ$  encircling the globe. In Fig. 8-17 the  $N$  values of the actual geoid in Europe are given. The geoid is above the ellipsoid (flattening 1/297.0) in all this area. The geoid distances vary from 7.5 to 43.5 m.

		$\lambda_o \pm 15^\circ$				$\lambda_o$				$\lambda_o \pm 5^\circ$				Squares $5^\circ \times 5^\circ$				$\lambda_o \pm 1^\circ$	
		Squares $5^\circ \times 5^\circ$				Squares $5^\circ \times 5^\circ$				Squares $5^\circ \times 5^\circ$				Squares $1^\circ \times 1^\circ$				$\lambda_o \pm 15^\circ$	
		2		3		4		5		6		7		8		9		10	
		1	2	3	4	1	2	3	4	5	6	7	8	9	10	1	2	3	4
50°		1	1	1	1	1	1	1	1	1	1	1	1	1	1	1	1	1	1
40°		2	2	2	2	2	2	2	2	2	2	2	2	2	2	2	2	2	2
30°		3	2	2	2	2	2	2	2	2	2	2	2	2	2	2	2	2	2
20°		4	3	3	3	3	3	3	3	3	3	3	3	3	3	3	3	3	3
0°		5	4	4	4	4	4	4	4	4	4	4	4	4	4	4	4	4	4
-10°		6	5	5	5	5	5	5	5	5	5	5	5	5	5	5	5	5	5
-20°		7	6	6	6	6	6	6	6	6	6	6	6	6	6	6	6	6	6
-30°		8	5	5	5	5	5	5	5	5	5	5	5	5	5	5	5	5	5
-40°		9	3	3	3	3	3	3	3	3	3	3	3	3	3	3	3	3	3
-50°		10	1	1	1	1	1	1	1	1	1	1	1	1	1	1	1	1	1
-60°		11	0	0	0	0	0	0	0	0	0	0	0	0	0	0	0	0	0

FIG. 8-16. Stokes' coefficients  $c_q$  (according to Tamm). Inside the  $40^\circ$  zero line and outside the other zero line,  $117^\circ$ , the coefficients  $c_q$  are positive; between the zero lines they are negative. All figures represent the undulation  $N$  of the geoid caused by the average gravity anomaly 1 mgal of the square  $5^\circ$  by  $5^\circ$ . The small diagram gives the corresponding coefficients for the division  $1^\circ$  by  $1^\circ$ .

The largest positive undulations are in Europe, the eastern part of the Atlantic, and the East Indies; the largest negative undulations are in India, Turkestan, and surrounding areas. Very interesting are the steep slopes of the geoid in Turkestan, about 40 m/10°, and between India and

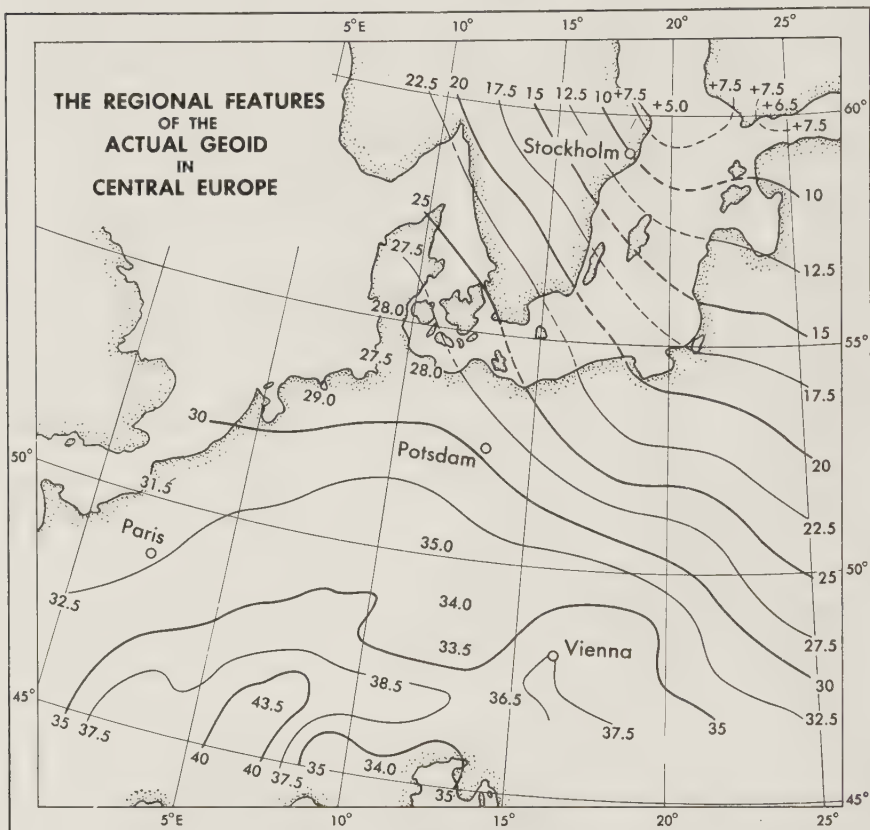


FIG. 8-17. Actual geoid of Europe, in meters (according to Tanni). Everywhere in Europe the geoid is above the ellipsoid.

the East Indian Archipelago, 95 m/30°. The latter slope is in harmony with the astronomic-geodetic determination of the geoid in Burma.

Tanni's geoid differs, of course, from Hirvonen's because Tanni had much more material to work with. Thus, Hirvonen's average  $N$  is  $\pm 50$  m, Tanni's only  $\pm 30$  m; however, in those areas where rather good gravity-station nets existed 25 years ago, e.g., in the United States and Europe, the agreement is reasonably good. Thus at the 12 European points common for both geoids the mean difference is  $-4$  m or, disregarding the sign, 12 m. At 10 common points of the United States the respective figures

are +7 and 13 m. The larger differences elsewhere are due mostly to the fact that Hirvonen completed the gravity field with hypothetical figures to a considerable degree, whereas Tanni's results were based on a greater number of actual measurements. Tanni states that the accuracy of his  $N$  values is of the order  $\pm 10$  m and in Central Europe considerably higher.

A suitable interpolation method inside the  $5^\circ$  by  $5^\circ$  squares must be found in order to get the regional correction for  $N$  obtained in the vicinity of the computation point from the mean gravity anomalies of the  $1^\circ$  by  $1^\circ$  square system instead of from the  $5^\circ$  by  $5^\circ$  squares. This correction is necessary because Stokes' function  $S(\psi)$  changes so rapidly with  $\psi$  in the neighborhood of the computation point that the mean coefficients  $c_q$  are only poor representations of the whole  $5^\circ$  by  $5^\circ$  squares. This is particularly true if the gravity anomalies themselves vary rapidly with  $\psi$ .

When studying the problem of interpolation, Tanni<sup>76</sup> came to the conclusion that linear interpolation is sufficiently accurate for the whole effect of all  $5^\circ$  by  $5^\circ$  squares except the nine closest, of which the middle square  $ABCD$  is the proper interpolation area (Fig. 8-18). For example, first compute for the corner point  $A$  the value  $N_1$  caused by the whole gravity field outside the nine inner squares of our figure. In the same way we compute similar values  $N_{II}$  at  $B$ ,  $N_{III}$  at  $C$ , and  $N_{IV}$  at  $D$ . In computing these values  $N_1$ ,  $N_{II}$ ,  $N_{III}$ , and  $N_{IV}$ , the square  $ABCD$ , as we have said, is the central one of the nine squares.

On the basis of the four corner values we can then obtain, by linear interpolation, the desired value net at  $1^\circ$  intervals for the whole square  $ABCD$ . The center of this square is an important control point, at which the difference between the interpolated values obtained from the values  $N_1$  and  $N_{III}$  and  $N_{II}$  and  $N_{IV}$ , respectively, will seldom be more than 1 m. Treating each of the other squares in succession as we did the middle square, we obtain at each point  $A$ ,  $B$ ,  $C$ ,  $D$ , etc., four values  $N_1$  to  $N_{IV}$  for each quadrant, so that at point  $C$ , say,  $N_{III}$  belongs to that nine-square system in which  $ABCD$  is the middle one but  $N_{IV}$  belongs to the similar system around the square  $BEFC$ , etc.

The effect of the nine omitted  $5^\circ$  by  $5^\circ$  squares must be computed on the basis of the  $1^\circ$  by  $1^\circ$  square system. At each corner point of the  $1^\circ$  by  $1^\circ$  square system—225 corner points all told—the summation must be made separately. The method is, of course, similar to that for the  $5^\circ$  by

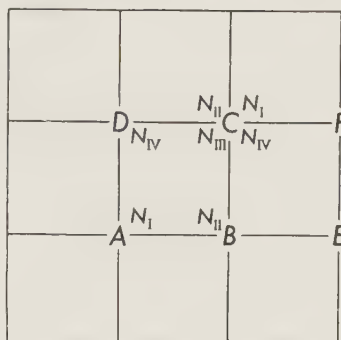


FIG. 8-18. To interpolate in the  $5^\circ$  by  $5^\circ$  square  $ABCD$ , four values of  $N$  for the effect of the area outside the  $15^\circ$  by  $15^\circ$  square must be computed at each corner point.

$5^\circ$  square system, the only difference being that we have to use the  $1^\circ$  by  $1^\circ$  coefficients  $c_g$  instead of the  $5^\circ$  by  $5^\circ$  coefficients  $c_g$ . As the factors are mostly smaller than 10 and the anomalies are rounded to 0 or 5 mgal, the work is relatively easy to accomplish. At the boundary points of each  $5^\circ$  by  $5^\circ$  square we get as controls two separately computed values, and at the corner points, four values. The small discrepancies of 0.1 to 0.3 m between these values are usually caused by the inaccuracies of the computation method.

We can summarize this interpolation method as follows. We compute for all corner points of the  $5^\circ$  by  $5^\circ$  squares the effect of the whole globe except the nine closest squares. The effect of this outer area can be interpolated to the corner points of the  $1^\circ$  by  $1^\circ$  system. The effect of the omitted nine nearest squares must be computed in the way described above at each corner point of the  $1^\circ$  by  $1^\circ$  system.\*

The result of Tanni's study is both interesting and encouraging. The regional correction for the  $N$  values in the area of Europe studied was generally from 0 to  $\pm 2$  m and only in a few extreme cases  $\pm 5$  m. Therefore it is hardly necessary to compute similar regional corrections on the basis of a still closer square system, e.g.,  $10'$  by  $10'$ , as its share would be only on the order of  $\pm 0.4$  m. Besides, the local corrections for the undulations of the geoid are best computed on the basis of astronomic-geodetic or gravimetric deflections of the vertical.

For the computation of  $\xi_g$  and  $\eta_g$  the gravity-anomaly field of the nearest neighborhood of the computation points is decisive, while the effect of the gravity-anomaly field beyond  $\psi = 20^\circ$  is small. The accuracy of  $N$  is, on the contrary, essentially dependent also upon our knowledge of the gravity anomalies of the far-lying regions, out to the antipode of the computation point, but the effect of the nearest neighborhood can be obtained from scarcer gravity material than is possible for  $\xi_g$  and  $\eta_g$ .

Since large gaps exist in the present gravity-anomaly map of the world, particularly in the Southern Hemisphere, we cannot get  $N$  with such high relative accuracy as we can  $\xi_g$  and  $\eta_g$ . According to Hirvonen,<sup>39</sup> the accuracy of the gravimetric  $N$ , even in Europe and America, is, on the basis of the present material, only  $\pm 10$  m; according to Vening Meinesz,<sup>32</sup> it is  $\pm 5$  m. The author (H.) believes that Hirvonen's estimate may be too pessimistic.

When we keep in mind that 6.4 m is only  $1/1,000,000$  of the radius of the earth, we can be quite satisfied even with an accuracy of  $\pm 10$  m. Furthermore, the *relative* accuracy of  $N$  obtained is much higher. We may have, for instance, the shape of the rather accurate geoid for Europe, but all  $N$  values of Europe may need a nearly constant correction, positive or negative after the sign of the effect of the remote unsurveyed areas.

\* If fast high-speed computers are available we can use the  $1^\circ$  by  $1^\circ$  system all around the world.

### C. Some Other Geoids

*Columbus geoid.* Through the generous and continuous support of the Air Force Cambridge Research Center it has been possible for The Ohio State University to collect gravity material, analyze it, and use it for com-

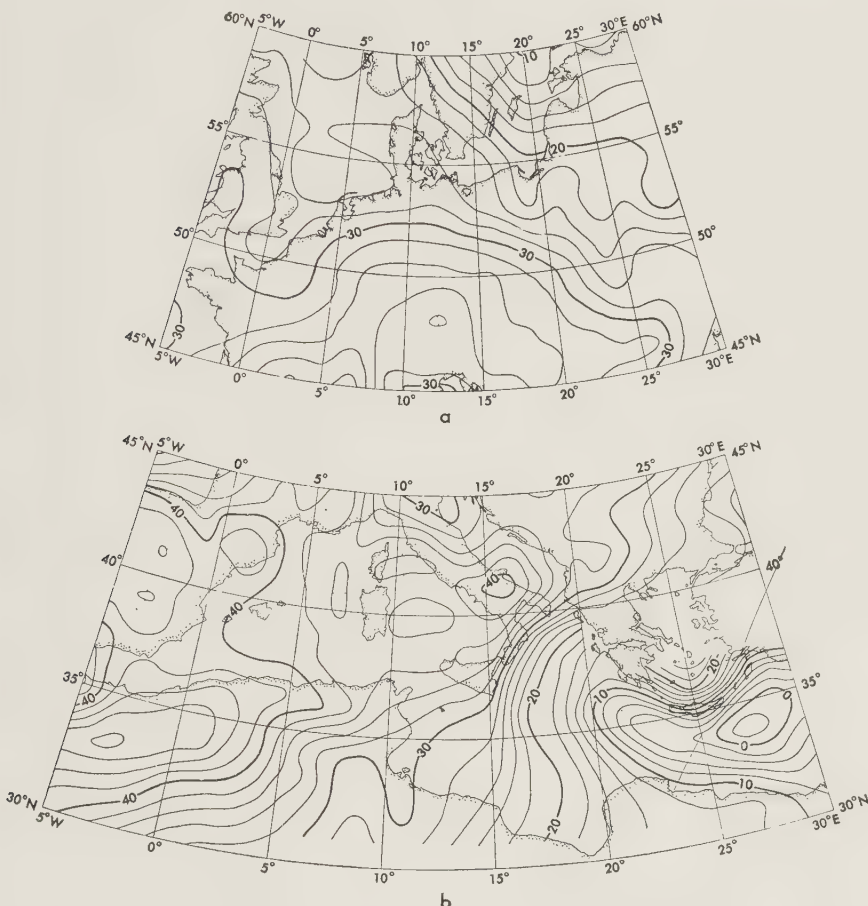


FIG. 8-19. Gravimetrically computed geoid for Europe. Contour interval: 2 m. (Mapping and Charting Research Laboratory, The Ohio State University Research Foundation.)

putations of the geoid.<sup>97, 98</sup> Since we have more than four times the amount of material that Tanni had, thanks to close cooperation among the agencies and scientists of thirty-five countries, it is clear that the new geoid will be more accurate than the old ones. The computations have been finished for the area between latitudes 60°N and 30°N and for the longitudes  $-5^{\circ}$  to  $+30^{\circ}$ . Figure 8-19 illustrates the obtained geoid of Europe.

It is interesting to note that the  $N$  values are positive for most of this area. From the value +10 meters at the point  $\varphi, 60^\circ; \lambda, +20^\circ$ , the geoid rises continuously southward and will be about 40 m in Spain and Italy. From Italy it will go down very fast and will be zero in the eastern part of the Mediterranean.

It is easy to see that the dimensions derived earlier in Europe from the measured arcs could not give the best values because the criterion,  $\Sigma(\xi^2 + \eta^2) = \min$ , cannot be true, since for this area both components are mostly positive;  $\xi$  is even  $3''$  to  $6''$ . As we have already mentioned, the dimensions of the earth computed by the Army Map Service recently have changed the equatorial radius value by more than 100 m because it could use superlong arcs from different continents. Still higher accuracy can be obtained when gravimetric evidence will also be applied.

Of course, we have computed the average deflections of the vertical  $\xi$  and  $\eta$  from the contour curves of the geoid. They, however, will not be good for any particular point, because  $\xi$  and  $\eta$  can change very fast from point to point, even more than  $10''/50$  km.

*Indian geoid.* Geoid studies have been carried out in India longer than in any other country.<sup>12a</sup> A century ago, when the famous Everest was Surveyor General of India, F. H. Pratt and G. B. Airy tried to explain why no reference ellipsoid could fit for the whole central meridian in India. Thanks to their work, as we have seen, India is the birthplace of the theory of isostatic equilibrium. Some decades later, the Geological Survey of India began a continuous program for precise astronomic determination of latitudes at many triangulation points. In addition, longitude, the observation of which was not easy at that time, was measured at 24 points and included in the triangulation chain. Attempted explanations of the deflections of the vertical failed because at that time they were believed to be caused by the local attraction of the mass anomalies close to the observation point. Not until the turn of the twentieth century, when some gravity data were also available, making the problem still more complicated, was Burrard, another Surveyor General of India, able to bring some order into the accumulated data on the deflections of the vertical.

When de Graaff Hunter became head of the Geodetic Division of the Geological Survey of India, he realized, as Hayford did in the United States, that one of the main theoretical problems of geodesy was the determination of the geoid, and consequently geoid studies in India began on a large scale. After the First World War the Survey of India began to draw geoid maps on the basis of astronomic observations carried out with very high accuracy at some 400 stations in India and Burma. It was very soon seen, however, that the deflections of the vertical change so fast from point to point that it would have been better to make ten times as many observations with ten times lower accuracy.

Since 1922, the Survey of India has published geoid maps in its annual geodetic reports. The rather accurate method of "geoidal sections" was used. From topographic maps with a scale of 1:63,000, based on geodetic triangulation, the geodetic latitude and longitude of the selected points at intervals of about 10 miles could be read with an accuracy of  $1''$ . As their astronomic latitude and longitude were observed with accuracy of better than  $1''$ , it was possible to get deflections of the vertical along the geoidal sections with an accuracy of approximately  $1''$ . Such geoidal sections extend now over 8000 miles in India and Burma. By the aid of this material rather accurate geoids have been drawn.

The aim of the geoidal sections is to provide values for deflections of the vertical which will make it possible for intermediate values to be interpolated to a probable error of  $1''$ . Assuming that in a geoidal section there are  $n + 1$  observed deflections with an accuracy of  $1''$  at intervals of  $k$  kilometers, the probable derived error  $E$  of relative geoidal elevations is  $E = 1000k\sqrt{n}/\rho$  m ( $\rho$ , radians =  $206,265''$ ), provided there are no systematical errors. If  $k = 25$  km,  $n = 400$ , and  $nk = 10,000$  km, or a quadrant of the earth, then  $E = 2.5$  m, again supposing there are no systematical errors in triangulation, astronomic observations, or the maps.

If  $nk = 1000$  km or  $n = 40$  the error  $E$  would be  $\sqrt{10}$  smaller, or approximately 0.8 m. This seems to show that the deflection method described above would yield the relative undulations  $N$  along a triangulation chain of 1000 km—astronomic-point interval of 25 km—with the same precision as the gravimetric method. In rugged mountains, where the deflections of the vertical change rapidly, the point interval must be much shorter than 25 km.

The limitation of this good method, like that of all astronomic-geodetic methods, is that it can be applied only in areas where accurate triangulations with many astronomic points exist.

*Rice's geoid.* From the adjusted deflections of the vertical of the West Indies area, Rice computed the geoid heights at 5-m intervals along the lines joining the stations and drew the geoid contours.<sup>71</sup> Although these contour lines allow one to determine the generalized geoid slope at any selected point, they are contours not of the real geoid but only of a surface which has the shape of the geoid in the area studied. To obtain the real geoid the real geoid height  $N$  must be known for at least one point of the studied area.

*Bomford's geoid.* Bomford<sup>3a</sup> computed the geoid of Europe in 1954, using solely the astronomic-geodetic  $\xi_a$  and  $\eta_a$  obtained from the geodetic coordinates  $\varphi$ ,  $\lambda$ ,  $A$  of the astronomic points of the European triangulation net (which had been adjusted at the suggestion of the U.S. Army Map Service by the U.S. Coast and Geodetic Survey under the leadership of Whitten<sup>85</sup>) by comparing the coordinates  $\varphi$ ,  $\lambda$ , and  $A$  with the astronomic

coordinates  $\varphi'$ ,  $\lambda'$ , and  $A'$ . As the initial point Bomford used the Helmert Tower in Potsdam, assuming for that point  $N = 0$ ,  $\xi_0 = +3.^{\circ}36$  and  $\eta_0 = +1.^{\circ}78$ .

Unfortunately there are several drawbacks to Bomford's method. First, he used the observed deflections of the vertical without any reduction. When we remember that  $\xi$  and  $\eta$  change very rapidly in the rough-mountain areas of Central Europe included in Bomford's study, we see that his result cannot be sufficiently accurate. The topographic-isostatic reduction of  $\xi_a$  and  $\eta_a$  would have improved his results essentially. Second, the deflection components  $\xi_0$  and  $\eta_0$  at Potsdam and the dimensions of the reference ellipsoid used in the computations influenced the results, as generally happens in the astronomic-geodetic method.

It is interesting to compare Bomford's and Tanni's geoids for this area, because the differences are generally larger than the  $N$  values themselves (Table 8-17). Obviously there must be some real reasons for this discrepancy. To study this problem the author<sup>31</sup> (H.) corrected the Bomford geoid so that the Potsdam values would be  $N = +27$  m,  $\xi_0 = 6.^{\circ}3$ , and  $\eta_0 = +2.^{\circ}8$ . The  $N$  value is taken from Tanni, while the  $\xi_0$  and  $\eta_0$  values are the average of the  $\xi_0$  and  $\eta_0$  obtained by Wolf<sup>88</sup> and Ledersteger.<sup>52</sup> The results of the correction are shown in Table 8-17.

The table shows that the residuals  $\Delta N$  (Tanni - corrected Bomford) are small, except in the small geoid-depression area of the Po Valley, where the difference is as great as 15 m. The residuals are large also at the three points on the Greenwich meridian and in Greece; this fact is easily understood since the gravity survey there is incomplete and astronomic data are scarce in the neighborhood of these points. The residual for the relatively small Po Valley geoid "hollow" is explained by the fact that Tanni's material was not sufficient to compute such small anomalies of the geoid.

Bomford's work shows the possibilities and limitations of the astronomic-geodetic method in practice. As we have said before, the astronomic-geodetic  $\xi_a$  and  $\eta_a$  can, if the distance between the astronomic-geodetic points is not too great, give the *shape* of the geoid but not the geoid itself. The geoid height  $N$  and the tilting between the ellipsoid and geoid, i.e., the real values of  $\xi$  and  $\eta$ , must be computed gravimetrically at least at the initial point of the geodetic system in question and, if possible, as a control, at several other points in the area covered by the geodetic system used.

The profile of the European geoid along longitude  $24^{\circ}$  computed by the U.S. Army Map Service<sup>8</sup> shows that Bomford's geoid needs an essential correction of its orientation, as had been predicted at the Rome Assembly of the IUGG (International Union of Geodesy and Geophysics) in 1954.

TABLE 8-17. TANNI'S GRAVIMETRIC AND BOMFORD'S ASTRONOMIC-GEODETIC GEOIDS FOR EUROPE

(In meters)

$\varphi$	$\lambda$	Tanni	Bomford	Corrected Bomford	Tanni - corr. Bomford
60°	15°	+14	+4	+17	-3
	20	+8	-4	+7	+1
	25	+7	-4	+5	+2
55	0	+30	-5	+19	+11
	5	+28	-2	+23	+5
	10	+27	+1	+24	+3
	15	+23	0	+22	+1
	20	+19	-3	+17	+2
50	0	+32	-11	+23	+9
	5	+33	-5	+28	+5
	10	+33	+2	+34	-1
	15	+33	+2	+33	0
	20	+30	+2	+31	-1
47.5	5	+37	-8	+30	+7
	10	+36	-3	+34	+2
	15	+36	+2	+37	-1
	20	+34	0	+34	0
45	5	+41	-10	+33	+8
	10	+39	-17	+24	+15
	15	+39	-4	+36	+3
	20	+37	-2	+36	+1
	25	+32	-2	+34	-2
42.5	12.5	+39	-10	+35	+4
40	0	+42	-25	+28	+14
	15	+39	-15	+34	+5
	20	+36	-23	+24	+12

This example indicates that the astronomic-geodetic method needs the help of the very flexible gravimetric method, which can be applied everywhere, even at sea, whereas measured arcs cover only a small part of the continents and do not exist at sea. Without doubt the best procedure would be to combine the gravimetric and astronomic-geodetic methods in so far as possible. If we had time to wait several decades, we could

carry out new arc measurements in the areas where no triangulations exist; if, however, we wish to get the detailed shape of the geoid within a few years, the gravimetric method must be used, and on as extensive a scale as possible.

For the gravimetric determination of the size and shape of the geoid we need to know as accurately as possible two fundamental quantities, the radius  $a$  of the reference ellipsoid and the equator gravity value  $\gamma_E$ . We know (Sec. 8-3D) how the combination of gravimetric and astronomic-geodetic method can give the most probable  $a$  value. As for the equator value of gravity  $\gamma_E$ , the gravity anomalies themselves yield it directly (Sec. 3-11).

The flattening  $\alpha$  and the  $\beta$  term of the gravity formula are not so important. If an incorrect value for  $\beta$  is used, the gravity anomalies, since they depend on the latitude, will give  $N$  values which also change systematically with the latitude. On the other hand, the flattening value, which depends on the  $\beta$  term, will also be incorrect, and therefore the resulting radius of curvature  $R$  of the reference ellipsoid will also be incorrect, though its error would also change systematically with the latitude. The errors of  $R$ , caused by a wrong  $\alpha$  value, and the errors of  $N$ , caused by a wrong  $\beta$  term, will compensate each other, so that the sum of  $R + N$  will be the same regardless of the errors in  $\alpha$  and  $\beta$ .

The gravimetric method for determining the fundamental quantities  $N$ ,  $\xi$ , and  $\eta$  has been developed especially since 1950 at the Mapping and Charting Research Laboratory of The Ohio State University. One project of these world-wide studies, supported by the Geophysics Research Directorate of the Air Force Research Center, Cambridge, Massachusetts, is to prepare three sets of world maps. One set is to give the geoid heights and the contour curves of  $N$  at the interval of 1 or 2 m, and the other two sets will give the lines of equal  $\xi$  and  $\eta$  components, respectively.<sup>97,98</sup> In the areas of adequate gravity material maps of larger scale are used than in regions of poor gravity information. The geoid computed gravimetrically in Columbus, Ohio, is almost correct in large parts of the world.

#### REFERENCES

1. U.S. Army Map Service: Rept. Rome Assembly IUGG, 1954.
2. Baglietto, Eduardo E.: Contributions to applied geodesy, Engineering Faculty, Buenos Aires University, Rept. Rome Assembly IUGG, 1954.
3. Bomford, G.: Geodesy, Oxford, London, 1952.
- 3a. ———: Liste des stations de déviation de la verticale rattachées au réseau européen, Presented at 10th Assembly IAG, Rome, 1954.
4. Bouguer, Pierre: La figure de la terre, Paris, 1749.
5. Bouguer Expedition: Mesures des trois premiers degrés du méridien dans l'hémisphère austral, tirée des observations des Mrs. de l'académie royale des sciences, envoyés par le roi sous l'équateur, par M. de la Condamine, Paris, 1751.

6. Bowie, William: Investigations of gravity and isostasy, USCGS Spec. Publ., no. 40, 1917.
7. Bullard, E. C.: The figure of the earth, Monthly Notices Roy. Astron. Soc., Geophys. Suppl., vol. 5, no. 6, 1948.
8. Chovitz, B., and Irene Fischer: A new determination of the figure of the earth from arcs, Trans. Am. Geophys. Union, vol. 37, p. 339, 1956.
9. Fischer, Irene: The deflection of the vertical in the Western and Central Mediterranean area, Bull. géod., no. 34, 1954.
10. Gauss, C. F.: *Theoria motus corporum coelestium in sectionibus conicis solem ambientium*, Hamburg, 1809.
11. de Graaff Hunter, J.: Rept. Oslo Assembly IUGG, 1948.
12. ———: The figure of the earth from gravity observations and the precision obtainable, Trans. Roy. Soc. (London), ser. A, vol. 234, 1935.
- 12a. ———: Observing and using geoidal deflections, Publ. Finn. Geod. Inst., no. 46, 1955.
13. Gromov, S. V.: The inversion method of Rudzki considered and extensively developed, Trudy Astron. Observatorii, Leningrad. Univ., vol. 16, 1952; The inversion of the deflection of the vertical, *ibid.*
14. Gulatee, B. L.: Deviation of the vertical in India, Geol. Survey India, Tech. Paper, no. 9, 1956.
15. Hales, A. L., and D. J. Gough: Measurements of gravity in Southern Africa, The Government Printer, Pretoria, 1950.
16. Hayford, J. F.: Supplementary investigation in 1909 of the figure of the earth and isostasy, USCGS, 1910.
17. ———: The figure of the earth and isostasy, from measurements in the United States, USCGS, 1909.
18. Heiskanen, W. A.: Untersuchungen über Schwerkraft und Isostasie, Publ. Finn. Geod. Inst., no. 4, 1924.
19. ———: Schwerkraft und isostatische Kompensation in Norwegen, *ibid.*, no. 5, 1926.
20. ———: Die Erddimensionen nach den europäischen Gradmessungen, *ibid.*, no. 6, 1926.
21. ———: Ist die Erde ein dreiachsiger Ellipsoid?, Gerlands Beitr. Geophys., vol. 19, 1928.
22. ———: Investigations on the gravity formula, Publ. Isos. Inst. IAG (Helsinki), no. 1, 1938.
23. ———: Intercontinental connection of the geodetic systems, Intern. Hydrograph. Rev., vol. 1, 1955.
24. ———: Relative significance of the different methods of modern geodesy, Trans. Am. Geophys. Union, vol. 35, no. 6, 1954.
26. ———: On the world geodetic system, Publ. Isos. Inst. IAG (Helsinki), no. 26, 1951; Publ. Ohio State Univ. Inst. Geod., Photogrammetry and Cartogr., no. 1.
27. ———: World gravity needs for geodetic purposes, Ohio State Univ. Mapping and Charting Research Lab., Tech. Paper, no. 118, 1950.
28. ———: On the isostatic structure of the earth's crust, Publ. Isos. Inst. IAG (Helsinki), no. 24, 1950.
29. ———: Rept. isostasy, Brussels Assembly IUGG, Trav. assoc. géod. (Paris), 1951.
30. ———: Symposium on geophysics and geophysical geodesy, Bull. géod., no. 31, 1952.
31. ———: Rept. isostasy, Rome Assembly IUGG, 1954.
32. ———: On the geodetic control systems, Geofis. pura e appl., vol. 22, 1952.
33. ———: The geodetic significance of world-wide gravity studies, Ohio State Univ. Mapping and Charting Research Lab., Tech. Paper, no. 124, 1950.

34. Helmert, F. R.: Der normale Teil der Schwerkraft im Meeresniveau, Ber. kgl. preuss. Akad. Wiss., vol. 14, p. 328, 1901.
35. ———: Neue Formeln für den Verlauf der Schwerkraft im Meeresniveau beim Festlande, *ibid.*, vol. 41, 1915.
36. ———: Die mathematischen und physikalischen Theorieen der höheren Geodäsie, Teubner, Leipzig, vol. 1, 1880, vol. 2, 1884.
37. Hirvonen, R. A.: On the precision obtainable for gravimetric determination of the geoid, Ohio State Univ. Mapping and Charting Research Lab., Tech. Paper, no. 171, 1953.
38. ———: The continental undulations of the geoid, Publ. Finn. Geod. Inst., no. 19, 1934.
39. ———: The removal of spherical harmonics of first order from a field of observed gravity anomalies, *ibid.*, no. 46, 1955.
40. ———: On the precision of the gravimetric determination of the geoid, Trans. Am. Geophys. Union, vol. 37, no. 1, 1956.
41. Jeffreys, H.: The figures of the earth and moon (Third paper), Monthly Notices Roy. Astron. Soc., Geophys. Suppl., vol. 5, no. 7, 1949.
42. ———: An application of the free air reduction of gravity, Gerlands Beitr. Geophys., vol. 31, p. 378, 1931.
43. Jordan, W., and O. Eggert: Handbuch der Vermessungskunde, 7th ed., Bd. 3, Metzlersche, Stuttgart, 1923.
44. Jung, K.: Figur der Erde, in S. Flugge (ed.), Handbuch der Physik, vol. 47, Geophysics, I, pp. 543–639, Springer, Berlin, 1956.
45. Kasansky, I.: Ein praktischer Versuch der gravimetrischen Bestimmung der Lotabweichungen, Verhandl. 7 Tagung balt. geod. Komm., Helsinki, 1935.
46. Kladivo, B.: Reduction de la pesanteur d'après Rudzki, Brno, 1940.
47. Kukkamäki, T. J., and R. A. Hirvonen: The Finnish solar eclipse expedition to the Gold Coast and Brazil 1947, Publ. Finn. Geod. Inst., no. 44, 1954.
48. Lambert, W. D., and F. W. Darling: Tables for determining the form of the geoid and its indirect effect on gravity, USCGS, Spec. Publ., no. 199, 1936.
49. ———: Deflections of the vertical from gravity anomalies, Trans. Am. Geophys. Union, vol. 28, no. 2, 1947.
50. Lambert, Walter D.: Discours présidentiel, Bull. géod., N.S., no. 22, 1951.
51. Ledersteiger, K.: Der Schrittweise Aufbau des europäischen Lotabweichungssystems und sein bestanschliessendes Ellipsoid, Österr. Z. Vermessungswesen (Vienna), Sonderheft 3, 1948.
52. ———: Die Bestimmung des mittleren Erdellipsoïdes und der absoluten Lage der Landestriangulationen, *ibid.*, Sonderheft 12, 1951.
53. Legendre, A. M.: Sur la methode des moindres carrés, 1806.
54. Lejay, Pierre, and Suzanne Coron: Tables pour le calcul des corrections isostatiques compte tenu de l'effet indirect, IAG, Spec. Publ., no. 4, 1950.
55. ———: A l'effet indirect et l'interprétation des anomalies gravimétriques, Ann. géophys., vol. 7, fasc. 3, 1951.
56. ———: Tables pour le calcul de l'effet indirect et la déformation du géoïde, Bull. géod., N.S., no. 8, 1948.
57. Markowitz, W.: The moon camera method, Ohio State Univ. Symposium, New era of geodesy, Bull. géod., no. 35, 1955.
58. Maupertuis, P. L. de: La figure de la terre, Paris, 1738.
59. Michailov, A.: Tables for the reduction of observed values of gravity by the method of condensation (in Russian), Publ. Lenin Univ. (Moscow), vol. 101, 1945.

60. Morelli, Carlo: Compensazione della rete internazionale della stazione di referimento per le misure di gravità relativa, Pubbl. fac. sci. e ing. univ. Trieste, no. 238, 1946.
61. Nares: Lecture Congress IAG, August, 1948, Bull. géod., no. 11, p. 16.
62. Niskanen, Erkki: World maps for the indirect effect of the undulations of the geoid on gravity anomalies, Publ. Isos. Inst. IAG (Helsinki), no. 7, 1941.
63. ———: Gravity formulas derived by the aid of the level land stations, *ibid.*, no. 16, 1945.
64. O'Keefe, J. A., and Pamela Anderson: The earth's equatorial radius and the distance of the moon, Bull. géod., no. 29, 1953.
65. Picard, J.: Mesure de la terre, 1671.
66. Pizetti, P.: Sopra il calcolo teorico delle deviazioni del geoide dall'ellissoide, Atti reale accad. sci. Torino, vol. 46, 1911.
67. Prey, A.: Darstellung der Höhen- und Tiefenverhältnisse der Erde durch eine Entwicklung nach Kugelfunktionen bis zur 16. Ordnung, Abhandl. Ges. Wiss. Göttingen, Math.-physik. Kl., N.F., vol. 11, no. 1, 1922.
68. ———: Zur Frage nach dem isostatischen Ausgleich der Erdrinde, Gerlands Beitr. Geophys., vol. 29, 1931.
69. Putnam, G. R.: Proc. Natl. Acad. Sci. U.S., vol. 14, p. 413, 1928.
70. Rice, D. A.: Generalised geoid slopes in the Caribbean area, Ohio State Univ. Symposium, New era of geodesy, Bull. géod., no. 35, 1955.
71. ———: Deflections of the vertical from gravity anomalies, *ibid.*, no. 25, 1952.
72. Sollins, A. D.: Tables for the computation of deflections of the vertical from gravity anomalies, Bull. géod., N.S., no. 6, 1947.
73. Somigliana, C.: Sul campo gravitazionale esterno del geoide ellipsoidico, Atti accad. nazl. Lincei Rend., Classe sci. fis. mat. e nat., 1930.
74. Vos van Steenwijk, J. E., baron de: Plumb-line deflections and geoid in Eastern Indonesia as derived from gravity, Publ. Neth. Geod. Comm., Delft, 1947.
75. Stokes, G. G.: On the variation of gravity and the surface of the earth, Trans. Cambridge Phil. Soc., vol. 8, p. 672, 1849.
76. Tanni, L.: The regional rise of the geoid in Central Europe, Publ. Isos. Inst. IAG (Helsinki), no. 22, 1949.
77. ———: On the continental undulations of the geoid as determined from the present gravity material, *ibid.*, no. 18, 1948.
78. Vening Meinesz, F. A.: A formula expressing the deflection of the plumb-line vertical in the gravity anomalies and some formulae for the gravity-field and the gravity-potential outside the geoid, Proc. Koninkl. Ned. Akad. Wetenschap., vol. 31, no. 3, 1928.
79. ———: Gravity expeditions at sea 1923–1938, vol. 4, Publ. Neth. Geod. Comm., Delftsche Uitgevers Mij, Delft, 1948.
80. ———: The equilibrium figure of the earth and the indirect isostatic or Bowie reduction, Proc. Koninkl. Ned. Akad. Wetenschap., vol. 44, no. 1, 1941.
82. ———: On the possibility of applying Stokes' theorem and the formula for the plumb-line deflection derived from it, Publ. Finn. Geod. Inst., no. 46, 1955.
83. ———: Physical geodesy, I, II, Koninkl. Ned. Akad. Wetenschap. Proc., ser. B, vol. 56, 1953.
84. Wiechert, E.: Über die Massenverteilung in Innern der Erde, Nachr. kgl. Ges. Wiss. Göttingen, vol. 221, 1897.
85. Whitten, C. A.: Adjustment of European triangulation, Rept. Brussels Assembly IUGG, 1951.

86. Wideland, Bror: Topographic-isostatic reduction of the Swedish gravity stations, Rikets allm. kartverk, Publ. no. 23, Stockholm, 1954.
87. ———: Geoid in Sweden, *ibid.*, no. 25, Stockholm, 1955.
88. Wolf, H.: Geoidvergleiche und absolute Lotabweichungen, Veröff. deutsch. geod. Komm., Reihe A, Heft 5, 1952.
89. Woppard, George P.: World wide gravity measurements conducted during the period June, 1949–January, 1952, Woods Hole Oceanog. Inst., ref. no. 52-59, 1952; 53-36, 1953; 54-53, 1954; 54-54, 1954.
90. ———: Report of the special committee on the geophysical and geological study of continents, 1952–1954, Trans. Am. Geophys. Union, vol. 36, pp. 695–709, 1955.
91. ———, J. C. Rose, and W. E. Bonini: The establishment of the international gravity standard, Trans. Am. Geophys. Union, vol. 37, pp. 143–153, 1956.
92. ——— and W. E. Bonini: A review of the factors affecting the accuracy of long-distance and intercontinental gravimeter measurements, Trans. Am. Geophys. Union, vol. 36, pp. 575–583, 1955.
93. Worzel, J. Lamar, and Maurice Ewing: Gravity measurements at sea, 1948 and 1949, *ibid.*, vol. 33, no. 3, 1951.
94. Ölander, V. R.: On the geoid in the Baltic area and the orientation of the Baltic ring, Publ. Finn. Geod. Inst., no. 38, 1950.
95. Darling, F. W.: Fundamental tables for the deflection of the vertical, USCGS Spec. Publ., no. 243, 1949.
96. de Graaff Hunter, J.: Presidential address at the General Assembly of the IUGG, Toronto, September, 1957.
97. Heiskanen, W. A.: Columbus geoid, Trans. Am. Geophys. Union, vol. 38, no. 6, 1957.
98. ———: Achievements of the world-wide gravity program of the Mapping and Charting Research Laboratory of The Ohio State University, Report for the General Assembly of the IUGG, Toronto, September, 1957.
99. ———: General report on the gravimetric computation of the undulations of the geoid,  $N_g$ , and the deflection of the vertical components  $\xi_g$  and  $\eta_g$ , Report for the General Assembly of the IUGG, Toronto, September, 1957.
100. Honkasalo, T.: Gravity survey and astro-gravimetric stations of the Finnish Geodetic Institute (in Swedish), Second Assembly of the Nordic Geodetic Commission, Helsinki, 1956.
101. ———: Gravity survey of the Baltic Sea, Symposium, Size and shape of the earth, Publ. Inst. Geod., Photogram. Cartog., Ohio State Univ., no. 7, 1957.
102. Kaula, W. M.: Accuracy of gravimetrically computed deflections of the vertical, Trans. Am. Geophys. Union, vol. 38, no. 3, 1957.
103. Netherland's report for the General Assembly of the IUGG, Toronto, September, 1957.
104. Uotila, U. A.: Determination of the shape of the geoid, Symposium, Size and shape of the earth, Publ. Inst. Geod., Photogram. Cartog., Ohio State Univ., no. 7, 1957.
105. Arnold, K.: Die Co-Geoide der Freiluftreduktion, Gerlands Beitr. Bd. 66, Leipzig, 1957.
106. de Graaff Hunter, J.: Legitimate deductions from geodetic observations, Festschrift C. F. Baeschlin, Zurich, 1957.
107. Ledersteger, Karl: Eine Modifikation der Freiluftreduktion, *ibid.*, 1957.
108. Levallois, J. J.: Sur la formule de Stokes et celles qui en dérivent, *ibid.*, 1957.
109. Tsuboi, C.: A new simple method for calculating the deflections of the vertical from gravity anomalies with the aid of the Bessel Fourier series, Proc. Japan Acad., vol. 30, p. 461, 1954.

## CHAPTER 9

### WORLD GEODETIC SYSTEM

#### 9-1. Conversion of Existing Geodetic Systems to the World Geodetic System

Any existing geodetic system at whose initial point very accurate astronomic measurements of latitude  $\varphi'_0$ , longitude  $\lambda'_0$ , and azimuth  $A'_0$  of one direction have been carried out could be used as the world geodetic system.<sup>6</sup> In addition, and this is essential, the absolute vertical-deflection components  $\xi_g$  and  $\eta_g$  must be known in order to obtain from  $\varphi'_0$ ,  $\lambda'_0$ , and  $A'_0$  the coordinates  $\varphi_0$ ,  $\lambda_0$ , and  $A_0$  equivalent to geodetic coordinates. For the relationships between the quantities  $\varphi'_0$ ,  $\varphi_0$ ,  $\lambda'_0$ ,  $\lambda_0$ , and  $A'_0$ ,  $A_0$  and the components  $\xi_g$  and  $\eta_g$  there exist the following equations:

$$\begin{aligned}\varphi_0 &= \varphi'_0 - \xi_g \\ \lambda_0 &= \lambda'_0 - \eta_g \sec \varphi \\ A_0 &= A'_0 - \eta_g \tan \varphi\end{aligned}\tag{9-1}$$

Since the astronomic coordinates refer to the geoid and the geodetic coordinates to the reference ellipsoid being used, the astronomic coordinates corrected by the deflections of the vertical give the latitude, longitude, and azimuth of the initial point on the ellipsoid.

The initial point of the world geodetic system could be, for instance, Meades Ranch in America, Potsdam in Europe, Pulkovo in Russia, or Dehra Dun in India, but as most control points have probably been computed in the European Potsdam system and in the American Meades Ranch system, either of these two is to be preferred; perhaps Meades Ranch, at which rather accurate  $\xi_g$  and  $\eta_g$  have been computed,<sup>8</sup> would be the best of all.

We get the coordinates  $\varphi$ ,  $\lambda$  and azimuth  $A$ , valid on the reference ellipsoid, of the initial point of any *other* existing geodetic system in a manner similar to that used before if we have made accurate astronomic observations  $\varphi'$ ,  $\lambda'$ ,  $A'$  and computed gravimetrically the accurate vertical-deflection components  $\xi_g$  and  $\eta_g$  at that point.

For our computation the equator value  $\gamma_E$  of the gravity formula is of basic significance, because in the gravimetric computation of the geoid

undulations  $N$  and the vertical-deflection components  $\xi$  and  $\eta$  we have to use the gravity-anomaly field of the whole earth. If the gravity anomalies were known everywhere in the world, it would do no harm to use gravity anomalies, say, 10 mgal too large; we would still obtain correct  $N$  values since the sum of Stokes' coefficients over the whole world is zero. The same thing applies to the vertical deflections. However, since there are large gravimetrically unsurveyed areas, we have to use the gravity anomaly zero in such areas because it corresponds to the complete isostatic equilibrium. If the equatorial value  $\gamma_E$  of the gravity formula would be, say, 10 mgal too high, then all gravity anomalies would be, on the average, 10 mgal too small. When we do not know this fact and use in the gravimetrically unsurveyed areas the anomaly zero, it is wrong by 10 mgal, the right value being  $-10$  mgal. These assumed values do not correspond to reality and can produce  $N$  values more than 10 m wrong.

When we need to, we can, of course, compute the *distance* along the reference ellipsoid between the initial points of any geodetic systems. For that purpose the dimensions of the reference ellipsoid are very important. The flattening  $\alpha$  is related to the gravity formula being used and cannot be altered. The significance of the equatorial radius  $a$  is great, because its error  $da$  affects the computations with full weight. The error  $ds$  of the distance  $s$  between the initial points in question will be, of course,

$$ds = \frac{s}{r} da \quad (9-2)$$

where  $r$  is the mean radius of curvature of the geodesic line  $s$ . As the difference  $r - a$ , however, is always less than 1 per cent of  $a$ , we can use instead of  $r$  the equatorial radius and get

$$ds = \frac{s}{a} da \quad (9-3)$$

The accuracy of the geodetic quantities  $\varphi$ ,  $\lambda$ , and  $A$  of the initial point is, according to Formula (9-1), dependent upon the errors  $d\xi_g$  and  $d\eta_g$  as well as upon the error of the astronomic position. If  $d\xi_g$  and  $d\eta_g$  are both  $0.^{\circ}5$ , the standard error  $m_1$  of the location of the initial point will be  $m_1 = \pm 0.^{\circ}5\sqrt{2} = 0.^{\circ}705 = 21.9$  m. The standard error caused by  $d\xi_g$ ,  $d\eta_g$  in the computed distances between the initial points is, of course,  $m_1\sqrt{2} = 1.^{\circ}00 = 31.4$  m. The errors of  $\xi_a$  and  $\eta_a$ , approximately  $0.^{\circ}2$  each, increase  $m_1\sqrt{2}$  very little; instead of 31.4 m we get 33.4 m. It is important to realize that the errors  $m_1$  and  $m_1\sqrt{2}$  are independent of the distance  $s$ ; they are the same regardless of whether  $s$  is 50, 500, or 10,000 km.

If  $\epsilon_0$  is the angle between the direction of the maximum deflection of the vertical  $\theta_0 = \sqrt{{\xi_0}^2 + {\eta_0}^2}$  and the geodesic line  $P_0P_1$  at the initial point  $P_0$ ,

and if  $\epsilon_1$  is the corresponding angle at the initial point  $P_1$  between  $\theta_1 = \sqrt{\xi_1^2 + \eta_1^2}$  and the geodesic line  $P_1P_0$ , then the whole error  $ds$  of the distance  $P_0P_1$  is

$$ds = \frac{s}{a} da + \frac{a}{\rho} (\theta_0 \cos \epsilon_0 + \theta_1 \cos \epsilon_1) \quad (9-4)$$

If we suppose that  $\xi_0 = \eta_0 = \xi_1 = \eta_1$  and therefore  $\theta_0 = \theta_1 = \xi \sqrt{2}$ , we get

$$ds = \frac{s}{a} da + \frac{a\sqrt{2}\xi}{\rho} (\cos \epsilon_0 + \cos \epsilon_1)$$

The standard error  $m_s$  of the distance  $s$  would therefore be

$$m_s = \pm \sqrt{\left(\frac{s}{a} da\right)^2 + \left(\frac{a\sqrt{2}\xi}{\rho}\right)^2 (\cos^2 \epsilon_0 + \cos^2 \epsilon_1)}$$

and its maximum value  $M$ , when  $\cos^2 \epsilon_0 = \cos^2 \epsilon_1 = 1$ , is

$$M = \pm \sqrt{\left(\frac{s}{a} da\right)^2 + 4 \frac{\xi^2}{\rho^2} a^2} \quad (9-5)$$

If  $da = 50$  m,  $s = a = 6378$  km, and  $\xi = 0.^{\circ}5$ , we get

$$M = \pm \sqrt{50^2 + 31^2} = \pm 59 \text{ meters} \quad (9-5a)$$

If  $da = 50$  m,  $s = a$ , and  $\xi = 1''$ , we get

$$M = \pm \sqrt{50^2 + 62^2} = \pm 80 \text{ meters} \quad (9-5b)$$

In the latter case the effect of the errors of  $a$  and  $\theta$  on the standard error of  $s$  will be nearly equal.

We must also know, however, the geoid heights  $N$  at the initial points to be able to project each initial point from the geoid to the reference ellipsoid being used. In this projection we can neglect the deflection of the vertical because even in the extreme case in which the mean deflection of the vertical is  $3.^{\circ}4$  (in fact the vertical deflections will never exceed  $1.^{\circ}5$ ) its effect would be only  $N \sin 3.^{\circ}4 = N/1000$ , or only 0.1 m if  $N = \pm 100$  m, which extreme value hardly exists. By the procedure mentioned previously we can localize exactly each initial point on the geoid.

The method described above allows us to convert the initial point of each existing geodetic system, and therefore the systems themselves, to the world geodetic system. Astronomic-geodetic computation of the coordinates of the control points of each geodetic system has been made, beginning from the astronomic coordinates of the initial point, either corrected

or uncorrected, for the deflection of the vertical. Therefore these control points must also be converted to the world geodetic system.

First it is necessary to compute the corrections  $d\xi$ ,  $d\eta$ , and  $dN$  of the deflection components and geoid distance  $N$  at the individual control points  $P$  resulting from the corrections  $\xi_g - \xi_0 = d\xi_0$ ,  $\eta_g - \eta_0 = d\eta_0$ , and  $dN_0$  at the initial point  $P_0$ . Here  $\xi_0$  and  $\eta_0$  are the old components used, and  $\xi_g$  and  $\eta_g$  are the gravimetrically computed absolute vertical-deflection components. The quantities  $d\xi$ ,  $d\eta$ , and  $dN$  can best be obtained from the formulas of Vening Meinesz<sup>9</sup>

$$\begin{aligned}
 d\xi &= \frac{R_0}{R} [\cos(\varphi - \varphi_0) - 2 \sin \varphi \sin \varphi_0 \sin^2 \frac{1}{2}(\lambda - \lambda_0)] d\xi_0 \\
 &\quad + \frac{r_0}{R} \sin \varphi \sin (\lambda - \lambda_0) d\eta_0 \\
 &\quad + \frac{1}{R} [\sin(\varphi - \varphi_0) - 2 \sin \varphi \cos \varphi_0 \sin^2 \frac{1}{2}(\lambda - \lambda_0)] dN_0 \\
 d\eta &= -\frac{R_0}{r} \sin \varphi_0 \sin (\lambda - \lambda_0) d\xi_0 + \frac{r_0}{r} \cos (\lambda - \lambda_0) d\eta_0 \\
 &\quad - \frac{1}{r} \cos \varphi_0 \sin (\lambda - \lambda_0) dN_0 \\
 dN &= -R_0 [\sin(\varphi - \varphi_0) + 2 \cos \varphi \sin \varphi_0 \sin^2 \frac{1}{2}(\lambda - \lambda_0)] d\xi_0 \\
 &\quad + r_0 \cos \varphi \sin (\lambda - \lambda_0) d\eta_0 \\
 &\quad + [\cos(\varphi - \varphi_0) - 2 \cos \varphi \cos \varphi_0 \sin^2 \frac{1}{2}(\lambda - \lambda_0)] dN_0
 \end{aligned} \tag{9-6}$$

where  $R_0$ ,  $R$  = radius of curvature of meridian at initial point  $P_0$  and point  $P$ , respectively

$r_0$ ,  $r$  = east-west radius of curvature at initial point  $P_0$  and point  $P$ , respectively

We use  $r$  instead of the usual  $N$  to represent the east-west radius of curvature because in our formulas  $N$  signifies geoid distance.

If  $P_0P$  is very long, we must use these complete formulas; but if  $P_0P < 300$  km in the east-west direction and  $< 1500$  km in the north-south direction, as is frequently the case inside the same geodetic system, and if we consider the quantities  $d\xi_0$ ,  $d\eta_0$ , and  $dN_0$  to be small and remember that the ratios  $R_0/R$ ,  $r_0/R$ ,  $R_0/r$ , and  $r_0/r$  differ from 1 always by less than 0.01, we can replace them by 1 and get the approximate formulas

$$d\xi = \cos(\varphi - \varphi_0) d\xi_0 + \sin \varphi \sin(\lambda - \lambda_0) d\eta_0 + \sin(\varphi - \varphi_0) \frac{dN_0}{a}$$

$$d\eta = -\sin \varphi_0 \sin(\lambda - \lambda_0) d\xi_0 + d\eta_0 - \cos \varphi_0 \sin(\lambda - \lambda_0) \frac{dN_0}{a} \quad (9-7)$$

$$\frac{dN}{a} = -\sin(\varphi - \varphi_0) d\xi_0 + \cos \varphi \sin(\lambda - \lambda_0) d\eta_0 + \cos(\varphi - \varphi_0) \frac{dN_0}{a}$$

These formulas are similar to Helmert's formulas,<sup>7</sup> which have generally been used until now.

The Vening Meinesz formulas are, however, more accurate. Vening Meinesz takes into account the fact that, because of the corrections  $d\xi_0$  and  $d\eta_0$  of the deflection of the vertical at the origin  $P_0$ , the geodesic line  $PP_0$  will change its length and will not make the same angle at  $P_0$  with any triangle side as before. He also takes into account the effect of the displacement  $dN_0$  at the origin, which previously had been neglected. If  $P_0P_1$  is only of the order of 200 km or less, as has generally been the case, these two effects are negligible, but if  $P_0P_1$  is of the order of the length of the earth's radius, they have to be considered. If  $\varphi - \varphi_0$  and  $\lambda - \lambda_0$  are close to 90°, the share of  $dN_0$  in  $d\xi$  is equal to  $(1 - \sin \varphi \cos \varphi_0)dN_0/a$  and in  $d\eta$  to  $\cos \varphi_0 dN_0/a$ . For example, since  $dN_0$  in Potsdam is about +30 m, according to the author (H.),<sup>6</sup> its effect on  $d\xi$  and on  $d\eta$  is, at a point, at approximately 90° latitude and 90° longitude, 1" and 0".6, respectively. The ratio between  $dN$  and  $dN_0$  is not zero but will vary with  $\cos(\varphi - \varphi_0)$ ,  $\cos \varphi$ ,  $\cos \varphi_0$ , and  $\sin^2 \frac{1}{2}(\lambda - \lambda_0)$ , as the last of Equations (9-6) shows.

If different reference ellipsoids have been used, we must convert the vertical-deflection components from the old ellipsoid to the reference ellipsoid of the world geodetic system. This is effected by means of formulas Vening Meinesz<sup>9</sup> computed in 1950. The complete formulas are complicated, but in most cases the following formulas are sufficient:

$$\begin{aligned} d\xi &= [\sin(\varphi - \varphi_0) - 2 \cos \varphi_0 \sin \varphi \sin^2 \frac{1}{2}(\lambda - \lambda_0)] \Delta\beta \\ &\quad - 4 \cos \varphi \cos \frac{1}{2}(\varphi + \varphi_0) \sin \frac{1}{2}(\varphi - \varphi_0) \Delta\alpha \\ &\quad - (2 + \frac{3}{4} \tan \varphi_0 \sin 4\varphi_0) \sin(\varphi - \varphi_0) \alpha \Delta\alpha \end{aligned}$$

$$d\eta = -\cos \varphi_0 \sin(\lambda - \lambda_0) \Delta\beta + \frac{1}{4} \sin \varphi_0 \sin 4\varphi_0 \sin(\lambda - \lambda_0) \alpha d\alpha \quad (9-8)$$

$$\begin{aligned} \frac{dN}{a} &= -2[\sin^2 \frac{1}{2}(\varphi - \varphi_0) + \cos \varphi_0 \cos \varphi \sin^2 \frac{1}{2}(\lambda - \lambda_0)] \Delta\beta \\ &\quad + 4 \cos^2 \frac{1}{2}(\varphi + \varphi_0) \sin^2 \frac{1}{2}(\varphi - \varphi_0) \Delta\alpha \end{aligned}$$

$$\Delta\beta = \frac{\Delta a}{a} + \sin^2 \varphi_0 \Delta\alpha$$

where  $\varphi_0, \lambda_0$  = geographic coordinates of initial point

$\varphi, \lambda$  = corresponding coordinates of computation point

$\Delta a, \Delta \alpha$  = corrections of adopted  $a$  and  $\alpha$  values

The corrected vertical-deflection components are  $\xi_c = \xi + d\xi$  and  $\eta_c = \eta + d\eta$ .

Therefore, when we have computed the absolute  $\xi_g$  and  $\eta_g$  at the initial points of different geodetic systems, it is relatively easy to convert the  $\xi$  and  $\eta$  values of all astronomic-geodetic points to the world geodetic system after the relative vertical-deflection components have been computed. Let us suppose that the triangulation and astronomic measurements are faultless; these converted  $\xi_c$  and  $\eta_c$  values will then be absolute (referred to the adopted ellipsoid). The errors occurring in the triangulation and in the astronomic measurements will, of course, make the  $\xi_c$  and  $\eta_c$  values less accurate.

If some parts of a local geoid have been computed with reference to the old geodetic system, we are able to convert the  $N$  values so obtained to the absolute  $N$  values. We have only to use the proper  $N$  value at the initial point and to compute the effect of the tilting of the geoid, i.e., of the differences  $\xi_g - \xi_0$  and  $\eta_g - \eta_0$ , and the effect of the adopted ellipsoid (if the international ellipsoid has not been used) on the  $N$  values at the other points.

This method must be used especially for all vertical-deflection stations in whose vicinity only a few, if any, gravity stations exist. The astronomic-geodetic method has given the shape of different local geoid fragments; the gravimetric method converts these fragments into parts of the actual geoid. In this way it is possible to convert all needed control points of any geodetic system into the world geodetic system regardless of what initial points and what reference ellipsoid have been used in computing the original astronomic-geodetic coordinates of these points.

## 9-2. Supercontrol Points

Triangulation is a rather accurate method and gives reliable coordinates for the triangulation points as far as relatively short chains, not exceeding 1000 km, are concerned. If the triangulation has continental dimensions of many thousand kilometers, the observation errors, particularly the systematic ones, can produce errors so large that the accuracy of such chains is questionable. The adjustment of the European triangulation nets under the leadership of Whitten,<sup>10</sup> in 1951, shows that the closure errors of the South European triangulations often are between 1:25,000 and 1:75,000.

No adjustment computation, however careful and theoretically correct it may be, can eliminate systematic errors, because it can correct only errors that are accidental, not systematic. The inner discrepancies of the

triangulation can, of course, be removed by the adjustment, but no one knows how erroneous the adjusted long distances actually are except when new triangulations are carried out, which happens rather seldom. The least-squares method of adjustment has drawbacks too, in that it gives too large corrections for the small angles even when the observational errors are accidental.

The discrepancy, for instance, between the old adjusted and the new adjusted triangulation of about 3000 km from Meades Ranch to Seattle, Washington, amounts to about 50 m, according to the U.S. Army Map Service. Thus, large errors can easily be produced in triangulations carried out under difficult conditions. The lateral refraction encountered in the measurement of angles when one or both sides run quite close to the earth's surface can, for instance, cause systematic errors of 1" to 2".

Likewise, the deflections of the vertical at observation points where the slope of sight lines are large give errors in measurement up to 3". It has not been possible to eliminate the sources of these errors simply because we do not know them.

With such errors in mind we urgently need the supercontrol points first advocated by Byrd,<sup>1</sup> who wrote, "Can supercontrol points be established at, say, intervals of 2000 to 6000 miles to control first-order triangulation? In my opinion, such points can and will be established within the next decade."

The basis for establishing these supercontrol points is found in Eqs. (9-1):

$$\begin{aligned}\varphi &= \varphi' - \xi \\ \lambda &= \lambda' - \eta_g \sec \varphi \\ A &= A' - \eta_g \tan \varphi\end{aligned}\tag{9-1a}$$

We get, therefore, the geodetic quantities  $\varphi$ ,  $\lambda$ , and  $A$  at any points where the astronomic quantities  $\varphi'$ ,  $\lambda'$ , and  $A'$  and the gravimetric vertical-deflection components  $\xi_g$  and  $\eta_g$  have been determined. We compute at least one such control point at or close to both ends of a long-range triangulation. For this purpose we need astronomic observations as accurate as possible and a good local gravity-station net in the vicinity of the selected astronomic-geodetic points of the triangulation.

Since, as we have seen in Sec. 9-1, the accuracy of the geodetic coordinates  $\varphi$  and  $\lambda$  is, in favorable cases, of the order of 20 to 30 m, the standard error of the distance of the triangulation would be 30 to 45 m. Long-range triangulations, where the errors are larger than this, can consequently be improved by these supercontrol points.

It is neither necessary nor wise to measure and compute these control points at the astronomic-geodetic end points of the triangulation chain if

the conditions there are not favorable. It is best to choose the supercontrol points in regions where the effect of the topography on the astronomic coordinates is small and the surrounding gravity-station net is, or can be made, sufficient for accurate computation of  $\xi_g$  and  $\eta_g$ . Even if these points are some hundred kilometers from the end points of the triangulation chain, the higher accuracy of the computed geodetic coordinates will more than compensate for the fact that the distance between these control points is shorter than the triangulation chain itself.

Supercontrol points would be useful in Alaska, Mexico, and Patagonia to control the western American arc measurements from Alaska to Patagonia, and in the neighborhood of Cairo, the equator, and Cape Town for the Cairo-Cape Town arc measurement, which was carried out under poor conditions in several places. Supercontrol points computed at a few locations in India and Burma would increase the accuracy of the important Indian arc measurement.

What is more important, supercontrol points can be used to control the rapid, but perhaps less accurate, quadrilaterals obtained by the Shoran-Hiran method. Using this method in conjunction with supercontrol points would be an excellent way to get map control sufficiently good for mapping the island arcs and wildernesses like the arctic and antarctic areas, Central Africa, and so on.

### 9-3. Control of Small-scale Maps

For controlling large-scale maps, with a scale of 1:2000 to 1:50,000, only triangulation, classic or modern, or traverse measuring gives sufficient accuracy, i.e., furnishes the maps with control points whose error is smaller than the drafting and reproducing accuracy of the maps, itself hardly greater than 0.3 mm. The corresponding accuracy of the control points, viz., 0.6 m for maps 1:2000, 3 m for maps 1:10,000, 6 m for maps 1:20,000, and 15 m for maps 1:50,000, can hardly be obtained by any other method.

If triangulation has been carried out, of course the triangulation points are also used as control points for small-scale maps. If, however, areas where no triangulations exist are to be mapped, say on a scale of 1:100,000 or 1:250,000, astronomic-gravimetric control has the great advantage of being fast. For instance, completing the triangulation from Cairo to Cape Town took 75 years, and, according to experts, the triangulation of Brazil would consume about 20 to 30 years.

Until recently, there was not enough gravity material for the astronomic-gravimetric method to be used, and the method itself could be developed only when a fast and accurate method of carrying out the necessary additional gravity surveys became available.

Now there are rather good gravity-station nets in many areas, and when necessary, they can be improved rapidly by making regional gravity sur-

veys with gravimeters along the highways and railroads and at other places with sufficient elevation control. The astronomic observations can be made with high accuracy in two or three clear nights.

Formula (9-1a) can be applied here also.<sup>2</sup> As the accuracy of the astronomic observations is higher than the accuracy of the gravimetric deflections of the vertical ( $0.^{\circ}3$  as against  $1.^{\circ}0$ ), the accuracy of  $\xi_g$  and  $\eta_g$  will essentially determine the accuracy of the astronomic-gravimetric control points. On 1:100,000 maps a drafting accuracy of 0.3 mm corresponds to 30 m, or the same accuracy as that given by this control method,  $1.^{\circ} = 30$  m. For maps on a smaller scale this map control is sufficient even when the gravity measurements do not allow higher accuracy than  $2.^{\circ}$  to  $3.^{\circ}$ , or 60 to 90 m. It is hardly possible to emphasize strongly enough the significance of this fast, inexpensive, and sufficiently accurate astronomic-gravimetric method.

When it is used in conjunction with triangulation, it is easy to convert large-scale maps of different areas to the same system. For instance, when cities, mining centers, or other types of valuable areas are separated from each other by mountains, oceans, or inaccessible wilderness, this is the method to be used. Each of these areas is covered with triangulations and traverses of the required accuracy, which give the control points needed.

To convert these local maps to the same system we have only to carry out very accurate astronomic observations at least at *one* point of *each* local survey and to measure an adequate local gravity-station net. The astronomic observations give the direction of the plumb line, and the gravimetric  $\xi_g$  and  $\eta_g$  give the correction of the plumb line to the normal of the reference ellipsoid. If a regional survey farther from these separated areas already exists, we shall get the geodetic quantities  $\varphi$  and  $\lambda$ , as referred to the reference ellipsoid adopted, even with an accuracy of 30 to 50 m.

In this way we obtain the geodetic coordinates  $\varphi$  and  $\lambda$  and the azimuth  $A$  [relatively accurately (probable error,  $1.^{\circ}$  to  $2.^{\circ}$ )] of one central control point of the mapped areas in question. Thus, on the basis of the local triangulation, there are accurate large-scale maps (1:2000, 1:20,000, or whatever the scale may be) which have been converted by the aid of the astronomic-gravimetric central control points to the world geodetic system. It

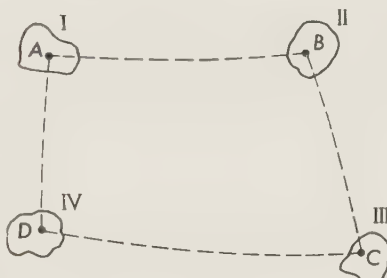


FIG. 9-1. Areas I, II, III, and IV, far from each other and covered by large-scale maps, can be converted without triangulation to the same system when at one point (*A*, *B*, *C*, *D*) of each area the astronomic latitude and longitude have been observed and gravimetric vertical-deflection components  $\xi_g$  and  $\eta_g$  have been computed.

should be emphasized particularly that no long triangulation between the mapped areas is needed.

The method is illustrated in Fig. 9-1. Areas I, II, III, and IV, far from each other, are covered by large-scale maps. If accurate astronomic observations have been made at the points  $A$ ,  $B$ ,  $C$ , and  $D$ , and if the surrounding gravity-station nets allow the computation of  $\xi_g$  and  $\eta_g$  with sufficient accuracy, the geodetic coordinates of these points can be computed; consequently, the isolated areas I, II, III, IV can be converted to the world geodetic system almost as accurately as if triangulation had been carried out between the areas.

#### 9-4. Other Applications

Since the undulations of the geoid  $N$  in very large areas exceed 20 m and even reach values of -40 to 60 m, and since the base lines of triangulations are referred to the geoid whereas the computations are carried out along the reference ellipsoid, the base lines are systematically too long in areas where the geoid is above the ellipsoid and too short in the "hollow" areas of geoid. This fact causes a systematic error which decreases the final accuracy of long-range triangulations regardless of the way it has been adjusted.

This source of error can be avoided only by *reducing the measured base lines from geoid to ellipsoid*. The reduction was impossible until recently simply because the geoid heights  $N$  were not known.

The reduction  $dL$  of the base line will be

$$dL = \frac{L}{R} N$$

where  $L$  = measured length of base line

$R$  = mean radius of curvature of ellipsoid at base line

$N$  = average geoid height along base line

Using the value  $R = 6370$  km, we get the relative reduction  $dL/L$  of the base line shown in Table 9-1.

TABLE 9-1. REDUCTION OF BASE LINE FROM GEOID TO ELLIPSOID

$N, \text{m}$	10	20	30	40	50	60	70	80	90	100
$10^5 \times dL/L$	0.15	0.31	0.47	0.63	0.79	0.94	1.11	1.25	1.41	1.57

In Central Europe the geoid height  $N$  is, according to the author (H.),<sup>6</sup> about +40 m, and in parts of India it is -30 m; therefore the average re-

duction from geoid to ellipsoid would be  $-1/150,000$  of the measured base line in Europe and  $+1/200,000$  in India.

The deflection of the vertical perpendicular to the direction of the triangle side introduces errors into the triangulation similar to those given by the inclination  $i$  of the horizontal axis of theodolite. The error is  $\theta_p \tan h$ , where  $\theta_p$  is the difference between the perpendicular deflection components at both ends of the triangulation side and  $h$  the elevation angle of the sight. In the mountains, where  $h$  can reach values of  $5^\circ$  and  $\theta_p$  can be  $10''$  to  $20''$ , this effect is considerable; for  $h = 5^\circ$ ,  $\theta_p = 20''$  it is no less than  $1''.8$ . It has been neglected until now because generally  $\theta_p$  is not known. This neglect has introduced systematic errors into the present triangulations.

The best method for escaping these errors may be to determine gravimetrically the deflection of the vertical at the observation points, to compute  $\theta_p$ , and to consider it in the adjustment computation. It must be kept in mind, however, that the determination of  $\theta_p$  in rough mountains is rather difficult because it presumes a good local gravity survey, which is easier to mention than to carry out. On the other hand, the deflections of the vertical computed on the basis of the topography of the surrounding area of the computation point can yield useful values for the effect.

### 9-5. Conclusions

It may be of interest to list here, at the end of these chapters on the geodetic achievements of physical geodesy, the problems this method is able to solve,<sup>2-5a</sup> alone and in connection with other measuring methods.

*Alone the gravimetric method can give:*

1. The flattening  $\alpha$  of the reference ellipsoid.
2. The undulations  $N$  of the geoid.
3. The vertical-deflection components  $\xi$  and  $\eta$  at any point, oceans and islands included.
4. The conversion of existing geodetic systems to the same world geodetic system.
5. The reduction of triangulation base lines from the geoid to the reference ellipsoid.
6. The correction of errors in triangulation in mountainous regions due to the effect of the deflections of the vertical.
7. Geophysical applications of gravity measurements, e.g., the isostatic study of the earth's interior and the exploration of oil fields and ore deposits.

*With astronomic observations the gravimetric method can:*

1. Control maps on a scale of 1:100,000 and on a smaller scale in areas where adequate triangulation is not available. The error of the control points, computed by the astronomic-gravimetric method, is of the order of 30 to 45 m, which is not larger than the drafting and reproducing errors of 1:100,000 maps.

2. Compute the distance between any points along the reference ellipsoid with an accuracy of about 50 m regardless of whether the points are 50 or 10,000 km apart.
3. Convert ellipsoidal distances to geoidal distances.
4. Establish geodetic supercontrol points for controlling the accuracy of long-range triangulation.

*With existing triangulations the gravimetric method can:*

Correct the dimensions of the reference ellipsoid.

It is the firm conviction of both of the authors that the gravimetric method is by far the best of the existing methods for solving the main problems of geodesy, i.e., to determine the shape of the geoid on the continents as well as at sea and to convert the existing geodetic systems to the world geodetic system. It can also give invaluable help in the computation of the dimensions of the reference ellipsoid.

#### REFERENCES

1. Byrd, W. O.: The modern mission of geodesy, Surveying and Mapping, October-December, 1952.
2. Heiskanen, W. A.: The role of gravimetry in geodesy, Surveying and Mapping, vol. 12, no. 1, 1952.
3. ———: Relative significance of the different methods of modern geodesy, Trans. Am. Geophys. Union, vol. 35, no. 6, 1954.
4. ———: The gravity program of the Mapping and Charting Research Laboratory of The Ohio State University, pamphlet distributed at Brussels Assembly IUGG, 1951.
5. ———: The geodetic significance of world-wide gravity studies, Ohio State Univ. Mapping and Charting Research Lab., Tech. Paper, no. 124, 1950.
- 5a. ———: On the world geodetic system, Publ. Finn. Geod. Inst., no. 39, 1951.
6. ———: Achievements of the world-wide gravity program of the Mapping and Charting Research Laboratory of the Ohio State University, Rept. for the General Assembly of the IUGG, Toronto, September, 1957.
7. Jordan, W., and O. Eggert: Handbuch der Vermessungskunde, 7th ed., Bd. 3, 2, pp. 424-428, Metzlersche, Stuttgart, 1923.
8. Rice, D. A.: Deflections of the vertical from gravity anomalies, Bull. géod., no. 25, 1952.
9. Vening Meinesz, F. A.: Bull. géod., N.S., no. 15, 1950.
10. Whitten, C. A.: Adjustment of European triangulation, Rept. Brussels Assembly IUGG, 1951.

## CHAPTER 10

### DEVIATIONS FROM ISOSTATIC EQUILIBRIUM

#### PART 10A

GENERAL CONSIDERATIONS. FORMULAS FOR ELASTIC, PLASTIC, AND  
SHEAR DEFORMATIONS OF THE CRUST. DEVELOPMENT OF  
GEOSYNCLINES

#### 10A-1. Introduction and Summary

If we find a mean isostatic anomaly, different from zero, in an area large enough to allow readjustment of the equilibrium by upward or downward bending of the crust, and if this mean anomaly thus cannot be attributed to the presence of unknown mass anomalies in the crust or to the application of a system of isostatic reduction not corresponding to the way in which the compensation actually occurs, we may conclude that there is a deviation from equilibrium in this area. We then have three possibilities: (1) that a cause of deviation is still present, (2) that such a cause has recently been present but is no longer there and that the equilibrium is now being readjusted, and (3) that the cause is gone but that the deviation from equilibrium is too small to bring about stresses exceeding the elastic limit of the plastic substratum.

It is a happy circumstance that in our time one instance of the second type is most probably occurring, viz., the readjustment of the equilibrium in Scandinavia and in Canada and Labrador following the disappearance of the heavy ice load of the glacial period. This phenomenon has been well investigated and is discussed in Part B of this chapter. Two important results can be derived: (1) a figure for the pseudo viscosity of the subcrustal layer, viz.,  $10^{22}$  poises, and (2) an estimate of the relaxation time, i.e., the period in which the readjustment reduces the deviation to  $1/e$  times its value.

As it is certain that at the present time the rise is still continuing, the actual negative gravity anomaly in the center of the rising area is clearly above the value prescribed by the elastic limit of the subcrustal layer, below which probably no further readjustment will occur. Thus we also obtain a maximum value for these limits.

We find a rather high speed for the adjustment phenomenon; the relaxation time proves to be less than 10,000 years for the breadth dimensions of about 1400 km of the rising area of Scandinavia. Though it is not yet absolutely clear how the relaxation time varies with the dimensions of the phenomenon, it is probably safe to conclude that, if the dimensions are not less than the crustal bending limit mentioned in the beginning of this section, the time cannot be much more than 100,000 years. This is short in comparison with geological periods.

As the crust in the areas of Scandinavia or Canada and Labrador certainly cannot be considered to be particularly mobile, we come to the important conclusion that isostatic readjustment phenomena cannot, in general, take more than a few hundred thousand years. Thus, deviations which can be assumed to have existed for a much greater time must belong to the first group, i.e., to the type of disturbance brought about by causes still at work or by causes active until recently.

These causes may be located in the crust or in the plastic subcrustal layer. For the crust there is the possibility of loading or unloading by sedimentation, erosion, and volcanism and perhaps also by an increase of thickness or by changes of state affecting the density, which may change the amount of matter in each vertical column. In general, these effects must result in sinking or rising of the crust by isostatic adjustment, and the cohesion of the crust may result in a regional adjustment of this equilibrium. The loading and unloading by ice, as mentioned above, is also in this category, as is loading or unloading by changes of sea level.

These latter phenomena take place quickly in comparison with the others, and the resulting lag of isostatic readjustment may cause anomalies for some time. Most of the other phenomena may be expected to be so slow that such a readjustment lag cannot give notable deviations from isostatic equilibrium. It may be pointed out, however, that, when there are fault planes through the crust, the equilibrium conditions are not covered by any of the existing systems of reduction, and therefore isostatic anomalies are to be expected after the reduction has been applied, though their mean value over a larger area must be zero.

If the fault planes are vertical, there probably will not be the same regional spreading in all the directions on which the regional reduction is based; nor is there purely local compensation; the equilibrium is more complicated. A certain approximation to smaller anomalies may perhaps be obtained by applying different radii of regionality for gravity profiles crossing the area in different directions, but obviously this cannot give more than a rough indication of where fault planes may be expected.

If the fault planes are tilted, the equilibrium position of the different crustal blocks between the faults is still more complicated, and notable topographic features at the surface of the crust may result. It is likely,

for example, that the great grabens can thus be explained. In Part D of this chapter, where we return to this subject with a more detailed investigation, we shall see that tilted fault planes probably can be attributed to horizontal stress release in the crust.

The crust may also be subjected to horizontal compression. When this stress is below the elastic limit of the crust, its effect is restricted to two consequences, an elastic compression, which has little importance for the isostatic anomaly, and a slight rising of the crust above its isostatic-equilibrium position, which is due to the small upward resultant of the compression caused by the earth's curvature; the result must be a small isostatic anomaly. These consequences are investigated in the next section.

More important is the study of the crustal deformation after the compression (here considered to be uniaxial) has exceeded the elastic limit. This leads to a plastic thickening of the crust, but because of the tendency toward isostatic equilibrium, a greater bulge is formed at the lower boundary than at the upper one. It will be seen that the resulting asymmetry in the crust causes a downbending of the crust, slow in the beginning but accelerating, and thus leads to a downbuckling of the crust. In Secs. 10A-4 to 10A-7 we deal with this phenomenon and apply these results to the important problems raised by geosynclines and by the belts of strong negative anomalies found in several island-arc areas. A study of these belts shows that we have to assume the existence of forces that prevent the strong deviations from equilibrium, over a breadth of 100 to 200 km, from disappearing, and the most probable explanation seems to be the lateral compression mentioned above. This force can also account for the first geosyncline stage of a gradually deepening trough in which sediments are laid down and for the strong subsequent folding and overthrusting of strata, found in many geosynclines. The later stages of high rising, and the development of a great mountain system in the period when most of the folding is past, can well be understood as the result of the readjustment of the isostatic equilibrium of the negative belt; it can take place when the lateral compression is sufficiently diminished to allow the local rising of the belt. In Part C of this chapter the island-arc areas, especially the Indonesian Archipelago, are studied in more detail.

Before taking up the problem of the plastic deformation of the crust in Sec. 10A-4, we begin by dealing in Sec. 10A-3 with the elastic deformation of the crust as a result of vertical loading and horizontal compression, which, even in the case of plastic deformation in a geosyncline belt, must occur in the neighboring areas; the supposition of plastic behavior in the adjacent areas as well cannot explain the observed facts.

Still another crustal reaction to horizontal compression is possible, especially if the stresses are not regularly distributed: the crust may give way by shear. There is hardly room for doubt that this reaction also occurs in

island-arc areas, particularly on the sides of the arc, e.g., in west Sumatra and east of the Philippines in the Indonesian Archipelago; as this whole archipelago probably moves toward the south-southeast with respect to the surrounding regions, the relative movements in the areas mentioned must be mainly shear. We deal with the formulas for this phenomenon in Sec. 10A-5, where we follow the theory of shear as applied to geology by Chamberlin and Shepard<sup>5</sup> and recently further elaborated by Anderson<sup>1</sup> and Hubbert.<sup>9</sup> In Part C of this chapter we apply these results to the study of island-arc areas.

Besides the types of crustal phenomena and corresponding anomaly distribution hitherto dealt with, there also exist more extensive fields of isostatic anomalies of the same sign. The problem of their origin is a difficult one and one about which little is known. As will be seen in Sec. 10A-6, fields of positive anomalies may possibly be connected with geosyncline development, but more research is needed before any final conclusion can be reached. It is also possible that systematic anomalies over great areas are caused by large thermal deviations in the earth. This question is clearly related to that of convection currents, which are discussed in Chap. 11, and in connection with which the difficult subject of thermal equilibrium in the earth must be raised. That deviations from thermal equilibrium exist seems at least possible. Finally, it is possible to imagine that great anomaly fields are caused by large areas in the earth having differences of state or chemical constitution, though up to the present, with one exception to be mentioned in Chap. 11, there is little evidence of such a cause.

### 10A-2. Horizontal Compression in the Crust below the Elastic Limit

Assuming that the stress is below the elastic limit, we can be sure (as we shall find in the next section) that it is also below the buckling limit of the crust and that, therefore, there is no wave formation of the crust because of buckling; we also assume that vertical loads or other causes of wave formation are all absent. As far as deformation is concerned, the effect is restricted to an elastic thickening of the crust, with a slight increase of the dimensions at right angles to it, according to Poisson's constant. We shall not go into detail about this deformation, which has no further bearing on our problems; a closer study of them can be found in Vening Meinesz,<sup>17</sup> pp. 40-44.

Another feature, however, brings about small isostatic anomalies and therefore requires examination. Because of the earth's curvature, the compression causes an upward resultant force, which affects the position of the crust, bringing it slightly above the position of isostatic equilibrium and so giving rise to a positive isostatic anomaly.

If we examine an element of the crust (Fig. 10A-1) of length  $dl$  and of

unit dimension at right angles to the figure, the equilibrium condition for the vertical components of the forces working on the element gives

$$\rho g T \, dl - p \, dl - \sigma T \frac{dl}{R} = 0$$

where  $\sigma$  = compressive stress

$p$  = pressure exerted by sub-crustal layer

$T$  = thickness of crust

$\rho$  = mean density of crust

$R$  = earth's radius

or, by dividing by  $dl$ ,

$$\rho g T - p - \frac{\sigma T}{R} = 0$$

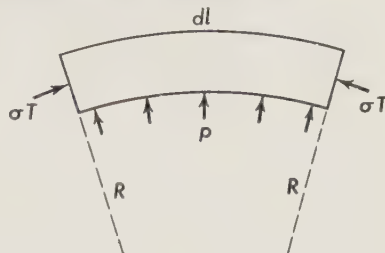


FIG. 10A-1. Earth crust under horizontal compression  $\sigma T$ .

According to this equation, equilibrium in this condition implies an excess of mass, per surface unit of the crust, of  $\sigma T/gR$  with respect to the normal isostatic equilibrium given by  $\rho g T = p$ . If  $\rho_s$  is the density of the plastic substratum, this excess of mass corresponds to a position of the crust which is higher than that of normal isostatic equilibrium, and the amount of rising is given by

$$c_\sigma = \frac{\sigma T}{\rho_s g R} \quad (10A-1)$$

The excess of mass brings about an isostatic anomaly of

$$A = \frac{2\pi k^2 \sigma T}{g R} \quad (10A-2)$$

By introducing the values for  $R$  (6371 km) and for  $k^2$  ( $6.67 \times 10^{-8}$ ) we obtain

$$A = 6.7 \times 10^{-11} \sigma T \text{ mgal} \quad \text{uniaxial compression} \quad (10A-3)$$

in which  $\sigma$  is expressed in dynes per square centimeter and  $T$  in kilometers.

It is clear that if the crust is also subjected to horizontal compressive stress at right angles to the plane of the figure, the anomaly must be twice as much, and so we have

$$A = 13.4 \times 10^{-11} \sigma T \text{ mgal} \quad \text{compression in all directions} \quad (10A-4)$$

The anomaly thus brought about by compression is small. If we assume a value for  $T$  of 35 km and a compression in all directions of  $2 \times 10^9$

dynes/cm<sup>2</sup> (which appears a rather high figure), we obtain an anomaly of 9.2 mgal. But this effect is not negligible, and we must take it into account. In cases of higher compression and of wave formation in the crust (to be dealt with in the next section) this anomaly must always be present in addition to the anomalies caused by the other processes.

In these paragraphs compressive stress is given a positive sign. As mentioned in Sec. 2-4, this convention is used throughout the book except in Part B of this chapter and in Chap. 11; the usage appears logical since compression is so common in the earth and tension so rare, although contrary to the general rule. For strain we also give a positive sign to a shortening of the dimensions. In Part B of this chapter and in Chap. 11, where we deal with current systems in the earth, it is best to keep to the normal system, as otherwise velocities will have the wrong sign. In those sections, therefore, stresses, including shear stresses, carry the opposite sign to those in all other chapters.

### 10A-3. Elastic Deformation of the Crust by Vertical Loading and Horizontal Compression

This section deals particularly with the wave formation of the crust as an elastic phenomenon; besides this deformation the effect dealt with in the previous section is also present. The assumption that the stresses are below the elastic limit does not exclude an investigation of the elastic buckling of the crust; when crustal dimensions and physical constants are introduced later, it will be found that the buckling-stress limit is above the elastic limit, but this fact does not affect the formulas.

Let us investigate the following two-dimensional case of crustal deformation. We consider a part of the crust of considerable length and of unit dimension at right angles to the plane of deformation, which is assumed to be vertical; we denote the thickness of the crust by  $T$ . In vertical cross sections perpendicular to the length dimension we suppose a normal-stress component of mean value  $\sigma$  and a vertical-shear component of mean value  $\tau$ ; the resultant force working on that cross section has, therefore, the components  $D = \sigma T$  and  $H = \tau T$ . We indicate the moment exerted by the normal-stress components in a cross section by  $M$ . The crust is further subjected to a reaction of the subcrustal layer, which exerts a pressure per surface unit denoted by  $p$ .

We introduce a coordinate  $x$  following the undeformed crust in the direction of the length dimension of the part considered and a vertical coordinate  $y$  (positive downward) which gives the deviations of the crust from the undeformed position. As the deformations are assumed to be of the elastic type, we can assume that  $\partial y / \partial x$  is small and  $\partial^2 y / \partial x^2$  very small.

We first consider an element  $dx$  of the crust (Fig. 10A-2). Indicating the earth's radius by  $R$  and the density of the substratum by  $\rho_s$ , we find

for the equilibrium conditions

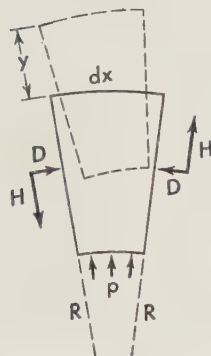


FIG. 10A-2. Deformed earth crust under vertical loads and uniaxial horizontal compression; dashed line represents original position.

$$\frac{\partial H}{\partial x} + D \left( \frac{1}{R} + \frac{\partial^2 y}{\partial x^2} \right) + p = 0 \quad (10A-5a)$$

$$-\frac{\partial D}{\partial x} + H \left( \frac{1}{R} + \frac{\partial^2 y}{\partial x^2} \right) = 0 \quad (10A-5b)$$

$$\frac{\partial M}{\partial x} - H = 0 \quad (10A-5c)$$

We have further

$$p = \rho_s g y \quad (10A-6)$$

and for the relation between stress and strain

$$\frac{\partial^2 y}{\partial x^2} = \frac{M}{f} \quad (10A-7a)$$

$$\text{with } f = \frac{m^2 ET^3}{12(m^2 - 1)} \quad (10A-7b)$$

where  $E$  is Young's modulus for the crust and  $m$  is Poisson's constant.

Introducing (10A-7a) into (10A-5c), we obtain

$$H = f \frac{\partial^3 y}{\partial x^3} \quad (10A-8a)$$

and applying this to (10A-5b), we have

$$\frac{\partial D}{\partial x} = f \left( \frac{1}{R} + \frac{\partial^2 y}{\partial x^2} \right) \frac{\partial^3 y}{\partial x^3}$$

Integrating,

$$D = \frac{1}{2} f \left( \frac{\partial^2 y}{\partial x^2} \right)^2 + \frac{f}{R} \frac{\partial^2 y}{\partial x^2} + D_0 \quad (10A-8b)$$

where  $D_0$  is the compression for  $y = 0$ , i.e., for the undeformed crust. We can neglect the first term.

Introducing (10A-6), (10A-8a), and (10A-8b) into (10A-5a) and again neglecting  $(\partial^2 y / \partial x^2)^2$ , we obtain the equation for  $y$

$$\frac{\partial^4 y}{\partial x^4} + \left( \frac{D_0}{f} + \frac{1}{R^2} \right) \frac{\partial^2 y}{\partial x^2} + \frac{D_0}{fR} + \frac{\rho_s g}{f} y = 0 \quad (10A-9)$$

We shall see that  $1/R^2$  is only 1/20,000 part of  $D_0/f$ , and so we can neglect it between the parentheses of the second term. We can eliminate the

constant term of this equation by introducing

$$z = y + \frac{D_0}{\rho_s g R} \quad (10A-10a)$$

and we obtain

$$\frac{\partial^4 z}{\partial x^4} + \frac{D_0}{f} \frac{\partial^2 z}{\partial x^2} + \frac{\rho_s g}{f} z = 0 \quad (10A-10b)$$

$z$  is the subsidence of the crust with respect to the position given by the term  $-D_0/\rho_s g R$  of Formula (10A-1); as  $c_\sigma$  represents a rising, its sign is negative here.

The solution of (10A-10) can easily be given. For simplifying the formulas we introduce a length  $l$  given by

$$l = \sqrt[4]{\frac{f}{\rho_s g}} = \sqrt[4]{\frac{m^2 ET^3}{12(m^2 - 1)\rho_s g}} \quad (10A-11a)$$

and a force  $D_b$  defined by

$$D_b = 2\rho_s g l^2 = \sqrt{\frac{m^2 ET^3 \rho_s g}{3(m^2 - 1)}} \quad (10A-11b)$$

Equation (10A-10b) becomes

$$l^4 \frac{\partial^4 z}{\partial x^4} + 2 \frac{D_0}{D_b} l^2 \frac{\partial^2 z}{\partial x^2} + z = 0 \quad (10A-11c)$$

If  $D_0 = D_b$ , the solution is simple; we find

$$z = a \cos \frac{x}{l} \quad (10A-12a)$$

in which  $a$  is an arbitrary integration constant, and so the compression  $D_b$  can cause a wave deformation of the crust of an amplitude which may increase indefinitely. It is clear, therefore, that  $D_b$  represents the buckling limit of the crust. As

$$\frac{D_b}{f} = 2 \frac{\rho_s g}{f} l^2 = \frac{2}{l^2}$$

and as  $l$  will prove to be of the order of  $\frac{1}{100}$  part of the earth's radius  $R$ , we thus find confirmation in the fact that  $1/R^2$  in the second term of Eq. (10A-9) is of the order of  $1/20,000$  part of the term  $D_0/f$ .

From (10A-11b) we find that the buckling stress  $\sigma_b$  is

$$\sigma_b = \frac{D_b}{T} = \sqrt{\frac{m^2 ET \rho_s g}{3(m^2 - 1)}} \quad (10A-12b)$$

and for the half wavelength  $L$  we find

$$L = \pi l = \pi \sqrt[4]{\frac{m^2 ET^3}{12(m^2 - 1)\rho_s g}} \quad (10A-12c)$$

For the values  $E = 10^{12}$  dynes/cm<sup>2</sup>,  $m = 4.1$ ,\*  $T = 35$  km (thickness of the rigid crust), and  $\rho_s = 3.27$ , we obtain

$$\begin{aligned} \sigma_b &= 63.2 \times 10^9 \text{ dynes/cm}^2 \\ L &= 185 \text{ km} \end{aligned} \quad (10A-13a)$$

When the whole phenomenon takes place under water, we must introduce a value for  $\rho_s$  of  $3.27 - 1.028 = 2.242$ , and we find

$$\begin{aligned} \sigma_b &= 52.3 \times 10^9 \text{ dynes/cm}^2 \\ L &= 203 \text{ km} \end{aligned} \quad (10A-13b)$$

In both cases the stress is far above the elastic limit of the crust, and so elastic buckling seems out of the question. This result was found by Smoluchowski<sup>16</sup> as early as 1909. He suggested that elastic buckling might perhaps still be possible if the crust consisted of different layers which could slip over each other without too much friction. If we suppose this friction to be entirely negligible, and if we assume a crust of  $n$  layers of equal thickness having densities increasing regularly downward by the same amount at each interface and capable of buckling more or less independently of each other, we can apply Formula (10A-12b) with values for  $T$  and for  $\rho_s$  which are each  $n$  times smaller, and so we find a buckling stress which is also  $n$  times smaller. Bringing down the values obtained for  $\sigma_b$  to figures of about  $2 \times 10^9$  dynes/cm<sup>2</sup> (which may still be too high) would require about 30 different layers sliding without friction over each other. Since this seems impossible, it does not appear to be a way out of the difficulty.

Another line has been proposed by Griggs,<sup>7</sup> who suggests the possibility of a downbulging of the crust caused by the sucking action of a descending column of a convection current, the current at the same time causing compression in the crust. This explanation obviously implies a phenomenon other than the elastic buckling dealt with here. Since we shall see in Part C of this chapter that such local convection currents do not seem to fit the data and conditions in the areas where narrow belts of negative gravity anomalies indicate the probability of buckling phenomena, we shall not deal with phenomena of the kind suggested by Griggs in this or the following section.

\* B. Gutenberg, Internal constitution of the earth, 2nd ed., pp. 64, 70, 1951.

A third way out of the difficulty is to assume plastic buckling of the crust by lateral compression above the elastic stress limit. We shall deal with this supposition in the next section, and in Part C we shall see that it seems to be in harmony with the data in the areas mentioned.

Returning to our equation (10A-11c) for elastic deformation of the crust, we shall now treat of its general solution when  $D_0$  has an arbitrary value. Since  $D_0$  can never be greater than the buckling value  $D_b$ , we can introduce an angle  $\beta$  given by

$$\frac{D_0}{D_b} = \cos 2\beta \quad (10A-14a)$$

$\beta$  can obviously vary from  $45^\circ$ , for  $D_0 = 0$ , to  $0^\circ$ , for  $D_0 = D_b$ . If we assume  $D_0$  to be below the elastic limit, we can suppose  $D_0$  to be less than  $0.035D_b$ , and so  $45^\circ > \beta > 44^\circ$ .

The solution of (10A-11c) is

$$z = Ae^{-(x/l) \sin \beta} \cos\left(\frac{x}{l} \cos \beta + \varphi\right) + A'e^{(x/l) \sin \beta} \cos\left(\frac{x}{l} \cos \beta + \varphi'\right) \quad (10A-14b)$$

in which  $A$ ,  $A'$ ,  $\varphi$ , and  $\varphi'$  are integration constants.

For  $D_0 < 0.035D_b$  we can introduce the mean value for  $\beta$  of  $44^\circ 30'$  and thus find with sufficient approximation that

$$z = Ae^{-0.700(x/l)} \cos\left(0.713\frac{x}{l} + \varphi\right) + A'e^{0.700(x/l)} \cos\left(0.713\frac{x}{l} + \varphi'\right) \quad (10A-14c)$$

The first terms of these formulas represent a wave dying out for increasing  $x$  and the second terms a wave increasing with  $x$ . These deformations are obviously caused by outward forces working on the crust in addition to the compression  $D_0$ , and evidently we must choose the constants  $A$  and  $A'$  in such a way that the waves decrease on both sides of the outward forces responsible for them.

We see that, as long as the compression  $D_0$  remains below the limit of elasticity, the effect of  $D_0$  is practically negligible; when  $D_0 = 0$ , we get

$$z = Ae^{-0.707(x/l)} \cos\left(0.707\frac{x}{l} + \varphi\right) + A'e^{0.707(x/l)} \cos\left(0.707\frac{x}{l} + \varphi'\right) \quad (10A-14d)$$

which is nearly identical to (10A-14c).

Starting with the case in which the outward forces work only in one cross section of the crust, we choose the origin of the  $x$  coordinate in that

cross section and get a formula for  $z$  with only one term on each side; for positive values of  $x$  the constant  $A'$  is zero, and for negative values of  $x$  the constant  $A$  is zero. The solution of more complicated cases, in which forces are at work in more than one cross section, can be built up by adding several of the simpler solutions together; as Eq. (10A-11c) is linear, this is allowable.

To introduce the boundary conditions for  $x = 0$ , and possibly also for other values of  $x$ , we can use the following set of formulas

$$z = A e^{-(x/l) \sin \beta} \cos \left( \frac{x}{l} \cos \beta + \varphi \right) \quad (10A-15a)$$

$$\frac{\partial z}{\partial x} = -\frac{A}{l} e^{-(x/l) \sin \beta} \sin \left( \frac{x}{l} \cos \beta + \varphi + \beta \right) \quad (10A-15b)$$

$$\frac{\partial^2 z}{\partial x^2} = -\frac{A}{l^2} e^{-(x/l) \sin \beta} \cos \left( \frac{x}{l} \cos \beta + \varphi + 2\beta \right) \quad (10A-15c)$$

$$\frac{\partial^3 z}{\partial x^3} = \frac{A}{l^3} e^{-(x/l) \sin \beta} \sin \left( \frac{x}{l} \cos \beta + \varphi + 3\beta \right) \quad (10A-15d)$$

combined with (10A-15e) and (10A-15f), which are derived from (10A-7a), (10A-8a), (10A-10a), and (10A-11a):

$$M = f \frac{\partial^2 z}{\partial x^2} = \rho_s g l^4 \frac{\partial^2 z}{\partial x^2} \quad (10A-15e)$$

$$H = f \frac{\partial^3 z}{\partial x^3} = \rho_s g l^4 \frac{\partial^3 z}{\partial x^3} \quad (10A-15f)$$

For  $\beta$  we can introduce a value of  $45^\circ$  (or somewhat less if we have reason to suspect the presence of lateral compression).

By means of these formulas we shall derive the solution of a few two-dimensional geophysical problems. First we shall study the crustal deformations caused by a vertical load  $P$ , positive or negative. We have met this problem before (Sec. 6-6) when dealing with two-dimensional regional isostatic reductions. It may be present where there are steep river valleys, e.g., the Grand Canyon and the upper Rhone Valley, or where there is sedimentation along continental coasts or loading of the crust by volcanic ranges along a crustal fault plane. We shall assume that the crust remains unbroken. We thus have the following two conditions for determining the two integration constants  $A$  and  $\varphi$  in (10A-15a). They both apply with respect to the point  $x = 0$ , which we shall indicate by the subindex 0.

Since the crust is unbroken, we get

$$\left( \frac{\partial z}{\partial x} \right)_0 = 0 \quad (10A-16a)$$

and so, because of (10A-15b), we have

$$\varphi = -\beta \quad (10A-16b)$$

The load  $P$  is carried by both the left and right halves of the crust, and so, because of (10A-15f), we have

$$\frac{\partial^3 z}{\partial x^3} = \frac{P}{2\rho_s gl^4} \quad (10A-17a)$$

Therefore (10A-15d) gives for  $x = 0$

$$A = \frac{P}{2\rho_s gl} \csc 2\beta \quad (10A-17b)$$

We thus obtain

$$z = \frac{P}{2\rho_s gl} \csc 2\beta e^{-(x/l) \sin \beta} \cos \left( \frac{x}{l} \cos \beta - \beta \right) \quad (10A-18a)$$

and for compression  $D_0$  below the limit of elasticity (thus  $\beta = 45^\circ$  or very near to it) we get

$$z = \frac{P}{2\rho_s gl} e^{-0.707(x/l)} \cos \left( 0.707 \frac{x}{l} - 45^\circ \right) \quad (10A-18b)$$

Figure 10A-3 gives the curve of the crustal deformation with a twentyfold exaggeration of the vertical ordinates.

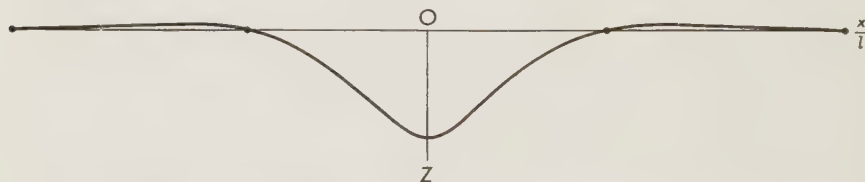


FIG. 10A-3. Deformation of floating earth crust under concentrated vertical load; vertical ordinates exaggerated twentyfold.

The second problem concerns the effect on a broken crust of a vertical load  $P$  working at the end of one half of it; the condition is, therefore, that no moment is working there on the crust. This problem is probably present where there are tilted fault planes through the crust, which is likely, for example, in the crustal parts adjoining a graben. We shall deal with these features in Part D of this chapter. The problem may also be

present in side areas of island arcs, where the main movement in the mobile belt is a sliding along a nearly vertical fault plane but where there is also a smaller component of movement of the thrust-faulting kind. We shall investigate these problems in Part C of this chapter.

For  $x = 0$  we now have the condition that the moment is zero, and so, according to (10A-15e), we obtain

$$\left( \frac{\partial^2 z}{\partial x^2} \right)_0 = 0 \quad (10A-19a)$$

and, because of (10A-15c),

$$\varphi = 90^\circ - 2\beta \quad (10A-19b)$$

The load  $P$  introduced in (10A-15f) gives

$$\left( \frac{\partial^3 z}{\partial x^3} \right)_0 = \frac{P}{\rho_s g l^4} \quad (10A-20a)$$

and using (10A-15d), for  $x = 0$  we derive

$$A = \frac{P}{\rho_s g l} \sec \beta \quad (10A-20b)$$

We thus obtain

$$z = - \frac{P}{\rho_s g l} \sec \beta e^{-(x/l) \sin \beta} \sin \left( \frac{x}{l} \cos \beta - 2\beta \right) \quad (10A-21a)$$

For  $D_0$  zero or relatively small we can introduce  $\beta = 45^\circ$  and find

$$z = 1.415 \frac{P}{\rho_s g l} e^{-0.707(x/l)} \cos \left( 0.707 \frac{x}{l} \right) \quad (10A-21b)$$

The curve thus obtained for the deformed crust is represented by Fig. 10A-4; the vertical ordinates are exaggerated twenty times.

The third problem is that of the deformation of the right half of the crust broken at  $O$  (again the left half is symmetrical to it) which is subjected to an upward force at  $O$ , the tilt of the crust there resulting from the phenomenon taking place at  $O$ . A probable example occurs in the crustal parts adjoining the deformed belt in Indonesia, which is marked by strong negative gravity anomalies and by tectonic activity.

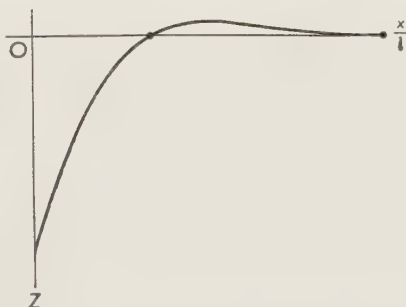


FIG. 10A-4. Deformation of floating earth crust broken at  $O$  and vertically loaded there; vertical ordinates exaggerated twentyfold.

We shall deal with it in Part C of this chapter. The tendency toward isostatic balance provides the upward force  $P$ , and the deformation is likely to impart a tilt to the adjoining crust on both sides of the belt. We shall want to study somewhat larger deformations, which probably are partly accompanied by plastic strain (see Sec. 10A-4).

We have now

$$P = -2H - 2D_0 \left( \frac{\partial z}{\partial x} \right)_0 = -2\rho_s gl^4 \left( \frac{\partial^3 z}{\partial x^3} \right)_0 - 4\rho_s gl^2 \cos 2\beta \left( \frac{\partial z}{\partial x} \right)_0 \quad (10A-22a)$$

and introducing (10A-15b) and (10A-15d)

$$P = 2\rho_s gl A \sin (\varphi - \beta) \quad (10A-22b)$$

The second condition concerns the tilt  $(\partial z / \partial x)_0$ , which is presumed known,

$$\left( \frac{\partial z}{\partial x} \right)_0 = -\frac{A}{l} \sin (\varphi + \beta) \quad (10A-23)$$

From (10A-22b) and (10A-23) we can derive  $A$  and  $\varphi$ . We find

$$\tan \varphi = \frac{-(P/2\rho_s gl^2) + (\partial z / \partial x)_0}{(P/2\rho_s gl^2) + (\partial z / \partial x)_0} \tan \beta$$

$$\text{and } A = \frac{P}{2\rho_s gl} \csc (\varphi - \beta) \quad (10A-24a)$$

$$\text{and so } z = \frac{P}{2\rho_s gl} \csc (\varphi - \beta) e^{-(x/l) \sin \beta} \cos \left( \frac{x}{l} \cos \beta + \varphi \right) \quad (10A-24b)$$

which, together with (10A-24a), gives the complete solution.

For  $(\partial z / \partial x)_0 = 0$  we have  $\varphi = -\beta$  and, as we might expect, we again get the solution for the first case, which is represented by Fig. 10A-3; the bending is now upward because  $P$  works in that sense.

When

$$\left( \frac{\partial z}{\partial x} \right)_0 = -\frac{P}{2\rho_s gl^2} \quad (10A-25a)$$

we find

$$\varphi = 90^\circ$$

and so we obtain

$$z = -\frac{P}{2\rho_s gl} \sec \beta e^{-(x/l) \sin \beta} \sin \left( \frac{x}{l} \cos \beta \right) \quad (10A-25b)$$

For not too large values of the compression  $D_0$  ( $\beta$  therefore about equal to  $45^\circ$ ) we get

$$z = -0.707 \frac{P}{\rho_s g l} e^{-0.707(x/l)} \sin \left( 0.707 \frac{x}{l} \right) \quad (10A-25c)$$

For  $\left( \frac{\partial z}{\partial x} \right)_0 = -\frac{P}{\rho_s g l^2}$  (10A-26a)

we obtain

$$\tan \varphi = 3 \tan \beta \quad (10A-26b)$$

and so for not too large compression  $D_0$  and  $\beta$  about equal to  $45^\circ$  we get

$$\tan \varphi = 3$$

$$\varphi = 71^\circ 34' \quad (10A-27a)$$

and so

$$z = 1.118 \frac{P}{\rho_s g l} e^{-0.707(x/l)} \cos \left( 0.707 \frac{x}{l} + 71^\circ 34' \right) \quad (10A-27b)$$

This solution is represented by Fig. 10A-5.

This curve is discussed in Part C of this chapter, dealing with island-arc areas, especially Indonesia. It can be pointed out here that the maximum

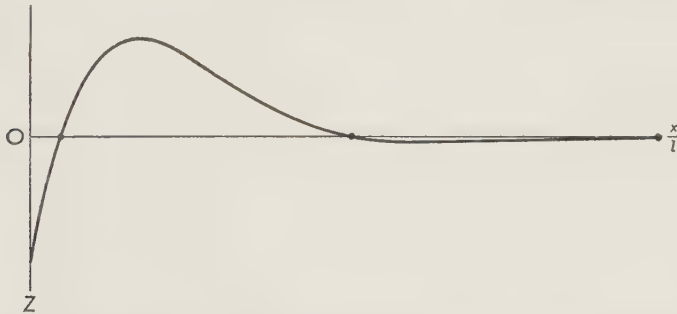


FIG. 10A-5. Deformation of floating earth crust broken at  $O$ , where crustal tilt is given by phenomenon. Crust subject to upward force at  $O$ . Only the right half is represented; vertical ordinate exaggerated twentyfold; the left half is symmetrical.

uplift of the crust occurs for a value of  $x$  of about  $1.6l$ . Since the phenomenon probably occurs under water, and since (10A-13b) gives for that case a value for  $L$  of 203 km and therefore for  $l$  of 65 km, it follows that the maximum positive gravity anomaly, accompanying the belt of strong negative anomalies on both sides, must be expected at a distance of more than 110 km outside the strongly deformed belt. This conclusion checks well with the map of the gravity anomalies in Indonesia and appears to confirm our elastic-wave theory of the earth's crust. Parts C and D of this chapter

will provide more confirmation, e.g., curves of the sea-bottom profiles which show the crustal bending directly, and further confirmation is found in the results for the degree of regionality of the isostatic reduction derived from gravity results in the areas of volcanic islands and in the Indonesian Archipelago. The values found for  $R$  of 174.3 to 232.4 km correspond to figures for  $l$  of 60 to 80 km, which check well with the values for  $l$  derived here of 60 and 65 km for continental and oceanic areas, respectively [Formulas (10A-13a) and (10A-13b)].

#### 10A-4. Plastic Deformation of the Crust by Horizontal Compression

In the preceding section it was shown that the downward buckling of the crust suggested by the belts of strong negative gravity anomalies and other phenomena in the tectonically active parts of island-arc areas cannot, even at the beginning, be of the purely elastic type; the buckling stress of an elastic crust about 35 km thick is more than twenty times the limit of elasticity. Another objection to assuming elastic buckling is that there are several reasons for believing that, although the subcrustal layer obviously is liable to flow, as is demonstrated, for example, by readjustments of isostatic equilibrium, it also has a limit of elasticity, probably of the order of about  $10 \text{ kg/cm}^2$ . Since the stress differences must exceed this limit before flow can set in, elastic buckling could not originate as a consequence of a small deviation from the crustal equilibrium position.

We shall see that plastic deformation can also lead to a downward buckling of the crust and that it is not open to the objection just mentioned. Long ago Bijlaard<sup>3,4</sup> suggested this possibility (in connection with the following treatment of the problem the reader is referred to Bijlaard's papers on the subject, especially those of 1935 and 1936). One of the views he brings forward is that elastic buckling can occur only at right angles to the compression while plastic buckling can occur at other angles, a fact which may explain the formation of arcs or more complicated patterns of the tectonic axis in areas where orogeny has occurred or is still taking place; such patterns are difficult to understand if elastic buckling is assumed. This question is taken up in Sec. 10A-7 and again in Part C of this chapter.

We can conclude that the supposition of elastic deformation at the start of the phenomenon presents several difficulties which can be avoided by assuming that from the beginning the deformation has a plastic character. We assume that in a belt of breadth  $2b$  the compression exceeds the elastic limit  $\sigma_l$  of the crust and causes a thickening  $h$  of the crust which disappears toward the edges of the belt. The thickening must proceed very slowly, probably not more than a few millimeters per year or even less; it obviously depends on the coefficient of apparent viscosity of the crustal rocks for stresses above their limit of elasticity. We do not know this coefficient, but we do know that it is considerably larger than the coefficient for

the suberustal matter, which (in Part B of this chapter) we shall find to be about  $0.7 \times 10^{22}$  to  $10^{22}$ ; for the crust we shall assume a mean value of  $10^{23}$ , but it might be half or twice that value.

Under these circumstances we can probably neglect the viscous resistance of the substratum to the development of the bulge at the lower boundary of the crust, and so we can expect the isostatic readjustment of the crust's equilibrium to keep pace with the crust's deformation, at least after the small elastic limit of the subcrustal layer has been exceeded. Since the difference  $\rho_s - \rho$  of the densities of the substratum and the surface rocks

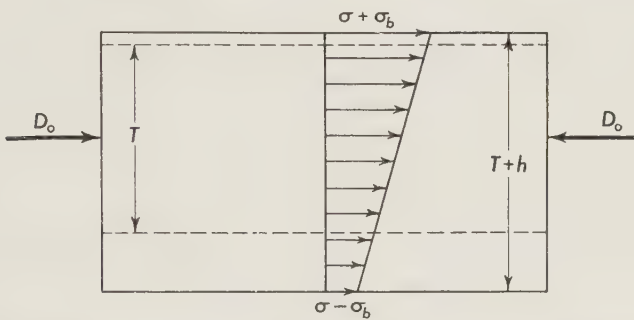


FIG. 10A-6. Floating earth crust thickened by uniaxial horizontal compression. Graph of horizontal compressive stress.

is much smaller than the density of the surface rocks  $\rho$  (usually the values  $\rho_s - \rho = 0.6$  and  $\rho = 2.67$  have been adopted), such a readjustment must mean a sinking of the crust, and we can therefore assume that the crustal thickening causes a larger bulge at the lower crustal boundary than at the surface.

As Fig. 10A-6 shows, this inequality causes an asymmetry of the crustal cross section with respect to the resultant  $D_0 = \sigma(T + h)$  of the compressional stresses, of which the mean value is indicated by  $\sigma$ , and so the stress at the surface of this section must be larger than at the base. If this difference is denoted by  $2\sigma_b$ , the stresses at the borders are  $\sigma + \sigma_b$  and  $\sigma - \sigma_b$ . The difference of stress must bring about a greater shortening at the surface of the crust than at the lower boundary, and so there is a further downbending; a geosyncline is formed. As this downbending increases the asymmetry of the crustal cross section with respect to the compressional resultant  $D_0$ , this process has an accelerating character. This phenomenon may eventually lead to crustal downbuckling accompanied by strong crustal shortening. The importance of these phenomena for geology and geophysics makes it desirable to elaborate the equations governing them.

We must, therefore, attack the difficult problem of combined elastic and plastic deformations. Before taking up the general equations, we have to

adopt a formula for the stress-strain relation in the plastic thickening and in the bending of the crust.

In accordance with Sec. 2-4 [Formula (2-13)], we shall assume all the constituents of the strain deviator  $D_d$  to consist, in the same ratio, of an elastic and a pseudo-viscous part. As this formula shows, the elastic parts are assumed to be proportional to the constituents of the stress deviator, and the differentials with respect to time of the pseudo-viscous parts are assumed to be proportional to the constituents of the stress deviator  $S_d$  minus those of the elastic-limit stress deviator  $(S_d)_l$  (supposed to have the same ratio of the constituents), according to the von Mises limit

$$D_d = \frac{1}{2\mu} S_d + (1 - \psi) \int_0^t \frac{1}{2\eta} S_d dt \quad (2-13)$$

in which  $\psi$  is a scalar given by

$$(S_d)_l = \psi S_d$$

For the crustal thickening we can omit the elastic part because it is small, and we can assume that the rigid crust on both sides of the plastic belt—which determines the position of the compressive-stress resultant  $D_0$ —is subject to nearly the same elastic deformation. So for the plastic thickening  $h$  we obtain

$$h = \int_0^t \frac{\sigma - \sigma_l}{2\eta} T dt \quad (10A-28a)$$

and, if we assume that, since  $t = 0$ ,  $\sigma - \sigma_l$  has been constant,

$$h = \frac{\sigma - \sigma_l}{2\eta} T t \quad (10A-28b)$$

For the values  $\sigma - \sigma_l = 200$  kg/cm<sup>2</sup>,  $T = 35$  km, and  $\eta = 10^{23}$  this gives a thickening of 1 mm/year, which seems an acceptable value.

For the bending we cannot omit the elastic deformation, as it plays its part in the beginning of the phenomenon. If we denote the difference in compressive strain at the crust's surface and lower boundary by  $2s_b$ , we have

$$s_b = \frac{\sigma_b}{E} + \int_0^t \frac{\sigma_b}{2\eta} dt \quad (10A-29a)$$

In this formula we have supposed that

$$\begin{aligned} \sigma_b &< \sigma - \sigma_l \\ \text{and so} \quad \sigma_l &< \sigma - \sigma_b \end{aligned} \quad (10A-29b)$$

As  $\sigma - \sigma_b$  is the smallest value of the compressive stress in the cross section, this condition implies that the deformation continues to be of the plastic

type everywhere. Wherever the bending exceeds the limit corresponding to this condition, the stresses in that part of the cross section are below the elastic limit, and only elastic deformations occur there. We shall avoid this complication by supposing the bending to be below this limit.

For integrating (10A-29a) we shall suppose that, since  $t = 0$ , the deformation has increased proportionally to  $t^n$ . By doing so and by choosing  $n$  in the right way we can represent different degrees of acceleration of the bending phenomenon reasonably well. We thus obtain

$$s_b = \frac{\sigma_b}{E} + \frac{\sigma_b t}{2(n+1)\eta} \quad (10A-30)$$

As the moment  $M$  in the crust corresponding to a value of  $\sigma_b$  is found by multiplying  $\sigma_b$  by  $\frac{1}{6}(T+h)^2$ , and as

$$s_b = \frac{1}{2}(T+h) \frac{d^2z}{dx^2}$$

where  $x$  is the horizontal coordinate and  $z$  the vertical one, positive downward, we find

$$\frac{d^2z}{dx^2} = \frac{12}{(T+h)^3} \left[ \frac{M}{E} + \frac{Mt}{2(n+1)\eta} \right]$$

If we take into account the lateral contraction given by Poisson's constant  $m$ , and if we realize that the whole phenomenon is two-dimensional and that the third dimension of the crust may be considered to be infinite, we have to add a factor  $(m^2 - 1)/m^2$ . As  $m$  may be estimated at 4.1 for the elastic deformation of the crustal rocks, and as it equals 2 for all viscous flow, we obtain

$$\begin{aligned} \frac{d^2z}{dx^2} &= \frac{12}{(T+h)^3} \left[ \frac{(m^2 - 1)M}{m^2 E} + \frac{3Mt}{8(n+1)\eta} \right] \\ &= \frac{11.28M}{(T+h)^3} \left[ \frac{1}{E} + 0.40 \frac{t}{(n+1)\eta} \right] \end{aligned} \quad (10A-31)$$

For  $E = 10^{12}$  dynes/cm<sup>2</sup> and  $\eta = 10^{23}$  poises we find that the viscous term equals the elastic term after a time interval given by

$$t_y = 8000(n+1) \text{ years} \quad (10A-32)$$

After this time the viscous term increasingly dominates, and so we can conclude that in geological periods the viscous deformation is by far the most important. The elastic term gradually becomes negligible as compared with the viscous term.

We now turn to the derivation of the equations for the deformation of the earth's crust. They are similar to those derived in Sec. 10A-3 for purely elastic deformation. In addition to the general compression by the horizontal force  $D_0 = (T + h)\sigma$ , there is not only the vertical reaction by the substratum of  $\rho_s g z$  per surface unit but also the effect of the crustal thickening  $h$ . Since without further crustal deformation this gives equal bulges of  $\frac{1}{2}h$  at the surface and at the lower boundary, the loading is given by  $(\rho_c - \frac{1}{2}\rho_s)gh$ , where  $\rho_c$  is the mean density of the crust. There may also be sedimentation, erosion, or a loading by water. If we suppose the undeformed crust's surface to have been situated at sea level, and if we assume that sedimentation and erosion continue to keep the surface at that level, we get a loading of  $(z - \frac{1}{2}h)\rho'g$ , where  $\rho'$  may have several meanings, viz., the density of water, of sediments, or of the surface layer of the crust; if the sedimentation or erosion is less than assumed, the effect is smaller, and we have to introduce a correspondingly smaller value for  $\rho'$ .

Together we get a loading per surface unit of the crust of

$$p = \rho'_s g z - (\rho_c - \frac{1}{2}\rho''_s)gh \quad (10A-33)$$

where  $\rho'_s = \rho_s - \rho'$  and  $\rho''_s = \rho_s + \rho'$

The sign of  $p$  is chosen positive upward. According to (10A-28),  $h$  increases with the time  $t$ ; it is also a function of the coordinate  $x$ .

As we shall assume the subcrustal density  $\rho_s$  to be 3.27, the density  $\rho'_s$  varies from 3.27 to 0.6 and  $\rho''_s$  varies from 3.27 to 5.94. For the oceans we may make the supposition that the whole crustal deformation occurs under water, and then  $\rho'_s$  varies from  $3.27 - 1.028 = 2.242$  to  $3.27 - 2.60 = 0.67$ ; the value 2.60 represents here the estimated maximum density of submarine sediments. In the same way we get for  $\rho''_s$  a variation from  $3.27 + 1.028 = 4.298$  to  $3.27 + 2.60 = 5.87$ .

To find the mean density  $\rho_c$  of the continental parts of the crust we must make a supposition about their constitution. If we assume a granitic and a basaltic layer of equal thickness, or if we assume a gradual change of constitution and density from granite at the surface to basalt at the bottom, we obtain

$$\text{For continents } \rho_c = \frac{1}{2}(2.67 + 3.00) = 2.835 \quad (10A-33a)$$

If we assume an oceanic crust with a mean density of 2.97 in the upper 10 per cent of its thickness and with subcrustal matter in the lower 90 per cent of density 3.27, we get

$$\text{For oceans } \rho_c = 3.24 \quad (10A-33b)$$

To derive the equation for the crustal deformation we can make use of Formulas (10A-5) to (10A-10) and Fig. 10A-2. For  $p$  we must introduce

the value given by (10A-33), and for the quantity  $f$  in Formula (10A-7a), which defines the stress-strain relation, we must use the value given by Formula (10A-31), which provides us with

$$\frac{1}{f} = \frac{11.28}{(T+h)^3} \left[ \frac{1}{E} + 0.40 \frac{t}{(n+1)\eta} \right] \quad (10A-34)$$

The introduction of Formula (10A-33) for  $p$  brings Eq. (10A-10b) into the form

$$\frac{\partial^4 z}{\partial x^4} + \frac{\sigma(T+h)}{f} \frac{\partial^2 z}{\partial x^2} + \frac{\rho'_s g}{f} z - (\rho_c - \frac{1}{2}\rho''_s) \frac{gh}{f} = 0 \quad (10A-35)$$

Before we can undertake its solution, we still have to define the way in which the crustal thickening  $h$  changes with  $x$ . We shall suppose that this variation is caused by a slightly smaller value of the elastic limit  $\sigma_l$  of the crustal matter in the plastic belt. For this belt we shall assume a value of  $h$  given by

$$h = \frac{1}{2}h_0 \left( 1 + \cos \pi \frac{x}{b} \right) \quad (10A-36)$$

with 
$$h = \frac{\sigma - \sigma_l}{2\eta} Tt \quad \text{and} \quad h_0 = \frac{(\sigma - \sigma_l)_0}{2\eta} Tt$$

in which the subindex 0 refers to the point  $x = 0$ . Outside the belt  $2b$  we assume  $h$  to be zero.

To solve (10A-35) combined with (10A-36) we can introduce

$$z = \frac{1}{2}ch_0 \left( 1 + \alpha \cos \pi \frac{x}{b} \right) + \xi \quad (10A-37a)$$

with 
$$c = \frac{\rho_c - \frac{1}{2}\rho''_s}{\rho'_s}$$

and we find that  $\xi$  has to satisfy Eq. (10A-35) without the last term and that  $\alpha$  is a constant given by

$$\alpha = \frac{1}{1 + L^4/b^4 - 2(L^2/b^2)(\sigma/\sigma_b)} \quad (10A-37b)$$

where  $L$  and  $\sigma_b$  mean the half wavelength and the buckling limit of the crust, as in Formulas (10A-12c) and (10A-12b), respectively, for the case

of purely elastic deformation. New formulas for them are found by introducing the value of  $1/f$  from Formula (10A-34):

$$L = 1.715 \sqrt[4]{\frac{(T+h)^3 E}{\rho'_s g \{1 + 0.40[tE/(n+1)\eta]\}}} \quad (10A-37c)$$

$$\sigma_b = 0.596 \sqrt{\frac{\rho'_s g (T+h) E}{1 + 0.40[tE/(n+1)\eta]}} \quad (10A-37d)$$

The value of  $\sigma_b$  represents the compressive stress which, working during a time  $t$ , causes buckling of a crustal belt of breadth  $L$  with frictionless hinges at both ends.

We must introduce into these formulas a value for  $h$  corresponding to the time  $t$  which is between the value,  $h_0$ , of  $h$  in the middle of the plastic belt and its mean value. Since the latter, according to Formula (10A-36), is  $\frac{1}{2}h_0$ , we shall put  $h = 0.8h_0$ .

The equation for  $\xi$ ,

$$\frac{\partial^4 \xi}{\partial x^4} + \frac{\sigma(T+h)}{f} \frac{\partial^2 \xi}{\partial x^2} + \frac{\rho'_s g}{f} \xi = 0 \quad (10A-38)$$

has the same form as Eq. (10A-11c) for the elastic deformation, and thus it is also the equation for  $z$  outside the belt, where we suppose that the deformation remains elastic. The solution of (10A-38) is identical with that of (10A-11c), and we shall again introduce the angle  $\beta$  given by

$$\frac{\sigma}{\sigma_b} = \cos 2\beta \quad (10A-14a)$$

We thus obtain the following solution of  $z$  for the belt  $2b$  and of  $z'$  and  $z''$  for the adjoining crustal parts to the left and right respectively. In the equations for  $z'$  and  $z''$  we place the primes on the other quantities as well; we suppose  $\sigma \leq \sigma_b$  for all three equations.

$$\begin{aligned} z &= A e^{\pi(x/L) \sin \beta} \cos \left( \pi \frac{x}{L} \cos \beta + \varphi_a \right) \\ &+ B e^{-\pi(x/L) \sin \beta} \cos \left( \pi \frac{x}{L} \cos \beta + \varphi_b \right) \\ &+ \frac{1}{2} c h_0 \left( 1 + \alpha \cos \pi \frac{x}{b} \right) \end{aligned} \quad (10A-39a)$$

$$z' = A'e^{-\pi(x/L') \sin \beta'} \cos \left( \pi \frac{x}{L'} \cos \beta' + \varphi' \right) \quad (10A-39b)$$

$$z'' = A''e^{\pi(x/L'') \sin \beta''} \cos \left( -\pi \frac{x}{L''} \cos \beta'' + \varphi'' \right) \quad (10A-39c)$$

in which  $A$ ,  $B$ ,  $A'$ ,  $A''$ ,  $\varphi_a$ ,  $\varphi_b$ ,  $\varphi'$ , and  $\varphi''$  are eight integration constants which are necessary and sufficient for ensuring that  $z$ ,  $\partial z/\partial x$ , the moment  $M$ , and the resultant shear  $H$  in cross sections are continuous in the transitions between the three parts. According to Formulas (10A-15e) and (10A-15f), the values of  $M$  and  $H$  are proportional to  $L^4(\partial^2 z/\partial x^2)$  and  $L^4(\partial^3 z/\partial x^3)$ , respectively. In each of Formulas (10A-39)  $x$  is measured from the same point in the middle of the plastic belt and is positive to the right.

This solution is valid for  $\sigma \leq \sigma_b$ . We shall see, however, that the conditions of the problem imply that for the plastic belt 2*b* values of  $\sigma > \sigma_b$  can also occur, but the elastic reaction of the areas on both sides prevents instantaneous buckling. To investigate the problem when  $\sigma > \sigma_b$  we need the formulas for  $\sigma > \sigma_b$  in the plastic belt. Putting

$$\frac{\sigma_b}{\sigma} = \sin 2\gamma \quad (10A-40a)$$

we find, for the plastic belt,

$$\begin{aligned} z = A \cos \left( \pi \sqrt{\tan \gamma} \frac{x}{b} + \varphi_a \right) + B \cos \left( \pi \sqrt{\cot \gamma} \frac{x}{b} + \varphi_b \right) \\ + \frac{1}{2} ch_0 \left( 1 + \alpha \cos \pi \frac{x}{b} \right) \quad (10A-40b) \end{aligned}$$

For the adjoining elastic areas Formulas (10A-39b) and (10A-39c) remain valid. We have to make the same adjustments in the conditions prevailing in the transition cross sections by means of the eight integration constants  $A$ ,  $B$ ,  $A'$ ,  $A''$ ,  $\varphi_a$ ,  $\varphi_b$ ,  $\varphi'$ , and  $\varphi''$ . The angle  $\gamma$  decreases with time from its value of  $45^\circ$  for  $\sigma = \sigma_b$ .

Before discussing these solutions, we must emphasize their limitations. To avoid the complications we should otherwise have to cope with we have dealt rather sketchily with the way the phenomenon changes with time, taking it into account only in the suppositions leading to Formulas (10A-28b), for the thickening  $h$ , and (10A-30), for the strain  $s_b$  caused by the bending. We cannot expect our solutions, therefore, to represent the shape assumed by the crust during more than a short period of the phenomenon. The half wavelength  $L$  is, for example, not constant, as it depends on  $t$  and on  $h$ , which is proportional to  $t$ . So the development of the

crustal deformation over a longer period must be complicated, as in each period a deformation with a different wavelength is added to the ones already existing. A closer investigation of the matter shows, however, that after a rapid shortening of  $L$  during the first few million years, a long period follows during which its variability is small. In Table 10A-1

TABLE 10A-1. CRUSTAL THICKENING  $h_0$  AND CRUSTAL SUBSIDENCE  $z_0$  AND  $\bar{z}_0$ 

$t_{my}$ , $10^6$ yr (1)	$\frac{h_0}{T}$ (2)	$\frac{T+h}{T}$ (3)	$\psi = \frac{L^0}{L}$ (4)	$F$ (5)	$\frac{F}{F_b} = \frac{\sigma}{\sigma_b}$ (6)	$\frac{z_0}{ch_0}$ (7)	$h_0$ , km (8)	$z_0$ , km (9)	$z_0 - \frac{1}{2}h_0$ , km (10)	$\bar{z}_0$ , km (11)	$\bar{z}_0 - \frac{1}{2}h_0$ , km (12)
0	0.0000	1.0000	1.00	1.00	0.0383	0.761	0.000	0.000	0.000	0.000	0.000
0.5	0.0158	1.0126	2.24	5.09	0.1947	0.793	0.552	0.212	-0.064	0.134	-0.142
1	0.0316	1.0252	2.63	7.08	0.2715	0.825	1.104	0.443	-0.099	0.279	-0.273
2	0.0631	1.0505	3.06	9.86	0.377	0.888	2.209	0.952	-0.152	0.599	-0.505
3	0.0947	1.0758	3.33	11.90	0.455	0.952	3.313	1.531	-0.122	0.965	-0.690
4	0.1262	1.1010	3.51	13.58	0.520	1.008	4.418	2.161	-0.048	1.360	-0.849
5	0.1578	1.1262	3.65	15.00	0.574	1.048	5.521	2.811	+0.050	1.770	-0.991
7.5	0.2367	1.1894	3.88	17.86	0.683	1.157	8.282	4.66	+0.52	2.931	-1.210
10	0.3156	1.2525	4.01	20.10	0.769	1.270	11.04	6.82	+1.30	4.29	-1.23
15	0.4733	1.3788	4.12	23.46	0.898	1.520	16.57	12.24	+3.96	7.71	-0.57
20	0.6312	1.5050	4.15	25.92	0.992	1.85	22.09	19.85	+8.80	12.50	+1.46
25	0.7890	1.6313	4.13	27.83	1.064	2.30	27.62	30.87	+17.06	19.42	+5.61
30	0.9468	1.7575	4.09	29.38	1.123	2.82	33.14	45.42	+28.85	28.58	+12.01

column 4 gives the ratio of the value  $L^0$  for  $t = 0$  to the value of  $L$  at the times given in column 1; according to Formula (10A-37c) this ratio  $\psi$  is given by

$$\psi = \left(1 + \frac{\sigma - \sigma_l}{2\eta} t\right)^{-\frac{3}{4}} \left[1 + 0.40 \frac{E}{(n+1)\eta} t\right]^{\frac{1}{4}} \quad (10A-41)$$

In this formula we have put  $n = 1.5$ , which is in harmony with the result obtained for the first 20 million years, and we have introduced  $\eta = 10^{23}$  poises,  $E = 10^{12}$  dynes/cm<sup>2</sup>,  $(\sigma - \sigma_l)_0 = 2 \times 10^8$  dynes/cm<sup>2</sup>, and  $\sigma - \sigma_l = 0.8(\sigma - \sigma_l)_0$ . The value  $L^0$  is the purely elastic half wavelength already dealt with in Sec. 10A-3. Examining Table 10A-1 and Fig. 10A-7, we see that between  $t = 4 \times 10^6$  years and  $t = 50 \times 10^6$  years the value of  $L$  differs from  $\frac{1}{4}L^0$  by less than 10 per cent.

We shall now assume that the half wavelength remains constant during the whole phenomenon and is equal to  $\frac{1}{4}L^0$ . Except for the first few million years, this is a fair approximation; the fact that we also assume that  $b = L$  or, in other words, that the plastic belt comprises only one wavelength  $2L$  makes it likely that the small variation of  $L$  does not greatly affect our deductions. On both sides of the belt  $2b$  the phenomenon has an elastic character, and so the half wavelengths  $L'$  and  $L''$  for these parts are equal to  $L^0 = 4L$ .

Our assumption of constant wavelength considerably simplifies our problem by allowing us to apply the formulas for the mixed elastic and plastic bending to the duration of the phenomenon. Though the integration of the plastic deformation over this whole period, as represented by Formulas (10A-29a) and (10A-30), is still an approximation, the great difficulty resulting from the integration of crustal deformations with varying wavelength has been removed.

For greater simplification of our problem we shall further assume that during the whole phenomenon the breadth  $2b$  of the plastic belt remains

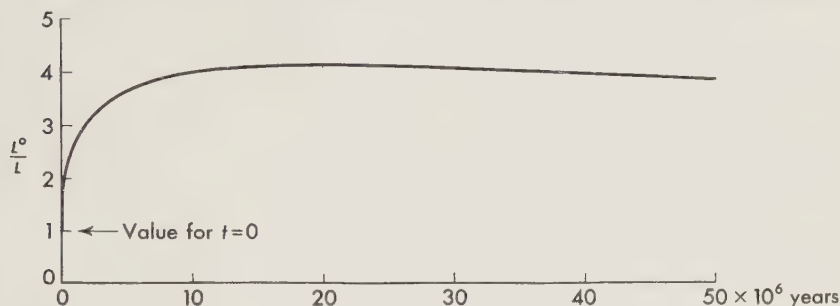


FIG. 10A-7. Ratio of half wavelength  $L^0$  of crust, for  $t = 0$ , to  $L$  for time  $t$  for plastic buckling of crust.

the same and that it is not affected by the crustal shortening connected with the plastic thickening.

Our supposition that  $b = L$  may be made acceptable in the following way. If the compressive stress  $\sigma$  slowly increases until it surpasses the elastic limit  $\sigma_l$  in the critical belt, the belt, because of the increase of  $\sigma$ , will gradually become broader until the moment when the breadth  $2b$  reaches the value  $2L$ . At that moment there is resonance with the wavelength  $2L$ , which, after the first stage of a few million years, dominates the crustal deformations, and it seems likely that the giving way of the crust maintains this coincidence. The exact coincidence of  $b$  and  $L$ , though simplifying the computations, is not necessary for our deductions; as long as the difference of  $b$  and  $L$  is not large, our conclusions will remain true.

We shall also suppose that  $\sigma$  has the same value over the whole breadth of the belt  $2b$  and over the areas on either side. According to Formula (10A-36) for  $\sigma - \sigma_l$ , this implies, as mentioned before, that the value of the elastic limit  $\sigma_l$  is somewhat less in the plastic belt than outside, where we assume that the whole crustal deformation remains of the elastic type. We shall further suppose that from the moment  $t = 0$ ,  $\sigma$  and  $\sigma - \sigma_l$  remain constant. For  $\sigma$  we shall adopt a value of  $2 \times 10^9$  dynes/cm<sup>2</sup>.

These suppositions have been made in order to simplify our problem. As, however, we assume that the thickness of the rigid crust increases pro-

portionally with time, our supposition that  $\sigma$  is constant implies that the total compression force working in the crust increases correspondingly. This assumption may likewise make acceptable our further assumption that the breadth of the plastic belt is constant, notwithstanding the crustal shortening in this belt. It is therefore obvious that there must be a change in the adjoining crustal matter from elastic to plastic behavior, which can be accounted for if the compressive force increases.

Since it is clear that we cannot expect these conditions to remain fulfilled indefinitely and that for longer periods the process must change its character, our treatment cannot give more than an approximation for the beginning stage of the phenomenon, during which the compression is still increasing.

There are other reasons why we cannot consider it as more than an approximation. In the first place, our equations are valid only for small deformations. This is still more evident than for the usual method of dealing with problems of purely elastic deformation because we assumed that the bending does not affect the supposition of plastic deformation in the central belt and elastic deformation in the areas on both sides, although the bending stresses must in both areas tend to cause a changed condition over the lower part of the cross section. In the central belt we can expect the downbending to cause tensile stresses which might bring part of the cross section back to elastic deformation, and in the adjoining areas the compression caused by the upbending may lead to plastic behavior. So it is probable that the deformation must soon reach a stage of complicated types of deformation of a mixed character.

In the second place, to appraise the solution given here we must realize that the whole concept of a rigid crust floating on a plastic substratum is a schematization of the actual conditions. We know that under the deep ocean basins the crust consists only of a thin layer of sediments and a 3- to 6-km layer with a density of about 3.0 (probably consisting of basalt, perhaps partly of dolomitized older sediments), bounded below by the M discontinuity, under which we find the ultrabasic rocks of the mantle, probably olivine. Hence it is clear that the lower boundary of the so-called rigid crust, below which, for example, flow for isostatic readjustment takes place, is situated deep in the ultrabasic layer. Thus there can be no doubt here that this boundary is determined not by a change in chemical composition but solely by temperature and pressure. Below the continents the M discontinuity seems to coincide more or less with the lower boundary of the rigid crust as derived from the degree of regionality of the isostatic compensation. Perhaps this coincidence is not fortuitous; in the course of this section we shall see that there is reason to suppose that continental matter descending below this depth melts and is carried away by subcrustal currents.

Our conclusion that, at least under the oceans, the boundary of the rigid crust is determined by temperature and pressure points to a gradual change of the physical constants of the rocks as the depth increases. We can assume that the value of the limit of elasticity  $\sigma_l$  drops from about  $3 \times 10^9$  dynes/cm<sup>2</sup> at the surface to about  $10^7$  dynes/cm<sup>2</sup> at the lower boundary of the crust and that the value of the dynamic viscosity  $\eta$  drops from  $5 \times 10^{23}$  to  $10^{22}$  poises over that distance.

These points of view and values are in harmony with our supposition of plastic behavior of the rigid crust under the effect of tectonic forces. We shall now assume the approximate mean values  $\sigma_l = 2 \times 10^9$  dynes/cm<sup>2</sup> and  $\eta = 10^{23}$  poises over the upper 35 km of the earth. According to the suppositions already made for  $\sigma$  and  $\sigma - \sigma_l$ , we assume the value of  $\sigma_l$  to be somewhat less in the plastic belt. We may add that in supposing the upper layer of 35 km in this belt to deform plastically, we can assume, in harmony with the views given here, that during these movements the upper few kilometers may show faulting and breaking; the low temperature of these rocks must render them more brittle than deeper parts of the crust, and the small pressure must allow disruptive phenomena to take place.

So the more complete picture given here of the deformations of the upper layers of the earth in tectonic belts is one of flow up to the surface, with great differences of viscosity at different depths. Our picture of a rigid crust floating on a less viscous substratum is no more than a schematic approximation introduced to provide a model that can be dealt with mathematically.

We complete the picture by assuming that the temperature conduction is so slow that during the periods of 20 to 30 million years considered here the downbuckled crustal matter retains its viscosity. Since the assumption cannot remain true for longer periods, an ultimate melting and flowing away of the crustal root under the continents must be expected.

Turning now to a discussion of the solution given by Formulas (10A-36) to (10A-40), we see that it follows from (10A-39) and (10A-40) that the crustal deformation strongly depends on the angles  $\beta$  and  $\gamma$ , i.e., on the ratio  $\sigma/\sigma_b$ . Since a constant value of  $2 \times 10^9$  dynes/cm<sup>2</sup> has been assumed for  $\sigma$ , the change with time in the ratio depends on a change in the buckling stress  $\sigma_b$ , which is given by Formula (10A-37d). We write the result in the form

$$\sigma_b^0 = \frac{\sigma_b^0}{F} \quad (10A-42a)$$

where  $\sigma_b^0 = 0.596 \sqrt{T \rho_s' g E}$  (10A-42b)

and  $F = \left[ 1 + 0.40 \frac{Et}{(n+1)\eta} \right]^{\frac{1}{2}} \left( 1 + \frac{\sigma - \sigma_l}{2\eta} t \right)^{-\frac{1}{2}}$  (10A-42c)

In these formulas  $\sigma_b^0$  represents the buckling stress for the time  $t = 0$ , or, in other words, for purely elastic buckling of the crust.  $F$  is a factor increasing with time. Introducing the values  $n = 1.5$ ,  $E = 10^{12}$  dynes/cm<sup>2</sup>,  $(\sigma - \sigma_l)_0 = 2 \times 10^8$  dynes/cm<sup>2</sup>, and  $\sigma - \sigma_l = 0.8(\sigma - \sigma_l)_0$ , and expressing  $t$  in millions of years, we obtain

$$F = (50.50t_{my} + 1)^{\frac{1}{2}}(1 + 0.02525t_{my})^{-\frac{1}{2}} \quad (10A-43)$$

Column 5 of Table 10A-1 shows how  $F$  increases with time, until, after  $10 \times 10^6$  years, it reaches a value of 20.10; after  $20 \times 10^6$  years, a value of 25.92; and after  $30 \times 10^6$  years, a value of 29.38. According to (10A-42a), the buckling stress  $\sigma_b$  diminishes in inverse ratio to these figures. Restricting our considerations now to geosynclines filled by sea water, we shall introduce  $\sigma_b^0 = 52.3 \times 10^9$  dynes/cm<sup>2</sup>, given for this case by Formula (10A-13b). The resulting values of the ratio  $\sigma/\sigma_b$  given in column 6 of Table 10A-1 provide us with the angles  $\beta$  and  $\gamma$  of our solutions (10A-39a) and (10A-40b), respectively. For the elastic deformation of the areas on both sides, as given by (10A-39b) and (10A-39c), we have in our example an angle  $\beta' = \beta'' = 44^\circ$ , derived from (10A-14a) by introducing  $\sigma = 2 \times 10^9$  dynes/cm<sup>2</sup> and  $\sigma_b = 52.3 \times 10^9$  dynes/cm<sup>2</sup>.

By using the respective boundary conditions connected with Formulas (10A-39) and (10A-40) we can now deduce the eight integration constants of these formulas as functions of the product  $ch_0$  and thus find the deformation  $z, z', z''$  of the crust's axis over the plastic belt and the elastic areas on either side. Assuming the same value of  $c$  over all parts, i.e., the same densities for the crust and for the subcrustal layer, and supposing the deformation to vanish at infinite distance on either side, we obtain a deformation curve which is symmetric with respect to the point  $x = 0$ , i.e., to the center of the geosyncline belt. In that case Formulas (10A-39) and (10A-40) give us the ratios  $z/ch_0$  and  $z'/ch_0 = z''/ch_0$ . The values  $z_0/ch_0$  thus found for the center of the geosyncline belt are listed in column 7 of Table 10A-1.

Sedimentation has been assumed absent in applying these results to two cases: (1) the development of a geosyncline in the ocean floor, i.e., a deep sea trench, where the mean crustal density  $\rho_c$  may be put at 3.24, and (2) a submerged continental geosyncline, for which  $\rho_c = 2.835$ . Values of  $z$  and other quantities relating to the second case are distinguished by a bar. We get

$$c = \frac{3.24 - \frac{1}{2}(3.27 + 1.028)}{3.27 - 1.028} = 0.486 \quad (10A-44)$$

$$\bar{c} = \frac{2.835 - \frac{1}{2}(3.27 + 1.028)}{3.27 - 1.028} = 0.306$$

Columns 9 and 11 of Table 10A-1 give the values of the subsiding  $z_0$  and  $\bar{z}_0$  of the crust's axis plane in the middle of the oceanic and continental

geosynclines, respectively, and 10 and 12 give the subsidence  $z_0 - \frac{1}{2}h_0$  and  $\bar{z}_0 - \frac{1}{2}h_0$  of the crust's surface at the same places. Columns 9 and 11 corroborate our surmise of an accelerated subsidence. The whole geosyncline development appears, however, to be extremely slow, taking periods of the order of 20 to 30 million years. It should be pointed out here that all time indications are based on a value of the mean pseudo viscosity  $\eta$  of the crust of  $10^{23}$  poises. If a higher figure should have to be adopted—which is

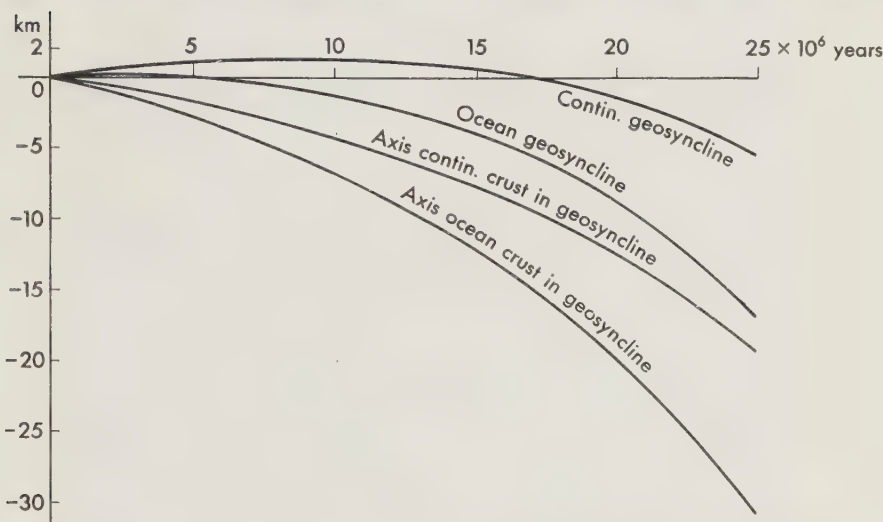


FIG. 10A-8. Time curves for surface and axis plane of earth crust in center of developing geosyncline for continental and oceanic areas.

quite possible—we should have to increase the times in the first column, and in the same ratio.

The acceleration is also clearly shown by Fig. 10A-8, which gives the curves, for both oceanic and continental areas, for the downward movement of the crustal axis plane and of the surface of the crust in the center of the geosyncline. As we expected, the geosyncline development has the character of a downbuckling of the crust. The velocity of the continental crust is smaller than that of the oceanic crust, which is no doubt due to the fact that, since the density of the continental crust is smaller, the energy needed to press it down into the heavier subcrustal matter is greater than that needed for the oceanic crust.

Examining more closely the conditions which lead to this crustal downbuckling, we find that plastic thickening plays a vital part. It brings about a downbending of the crust, which causes bending stresses in crustal cross sections; the stresses, in turn, cause plastic flow, which very slowly leads to displacements attaining the critical value needed for downbuckling. If

there had been no crustal downbending by plastic thickening, only small bending stresses caused by incidental disturbances could be expected, and they could not last long enough to bring about the plastic deformation corresponding to the geosyncline formation. It should be noted that the plastic thickening of the crust, which brings about a finite bending, distinguishes crustal downbuckling from the buckling of a vertical column under compression; here if the elastic-buckling limit of the compressive stress is considerably higher than the limit of elasticity, it is uncertain whether plastic buckling will occur at all or whether the column will continue to give way by plastic thickening and shortening.

Mentioned at the beginning of this section was the fact that the decisive part played in the downbuckling by plastic thickening of the crust can explain the complicated pattern of tectonic orogeny; this question is dealt with in Sec. 10A-7.

The thickening of the crust which accompanies the downbuckling causes the crustal surface to rise initially. In Table 10A-1 we see that for the oceanic crust this does not yield a higher elevation than about 150 m. After  $4\frac{1}{2}$  million years the ridge has disappeared, and the subsidence starts at an increasing rate; 10 million years later the geosyncline has reached a depth of about  $3\frac{1}{2}$  km. For the continental crust the initial rising attains a height of more than 1200 m, and more than 16 million years must pass before it disappears and the subsidence begins; \* but after 10 million years more the geosyncline has already attained a depth of about  $7\frac{1}{2}$  km.

It is questionable, however, whether this last figure is valid, and this is also true for other figures of the lower lines of Table 10A-1. The uncertainty is not caused by exceeding the limit given by  $\sigma = \sigma_b$ , though at that stage the mathematical treatment passes through a singularity which requires a shift from Formula (10A-39a) to (10A-40); the values obtained for  $z/ch_0$  remain continuous. But, as we have already mentioned, the formulas are no longer applicable for large deformations. If the downbuckling continues, two developments may be expected. In the first place, the upper strata of the crust, because of the downbending, must be subjected to much stronger horizontal compression than is found elsewhere in the crust, and so some folding phenomena can be expected in those strata. In the second place (and this phenomenon is more important), probably the deformation gradually leads to such a deepening of the syncline that it more or less assumes the shape of a downbulging in the central part of the plastic belt. We may, for example, imagine that the horizontal stress  $\sigma$  by pressing the

\* In this connection we must realize that, since we have chosen the value of  $\rho_s' = 2.242$  for a submerged geosyncline, our conclusions are valid only if we suppose either that the continental surface was originally at a depth of at least 1200 m or that the surface, in rising above sea level, was attacked by erosion and thus lowered to  $2.242/3.27 = 0.686$  times its height.

sides together gradually tends to make the syncline narrower. A tentative representation of this phenomenon is given by Fig. 10A-9, which shows five successive stages of an experiment by Kuenen<sup>11</sup> during which he subjected

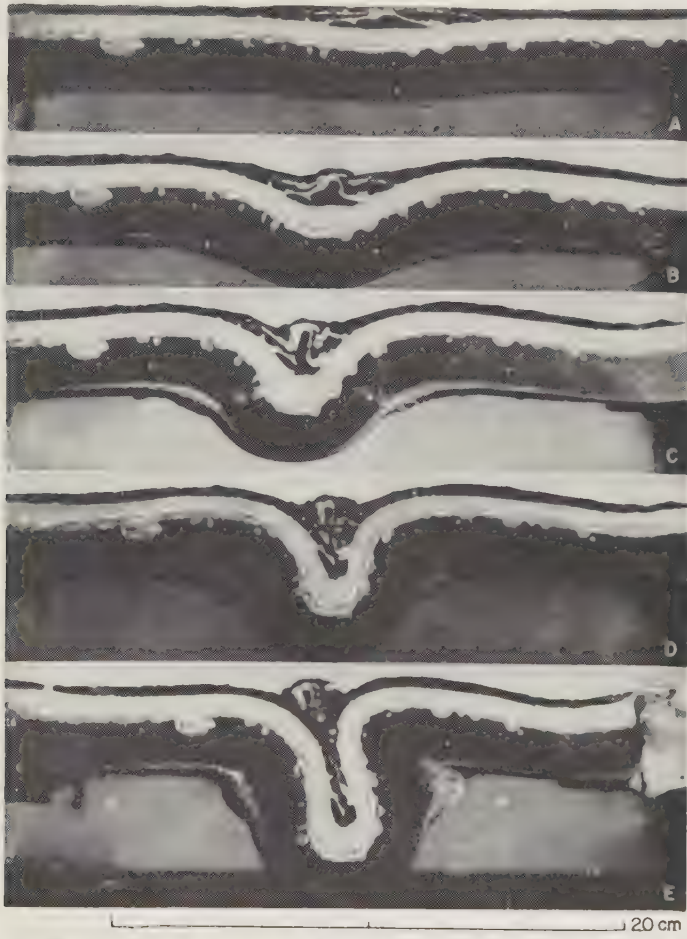


FIG. 10A-9. Five successive stages of Kuenen's experiments on buckling of a floating plastic layer under uniaxial horizontal compression.

mixtures of wax and paraffin floating on water to horizontal compression. To represent the weakness of sediments with respect to the deeper parts of the crust as well as possible, he used three layers of increasing viscosity from surface to bottom.

It is likely that during this phase of the phenomenon, which can be called the catastrophic or downbulging phase, a much greater shortening of the upper layers of the crust in the central part of the belt occurs than

the general shortening of the crust which has been going on during the whole geosyncline development. Great folding and overthrusting of the surface layers may result. Whether or not this last process takes place must depend on the question of whether or not there are incompetent sediments; when they are present, they are probably squeezed out so that they do not follow the downward movement of the crust in the central zone. As two examples of such different behavior we may mention the Alpine system, where great overthrusts have occurred, and the Pyrenees, where overthrusts are much less apparent though the scaly structure points to the catastrophic stage's having been present.

It is difficult to say at what period the catastrophic stage sets in; probably it is a gradual development. For the oceanic geosyncline it is likely to occur, according to our time scale, at a period between 10 and 20 million years, and for the continental one between 20 and 30 million years. If there is a geosyncline development on the continental margin, where geosynclines so often are located, the difference in velocity for the two types must lead to an asymmetric development in which the oceanic side subsides at greater velocity than the continental side, and the catastrophic deformation must take place on the oceanic side. The continental side must give the impression of overriding the oceanic side. These conclusions are in remarkable agreement with the facts, which are dealt with in Part C of this chapter. The increasing difference in level of the crust's surface on both sides must lead to great shear planes, caused by the crustal compression and marked by intermediate and deep earthquake foci. They dip down below the continental side of the geosyncline.

Sedimentation, which is more likely to occur on and near the continents than in most oceanic geosynclines, can also strongly affect the phenomenon. If the sedimentation follows the syncline development so quickly that the loading can be considered to occur at the same time, it can be taken into account by choosing  $\rho'$  equal to its density. If  $\rho' = 2.4$ , the constant  $c$  becomes zero, and there would not be any movement of the crust; the sedimentation would block the syncline formation. If, however, the sedimentation is lagging behind, or if it is less complete, the effects are more complicated. A further change of the process results if the sediments are consolidating. These problems will not be discussed further; it is clear that sedimentation can cause deviations from the two types of geosyncline development dealt with here.

Hitherto it has been assumed that the value of the compressive stress remains constant during the whole phenomenon. It is probable, however, that during these long time intervals variations of  $\sigma$  occur, which must also greatly influence the development of the phenomenon. If, for example, during the period, of many million years, of formation of a geosyncline,  $\sigma$  diminishes in the same ratio as  $\sigma_b$  and gets below the elastic limit  $\sigma_l$ , the

thickness of the crust and the depth of the geosyncline must remain stable, and so the development is interrupted. If  $\sigma$  decreases more than this, or if it vanishes entirely, a slow relaxation of the stresses can be expected, but the thickening of the crustal layers remains present. The belts of negative anomalies which appeared during the development of the geosyncline (to be discussed presently) will slowly disappear; the crust tends to resume isostatic equilibrium. Since the return to equilibrium must be accomplished by a rising of the geosynclinal belt, on the continents it leads to a high mountain range, the elevation of which is determined by the degree of thickening of the crust. If the relaxation of the stresses occurred after the catastrophic stage of compression had been reached, the mountain range may show strong folding and overthrusting; if it occurred at an earlier date, the mountain system shows little folding or overthrusting, except perhaps minor effects caused by gravimetric sliding, for which the rising movements must create appropriate conditions. Some folding may have been brought about by the great compression to which the surface layers of the crust were subjected during the quiet geosyncline stage preceding the catastrophic period. An example of a high mountain range without much folding whose origin can probably be thus explained is the High Atlas in Morocco.

The development of an oceanic geosyncline during the relaxation stage cannot be the same. Because of the small difference between the mean densities of the crust and the subcrustal layer, the bottom of the trench cannot rise to an elevation greater than about 500 m during the readjustment of the isostatic equilibrium, and so the development of only a low ridge can be expected. If, on the other hand, great masses of sediments have been deposited in the trench, and if they have been consolidated to rock consistency, the readjustment of equilibrium will lead to a higher ridge; it does not seem likely, however, that the elevation will ever amount to more than some 2 km. It is possible that some of the submarine ridges known to exist in the oceans originated in this way.

Though we may be reasonably sure about the final stage to which the relaxation leads, the course of events during the relaxation may be complicated and must depend on the way in which the compression diminishes. We shall not enter into a discussion of these problems here.

#### 10A-5. Later History of Geosyncline Belts; Subcrustal Flow of Crustal Matter; Mittelgebirge; Thickness of Continents

The last part of the history of a geosyncline must be different for continental and oceanic areas; we shall start by discussing the first type. The high mountain range arising in the continental synclinal belt can be expected to disappear gradually by two processes: (1) erosion by water or ice breaks the range down at the surface; (2) it can be surmised that after a

long time interval the light downbuckled root below the normal depth of the M discontinuity must assume the temperature normally present at that depth and thus gradually reach an apparent viscosity  $\eta_s$  of  $10^{22}$  poises. This process, which might be called "melting," must lead to the flattening of the root and its spreading under the "foreland" of the range. The amount of light crustal mass is thus diminished below the range itself and increased below the adjoining areas, and the isostatic adjustment of these mass changes must cause a subsidence of the range and a rise of the foreland.

This phenomenon can probably be recognized in the history of the Alps, and it may explain the rising of the French and German *Mittelgebirge*. The period of their creation followed the Alpine orogeny in the way we might expect, and the fact that they were caused mainly by rising and show only weak folding is in harmony with our hypothesis. The moderate folding may be explained by the drag resulting from the slow subcrustal current of root matter.

We may ask whether we can thus explain why the *Mittelgebirge* came into being only on the north and west sides of the Alps and not on the Italian side. It seems likely that this question can be answered by our supposition of a small limit of elasticity in the subcrustal material. It can be assumed that this limit is first surpassed outside the Alpine arc, where the flow finds more room than on the inside, and that thus the subcrustal flow originates to the west and north of the Alps. When this has occurred, however, it can be supposed that the limit toward the Italian side will never be reached and that therefore flow toward that side can no longer originate.

We thus can account satisfactorily for the origin of *Mittelgebirge* and for the way they surround the main Alpine orogenesis. We can likewise explain what became of the enormous subcrustal root corresponding to the large crustal shortening of several hundred kilometers which is indicated by the great folding and overthrusting of the surface layers in the Alpine area, and only part of which can be accounted for by gravitational sliding. We may estimate the shortening at 200 to 300 km, and so, if we put the crust's thickness at 30 km, the excess of crustal matter in each cross section is  $6000$  to  $9000$   $\text{km}^2$ . Assuming that the present cross section of the Alps is  $150 \times 2.5 = 375 \text{ km}^2$ , the corresponding excess is  $5.45 \times 375 = 2040 \text{ km}^2$ . So, if there had not been any root spreading, we should have to suppose that  $3960$  to  $6960 \text{ km}^2$  disappeared by erosion, i.e., 10.6 to 18.6 times the total volume of the Alps. This amount appears far too large and also leads to the question of where all this matter went.

The root-spreading hypothesis can give an adequate answer. If we adopt a mean breadth of the *Mittelgebirge* of 600 km, a length twice that of the Alps, a mean height of 0.6 km, and, therefore, a mean increase of crustal

thickness of  $5.45 \times 0.6 = 3.27$  km, we can thus account for  $2 \times 600 \times 3.27 = 3920$  km<sup>2</sup> for each Alpine cross section, and so the erosion would have had to carry away only 40 to 3040 km<sup>2</sup>. As the actual cross section of Alps +  $2 \times$  *Mittelgebirge* equals  $375 + 720 = 1095$  km<sup>2</sup>, this amounts to 0.04 to 2.78 times the present topography, it is easy to choose an intermediate value of the crustal shortening which fulfills the conditions. It must be emphasized that the computation is based on rough estimates. It is clear, however, that without the hypothesis of root spreading we get into serious difficulties.

By adopting this hypothesis we can also understand why the depth of the M discontinuity more or less coincides with the depth of the lower boundary of the rigid crust, which we have defined as the depth where the plasticity becomes small enough for perceptible flow to be possible. If the depth of the M discontinuity becomes larger, as is true for the geosynclinal root, flow would, at least in the long run, remove the lighter crustal matter below it. We might suppose, however, that because of the elastic limit which has to be overcome before flow can start, a slight inclination of the M discontinuity can be maintained. For large continents this could lead to a somewhat greater depth of the M discontinuity in the central area, which seems to agree with the seismic results obtained so far.

The melting of the downbuckled root, which may well contain sedimentary constituents, and the subsequent consolidation of this crustal matter may give a satisfactory explanation of the formation of granite. The high temperature and the high pressure are exactly the conditions appropriate for granitization. The conviction expressed by Read<sup>13</sup> that nearly every mountain range is characterized by its own granite is a strong argument in favor of this hypothesis.

The later history of oceanic geosynclines is much simpler. In the first place, there is no erosion to break down the low ridge formed in the geosyncline. In the second place, it is unlikely that the thin layer situated on top of the ultrabasic, which forms the main part of the crust, can subside by downbuckling to a sufficient depth to be involved in the root melting. Thus the root consists entirely of ultrabasic matter, and the melting cannot lead to subcrustal currents. Since both effects attacking mountain ranges on the continents are absent here, it appears likely that the low ridge is permanent. Perhaps, however, it will gradually be swamped in the layer of sediments which probably will be slowly deposited on the ocean floor. It is not certain whether such geosynclinal low ridges have come into being at a sufficient distance from continents or islands to be devoid of sediments. If sedimentation takes place in the oceanic geosyncline, a phenomenon intermediate between the continental and oceanic types must result.

### 10A-6. Further Discussion of Crustal Deformation; Gravity Anomalies

Taking up a further discussion of the deformation as given by Formulas (10A-39) and (10A-40), we shall continue to restrict ourselves to the symmetric case. We shall give the formulas for  $z/ch_0$  and  $z'/ch_0$  for two arbitrary values of  $\sigma/\sigma_b$ , the first where  $\sigma/\sigma_b < 1$  and the second where  $\sigma/\sigma_b > 1$ . Expressing  $x$ ,  $z$ , and  $h_0$  in kilometers, we obtain for the times  $t = 14.1 \times 10^6$  years and  $t = 28.2 \times 10^6$  years:

$$\text{I. } t = 14.1 \times 10^6 \text{ years} \quad \frac{\sigma}{\sigma_b} = 0.875 \quad \sin \beta = 0.25$$

$$\text{Inside plastic belt} \quad -b \leq x \leq +b \quad b = 50 \text{ km}$$

$$\begin{aligned} \frac{z}{ch_0} = & 0.583e^{0.01578x} \cos (3^\circ 486x - 156^\circ 95) \\ & + 0.583e^{-0.01578x} \cos (3^\circ 486x + 156^\circ 95) + 0.5 + 2 \cos 3^\circ 6x \end{aligned} \quad (10A-45a)$$

$$\text{Outside plastic belt} \quad x \geq b$$

$$\frac{z'}{ch_0} = 0.096e^{-0.0109x} \cos (0^\circ 647x + 116^\circ 9) \quad (10A-45b)$$

$$\frac{z_0}{ch_0} = 1.427 \quad (10A-45c)$$

$$h_0 = 15.58 \text{ km} \quad (10A-45d)$$

$$\text{II. } t = 28.2 \times 10^6 \text{ years} \quad \frac{\sigma}{\sigma_b} = 1.101 \quad \tan \gamma = 0.64$$

$$\text{Inside plastic belt} \quad -b \leq x \leq +b \quad b = 50 \text{ km}$$

$$\frac{z}{ch_0} = 2.927 \cos 2^\circ 88x + 1.666 \cos 4^\circ 50x + 0.5 - 2.47 \cos 3^\circ 6x \quad (10A-46a)$$

$$\text{Outside plastic belt} \quad x \geq b$$

$$\frac{z'}{ch_0} = 0.992e^{-0.0109x} \cos (0^\circ 647x + 144^\circ 6) \quad (10A-46b)$$

$$\frac{z_0}{ch_0} = 2.62 \quad (10A-46c)$$

$$h_0 = 31.10 \text{ km} \quad (10A-46d)$$

Figure 10A-10 represents these curves on a true vertical scale for an oceanic geosyncline for which  $c = 0.486$ . They are in good agreement

with the first stages of Kuenen's experiments (Fig. 10A-9), but it must be realized that our formulas are based on elastic deformation in the adjoining areas while in the experiments the deformation is plastic throughout. This fact is expressed in the four-times-larger wavelength shown by Fig. 10A-10. The two curves also clearly reveal the accelerating character of the phenomenon. The subsidence in the center is nearly four times more in the second stage than in the first, though the time  $t$  is only twice as long. It is evident, however, that for the second stage the deformations are so

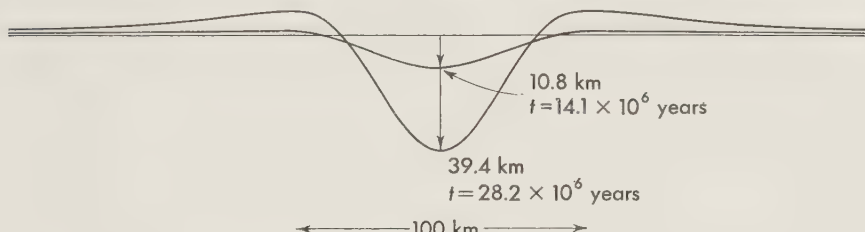


FIG. 10A-10. Two stages, for  $t = 14.1$  million years and  $t = 28.2$  million years, of plastic crustal downbuckling of oceanic crust; on true vertical scale.

large that the formulas can no longer be valid. Even in the first stage their validity is already doubtful; the lower boundary of the crust is found at a depth of 18.6 km. We must also remember that in reality there cannot be a sudden transition between plastic and elastic deformation. We therefore cannot expect our curves to be more than an approximation.

Examining the upward waves on either side, we see that their height is still increasing more than the depth of the geosyncline itself is; the ratio of these heights in the two curves is about 15. We shall presently come back to this point.

Figure 10A-11 shows the deformation of the upper and lower boundaries of the crust and of its axis given by the formulas for a time  $t = 15.56 \times 10^6$  years. After that period the depth of the trench at the surface is 4.5 km, and so this stage must approximately represent the deep ocean trenches

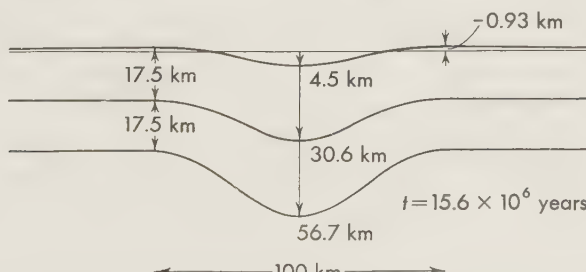


FIG. 10A-11. Plastic crustal downbuckling of oceanic crust on true vertical scale; upper and lower crustal boundaries and axis plane.

found in the Pacific and north of Puerto Rico. The formulas give for that time a thickening of the crust of 17.18 km, i.e., of 49 per cent of the crust's thickness, and this figure is in harmony with the important result found by Raitt (see Ref. 48 of Chap. 2) in the Tonga Trench, where his seismic data show for the layer of density 3.0 a thickness of about 8 km, while to the east of the trench he obtained a normal value of 5 km.

It is clear that the downbuckling of the crust in the geosyncline can explain the belts of negative gravity anomalies found in the East and West Indies; the crust in those belts is pressed down several kilometers lower than its isostatic-equilibrium position, thus representing a strong mass deficiency. In Part C of this chapter the gravity profiles over these belts, especially the Indonesian Archipelago, are discussed. These profiles are in harmony with the deformation curves found here; they also show the positive anomalies that must be expected over the upbending waves in the adjoining areas. A point which has hitherto lacked a clear explanation is the fact that, notwithstanding the belts of strong negative anomalies, the gravity field over the whole Indonesian Archipelago, including those belts, shows a positive mean gravity anomaly of about 25 mgal. Of this anomaly, about 5 mgal can be accounted for as the result of the uniaxial compression of the crust, which is given by Formula (10A-3) and so about 20 mgal still have to be explained. Our formulas provide an indication of the possible answer.

To determine the mean anomaly over the whole area we integrate Formulas (10A-39) and (10A-40) for  $z$ ,  $z'$ , and  $z''$  over the entire cross section of the geosynclinal belt and adjoining areas, i.e., from  $x = -\infty$  to  $x = +\infty$ , and multiply this result by  $\rho'_s$  to obtain the mass deficiency caused by the displacement of the crustal axis. Subtracting the mass deficiency from the mass excess caused by the thickening of the crust, we find the total excess of mass brought about by the phenomenon. After multiplying the excess by  $2\pi k^2$  ( $k^2$  is Newton's constant of attraction) to find the integral of the gravity anomalies over the entire cross section, we assume the larger part to be caused by the anomalies over the central area 300 km wide and find the mean anomaly  $A_m$  by dividing our result by 300. We again take into account the fact that we can assume the wavelength  $L'$  in the adjoining areas to equal four times the wavelength  $L$  in the plastic belt and obtain for  $\sigma \leq \sigma_b$

$$\begin{aligned} A_m = & -4k^2 \rho'_s \frac{LA}{300} [e^{\pi \sin \beta} \sin (\pi \cos \beta - \varphi + \beta) \\ & + e^{-\pi \sin \beta} \sin (\pi \cos \beta + \varphi - \beta)] \\ & + 16k^2 \rho'_s \frac{LA'}{300} e^{-(\pi/4) \sin \beta'} \sin \left( \frac{\pi}{4} \cos \beta' + \varphi' - \beta' \right) \quad (10A-47a) \end{aligned}$$

and for  $\sigma > \sigma_b$

$$A_m = -4k^2 \rho_s' \frac{L}{300} [A \sqrt{\cot \gamma} \sin(\pi \sqrt{\tan \gamma}) + B \sqrt{\tan \gamma} \sin(\pi \sqrt{\cot \gamma})] + 16k^2 \rho_s' \frac{LA'}{300} e^{-(\pi/4) \sin \beta'} \sin\left(\frac{\pi}{4} \cos \beta' + \varphi' - \beta'\right) \quad (10A-47b)$$

The results are given by Fig. 10A-12. Instead of representing  $A_m$  as a function of  $\sigma/\sigma_b$ , we have replaced this coordinate by the time  $t$ , using

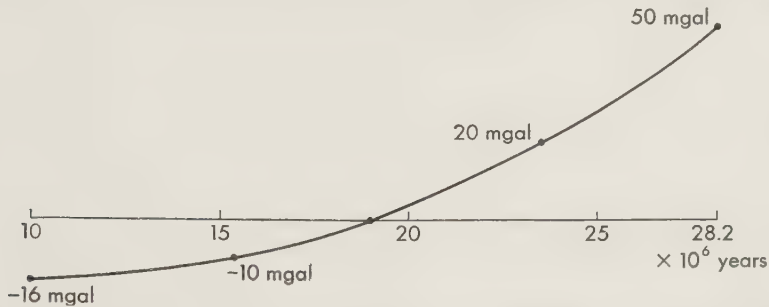


FIG. 10A-12. Mean gravity anomaly over geosyncline area extended to 150-km distance from axis to both sides.

Table 10A-1. The curve shows that for values of  $t$  larger than about  $19 \times 10^6$  years of our time scale the mean anomaly becomes positive. To obtain a mean anomaly of 20 mgal we should have to assume that the compression  $\sigma$  continued for about  $23.5 \times 10^6$  years. It is evident that by that time the deformation has become so large that the phenomenon must be in the catastrophic stage, and our formulas are no longer valid. It is therefore questionable whether this explanation of the positive anomalies remains valid.

The cause of the increasing mean positive anomaly for greater deformations of the crust must no doubt be sought in the result of the compression  $\sigma$  together with the increasing upbending of the crust over broad areas adjoining the geosyncline. The effect is comparable to that of the earth's curvature combined with the compression in the crust, for which we have derived Formula (10A-3). The strongly increasing upbending has already been mentioned above.

#### 10A-7. Preferred Starting Direction of Plastic Deformation by Uniaxial Compression

We now come to a subject broached at the beginning of Sec. 10A-4, viz., under what angle, with respect to the direction of the compressive stress,

does the plastic deformation of the crust originate? As mentioned earlier, Bijlaard<sup>3,4</sup> has shown that, if elastic downbuckling of the crust is possible, it must occur in strips at right angles to the compression but that the same is not true for plastic deformation. It is well known that in a plate subjected to a single stress direction such deformation occurs at an angle of about 55° with the stress; this direction is shown, for example, by the development of Hartmann's lines at the moment the limit of elasticity is surpassed. Bijlaard and later van Iterson<sup>10</sup> gave an explanation of this behavior and derived a formula for the angle which occurs in the more general case of other stress conditions in the plate. Bijlaard's views can be summarized as follows.

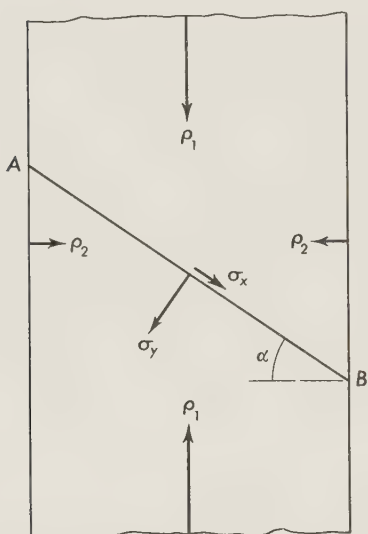


FIG. 10A-13. Plastic deformation in belt  $AB$  of broad strip subjected to compressive stresses  $\rho_1$  and  $\rho_2$ .

We imagine a plate of a thickness small with respect to the dimensions in the other senses to be subjected to stresses in the sense of the plate and constant over a certain area. We can assume that these conditions are fulfilled in the earth's crust. Let  $\rho_1$  and  $\rho_2$  be the principal stresses working in a broad strip (Fig. 10A-13) in the sense of, and at right angles to, the strip. Assuming the plastic deformation to occur in the belt  $AB$ , Bijlaard's supposition is that the direction of this belt adjusts itself in such a way that during the plastic deformation the dimension in the sense of the belt does not change.

the view that a continuously growing

change in length in that sense would imply great loss of energy, which, because of the small thickness of the plate, is not true for a change of thickness of the belt.

In plastic deformation the value of Poisson's constant for the speed of deformation is such that the volume does not change; since  $m = 2$ , the stress  $\sigma_x$ , in the sense of the belt, must be half of  $\sigma_y$ , at right angles to it, for the lateral effect of  $\sigma_y$  to compensate the direct effect of  $\sigma_x$  exactly. In the usual representation (Fig. 10A-14) of the stresses of a two-dimensional stress situation by a Mohr's circle, our condition amounts to the relation  $MP = \frac{1}{3}OM$ , and so

$$\cos 2\alpha = \frac{1}{3} \frac{\rho_1 + \rho_2}{\rho_1 - \rho_2} \quad (10A-48)$$

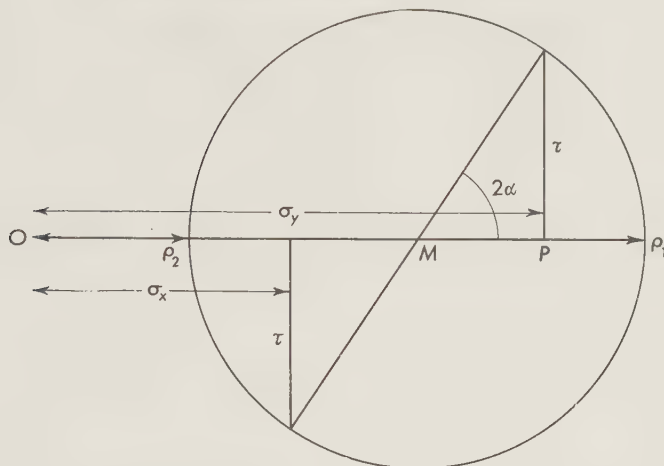


FIG. 10A-14. Mohr's circle for stress in Fig. 10A-13.

For  $\rho_2 = 0$ , i.e., for uniaxial compression in the strip, this gives  $2\alpha = 70^\circ 31' 7$ , or  $\alpha = 35^\circ 15' 9$ , in agreement with the experimental results.

Bijlaard<sup>3,4</sup> has proved that our conclusion, defined in Formula (10A-48), is in harmony with the Huber-Hencky-von Mises criterion, mentioned in Sec. 2-4.

We return to these results in Part C of this chapter, where we shall find that they can, in general, offer a satisfactory explanation of the complicated trends of tectonic belts.

For  $2\alpha = 70^\circ 31' 7$  Fig. 10A-14 gives us a shear stress

$$\tau = \frac{1}{2}(\rho_1 - \rho_2) \sin 2\alpha = 0.472(\rho_1 - \rho_2) \quad (10A-49a)$$

and a compression

$$\begin{aligned} \sigma &= \frac{1}{2}(\rho_1 + \rho_2) + \frac{1}{2}(\rho_1 - \rho_2) \cos 2\alpha \\ &= \frac{1}{2}(\rho_1 + \rho_2) + 0.167(\rho_1 - \rho_2) \end{aligned} \quad (10A-49b)$$

For  $\rho_2 = 0$  this becomes

$$\tau = 0.472\rho_1 \quad (10A-49c)$$

$$\sigma = 0.667\rho_1 \quad (10A-49d)$$

So we see that the compression is accompanied by considerable shear stress. In Part C we shall find reason to suppose that this shear takes place in the volcanic arc on the inside of the tectonic arc.

### 10A-8. Faulting and Shear Phenomena in the Crust

There is still another reaction of the crust to stress which, although it consists chiefly in fracturing and shear, also shows some compression in a direction perpendicular to the belt of deformation. The main phenomenon is shear. It appears to occur at the sides of island arcs.

The problem can probably be stated best by asking in what direction an interface will form in the crust when two large crustal areas on both sides are moving at a relatively small, possibly zero, angle with respect to the interface. If the angle differs from zero, the relative movement must imply a small component at right angles to the interface, which probably causes the crustal block on one side of the fault to override that on the other side. This seems to have occurred, for example, in a belt outside Sumatra in the Indonesian arc.

In dealing with this problem we shall start with ideas introduced by Coulomb in 1776, further established by Rankine, applied to geology by Chamberlin and Shepard<sup>5</sup> (pp. 511–512) and more recently by Anderson<sup>1</sup> (1942), Hubbert,<sup>9</sup> and Hafner.<sup>8</sup>

Coulomb stated the view that the resistance to fracture consists of two parts: a limit of cohesion  $c$ , which has to be surpassed, is combined with an internal friction given by  $\sigma \tan \varphi$ , where  $\sigma$  is the normal component of the stress working on the critical cross section and  $\varphi$  is the angle of internal

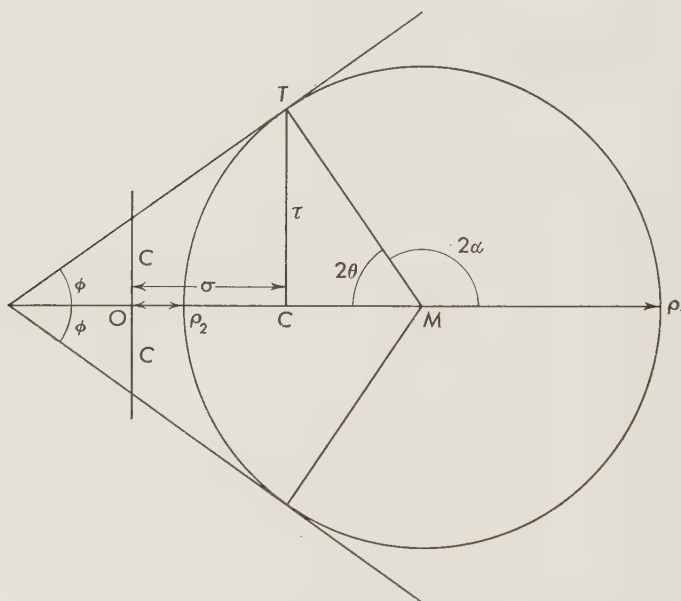


FIG. 10A-15. Mohr's diagram for shear fracturing of earth crust.

friction. Using Mohr's diagram, this hypothesis involves having the fracture occur when the stress circle is tangent to two lines enclosing angles  $\varphi$  with the horizontal axis (see Fig. 10A-15). The critical shear stress is given by  $TC$ , and the angle enclosed by the shear plane and the plane in which the greatest principal stress works is given by

$$\alpha = 45^\circ + \frac{1}{2}\varphi \quad (10A-50a)$$

Thus the angle  $\theta$  between the shear plane and the greatest principal stress  $\rho_1$  is

$$\theta = 45^\circ - \frac{1}{2}\varphi \quad (10A-50b)$$

According to Coulomb's ideas, the shear stress is

$$\tau = c + \sigma \tan \varphi \quad (10A-51)$$

and the difference of the principal stresses is

$$\rho_1 - \rho_2 = 2c \cos \varphi + (\rho_1 + \rho_2) \sin \varphi \quad (10A-52)$$

Figure 10A-15 shows that the fracture shear does not occur in the cross section where the shear is maximum.

Anderson, Hubbert, and Hafner are confident that this theory of fracture is valid for the behavior of rocks in faulting and folding and "appears to afford a basis of understanding for a variety of empirically well known geologic structures." \* We here apply it to faulting of the crust as a whole, and in Part C of this chapter we shall see that it seems to give satisfactory results for island arcs. We should perhaps assume that in the deeper layers of the crust, under the effect of great hydrostatic pressure, the shear has a more plastic character, but we must believe that for the crust as a whole the shear along a fault plane dominates the phenomenon.

The stress limit above which shear faulting sets in probably is not independent of the third principal stress, as might appear from Coulomb's fracture theory, but, although it seems likely that the third stress plays a part, little is known about the effect of triaxial stress. The approach taken in this matter by different authors, e.g., Goguel<sup>6</sup> (p. 143), Hubbert<sup>9</sup> (p. 364), is to use the results obtained in many experiments for cases in which the two smaller principal stresses are equal; in those cases we can continue to use Mohr's diagram.

Several tests on rocks have been made to determine the angle  $\varphi$  of internal friction or  $\theta$  between the shear plane and the greatest principal stress. Hubbert<sup>9</sup> (p. 364) mentions the results for marble, which was found to be brittle for low pressure  $\rho_2$  but to flow at higher values of  $\rho_2$ ; the angles  $\varphi$  varied from  $40^\circ$  (so  $\theta = 25^\circ$ ) at the beginning to  $0^\circ$  ( $\theta = 45^\circ$ ) at the end;

\* Abstracted from Hubbert.<sup>9</sup>

the envelopes of the Mohr's circles were convex outward. Triaxial tests on concrete reported by Ros and Eichinger<sup>14</sup> in 1928 showed  $\theta$  observed directly to vary from  $22^\circ$  to  $33^\circ$  (so  $\varphi = 46^\circ$  to  $24^\circ$ ). Other tests on concrete made by Blanks and McHenry<sup>2</sup> in 1945 gave values for  $\varphi$  of  $35^\circ$  ( $\theta = 27.5^\circ$ ). In 1942 Nijboer's tests<sup>12</sup> on asphalt aggregates, made to find their resistance to plastic deformation, generally gave straight envelopes for the Mohr's circles, and the majority showed  $\varphi$  to be  $28^\circ \pm 4^\circ$  ( $\theta = 31^\circ \pm 2^\circ$ ). In 1948 a large number of experiments on different kinds of rock were published by Goguel.<sup>6</sup> Of this valuable material one result for an old type of rock may be mentioned here, viz., for a permian shale of the *dôme du Barrot* he found (p. 194) an envelope of two Mohr's circles showing a value of  $\varphi$  of about  $40^\circ$  ( $\theta = 25^\circ$ ). Hubbert also mentions (p. 364) data for normal and reverse faults, where  $\theta$  is between  $20^\circ$  and  $40^\circ$  ( $\varphi = 50^\circ$  to  $10^\circ$ ), and gives the result found by Sax,<sup>15</sup> viz., a peak frequency for a great many normal faults of  $\theta$  of  $27^\circ$  ( $\varphi = 36^\circ$ ). These field observations are seen to be in good agreement with experimental results.

It can be concluded that a value for  $\theta$  of about  $27^\circ$  is probably an acceptable estimate, but it must be realized that this is only a vague indication for the crust as a whole, where other rocks and much greater hydrostatic pressures occur. For this angle Fig. 10A-15 gives the following values for the shear-stress and normal-stress components in the critical fault plane:

$$\tau = \frac{1}{2}(\rho_1 - \rho_2) \sin 2\theta = 0.404(\rho_1 - \rho_2) \quad (10A-53a)$$

$$\begin{aligned} \sigma &= \frac{1}{2}(\rho_1 + \rho_2) - \frac{1}{2}(\rho_1 - \rho_2) \cos 2\theta \\ &= 0.5(\rho_1 + \rho_2) - 0.294(\rho_1 - \rho_2) \end{aligned} \quad (10A-53b)$$

which for  $\rho_2 = 0$  provides us with the values

$$\tau = 0.404\rho_1 \quad (10A-53c)$$

$$\sigma = 0.206\rho_1 \quad (10A-53d)$$

This normal stress probably causes the crust in the island ridge west of Sumatra to override the adjacent crust in the Indian Ocean. In Part C of this chapter we shall find that after some time the resulting crustal thickening, because it strengthens the crust, probably brings about a shift of the shear belt toward the inside of the arc, i.e., to Sumatra. This may be the explanation of a second arc accompanying the main tectonic arc on the inside and having volcanic character.

With our present knowledge it is difficult to determine when, as discussed in this section, shear faulting takes place and when, as discussed in the previous section, plastic downbuckling occurs in belts, making an angle generally of  $55^\circ$  with the main compressive stress. Downbuckling corresponds to the Huber-Hencky-von Mises criterion, mentioned in Sec. 2-4,

but shear faulting does not. More evidence is needed from actual places where one phenomenon or the other can be supposed to have taken place.

It is clear that shear faulting of the crust may be furthered by the presence of zones of weakness in the earth's crust, and in Chap. 12 it is shown that such zones can be expected. There is fairly strong evidence, especially from geomagnetic sources, that the poles have moved with respect to the earth's surface, and the only possible explanation of this is that the crust as a whole has moved over the earth's interior. When such movements took place for the first time, at the beginning of the earth's history, they must have caused strong stresses in the crust because of the flattening. The stresses must have divided the crust into a number of blocks separated by zones of shear, which have remained zones of weakness in the crust.

To suppose that such weak belts exist in the Sumatra and Philippine regions of the Indonesian arc is in harmony with the pattern of these zones given in Chap. 12 and leads to the tentative hypothesis that the shear faulting of the crust occurs only in zones of weakness in the crust. As such belts do not meet the condition of isotropy, which is assumed for the Huber-Hencky-von Mises criterion, it can be understood that shear faulting of the crust does not satisfy this criterion.

If this hypothesis is true, the wings of the island arcs could develop only if they coincided with zones of weakness in the crust. It is remarkable that the pattern of these belts (see Chap. 12) is in agreement with the hypothesis in most of the arcs. The evidence, however, is not sufficient to justify a final decision.

When the two types of deformation belts, i.e., the plastic downbuckling and the shear-faulting zones, occur in adjoining parts of island arcs, they must enclose an angle of about  $55^\circ - 27^\circ = 28^\circ$ . We can recognize such an angle in the trends of several arcs, e.g., in the Indonesian arc between Sumatra and Java and in the Antillean arc between Martinique and Saint Lucia.

#### REFERENCES

1. Anderson, E. M.: The dynamics of faulting, 2nd ed., Oliver & Boyd, Edinburgh, 1951.
2. Blanks, R. F., and D. McHenry: Large triaxial testing machine built by Bureau of Reclamation, Eng. News-Record, vol. 135, pp. 171-173, 1945.
3. Bijlaard, P. P.: Beschouwingen over de knikzekerheid en de plastische vervormingen van de aardkorst in verband met de geologie van de Indische Archipel (Summary in German), Ingr. Ned. Indië, vol. 11, pp. 135-156, 1935.
4. ———: Théorie des déformations plastiques et locales par rapport aux anomalies négatives de la gravité, aux fosses océaniques, aux géosynclinaux, etc., Rapp. congr. Edimbourg UGGI, 1936.
5. Chamberlin, R. T., and F. P. Shepard: Some experiments in folding, J. Geol., vol. 31, pp. 490-512, 1923.

6. Goguel, J.: Introduction à l'étude mécanique des déformations de l'écorce terrestre, Mém. carte géol. détaillée France, 2nd ed., Imprimerie Nationale, Paris, 1948.
7. Griggs, D.: A theory of mountain building, Am. J. Sci., vol. 237, pp. 611–650, 1939.
8. Hafner, W.: Stress distributions and faulting, Bull. Geol. Soc. Amer., vol. 62, pp. 373–398, 1951.
9. Hubbert, M. King: Mechanical basis for certain familiar geologic structures, Bull. Geol. Soc. Amer., vol. 62, pp. 355–372, 1951.
10. Iterson, F. K. Th. van: Plasticiteitsleer, Kluwer, Deventer, 1945.
11. Kuennen, Ph. H.: The negative isostatic anomalies in the East Indies, Leidsche Geol. Mededeel., vol. 8, pp. 169–214, 1936.
12. Nijboer, L. W.: Onderzoek naar den weerstand van bitumen-mineraal-aggregaat mengsels tegen plastische deformatie, Noord-Hollandsche Uitgevers Mij, Amsterdam, 1942.
13. Read, H. H.: Granite series in mobile belts, Columbia Univ. Symposium, The crust of the earth, Abstracts, p. 42, New York, 1954.
14. Ros, H. C. M., and A. Eichinger: Experimental attempt to solve the problem of failure in nonmetallic materials, Federal Mat. Testing Lab., Eidgenossische Technische Hochschule, Zürich, Rept. no. 28, 1928.
15. Sax, H. G. J.: De tectoniek van het carboon in het Zuid Limburgsche mijngebied, Mededel. Geol. Sticht., ser. C-I-I, no. 3, pp. 1–77, 1946.
16. Smoluchowski, M.: Anz. Akad. Wiss. Krakau, Math.-naturw. Kl., vol. 2, pp. 3ff., 1909.
17. Vening Meinesz, F. A.: Gravity expeditions at sea, vol. 2, Publ. Neth. Geod. Comm., Waltman, Delft, 1934.
18. ———: Earth's crust deformations in geosynclines, Proc. Koninkl. Ned. Akad. Wetensch., ser. B, vol. 53, pp. 27–46, 1950.
19. ———: Earth-crust movements in the Netherlands resulting from Fennoscandian postglacial isostatic readjustment and Alpine foreland rising, Proc. Koninkl. Ned. Akad. Wetensch., ser. B, vol. 57, pp. 142–155, 1954.
20. ———: Plastic buckling of the earth's crust: The origin of geosynclines; "The crust of the earth," Geol. Soc. Amer. Spec. Paper 62, 1955.
21. ———: The geophysical history of a geosyncline, Proc. Koninkl. Ned. Akad. Wetensch., ser. B, vol. 60, pp. 126–140, 1956.

## PART 10B

### POSTGLACIAL READJUSTMENT OF CRUSTAL EQUILIBRIUM. ISOSTATIC READJUSTMENT

#### 10B-1. General Considerations; Readjustment Determined by Subcrustal Phenomena

It was mentioned in Sec. 10A-1 that there are two large continental areas, viz., Fennoscandia and a part of North America, which were covered with ice in the glacial period and which, since its disappearance, show clear evidence of rising. This rising can be traced in systems of uplifted shorelines and by precise leveling, which shows that it is still going on at present.

It can be assumed that in these areas the earth's crust was pressed down by the weight of the ice load and that, after the ice melted away, the crust started readjusting its isostatic balance. This explanation of the rising is supported by two facts: the area of rising coincides satisfactorily with the area covered by ice, and the shorelines show that the way in which the speed of rising diminishes with time checks not too badly with the  $e$  curve to be expected. Further support is given by the observed negative gravity anomalies of about 20 mgal, which show that the areas have not yet attained complete isostatic equilibrium.

In this section we deal first with recent theoretical investigations of the mechanical and hydrodynamical aspects of these isostatic-adjustment processes made by Haskell,<sup>4,5</sup> Niskanen,<sup>10-12</sup> and the author (V. M.),<sup>14</sup> and then we examine the extensive evidence for these vertical movements of the crust and draw some provisional conclusions from them.

The treatment given by Haskell and the author starts from the assumption that the floating crust does not materially affect the phenomenon but follows more or less accurately the surface movement of the plastic subcrustal layer. Contrary to this assumption is the suggestion that under the weight of the ice the crust sank by elastic deformation and that later the resulting elastic stresses vanished by slow relaxation. It has further been suggested that in the period after the unloading by the disappearance of the ice the crust resisted the rising tendency elastically and thus took part in making the process go slower. This would have brought the rising speed back to that of the slow creep and decay of the elastic resistance of the crust. The pseudo viscosity of the subcrustal layer would thus

amount to  $\eta = 5 \times 10^{21}$  poises, i.e., a value essentially smaller than that found by attributing the whole delaying effect to the viscosity of the subcrustal flow.

This point of view can hardly correspond to the facts. Even supposing that, when the ice disappeared, the crust had lost by relaxation the elastic stresses incurred during the loading period, it is easy to prove that its upward bending prevents only  $\frac{1}{36}$  per cent of the original downbending from disappearing and that this small effect is negligible with respect to the main rising phenomenon. If the original downbending had a two-dimensional character represented by

$$\zeta = \zeta_0 \sin \pi \frac{x}{L} \quad (10B-1)$$

where  $x$  = horizontal coordinate

$\zeta$  = sinking

$L$  = breadth of loaded area

$\zeta_0$  = maximum sinking in axis

the upward pressure  $p$  working on the crust after the ice had disappeared would be

$$p = \rho g \zeta = \rho g \zeta_0 \sin \pi \frac{x}{L} \quad (10B-2)$$

where  $\rho$  is the density of the subcrustal layer. This pressure would cause a moment  $M$  in the crust, which, per centimeter of the third dimension, is given by

$$M = \rho g \zeta_0 \frac{L^2}{\pi^2} \sin \pi \frac{x}{L} \quad (10B-3)$$

If the thickness of the crust is again indicated by  $T$ , we find the following equation for the upbending  $-z$  ( $z$  is taken positive downward)

$$\frac{\partial^2 z}{\partial x^2} = 12 \frac{\rho g \zeta_0}{ET^3} \frac{L^2}{\pi^2} \sin \pi \frac{x}{L} \quad (10B-4)$$

of which the solution is

$$z = -12 \frac{\rho g \zeta_0}{ET^3} \frac{L^4}{\pi^4} \sin \pi \frac{x}{L} \quad (10B-5)$$

This is proportional to the original downbending  $\zeta$ . We can write

$$z = -12 \frac{\rho g}{ET^3} \frac{L^4}{\pi^4} \zeta \quad (10B-6)$$

Introducing  $\rho = 3.27$

$$E = 1,000,000 \text{ kg/cm}^2 = 10^9 g \text{ dynes/cm}^2$$

$$T = 35 \text{ km}$$

$$L = 1400 \text{ km}$$

we obtain

$$z = -3600\xi \quad (10B-7)$$

and so we come to the conclusion that  $\frac{1}{3600}M$  of the moment  $M$  caused by the upward pressure  $p$  [Formula (10B-3)] is sufficient to bring about an elastic upbending of the crust completely neutralizing its original downbending. So, obviously, practically the entire upward pressure serves to overcome the pseudo-viscous resistance of the subcrustal layer, and it is this last effect which determines the speed of rising.

For the bending stress  $\sigma$  and  $-\sigma$  in the upper and lower boundary, respectively, of the crust corresponding to  $\frac{1}{3600}M$  we find

$$\sigma = \frac{6}{T^2} \times \frac{M}{3600} = \frac{\rho g \xi_0}{600 T^2} \frac{L^2}{\pi^2} \sin \pi \frac{x}{L} \quad (10B-8)$$

$\sigma$  has its maximum value in the axis of the upbending, and when the value for  $\xi_0$  of 500 m given by the evidence in Fennoscandia is introduced, Formula (10B-8) yields a maximum value for  $\sigma$  of 44 kg/cm<sup>2</sup>. So, even if the whole downbending has disappeared, the stress will be small; and since by now probably about one-half the stress has vanished, the present stress will be only about 22 kg/cm<sup>2</sup>, even if we do not assume that it has already been diminished by relaxation during the period of about 10,000 years since the rising started. It seems hardly likely, therefore, that breaking of the crust could have occurred, but the hinge lines suggested by Sauramo<sup>13</sup> may have developed because of the presence of fault planes through the crust caused by other phenomena.

Returning to our previous result, we arrive at the important statement that the crust, although it has followed the rising in the postglacial period, has played no appreciable part in the phenomenon; therefore, the rising cannot provide any indication of the physical properties of the crust. This fact simplifies the problem and makes it possible to neglect the crust and deal solely with the reaction of the plastic subcrustal layer, the properties of which are thereby freed of uncertainties resulting from possible interference by crustal reactions.

## 10B-2. Subcrustal Reaction to Loading or Unloading of the Crust

The quickest reaction to loading or unloading of the crust in which the crust also takes part is the elastic reaction. It has been investigated by

Daly<sup>1</sup> and Darwin.<sup>2</sup> Assuming a sinusoidal shape for the load, Darwin found an uplift  $H$  in the center of

$$H = \frac{ghr\rho}{2\pi\mu} \quad (10B-9)$$

where  $h$  = height load in center

$r$  = radius of load

$\rho$  = density of load

$\mu$  = elastic-shear modulus in the earth

$H$  is assumed to be constant over the area and depth involved. When we apply this formula, in the next section, we shall find good agreement with Daly's estimate of 100 m for Fennoscandia.

A second reaction, also quicker than the effect of viscous flow of the substratum, can be expected to take place in connection with the supposed presence in the mantle of a transition layer at the depth between 200 and 900 km separating the olivine in the orthorhombic phase from a presumed denser phase, perhaps cubic (see Sec. 11-2, where the subject is dealt with in greater detail). The densities of the two phases, reduced to surface pressure and temperature, can be estimated at 3.3 and 4.0, respectively. As mentioned in Sec. 11-2, the release of pressure caused by the crustal unloading can be expected to effect the transition of a certain amount of the denser phase to the lighter one and, as a result, a rising at the surface. The reaction must occur fairly quickly, although, because of the intervening plastic layer of 200 km, it is not so rapid as the elastic rebound. It must stop at a given moment because the transition absorbs heat and the corresponding decrease of the temperature must restore the equilibrium of the two phases. Since the thermal conductivity in the earth is exceedingly small, it cannot affect this change of temperature perceptibly.

The rising at the surface gradually brought about by the viscous flow of the substratum must be accompanied by a reversal of both reactions. The loading causes an elastic reaction in the opposite sense, and the pressure increases again in the transition layer, where a reversed phenomenon must also take place; the rising at the surface must now be diminished by an elastic sinking as well as by a subsidence in accord with the transition of lighter into denser phase.

It can be seen that the presence of the transition layer must increase the rising at the beginning of the isostatic readjustment and decrease it afterwards. The amount of both effects cannot be estimated because the transition heat of the process is unknown. The effect has opposite sign for the isostatic readjustment after a fairly sudden loading of the crust, and so it can again be said that in the beginning the readjustment is accelerated and afterwards delayed.

We now take up the main isostatic readjustment effect, viz., that of

the pseudo-viscous flow in the subcrustal layer. In doing so we shall limit ourselves to the simple case in which the distribution of the loading and unloading of the crust has a harmonic character in  $x$  and  $y$  in the horizontal plane, and we shall neglect the earth's curvature. Although we know that the subcrustal layer behaves as a plastic substance and has a small limit of elasticity (probably about  $10^7$  dynes/cm $^2$ ), which has to be overcome before flow can set in, we shall assume it to react like a Newtonian fluid, i.e., one without any such limit, and with a strain velocity proportional to the stress deviator. We can then apply the equations for viscous fluids. As the velocity components  $u$ ,  $v$ ,  $w$  are small—probably of the order of 1 cm/year—we can neglect the squares and products of these quantities. We shall assume incompressibility. Denoting the pressure by  $p$ , the equations become

$$\rho \frac{\partial u}{\partial t} = - \frac{\partial p}{\partial x} + \eta \nabla^2 u \quad \Delta^2 = \frac{\partial^2}{\partial x^2} + \frac{\partial^2}{\partial y^2} + \frac{\partial^2}{\partial z^2} \quad (10B-10a)$$

$$\rho \frac{\partial v}{\partial t} = - \frac{\partial p}{\partial y} + \eta \nabla^2 v \quad (10B-10b)$$

$$\rho \frac{\partial w}{\partial t} = - \frac{\partial p}{\partial z} + \eta \nabla^2 w + \rho g \quad (10B-10c)$$

$$\frac{\partial u}{\partial x} + \frac{\partial v}{\partial y} + \frac{\partial w}{\partial z} = 0 \quad (10B-11)$$

Here and in Chap. 11 we have kept the usual sign for stresses, giving tension a positive sign and thus reversing the signs given stresses elsewhere in this book. We thus have

$$p = -\frac{1}{3}(\sigma_x + \sigma_y + \sigma_z) \quad (10B-12)$$

and for the relations of stresses and velocities

$$\sigma_x = -p + 2\eta \frac{\partial u}{\partial x} \quad (10B-13a)$$

$$\sigma_y = -p + 2\eta \frac{\partial v}{\partial y} \quad (10B-13b)$$

$$\sigma_z = -p + 2\eta \frac{\partial w}{\partial z} \quad (10B-13c)$$

$$\tau_x = \eta \left( \frac{\partial w}{\partial y} + \frac{\partial v}{\partial z} \right) \quad (10B-13d)$$

$$\tau_y = \eta \left( \frac{\partial u}{\partial z} + \frac{\partial w}{\partial x} \right) \quad (10B-13e)$$

$$\tau_z = \eta \left( \frac{\partial v}{\partial x} + \frac{\partial u}{\partial y} \right) \quad (10B-13f)$$

According to our assumption of a harmonic distribution in the  $x$  and  $y$  directions, and supposing the main phenomenon to be a slow approach to equilibrium, we shall further assume  $u$ ,  $v$ ,  $w$ , and  $p$  to be functions of  $z$  multiplied by

$$Ke^{-kt} = \cos lx \cos mye^{-kt} \quad (10B-14)$$

$K$  is a harmonic function of  $x$  and  $y$  which fulfills the equation

$$\nabla^2 K + f^2 K = 0 \quad \text{with} \quad f^2 = l^2 + m^2 \quad (10B-15)$$

This leads to the following solution, which fulfills (10B-11):

$$\begin{aligned} u &= \frac{1}{f^2} \frac{\partial w_0}{\partial z_0} \frac{\partial K}{\partial x} e^{-kt} & w &= w_0 Ke^{-kt} \\ v &= \frac{1}{f^2} \frac{\partial w_0}{\partial z_0} \frac{\partial K}{\partial y} e^{-kt} & p &= p_0 Ke^{-kt} + \rho g z \end{aligned} \quad (10B-16)$$

in which  $w_0$  and  $p_0$  are functions of  $z$  only. Introducing (10B-16) into (10B-10a) or (10B-10b) and dividing by  $(\partial K / \partial x)e^{-kt}$  and  $(\partial K / \partial y)e^{-kt}$ , respectively, we obtain

$$p_0 = - \left( \eta - \frac{\rho k}{f^2} \right) \frac{\partial w_0}{\partial z} + \frac{\eta}{f^2} \frac{\partial^3 w_0}{\partial z^3} \quad (10B-17)$$

Introducing both this formula and (10B-16) into (10B-10c) and dividing by  $(\eta/f^2)Ke^{-kt}$ , we find the following equation for  $w_0$ :

$$\frac{\partial^4 w_0}{\partial z^4} - \left( 2f^2 - \frac{\rho k}{\eta} \right) \frac{\partial^2 w_0}{\partial z^2} + f^2 \left( f^2 - \frac{\rho k}{\eta} \right) w_0 = 0 \quad (10B-18)$$

If we put

$$f^2 - \frac{\rho k}{\eta} = s^2 \quad (10B-19a)$$

the solution is

$$w_0 = A_1 e^{-fz} + B_1 e^{fz} + A_2 e^{-sz} + B_2 e^{sz} \quad (10B-19b)$$

Our supposition that the time dependence of the phenomenon is simply given by the factor  $e^{-kt}$  is confirmed by our solution; after this factor is introduced, the time vanishes from the equations.

Examining Formulas (10B-19) for  $w_0$ , we see that, if we apply them to the earth,  $\rho k/\eta$  is negligible with respect to  $f^2$ . For Fennoscandia we can put  $k = 2.3 \times 10^{-12}$  sec $^{-1}$ ,  $f = \pi/1.4 \times 10^8 = 2.2 \times 10^{-8}$  cm $^{-1}$ , and therefore  $f^2 = 5 \times 10^{-16}$  cm $^{-2}$ ; since  $\rho = 3.3$  and  $\eta = 1.5 \times 10^{22}$ , we have  $\rho k/\eta = 5 \times 10^{-33}$  cm $^{-2}$ . So the ratio of this quantity to  $f^2$  is of the order of  $10^{-17}$  and is therefore entirely negligible.

Hence we may neglect the difference of  $f$  and  $s$ . As this leads to two pairs of equal roots of the equation which gives the solution of (10B-18), that solution now assumes the form

$$w_0 = -A(qz + 1)e^{-fz} + B(nz + 1)e^{fz} \quad (10B-19c)$$

where  $A$ ,  $B$ ,  $q$ , and  $n$  are the four integration constants. They can be derived from the boundary conditions. If we assume that for  $z = \infty$  the velocity components vanish, we have  $B = 0$ , and the second term of  $w_0$  disappears.

The factors of  $u$  and  $v$ , which are dependent on  $z$ , are proportional to  $\partial w_0 / \partial z$ , which now is given by

$$\frac{\partial w_0}{\partial z} = A(fqz + f - q)e^{-fz} \quad (10B-20a)$$

and the factors, containing  $z$ , of  $\tau_x$  and  $\tau_y$  [Formulas (10B-13d) and (10B-13e)] are proportional to

$$w_0 + \frac{1}{f^2} \frac{\partial^2 w_0}{\partial z^2} = -2 \frac{A}{f} (fqz + f - q)e^{-fz} \quad (10B-20b)$$

Our second boundary condition is  $\tau_x = \tau_y = 0$  for  $z = 0$ . From Formulas (10B-20) it follows that this implies  $q = f$  and that then  $u$  and  $v$  also vanish for  $z = 0$ . This is in harmony with the fact that the readjustment of isostatic equilibrium in Fennoscandia and in North America does not seem to be accompanied by folding of the crust.

We are now able to write down the complete solution.

$$u = Az \frac{\partial K}{\partial x} e^{-fz-kt} \quad (10B-21a)$$

$$v = Az \frac{\partial K}{\partial y} e^{-fz-kt} \quad (10B-21b)$$

$$w = -A(fz + 1)Ke^{-fz-kt} \quad (10B-21c)$$

As  $p_0 = -\eta \left( \frac{\partial w_0}{\partial z} - \frac{1}{f^2} \frac{\partial^3 w_0}{\partial z^3} \right) = -2\eta f A e^{-fz}$

we find

$$p = \rho g z - 2\eta A f K e^{-fz-kt} \quad (10B-22a)$$

and

$$\sigma_x = -\rho g z + 2\eta A \left( fK + z \frac{\partial^2 K}{\partial x^2} \right) e^{-fz-kt} \quad (10B-22b)$$

$$\sigma_y = -\rho g z + 2\eta A \left( fK + z \frac{\partial^2 K}{\partial y^2} \right) e^{-fz-kt} \quad (10B-22c)$$

$$\sigma_z = -\rho g z + 2\eta A (1 + fz) f K e^{-fz-kt} \quad (10B-22d)$$

$$\tau_x = -2\eta A fz \frac{\partial K}{\partial y} e^{-fz-kt} \quad (10B-22e)$$

$$\tau_y = -2\eta A fz \frac{\partial K}{\partial x} e^{-fz-kt} \quad (10B-22f)$$

$$\tau_z = 2\eta A z \frac{\partial^2 K}{\partial x \partial y} e^{-fz-kt} \quad (10B-22g)$$

Obviously, the value of  $\sigma_z$  for  $z = 0$  equals the vertical deviation from equilibrium at the surface, which we shall denote by  $\xi$ , multiplied by  $\rho g$ . Hence we find

$$\xi = \frac{2\eta f}{\rho g} A K e^{-kt} \quad (10B-23)$$

and since the differential  $\dot{\xi}$  of  $\xi$  with respect to the time must equal the value of  $w$  for  $z = 0$ , we obtain

$$-\frac{2\eta f}{\rho g} k A K e^{-kt} = -A K e^{-kt}$$

or

$$k = \frac{\dot{\xi}}{\xi} = \frac{\rho g}{2\eta f} \quad (10B-24)$$

As  $f$  is inversely proportional to the linear dimensions of the harmonic distribution, the formula shows the readjustment velocity  $\dot{\xi}$  to be proportional to the linear dimensions (we return later to this important result).

The values of  $\xi$  and  $\dot{\xi}$  at the surface can be measured in so far as we can succeed in taking into account the effects of the elastic rebound and of the transition layer between 200 and 900 km, and thus the formula enables us to derive  $\eta$ .

Our solution, however, is based on a harmonic distribution of these quantities, i.e., distribution proportional to the formula

$$K = \cos lx \cos my$$

and so whenever the distribution is not harmonic, e.g., the postglacial rise of Fennoscandia, it will require a development either in a two-dimensional Fourier series or, if the problem is two-dimensional, in a simple Fourier series.

The solution for a spherical harmonic distribution can be given in a similar way and is useful, for example, for an axisymmetric distribution of the loading or unloading of the crust (for this development and solution see Niskanen<sup>11</sup>).

Evidence for the Fennoscandian phenomena has been given by experiments which were made with oil of high viscosity, provided by De Nederlandsche Aardolie Maatschappij, and which were carried out by B. J. Collette at the Mineralogical and Geological Institute in Utrecht. A flat circular depression was made in the oil surface, and observation of the subsequent readjustment of the equilibrium showed, at the border of the depression, a circular rising belt which came above the original oil surface. This result agrees with the harmonic-distribution solution given in this section: the original depression of the oil surface develops in harmonic waves, and since the longer waves disappear more quickly, the shorter upward waves around the central part of the depression rise above the original surface.\*

### 10B-3. Evidence in Fennoscandia; Approximate Conclusions about $\eta$

The evidence of postglacial isostatic readjustment in Fennoscandia is clearer and more extensive than in North America. The data are of three types. (1) The geological evidence from old shorelines and varves gives the relative position of the ground with respect to sea level during the whole period since the ice disappeared. It is apparent that use of this evidence requires a study of the changes of sea level during the period. (2) Tide gauges and marigraphs give indications of the relative movements with respect to sea level at the present time. Care must be taken to investigate the reliability of these indications because of possible changes of gauge position with respect to the ground. (3) Leveling operations repeated after sufficient time intervals give important results and make it possible to get accurate data on differences in rising throughout a whole country. Especially noteworthy is the high-precision leveling carried out in Finland in 1892 to 1910 and repeated with still higher precision since 1933. (For details see Kukkamäki,<sup>7</sup> who played a leading part in these important operations, and Kääriäinen,<sup>6</sup> who gives an extensive summary of the history and data regarding the Fennoscandian phenomena, the complete results of the second leveling survey, and the rate of rising derived therefrom for the Finnish territory.)

\* A paper on the results of these experiments and on the application of the harmonic-distribution solution given here to the Fennoscandian postglacial uplift is to be published.

TABLE 10B-1. POSTGLACIAL DEPRESSION  $d$  AND VELOCITY OF UPLIFT  $w_0$  IN THE CENTRAL PART OF FENNOSCANDIA (ÅNGERMANLAND)

$t$ , years (1)	$d$ , m (2)	$d'$ , m (3)	$w'_0$ , cm/year (4)	$k \times 10^{12}$ , sec $^{-1}$ (5)	$w_0$ , cm/year (6)	$w'_0 - w_0$ , cm/year (7)
8000 b.c.	556	556	22.1	12.60	10.53	11.6
6800	376	347	11.8	9.96	7.12	4.7
6000	306	266	6.86	7.11	5.79	1.07
5000	273	229	3.76	4.37	5.17	-1.41
4000	244	194	3.06	3.95	4.62	-1.56
3000	220	166	2.51	3.62	4.16	-1.65
2000	200	142	2.09	3.31	3.79	-1.70
1000	184	124	1.78	3.07	3.48	-1.70
0	170	108	1.56	2.91	3.22	-1.66
A.D. 1000	157	93	1.41	2.84	2.97	-1.56
1950	146	80	1.31	2.84	2.76	-1.45

In the ensuing short summary of the data and their implications we use the data provided by Daly,<sup>1</sup> Nansen,<sup>9</sup> Lidén,<sup>8</sup> Sauramo,<sup>13</sup> and Gutenberg.<sup>3</sup> The best and most consistent figures can be given for the central area, which is generally assumed to be in Ångermanland, on the west coast of the Gulf of Bothnia. Column 2 of Table 10B-1 gives the values of the depression  $d$  in meters as given by Nansen but with 146 m added for the amount we can assume to be still present at this time. The value of the added amount is derived from the mean negative anomaly in the area, which may be estimated at about -20 mgal. The oldest value, 556 m, is derived from the figure given in 1928 by Nansen<sup>9</sup> (p. 63), i.e., 270 m for the depression before the year 6800 b.c.; the total depression of 646 m thus obtained is diminished by 90 m to allow for the elastic rebound as given by Formula (10B-9). The value 90 m is obtained by introducing for  $h\rho$  the product of 646 m multiplied by  $\rho = 3.27$ , which can be expected to equal the corresponding product for the ice load, and by putting  $r = 1100$  km and  $\mu = 4 \times 10^{11}$  dynes/cm $^2$ . On the fictitious supposition that the ice load corresponding to the maximum depression of 556 m disappeared suddenly, the moment of its disappearance is estimated as 8000 b.c. For the years 1000 b.c., 0, and A.D. 1000 the figures for  $d$  have been interpolated between the values for 2000 b.c. and A.D. 1950. For the latter period the present rising in Ångermanland of 1.1 cm/year found by precise leveling has also been taken into account.

During the whole course of the phenomenon the change of the depression  $d$  must have consisted of the three parts mentioned in Sec. 10B-2. The

main part is the decrease caused by the subcrustal flow, for which we derived formulas in the preceding section. This decrease is diminished by two effects: (1) the elastic compression resulting from the increase of pressure caused by the decrease of the depression  $d$  and (2) the transition from the lighter to the denser phase in the layer between 200 and 900 km depth, which occurs for the same reason. Of these two effects, the elastic one can be determined. The determination has been made, and the results have been subtracted from the values of  $d$ ; column 3 of Table 10B-1 lists the figures for the corrected depression  $d'$  thus obtained.

Column 4 gives the figures for the rising  $w'_0$ , in centimeters per year, derived from  $d'$ . They represent the rising through subcrustal flow combined with the effect of the phase transition in the layer between 200 and 900 km depth.

For a further investigation of the problem we must develop the distribution of the depression over the whole area in a double Fourier series or in spherical harmonics (Niskanen<sup>11</sup>) and use the solution of the preceding section. We shall not carry this out but refer again to the publication mentioned above (see footnote on page 365). We shall accept here the approximate solution based on the supposition that the Fennoscandian unloaded area forms part of a region where the loading and unloading are harmonically distributed.

If we start by neglecting the effect of the transition layer, we can derive for each moment, by means of Formula (10B-24), the quantity  $k$  by dividing the values of column 4 by those of column 2. To change the time unit to seconds and the length unit to centimeters we multiply the quotients by  $3.17 \times 10^{-10}$ . The results are listed in column 5.

It can be assumed that the variations of these values are caused mainly by the phase transitions in the layer from 200 to 900 km depth. At the beginning of the adjustment phenomenon they must have been caused by the pressure release resulting from the ice removal and the corresponding transition from the denser to the lighter phase which brought about the high figures of  $w'_0$  and  $k$  at 8000 and 6800 B.C. During the further course of the phenomenon the gradual restoring of the isostatic balance must have had the opposite effect, though at a slower rate; the increase of pressure must have led to a transition of the lighter to the denser phase. This transition must have caused the velocity of rising to diminish at a lower rate than the rate of increase at the start, and, if it is assumed that at the end the original ratio of the two phases has been reestablished, the integral of  $w'_0$  at that moment with respect to time must be undisturbed. Thus we arrive at the rough estimate that the undisturbed value of  $k$  must be about  $6 \times 10^{-12} \text{ sec}^{-1}$ .

Column 6 of Table 10B-1 gives the values of  $w_0$ , in centimeters per year, based on this value of  $k$ . They are derived by multiplying the values of

$d$  of column 1 by  $6 \times 10^{-12} / 3.17 \times 10^{-10} = 0.01893$ . Column 7 lists the differences  $w'_0 - w_0$  which we assume to have been caused by the phase transitions and the integral of which with respect to time we thus suppose (if our estimate of  $k$  has been right) to vanish toward the end of the phenomenon. From the values of this column it appears likely that this condition will be reasonably well fulfilled, but since no details of the phase-transition phenomena or of the time and distribution of the unloading of the crust by ice removal are known, no definite conclusion is possible. From closer investigation, however, it seems likely that  $k$  must be between  $5 \times 10^{-12}$  and  $7 \times 10^{-12} \text{ sec}^{-1}$ . At any rate, this represents an accuracy which we cannot expect to surpass.

By means of (10B-24) it is simple, once  $k$  is known, to derive  $\eta$ . For Fennoscandia we can assume  $f = \pi / 1.2 \times 10^8 = 2.62 \times 10^{-8}$ , which corresponds to dimensions for the depression of 1400 km in one direction and 2300 km at right angles to it. This, combined with  $\rho = 3.27$  and  $k = 6 \times 10^{-12} \text{ sec}^{-1}$ , leads to

$$\eta = 1.02 \times 10^{22} \text{ poises} \quad (10B-25a)$$

while for values of  $k$  of  $5 \times 10^{-12}$  and  $7 \times 10^{-12} \text{ sec}^{-1}$  we find  $\eta = 1.22 \times 10^{22}$  and  $0.87 \times 10^{22}$  poises, respectively. It is probable, however, that these values are too high. The supposition of a harmonic distribution implies four areas around Fennoscandia having an elevation equal to the depression there, which must favor the subcrustal current leading to the readjustment of isostatic equilibrium. If we assume that this adds 50 per cent to the readjustment velocity, we come to an estimate for  $\eta$  of the order of

$$\eta = 10^{22} \text{ poises} \quad (10B-25b)$$

In view of the uncertainties involved in the data and treatment of the problem, we cannot consider this as more than an estimate of the order of magnitude of  $\eta$ .

In North America the phenomena have no doubt covered a much larger area than in Europe and have certainly been more complicated because of their geographical distribution. We know that at present both rising and sinking occur, and under the circumstances this fact can hardly surprise us. The movements and the gravity field are not sufficiently well known at the present time for even an attempt at explanation, and the same is true of other glaciated and deglaciated areas in the Northern Hemisphere.

#### 10B-4. Conclusions about the Rate of Readjustment of Isostatic Equilibrium

The Fennoscandian phenomena can be used to derive a rate of isostatic adjustment which is probably generally valid for all cases of deviation

from equilibrium caused by phenomena occurring in the crust or at the surface of the subcrustal layer. Since the effects of elastic behavior and of transitions of phase in the layer from 200 to 900 km depth are proportional to the same pressure differences dominating the main effect (that of plastic flow in the subcrustal layer), it can be expected that all vertical-velocity components will more or less satisfy the equations of Sec. 10B-2 derived for the latter phenomenon, especially (10B-24). The effects of phase transitions, however, appear to have a time lag with respect to the flow phenomenon, and this lag, as shown in the preceding section, is a disturbing influence.

From the Fennoscandian data we derived a value for  $k$  of about  $6 \times 10^{-12} \text{ cm}^{-1}$ , which leads to a relaxation time  $t_r$  (during which the deviation from isostasy diminishes to  $1/e$  of its value) of about  $t_r = 1/k = 0.167 \times 10^{12} \text{ sec} = 5280 \text{ years}$ . From columns 2 and 5 of Table 10B-1 we may conclude that this result checks reasonably well with the values of  $d$  and  $k$  in Fennoscandia, although the effect of the phase transition in the layer from 200 to 900 km depth causes the phenomenon to proceed at greater velocity in the beginning and more slowly afterwards.

As Formula (10B-24) shows,  $k$  is proportional to the dimension  $L = \pi/f$  of the phenomenon, and so  $t_r L$  equals the same constant for all cases of deviations from isostasy. Since for Fennoscandia we can assume  $L = 1.2 \text{ Mm}$  ( $1 \text{ Mm} = 1 \text{ megameter} = 1000 \text{ km}$ ), we obtain in general

$$t_r L = 6.3 \text{ Mm } y_m \quad (10B-26a)$$

in which  $t_r$  is expressed in the unit of 1000 years, which we indicate by  $y_m$ .

In this formula,  $L$  is the horizontal dimension, in megameters, of a depression which in the second horizontal direction has infinite dimension. From the second formula of (10B-15) it follows that if in the second direction the depression has a dimension of  $M \text{ Mm}$ , Formula (10B-26a) becomes

$$\frac{t_r LM}{\sqrt{L^2 + M^2}} = 6.3 \text{ Mm } y_m \quad (10B-26b)$$

From our considerations it follows that the same relaxation time  $t_r$  is valid not only for the subsidence or elevation corresponding to the deviation from isostasy but also for the vertical velocity in the center of the deviation area. It need not be emphasized that Formulas (10B-26) are only approximate in character.

#### REFERENCES

1. Daly, Reginald: The changing world of the ice age, Yale University Press, New Haven, Conn., 1934.
2. Darwin, George: Phil. Mag., ser. 5, vol. 14, p. 409, 1882.

3. Gutenberg, B.: Changes in sea level, postglacial uplift, and mobility of the earth's interior, *Bull. Geol. Soc. Amer.*, vol. 52, pp. 721–772, 1941.
4. Haskell, N. A.: The motion of a viscous fluid under a surface load, *Physics*, vol. 6, no. 8, 1935; vol. 7, no. 2, 1936.
5. ———: The viscosity of the asthenosphere, *Am. J. Sci.*, vol. 33, 1937.
6. Kääriäinen, E.: On the recent uplift of the earth's crust in Finland, *Publ. Finn. Geod. Inst.*, no. 42, 1953.
7. Kukkamiäki, T. J.: Über zwei dem Präzisionsnivelllement sich anschliessende Fragen, *Publ. Finn. Geod. Inst.*, no. 26, 1939.
8. Lidén, R.: Den senkvartära strandförskjutningens förlopp och kronologi i Ångermanland, *Geol. Fören. i Stockholm Förh.*, vol. 60, no. 3, 1938.
9. Nansen, F.: The earth's crust, its surface forms, and isostatic adjustment, *Avhandl. Norske Videnskaps-Akad. Oslo, I. Mat.-Naturv. Kl.*, vol. 12, 1928.
10. Niskanen, Erkki: On the upheaval of land in Fennoscandia, *Ann. Acad. Sci. Fenniae*, ser. A, III, no. 10, 1939.
11. ———: On the viscosity of the earth's interior and crust, *ibid.*, no. 15, 1948.
12. ———: On the elastic resistance of the earth's crust, *ibid.*, no. 21, 1949.
13. Sauramo, M. R.: The mode of the land upheaval in Fennoscandia during late quaternary time, *Bull. comm. géol. Finlande*, no. 125, 1939.
14. Vening Meinesz, F. A.: The determination of the earth's plasticity from the postglacial uplift of Scandinavia; isostatic adjustment, *Proc. Koninkl. Ned. Akad. Wetensch.*, vol. 40, no. 8, pp. 654–662, 1937.

**PART 10C**  
**ISLAND-ARC AREAS**

### **10C-1. Introduction**

Belts of large negative gravity anomalies are found in many island-arc areas; they are 100 to 200 km wide and usually coincide with islands where the geology shows strong folding and overthrusting. In this part we deal especially with one of these areas, Indonesia, for which the geological and geophysical data are fairly complete, and then we consider the facts known for a few other areas.

Map 10C-1 is a bathymetric map of the Indonesian Archipelago showing the deep basins in the eastern part and three deep trenches: the Java Trench, south of a submarine ridge parallel to the south coast of Java, where the deepest sounding gave 7140 m depth; the Weber Deep, east of the Banda Sea, where a depth of 7440 m has been found; and the southern part of the Philippine Trench, which shows a depth of about 9600 m at the edge of the map but for which figures exceeding 10,000 m have been obtained further north. A fourth trench, the Palao Trench, is just visible in the northeast corner of the map; it is outside the archipelago. Of the deep basins of roughly 5000 m depth, the Celebes Sea shows the deepest figure of 5590 m. The Molucca Sea comprises the Morotai Basin, with a maximum depth of 3890 m north of the island of Halmahera; the Gorontalo Basin, south of the little town of that name, with a depth of 4180 m; and a southeast corner with a maximum figure of 4750 m. The Banda Sea comprises a northern basin with a maximum depth of 5800 m, a main part with a depth of 5400 m southeast of the small volcanic island of Gunung Api, and a western prolongation in the Flores Deep, where a depth of 5140 m has been found. The Java Sea and the sea between Borneo, Sumatra, and Malacca are shallow; their depth does not exceed 70 m. The Java Sea is a shelf sea, which no doubt originated after the ice melted at the end of the glacial period, and in it river beds can be found in the prolongation of rivers of Borneo, Sumatra, and Java. These three islands, therefore, belong to the Asiatic continent. Whether the deep basins in the eastern part of the archipelago are old is uncertain; many geologists consider it probable that many of them, at least, originated in the last 5,000,000 years.

Map 10C-2 shows the gravity anomalies over the water-covered parts and in several harbors. The anomalies have been subjected to the reduction for topography and isostatic compensation according to the regional Airy system for a thickness  $T$  of the crust of 30 km and a radius  $R$  of regional spreading of 174.3 km.\* The major features of this field are the strongly negative belts already mentioned and weaker positive belts accompanying them on both sides; in the deep basins of the eastern part the anomalies are positive. Part of the latter may be caused by the regional reduction of the steep slopes surrounding the basins, which, in so far as they are not volcanic, are likely to be caused by flexures and faulting and thus are probably locally compensated.

The main negative belt coincides with the islands west of Sumatra, where it is probably the continuation, via the Nicobar and Andaman Islands, of the belt in Burma discussed by Evans and Crompton;<sup>5</sup> it continues over the submarine ridge south of Java and then—after a short interruption and a lateral shift near Sumba—along Timor, over the Tanimbar Islands, the Kai Islands, and Ceram, after which a short branch stops west of Buru, and another branch connects it with the second belt. The latter, from the east arm of Celebes, runs between the north arm of that island and Halmahera and further north via the Talaud Islands toward the Philippine Trench. The first belt has long stretches of regular intensity and course; in the stretches where its direction is northwest-southeast the negative anomalies are weaker. The second belt is less regular; it shows two areas of very large anomalies: one over the Molucca Sea, where a value of  $-204$  mgal is found, and one south of the Talaud Islands, where an anomaly of  $-157$  mgal occurs.

In view of the large deviations from isostatic equilibrium in these belts and the fact that the islands situated in them, e.g., Timor, Ceram, and east Celebes, show marked folding and overthrusting, we can conclude that during the last period of great tectonic activity the crust in these zones was subjected to strong lateral compression. According to Umbgrove,<sup>15-17</sup> this deformation must be dated in the upper Miocene. The seismic action over and near these belts indicates that this activity is still continuing.

In Sec. 10A-4 it was shown that lateral compression of the crust above the limit of elasticity must lead to plastic thickening of the crust combined with downbuckling, which presses the crust into a position considerably lower than that of its isostatic equilibrium. Since this evidently must cause a belt of strong negative anomalies, our hypothesis is in harmony with the gravity results. On the sides of the arc, viz., west of

\* The anomalies of the map have not been subjected to the indirect reduction mentioned in Sec. 6-2E. This is a small reduction, usually not more than 3 mgal; its value in the Indonesian stations can be found in Vening Meinesz,<sup>18</sup> pp. 150-233.

Sumatra, east of the Philippine Islands, and southeast of Ceram, the negative anomalies are smaller and so the downpressing seems to be weaker there; at the same time we have evidence there of transcurrent, or "wrench," faulting (Anderson<sup>1</sup>), which would be in agreement with the supposition that the relative movement of the two crustal blocks on both sides of the belt is of the type dealt with in Sec. 10A-8, with only a small compressive component at right angles to the belt. This result fits if we simply picture the cause of the whole Indonesian belt system as the relative movement of two great crustal blocks inside the arc to the south-southeast with respect to the crust outside the arc. The two directions of movement of the blocks are indicated by the arrows on the map; they diverge slightly.

If these directions are identified with uniaxial stress systems working on the blocks, we find that nearly everywhere the parts of the belts where the anomalies are strong, and where downbuckling is therefore the principal phenomenon, make angles of about  $55^\circ$  with the compressive stress. This fact is in good agreement with the results derived in Sec. 10A-7 and again favors our buckling hypothesis. The same may be said regarding the angles between the wrench-faulting parts of the belts, which enclose angles of about  $27^\circ$  with the direction of the compressive stress, thus checking with the results arrived at in Sec. 10A-8. The axes of the islands of Sumatra and Java thus make angles with each other of about  $28^\circ = 55^\circ - 27^\circ$ . Thus we shall see that almost the entire complicated pattern of the tectonic axis in the Indonesian Archipelago can be understood.

In Sec. 10C-2 we examine in more detail the parts of the belts where the strong negative anomalies point to downbuckling as the main phenomenon. In Sec. 10C-3 we deal with the wrench-faulting parts, and in Sec. 10C-4 with the inner arc, which in general has a volcanic character. Its origin may perhaps be accounted for by shear planes taking over the wrench faulting from the tectonic arc.

The questions of the origin of the stress fields resulting in crustal deformations in island-arc areas, of the causes of the intermediate and deep earthquakes occurring there, and of the subsidence of the deep basins are taken up in a study of convection currents in Chap. 11.

### 10C-2. The Downbuckled Belts

The longest downbuckled belt of the Indonesian Archipelago runs from Sunda Strait up to a point past the Kai Islands. Near Sumba an interruption is found. The western part of this belt has a remarkably linear character, which again provides an argument in favor of the buckling hypothesis; if chemical-differentiation processes were the cause of the anomaly belt (van Bemmelen<sup>2</sup>), a more patchy and less linear pattern would have to be anticipated.

The belt shows a great variety of topographic features. South of Java it follows a submarine ridge, of which the highest point comes up to a depth of 1200 m, and which is situated between a trough to the north, of a depth to 3900 m, and a deeper one to the south, of a depth to 7140 m. Further east the belt runs over the trough along the south coast of the island of Timor and still further east over shallow depths alternating with the low Tanimbar and Kai island groups.

Still greater differences are found in the West Indies, where the belt of negative gravity anomalies coincides with the strait north of Haiti, which reaches a depth of about 4000 m, then with the Puerto Rico Trench, where the depths amount to 9200 m, next with the normal ocean depths of 5500 to 6000 m, and finally with the islands of Barbados, Tobago, and Trinidad, between which depths to 1500 m are found.

The strong negative anomalies show that, notwithstanding these different topographic features, the crust must everywhere have been subjected to a common phenomenon. The downbuckling hypothesis fits this requirement. It keeps the crust below its isostatic-equilibrium position and thus causes a deficiency of mass independent of other processes affecting the crust. In the Puerto Rico Trench a great part of the mass deficiency causing the negative anomalies is represented by the trench itself, which shows the downbuckling process of the crust directly. The seismic investigations of Ewing<sup>6</sup> and his collaborators have proved this trench to be deeper than shown by soundings; it is partly filled with unconsolidated sediments, but their depth could not be determined.

Since isostatic reduction of the gravity anomalies transfers the deficiencies of matter from the surface to the lower boundary of the crust, the belt of negative isostatic anomalies must be somewhat broader than the mass-deficiency belt itself.

Some differences of topographic elevation along the belts may have been caused by relaxation of the stresses, for which we find evidence in the eastern half of the Indonesian Archipelago. During the Pliocene, for example, the island of Ceram, the Kai Islands, the Tanimbar Islands, and Timor show graben formation which (see Part D of this chapter) points to tension, at least in the upper layers of the crust. This can obviously be considered as evidence of upbending in the belt and hence as a relaxation phenomenon which might explain the continued rising taking place since the Pleistocene and still continuing.

It is likely, however, that in the present period there is again compression in the belt; the crustal movements during earthquakes in Sumatra and the Philippine Islands, with right-handed and left-handed wrench faulting, respectively, point to it. If so, the present strong rising of the islands already mentioned would be the effect of new wave formation of short wavelength, which may have been prepared by the former relaxation

movements. More research is needed to make sure of this supposition. In Timor the situation seems still more complicated; recent gravimetric research in the eastern part by de Snoo (Texeira<sup>14</sup>) shows that this island, which in the Pleistocene rose in a spectacular way above sea level and even now has an elevation of 2920 m in the center, is presently situated on the northern flank of the belt of negative anomalies. Since positive anomalies of more than 150 mgal have been found on the northeast coast, it is clear that now, at least, the strong rising is due to a new wave formation and is not a relaxation phenomenon. Here again more research is needed before a satisfactory interpretation can be given.

The two north-south profiles over West Java and Bali Strait represented in Figs. 10C-1 and 10C-2 show the topography (tenfold vertical exaggeration) and the gravity anomalies after reduction for the topography and the isostatic compensation. The isostatic reduction has been made according to four different systems of compensation, each corresponding to an anomaly curve in the figures and each based on the Airy principle; the first two systems assume local compensation with  $T = 20$  km and  $T = 30$  km, respectively; the third,  $T = 30$  km and a radius  $R$  of regionality of the compensation of 116.2 km; and the fourth,  $T = 30$  km and  $R = 232.4$  km. The anomaly map (Map 10C-2) is based on  $T = 30$  km and  $R = 174.3$  km, and so it gives anomalies close to the mean of the last two of these four systems of reduction. The regional isostatic systems give the simplest anomaly pattern in the archipelago. We shall not discuss these two gravity profiles in detail, but we may note that the right half of the curves for regional compensation checks well with the anomalies corresponding to the plastic thickening and downbuckling as derived in Secs. 10A-4 to 10A-6. We clearly see the effect of the fairly narrow downbuckled wave, which in Indonesia has no doubt reached the catastrophic stage of deformation, a conclusion that also follows from the great folding and overthrusting found on Timor. We also notice the broader elastic upward wave to the right of the downbuckled part. To the left the profiles are more complicated because of a second crustal wave over Java, viz., an idiogeosyncline, as Umbgrove<sup>15-17</sup> calls it, which has not reached the catastrophic stage, and which, therefore, shows much smaller anomalies than the main belt. It carries oil.

The two topographic profiles, especially that of Fig. 10C-2, are likewise suggestive in connection with crustal deformation. The troughs on both sides of the ridge over the belt of negative anomalies indicate the downbuckling, which in the axis is hidden by matter insufficiently competent to follow the downward movement. As the matter is probably composed mainly of sediments, it is easy to understand why the trough on the ocean side is deeper than the one on the continental side. On the ocean side of this deeper trough the topographic profile of Fig. 10C-2

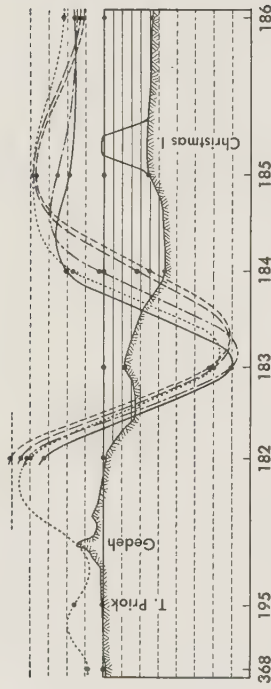


Fig. 10C-1. Gravity profile over Djakarta and Christmas Island. Local isostatic anomalies ( $T = 20$  km) indicated by short-dashed lines; local isostatic anomalies ( $T = 30$  km) indicated by long-dashed lines; regional isostatic anomalies ( $T = 30$  km,  $R = 116.2$  km) indicated by dotted lines; regional isostatic anomalies ( $T = 30$  km,  $R = 232.4$  km) indicated by solid lines; Hayford-Bowie isostatic anomalies indicated by dots. Horizontal scale, 1:8,240,000; vertical scale, 1:824,000; line interval in oceans = 1000 m = 10 mgal; line interval elsewhere = 2000 m = 20 mgal.

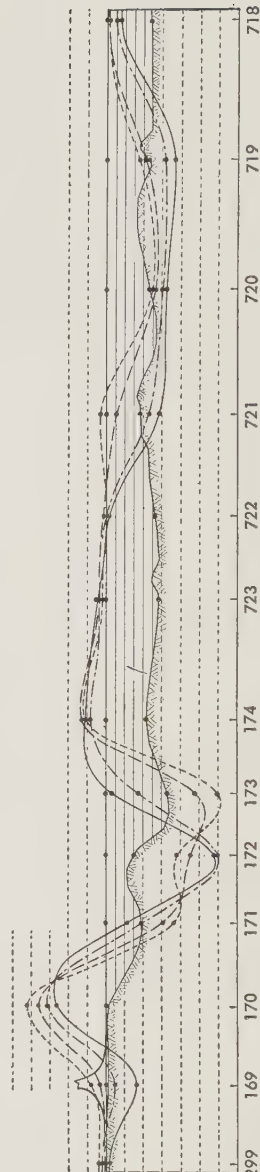


Fig. 10C-2. Gravity profile over Bali Strait, continued through the Indian Ocean up to the Northwest Cape of Australia.

shows clearly the upward elastic wave suspected, but the presence of Christmas Island (Fig. 10C-1), which represents a load on the crust, no doubt complicates matters by preventing the wave from developing fully.

Map 10C-2 shows how most of the pattern of the two strong negative anomaly belts of the Indonesian Archipelago can be explained by Bijlaard's<sup>4</sup> theory of plastic deformation in thin plates (Sec. 10A-7). As mentioned before, uniaxial compressive stress must lead to deformation belts making angles of 55° with the stress. This angle is realized in many places: in the two wings of the northern belt that run from the Molucca Sea to east Celebes and from the Molucca Sea to the north-northeast; in the direction of the belt over Ceram; in the two wings of the southern belt meeting at the southwest tip of the Tanimbar Islands; and, lastly, in the long part of the southern belt from Sunda Strait to Sumba. Although the western portion of this last part does make an angle of about 55° with the arrow on the map indicating the direction of the compression, toward the east the angle gradually increases, and thus the belt is slightly curved. The curvature can perhaps be accounted for by the fact that the plastic flow can be expected to have a component in the direction of the belt toward the east (Bijlaard<sup>4</sup>), which might give rise to a secondary compressive stress in the eastern part of the belt. According to Formula (10A-48), a value  $\rho_2 = 0.4\rho_1$  corresponds to  $\alpha = 20^\circ$  and therefore to an angle between the plastic belt and the main compressive stress of 70°, which checks with the angle shown by Map 10C-2 near the island of Lombok.

It is interesting to notice that the inner arc, i.e., the volcanic arc, shows hardly any curvature over Java, Bali, Lombok, and Sumbawa; nor does it do so further to the east, where the tectonic arc over Sumba, Rotti, and Timor deviates strongly to the south (see Sec. 10C-4).

The gravity field over the area of Sumba and Timor is not known sufficiently well to allow interpretation of the trend of the belt in that part, and so we must refrain from attempting an explanation.

### 10C-3. The Wrench-faulting Parts of the Belts

If we assume that in the whole western part of the archipelago both the relative movement and the uniaxial compressive stress have the direction given by the arrow in Map 10C-2, the angle made with the belt west of Sumatra is about 27°. This figure is in harmony with the supposition that the principal phenomenon here has the character of wrench faulting. At the same time, the component of the stress at right angles to the belt, which, as we saw (Sec. 10A-8), must have a value of 0.206 times the total compressive stress, causes compression of the crust and brings about a belt of negative anomalies weaker than, for example, south of Java.

In Sec. 10A-8 we found that the component of the stress parallel to the belt must have a value of 0.404 times the total compressive stress. It causes right-handed wrench faulting, which agrees with what has been observed (although not in a fault plane in the belt itself but in a parallel plane in the western zone of Sumatra). That the Sumatra block moves to the southeast with respect to the Indian Ocean block was found by Muller,<sup>13</sup> who made a new triangulation after the earthquake of May, 1892. The results showed that several triangulation points northeast of a fault plane had shifted, on the average, about 2 m to the southeast with respect to a set of points southwest of the plane, along which the faulting had obviously taken place; the plane was parallel to the belt of negative anomalies.

It is difficult to say whether shear is also going on in the belt itself at present, but it most likely has at least begun there. The compressive-stress component probably does not exceed the elastic limit and is therefore too small to cause plastic thickening and downbuckling. It is easier to understand the downpressing of crustal matter in the belt, as proved by the negative anomalies, if it is assumed that the wrench shear occurred not in a vertical fault plane but, under the effect of the compressive stress component, in an inclined plane, thereby causing the crustal block on the Sumatra side to override, more or less, that on the Indian Ocean side. The resulting concentration of crustal matter in the belt is responsible for the negative anomalies.

The topographic profiles at right angles to the belt (Figs. 10C-3 and 10C-4) are in good agreement with this hypothesis, as they show a downpressing of the floor of the Indian Ocean at the foot of the outward island slope and a broad upbending further out to sea which closely resemble the elastic-bending curve of the crust (Fig. 10A-4) derived for a broken crust loaded at the end with a force  $P$ . Figures 10C-3 and 10C-4 give the gravity and topography profiles through the ports of Padang and Benkulen, respectively.

In the four gravity-anomaly profiles of each of these figures (which give the anomalies reduced as in Figs. 10C-1 and 10C-2) the curves for the two regional isostatic anomalies are again somewhat simpler than those for the local anomalies. Since the regional isostatic anomalies over the Indian Ocean are in harmony with the topography of the upbending crustal wave, it can be concluded that this wave is probably a deviation of equilibrium caused by the load exerted on the crust in the belt.

An interesting conclusion can be drawn from the earthquake foci in this area. Figure 10C-5 shows three maps by Koning<sup>11</sup> of the foci in the Indonesian Archipelago between 0 and 50, 50 and 100, and 100 and 150 km depth. Examining these maps, we see that many foci west of, or over, Sumatra and south of Java are deeper than 50 km and that some are even

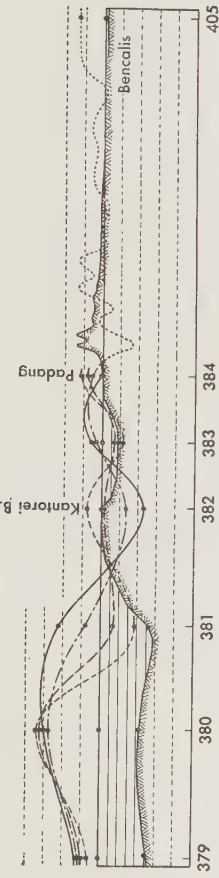


FIG. 10C-3. Gravity profile over Padang.

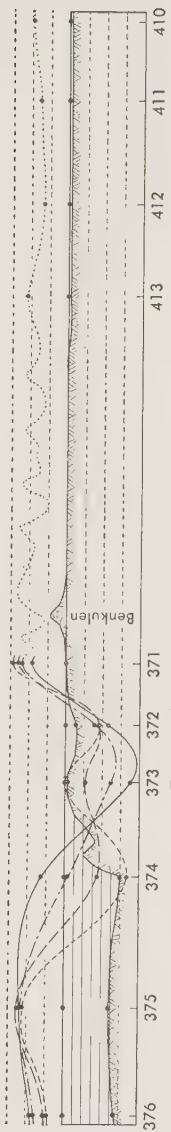


FIG. 10C-4. Gravity profile over Benkulen.

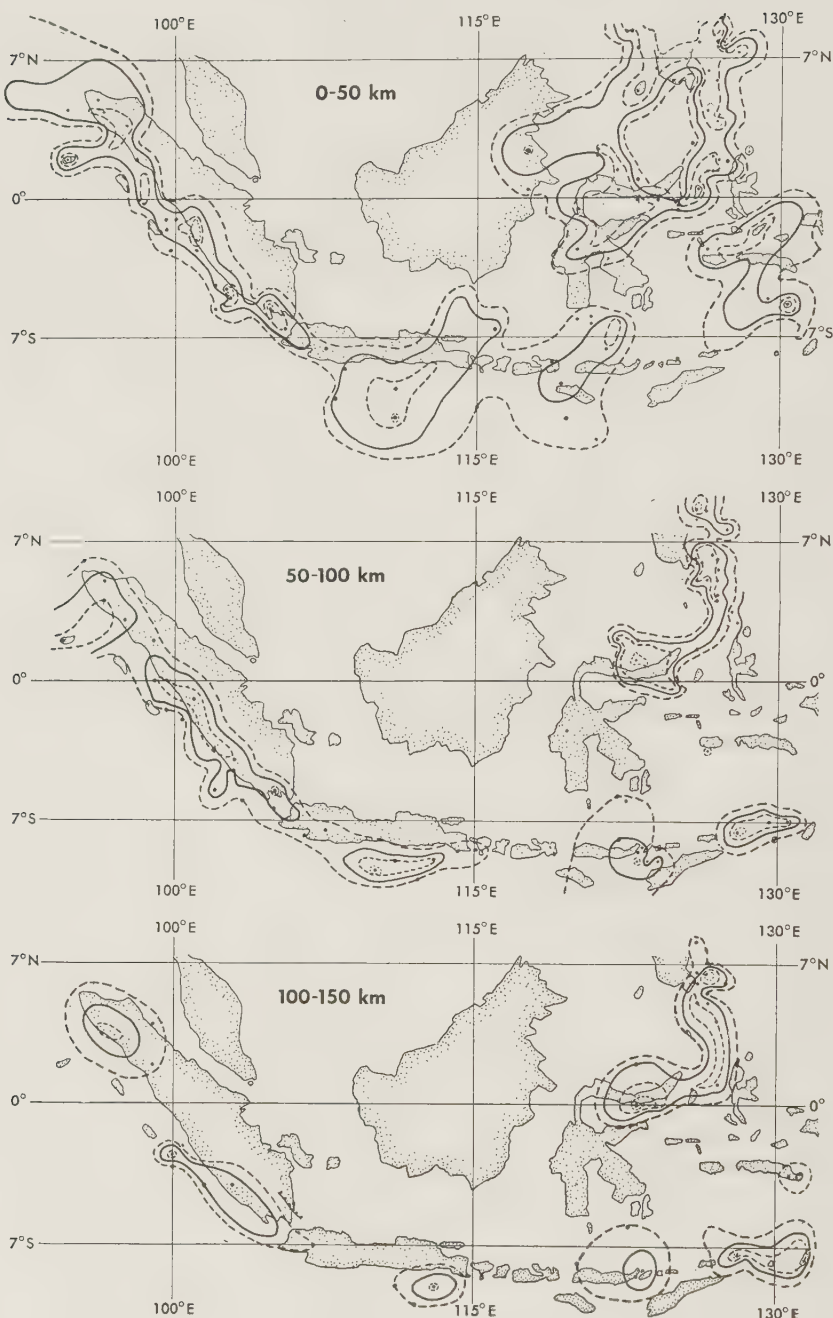


FIG. 10C-5. Seismic maps of foci up to depths of 150 km by Koning.<sup>8</sup>

deeper than 100 km. We notice that the deepest ones west of Sumatra occur in the areas in the northern and southern parts of the anomaly belt where the anomalies are largest. Still, even there we should not expect the crustal downpressing to reach deeper than 50 km, and so it seems that the sudden deformations connected with it go deeper down in the subcrustal matter than might be anticipated. Attention should be drawn, however, to the statement in Sec. 2-3 about the boundary between the crust and the plastic substratum. Such a boundary is no more than a schematic picture, and we probably have to assume a gradual transition of the physical constants, e.g., the modulus of pseudo viscosity and the limit of elasticity. Sudden changes of stress, such as those brought about by a giving way of the "crust," may no doubt be propagated to greater depth, and there lead to rupture.

The crustal phenomenon found east of the Philippine Islands is probably similar to that found west of Sumatra, viz., a wrench faulting under an angle of between  $20^\circ$  and  $27^\circ$  with the compressive stress. Here again there are at the present time parallel fault planes on the inside of the deep trench, which here represents the belt of negative anomalies. During earthquakes these fault planes seem to work as anticipated: the western block moves to the south-southeast with respect to the eastern block, resulting in left-handed wrench faulting (Brouwer<sup>3</sup>). In Fig. 10C-6 the gravity anomalies and the topography are given—though not in great detail—for a profile over the trench east of Surigao Strait made during one of the earlier expeditions. As far as can be ascertained from these data, the profile of the topography is in harmony with the hypothesis of a downpressing of the floor of the Pacific Ocean by the continental crust of the Philippine Islands. The same conclusion can be drawn from the gravity anomalies (the four anomaly curves have the same meaning as before). The main deficiency of mass here is obviously the trench itself, a fact that can be demonstrated as follows. If the deficiency is transferred to the lower boundary of the crust by isostatic reduction, the anomalies nearly disappear in the curve for the regional reduction, which spreads the compensation masses over an area nearly 500 km in diameter.

Hence we can probably conclude that a trench can originate not only by crustal thickening and downbuckling of the crust but also as the result of a phenomenon characterized mainly by shear. In that event the com-

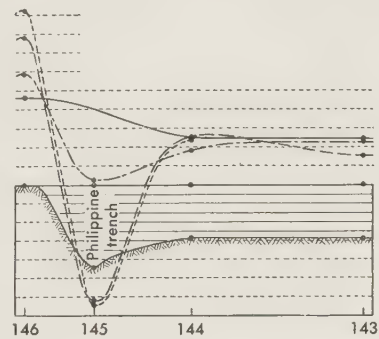


FIG. 10C-6. Gravity profile over Surigao Strait.

pressive stress component is too small to exceed the limit of elasticity and therefore cannot cause plastic thickening of the crust. It makes the crustal shear plane deviate from the vertical and tilt sufficiently to cause not only wrench faulting but also some thrust faulting. Besides the horizontal displacement along the fault plane, therefore, a pressing down of the ocean floor and a rising of the continental side occur. If there is no disturbing effect due to sedimentation, the negative anomaly ought to correspond entirely to the mass deficiency given by multiplying the volume of the trench by the density  $\rho_s$  of the subcrustal matter diminished by the density  $\rho_w$  of sea water. For the Philippine Trench this seems to be true.

It is clear that in an island arc this type of trench can develop only on the wings of the arc, while in the central part a trench must originate by plastic crustal thickening and downbuckling, e.g., the trench south of Java.

The last parts of the belt of negative anomalies in Indonesia, which probably have not been subjected to strong crustal downbuckling, are those running from the Kai Islands to the east corner of the island of Ceram and from west Ceram to the northwest. Both parts are more or less parallel to the direction of the supposed uniaxial compression, and so the relative movement of the blocks on both sides of the belt must be mainly shear movement. The weakness of the anomalies in these parts is therefore in harmony with our suppositions.

#### 10C-4. The Volcanic Arc

In the Indonesian Archipelago the distance between the tectonic and volcanic arcs generally varies between 180 and 250 km, and these figures usually seem valid for other island arcs.

Two properties of the volcanic arc can be stated. First, the volcanic arc is always the inner one with respect to the tectonic arc, where the main crustal deformations occur; or, stated in more detail, volcanoes usually occur on the concave side of the tectonic arc and never on the convex side. In the present period, for example, the volcanoes of the southern Indonesian arc are interrupted north of Timor, where the tectonic arc reverses its curvature. Another interesting volcanic distribution is found around the Molucca Sea, where volcanoes occur on the east side as well as on the northwest side, but here two tectonic arcs join, and the north Celebes-Sangihe Island volcanic arc and the Ternate-Batjan row of volcanoes both obey the rule. If the tectonic arc is straight, the volcanoes usually occur on the continental side, as they do, for example, in Sumatra.

Second, the volcanic arc usually is more regular and nearer a straight line than the tectonic arc. A striking example is the Sunda Islands arc.

The row of volcanoes over Java, Bali, and Lombok is practically a straight line, which, in the Sunda Strait, makes an angle with the straight line of volcanoes over Sumatra; however, both the belt of negative gravity anomalies and the submarine ridge more or less coinciding with it show a smooth curve to the southwest of the Sunda Strait and follow a curved track south of Java. Further to the east the tectonic arc is irregular, showing two outward bulges in the Sumba-Timor and in Tanimbar Islands areas, while the volcanic arc follows a regular course over the whole distance and for two-thirds of it is close to a straight line.

This second property, the tendency of the volcanic arc to be straight, points to its being connected with fault planes in the crust. Since such planes can never be so smooth that wrench faulting along them would not open opportunities for the magma to rise to the surface, their coincidence can be understood with volcanoes. In harmony with this point of view is the fact that in Sunda Strait, where the two fault planes—perhaps we should say fault zones—through Sumatra and Java meet, is found the particularly active volcano of Krakatoa. A stronger proof is the fact that we know the volcanic zone of Sumatra to be subject to wrench faulting along fault planes parallel to the axis of the island; in Sec. 10C-3 we noted how these movements form a component of the relative movement of the large crustal blocks of the archipelago which is the base of the great tectonic phenomena. Attributing the presence of the volcanoes to this wrench-faulting activity seems indicated.

We saw that the wrench faulting in Sumatra probably occurred originally in the tectonic belt. The reason why at least part of that movement now takes place in a parallel zone inside the tectonic belt probably is the increased resistance against shear in the belt, resulting from the concentration of crustal matter there.

The same conclusions obviously apply to the central part of the belt, where the volcanoes can also be attributed to faulting along planes more or less parallel to, though straighter than, the tectonic belt. In these areas the belt is thickening and downbuckling in a direction tending to make an angle of  $55^\circ$  with the compressive stress. As shown in Sec. 10A-7, the stress component parallel to the belt in this case is slightly larger than in the wrench-faulting parts, where it is about 0.404 times the total compressive stress; here it is 0.472 times the total stress. It is clear that in the downbuckling areas, where the concentration of crustal matter is so much greater than in the wrench-faulting areas, the tendency toward a shear release in another zone must be at least as great. It is also clear why that zone has no tendency to follow the detailed curves of the tectonic arc.

Two points, however, have to be accounted for. In the first place, why is it that the shear release occurs at so great a distance, viz., 180 to

250 km? The explanation probably lies in the broad upbending crustal waves on both sides of the thickened downbuckled belt, which cause excess compression in the lower half of the crust, thus preventing the occurrence of faults through which magma can rise to the surface. The fact that the fault planes must therefore originate outside this area checks with the distance mentioned. It seems likely that, if zones of crustal weakness occur, because of older deformation phenomena, the fault planes originate there.

The second question arises when the tectonic belt exhibits a curve over great distances, viz., why do the volcanoes always develop on the concave side of the curve and never on the convex side? This does not seem difficult to explain. It is likely that the crust has to approach the plastic belt, where it is subject to downbuckling, at right angles to the belt; when the belt is curved, the movement causes tension in the direction of the belt on the concave side and compression on the convex side. Hence, on the inside of the curve a release of pressure can be expected, which must be favorable for initiation of volcanic activity, while on the outside the excess of pressure must exclude it.

Near irregularly curved parts of the tectonic belt the area between it and the volcanic belt must be subject to complicated stress situations. This must be especially true near the Sunda Strait, where the volcanic belt shows a sudden change of direction, and also in the parts where irregular curves of the tectonic belt are not followed by the volcanic belt, e.g., in the Sumba-Timor and the Tanimbar Islands areas. There are many complications involved, but we shall not enter into a detailed discussion of them here.

According to our hypothesis, then, the volcanic arc is caused by the fact that, owing to the plastic character of the crustal deformations, the direction of the tectonic arc almost nowhere occurs at right angles to the compressive stress and by the fact that a shear component of this stress is therefore everywhere present, bringing about wrench faulting combined with volcanic activity in a second arc, interior to the first, at a distance of 180 to 250 km. Several of the resulting volcanoes, if not all, rise above sea level, which is also true when the tectonic arc is submerged and possibly even when it is represented only by a deep trench. Hence we can conclude that when only one island arc is visible, it must be the volcanic one; but a second arc, not visible above sea level, must exist. This point of view is confirmed by the facts; if there is only one arc, it consists of a row of volcanic islands.

In the East and West Indies, the volcanic arc is characterized by large islands on the wings of the arc, viz., Sumatra, the Philippine Islands, Haiti, and Puerto Rico.

### 10C-5. General Discussion of Island Arcs; Caribbean Arc

Our study of the Indonesian Archipelago has shown that we can understand a great part of the topography, gravity field, and tectonic phenomena on the basis of the two different types of crustal reaction to stresses discussed in Part A of this chapter and by assuming a regular stress field over the whole area, which causes a relative movement, with respect to the surrounding crust, of only two great crustal blocks. In the northeastern part of the archipelago complications of this simple picture develop, which can probably be attributed to the presence of another arc over the Palao Trench running toward Halmahera and to the New Guinea geosyncline. In the Molucca Sea the two Indonesian belts merge in a triangular area of especially strong anomalies, and in the northern belt an interruption occurs, between north Celebes and north Halmahera, where the anomalies are weak.

In the more regular parts, the belt of negative anomalies has a linear character, and the inner arc, which is characterized by volcanoes, is still more regular in shape. The arc consists of different linear parts, but a slight curvature caused by a general change of stress direction may occur. Each part is characterized by one of the two types of crustal deformation, and often the transition is abrupt, e.g., in the volcanic arc in the Sunda Strait. Although older tectonic trends may determine the location of the inner, volcanic arc, it probably cannot approach the tectonic arc closely.

Despite some indications that the general picture obtained for the Indonesian Archipelago is valid for all other island arcs, definite conclusions cannot be drawn before more is known. The best-surveyed area is the northern and eastern part of the Caribbean arc, of which the topography, geology, and gravity anomalies are known (see the geological and geophysical work of Hess<sup>7,8,10</sup> and his collaborators), as well as seismic data (Ewing<sup>6</sup> and his collaborators). From Haiti to the meridian of 65°W in Venezuela the belt of negative anomalies is in good agreement with deductions accumulated from the study of the Indonesian Archipelago. If we assume that this whole crustal block undergoes uniaxial compression in an azimuth of about N35°E, we find that the three parts in which the belt shows strong anomalies, viz., from Haiti to northeast of the Anegada Passage, from northeast of Anguilla to east of St. Vincent, and from Trinidad to the 65th meridian, make angles of 55° with the compressive stress. The same is true for the corresponding parts of the volcanic arc on the inside. Moreover, the volcanic arc clearly consists of straight parts in these same areas; between Martinique and St. Vincent it changes its direction from an azimuth of about N20°W to about N16°E, and the belt of negative anomalies does likewise. The fact that both belts thus make an angle of about 19° there with the supposed direction of compres-

sion points to wrench faulting of the crust. This conclusion is supported by the fact that the negative anomalies are much weaker there and by the existence of troughs on both sides, the Grenada and Tobago Troughs.

The negative anomalies in the belt from Trinidad to the 65th meridian are particularly strong; the values found here of over -200 mgal are similar to those found in the Molucca Sea. In both places the belt is interrupted on each side, and it is easy to understand that a more strongly concentrated downbuckling in the central part results.

West of the 65th meridian the belt of negative anomalies seems to shift to the north, probably in echelon form, and it reappears north of the island of Curaçao. The northern part of the belt of negative anomalies stops near eastern Cuba, which might lead to the hypothesis that the compressive stress mentioned before is caused by a north-northeastward movement of the South American continent; the stress direction of N35°E suggests that the Beata Ridge might mark the western boundary of this movement, which may have caused the curious twist of the isthmus near Panama. The shift of axis of the isthmus amounts to 100 to 200 km, pointing to an equal displacement of South America relative to Central America.

We shall not further enlarge on this island arc or go deep into the study of others. In Japan and its neighborhood gravity observations have also been made. The presence of a deep trench, a belt of strong negative anomalies, and great seismic and volcanic activity indicates large crustal deformation of the same type as in other island-arc areas, but the belt of anomalies is irregular and will be difficult to interpret until better investigations are made of the neighboring areas and the arcs, which meet there, of the Kurile, Bonin, and Ryukyu Islands. Although the topography is now well known, thanks to the study and mapping of a great part of the area by Hess,<sup>9</sup> large parts of the gravity field are still lacking.

The great activity in geophysical research in Japan has already produced important results for the more detailed deformations of the upper layers of the crust and has demonstrated the presence of many crustal blocks which may start moving during earthquakes (Miyabe<sup>12</sup>). The general tendency is for these blocks to move toward the Japan Trench.

Blocks of the same kind and evidence for their movement during earthquakes have also been found in California, where different fault zones may become active. Several zones are more or less parallel to the coast; of these, the San Andreas fault is best known. They all show right-handed wrench faulting, while the faults directed toward the desert are left-handed. Morphological and geological evidence shows that along the San Andreas fault, for example, the movements have continued in the same sense for long periods. Displacements of several kilometers have been noted.

Returning to the subject of island arcs, the study of which is hampered by the lack of data, we have one further point to make. When we examine the larger arcs, e.g., the Bonin-Marianas arc and the Tonga Trench, we find long straight (or nearly straight) sections, which points to the truth of our surmise that the arcs consist mainly of such nearly straight parts whose directions are related to a regular stress field. In the Bonin-Marianas arc we notice a feature also found in the Indonesian Archipelago: the volcanic arc may be nearly or entirely straight, but the tectonic arc, which here consists mainly of deep trenches, may show bulges and deviations.

## REFERENCES

1. Anderson, E. M.: The dynamics of faulting, 2nd ed., Oliver & Boyd, Edinburgh, 1951.
2. Bemmelen, R. W. van: The geology of Indonesia, Government Printing Office, The Hague, 1949.
3. Brouwer, H. A.: The movements of island arcs, Quart. J. Geol. Soc. London, vol. 106, pp. 231-239, 1951.
4. Bijlaard, P. P.: Théorie des déformations plastiques et locales par rapport aux anomalies négatives de la gravité, aux fosses océaniques, aux géosynclinaux, etc. Rapp. congr. Edimbourg UGGI, 1936.
5. Evans, P., and W. Crompton: Geological factors in gravity interpretation illustrated by evidence from India and Burma, Quart. J. Geol. Soc. London, vol. 102, pp. 211-249, 1946.
6. Ewing, Maurice, and J. Lamâr Worzel: Gravity anomalies and structure of the West Indies, I, Bull. Geol. Soc. Amer., vol. 65, pp. 165-174, 1954.
7. Hess, Harry H.: Interpretation of geological and geophysical observations, Report Navy-Princeton Gravity Expedition to the West Indies in 1932, pp. 27-53, U.S. Navy Hydrographic Office, Washington, D.C., 1933.
8. ———: Gravity anomalies and island-arc structure with particular reference to the West Indies, Proc. Am. Phil. Soc., vol. 79, no. 1, pp. 71-96, 1938.
9. ———: Major structural features of the western North Pacific, an interpretation of H.O. 5485 Bathymetric Chart, Korea to New Guinea, Bull. Geol. Soc. Amer., vol. 59, pp. 417-446, 1948.
10. ——— and collaborators: Caribbean research project, Bull. Geol. Soc. Amer., vol. 64, pp. 1-96, 1953.
11. Koning, L. P. G.: Earthquakes in relation to their geographical distribution, depth and magnitude, I: The East Indian Archipelago, Koninkl. Ned. Akad. Wetensch. Proc., ser. B, vol. 55, pp. 60-77, 1952.
12. Miyabe, N.: Notes on the block structure of the earth's crust, Scientia (Milan), vol. 59, annus 30, pp. 15-19, 1936.
13. Muller, J. J. A.: De verplaatsing van eenige triangulatiepilaren in Tapanoeli, tengevolge van de aardbeving van 17/5/1892, Verhandel. Koninkl. Akad. Wetensch. Amsterdam, Afdel. Natuurk. sec. 1, vol. 3, pp. 3-26, 1895.
14. Texeira, Carlos: As anomalias da gravidade na parte portuguesa da ilha de Timor, Garcia de Orta, vol. 1, pp. 211-217, 1954.
15. Umbgrove, J. H. F.: The relation between geology and gravity field, in the East Indian Archipelago; A short survey of theories on the origin of the East Indian

- Archipelago, chaps. 6, 7 in F. A. Vening Meinesz, Gravity expeditions at sea, vol. 2, Publ. Neth. Geod. Comm., Waltman, Delft, 1934.
16. Umbgrove, J. H. F.: Geological history of the East Indies, Bull. Am. Assoc. Petroleum Geol., vol. 22, pp. 1-70, 1938.
17. ———: Structural history of the East Indies, Cambridge, London, 1949.
18. Vening Meinesz, F. A.: Gravity expeditions at sea, vol. 4, Publ. Neth. Geod. Comm., Delftsche Uitgevers Mij, Delft, 1948.
- 18a. ———: A third arc in many island arc areas, Proc. Koninkl. Ned. Akad. Wetensch., ser. B, vol. 54, pp. 432-442, 1951.
19. ———: Indonesian Archipelago: A geophysical study, Bull. Geol. Soc. Amer., vol. 65, pp. 143-164, 1954.

*A Few References to Maps of Island-arc Areas*

20. Bruyn, J. W. de: Isogram maps of Caribbean Sea and surroundings and of South-east Asia, World Petroleum Congr., Proc., 3rd Congr. Hague, 1951, pp. 598-612.
21. Dietz, R. S.: Marine geology of northwestern Pacific: Description of Japanese Bathymetric Chart 6901, Bull. Geol. Soc. Amer., vol. 65, pp. 1199-1224, 1954.
22. Ewing, Maurice, and Harry H. Hess: Provisional isostatic gravity anomaly map, Proc. Am. Phil. Soc., vol. 79, p. 96, 1938.
23. Hess, Harry H.: See ref. 7.
24. Riel, P. M. van: Snellius expedition, Bathymetric map of the Indonesian Archipelago, vol. 2, Oceanography, part 2, Kemink en Zoon, Utrecht, 1935; also in F. A. Vening Meinesz, Gravity expeditions at sea, vol. 2, Publ. Neth. Geod. Comm., Waltman, Delft, 1934.
25. Vening Meinesz, F. A.: Gravity anomaly maps of the Indonesian Archipelago, in Gravity expeditions at sea, vol. 2, Publ. Neth. Geod. Comm., Waltman, Delft, 1934; vol. 4, Delftsche Uitgevers Mij, Delft, 1954.

**PART 10D**  
**STRESS RELEASE IN THE CRUST. TILTED FAULT PLANES. GRABEN  
FORMATION**

#### **10D-1. Introduction**

In this part we investigate horizontal uniaxial stress release in the crust, especially in the continental crust. We shall see that it can be expected to lead to a tilted fault plane and, as a consequence, to a second tilted fault plane converging downward with respect to the first, and then to the formation of a graben between them in the manner mentioned by Taber<sup>6</sup> in 1927. In dealing with these problems we keep to the usual simplification of an elastically deforming crust floating on a plastic substratum, and so we assume that the stresses in the crust do not exceed the limit of elasticity,  $\sigma_l = 2000 \text{ kg/cm}^2$ , of the crust. In view of the gradual decrease of this limit with depth and of the pseudo-viscosity modulus, the simplification is no doubt a schematization of the real conditions.

Bullard's important report<sup>2</sup> on his gravity research in East Africa has advanced the theory that grabens have originated as a consequence of compression. He assumes two tilted fault planes diverging downward and a more or less wedge-shaped part of the crust between, which is forced down by the compression. One of his arguments is the explanation thus obtained of the belts of moderate negative anomalies he found over the grabens. The hypothesis given here, however, also accounts for the anomaly belts; it is supported by the following two arguments.

In the first place, it can be shown that, when tilted fault planes are caused by compression, they make a smaller angle with the plane of the crust than when they are caused by tension, in which case the tilt checks with the slopes occurring on the sides of the graben. In the second place, it is unlikely that compression in the crust could cause such widely different crustal deformations as thickening and downbuckling of the crust on the one hand and faulting and graben formation on the other.

Nevertheless, Bullard's explanation is not impossible, and perhaps the long and nearly straight escarpments found by Menard<sup>5</sup> in the Pacific, which in some parts are accompanied by grabens, e.g., the Mendocino escarpment, can be attributed to wrench faulting combined with a thrust-faulting component, i.e., more or less in the manner discussed in Sec.

10C-3 for the belt west of Sumatra. If such a combination of wrench faulting and compression occurs in a purely oceanic crust, it probably leads to the formation of escarpments and grabens, and the latter would thus originate in a manner similar to that called for in Bullard's hypothesis. We shall not enter into a discussion of these remarkable features; more research, e.g., along seismic and gravimetric lines, seems desirable before a definite conclusion can be attempted.

The last section of this part of Chap. 10 is devoted to the gravity anomalies found by Bullard<sup>2</sup> in the graben areas of East Africa and to a short discussion of later developments to be expected in graben areas. Both these problems are fraught with uncertainties.

#### 10D-2. Faulting and Graben Development as a Consequence of Uniaxial Stress Release in the Crust

Our problem is divided into two stages, the development of the first tilted fault plane (Fig. 10D-1a) and that of the second (Fig. 10D-1b), which entails the forming of a graben (Fig. 10D-1c). Applying the theory

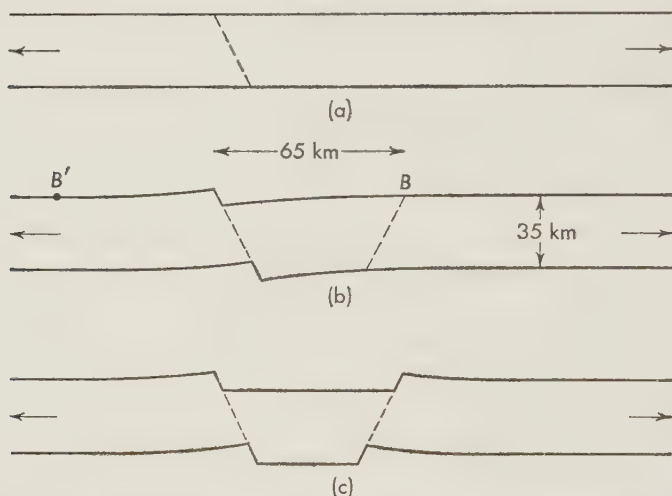


FIG. 10D-1. The development of a graben. (Figs. 7a, 7b, and 7c of "Les graben africains, etc." Institut. roy. colonial belge, Bull. 1950, 2.)

of faulting of Anderson,<sup>1</sup> Hubbert,<sup>4</sup> and Hafner,<sup>3</sup> as briefly treated in Sec. 10A-8, to the crust as a whole, we see that, if a gradually increasing horizontal tension or stress release occurs in the crust, it must unavoidably lead to a normal faulting phenomenon along a tilted fault plane. According to Sec. 10A-8, we can estimate the angle of hade of this fault at about  $27^\circ$  and the angle of dip, therefore, at about  $63^\circ$ . These figures seem to be in

harmony with the slopes of a graben side, whereas compression in the crust would cause thrust faulting to take place at an angle of slope of not more than about  $27^\circ$ . Hence we have another argument in favor of graben formation by stress release rather than compression.

We shall not discuss the details of the faulting process. At the surface, where we can assume that it starts, it no doubt has the character of a fracture, but deeper down it must be rendered more plastic by the high pressure. If the separation of both crustal halves continues, one side must bend downward and the other upward, and the motion lasts until the isostatic equilibrium is readjusted on both sides. Should the movement continue further, an interruption of the crust would occur if no other development, viz., a second faulting, took place. In this case further stretching of the crust occurs in the second fault zone and leads to the formation of a graben (Fig. 10D-1c). It is clear that the faulting phenomena may give rise to volcanic activity, which is borne out by the facts; e.g., the graben areas in East Africa are marked by the presence of many volcanoes.

To investigate whether the downbending of the crust, caused by the movement along the first fault plane, can lead to fracture at the place where the bending causes a maximum curvature and therefore a maximum tensile stress at the surface, we have first to determine the downward

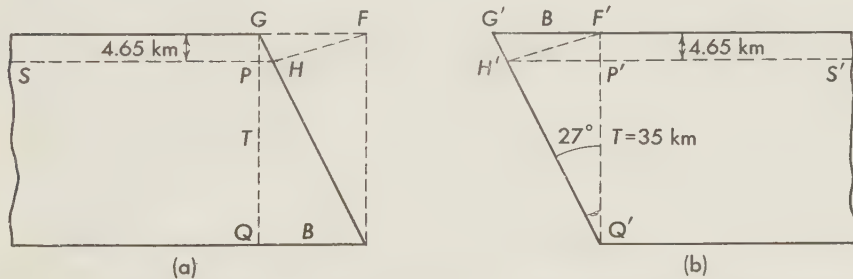


FIG. 10D-2. The parts of the crust on both sides of a fault. (Figs. 8a and 8b of "Les graben africains, etc." Institut. roy. colonial belge, Bull. 1950, 2.)

force caused by the first fault plane. Figure 10D-2 shows both sides of the crust in the undeformed state. The surface the substratum would have if no crust were present is indicated by a dashed line; if  $\rho_s$  is the subcrustal density and  $\rho_c$  the mean density of the crust, the surface must be situated at a distance of approximately  $T(\rho_s - \rho_c)/\rho_s$  below the surface of the crust. Figure 10D-2 shows that, if the crust is homogeneous, both sides of it would be in equilibrium if we could add the block  $GFH$  to the left side and remove the congruous block  $G'F'H'$  from the right side. Hence, the weight  $P$  of these blocks represents the force pressing down

the right side and pushing up the left side of the crust. Assuming the crust to consist of two layers of equal thickness, e.g., granitic and basaltic, of densities  $\rho_c - \Delta$  and  $\rho_c + \Delta$ , we have to apply a small correction proportional to  $\Delta$ . We then have

$$P = \left[ \frac{\rho_c(\rho_s - \rho_c)}{2\rho_s} - \frac{1}{4}\Delta \right] gT^2 \tan \theta \quad (10D-1)$$

where we can assume  $T = 35$  km and  $\theta = 27^\circ$ .

The bending curves of both sides of the crust are given by Formula (10A-21b), where this type of crustal bending has been dealt with. Substituting, in this formula, the value of  $P$  and putting  $l = L/\pi$  [see (10A-12c)], we obtain

$$z = \pm \frac{1}{2}\pi\sqrt{2} \left[ \frac{\rho_c(\rho_s - \rho_c)}{\rho_s^2} - \frac{\Delta}{2\rho_s} \right] \frac{T^2}{L} \tan \theta e^{-\frac{1}{2}\pi\sqrt{2}(x/L)} \cos \left( 0.707 \times 180^\circ \frac{x}{L} \right) \quad (10D-2a)$$

Putting  $\rho_c = 2.835$ ,  $\rho_s = 3.27$ ,  $\Delta = 0.165$ ,  $\theta = 27^\circ$ , and  $L = 185$  km [see (10A-13a)], we get

$$z = \pm 0.675 e^{-2.221(x/L)} \cos \left( 127.3 \frac{x}{L} \right) \text{km} \quad (10D-2b)$$

The moment  $M$  of the stresses working in cross sections of the crust is given by (10A-15c) and (10A-15e), and as the maximum stress  $\sigma_b$  at the surface and the lower boundary of the crust equals  $\pm 6M/T^2$ , we obtain

$$\sigma_b = \pm \frac{6}{T^2} \frac{\rho_s g L^2}{\pi^2} \times 0.675 \times 10^5 e^{-2.221(x/L)} \sin \left( 127.3 \frac{x}{L} \right) \text{dynes/cm}^2$$

which gives

$$\sigma_b = 3.68 e^{-2.221(x/L)} \sin \left( 127.3 \frac{x}{L} \right) \times 10^9 \text{ dynes/cm}^2 \quad (10D-3)$$

We obtain the distance  $x_m$  from the force  $P$ , where  $M$  and  $\sigma_b$  are maximum, by equating Formula (10A-15d) for  $\partial^3 z / \partial x^3$  to zero. This provides us with

$$127.3 \frac{x_m}{L} + \varphi + 3\beta = 127.3 \frac{x_m}{L} + 135^\circ = 180^\circ$$

from which it follows that

$$x_m = 0.354L = 65 \text{ km} \quad (10D-4)$$

We can therefore expect a second fault plane at about this distance, which thus represents the most probable width of the graben. In view of

the uncertainties in our assumptions, this value is in remarkably good agreement with the facts.

Introducing this value of  $x_m$  in (10D-3), we obtain a maximum value of  $\sigma_b$  of

$$\sigma_{bm} = 3.68e^{-(\pi/4)} \sin 45^\circ \times 10^9 = 1.18 \times 10^9 \text{ dynes/cm}^2 \quad (10D-5)$$

A tensile stress of this amount at the surface of the crust without doubt leads to fracturing; laboratory experiments have shown the breaking strength of granite, for example, to be of the order of  $1 \times 10^9$  dynes/cm<sup>2</sup>. Thus we may feel certain that a fault will develop on the downbending side, but the same cannot be true on the upbending side, where, at the surface, a compressive stress of this magnitude cannot bring about fracturing, while at the lower boundary of the crust, where a considerable hydrostatic stress is added, it is obviously even less possible.

Once the shear has started at the surface, we can expect the faulting to continue in the direction indicated by the theory for normal faulting, i.e., at a dip of about  $63^\circ$ ; the tension connected with the crustal bending must play the same part as the stress release does over the whole crust during the genesis of the first fault. It is more difficult to explain why the second fault plane should dip toward the first instead of originating in a parallel direction, and it seems possible that the latter development also occurs; it would lead to tilted blocks in the way shown by Fig. 10D-3.

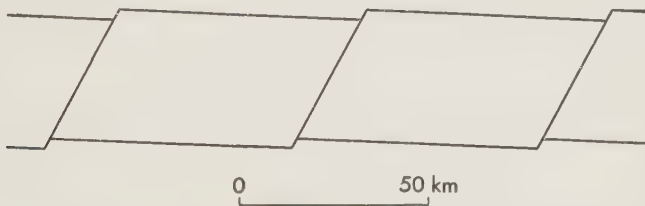


FIG. 10D-3. Tilted blocks when the fault planes are parallel.

We shall not go into details here but mention only that if the lengthening of the crust is sufficient to allow each block to settle independently in isostatic equilibrium, the surfaces will get a tilt of about 2.4 per cent, which, over a distance of 65 km, amounts to escarpments between them with a height of 1500 to 1600 m.

Returning to the other case, we see clearly that once the second fault plane has come into being, the whole phenomenon is symmetrical, and we can assume that the central block resumes its horizontal position and thus the graben is formed. If the separation of the outer blocks continues, it must reach a depth corresponding to isostatic equilibrium. We can easily determine this depth. Denoting by  $b$  the width between the two

graben slopes at the level of the free substratum surface, i.e., of the dashed line in Fig. 10D-2, and by  $d$  the subsiding of the central block with respect to its original position, we may put, approximately,

$$\rho_s g b d = 2P \quad (10D-6a)$$

and so obtain

$$d = \frac{2P}{\rho_s g b} = \left[ \frac{\rho_c(\rho_s - \rho_c)}{\rho_s^2} - \frac{\Delta}{2\rho_s} \right] \frac{T^2}{b} \tan \theta = 0.865 \text{ km} \quad (10D-6b)$$

To derive this figure we have introduced for  $b$  the value 65 km, obtained for  $x_m$ . Examining it more closely, we find that, together with the approximation of (10D-6a), we make an error of less than 1.5 km, obviously insignificant in view of the uncertainties in our assumptions.

Using the result found in (10D-2b), we obtain a value for the depth of the graben of about 1540 m; the graben floor has subsided about 860 m, and the sides have risen about 680 m. The entire profile is given by Fig. 10D-4; the vertical dimensions are exaggerated five times, but the angle of hade of the faults has been kept at 27°.



FIG. 10D-4. Graben development when the fault planes converge.

These results are in satisfactory agreement with the actual profiles found in existing grabens, and so our hypothesis that grabens are caused by tension, or at least stress release in the crust, seems well founded. It may be mentioned that in many respects these deductions are similar to those given by Bullard<sup>2</sup> in his report on the gravity results in East Africa.

We may add that if the stress release does not continue long enough for complete graben development to take place, the phenomenon is interrupted. The Manyara graben mentioned by Bullard<sup>2</sup> (p. 516) may be a place where the second fault did not develop.

### 10D-3. Bullard's Gravity Results in Graben Areas; Later Development in Graben Areas

Figure 10D-5 shows, on true vertical scale, the lower boundary of the crust according to our hypothesis and the boundary corresponding to the Airy-Heiskanen isostatic reduction method for the crustal thickness adopted here,  $T = 35$  km. Examination of these two boundaries shows why Bullard found negative anomalies over the grabens and weaker positive belts in the adjoining areas. Still, these anomalies are somewhat larger than can be accounted for by the differences in mass indicated in Fig. 10D-5; Bullard's isostatic anomalies over the grabens are of the

order of  $-50$  mgal, while our graben hypothesis gives  $-37.3$  mgal. The difference cannot be explained by the fact that Bullard used the Hayford isostatic reduction.

On the basis of his compression hypothesis, Bullard found a similar discrepancy, and this led him to assume a slight downbuckling of the central block. Since that assumption obviously is not in harmony with the tension hypothesis here advocated, we must find another explanation.

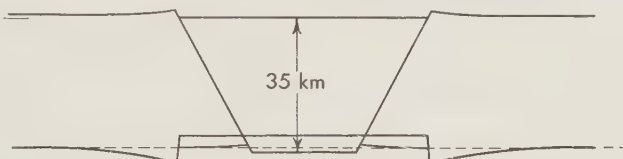


FIG. 10D-5. Cross section of a graben on true vertical scale; lower crustal boundaries according to our theory and to Airy-Heiskanen hypothesis of isostasy.

We can assume that a graben is subject to quick sedimentation, which, as long as the stress is still present, must cause subsidence of the central block to readjust its floating equilibrium. If the block is free to readjust completely, a sediment layer with a thickness of  $1.4$  km and a density of  $2.50$  in the graben would cause a further  $1.1$ -km subsidence of the central block, and the resulting mass deficiencies would agree with Bullard's anomaly of  $-50$  mgal. These anomaly computations have been made on the assumption that the crust consists of two equal layers, of densities of  $2.67$  and  $3.00$ , respectively.

The later history of a graben probably includes a gradual complete filling in by sediments; and probably, but at a much slower rate, the lower part of the central block, in so far as it extends below the normal position of the M discontinuity, melts and, at least partially, flows away along the lower crustal boundary, i.e., in the manner discussed in Sec. 10A-5 for the much larger roots of geosyncline belts.

Graben development as a consequence of stress release in the crust, as discussed here, is obviously possible only for the continental crust. In the oceans, where in addition to a thin layer of sediments there is a layer only up to  $5$  km thick of a density of about  $3$  on top of the ultrabasic rock, the upward and downward forces caused by tilted fault planes must be so much smaller that no grabens of any significance can form.

#### REFERENCES

1. Anderson, E. M.: The dynamics of faulting, 2nd ed., Oliver & Boyd, Edinburgh, 1951.
2. Bullard, E. C.: Gravity measurements in East Africa, Trans. Roy. Soc. (London), ser. A, vol. 235, no. 757, pp. 445-531, 1936.

3. Hafner, W.: Stress distributions and faulting, Bull. Geol. Soc. Amer., vol. 62, pp. 373-398, 1951.
4. Hubbert, M. King: Mechanical basis for certain familiar geologic structures, Bull. Geol. Soc. Amer., vol. 62, pp. 355-372, 1951.
5. Menard, H. W., and R. S. Dietz: Mendocino submarine escarpment, J. Geol., vol. 60, pp. 266-278, 1952.
6. Taber, S.: Fault troughs, J. Geol., vol. 35, pp. 557-606, 1927.
7. Vening Meinesz, F. A.: Les graben africains, résultat de compression ou de tension dans la croûte terrestre?, Inst. roy. colonial belge, Bull., vol. 21, pp. 539-552, 1950.

## CHAPTER 11

# CONVECTION CURRENTS IN THE EARTH. ORIGIN OF CONTINENTS AND OCEANS. GREAT GEOSYNCLINE BELTS

### 11-1. Introduction and Summary

There are many arguments to support the theory that great current systems exist in the mantle and are caused by temperature differences. In the first place, it is difficult to give any other explanation of the crustal deformations in the island-arc areas in Indonesia, off the east coast of Asia, and in the West Indies. In Part 10C it was seen that in Indonesia the character and distribution of the crustal deformations point to a south-southeastward movement of the whole Indonesian crustal block with respect to the surrounding area, and since the cross section has a breadth of more than 3000 km and the directions on the edges of the block diverge only slightly, a subcrustal current of continental size is indicated. Further support lies in the fact that all the island arcs on the east coast of Asia are similar in shape to the Indonesian arc.

The suggestion that the crustal deformations are caused by contraction is invalidated by their very character. If they were, the sides of the Indonesian arc, for example, would show a much greater compression and less, if any, shear. Actually, as was pointed out in Sec. 10C-3, wrench faulting is the principal phenomenon there. Yet another reason for attributing the crustal deformations to subcrustal currents rather than contraction is the fact that elsewhere in the crust grabens have been formed, e.g., in great parts of East Africa, including probably the Red Sea and the Gulfs of Suez and Akaba with the Dead Sea rift valley, and the upper Rhine valley between the Black Forest and the Vosges; since grabens strongly indicate tension or, at least, stress release, they are not reconcilable with the hypothesis of contraction.

As noted in Sec. 10C-5, the gravity field in the Caribbean area also points to a large system of subcrustal flow. From the gravity data we can probably infer a relative movement to the north-northeast of the South American continent with respect to the Antillean arc, and here again the supposi-

tion of a great subcrustal current system is more acceptable than the contraction hypothesis.

Another reason for coming to this conclusion is the size of the crustal shortening found in folded mountain systems, e.g., the Alps. For the Alps we have to assume at least 200 to 300 km (Heim<sup>10</sup>), which the hypothesis of thermal contraction can hardly explain; Jeffreys<sup>12</sup> shows the unlikelihood of such a crustal shortening's taking place by thermal contraction during the available period of about 150 million years.

A further argument in favor of subcrustal current systems of continental dimensions is provided by the evidence of polar wandering gathered recently from the magnetization of rocks by Runcorn<sup>13</sup> and his collaborators. He bases his conclusion on the evidence of late Tertiary and Quaternary rocks, which show that the magnetic-dipole axis of the earth tends to coincide roughly with the rotation axis, though the sign of the magnetic dipole may be reversed from time to time. Starting from this observed fact, it is difficult to interpret the large systematic deviations in the direction of magnetization of rocks of older periods as anything but evidence of changes in the position of the rotation axis relative to these rocks. The data obtained are in harmony with the hypothesis that the crust of the earth more or less remains a whole, though relative movements of a few hundred kilometers of different parts with respect to each other are not excluded. So, as far as the present data go, the conclusion seems to be that the crust as a whole has moved with respect to the rotation axis.

In Chap. 12 we shall find that there is also some evidence of large polar wandering, given by systems of preferred directions of the earth's topographic features. Since the probable cause is the plastic deformation and shear of the crust resulting from the change in the axis of flattening of the earth, polar wandering is again indicated, though probably at a very early period of the earth's history.

As it is extremely unlikely that the rotation axis of the earth could have changed over large angles with respect to the mass of the earth as a whole, it is safe to conclude that the polar change must be caused by a movement of the crust over the earth's interior. If we assume large-scale subcrustal currents, such a movement does not appear unlikely. Since it is improbable that the forces exerted on the crustal shell by world-wide current systems would be in equilibrium, a moment of the drag forces must unavoidably move the shell over the interior. As a consequence, we must assume that, referred to a coordinate system fixed in space, with respect to which the earth's rotation axis is also fixed, the larger part of the relative shift will be effected by the crustal shell and the much smaller part, in contrary direction, by the earth's interior. In this way the polar wandering is easily explained, whereas without large-scale current systems it would be hard to understand.

It was pointed out to the author (V. M.) by his colleague W. Nieuwenkamp that a further argument in favor of great convection currents in the mantle can be derived from Bowen's views<sup>6</sup> on the formation of basalt. According to him, release of pressure causes selective fusion of peridotite to give basaltic magma and olivine, the latter remaining in the solid state. Bowen asks how it is possible to explain continuous formation of basaltic magma throughout the earth's history, for selective fusion of the peridotite in the upper layer of the mantle must soon have caused the layer to lose its basaltic constituents and become barren. It is clear that episodically repeating convection currents in the mantle during the earth's history can provide an explanation; at each recurrence they must have brought to the surface new peridotite, which produced new basaltic magma. These considerations lead us to suppose that perhaps the slight difference in density between peridotite and olivine contributed to the energy available for the convection currents, which must have been provided chiefly by the earth's cooling.

In Secs. 11-6 to 11-8 we find still another argument to favor the existence of great current systems in the mantle while the present distribution of continents and oceans was originating; we find that the development in spherical harmonics (Prey<sup>15</sup>) of the earth's topography shows curiously regular features—hardly explainable except by current systems in the mantle.

Resuming, it can be said that the evidence for great current systems in the mantle during some periods of the earth's history is rather overwhelming, and actual tectonic activity in the earth makes it likely that such a current system is active now. The episodic character of tectonic revolutions (of which one of the most eloquent and well-founded expositions has been given by Umbgrove<sup>20</sup>) points to an episodic character for the current systems as well. It can probably be assumed that during the earth's existence, now estimated to have lasted about  $5 \times 10^9$  years, there have been some 10 to 20 tectonically active periods, each consisting of a number of particularly violent episodes.

Probably the current systems are chiefly the result of temperature gradients caused by the earth's cooling at the surface, which make the mantle unstable; this effect is increased by the occurrence of phase changes in the olivine of which the mantle consists. If it were necessary for us to seek the causes in irreversible chemical processes, we should find it difficult to explain the above-mentioned frequent repetitions, which, at least as far as we know from the last few revolutions, are more or less identical in character.

In 1939 Griggs<sup>8</sup> suggested that the episodicity is caused by the small limit of elasticity in the mantle which has to be overcome before flow can set in. As mentioned before, the limit of elasticity cannot be much more than  $10^7$  dynes/cm<sup>2</sup>, for otherwise we should find greater deviations from isostasy. The consequence of the elastic limit, if the temperature gradient

has no horizontal component, and if there is no other cause of stress differences in the horizontal sense, must be that no movement can start, and the elastic limit thus acts as stabilizer. Only when there is present, in addition to the downward gradient caused by the earth's cooling, a horizontal temperature gradient of sufficient degree or another adequate effect can pressure differences in this sense arise and cause the elastic limit to be exceeded and flow to start.

Thus is formed a vertical convection circuit, consisting of a horizontal flow at the surface, a descending column, a horizontal flow back at greater depth, and an ascending column closing the circuit. Once started, the flow accelerates because the upper, colder layer is carried along in the descending column and the lower, hotter layer in the ascending column. Hence the temperature difference and therefore the density difference between the columns increase, and consequently the velocity does too. Because these differences become maximum after about a quarter revolution, the same must be true of the velocity. From this moment the temperature difference and therefore the velocity diminish, until after about a half revolution the flow stops. The colder, denser matter then is down and the hotter, lighter matter up; stability has been reestablished.

In this short summary of the phenomenon we have neglected thermal conduction, but as it is extremely slow, its effect is probably small; it obviously tends to reduce the temperature differences and therefore the velocity and duration of flow.

The thermal convection flow discussed here makes only a half turn or, because of a small effect of conduction and of the elastic limit, slightly less. The reestablishment of thermal stability is marked by an upward temperature gradient. No new current system can be generated until the earth's cooling has again caused a sufficient downward temperature gradient and a trigger effect, e.g., a horizontal temperature gradient, for getting the system started. Thus we can understand the episodic character of tectonic activity; we could hardly expect the phenomenon to be accurately periodic. It is evident that we have thus found another argument for the hypothesis of current systems in the mantle; it solves the difficult major geological problem of episodic tectonic activity.

From the theory of episodic convection a second argument can be derived. We can expect the ascending column of a convection current to be found under continents because there the greater amount of radioactive matter in the continental crust, compared with the oceanic crust, causes a higher temperature. Since there must be a rise of temperature in this column before and during the period of the first great tectonic activity of a revolutionary cycle, thermal expansion during that time and a consequent rise of the earth's surface must result. This checks remarkably well with the regression in that period noted by geologists, while the long periods of rest be-

tween revolutionary cycles are characterized by transgression. The causes of transgression are undoubtedly, first, the disappearance of the higher temperature and, second, accelerated cooling of the earth in the areas where convection occurred and the consequent lowering of the earth's surface by thermal contraction.

Two objections to thermal convection in the mantle can be advanced. The first is that a homogeneous mantle is required; according to Birch,<sup>4</sup> homogeneity may exist in the upper 200 km and the lower 2000 km, where the densities derived from seismic velocities appear to be constant when reduced to surface conditions of pressure and temperature, but not in the intervening zone. In the upper 200 km the reduced-density figure is about 3.3; between 900 and 2900 km it is about 4.0; but between 200 and 900 km a gradual change from the first to the second figure probably takes place. No clear discontinuity has been found in this transition zone.

If the density change is connected with a change in chemical constitution, thermal convection probably could not break through the transition zone, and though it perhaps would not be impossible for the current to be confined to the thick lower layer of the mantle and for the drag exerted by the current to be transmitted to the crust by the intervening zone, such a process presents complications. We should certainly have to expect a clear discontinuity at the surface of the lower mantle layer. None has been found.

If, however, the density change is connected with a change of state of the mantle rocks, the difficulties disappear. As we shall see (Sec. 11-2), convection currents can then not only break through the layer of density change, but such phase changes must even promote their coming into being. It is easily seen that this transition layer must have a certain thickness, which can, no doubt, amount to 700 km. Thus arise interesting possibilities even of explaining the vertical temperature gradients at the earth's surface, which have been found to be about equal for oceanic and continental areas notwithstanding the difference in radioactive constituents in the upper layers.

The second objection to the hypothesis of convection currents in the mantle during each orogenic cycle is centered in the problem of explaining the development, in only 100 to 300 million years, of the downward temperature gradient needed for a new orogenic cycle after the last half-turn convection current has brought the colder layer down and the hotter layer up. In view of the extremely small value for thermal conductivity in the earth, Birch estimated that a much longer period would be needed.

The explanation is probably convection in the upper and lower halves of the mantle (see Sec. 11-9). There is much evidence in favor of convection cells having dimensions of 500 to 1000 km. In the first place, deep and intermediate earthquake foci point to shear stresses at those depths, which

are hard to understand without assuming a subcrustal current system of such dimensions. To assume only a shear plane dipping down under the continent, as has often been done, makes explanation of the shear stresses difficult.

In the second place, convection currents can clarify the origin of deep basins inside island arcs, which many geologists, e.g., Umbgrove,<sup>19</sup> believe to have developed only recently. The trigger effect that starts the currents can probably be attributed to local temperature differences caused by a concentration in the surrounding geosyncline belt of crustal matter containing more radioactive constituents than the deeper rocks. In the required trigger effect a part may also be played, especially in causing deep earthquakes, by vertical movement of the geosyncline belt, either a subsidence or a rising. Seismic data show that the shear in the focus area may have the character either of normal or reverse faulting.

Besides this evidence, spherical harmonic analysis of the earth's topography shows the presence of waves whose terms point to current systems of about 1400 and 2000 km diameter (see Sec. 11-9).

Lastly the topography of the Indonesian Archipelago indicates that possibly we shall also have to assume the occurrence of still smaller systems of convection, which, for example, could have caused the Gulf of Tomini, between north and east Celebes, the Gulf of Boni, between south and southeast Celebes, and the gulf of Makassar, between Celebes and Borneo. If these subsidences were indeed caused by convection, their dimensions would point to a current that was restricted to the upper few hundred kilometers of the mantle, which are probably homogeneous. All the other types of convection current mentioned here would have had to break through, or at least into, the layer of density transition between 200 and 900 km depth. All types of current must promote a more rapid change from the stable temperature distribution, i.e., the upward temperature gradient left by the preceding orogenic cycle, to the unstable system, i.e., the downward temperature gradient required for the next cycle; they thus explain how the change can take place in only a few hundred million years.

To conclude this introductory section let us summarize the balance of this chapter: Sec. 11-2 treats of the transition layer between 200 and 900 km depth; Secs. 11-3, 11-4, and 11-5 give convection equations and formulas for, respectively, a plane layer, a spherical shell (especially the mantle), and a sphere as a whole; Sec. 11-6 discusses Prey's development in spherical harmonics of the earth's topography; Sec. 11-7 deals with the first-order term of this development and with the origin of the core and of an ur continent; Sec. 11-8 examines the hypothesis that the ur continent broke up into the existing continents; Sec. 11-9 attempts an early history of the earth; and Sec. 11-10 discusses the hypothesis of smaller convection systems below the crust which cause the deep basins in the island-arc areas.

## 11-2. The Density-transition Layer from 200 to 900 km Depth

If, in connection with many arguments in favor of the hypothesis of subcrustal currents, we suppose that they can break through the density-transition layer between 200 and 900 km depth,\* we must assume that the mantle is chemically homogeneous and that the density difference of about 0.7 between the upper 200 km and the lower 2000 km is caused by a difference of modification.† The figure of 0.7 was derived by Birch<sup>4</sup> from the densities that follow from seismic velocities reduced to surface conditions of temperature and pressure. The mantle probably consists of olivine. We know of no modification of olivine that can explain this density difference, but Elsasser<sup>7</sup> mentions Bernal's suggestion<sup>3</sup> of the probability that under great pressure the rhombic phase changes to a denser cubic phase. We shall presently see that some local segregation of the magnesium and iron components of the olivine probably also occurs in the transition layer.

Assuming that under great pressure a phase change does occur, we shall discuss the following two questions in order:

1. Is it a tenable assumption that between two phases there exists a transition layer some 700 km thick having a certain stability?
2. What effects can we expect from loading or unloading of the crust or from a subcrustal current breaking through the transition layer?

We shall find an affirmative answer to the first question, and we shall find discussion of the second question giving the important result that the presence of the transition layer causes increased instability in the mantle and thus promotes convection currents, and explaining the unexpected fact that the temperature gradients found over continents and oceans are about equal, notwithstanding the difference in radioactivity of their respective crusts.

If the two phases exist together between 200 and 900 km depth, we must assume that over that interval the temperature at each depth is influenced by the phase equilibrium. We must, therefore, expect that a change of temperature or pressure must bring about phase transitions.

It can be assumed that the change from the denser to the lighter phase requires a certain heat of transition which is liberated when the change is reversed. This energy tends to stabilize the coexistence of both phases over the full height of the transition layer. If at a given depth some crystals of the lighter phase change into the denser one, the heat set free raises the temperature and thus causes just enough of the denser phase to start changing into the lighter for the consumption of energy to restore the tempera-

\* The latest views are that the boundaries are probably better put at 500 and 900 km depth. These values were used for the computations mentioned on page 407.

† For this subject see also a paper by A. E. Ringwood (Department of Geology, University of Melbourne): "The Olivine Spinel Transition in the Earth's Mantle," *Nature*, vol. 178, pp. 1303-1304, 1956.

ture to the value corresponding to that depth. The situation is thus restored. The result is the same when a change occurs in the other direction, i.e., from the denser phase to the lighter, which requires energy and thus lowers the temperature to the degree needed for readjusting the situation. So, as far as incidental deviations are concerned, the situation is stable.

It is hardly necessary to emphasize that, in view of the interchange of heat in the zone of coincidence, the earth's temperature-pressure curve may deviate there from the course it would have followed had this phase change not taken place.

We can write the following equations. Outside the transition layer we have

$$\mu \frac{\partial^2 \theta}{\partial z^2} - w_0 \frac{\partial \theta}{\partial z} - \frac{\partial \theta}{\partial t} = 0 \quad (11-1a)$$

where  $\theta$  = temperature

$z$  = depth coordinate

$w_0$  = vertical component of a possible velocity positive downward

$\mu$  = thermometric conductivity = thermal conductivity  $\lambda$  divided by specific heat  $c$  and density  $\rho$

Since we assume  $\theta$  inside the transition layer to be equal to the critical temperature  $F(p)$  at which, for a pressure  $p$ , the phase transition occurs, we obtain

$$\mu \left( \frac{\partial p}{\partial z} \right)^2 \frac{\partial^2 F}{\partial p^2} + \mu \frac{\partial^2 p}{\partial z^2} \frac{\partial F}{\partial p} - w_0 \frac{\partial p}{\partial z} \frac{\partial F}{\partial p} - \frac{\partial p}{\partial t} \frac{\partial F}{\partial p} + \frac{K}{c} \frac{\partial q}{\partial t} = 0 \quad (11-1b)$$

where  $q$  = percentage of heavier phase

$c$  = specific heat

$K$  = transition heat in calories per gram

In the above equations the quantities  $\mu$  and  $c$  may differ for the heavy and the light modifications, and, as the density is different, so also will  $\partial p / \partial z$ . For the transition layer, where these modifications are coexistent, we must expect intermediate values varying (probably almost linearly) with the percentage  $q$ . This fact introduces into the development of solutions for these equations additional complications which are difficult to handle. To begin with, the solutions obviously must depend on the initial conditions for each particular case.

Taking up our second question, we first examine the effect of removing a load from the earth's surface, e.g., the ice layer of the glacial period (see Part B of Chap. 10). The disappearance of the ice must have brought about a release of pressure down to a great depth, which disturbed the

balance in the transition layer and started the transition of part of the heavy phase into the lighter phase. The heat thus absorbed must have lowered the temperature until the equilibrium was restored and the transition stopped. The whole phenomenon must have taken a fairly short time and must have caused a rising of the earth's surface. We can thus explain the fact, mentioned in Part B of Chap. 10, that, after the removal of the ice, in addition to the elastic rebound, there occurred a rising greater than the amount corresponding to the pseudo-viscous flow of the subcrustal layer dealt with in that chapter. When such a flow later gradually restores the normal pressure, a reversed phenomenon takes place, retarding the rising and restoring the temperature at greater depths.

We turn now to the effect of a subcrustal current breaking through the transition layer. If it is assumed that the heat conduction is too slow to have an appreciable influence, the temperature distribution of a vertically rising column cannot be affected by it, while the pressure diminishes according to the amount of vertical displacement. As a consequence, the phase equilibrium is disturbed over the whole column, which leads part of the matter of heavier phase to change into the lighter phase. The corresponding consumption of heat brings about a lowering of the temperature and consequently brings a readjustment of the temperature at the lower pressure. For the subsiding column the reverse takes place; in both columns the phase transition restores the phase equilibrium.

This leads to the following equations. We shall first consider the subsiding column of the current. Of a particle at a certain level, having a downward velocity component  $w_0$ , so much is changed of the light phase that the heat produced— $K$  cal/g—raises the temperature of the particle until the temperature at the depth attained is restored. As this process requires a heat per second of  $c w_0 \frac{\partial F}{\partial z}$  calories, the amount of the heavy phase produced is  $(c w_0 / K) (\partial F / \partial z)$  g/sec. This partly serves to provide the increase of the percentage  $q$  of the heavy phase corresponding to the downward velocity  $w_0$ , viz.,  $w_0 \frac{\partial q}{\partial z}$ , and partly gives an increase  $\frac{\partial q}{\partial t}$  at this level. For this increase we thus get the following formula:

$$\frac{\partial q}{\partial t} = \left( \frac{c}{K} \frac{\partial F}{\partial z} - \frac{\partial q}{\partial z} \right) w_0 \quad (11-1c)$$

It is easy to see that for the rising column we find the same formula, but the sign of  $w_0$  is here reversed, so  $\frac{\partial q}{\partial t}$  is negative. If we denote the difference of the densities of the two phases of olivine by  $\Delta\rho$  we find that the vertical velocity causes changes of density in both columns given by

$$d = \Delta\rho \frac{\partial q}{\partial t} = \left( \frac{c}{K} \frac{\partial F}{\partial z} - \frac{\partial q}{\partial z} \right) w_0 \Delta\rho \quad (11-1d)$$

Carrying out a rough integration over the full height of the transition layer, assuming for this purpose that  $c$ ,  $K$ ,  $w_0$ , and  $\Delta\rho$  are constant, and indicating the difference of the temperatures at the bottom and top of the transition layer by  $\Delta\theta$ , we obtain for the density increase over each of the current columns

$$D = \left( \frac{c \Delta\theta}{K} - 1 \right) w_0 \Delta\rho \quad (11-1e)$$

The weight of this excess, respectively deficiency, of mass is positive for the subsiding column, and negative, i.e., working upwards, for the rising one. These forces represent the contributions of the transition layer to the driving power of the convection current.

It is easy to see that if this layer were homogeneous with a density  $\rho$  and a thermal volume-expansion coefficient  $\alpha_t$ , the value  $D'$  of the density excess, respectively deficiency, would be

$$D' = \alpha_t \Delta\theta w_0 \rho \quad (11-1f)$$

The ratio  $D/D'$  is, therefore, given by

$$\frac{D}{D'} = \frac{\Delta\rho}{\rho \alpha_t \Delta\theta} \left( \frac{c \Delta\theta}{K} - 1 \right) \quad (11-1g)$$

We can introduce  $\Delta\rho = 0.7$ ,  $\rho = 1/2(3.3 + 4.0) = 3.65$ ,  $c = 0.20$ , and  $\alpha_t = 2 \times 10^{-5}$ , and we obtain

$$\frac{D}{D'} = \frac{9,590}{\Delta\theta} \left( 0.2 \frac{\Delta\theta}{K} - 1 \right) \quad (11-1h)$$

The transition heat  $K$  obeys Clapeyron's law, which gives

$$\frac{dP}{dT} = \frac{KA}{T \Delta V} \quad (11-1i)$$

where  $P$  is the pressure,  $T$  the absolute temperature,  $\Delta V$  the change of volume  $V$  by the phase transition, and  $A$  the heat equivalent ( $4.19 \times 10^7$ ). The transition heat  $K$  equals the increase  $\Delta H$  of the enthalpy  $H$  (which is the sum of the energy  $U$  and the product  $PV$ ), and  $\Delta H = T \Delta S$ , where  $\Delta S$  represents the increase of the entropy. We may probably put  $\Delta S = 0.1$  cal/deg per g. Introducing this in (11-1i), applied to 1 g, and putting  $dP = \rho g dz$  (at the depths between 500 and 900 km we may put  $g = 998$  cm/sec<sup>2</sup>), we obtain  $dT/dz = 4.686^\circ/\text{km}$  and so  $\Delta\theta = 1875^\circ$ . Putting the temperature at 500 km depth at  $800^\circ = 1073^\circ\text{K}$  (absolute temperature) we find a mean absolute temperature in the transition layer of  $2010^\circ\text{K}$  and a

mean value of  $K$  of 201 cal. This leads to a value of  $D/D'$  of 4.4, and so we may conclude that a convection current cannot only break through the transition layer, but that this layer gives an increase of instability by a factor 4.4. So this layer seems to promote such currents.

The conclusions obtained about the temperatures in the transition layer are, however, not satisfactory. A temperature of nearly  $2700^{\circ}$  at a depth of 900 km does not appear to leave enough difference from that of about  $4000^{\circ}$ , which we must assume to be present at the depth of 5,100 km (below which the NiFe of the inner core is probably in a solid state), to allow the surface of the core at a depth of 2,900 km to undergo enough cooling to explain convection currents in the outer part of the core. Such currents are needed for the present theory of geomagnetism.

For these problems of petrography and thermodynamics the author (V.M.) had the assistance of Dr. W. Nieuwenkamp, Professor of Petrography and Mineralogy at the University of Utrecht and Dr. E. J. W. Verwey, Director of the Philips Research Laboratories at Eindhoven, and especially of Dr. J. L. Meijering, scientist of this laboratory. Dr. Meijering found a way out of the difficulty by assuming a certain amount of local segregation of the two components of the olivine, the magnesium and iron silicates. This hypothesis provides one more degree of liberty and thus allows the reduction of the great temperature increase between the depths of 500 and 900 km to a more acceptable value, while maintaining the possibility of convection currents. For details the reader may be referred to a paper by J. L. Meijering and C. J. M. Rooymans in *Proc. Koninkl. Ned. Akad. Wetenschap.*, ser. B, 1958.

We can assume that in the present period current systems are occurring throughout the whole mantle. Since the temperature is higher below the continents, because the amount of radioactivity is greater in the continental crust than in the oceanic crust, rising currents doubtless originate below the continents and subsiding currents below the oceans; but the phase changes in the transition layer must lead to a reduction of the temperature gradients above the rising currents and an increase of those above the subsiding ones, which may explain the surprising fact that, notwithstanding the difference of crustal radioactivity, the gradients recently found under the oceans have about the same value as those obtained in the continents. If, however, our interpretation is right, it appears probable that this result will not be found everywhere; in areas where no subcrustal currents occur we can expect greater temperature gradients in the continental crust and smaller ones in the oceanic crust.

The rising of the surface, caused by the change of heavy phase to light phase in the rising current, is also in good agreement with the regressions found in the first period of an orogenic cycle. Therefore, the conclusions we draw from the hypothesis of a convection current breaking through a

phase-transition layer are in remarkable harmony with the observed facts, thus providing further confirmation of our hypothesis of subcrustal currents.

### 11-3. Thermal Convection in a Plane Layer

We begin with a summary of Rayleigh's treatment<sup>16</sup> of thermal convection in a plane layer; application to a sphere is made in Secs. 11-4 and 11-5. Rayleigh treats of convection in an ideal fluid, in which the smallest pressure difference sets flow going. The earth's mantle deviates from this pattern in two ways. First, the pressure difference has to exceed an elastic limit before flow can start. As shown in Sec. 11-1, for thermal convection this leads to two requirements, viz., the storing of a certain potential energy in the form of a downward temperature gradient and a trigger effect of finite size for starting the flow. The flow reaches its maximum velocity after about a quarter revolution and stops after about a half revolution. Stable equilibrium is then restored; the downward temperature gradient has disappeared, and an upward one has formed. Mathematical treatment of the phenomenon is difficult. The second deviation, even more difficult to take into account mathematically, is the fact that most currents in the mantle have to break through or into the zone of density transition between 200 and 900 km depth. We examined this question briefly in the preceding section.

In this and the following section we confine ourselves to the ideal fluid discussed by Rayleigh, and in subsequent sections we try to draw conclusions from it for the more difficult conditions in the earth. Convection is possible in an ideal fluid if, as Rayleigh shows, the downward temperature gradient exceeds a certain minimum value. Then the velocity of the current increases with time. When the gradient is equal to the minimum value, a stationary current is possible, and when it is smaller, a flow that has been started dies out again.

Rayleigh separates the temperature  $\theta$  and the pressure  $p$  into (1) a part corresponding to zero flow with a downward temperature gradient  $\beta$  and a vertical pressure gradient  $gp' - \alpha_t g p' \theta$ , where  $\rho'$  is the density and  $\alpha_t$  the thermal volume-expansion coefficient, and (2) a part connected with the current, which henceforth we shall indicate by  $\theta$  and  $p$ . Rayleigh follows Boussinesq<sup>5</sup> in assuming that we can neglect the effect of pressure on density and that the only temperature effect is that caused by the density change affecting the gravity influence.

We shall confine ourselves to the discussion of stationary convection, i.e., to  $\partial/\partial t = 0$  for all quantities, and we shall assume the velocities to be so small that the derivative with respect to time,  $d/dt$ , for a moving particle can be neglected. If the  $z$  coordinate is chosen positive in the direction of gravity, and if  $u$ ,  $v$ , and  $w$  are the components of the velocity and  $\eta$  the viscosity modulus, the equations of movement now reduce to

$$-\frac{\partial p}{\partial x} + \eta \nabla^2 u = 0 \quad (11-2a)$$

$$-\frac{\partial p}{\partial y} + \eta \nabla^2 v = 0 \quad (11-2b)$$

$$-\frac{\partial p}{\partial z} + \eta \nabla^2 w - \alpha_t \rho' g \theta = 0 \quad (11-2c)$$

$$\frac{\partial u}{\partial x} + \frac{\partial v}{\partial y} + \frac{\partial w}{\partial z} = 0 \quad (11-3)$$

If the thermal conductivity is  $\mu$ , the heat equation gives

$$\mu \nabla^2 \theta = \beta w \quad (11-4)$$

To solve these equations Rayleigh supposes the quantities  $u$ ,  $v$ ,  $w$ , and  $p$  to be functions of  $z$  multiplied by

$$K = \cos lx \cos my \quad (11-5)$$

This is a harmonic function of  $x$  and  $y$  which can also be given by

$$\nabla^2 K + f^2 K = 0 \quad \text{with} \quad f^2 = l^2 + m^2 \quad (11-6)$$

of which (11-5) is the general solution. Rayleigh's supposition leads to the following solution:

$$\begin{aligned} u &= v_0 \frac{\partial K}{\partial x} & v &= v_0 \frac{\partial K}{\partial y} & w &= w_0 K \\ \theta &= \theta_0 K & p &= p_0 K \end{aligned} \quad (11-7)$$

in which  $v_0$ ,  $w_0$ ,  $\theta_0$ , and  $p_0$  are functions only of  $z$ .

Introducing these formulas in Eqs. (11-2a), (11-2b), and (11-3), and eliminating  $v_0$ , we obtain

$$p_0 + \eta \frac{\partial w_0}{\partial z} - \frac{\eta}{f^2} \frac{\partial^3 w_0}{\partial z^3} = 0 \quad (11-8)$$

Differentiating this with respect to  $z$ , and assuming that we can neglect  $\partial \eta / \partial z$ , we find  $\partial p_0 / \partial z$ , and by introducing both this and Formulas (11-7) into (11-2c) we obtain

$$\frac{\partial^4 w_0}{\partial z^4} - 2f^2 \frac{\partial^2 w_0}{\partial z^2} + f^4 w_0 + \frac{\alpha_t \rho' g}{\eta} f^2 \theta_0 = 0 \quad (11-9)$$

Equation (11-4) combined with (11-7) gives

$$\frac{\beta}{\mu} w_0 - \frac{\partial^2 \theta}{\partial z^2} + f^2 \theta_0 = 0 \quad (11-10)$$

We have thus found two equations for  $w_0$  and  $\theta_0$ , of which the first may be called the equation of motion and the second the equation of heat conduction.

If  $w_0$  has been derived, we can obtain  $v_0$  from the following equation, found by combining (11-3) with (11-7),

$$v_0 = \frac{1}{f^2} \frac{\partial w_0}{\partial z} \quad (11-11)$$

We can derive  $p_0$  from (11-8). By means of (11-7) we now obtain the three components of the velocity, the pressure  $p$ , and the temperature  $\theta$ . We shall determine later the stresses connected with this current system.

When we assume the quantities  $\eta$ ,  $\alpha_t$ , and  $\rho'$  to be constant over the entire depth of the layer, the elimination of  $\theta_0$  from Eqs. (11-9) and (11-10) is simple. By means of (11-10) we express  $\theta_0$  in  $w_0$ , and introducing this into (11-9), we obtain Rayleigh's equation

$$\frac{\partial^6 w_0}{\partial z^6} - 3f^2 \frac{\partial^4 w_0}{\partial z^4} + 3f^4 \frac{\partial^2 w_0}{\partial z^2} - f^6 w_0 + \frac{\alpha_t \rho' g \beta}{\eta \mu} f^2 w_0 = 0 \quad (11-12)$$

The solution is

$$w_0 = A_1 e^{is_1 z} + A_2 e^{is_2 z} + \cdots + A_6 e^{is_6 z} \quad (11-13a)$$

in which  $A_1, A_2, \dots, A_6$  are integration constants and  $s_1, s_2, \dots, s_6$  the six roots of the equation

$$(s^2 + f^2)^3 = \frac{\alpha_t \rho' g \beta}{\eta \mu} f^2 \quad (11-13b)$$

By means of the integration constants we can adapt the solution to the conditions at the upper and lower boundaries of the fluid. For both surfaces we shall have to put  $w_0 = 0$  and, if we assume no horizontal temperature gradients at those surfaces, also  $\theta = 0$ . For the last two conditions Rayleigh assumes for both surfaces  $\partial^2 w_0 / \partial z^2 = 0$ , which is fulfilled if the shearing stresses on these surfaces are zero. These assumptions give a particularly simple solution; we obtain

$$w_0 = A \sin qz \quad (11-14a)$$

$$\text{with } q^2 = \sqrt[3]{\frac{\alpha_t \rho' g \beta}{\eta \mu}} f^2 - f^2 \quad (11-14b)$$

The thickness  $D$  of the layer is given by

$$D = \frac{\pi}{q} \quad (11-14c)$$

It is interesting to determine for what horizontal dimensions of the current the thickness becomes a minimum. We can assume that for infinite

horizontal dimensions of the fluid layer the horizontal dimensions of the current will adjust themselves at those values, and so we determine the value of  $f$  for this condition. To obtain the minimum of  $D$  we introduce  $s = q$  into (11-13b) and put  $d(q^2)/d(f^2) = 0$ . We find

$$3(q^2 + f^2)^2 = \frac{\alpha_t \rho' g \beta}{\eta \mu} \quad (11-15a)$$

and introducing this into (11-13b), in which  $s = q$ , we obtain

$$q^2 = 2f^2 \quad (11-15b)$$

For the two-dimensional case, (11-6) indicates that  $f = l$ , and for the square current fields of rising and descending columns ( $l = m$ ),  $f = l\sqrt{2}$ . If we denote the horizontal dimensions of the current fields by  $L$  and  $L'$ , respectively, we get

$$L = D\sqrt{2} \quad \text{with} \quad L = \frac{\pi}{f} \quad (11-16a)$$

$$L' = 2D \quad \text{with} \quad L' = \frac{\pi}{l} = \frac{\pi}{m} \quad (11-16b)$$

From (11-15) we derive for the value of  $D = \pi/q$

$$D = \pi \sqrt[4]{\frac{27\eta\mu}{4\alpha_t \rho' g \beta}} \quad (11-17)$$

As Rayleigh shows, this is the minimum thickness for which convection is possible for a given value of the temperature gradient  $\beta$ . If  $D$  is given, we can also derive the minimum gradient  $\beta$  required. These minima are valid only when  $\partial^2 w_0 / \partial z^2 = 0$  at both boundaries and the horizontal dimensions can adjust themselves freely. For other cases both  $D$  and  $\beta$  have to be somewhat larger. To characterize these different conditions Jeffreys<sup>11</sup> introduced the quantity  $\lambda$ , of zero dimension, which for a thickness  $h$  is given by

$$\lambda = \frac{\alpha_t \rho' g \beta}{\eta \mu} h^4 \quad (11-18)$$

The quantity  $\lambda$  dominates the convection possibilities. For the most favorable conditions, for which we found the value of  $D$  given in (11-17), it amounts to

$$\lambda = \frac{27\pi^4}{4} = 657.50 \quad (11-19)$$

This is its minimum value.

To determine the stresses connected with the convection-current system we make use of the general expressions for the stresses in a viscous fluid

under the conditions mentioned in the beginning of this section:

$$\begin{aligned}\sigma_x &= -p + 2\eta \frac{\partial u}{\partial x} & \tau_x &= \eta \left( \frac{\partial w}{\partial y} + \frac{\partial v}{\partial z} \right) \\ \sigma_y &= -p + 2\eta \frac{\partial v}{\partial y} & \tau_y &= \eta \left( \frac{\partial u}{\partial z} + \frac{\partial w}{\partial x} \right) \\ \sigma_z &= -p + 2\eta \frac{\partial w}{\partial z} & \tau_z &= \eta \left( \frac{\partial v}{\partial x} + \frac{\partial u}{\partial y} \right)\end{aligned}\quad (11-20)$$

Since we have kept to the normal system in these formulas, giving tension a positive sign, all the stresses, including the shear stresses, are opposite in sign to those elsewhere in this book; this convention is continued throughout this chapter. By introducing (11-7) into these formulas we obtain

$$\begin{aligned}\sigma_x &= -p_0 K + 2\eta v_0 \frac{\partial^2 K}{\partial x^2} & \tau_x &= \eta \left( w_0 + \frac{\partial v_0}{\partial z} \right) \frac{\partial K}{\partial y} \\ \sigma_y &= -p_0 K + 2\eta v_0 \frac{\partial^2 K}{\partial y^2} & \tau_y &= \eta \left( w_0 + \frac{\partial v_0}{\partial z} \right) \frac{\partial K}{\partial x} \\ \sigma_z &= -p_0 K + 2\eta \frac{\partial w_0}{\partial z} K & \tau_z &= 2\eta v_0 \frac{\partial^2 K}{\partial x \partial y}\end{aligned}\quad (11-21)$$

By means of these formulas, and using the solution developed for  $w_0$  and the expressions (11-8) for  $p_0$  and (11-11) for  $v_0$ , we can derive the stresses for convection-current systems. We shall not examine them further here.

#### 11-4. Thermal Convection in a Spherical Shell

We shall make the same assumptions and follow the same procedure as in the preceding section. The formulas are the same except for their numbers, which are higher by 20 than those in Sec. 11-3. When we introduce spherical coordinates, radius  $\rho$ , polar distance  $\vartheta$ , and longitude  $\lambda$ , and indicate the components of the velocity by  $v_\rho$ ,  $v_\vartheta$ , and  $v_\lambda$ , the equations of motion (11-2) become

$$-\frac{1}{\rho} \frac{\partial \rho}{\partial \vartheta} + \eta \nabla^2 v_\vartheta + \frac{2\eta}{\rho^2} \frac{\partial v_\rho}{\partial \vartheta} - \frac{\eta}{\rho^2 \sin^2 \vartheta} v_\vartheta - \frac{2\eta \cot \vartheta}{\rho^2 \sin \vartheta} \frac{\partial v_\lambda}{\partial \lambda} = 0 \quad (11-22a)$$

$$-\frac{1}{\rho \sin \vartheta} \frac{\partial p}{\partial \lambda} + \eta \nabla^2 v_\lambda + \frac{2\eta}{\rho^2 \sin^2 \vartheta} \frac{\partial v_\rho}{\partial \lambda} + \frac{2\eta \cot \vartheta}{\rho^2 \sin \vartheta} \frac{\partial v_\vartheta}{\partial \lambda} - \frac{\eta}{\rho^2 \sin^2 \vartheta} v_\lambda = 0 \quad (11-22b)$$

$$-\frac{\partial p}{\partial \rho} + \eta \nabla^2 v_\rho - \frac{2\eta}{\rho^2} v_\rho - \frac{2\eta}{\rho^2} \frac{\partial v_\vartheta}{\partial \vartheta} - \frac{2\eta}{\rho^2} \cot \vartheta v_\vartheta - \frac{2\eta}{\rho^2 \sin^2 \vartheta} \frac{\partial v_\lambda}{\partial \lambda} + \alpha_t \rho' g \theta = 0 \quad (11-22c)$$

while (11-3) and (11-4) take the form

$$\frac{1}{\rho} \frac{\partial v_\vartheta}{\partial \vartheta} + \frac{v_\vartheta}{\rho} \cot \vartheta + \frac{1}{\rho \sin \vartheta} \frac{\partial v_\lambda}{\partial \lambda} + \frac{\partial v_\rho}{\partial \rho} + 2 \frac{v_\rho}{\rho} = 0 \quad (11-23)$$

$$-\mu \nabla^2 \theta = \beta v_\rho \quad (11-24)$$

Rayleigh's harmonic function  $K$ , as given by (11-5) or (11-6), can now be replaced by a spherical harmonic function  $Y_n$  of arbitrary order  $n$  given by

$$\nabla^2 Y_n + \frac{n(n+1)}{\rho^2} Y_n = 0 \quad (11-25)$$

where  $\nabla^2 Y_n = \frac{1}{\rho^2} \frac{\partial^2 Y_n}{\partial \vartheta^2} + \frac{1}{\sin^2 \vartheta} \frac{\partial^2 Y_n}{\partial \lambda^2} + \cot \vartheta \frac{\partial Y_n}{\partial \vartheta}$  (11-26)

and this leads to the solution

$$\begin{aligned} v_\vartheta &= v_0 \frac{\partial Y_n}{\partial \vartheta} & v_\lambda &= \frac{v_0}{\sin \vartheta} \frac{\partial Y_n}{\partial \lambda} & v_\rho &= w_0 Y_n \\ \theta &= \theta_0 Y_n & p &= p_0 Y_n \end{aligned} \quad (11-27)$$

in which  $v_0$ ,  $w_0$ ,  $\theta_0$ , and  $p_0$  are functions only of  $\rho$ .

Introducing (11-27) into Eqs. (11-22a), (11-22b), and (11-23), we get

$$p_0 + \eta \frac{n^2 + n - 6}{n(n+1)} \frac{\partial w_0}{\partial \rho} - \eta \frac{6}{n(n+1)} \rho \frac{\partial^2 w_0}{\partial \rho^2} - \eta \frac{1}{n(n+1)} \rho^2 \frac{\partial^3 w_0}{\partial \rho^3} = 0 \quad (11-28)$$

By differentiating this with respect to  $\rho$  and by assuming that we can again neglect  $\partial \eta / \partial \rho$  we obtain  $\partial p_0 / \partial \rho$ , and by introducing both this and Formulas (11-27) into (11-22c) we get the equation of motion

$$\begin{aligned} \frac{\partial^4 w_0}{\partial \rho^4} + \frac{8}{\rho} \frac{\partial^3 w_0}{\partial \rho^3} - \frac{2(n^2 + n - 6)}{\rho^2} \frac{\partial^2 w_0}{\partial \rho^2} - \frac{4n(n+1)}{\rho^3} \frac{\partial w_0}{\partial \rho} \\ + (n-1)n(n+1)(n+2) \frac{w_0}{\rho^4} - n(n+1) \frac{\alpha_t \rho' g \theta_0}{\eta} \frac{\partial \theta_0}{\partial \rho} = 0 \quad (11-29) \end{aligned}$$

We find the equation of heat conduction corresponding to (11-10) by introducing (11-27) into (11-24)

$$\frac{\beta}{\mu} w_0 + \frac{\partial^2 \theta_0}{\partial \rho^2} + \frac{2}{\rho} \frac{\partial \theta_0}{\partial \rho} - n(n+1) \frac{\theta_0}{\rho^2} = 0 \quad (11-30)$$

We thus have obtained the two equations in  $w_0$  and  $\theta_0$  for the spherical shell which correspond to (11-9) and (11-10) for the plane fluid layer. By introducing (11-27) into (11-23) we find the equation expressing  $v_0$  in  $w_0$

$$v_0 = \frac{1}{n(n+1)} \left( \rho \frac{\partial w_0}{\partial \rho} + 2w_0 \right) \quad (11-31)$$

Comparing the plane-layer solution to the one here developed for the spherical shell, we see that the respective horizontal distributions of the current systems given by (11-6) and (11-25) merge into each other when we put

$$f^2 = \frac{n(n+1)}{\rho^2} \quad (11-32)$$

and assume that both  $n$  and  $\rho$  become large. The two distributions display a great variability for the same value of  $f$  and  $n$ , respectively. For the plane layer we can still choose the wavelength in the  $x$  and  $y$  directions as long as  $l^2 + m^2 = f^2$ , and for the spherical shell we can dispose of  $2n+1$  coefficients of the terms constituting the spherical harmonic of the order  $n$ .

If we again assume the quantities  $\eta$ ,  $\alpha_t$ , and  $\rho'$  to be constant over the entire depth of the spherical shell, the elimination of  $\theta_0$  from Eqs. (11-29) and (11-30) presents no difficulties. Expressing  $\theta_0$  in terms of  $w_0$  by means of (11-30), and introducing the result into (11-29), we obtain

$$\begin{aligned} & \frac{\partial^6 w_0}{\partial \rho^6} + \frac{14}{\rho} \frac{\partial^5 w_0}{\partial \rho^5} - \frac{(3n^2 + 3n - 50)}{\rho^2} \frac{\partial^4 w_0}{\partial \rho^4} - \frac{8(2n^2 + 2n - 5)}{\rho^3} \frac{\partial^3 w_0}{\partial \rho^3} \\ & + \frac{n(n+1)(3n^2 + 3n - 14)}{\rho^4} \frac{\partial^2 w_0}{\partial \rho^2} + \frac{2n(n+1)(n^2 + n + 2)}{\rho^5} \frac{\partial w_0}{\partial \rho} \\ & - (n-1)^2 n(n+1)(n+2)^2 \frac{w_0}{\rho^6} + n(n+1) \frac{\alpha_t \rho' g \beta}{\eta \mu} \frac{w_0}{\rho^2} = 0 \end{aligned} \quad (11-33a)$$

If the last term is a whole rational function of  $\rho$ , the equation can be solved. If

$$\frac{\alpha_t \rho' g \beta}{\eta \mu} w_0 = C \rho^s \quad (11-33b)$$

the solution is

$$w_0 = D\rho^{s+4} + E\rho^{n+2} + F\rho^{n+1} + G\rho^{n-1} + \frac{H}{\rho^{n-1}} + \frac{I}{\rho^n} + \frac{K}{\rho^{n+2}} \quad (11-33c)$$

in which  $E, F, G, H, I$ , and  $K$  are integration constants which can be adapted to the six boundary conditions at the upper and lower surfaces and  $D$  is given by

$$D = \frac{n(n+1)C}{(n-s-2)(n-s-3)(n-s-5)(n+s+3)(n+s+4)(n+s+6)} \quad (11-33d)$$

If  $s$  has such a value that one of the factors of the denominator vanishes, the first term of the solution becomes

$$D'\rho^{s+4} \ln \rho \quad (11-33e)$$

for which  $D'$  can be found without difficulty.

We can now derive a solution of our problem by putting the left member of (11-33b) equal to an acceptable rational function of  $\rho$  and deduce  $w_0$  by means of Formulas (11-33). By dividing the chosen function by the value of  $w_0$  we obtain the value of  $\alpha_t \rho' g \beta / \eta \mu$ , as a function of  $\rho$ , for which our solution is valid. We can repeat this for other functions of  $\rho$  and thus determine how the current depends on different values of the temperature gradient and other physical quantities over the thickness of the spherical shell.

Instead of deriving the solution this way, we can also do it in two stages. By substituting for  $\beta w_0 / \mu$  a rational function of  $\rho$  we can first solve Eq. (11-30) and then solve (11-29) by introducing therein the value of  $\theta_0$  thus obtained as a rational function of  $\rho$ . The value found for  $w_0$  can be substituted in  $\beta w_0 / \mu$ , and the result provides the value of  $\beta / \mu$  for which our solution is valid.

This two-stage solution has the advantage of simplifying fulfillment of the six boundary conditions and allowing a clearer view of our assumptions regarding the different physical quantities of the problem. We thus eliminate some of the differentiation uncertainties that were unavoidable in deriving (11-33a).

To find the solution of (11-30) when  $\beta w_0 / \mu$  is a rational function of  $\rho$  we put

$$\frac{\beta}{\mu} w_0 = \frac{C \rho^s}{R^{s+2}} \quad (11-34a)$$

which gives

$$\theta_0 = \frac{C}{(n-s-2)(n+s+3)} \left(\frac{\rho}{R}\right)^{s+2} + A \left(\frac{\rho}{R}\right)^n + B \left(\frac{\rho}{R}\right)^{-(n+1)} \quad (11-34b)$$

or, if  $s = n - 2$  or  $s = -(n + 3)$ ,

$$\theta_0 = \frac{C}{2s+5} \left( \frac{\rho}{R} \right)^{s+2} \ln \frac{\rho}{R} + A \left( \frac{\rho}{R} \right)^n + B \left( \frac{\rho}{R} \right)^{-(n+1)} \quad (11-34c)$$

In these equations  $A$  and  $B$  are integration constants which can be derived from the boundary conditions on the outer and inner surfaces ( $\rho = R$  and  $r$ , respectively). As we assume that no horizontal gradients are present, we have for both surfaces  $\theta_0 = 0$  and further  $w_0 = 0$  and so likewise  $\beta w_0/\mu = 0$ , which leads to the assumption that the last quantity has the factors  $(R - \rho)(\rho - r)$ .

In applying our formulas to convection in the mantle of the earth we suppose the gradient to diminish from top to bottom, and so we assume

$$\frac{\beta}{\mu} w_0 = \frac{C}{R^5} \rho(R - \rho)(\rho - r) \quad (11-35)$$

When we consecutively apply Formulas (11-34) to the cases  $n = 1, n = 2, \dots, n = 7$  and indicate the ratio  $\rho/R$  by  $\epsilon$  (boundaries  $\epsilon = 1$  and  $\epsilon = \frac{6}{11}$ ), supposition (11-35) leads to the following formulas for  $\theta_0$ :

$$n = 1 \quad \frac{\theta_0}{C} = \frac{1}{28}\epsilon^5 - \frac{1}{198}\epsilon^4 + \frac{3}{55}\epsilon^3 - 0.00419674\epsilon - 0.00020441\epsilon^{-2} \quad (11-36a)$$

$$n = 2 \quad \frac{\theta_0}{C} = \frac{1}{24}\epsilon^5 - \frac{1}{154}\epsilon^4 + \frac{1}{11}\epsilon^3 - 0.02211922\epsilon^2 - 0.000066930\epsilon^{-3} \quad (11-36b)$$

$$n = 3 \quad \frac{\theta_0}{C} = \frac{1}{18}\epsilon^5 - \frac{1}{88}\epsilon^4 + \frac{6}{77}\epsilon^3 \ln \epsilon + 0.13764888\epsilon^3 - 0.000022617\epsilon^{-4} \quad (11-36c)$$

$$n = 4 \quad \frac{\theta_0}{C} = \frac{1}{10}\epsilon^5 - \frac{1}{99}\epsilon^4 \ln \epsilon - \frac{3}{44}\epsilon^3 - 0.03181040\epsilon^4 - 0.0000077743\epsilon^{-5} \quad (11-36d)$$

$$n = 5 \quad \frac{\theta_0}{C} = \frac{1}{11}\epsilon^5 + \frac{1}{110}\epsilon^4 - \frac{1}{33}\epsilon^3 - 0.12423970\epsilon^5 - 0.0000027192\epsilon^{-6} \quad (11-36e)$$

$$n = 6 \quad \frac{\theta_0}{C} = -\frac{1}{12}\epsilon^5 + \frac{1}{242}\epsilon^4 - \frac{1}{55}\epsilon^3 + 0.03126819\epsilon^6 - 0.00000097022\epsilon^{-7} \quad (11-36f)$$

$$n = 7 \quad \frac{\theta_0}{C} = -\frac{1}{26}\epsilon^5 + \frac{1}{396}\epsilon^4 - \frac{3}{242}\epsilon^3 + 0.007929295\epsilon^7 - 0.00000035358\epsilon^{-8} \quad (11-36g)$$

Introducing these values of  $\theta_0$  into Eq. (11-29), we can proceed to the derivation of  $w_0$ . In doing so we shall neglect the change of modification which probably occurs between 200 and 900 km depth. We shall also assume that the ratio  $\alpha_t \rho' g / \eta$  is constant over the entire mantle, although such an assumption is obviously not true. In the upper part of the mantle gravity still increases, but lower down it must diminish. Contrary behavior can be assumed for the pseudo viscosity  $\eta$ : in the upper part the increase of temperature is probably more effective in making  $\eta$  smaller than the increase of pressure is in making it larger. Lower down, where the increase of temperature becomes progressively smaller, the effect of the increase of pressure can be expected to dominate. The discrepancies between our assumptions and the real conditions in the mantle notwithstanding, we proceed with our solution.

We shall consider consecutively the two types of terms our solution of  $\theta_0$  consists of. If the last term of (11-29) has the form

$$n(n+1) \frac{\alpha_t \rho' g \theta_0}{\eta} \frac{D}{\rho^2} = n(n+1) \frac{D}{R^4} \epsilon^{t-2} \quad (11-37a)$$

the solution for  $w_0$  takes the shape

$$w_0 = \frac{n(n+1)D}{(n+1-t)(n-1-t)(n+t)(n+2+t)} \epsilon^t + E\epsilon^{n+1} + F\epsilon^{n-1} + G\epsilon^{-n} + H\epsilon^{-(n+2)} \quad (11-37b)$$

in which  $E$ ,  $F$ ,  $G$ , and  $H$  are integration constants. If, however,

$$t = n+1 \quad t = n-1 \quad t = -n \quad \text{or} \quad t = -n-2 \quad (11-37c)$$

we obtain

$$w_0 = - \frac{n(n+1)D}{(2t+1)[(n+1-t)(n+2+t) + (n-1-t)(n+t)]} \epsilon^t \ln \epsilon + E\epsilon^{n+1} + F\epsilon^{n-1} + G\epsilon^{-n} + H\epsilon^{-(n+2)} \quad (11-37d)$$

If the last term of (11-29) has the form

$$n(n+1) \frac{\alpha_t \rho' g \theta_0}{\eta} \frac{D'}{\rho^2} = n(n+1) \frac{D'}{R^4} \epsilon^{t-2} \ln \epsilon \quad (11-38a)$$

the solution is

$$w_0 = \frac{n(n+1)D'}{(n+1-t)(n-1-t)(n+t)(n+2+t)} \epsilon^t \ln \epsilon + \frac{2n(n+1)(2t+1)[(n-t)(n+1+t) + 1]D'}{(n+1-t)^2(n-1-t)^2(n+t)^2(n+2+t)^2} \epsilon^t + E\epsilon^{n+1} + F\epsilon^{n-1} + G\epsilon^{-n} + H\epsilon^{-(n+2)} \quad (11-38b)$$

These formulas cover all the possibilities the solution for  $\theta_0$  leads to, and so the solution for  $w_0$  can be derived. The four integration constants must be chosen in such a way as to fulfill the boundary conditions at the outer and inner surfaces of the mantle.

One of these conditions is obviously  $w_0 = 0$ . For the other we shall choose Rayleigh's condition for the plane case, viz., the assumption that the shear stress on both surfaces is zero. For the lower boundary, where the mantle touches the fluid core, this is no doubt true. For the upper boundary it is probably acceptable to neglect the resistance the crust offers to the large current systems throughout the whole mantle we are now considering, but for smaller systems (see Sec. 11-9) it is not true.

According to the formulas we shall presently derive for the shear stresses, the second condition amounts to

$$\frac{\partial v_0}{\partial \rho} - \frac{v_0}{\rho} + \frac{w_0}{\rho} = 0 \quad (11-39)$$

Combining this with the first condition,  $w_0 = 0$ , and with the incompressibility equation (11-31) we can put the second condition into the form

$$2 \frac{\partial w_0}{\partial \rho} + \rho \frac{\partial^2 w_0}{\partial \rho^2} = 0 \quad \text{or} \quad \frac{\partial^2}{\partial \rho^2} (\rho w_0) = 0 \quad (11-40)$$

The results thus obtained for  $w_0$  for  $n = 1, n = 2, \dots, n = 7$  are given in the appendix to this chapter. By means of (11-31)  $v_0$  can be derived, and by means of (11-27) the three components of the current velocity can be derived. The pressure  $p$  follows from (11-28) combined with (11-27).

It is now simple to derive the value for each point of Jeffreys's quantity  $\lambda$  given by (11-18). If we define it here by putting the thickness  $h = R - r$ , we obtain

$$\lambda = \frac{\alpha_t \rho g \beta}{\eta \mu} (R - r)^4 = \frac{\rho (R - \rho)(\rho - r)(R - r)^4}{(w_0/D) R^7} \quad (11-41)$$

These quantities  $\lambda$ , however, are not constant over the area of the currents; they vary with depth. We shall find their mean values in two ways, viz., by taking the mean over the depth and over the volume. Table 11-1 for currents over the whole mantle is derived from the formulas for  $w_0$  in the appendix to this chapter.

The mean values in the two lists have nearly the same ratio. Their minimum is at  $n = 3$ , but they are only slightly larger for  $n = 4$ . The values for  $n = 3$  and  $n = 4$  are somewhat greater than the minimum value of 657.50 found in (11-19) for the plane layer, but the difference is not large. We must remember, however, that several of our assumptions about the physical constants are probably untrue and that we have neglected the

TABLE 11-1. VALUES OF  $\lambda$  FOR MANTLE CURRENTS

$n$	Mean over depth $\lambda_m$	Mean over volume $\lambda'_m$	Ratio $\lambda'_m/\lambda_m$
1	1949	2215	1.136
2	933	1058	1.134
3	741	837	1.130
4	760	854	1.124
5	882	986	1.118
6	1094	1210	1.106
7	1394	1532	1.099

important factor of phase transition in the layer between 200 and 900 km depth; nevertheless, in Sec. 11-8, when we return to these results, we find that there are good reasons for trusting them. From the figures obtained here it would seem that for a slowly increasing downward temperature gradient  $\beta$  in the mantle, a current distribution according to third- and fourth-order spherical harmonics would be the most likely.

To derive the stresses connected with the convection currents we have to begin by expressing in spherical coordinates the equations (11-20) giving the relations between stresses and velocities. We keep to the assumption that the effects of temperature differences can be neglected except in so far as they influence the gravity effect. We also keep the normal sign convention, according to which tension gets a positive sign; the formulas thus derived for both normal-stress and shear-stress components are therefore opposite in sign to those elsewhere in this book. We obtain

$$\begin{aligned} \sigma_\vartheta &= -p + 2\eta \left( \frac{1}{\rho} \frac{\partial v_\vartheta}{\partial \vartheta} + \frac{v_\rho}{\rho} \right) \\ \sigma_\lambda &= -p + 2\eta \left( \frac{1}{\rho \sin \vartheta} \frac{\partial v_\lambda}{\partial \lambda} + \frac{v_\rho}{\rho} + \cot \vartheta \frac{v_\vartheta}{\rho} \right) \\ \sigma_\rho &= -p + 2\eta \frac{\partial v_\rho}{\partial \rho} \\ \tau_\vartheta &= \eta \left( \frac{\partial v_\lambda}{\partial \rho} + \frac{1}{\rho \sin \vartheta} \frac{\partial v_\rho}{\partial \lambda} - \frac{v_\lambda}{\rho} \right) \\ \tau_\lambda &= \eta \left( \frac{\partial v_\vartheta}{\partial \rho} + \frac{1}{\rho} \frac{\partial v_\rho}{\partial \vartheta} - \frac{v_\vartheta}{\rho} \right) \\ \tau_\rho &= \eta \left( \frac{1}{\rho \sin \vartheta} \frac{\partial v_\vartheta}{\partial \lambda} + \frac{1}{\rho} \frac{\partial v_\lambda}{\partial \vartheta} - \cot \vartheta \frac{v_\lambda}{\rho} \right) \end{aligned} \quad (11-42)$$

After introduction of Formulas (11-27) the expressions become

$$\begin{aligned}
 \sigma_\vartheta &= \left( -p_0 + 2\eta \frac{w_0}{\rho} \right) Y_n + 2\eta \frac{v_0}{\rho} \frac{\partial^2 Y_n}{\partial \vartheta^2} \\
 \sigma_\lambda &= \left[ -p_0 - 2\eta \left( \frac{w_0}{\rho} + \frac{\partial w_0}{\partial \rho} \right) \right] Y_n - 2\eta \frac{v_0}{\rho} \frac{\partial^2 Y_n}{\partial \vartheta^2} \\
 \sigma_\rho &= \left( -p_0 + 2\eta \frac{\partial w_0}{\partial \rho} \right) Y_n \\
 \tau_\vartheta &= \eta \frac{1}{\sin \vartheta} \left( \frac{\partial v_0}{\partial \rho} + \frac{w_0 - v_0}{\rho} \right) \frac{\partial Y_n}{\partial \lambda} \\
 \tau_\lambda &= \eta \left( \frac{\partial v_0}{\partial \rho} + \frac{w_0 - v_0}{\rho} \right) \frac{\partial Y_n}{\partial \vartheta} \\
 \tau_\rho &= 2\eta \frac{v_0}{\rho \sin \vartheta} \left( \frac{\partial^2 Y_n}{\partial \vartheta \partial \lambda} - \cot \vartheta \frac{\partial Y_n}{\partial \lambda} \right)
 \end{aligned} \tag{11-43}$$

which, on substitution of the values of  $v_0$  and  $w_0$ , give us the stresses for the convection-current systems.

It is important to notice that, since the formulas for  $\sigma_\vartheta$ ,  $\sigma_\lambda$ ,  $\tau_\rho$ ,  $\tau_\vartheta$ , and  $\tau_\lambda$  contain differential quotients of the spherical harmonic  $Y_n$ , they depend not only on the order of  $Y_n$  but also on the  $2n + 1$  terms which together constitute  $Y_n$ . Two conclusions follow.

In the first place, since deep and intermediate earthquakes are connected with shear stresses, we must assume that, if they are a consequence of convection currents, their distribution and focal phenomena must depend not only on the order of the spherical harmonic but also on individual terms of it. In the second place, the same double dependence must be true for the way the currents originate and for their distribution. As we can assume that there is in the mantle a certain elastic-stress limit that must be exceeded before flow develops, the areas where it is exceeded are of great importance for the distribution of the current systems which form. If, for example, we assume that the stress limit for flowoff, in horizontal sense, at the surface of a rising column is first surpassed in one direction only, it is probable that the original direction remains the only one in which flow starts, because the stress limit in other directions in the horizontal plane is never exceeded after flowoff in one direction has once begun.

The equations of this section obviously can also be applied to convection in layers extending over only part of the depth of the mantle.

### 11-5. Thermal Convection in the Entire Globe

It is simple to apply the equations and formulas of the preceding section to convection in the entire globe. Although world-wide convection certainly is not applicable to the earth as it is now, in an early phase of the earth's history the conditions may have been such that it was possible (see Sec. 11-7), and there is some evidence of its having occurred.

All the equations and corresponding discussion of the preceding section up to Formulas (11-34b) and (11-34c) can be applied without change. Since for these two formulas the value of the integration constant  $B$  must obviously be zero, we can now write

$$\theta_0 = \frac{C}{(-n + 2 + s)(n + 3 + s)} (1 - e^{-n+2+s}) e^n \quad (11-44a)$$

and if  $s = n - 2$  or  $s = -(n + 3)$ ,

$$\theta_0 = \frac{C}{2s + 5} e^{s+2} \ln s \quad (11-44b)$$

For the assumption of how the quantity  $\beta w_0/\mu$  diminishes from the surface to the center of the earth we introduce

$$\frac{\beta}{\mu} w_0 = \frac{C}{R^{p+3}} \rho^p (R - \rho) \quad (11-45)$$

which allows us to adopt more than one supposition by choosing different values of  $p$ . For the order  $n$  of the spherical-harmonic distribution we shall take no higher values than  $n = 3$ ; it is obviously improbable that greater values occur. We shall adopt consecutively

$$\begin{aligned} n &= 1 & p &= 1 \text{ and } p = 4 \\ n &= 2 & p &= 2 \text{ and } p = 5 \\ n &= 3 & p &= 2 \text{ and } p = 5 \end{aligned} \quad (11-46)$$

Since  $s = n - 2$  and  $s = -(n + 3)$  do not occur for these values, we can continue to use (11-44a). The results for our six cases can be given in the following general formula:

$$\begin{aligned} \theta_0 = & - \frac{C}{(n - p - 2)(n + p + 3)} (1 - e^{-n+p+2}) e^n \\ & + \frac{C}{(n - p - 3)(n + p + 4)} (1 - e^{-n+p+3}) e^n \end{aligned} \quad (11-47)$$

Introducing this value of  $\theta$  into (11-29), we can once more make use of Formulas (11-37) to find the solution for  $w_0$ . We shall again assume that the ratio  $\alpha_t \rho' g / \eta$  is constant, which is still more questionable than it was for convection in the mantle. We also keep to the same boundary conditions and assume that at the surface both  $w_0$  and the shear stresses are zero. The results thus obtained for  $w_0$  for our six cases are given in the appendix to this chapter (page 442).

Defining Jeffreys's quantity  $\lambda$  by substituting the radius  $R$  of the globe for the thickness  $h$  of the layer, we now get

$$\lambda = \frac{\alpha_t \rho' g \beta}{\eta \mu} R^4 = \frac{\rho^p (R - \rho)}{(w_0/D) R^{p+1}} \quad (11-48)$$

Introducing the radius  $R$  of the earth and taking once more the mean of the values thus obtained for  $\lambda$  in two ways, over the radius and over the volume, gives the values shown in Table 11-2.

TABLE 11-2. VALUES OF  $\lambda$  FOR CURRENTS THROUGH THE ENTIRE EARTH

$n$	$p$	Mean over radius $\lambda_m$	Mean over volume $\lambda'_m$	Ratio $\lambda'_m/\lambda_m$
1	1	928	1493	1.608
2	2	1828	3145	1.721
3	2	3610	5125	1.420
1	4	1522	3315	2.178
2	5	2563	5735	2.238
3	5	3811	8354	2.192

We see that the ratios of the two mean values fluctuate somewhat more than for mantle currents but that for the three low values of  $p$  and for the three higher values of  $p$  they are still in fair agreement. When we consider that the two groups refer to widely different temperature distributions but that the results have one thing in common—the fact that in each group the value of  $\lambda$  for  $n = 1$  is much smaller than for  $n = 2$  and  $n = 3$ —we can safely conclude that for convection in the entire globe first-order spherical harmonic distribution is more likely than a higher-order distribution. This is a remarkable result, especially in view of the asymmetry of the current distribution, which at first glance might seem improbable. We shall return to this conclusion in Sec. 11-7.

Figure 11-1 and 2 shows the current system according to the first-order spherical harmonic distribution for a temperature distribution corresponding to  $p = 1$ . The dashed curves give the velocity distribution in the verti-

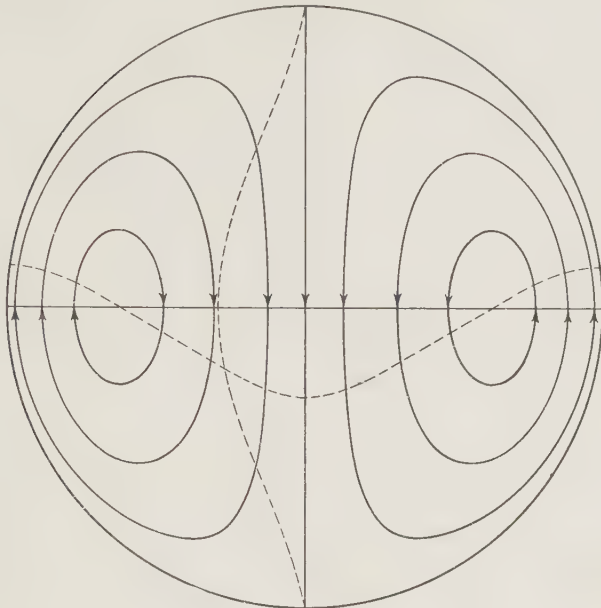


FIG. 11-1 and 2. First-order current system in the earth for  $p = 1$ ; dashed curves give the velocity distribution in the vertical axis and in the plane at right angles to it.

cal axis and in the plane at right angles to it. The large diameter of the central current and the relatively small diameter of the return current, which flows back over the whole circumference of the globe, should be noted.

Formulas (11-43) remain valid for stresses connected with global convection currents. By substituting the values of  $v_0$  and  $w_0$  we obtain the stress distribution. To obtain  $v_0$  and  $p_0$  we can apply the same formulas, (11-31) and (11-28), as for the mantle currents and thus find the velocity and pressure distributions by means of (11-27).

#### 11-6. Topography of the Earth Developed in Spherical Harmonics; Convection Currents as the Cause of Its Distribution

In 1922 Prey<sup>15</sup> published a development in spherical harmonics up to the 16th order of the topography of the earth. Figure 11-3 shows the representation he obtained. Little attention has been paid to this great work, which took several years to accomplish. It is true, of course, that the 289 coefficients published present an irregular picture, apparently without any features of interest.

In 1950 the author<sup>22-24</sup> (V.M.) undertook a study of Prey's figures which revealed remarkable characteristics and led to important conclusions. The investigation was based on the author's experience, obtained during the

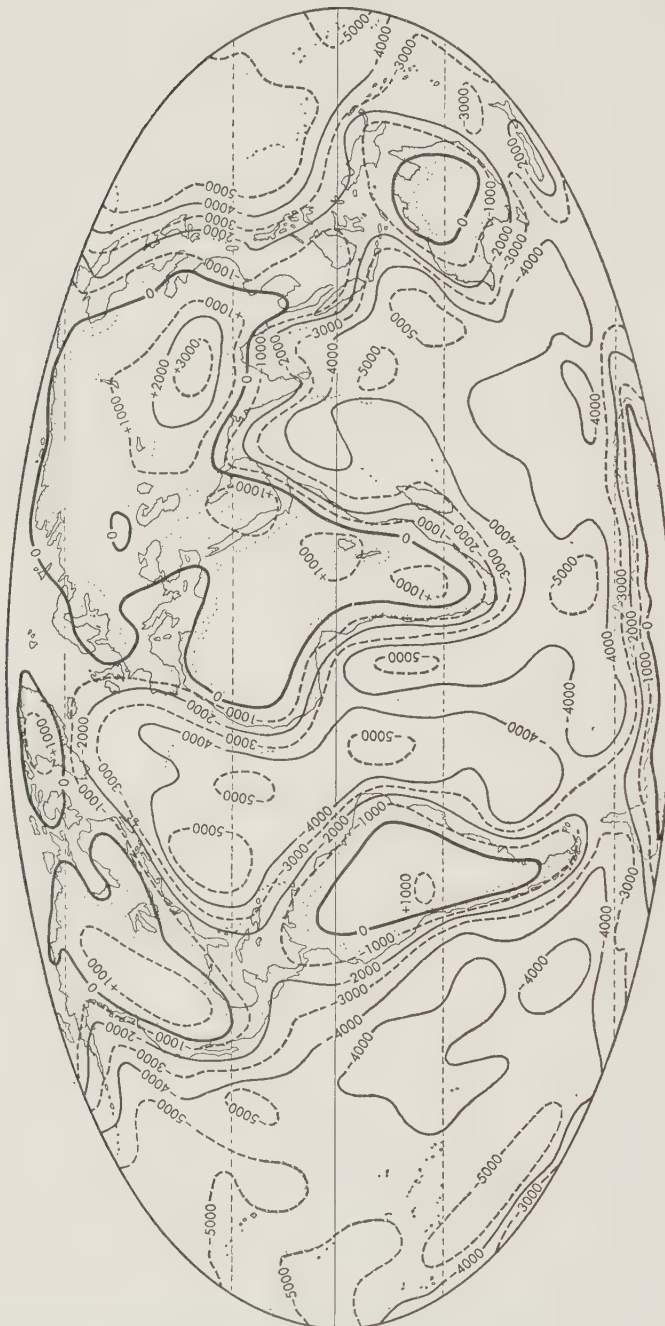


FIG. 11-3. The earth's topography as given by Prey's development in spherical harmonics up to the 16th order.

study of convection in the earth, that the basic equations governing the distribution of current systems contain only the order  $n$  of the spherical harmonic terms and not the individual  $2n + 1$  constituent terms of which they consist. This fact led him to determine for each of the 16 orders the mean value of the topography corresponding to all the constituent terms, taken together, of a given order, which was carried out by deriving the root mean square of the elevations of that topography.

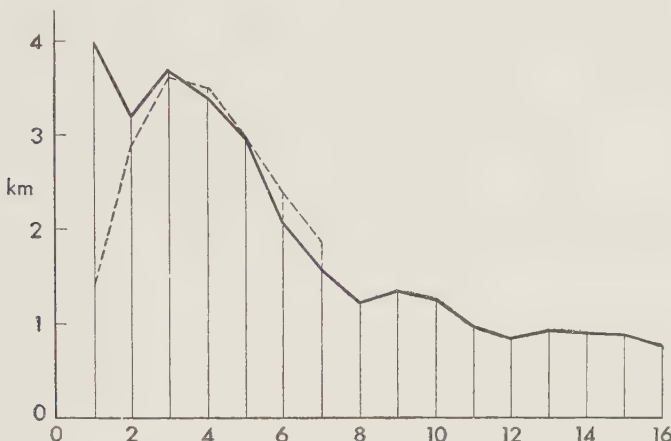


FIG. 11-4. Mean values over the earth's surface of the 16 first terms of the spherical-harmonic development of the thickness of the sialic crust.

To his surprise, the 16 results obtained formed a regular curve of the type given in Fig. 11-4, which shows a gradual decrease of the amplitudes for higher orders together with a wave character that will be analyzed presently. It can be concluded that the main lines of the earth's topography must have originated according to some fairly simple laws. If, as might well have been expected, they had been caused by some haphazard combination of a great many unrelated phenomena, the curve would have been quite irregular, with random deviations.

Since, because of isostasy, the topography, in its major features, is determined by the weight of the crustal columns, which, in turn, determines its equilibrium position, and since this weight depends on the thicknesses of the crustal layers, the way these thicknesses vary over the earth's surface is the fundamental problem. Taking it in its simplest form, we shall use here the common schematic picture of a uniform sialic crust of density 2.67 and below it the ultrabasic rocks of density 3.27, and we shall derive the thickness of this layer from the topography. In doing so we shall also have to take into account the weight of the sea water in the oceans, for which we shall assume a density of 1.028.

To make such isostatic studies possible, Prey carried out two spherical-harmonic developments, both up to the 16th order, and thanks to that fact, we are able to derive from his two tables the coefficients of development of the sialic thickness. Prey's table A gives the coefficients for the complete topography of the solid surface of the earth, and his table B gives those for the topography of the ocean floors combined with zero elevation for the parts of the crust above sea water.

For the assumed densities the normal thickness of the continental sialic crust is increased by  $1 + 2.67/0.6 = 5.45$  times the elevation of the topography, but for the oceanic crust a density of  $2.67 - 1.028 = 1.642$  must be attributed to the ocean depth, which can be considered as negative elevation, and so the sialic thickness is here diminished by  $1 + 1.642/0.6 = 3.737$  times the depth. Hence we find the coefficients of the development of the sialic thickness in spherical harmonics by multiplying the coefficients of Prey's table A by 5.45 and by subtracting  $5.45 - 3.737 = 1.713$  times the coefficients of his table B. We can obviously arrive at the same result by diminishing the coefficients of table A by  $1.713/5.45 = 0.3143$  times those of table B and multiplying the result by 5.45.

According to Formula (3-12b), the complete development has the form

$$Y_n = a_n P_n + a_{n1} P_n^{-1} \cos \lambda + \cdots + a_{np} P_n^{-p} \cos p\lambda + \cdots + a_{nn} P_n^{-n} \cos n\lambda \\ + b_{n1} P_n^{-1} \sin \lambda + \cdots + b_{np} P_n^{-p} \sin p\lambda + \cdots + b_{nn} P_n^{-n} \sin n\lambda \quad (11-49)$$

To derive the mean square over the whole earth we can make use of (3-14) to (3-16), and we obtain

$$|(Y_n)^2| = \frac{1}{2n+1} a_n^2 + \frac{1}{2(2n+1)} \frac{(n+1)!}{(n-1)!} (a_{n1}^2 + b_{n1}^2) + \cdots \\ + \frac{1}{2(2n+1)} \frac{(n+p)!}{(n-p)!} (a_{np}^2 + b_{np}^2) + \cdots \\ + \frac{(2n)!}{2(2n+1)} (a_{nn}^2 + b_{nn}^2) \quad (11-50)$$

The root of this quantity is the mean value  $h_m$  of the  $n$ th-order spherical harmonic part of the topography over the earth's surface.

To simplify the computation of the mean value of this and other linear functions of the two topographies as represented by Prey's tables A and B, we have determined separately the mean values  $|(Y'_n)^2|$  of the series  $Y'_n$  with the coefficients  $a, b$  of table A,  $|(Y'_n)^2|$  of the series  $Y'_n$  with the coefficients  $a', b'$  of the table B, and  $|(Y_n Y'_n)|$  of the product of both series. For the last mean value we must evidently replace, in Formula (11-50), the quantities  $a_n^2, a_{n1}^2, b_{n1}^2, a_{np}^2, b_{np}^2, a_{nn}^2$ , and  $b_{nn}^2$  by  $a_n a'_n, a_{n1} a'_{n1}, b_{n1} b'_{n1}, a_{np} a'_{np}, b_{np} b'_{np}, a_{nn} a'_{nn}$ , and  $b_{nn} b'_{nn}$ . Table 11-3 shows these three sets of mean values

TABLE 11-3. LISTS OF SPHERICAL HARMONIC TERMS

$$(Y_n'' = Y_n - 0.3143 Y'_n)$$

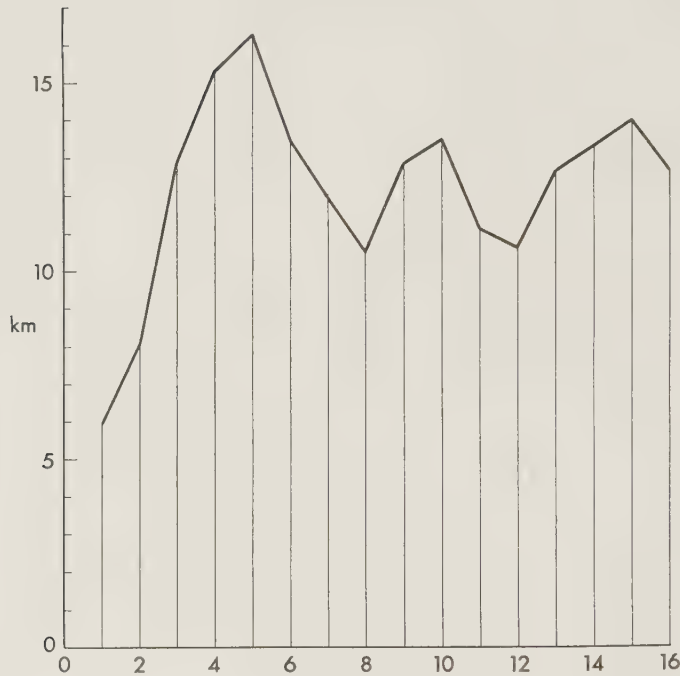
$n$ (1)	$ (Y_n)^2 , \text{ km}^2$ (2)	$\sqrt{ (Y_n)^2 }, \text{ km}$ (3)	$ (Y'_n)^2 , \text{ km}^2$ (4)	$ Y_n Y'_n , \text{ km}^2$ (5)	$ (Y_n'')^2 , \text{ km}^2$ (6)	$5.45 \sqrt{ (Y_n'')^2 }, \text{ km}$ (7)	$\frac{(7)}{(3)} \times \frac{(7)}{(9)}$	$n^{\frac{1}{2}}(n+1)^{\frac{1}{2}}$
0		-2.456				-8.791		
1	1.1036	1.055	0.8556	0.9722	0.5770	4.140	3.92	5.86
2	0.6760	0.822	0.5315	0.5971	0.3532	3.239	3.94	7.93
3	0.8667	0.931	0.6477	0.7450	0.4625	3.706	3.98	12.83
4	0.7221	0.850	0.5293	0.6157	0.3924	3.414	4.01	15.28
5	0.5640	0.751	0.3948	0.4870	0.2969	2.970	3.96	16.27
6	0.2597	0.510	0.1801	0.2088	0.1462	2.084	4.09	13.51
7	0.1730	0.416	0.1610	0.1626	0.0867	1.605	3.86	12.02
8	0.09573	0.309	0.07720	0.08213	0.05072	1.228	3.98	10.42
9	0.10805	0.3287	0.07702	0.08750	0.06066	1.342	4.08	12.74
10	0.09880	0.3143	0.06941	0.08034	0.05514	1.278	4.06	13.40
11	0.05563	0.2359	0.03943	0.04475	0.03140	0.966	4.10	11.10
12	0.04194	0.2048	0.02913	0.03296	0.02410	0.846	4.13	10.57
13	0.05521	0.2350	0.04552	0.04864	0.02913	0.930	3.96	12.55
14	0.05186	0.2277	0.04188	0.04480	0.02784	0.910	4.00	13.19
15	0.04750	0.2179	0.03180	0.03790	0.02682	0.893	4.10	13.83
16	0.03276	0.1810	0.02202	0.02457	0.01950	0.761	4.20	12.55

for the orders 1 to 16 in columns 2, 4, and 5; column 3 gives the roots of the values of column 2, i.e., the mean value of the topographies corresponding to the 16 orders of spherical harmonics, and column 6 lists the mean values  $|(Y_n'')^2|$  given by

$$\begin{aligned} |(Y_n'')^2| &= |(Y_n - 0.3143 Y'_n)^2| \\ &= |(Y_n)^2| - 0.6286 |Y_n Y'_n| + 0.3143^2 |(Y'_n)^2| \quad (11-51) \end{aligned}$$

Column 7 lists the roots of these values multiplied by 5.45, which thus represent the mean values over the earth's surface of the 16 parts of the thickness of the sialic crust corresponding to the complete 16 terms of its development in spherical harmonics up to the 16th order. The values of column 7 have been represented in Fig. 11-4, which shows the same properties of regularity and periodicity as the list of spherical harmonic terms of the topography in column 3. This fact is clearly visible in column 8, where the ratios of the values of columns 3 and 7 show only slight variation.

Column 9 lists the values of column 7 multiplied by  $n^{\frac{1}{2}}(n+1)^{\frac{1}{2}}$ ; the curve for these values is represented in Fig. 11-5, where it can be seen that the general decrease of the ordinates with increasing  $n$  has disappeared and that the periodic character, especially for the higher values of  $n$ , is still

FIG. 11-5. Ordinates of Fig. 11-4 multiplied by  $n^{1/2}(n + 1)^{1/2}$ .

more marked than in Fig. 11-4; the three waves in Fig. 11-5 are almost equidistant. Both curves have a remarkably regular character. Before analyzing them further we shall first discuss the meaning of the multiplication of the ordinates of Fig. 11-4 by  $n^{1/2}(n + 1)^{1/2}$  by means of which we obtained the curve of Fig. 11-5. The operation is based on the fact, expressed in Formula (11-32), that many spherical problems, for which the distribution over the sphere of radius  $\rho$  is given by a spherical harmonic  $Y_n$ , can, for large  $\rho$ , merge into plane problems, for which the distribution is given by the plane harmonic function  $K$ , given by

$$\nabla^2 K + f^2 K = 0 \quad (11-6)$$

$$\text{if} \quad f^2 = \frac{n(n + 1)}{\rho^2} \quad (11-32)$$

For  $f^2$  we can write

$$f^2 = l^2 + m^2 = \frac{\pi^2}{L_x^2} + \frac{\pi^2}{L_y^2} \quad (11-52)$$

where  $L_x$  and  $L_y$  are the half wavelengths, in the  $x$  and  $y$  directions, of the plane harmonic function  $K$ .

Since multiplication of the ordinates of Fig. 11-4 by  $n^{\frac{1}{2}}(n + 1)^{\frac{1}{2}}$  has the effect of dividing each of them by the horizontal dimensions of the harmonic distribution over the earth corresponding to the given ordinate, we come to the conclusion that the second and third waves of our development, which are (Fig. 11-4) nearly the same size as the first wave, correspond to topographic features with elevations roughly proportional to their horizontal dimensions. To obtain a rough idea of these dimensions we may combine (11-32) with (11-52), put  $L_x = L_y = L$ , and thus obtain

$$L = \frac{\pi\sqrt{2}}{f} = \frac{\pi R\sqrt{2}}{n^{\frac{1}{2}}(n + 1)^{\frac{1}{2}}} = \frac{28.400}{n^{\frac{1}{2}}(n + 1)^{\frac{1}{2}}} \text{ km} \quad (11-53a)$$

which, for the three waves of Fig. 11-4, gives

$$\begin{aligned} n &= 4\frac{1}{2} & L &= 5700 \text{ km} \\ n &= 9\frac{1}{2} & L &= 2800 \text{ km} \\ n &= 14\frac{1}{2} & L &= 1900 \text{ km} \end{aligned} \quad (11-53b)$$

The first wave is evidently of continental dimensions. Figure 11-4 shows that, besides these three waves and the general decrease of the ordinates for higher orders connected with the rough proportionality of vertical and horizontal dimensions of the great topographic features, there is a large 1st-order term. It obviously corresponds to the well-known fact that in one hemisphere land abounds and in the other sea. The fact that the term does not appear in Fig. 11-5 indicates that its elevation is not proportional to the dimensions in the same ratio as the other waves. Since the land hemisphere does not have the same topographic character as the continents —it is split up into widely separated blocks—such a result might have been anticipated.

In the following sections, where we attempt an interpretation of our findings, we shall see that the hypothesis of convection currents in the earth can probably provide a satisfactory explanation, at least for the most part. We can point out here that the most prominent spherical harmonics of the first large waves are the 3rd- and 4th-order terms and that they constitute just those terms which are the most likely to dominate in the distribution of convection currents in the mantle. The fact that the second and third waves have respective horizontal dimensions of about one-half and one-third those of the mantle currents is clearly in harmony with our hypothesis because we can expect smaller current systems in the mantle to break the mantle up into two, three, or more separate layers of cells. Finally, we can point out that for currents in the entire globe the 1st-order term is the preferred mode. The presence of such a term in the earth's topography seems to indicate that currents of that type have also occurred

in the earth. If this is true, it is likely that they took place in the first phase of the earth's history.

In the next section we start by dealing with a question which has first to be settled: can we indeed expect current systems in the earth to have swept together the sialic surface layer in blocks distributed according to the same spherical harmonic function  $Y_n$  that determined the current distribution?

### 11-7. First-order Term of the Topography; Origin of the Core and of an Ur Continent

Before discussing the 1st-order term of the development in spherical harmonics, we take up the question just raised of whether subcrustal current systems (as dealt with in Secs. 11-4 and 11-5) in which the vertical-velocity component  $v_\rho$  is distributed according to a spherical harmonic  $Y_n$  can be expected to leave lighter sialic matter behind at the surface in blocks also distributed according to  $Y_n$ . In Formula (11-27) we have assumed  $v_\rho = w_0 Y_n$ , in which  $w_0$  is a function only of  $\rho$  and is assumed to vanish at the surface.

According to our assumption of incompressibility, we know that the convergence of the horizontal-velocity component—which in  $xy$  coordinates would be given by  $-\partial u / \partial x - \partial v / \partial y$ —equals  $\partial v_\rho / \partial \rho = (\partial w_0 / \partial \rho) Y_n$ . If we suppose that no lighter matter is carried downward, the amount of sial left behind per unit of time would everywhere be proportional to this quantity and therefore to  $Y_n$ ; but since it remains floating on the current, it must have a tendency to be carried along with it. The result must be that the sial is pushed together until the effect of gravity prevents further piling up, and we must therefore expect it to be more or less concentrated over the central areas of the descending columns. So, in developing the distribution of sial in spherical harmonics, it is evident that the term  $Y_n$  must be strongly present, but higher-order terms representing the deviations from  $Y_n$  must also be expected.

As mentioned in Sec. 11-6, we may explain the 1st-order term of the earth's topography by assuming a 1st-order current system in an early phase of the earth's history. In doing so we must suppose that the earth was homogeneous at that time, or such a system would be extremely unlikely. We have seen (Sec. 11-5) that, if the earth was homogeneous, a current of the 1st order, as shown in Fig. 11-1 and 2, is by far the most probable. Thus the origin of the 1st-order term of the topography is pushed back to the beginning of the earth's history, before the core had formed, practically excluding the possibility that the distribution of the current system also contained the series of terms of the 3rd up to the 6th order, which, as we saw, correspond to a current system in the mantle. We can therefore safely conclude that the current system in the mantle (to be dealt

with in the next section) came into being at a later period. We can assume that the 1st-order system brought about not only the formation of the 1st-order term of the sial distribution but also the core; while the current was passing through the center, it must have left the heavier constituents behind when it was rising against gravity. We must obtain a welcome explanation of how it was possible that the nickel-iron core, during the 4 to 5 billion years of the earth's existence, was differentiated from the mantle constituents. As is well known, many geophysicists and physicists, e.g., Kuhn and Rittmann,<sup>14</sup> have expressed serious doubts about the possibility of such a differentiation in that length of time, and without a current system of the type suggested, their opinion would no doubt be valid. In this connection it is worthwhile mentioning that the core has a diameter of 54.5 per cent of the earth's diameter while Fig. 11-1 and 2), the current through the center has a larger diameter, *viz.*, 62.5 per cent. It seems probable, however, that during the later part of the core formation the current gradually assumed a 2nd-order, or perhaps even a 3rd-order, spherical-harmonic character; the core development itself must clearly have brought the 1st-order term in the current to an end.

Acceptance of the hypothesis of a 1st-order current system in the beginning of the earth's history leads to the question whether such an asymmetrical phenomenon could have originated by itself. This is not impossible; at that early time the earth's interior might have behaved like a Newtonian fluid without any elastic limit, and then cooling might have led to the current system without any appreciable trigger effect. If conditions were different, however, a 1st-order phenomenon for starting the current has to be assumed; an obvious answer is some effect of the moon, which, during its early history, is believed to have been close to the earth. If, according to Berlage's<sup>2</sup> theory, the earth had a second moon that fell onto the earth, the great disturbance and the higher temperatures in the impact area might well have started the 1st-order current system. Either possibility might also be the sole cause of the sialic ur continent, but the author (V. M.) is not inclined to take this view; we require an explanation of the origin not only of the sial but also of the core. According to Berlage, the second moon could not have had enough mass to provide all the sial.

If we assume that the origin was a 1st-order current system for which the distribution  $K_1$  had the simple form  $K_1 = \cos \psi$ , it is interesting to note that—in view of the present area of the sial, one-third of the earth's surface, and neglecting any change in size of that area (which clearly is possible)—we come to the conclusion that the current compressed the sial area to two-thirds that of the descending column, which occupied half of the sphere. If it was circular, its geocentric angular radius would thus be equal to  $\arccos \frac{1}{3} = 70^\circ 53$ . The border probably showed, however, some irregularities corresponding to 2nd- and perhaps 3rd-order current terms.

The undeformed elevation at an arbitrary point of a sialic shield distributed according to a 1st-order harmonic is given by  $a \cos \vartheta$ , where  $a$  is the elevation at the center and  $\vartheta$  the geocentric angular distance from the arbitrary point to the center. At the border of the compressed sial area, where  $\vartheta = \arccos \frac{1}{3}$ , the undeformed elevation would therefore be  $a/3$ , the elevations being taken with respect to the free ultrabasic surface.

Since we found the depth of the ultrabasic surface, covered only by sea water, to be 6800 m below sea level (Sec. 2-1), the depth of the free ultrabasic surface would be  $6800(3.27 - 1.028)/3.27 = 4660$  m below sea level; and since Prey's figures for the 1st-order term give a value of 1820 m above sea level, we obtain a value for  $a$  of about 6480 m and for  $a/3$  of about 2160 m. This would still be about 2500 m below sea level, and so we have to suppose that compression has increased the border thickness to about twice its original value, to bring the border up to sea level in the present conditions. This supposition appears acceptable. We must emphasize the uncertainties of these figures, as many changes may have occurred.

The value 1820 m of the maximum elevation of the present 1st-order term is in good agreement with the mean elevation of the different continents, which over the whole earth is 850 m. Here again we must be careful not to attach too much importance to this agreement; we have mentioned elsewhere that the elevations of the continents above sea level may depend on melting temperatures of the sial at their lower boundaries, and if they do, the elevations would have no relation to the elevation of the ur continent.

#### 11-8. Waves of 2nd- to 7th-, 8th- to 11th-, and 12th- to 16th-order Terms of the Topography; Origin of Continents and Oceans

The regular trend of each group of these terms points to a common physical origin. As we have already mentioned, the theory of subcrustal currents is in close harmony with the facts; for the first group we assume currents through the whole mantle; for the second, in the upper half; and for the last, in the upper third.

The indications for the first group are particularly strong. In Sec. 11-4 we saw that in mantle currents we can expect the 3rd- and 4th-order terms to dominate in the distribution over the sphere, which is exactly what Fig. 11-4 shows. We can pursue the comparison still further. If for the orders 1 to 7 we take the inverse values of  $\lambda_m$  and  $\lambda'_m$  given in Table 11-1, we see that they show a striking correlation with the values of column 7 in Table 11-3 represented in Fig. 11-4. In this figure the dashed curve gives the mean values of  $2700/\lambda_m$  and  $3050/\lambda'_m$  (these two quotients are nearly identical), and, with the exception of the first term, it is very close to the main curve. For  $n = 1$  the major part of the ordinate is due to the current of the first convection stage dealt with in the last section, and only a small

part is due to the mantle current discussed here. As we have mentioned, during the first convection stage probably 2nd-order (and perhaps even 3rd-order) currents also occurred, which may explain the smaller deviations in those ordinates (see also Vening Meinesz,<sup>22</sup> p. 543). As a whole, the agreement of the first seven terms with the curve of Fig. 11-4 is such that it can be considered convincing proof of our hypothesis that convection currents in the earth caused the irregularities in the thickness of the sialic layer and thereby the earth's main topographic lines. The fact that the reciprocal values of the figures for Jeffreys's quantity  $\lambda_m$  for the currents are found to be so nearly proportional to the terms of the spherical harmonic development of the crustal thickness, though not surprising, still lacks a complete explanation (Vening Meinesz,<sup>22</sup> p. 546). The problem is complicated by the fact that the earth is probably subject not to steady convection but to half-turn convection and that there is a density-transition layer between 200 and 900 km depth.

The main effect of the second convection stage in the earth has no doubt been the dividing of the ur continent into the present continents and the development of a belt of narrower oceans—the Atlantic and Indian Oceans and the Arctic Sea—over the rising currents (by oceans and seas we here mean the basins formed by the solid crust). The relative westward movement of North and South America thus formed the Atlantic, and relative southward and southeastward movements of the Antarctic continent and Australia, respectively, formed the Indian Ocean. It has long since drawn the attention of many geologists and geophysicists that the west and east coasts of the Atlantic show a striking similarity, as do some other coasts. The resulting supposition that they may once have been in contact with each other has, for example, been the main basis for Wegener's theory of the migration of continents, by which the present status developed from one ur continent. According to our views, the coastal analogies are much older and date from the second convection stage in the earth. They thus suggest that enough time must have elapsed after the first stage for the sialic ur continent to become more or less rigid, because otherwise the shapes could not have lasted until the present time.

Two reasons for this time interval can be given. In the first place, the outer mantle layer had to become cool enough to cause sufficient instability for the start of the second convection stage; in the second place, a trigger effect was required, which doubtless was the higher temperature below the ur continent caused by the greater radioactivity of the sial. The higher temperature must have led to rising currents below the continent, which caused it to be torn apart. Both temperature gradients must have taken time to develop.

The question arises of why the ocean floor did not also become rigid during this time, thus preventing the sialic parts of the ur continent from

floating apart at the time of the second convection stage. The explanation is probably that the ocean floor was not yet covered by a layer of lighter matter and that therefore the rigid floes at the surface caused by the cooling had greater density than the matter below and subsided. Hence the surface must have remained sufficiently plastic to take part in the current system and to allow the sialic parts to be carried along by the flow and to be left behind above the descending currents.

The fact that great parts of the continental coasts show similarities makes it probable that the major lines of continental shapes date from the time of the second convection stage. Since, however, the shapes include spherical harmonic terms not only of the 2nd to 7th but also of higher order, it is safe to conclude that the current systems also comprised systems of smaller dimensions. This is a further indication that the two higher-order groups of terms dealt with in this section are indeed also connected with currents in the mantle.

This result is not surprising. The cooling of the outer half of the mantle required for the great current system must have been the result of smaller systems of currents, probably started with the smallest mode possible at a period when the cooling of the earth, caused by radiation, had proceeded to a sufficient depth; a trigger effect undoubtedly took place, probably also caused by differences in radioactivity at the surface. Gradually convection currents must have developed, increasing in size until they assumed thicknesses of one-third and one-half, respectively, of the mantle, corresponding to the two groups of terms, and the process must have prepared the way for the large current system which brought the whole mantle into movement.

As Birch<sup>4</sup> has pointed out, to accomplish this result radiation and temperature conduction acting alone would have had to continue for more than 1 billion years, and in view of the time interval of a few hundred million years between the great orogenetic periods of the earth, such a length of time obviously does not agree with the facts; it is especially unlikely for the second convection stage, which must have occurred at a time when the ocean floors were still plastic. Therefore, the smaller convection systems must have been present before the large system and doubtless continued along with it.

It is interesting to note that the two largest oceans originating during the second convection stage both have a large submarine ridge in the middle, the Mid-Atlantic and the Mid-Indian Ocean Ridges. It is not known whether they contain sial. If so, they might have been caused by a thin sial floe remaining present above the central part of the rising current at the point where the horizontal velocity at the surface vanishes. A more probable cause, however, is a possibility discussed in the next section.

### 11-9. Early History of the Earth; Large Geosynclines; Crustal Shear Pattern

In the preceding two sections we came to some conclusions about the earliest history of the earth and its crust. We shall now make an attempt at continuing that history.

It is likely that during the period after the second convection stage, when the olivine crust between the continental shields gradually solidified, basaltic magma came to the surface and formed a layer on top of the olivine. Crystallization of olivine leaves a basaltic melt (Bowen,<sup>6</sup> pp. 315-320), which is still fluid, and since it is lighter, it must have reached the surface, at least in part, thus forming the thin basaltic layer 3 to 6 km thick found in the deeper ocean basins. The depth in the deepest parts of these basins of more than 6000 m points to the layer's being still thinner or perhaps even absent. Under the continents the basalt must have been added to the continental crust, which is assumed to consist of basalt in its lowest part.

In the ocean areas the basaltic layer must have promoted the consolidation of the crust. It is probably safe to assume that during the third great convection stage of the earth, which also must have been prepared for by cooling and by smaller current systems, the crust under the oceans was already rigid enough to prevent great translations of sialic blocks. The preparation process must have been characterized not only by smaller convection systems at the surface of the mantle but also, as pointed out to the author (V. M.) by his colleague E. F. M. van der Held, by similar current systems in the lowest layer of the mantle, where the second convection system must have left a large temperature difference with respect to the surface layer of the core. Here also the dimensions of the currents must gradually have increased until, eventually, the upper and lower current systems approached each other sufficiently in the central mantle layer (which up to that time must have been stable) to break through and establish a current system in the whole mantle.

Whether such current systems in the lowest mantle layer had occurred before, during the preparation of the second convection stage, may be left undecided; the answer depends on whether the first convection stage left behind sufficiently large temperature differences between the core and the inner boundary layer of the mantle.

Because of the great radioactivity of the sial, the third stage (and, we may add, all later great convection stages of the earth's history) must again have been characterized by rising currents under the continents flowing off toward adjacent oceans or seas. Their effect on the crust, however, must now have been limited mainly to the formation of geosyncline belts, in which the crust was pushed together. From the beginning, the crustal shortening in the belts was probably not more than a few hundred kilo-

meters. The two major geosyncline belts may have originated previously during the earliest stages. The circumPacific belt was probably initiated by lateral compression of the ur continent in the period of its formation, and the development of the great *Thețys* geosyncline may well have been determined by the second convection stage, during which the ur continent was drawn apart. The Asiatic part of this geosyncline corresponds to the compression above the descending current around the ascending current under the Indian Ocean. In view of the enormous thickening of the crust in southern and central Asia, we can safely assume that this part of the geosyncline has been particularly active. Its western continuation in the Mediterranean belt has no doubt also been the seat of great tectonic activity.

The smaller currents preparing for the great convection stages probably were often located in belts bordering the continental sial shields, under which the horizontal temperature gradient caused by the difference in radioactivity of the sial and the adjacent oceanic rocks must have been large. As we shall see in the next section, the smaller currents may often have been connected with geosyncline phenomena, thus leading to deep basins in island-arc areas.

It appears possible that the Mid-Atlantic and Mid-Indian Ocean Ridges were likewise formed by smaller convection systems working throughout the preparation of the third great convection stage, when the crust under the oceans was not yet strong but already was covered by a basaltic layer, which was concentrated in a thicker belt by the pushing together of the crust. We need not emphasize the hypothetical character of this supposition.

From the considerations of this and the preceding sections it follows that at least the first great mantle current systems in the beginning of the earth's history were world-wide; we can hardly doubt that the splitting up of the ur continent occurred in the same convection period. According to the equations given in Secs. 11-4 and 11-5, convection in a fluid spherical shell without limit of elasticity must involve the whole shell. At the present time, however, many data indicate that there is a limit of elasticity in the mantle, though a small one. That it must affect the distribution of a convection-current system follows from the fact that, according to Formulas (11-43), the stresses caused by such a current system depend not only on a spherical harmonic function  $Y_n$  but also on derivates of  $Y_n$  with respect to the coordinates  $\vartheta$  and  $\lambda$ . As a result, if the stress difference increases, the limit of elasticity must first be surpassed in some areas and directions, and this fact obviously continues to affect the current distribution; it is likely that in other areas and directions the limit is never reached. Under these conditions a convection system in a spherical shell is not complete, and for

higher-order spherical-harmonic distribution it may not even be world-wide. Therefore, although the tendency must have been toward world-wide orogeny in a certain period of revolution, the activity may have been only regional. Because of the fairly irregular way in which the continents are distributed, and because of the elapsed time between the first and second convection stages, we can assume that in the first part of the earth's history a limit of elasticity already existed in the mantle. It is difficult to say, however, whether the limit has increased or remained stable since that time.

After the crust had become a more or less rigid whole, the limit of elasticity must have had an important consequence which led to still another crustal phenomenon. We can prove that when a convection system in a spherical shell is complete, it does not exert a moment of force on a rigid crustal shell floating on it, but when it is not complete, as must have been true for the earth, the moment generally is not zero, and the crust must have been subjected to relative rotations with regard to the earth's interior. If the earth's surface were spherical, and if irregular frictional effects can be neglected, such a relative movement would not bring about crustal deformation; but the earth is flattened, and for that reason stresses are caused by the change in direction of the axis of flattening of the crustal shell. When we study this problem in the next chapter, we find that for continued movement we can expect shear in the crust in a world-wide pattern. There is a good deal of evidence that in the beginning of the earth's history such a phenomenon indeed took place. It is clear that these crustal rotations must have been accompanied by movements of the crust with respect to the pole, determined by the condition that the total moment of momentum of crust and earth's interior together must have remained constant. Every orogenic revolution stage in the earth must have been accompanied by such crustal rotations and polar movements, and the latter indeed have been indicated by the study of the magnetization of rocks dating from different periods. Assuming that the first crustal shearing phenomenon divided the crust into a number of blocks and that the belts between have remained zones of weakness, we can suppose, in general, that later polar movements caused the crustal shell to adapt to the new axis of flattening by relative movement of blocks. Probably no development of new zones of shear occurred, though exceptions appear possible.

In the same way it seems unlikely that the slow decrease of the flattening caused by the slowing down by tidal friction of the earth's rotation has ever subjected the crust to a new shear pattern. No doubt the extremely slow adaptation of the crustal shell to the diminished flattening also could have been achieved by readjustment of the relative positions of the crustal blocks.

### 11-10. Deep Basins in Island-arc Areas; Deep and Intermediate Earthquakes

As is well known, most geologists consider it likely that the deep basins in the eastern half of the Indonesian Archipelago, i.e., the southern and northern Banda Basins and the Celebes Sea, have recently subsided. Whereas the last great folding activity in the surrounding tectonic arc probably occurred about 20 million years ago, this subsidence is not older than about 5 million years and may even have taken place 1 or 2 million years ago. Similar views are held for the Caribbean Sea, the Gulf of Mexico, and, according to Kuenen, for the Mediterranean north and northwest of Corsica.

In keeping with the point of view expressed in this chapter, we can probably attribute the subsidence to convection currents of small dimensions preparing the way for the larger systems discussed before and suppose that the trigger effect for releasing the energy built up by cooling was provided by the horizontal temperature gradient that resulted from the concentration of sial in the tectonic arc during the last folding period.

By estimating the radioactive effects of the excess of sial we find a time of about 15 to 20 million years needed to raise the temperature around the sialic root by 80 to 100°. As the corresponding thermal expansion raises the surface by about 100 m, the resulting stress differences are of the order

of  $1.2 \times 10^7$  dynes/cm<sup>2</sup>, which appears sufficient for starting the current (Vening Meinesz,<sup>21</sup> pp. 41-45).

In the Banda arc, the horizontal dimension  $L$  is given by the radius of the arc of about 300 to 350 km, which, according to (11-53a), corresponds to a value of the order  $n$  of a spherical-harmonic development of about 43. When the formulas of Sec. 11-4 are followed, the horizontal dimensions lead to a current-layer thickness of about 240 km. This figure, however, is based on a downward temperature gradient  $\beta$  constant over the whole height, which probably does not hold true; the gradient kind given by  $\beta = \beta_0 e^{-mz}$  °C/km, in

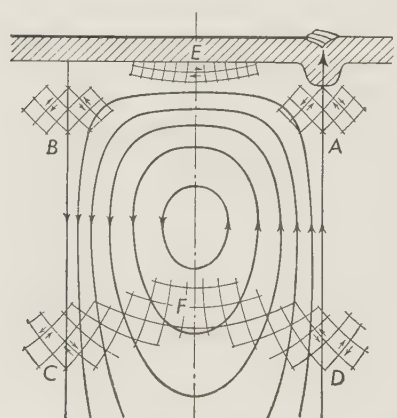


FIG. 11-6. Vertical cross section of convection current showing areas of maximum shear stress.

is more likely to obey a law of the form  $\beta = \beta_0 e^{-mz}$  °C/km, in which  $\beta_0$  is a constant, e.g., 10. Thanks to a method indicated by J. G. van de Corput, the equation of motion (11-33a) can also be solved for this case, and the results thus obtained (Vening Meinesz,<sup>21</sup> pp. 46-54)

are represented by Fig. 11-6. We see that the current now reaches much deeper. For our dimensions considerable stresses are found for depths over 500 km, and the current reaches deeper down still.

According to Sec. 11-2, therefore, we can assume that the current breaks into the density-transition layer at 200 to 900 km depth and that the subsiding column thus leads to an upward shift of this layer. Since the shift in the column must cause an increase in the denser modification of the olivine of the mantle, the surface must subside. Thus we can satisfactorily explain both the development of the deep basin and the time lag of the order of 15 to 20 million years following the last great tectonic activity in the arc around the basin. Because temperature changes in the subsiding column must be extremely slow, we can likewise understand why the basin persists for a long time after its formation. As the density difference of the two modifications of olivine must be 0.7, a subsidence of the basin of 5 km must correspond to an upward shift of the transition layer of  $5 \times 4.0/0.7 = 28.6$  km, which appears to be an acceptable value.

The rising current below the tectonic arc around the basin can be expected to cause a lowering of the transition layer there, which must be accompanied by a rising of the arc. Because the area of the arc is greater than that of the basin, we can assume that the amount of rising is smaller than the corresponding basin subsidence, which seems to agree to the facts; the arc has probably risen not more than a few thousand meters, possibly less.

It is difficult to predict gravity over the basin. The fact that the current columns probably have more or less maintained their isostatic equilibrium would not lead to large anomalies, though differences in depth of mass excesses and mass deficiencies may cause anomalies of some size. Since isostatic compensation for a basin bounded by faults and flexures is likely to have a local character, the map of local isostatic anomalies is best for our purpose. The anomalies of 30 to 40 mgal it shows over the Banda Basin are about the same as those found over the Java Sea, where no basins are present, and are therefore in harmony with our vague, tentative conclusion.

We may here briefly discuss the distribution of earthquake foci in the Indonesian Archipelago. Most of the normal foci are distributed over the tectonic and volcanic belts, the crustal deformations of which were discussed in Parts A and C of Chap. 10. The deep foci show some correlation with the deep basins discussed here. The mechanism in the center was determined for one of them by Koning<sup>13</sup> and for two others by Ritsema,<sup>17</sup> and in all three shear was found along a fault plane dipping down toward the Asiatic side. The relative movement of all three agrees with the rising of the tectonic belt with respect to the crust on the Asiatic side, which we know to be occurring at present because of the raised shorelines. We have attributed the rising to a renewal of the crustal compression and the formation of a short upward wave (see Part C of Chap. 10). In connection

with our present subject, it is worthwhile noticing that the deep and intermediate foci seem to coincide with the areas *C* and *A* in Fig. 11-6, which indicate the location of the maximum shear stresses, and that the direction of the relative movement for deep earthquakes checks with that determined by Koning and Ritsema. The sense of the relative movement for intermediate foci has not yet been determined.

From these results we can probably conclude that the stresses connected with the convection current play a part in the genesis of deep and intermediate earthquakes and more or less determine their location and depth, but since deep earthquakes also occur north of Java, where no basin has developed, the crustal deformation appears to be the main factor bringing the tilted fault plane into action. A closer study of deep and intermediate earthquakes and of the tilted fault planes connected with them can be found in the important work on these subjects by Benioff.<sup>1</sup>

Probably most deep basins in island-arc areas have been caused in the same way by small- or moderate-sized convection currents, which, no doubt, have usually resulted from trigger effects associated with horizontal temperature gradients connected with sial concentrations of tectonic origin. In this way these processes contribute to the development of deep basins in the great geosyncline belts and at the same time help prepare the conditions for the larger current systems discussed in this chapter.

#### REFERENCES

1. Benioff, H.: Orogenesis and deep crustal structure, additional evidence from seismology, *Bull. Geol. Soc. Amer.*, vol. 65, pp. 385-400, 1954.
2. Berlage, H. P.: Remarks on the origin of satellites in general and of the metamorphosis of the systems of Neptune and the earth in particular, *Proc. Koninkl. Ned. Akad. Wetensch., ser. B*, vol. 57, pp. 452-463, 1954.
3. Bernal, J. D.: *Observatory*, vol. 59, p. 268, 1936.
4. Birch, Francis: Remarks on the structure of the mantle, and its bearing upon the possibility of convection-currents, *Trans. Am. Geophys. Union*, vol. 32, pp. 533-534, 1951.
5. Boussinesq, J.: *Théorie analytique de la chaleur*, p. 172, 1903.
6. Bowen, N. L.: *The evolution of igneous rocks*, Princeton University Press, Princeton, N. J., 1928.
7. Elsasser, W. M.: The earth's interior and geomagnetism, *Rev. Modern Phys.*, vol. 22, pp. 1-35, 1950.
8. Griggs, D.: A theory of mountain building, *Am. J. Sci.*, vol. 237, pp. 611-650, 1939.
9. Gutenberg, B.: The cooling of the earth and the temperature in its interior, in B. Gutenberg (ed.), *Internal constitution of the earth*, 2nd ed., pp. 150-165, Dover, New York, 1951.
10. Heim, A.: *Geologie der Schweiz*, vol. 2, Tauchnitz, Leipzig, 1921.
- 10a. Honda, H., and A. Masatuka: On the mechanisms of the earthquakes and the stresses producing them in Japan and its vicinity, *Sci. Rep. Tōhoku Univ., ser. 5, Geophys.*, vol. 4, no. 1, 1952.

11. Jeffreys, H.: The earth, 2nd ed., Cambridge, London, 1929.
12. ———: *Ibid.*, 3rd ed., Cambridge, London, 1952.
13. Koning, L. P. G.: Over het mechanisme in den haard van diepe aardbevingen, Doctoral thesis, University of Amsterdam, Jacob van Kampen, Amsterdam, 1941.
- 13a. Kuenen, Ph. H., A. Faure-Murat, M. Lanteaume, and P. Fallot: Observations sur les Flyschs des Alpes Maritimes Françaises et Italiennes, Bull. soc. géol. France, 6me sér., T. VII, pp. 1-26, 1957.
14. Kuhn, W., and A. Rittmann: Ueber den Zustand des Erdinnern und seine Entstehung aus einem homogenen Urzustand, Geol. Rundschau, vol. 32, pp. 215-256, 1941.
15. Frey, A.: Darstellung der Höhen- und Tiefenverhältnisse der Erde durch eine Entwicklung nach Kugelfunktionen bis zur 16. Ordnung, Abhandl. Ges. Wiss. Göttingen, Math.-physik. Kl., N.F., vol. 11, no. 1, 1922.
16. Rayleigh, Lord J. W. Strutt: On convection currents in a horizontal layer of fluid, when the higher temperature is on the under side, Phil. Mag. (6), vol. 32, pp. 529ff, 1916.
17. Ritsema, A. R.: Over diepe aardbevingen in de indische archipel, Doctoral thesis, University of Utrecht, Wed. J. Ahrend en Zn, Rotterdam, 1952.
18. Runcorn, S. K.: The earth's core, Trans. Am. Geophys. Union, vol. 35, pp. 49-63, 1954.
19. Umbgrove, J. H. F.: Geological history of the East Indies, Bull. Am. Assoc. Petroleum Geol., vol. 22, pp. 1-70, 1938.
20. ———: The pulse of the earth, 2nd ed., Martinus Nijhoff, The Hague, 1947.
21. Vening Meinesz, F. A.: Gravity expeditions at sea, vol. 4, Publ. Neth. Geod. Comm., Delftsche Uitgevers Mij, Delft, 1948.
- 21a. ———: About mountain-formation on the earth, Proc. Koninkl. Ned. Akad. Wetensch., ser. B, vol. 51, no. 8, 1948.
22. ———: Convection-currents in the earth and the origin of the continents, Proc. Koninkl. Ned. Akad. Wetensch., ser. B, vol. 55, pp. 527-553, 1952.
23. ———: A remarkable feature of the earth's topography, origin of continents and oceans, *ibid.*, vol. 54, pp. 212-228, 1951.
24. ———: The origin of continents and oceans, Geol. en Mijnbouw, N.S., vol. 14, pp. 373-384, 1952.
25. ———: Correlation between geomagnetic field and tectonic movements?, Proc. Koninkl. Ned. Akad. Wetensch., ser. B, vol. 57, no. 3, 1954.
26. ———: A phase-transition layer between 200 and 900 km depth in the earth?, Proc. Koninkl. Ned. Akad. Wetensch., ser. B, vol. 59, no. 1, 1956.
27. ———: Instability in the earth's mantle because of the phase-transition-layer, Proc. Koninkl. Ned. Akad. Wetensch., ser. B, vol. 60, no. 5, 1957; second paper, *ibid.*, vol. 61, no. 1, 1958.

## CONVECTION CURRENTS IN A SPHERICAL SHELL

Formulas for  $w_0$  (vertical speed in the axis of the sinking column, positive downwards);  $D$  is an arbitrary constant having the dimensions of a speed.

$$\begin{aligned}
 n = 1; w_0/D &= 0.00002551020\rho^7 - 0.00011356957\rho^6 + 0.00015151515\rho^5 \\
 &\quad - 0.0001165762\rho^8 + 0.000068137 \ln \rho + 0.00002091826\rho^2 \\
 &\quad + 0.0000126878 + 0.0000193202\rho^{-1} + 0.00000019407\rho^{-5} \\
 n = 2; w_0/D &= 0.00010521886\rho^7 - 0.0005194806\rho^6 + 0.00108225108\rho^5 \\
 &\quad - 0.0009216342\rho^4 - 0.000016732\rho^{-1} + 0.0002647779\rho^3 \\
 &\quad + 0.00090351182\rho + 0.000002823423\rho^{-2} + 0.0000000125164\rho^{-4} \\
 n = 3; w_0/D &= 0.00037037037\rho^7 - 0.00292699724\rho^6 + 0.000811015\rho^5 \\
 &\quad + 0.0038961039\rho^5 \ln \rho - 0.0000037695\rho^{-2} + 0.001751144\rho^4 \\
 &\quad - 0.0000024478\rho^2 + 0.00000063216\rho^{-3} + 0.00000005435\rho^{-5} \\
 n = 4; w_0/D &= 0.0017482518\rho^7 + 0.012701516\rho^6 - 0.009539844\rho^6 \ln \rho \\
 &\quad - 0.0068870523\rho^5 \ln \rho - 0.00000107976\rho^{-3} - 0.01434443957\rho^5 \\
 &\quad - 0.00010444230\rho^3 + 0.0000017397\rho^{-4} + 0.00000002013\rho^{-6} \\
 n = 5; w_0/D &= -0.015447683\rho^7 + 0.005411255\rho^7 \ln \rho + 0.016211064\rho^6 \ln \rho \\
 &\quad + 0.0075757376\rho^5 - 0.00000033990\rho^{-4} + 0.00856562676\rho^6 \\
 &\quad - 0.00069342767\rho^4 + 0.000000057216\rho^{-5} + 0.000000006877\rho^{-7} \\
 n = 6; w_0/D &= -0.008974358\rho^7 \ln \rho - 0.0175619835\rho^6 \\
 &\quad + 0.00267005722\rho^5 \ln \rho + 0.001954262\rho^8 - 0.000000113192\rho^{-5} \\
 &\quad + 0.00899647661\rho^7 + 0.00661133482\rho^5 + 0.00000002133\rho^{-6} \\
 &\quad + 0.000000002244\rho^{-8} \\
 n = 7; w_0/D &= 0.009615385\rho^7 - 0.006164206\rho^6 \ln \rho - 0.00137741046\rho^5 \\
 &\quad + 0.00051393578\rho^9 - 0.000000039287\rho^{-6} - 0.0031893014\rho^8 \\
 &\quad - 0.0055625788\rho^6 + 0.000000008539\rho^{-7} + 0.0000000007073\rho^{-9}
 \end{aligned}$$

## CONVECTION CURRENTS IN THE WHOLE EARTH

Formulas for  $w_0$  (vertical speed in the axis of the sinking columns, positive downwards);  $D$  is an arbitrary constant having the dimensions of a speed.

$$\begin{aligned}
 n = 1, p = 1; w_0/D &= \frac{1}{18}[-0.005000\rho^5 + 0.001323\rho^6 + 0.022222\rho^3 \\
 &\quad - 0.028704\rho^2 + 0.010158] \\
 n = 1, p = 4; w_0/D &= \frac{1}{360}[-0.003788\rho^8 + 0.001764\rho^9 + 0.06482\rho^3 \\
 &\quad - 0.11063\rho^2 + 0.04784] \\
 n = 2, p = 2; w_0/D &= \frac{1}{8}[-0.002857\rho^6 + 0.000842\rho^7 + 0.009921\rho^4 \\
 &\quad - 0.010974\rho^3 + 0.003069\rho] \\
 n = 2, p = 5; w_0/D &= \frac{1}{22}[-0.000385\rho^9 + 0.000189\rho^{10} + 0.004444\rho^4 \\
 &\quad - 0.006656\rho^3 + 0.002407\rho] \\
 n = 3, p = 2; w_0/D &= \frac{1}{12}[-0.022727\rho^6 + 0.004444\rho^7 + 0.041667\rho^5 \\
 &\quad - 0.028860\rho^4 + 0.005476\rho^2] \\
 n = 3, p = 5; w_0/D &= \frac{1}{20}[-0.000928\rho^9 + 0.000427\rho^{10} + 0.006061\rho^5 \\
 &\quad - 0.007998\rho^4 + 0.002438\rho^2]
 \end{aligned}$$

## CHAPTER 12

### POLAR MIGRATIONS. SHEAR PATTERN OF THE EARTH'S CRUST

#### 12-1. Introduction; Formulas for Elastic Deformation of a Crustal Shell with Change in Axis of Flattening

The evidence in favor of migrations of the poles with respect to the earth's crust, caused by movements of the crust over the earth's interior, leads to the problem of how the rigid crustal shell adapted itself to a change in direction of the axis of flattening. Attention has long been called to a certain pattern existing in the topography and geology of the earth; the investigations of such *Lineamenttektoniker* as Daubrée,<sup>1</sup> Sederholm,<sup>3</sup> and Sonder<sup>4</sup> on this subject are well known. The question arises whether the pattern can perhaps be explained by this adaptation of the crust; we shall find that the answer is affirmative. The pattern points to a planetary phenomenon, and a study<sup>5</sup> by the author (V. M.) has shown that of two possible processes—a shift of the polar axis with respect to the crust and a decrease of the earth's flattening, both of which are presumed to have occurred—the first can indeed have caused a pattern which checks with observation. The polar shift must have caused the crust to split up into blocks, and it is likely that the second process, the slow decrease of the earth's flattening, has caused only a readjustment of the relative position of the blocks.

As we saw in Sec. 11-9, the breaking up of the crust into blocks probably happened in the beginning of the earth's history, and in this chapter we shall study the problems connected with the process (for a more detailed treatment we may again refer to the author's paper<sup>5</sup>).

The crust, which for the present purpose we suppose to be homogeneous, isotropic, and of uniform thickness  $T$ , is obviously too weak to interfere with the process whereby the earth keeps to its equilibrium figure after the axis of flattening has changed its position relative to the crust and also, therefore, slightly relative to the masses of the earth's interior; it can easily be proved that in this respect the moment of the stresses in a crustal cross section is negligible. We shall therefore assume that the normal stress in such a cross section is constant over its thickness, and we shall neglect the vertical component of the shear stress in the cross section.

During the polar shift, each part of the crust moves vertically over a distance which will be denoted by  $s_p$  and which can be derived from the amount of the shift and of the flattening  $\alpha$ . For the solution of our problem we can treat the crust as a thin spherical shell of radius  $R$ . Let  $\vartheta$  and  $\lambda$  be polar coordinates with respect to an axis through the earth's center perpendicular to the plane through the initial position  $MP'$  of the axis of rotation of the earth and its final position  $MP''$  (see Fig. 12-1),  $\vartheta$  being the angle between this axis and the radius vector of the crustal element considered, and  $\lambda$  being the angle between the plane through this radius vector and the axis and an arbitrary zero plane through the axis, for which we choose the plane through the axis of rotation of the earth in its final position  $MP''$ . Let  $\sigma_\vartheta$  and  $\sigma_\lambda$  be the normal components of the stresses working in cross sections of the crust corresponding to these coordinates and  $\sigma_p$  be the normal component of the stresses in planes parallel to the crust, all taken positive for compression; let  $\tau$  be the shear stress in the  $\vartheta$  and  $\lambda$  coordinate planes and parallel to the crust, taking the sign positive if, looking from the inside of the earth, we have a right-handed twist to a circular segment round the axis. (All stress components thus are opposite in sign to those in the paper<sup>5</sup> referred to above.) While we assume that  $\sigma_\vartheta$ ,  $\sigma_\lambda$ , and  $\tau$  are constant over the thickness  $T$ , we find that  $\sigma_p$  increases linearly with depth from a value of zero at the surface to a value of  $\sigma_r$  at the lower boundary of the crust.

For an elemental crustal prism  $ABCDA'B'C'D'$ , extending over the full thickness  $T$  of the crust (see Fig. 12-2) we obtain the following conditions of equilibrium:

$$(\sigma_\lambda - \sigma_\vartheta) \cos \vartheta - \frac{\partial \sigma_\vartheta}{\partial \vartheta} \sin \vartheta + \frac{\partial \tau}{\partial \lambda} = 0 \quad (12-1a)$$

$$\frac{\partial \sigma_\lambda}{\partial \lambda} - \frac{\partial \tau}{\partial \vartheta} \sin \vartheta - 2\tau \cos \vartheta = 0 \quad (12-1b)$$

$$\sigma_r = -(\sigma_\lambda + \sigma_\vartheta) \frac{T}{R} \quad (12-1c)$$

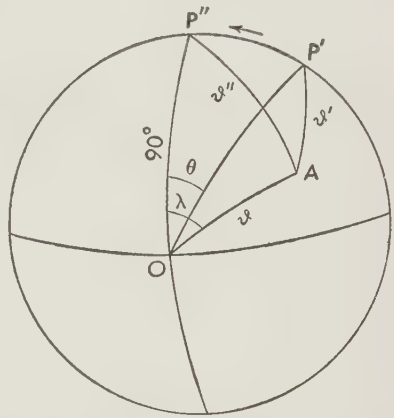


FIG. 12-1. Pole rotated counterclockwise over angle  $\theta$  from  $P'$  to  $P''$ . The angle  $\lambda$  is counted clockwise from  $OP''$ .

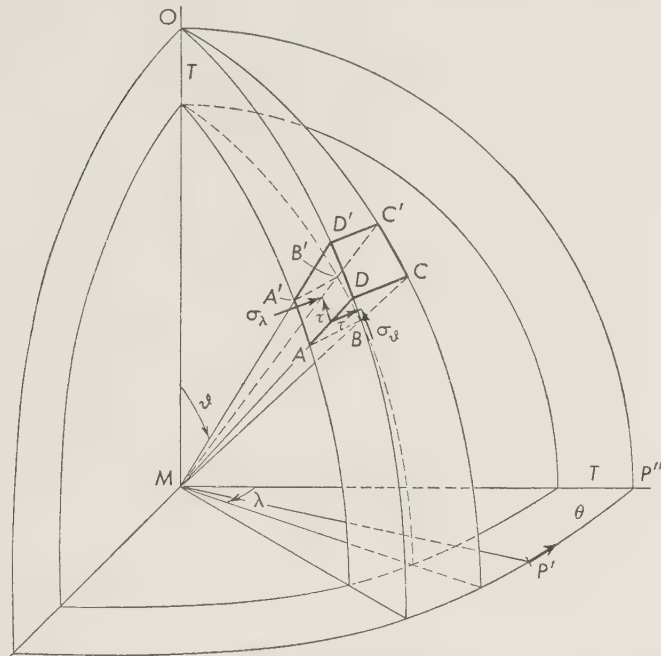


FIG. 12-2. Coordinate system for spherical crustal shell of the earth; axis  $OM$  perpendicular to initial position  $OP'$  and final position  $OP''$  of axis of daily rotation of the earth.

Applying the last formula to a crustal layer from the surface to a depth  $z$ , we find  $\sigma_\rho = -(\sigma_\lambda + \sigma_\theta)z/R$ , which confirms our statement that  $\sigma_\rho$  increases linearly with the depth  $z$ . We can also conclude that both  $\sigma_\tau$  and  $\sigma_\rho$  are of the order of less than 1 per cent of the stresses  $\sigma_\theta$  and  $\sigma_\lambda$ , and so we shall neglect them just as we did the flattening of the shell.

To express the relations between the stresses and the deformations we introduce the three components of the translation  $s$  in the direction of the three coordinates  $s_\rho$ ,  $s_\theta$ , and  $s_\lambda$  and also the two quantities determining the elastic deformation, the shear modulus  $\mu$  and Poisson's constant  $m$ . We obtain

$$-\sigma_\theta + \frac{1}{m} \sigma_\lambda = \frac{2(m+1)\mu}{mR} \left( \frac{\partial s_\theta}{\partial \vartheta} + s_\rho \right) \quad (12-2a)$$

$$-\sigma_\lambda + \frac{1}{m} \sigma_\theta = \frac{2(m+1)\mu}{mR} \left( s_\theta \cot \vartheta + \frac{\partial s_\lambda}{\partial \lambda} \csc \vartheta + s_\rho \right) \quad (12-2b)$$

$$\tau = \frac{\mu}{R} \left( \frac{\partial s_\theta}{\partial \lambda} \csc \vartheta + \frac{\partial s_\lambda}{\partial \vartheta} - s_\lambda \cot \vartheta \right) \quad (12-2c)$$

Formulas (12-1) and (12-2) determine the general solution for the stresses and the elastic deformation of a thin spherical shell. In our case the vertical component  $s_\rho$  is given, and to find the five unknown quantities  $\sigma_\vartheta$ ,  $\sigma_\lambda$ ,  $\tau$ ,  $s_\vartheta$ , and  $s_\lambda$  we use the five equations (12-1a), (12-1b), (12-2a), (12-2b), and (12-2c).

To the first order of flattening  $\alpha$  the radius vector of a rotation ellipsoid is given by  $R = \alpha R(\cos^2 \vartheta' - \frac{1}{3})$ , where  $\vartheta'$  is the geocentric colatitude. Assuming that the axis of rotation of the earth has migrated from  $P'$  (see Fig. 12-1) to a point  $P''$  at a distance  $\theta$  from the old position, it is simple to derive the difference  $s_\rho$  of the radii vectores in an arbitrary direction  $A$  (old and new colatitudes  $\vartheta'$  and  $\vartheta''$ , respectively) to the ellipsoids in the old and new positions. As we have chosen the axis of our spherical coordinate system at the intersection of the equator planes corresponding to the two positions, which is in fact the axis round which the crustal shell has rotated over the angle  $\theta$ , and as we reckon  $\lambda$  from the great circle through the pole in its final position  $P''$ , we obtain

$$s_\rho = \alpha R(\cos^2 \vartheta' - \cos^2 \vartheta'') = \alpha R \sin \theta \sin^2 \vartheta \sin(2\lambda - \theta) \quad (12-3a)$$

Introducing this into Eqs. (12-1) and (12-2), we can derive the following solution

$$\sigma_\vartheta = -\frac{2(m+1)}{5m+1} \alpha \mu \sin \theta (\sin^2 \vartheta + 2) \sin(2\lambda - \theta) \quad (12-3b)$$

$$\sigma_\lambda = -\frac{2(m+1)}{5m+1} \alpha \mu \sin \theta (3 \sin^2 \vartheta - 2) \sin(2\lambda - \theta) \quad (12-3c)$$

$$\tau = \frac{4(m+1)}{5m+1} \alpha \mu \sin \theta \cos \vartheta \cos(2\lambda - \theta) \quad (12-3d)$$

$$s_\vartheta = \frac{2(m+1)}{5m+1} \alpha R \sin \theta \sin \vartheta \cos \vartheta \sin(2\lambda - \theta) \quad (12-3e)$$

$$s_\lambda = \frac{2(m+1)}{5m+1} \alpha R \sin \theta \sin \vartheta \cos \vartheta \sin(2\lambda - \theta) \quad (12-3f)$$

We may note that the stresses and translations are dependent not on the thickness  $T$  of the crust but on the initial and final positions with respect to the crust of the polar axis, even though from  $P'$  to  $P''$  it may have described an irregular curve, with the restriction that during its migration it never before attained the critical distance  $\theta$  from its initial position. The complementary fact can be stated as follows: with the same restriction, the crust may have had an irregular movement in the opposite sense with

respect to the rotation axis, which, as far as these phenomena are concerned, must have remained stable in space.

Examining the equations obtained, we see that in two great circles through the origin  $O$ , given by  $\lambda = \frac{1}{2}\theta$  and  $\lambda = \frac{1}{2}\theta + 90^\circ$ , the stresses  $\sigma_\vartheta$  and  $\sigma_\lambda$  vanish, and so we have pure shear. According to (12-3d), the shear stress is maximum at the origin, where the two circles intersect at right angles, and amounts to

$$\tau_m = \frac{4(m+1)}{5m+1} \alpha\mu \sin \theta \quad (12-4)$$

Like the other stresses,  $\tau_m$  is maximum for  $\theta = 90^\circ$ , and the same is true for the translations. They diminish again for greater polar shift. For  $m = 4.1$  and  $\mu = 4 \times 10^{11}$  dynes/cm<sup>2</sup> and for the present flattening of 1/297, we find the maximum value of  $\tau$  to be  $1.28 \times 10^9$  dynes/cm<sup>2</sup>. Hence the stress is considerable and may well lead to the crust's giving way. As, however, the phenomenon must already have occurred at an early stage of the earth's history, we probably have to introduce a flattening at least twice as large. This leads to a value for  $\tau_m$  of about  $2.6 \times 10^9$  dynes/cm<sup>2</sup>, which is certainly more than the crust can stand.

For the two great circles through the origin which bisect the right angles between the previous pair and which, therefore, are given by  $\lambda = \frac{1}{2}\theta - 45^\circ$  and  $\lambda = \frac{1}{2}\theta + 45^\circ$ , Formula (12-3d) indicates that  $\tau$  vanishes and that the same is true for  $\vartheta = 90^\circ$ , viz., for the meridian through the initial and final positions of the pole. For this meridian we further see that everywhere  $\sigma_\vartheta = 3\sigma_\lambda$ . The maximum absolute values of  $\sigma_\vartheta$  are found at the intersections of this meridian with the two great circles; for the first there is maximum compression and for the second, maximum tension. For both, the absolute value is given by

$$\sigma_\vartheta = \frac{6(m+1)}{5m+1} \alpha\mu \sin \theta \quad (12-5)$$

which, for the above values of  $m$  and  $\mu$  and for  $\theta = 90^\circ$  and  $\alpha = 1/297$ , gives  $1.92 \times 10^{11}$  dynes/cm<sup>2</sup> and, for the early period, when the flattening was double the present value,  $3.8 \times 10^{11}$  dynes/cm<sup>2</sup>.

We come to the conclusion that a large shift of the poles—in the present period as in an early period—must lead to stresses that the crust cannot stand; if such a shift has occurred, it therefore must have caused permanent crustal deformations. A small polar movement, for which  $\sin \theta$  would be small, would not have had any effect.

## 12-2. Crustal Pattern Caused by Polar Migration

To derive the pattern of the permanent deformation caused by the crustal stresses dealt with in the last section we shall follow Bijlaard's

theory (briefly treated in Sec. 10A-7) of plastic deformation in a thin plate. As shown by Fig. 10A-14 and Formula (10A-48), the angle  $\psi$  between the cross section on which the largest of the principal stresses  $\rho_1$  and  $\rho_2$  works and the belt of permanent deformation is given by

$$\cos 2\psi = \frac{1}{3} \frac{\rho_1 + \rho_2}{\rho_1 - \rho_2}$$

Using Mohr's circle and Formulas (12-3), we can derive the angle  $\varphi$  between the direction of  $\rho_1$  at an arbitrary station  $A$  on the earth's surface and the great circle to the origin  $O$  from

$$\tan 2\varphi = \frac{2\tau}{\sigma_\vartheta - \sigma_\lambda} = - \frac{2 \cos \vartheta}{1 + \cos^2 \vartheta} \cot (2\lambda - \theta) \quad (12-6)$$

Mohr's circle further gives

$$\rho_1 = \frac{1}{2}(\sigma_\vartheta + \sigma_\lambda) + \frac{1}{2}(\sigma_\vartheta - \sigma_\lambda) \sec 2\varphi$$

$$\rho_2 = \frac{1}{2}(\sigma_\vartheta + \sigma_\lambda) - \frac{1}{2}(\sigma_\vartheta - \sigma_\lambda) \sec 2\varphi$$

We thus obtain  $\psi$  from

$$\cos 2\psi = \frac{1}{3} \frac{\sigma_\vartheta + \sigma_\lambda}{\sigma_\vartheta - \sigma_\lambda} \cos 2\varphi = \frac{2}{3} \frac{\sin^2 \vartheta}{1 + \cos^2 \vartheta} \cos 2\varphi \quad (12-7)$$

The two cross sections in which, according to Bijlaard's theory, plastic deformation can occur enclose angles of  $\varphi + \psi$  and  $\varphi - \psi$  with the great circle through the origin. Our formulas enable us to derive the angles for each station at the earth's surface. Figure 12-3 gives the result in stereographic projection for a hemisphere around the origin and bounded, therefore, by the meridian containing the initial and the final positions of the pole. For the second hemisphere the directions are identical. The figure has to be turned clockwise through an angle  $\frac{1}{2}\theta$  to bring the pole into its new position on top. As it is, the pole in its new position is  $\frac{1}{2}\theta$  to the left of  $A$  and in its initial position  $\frac{1}{2}\theta$  to the right.

In addition to finding for each point the two directions in which plastic deformation can be expected, it is also important to know where the elastic limit will be reached first. According to the discussion in Sec. 2-4, for this purpose we shall derive the Huber-Hencky stress  $\sigma_v$  given by Formula (2-11). Using (12-3), we obtain

$$\sigma_v = \frac{2(m+1)}{5m+1} \alpha \mu \sin \theta \sqrt{7 \sin^4 \vartheta \sin^2(2\lambda - \theta) + 12 \cos^2 \vartheta} \quad (12-8a)$$

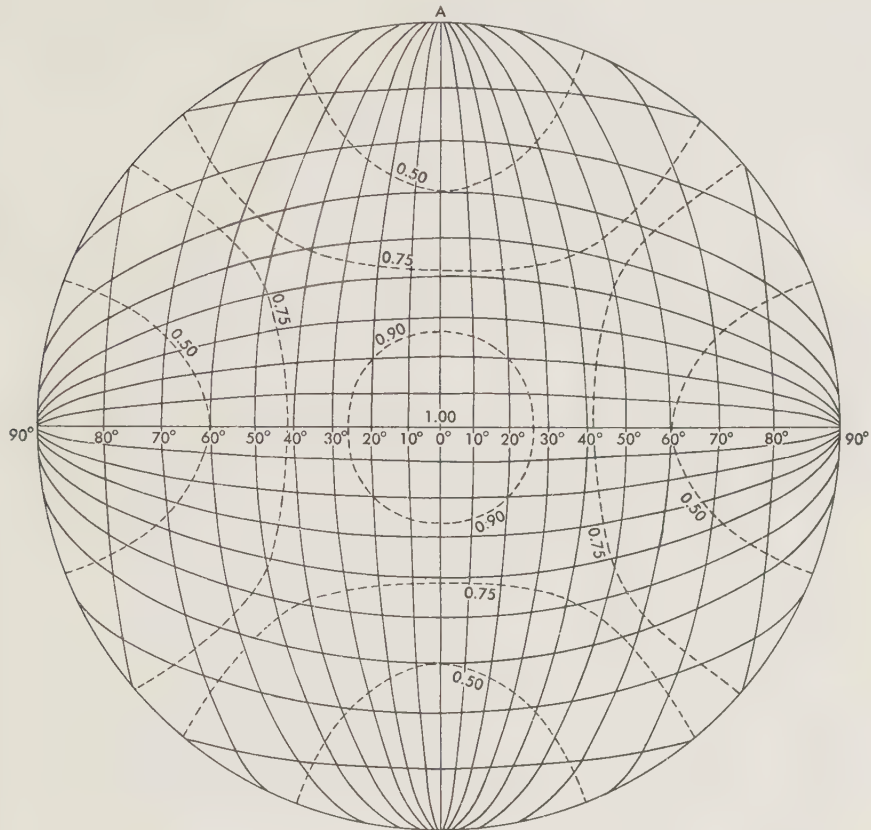


FIG. 12-3. Shear pattern in stereographic projection of the half sphere for infinitesimal shift of the poles; for shift over the angle  $\theta$  the figure has to be rotated clockwise over  $\theta/2$ . The dashed lines indicate the Huber-Hencky stress limit  $\sigma_v$ , divided by its maximum value  $\sigma_{vm}$ .

This function reaches a maximum value  $\sigma_{vm}$  at the origin. If we divide the function by this value, we get

$$\frac{\sigma_v}{\sigma_{vm}} = \sqrt{\frac{7}{12} \sin^4 \vartheta \sin^2 (2\lambda - \theta) + \cos^2 \vartheta} \quad (12-8b)$$

In Fig. 12-3 the broken-line curves represent values of this ratio of 90, 75, and 50 per cent. In the center it is 1.00, and at the ends of the horizontal and vertical diameters it is zero.

We further have

$$\sigma_v = \frac{4(m+1)\sqrt{3}}{5m+1} \alpha \mu \sin \theta \quad (12-8c)$$

which, for the values of  $m = 4.1$  and  $\mu = 4 \times 10^{11}$  dynes/cm<sup>2</sup> already introduced and for  $\theta = 90^\circ$ , give

$$\text{For } \alpha = 1/297 \quad \sigma_v = 2.22 \times 10^9 \text{ dynes/cm}^2$$

$$\text{For } \alpha = 2/297 \quad \sigma_v = 4.43 \times 10^9 \text{ dynes/cm}^2$$

These values confirm the views we have already expressed. Even for the present flattening the value of  $\sigma_v$  is above the elastic limit, and it is still more evidently so for double the value of the flattening, or more, which we must assume at the early period when we suppose the phenomenon to have happened.

From Fig. 12-3 we can obtain a clear view of the patterns of crustal deformation which a shift of the poles can cause in an unbroken crustal shell. Once the crust has been broken into blocks, we cannot expect it to have reacted to later migrations other than by a readjustment of the blocks.

### 12-3. The Pattern Present in the Earth's Crust; Polar-flight Forces Too Small to Have Been the Cause

The pattern present in the earth's crust is most clearly shown at the earth's surface in the topography, but other indications are given by geological patterns, fault patterns, seismic patterns, and gravity-anomaly fields. In studying the matter the author (V. M.) found that the pattern according to Fig. 12-3, of which the situation on the earth's surface could be adapted to the topographic pattern of the North Atlantic sea floor, thus practically fits the data from all sources over the whole earth's surface. This situation corresponds to a position of the origin  $O$  of the spherical coordinates on the present equator at  $0^\circ$  longitude, and a position of the top  $A$  which is in the middle between the initial and final positions of the pole, at  $55^\circ\text{N}$  and  $90^\circ\text{E}$ . As the pattern of Fig. 12-3 is symmetric with respect to the middle meridian and the equator, point  $A$  may also be placed at one of the positions  $35^\circ\text{S}$  and  $90^\circ\text{E}$ ,  $35^\circ\text{N}$  and  $90^\circ\text{W}$ , or  $55^\circ\text{S}$  and  $90^\circ\text{W}$ . When the shearing catastrophe occurred, the pole moved along an arbitrary path from an initial to a final position, both positions on the great circle formed by the meridians  $90^\circ\text{E}$  and  $90^\circ\text{W}$  and symmetrically situated with respect to one of these four points. Since recent data on the magnetization of rocks indicate that since that time the poles have probably moved, it appears a coincidence that at present the poles are again located on that great circle. If the poles have not moved since that time, the polar movement leading to the crustal catastrophe must have occurred from a position at  $20^\circ\text{N}$  and  $90^\circ\text{E}$  to the present position of the North Pole, i.e., over an arc of  $70^\circ$ . Though the path is arbitrary, we must obviously assume that

it has not passed through points at a greater distance from the initial position than the final position.

The pattern of the earth's crust originating in one of these ways is represented in Mercator's projection in Fig. 12-4. We shall not enlarge on the correlation of this net to topographic, geological, seismological and gravimetric features (see Vening Meinesz<sup>6</sup>), but one correlation merits examination here, viz., that of the continental borders with the net, e.g., the east coast of South America combined with the northwest coast of Africa and the east coast of Spain in one continuous deformation zone; the east coast of Africa and Arabia with the east side of the Pakistan mountain ranges in another such zone; the main parts of Australia's coasts; and the east coast of Asia. Probably the correlation can be explained by the hypothesis that, because of sedimentation, the border zones of the continents are zones of crustal weakness. If so, the crustal shearing catastrophe must have taken place at a stage of the polar shift when the shearing could follow the border zones for large distances.

The question arises of whether the polar shift could have been caused by the tendency of centrifugal forces to bring the continental shields toward the equator. The tendency results from the fact that the center of gravity of the continental sial blocks is higher than the center of gravity of the ultrabasic masses they displace, while the corresponding difference in height is much smaller for the oceanic crust. As is well known, this tendency has often been cited as a polar-flight tendency of the continents. We shall examine how much polar shift these forces can accomplish.

The energy of elastic deformation is, in general, given by the following formula

$$A = \frac{1}{4\mu} (\sigma_x^2 + \sigma_y^2 + \sigma_z^2) + \frac{1}{2\mu} (\tau_x^2 + \tau_y^2 + \tau_z^2) - \frac{1}{4(m+1)\mu} (\sigma_x + \sigma_y + \sigma_z)^2 \quad (12-9)$$

For our case it reduces to

$$A = \frac{1}{4\mu} (\sigma_\vartheta^2 + \sigma_\lambda^2 + 2\tau^2) - \frac{1}{4(m+1)\mu} (\sigma_\vartheta + \sigma_\lambda)^2 \quad (12-10)$$

Introducing (12-3) and integrating over the whole crust, we obtain

$$A = \frac{64(m+1)}{15(5m+1)} \pi \alpha^2 \mu T R^2 \sin^2 \theta \quad (12-11)$$

which agrees with the formula Kuiper<sup>2</sup> found for  $m = 3$  in his study of polar shifts caused by polar-flight forces. Differentiating this formula with respect to  $\theta$ , and neglecting the part needed for overcoming friction,

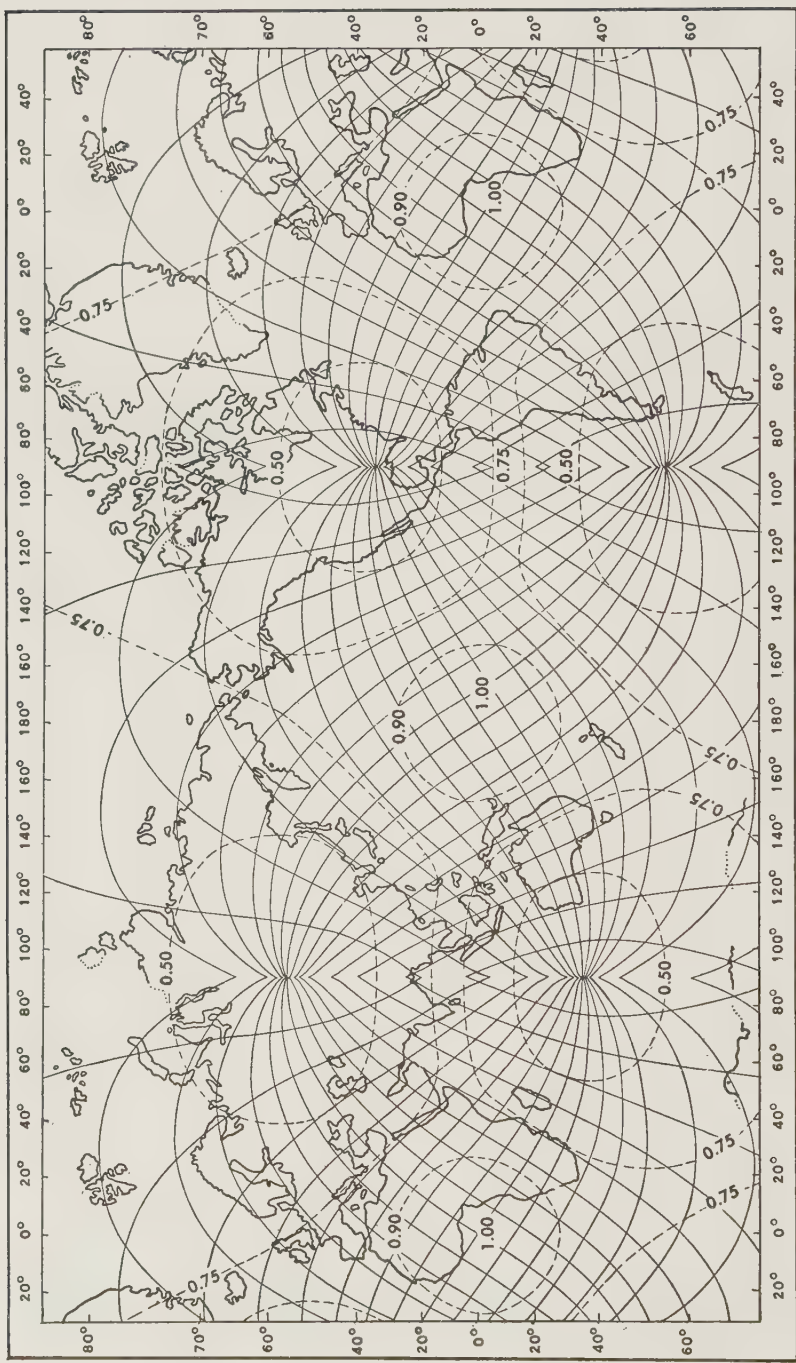


FIG. 12.4. Shear pattern in Mercator's projection for a shift of the poles over  $70^\circ$  along the meridian of  $90^\circ$  longitude; the dashed lines show the Huber-Hencky stress limit  $\sigma_v$  (zero at points where shear pattern concentrates), divided by its maximum value  $\sigma_{vm}$ .

for the moment of forces  $M$  around the axis through the origin  $O$  of our spherical coordinates required for the polar shift  $\theta$  we find

$$M = \frac{64(m+1)}{15(5m+1)} \pi \alpha^2 \mu T R^2 \sin 2\theta \quad (12-12a)$$

For  $m = 4.1$ ,  $\mu = 4 \times 10^{11}$  dynes/cm<sup>2</sup>,  $\alpha = 1/297$ ,  $T = 35$  km,  $R = 6371$  km we obtain

$$M = 2.05 \times 10^{31} \sin 2\theta \text{ dyne-cm} \quad (12-12b)$$

For twice the flattening we find four times as much.

For the present  $M_p$  of the polar-flight forces Kuiper<sup>2</sup> derived a value of about  $3 \times 10^{30}$  dyne-cm. We see that, if we neglect friction, these forces can bring about a polar shift over an angle  $\theta_p$  given by  $\sin 2\theta_p = 3/20.5$ , and so  $\theta_p = 4^\circ 12'$ , which corresponds to a critical stress  $\sigma_v$  of  $1.63 \times 10^8$  dynes/cm<sup>2</sup>. This is certainly insufficient to cause permanent deformation in the crust, and for the period when the flattening was twice as much the critical stress would have been about four times less. Thus we may conclude that the polar-flight forces are far too small to produce either the polar shifts required to give a pattern of permanent crustal deformation or those presumed on the basis of rock-magnetization data. We therefore come back to our original conclusion: the polar shifts believed to have occurred could not have taken place without currents in the mantle.

#### REFERENCES

1. Daubrée, A.: *Synthetische Studien zur Experimentalgeologie*, Brunswick, 1880.
2. Kuiper, H.: *Poolbewegingen tengevolge van poolvluchtkracht*, Doctoral thesis, University of Utrecht, N. Hollandsche Uitg. Mij, Amsterdam, 1943.
3. Sederholm, J. J.: *Weitere Mitteilungen über Bruchspalten und Geomorphologie*, Bull. comm. géol. Finlande, no. 37, 1913.
4. Sonder, R. A.: *Die Lineamenttektonik und ihre Probleme*, Eclogae Geol. Helv., vol. 31, pp. 199–238, 1938.
5. Vening Meinesz, F. A.: *Topography and gravity in the North Atlantic Ocean*, Proc. Koninkl. Ned. Akad. Wetensch., ser. B, vol. 45, no. 2, 1942.
6. ———: *Shear patterns of the earth's crust*, Trans. Am. Geophys. Union, vol. 28, pp. 1–61, 1947.



## NAME INDEX

- Aardolie Mij., Nederlandsche, 365  
Adams, J. C., 127  
Adams, L. H., 12, 221  
Airy, G. B., 126, 128, 129, 135, 145, 230,  
    290  
Anderson, E. M., 314, 352, 373, 390  
Anderson, Pamela, 297  
Aristotle, 225
- Baeyer, J. J., 228  
Baglietto, Eduardo E., 275, 294  
Baily, F., 155  
Ballarin, S., 168, 185  
Bancroft, D., 22  
Bauer, L. A., 28  
Bemmelen, R. W. van, 28, 373  
Benioff, H., 13, 23, 440  
Berlage, H. P., 431  
Bernal, J. D., 403  
Berroth, A., 75, 230  
Bessel, F. W., 228, 230  
Bijlaard, P. P., 20, 326, 350, 377, 447  
Birch, Francis, 9, 11, 12, 22, 170, 184, 403,  
    434  
Blanks, R. F., 354  
Boer, J. de, 25  
Bomford, G., 121, 234, 291–294  
Bonini, W. E., 123  
Bonsdorff, A., 230  
Bonsdorff, I., 129, 130, 145, 204, 220  
Bosecovich, R. J., 126, 145  
Bouguer, Pierre, 126, 145, 153, 184, 227,  
    228, 230, 294  
Boussinesq, J., 408  
Bowen, N. L., 435  
Bowie, William, 75, 78, 83, 131, 132, 137,  
    142, 145, 159, 162, 165, 166, 183, 184,  
    188, 220, 230, 249, 295  
Boys, C. V., 155
- Braun, K. F., 155  
Bridgman, P. W., 13, 23  
Brouwer, D., 29, 56  
Brouwer, H. A., 381  
Browne, B. C., 75, 97, 100, 116, 121  
Bruyn, J. W. de, 178, 184  
Bullard, E. C., 7, 28, 29, 56–58, 75, 164,  
    172, 185, 192, 220, 230, 295, 389, 390  
Bullen, K. E., 9–11, 25, 56, 57  
Burgess, G. K., 155  
Burrard, F. E., 290  
Byerly, P., 6  
Byrd, W. O., 305, 310
- Callandraeu, O., 40, 48  
Carlheim-Gyllensköld, 28  
Cassini, Jacques, 227  
Cassini, Jean D., 227  
Cassinis, G., 52, 74, 83, 132, 164, 166, 168,  
    183, 185  
Cavendish, Henry, 155  
Chamberlin, R. T., 314, 352  
Chovitz, B., 292, 295  
Chrzanowski, Peter, 155  
Cizancourt, H. de, 144, 145  
Clairaut, A. C., 50, 52, 56, 173  
Clarke, A. R., 229, 230, 234  
Clarkson, H. N., 122  
Clausen, Th., 56  
Collette, B. J., 242, 365  
Cooper, R. I. B., 172, 185  
Coron, Suzanne, 178, 185  
Corput, J. G. van de, 438  
Coulomb, C. A. de, 352, 353  
Crompton, W., 190, 220, 372
- Daly, Reginald A., 143, 145, 170, 214, 360,  
    366

- Darling, F. W., 9, 66, 136, 146, 174, 186, 255, 279, 284, 298  
 Darwin, G. H., 56, 57, 173, 360  
 da Vinci, Leonardo, 125, 126  
 Delambre, J. B. J., 230  
 Delaney, John P., 125, 126, 145  
 Deslandres, H. A., 128  
 Dobrin, Milton B., 121  
 Dore, P., 168, 185  
 Dutton, C. E., 130, 145
- Eggert, O., 296, 310  
 Eichinger, A., 354  
 Einstein, Albert, 128  
 Elsasser, W. M., 11, 12, 25–29, 403  
 Eötvös, R., 155  
 Eratosthenes, 226, 228  
 Erola, V., 172, 185, 203, 220  
 Eucken, A., 25  
 Evans, P., 171, 185, 190, 220, 372  
 Everest, G., 230, 234, 290  
 Ewing, Maurice, 7, 117, 170, 205, 210, 211, 219, 220, 298, 374, 385
- Field, R. H., 94  
 Fischer, Irene, 275, 276, 292, 295
- Gaskell, 211  
 Gauss, K. F., 228, 295  
 Gay, Malcolm W., 122  
 Glennie, E. A., 97, 182, 185  
 Goguel, J., 13, 18, 23, 353, 354  
 Gough, D. J., 178, 185, 203, 220, 295  
 Graaff Hunter, J. de, 73, 150, 185, 243–245, 249, 271, 290, 295, 298  
 Griggs, D., 13, 23, 24, 319  
 Gromov, S. V., 158, 185, 243, 295  
 Gulatee, B. L., 97, 122, 234, 295  
 Gutenberg, B., 6, 7, 13, 14, 21–25, 185, 205, 220, 366, 403
- Hafner, W., 352, 353, 390  
 Hale, G. E., 128  
 Hales, A. L., 156, 178, 185, 203, 220, 245, 295  
 Hall, James, 130  
 Haskell, N. A., 357
- Hayford, J. F., 52, 83, 129, 131, 132, 142, 145, 153, 159–166, 169, 175, 183, 185, 229, 230, 245, 255, 256, 295  
 Hecker, O., 97, 103, 122  
 Heiskanen, W. A., 52, 74, 75, 77–79, 83, 85, 94, 103, 122, 132, 135, 141, 143, 145, 150, 164, 166, 167, 169, 176–178, 181, 185, 188, 199, 203, 211, 220, 222, 223, 229–231, 234–237, 243, 245, 247, 249, 278, 288, 289, 292, 294, 295, 298, 299, 303, 307–310  
 Held, E. F. H. van der, 435  
 Helmert, F. R., 42, 56, 65, 75, 78, 79, 83, 129, 131, 145, 156, 166, 185, 186, 230, 243, 247, 252, 258, 279, 296, 303
- Hersey, 211  
 Hertz, 138  
 Hess, Harry, 205, 209, 220, 385, 386  
 Heyl, Paul R., 155  
 Hilbert, D., 128  
 Hill, M. N., 7  
 Hirvonen, R. A., 73, 86, 122, 241, 243, 247, 249, 271–273, 277, 282, 286–288, 296  
 Hodgson, 210  
 Holopainen, Paavo E., 193, 194, 199, 203, 220
- Homer, 225  
 Honkasalo, T., 121, 122, 262–264, 267, 273, 275, 298  
 Hough, Floyd W., 230  
 Hoyt, 205, 206  
 Hubbert, M. King, 314, 352–354, 390  
 Hughson, W. G., 189, 220  
 Huygens, C., 227, 228
- Innes, M. J. S., 121, 122  
 Ivanov, V. K., 230
- Jamieson, J., 130  
 Janssen, P. J. C., 128  
 Jeffreys, H., 6, 9, 12, 13, 20–22, 25, 75, 229–231, 243, 296  
 Jolly, P. von, 155  
 Jordan, W., 225, 296, 310  
 Jung, K., 296
- Kaarainen, E., 212, 213, 220, 365  
 Kasansky, I., 262, 267, 296

- Kater, Henry, 153  
 Katz, 210  
 Kaula, W. M., 273, 298  
 Kivioja, L., 177, 181, 186  
 Kladivo, B., 158, 186, 243, 296  
 Kobold, F., 150, 186  
 Koning, L. P. G., 378, 380, 439, 440  
 Korringa, J., 25  
 Kossmat, F., 220  
 Krassowski, F. N., 229, 230, 232, 234  
 Krigar-Menzel, O., 155  
 Kronig, R., 25  
 Kuennen, Ph. H., 7, 341  
 Kuhn, W., 25, 431  
 Kuiper, H., 450  
 Kukkamaki, T. J., 121, 183, 186, 212, 213,  
     220, 235, 296, 365  
 LaCoste, L. J. B., 109, 120, 122  
 Lambert, W. D., 9, 54, 66, 136, 146, 148,  
     158, 174, 186, 243, 249, 279, 284, 296  
 Laughton, L. S., 7  
 Ledersteger, K., 230–232, 292, 296  
 Lee, A. W., 6  
 Leet, L. D., 6, 210  
 Legendre, A. M., 296  
 Lehner, Mariette, 138, 145  
 Lejay, Pierre, 87, 97, 102, 122, 174, 186,  
     243, 245, 249  
 Leverrier, U. J. J., 127  
 Lidén, R., 366  
 Lockyer, J. N., 128
- Macelwane, J. B., 7  
 McHenry, 354  
 Markowitz, W., 235, 296  
 Maupertuis, P. L. M. de, 227, 228, 230, 296  
 Meijering, J. L., 407  
 Meissner, E. F. S., 22  
 Menard, H. W., 389  
 Michailov, A., 243, 296  
 Miller, A. H., 189, 220  
 Milne, 210  
 Miyabe, N., 386  
 Mohorovičić, 6, 205  
 Morelli, Carlo, 75, 85, 94, 121, 122, 123,  
     178, 186, 203, 220, 245, 297  
 Muller, J. J. A., 378  
 Munk, W., 29
- Nansen, F., 366  
 Nares, 232, 233, 297  
 Nederlandsche Aardolie My., 365  
 Newcomb, S., 25  
 Newton, Isaac, 227, 228  
 Niethammer, T. H., 132  
 Nieuwenkamp, W., 407  
 Niskanen, Erkki, 79, 83, 138, 145, 177,  
     181, 186, 214, 215, 220, 230, 249, 297,  
     357, 365, 367  
 Nørgaard, G., 107, 109  
 Nuotio, U., 169, 177  
 Nyboer, L. W., 354
- O'Keefe, J. A., 235, 297  
 Olander, V. R., 232–234, 298  
 Ors, Inglada, 132  
 Outhier, 227
- Pepper, T. B., 113, 122  
 Pesonen, U., 95, 96, 122  
 Picard, J., 226, 297  
 Pizetti, P., 297  
 Poincaré, H., 173  
 Poisson, D., 139, 153, 186  
 Poynting, J. H., 155  
 Pratt, J. H., 126, 127, 129, 131, 132, 145,  
     230, 290  
 Press, Frank, 210  
 Prey, A., 249, 297, 423, 424, 426  
 Putnam, G. R., 129, 142, 146, 245, 297  
 Pythagoras, 225
- Rainesalo, A., 162, 186  
 Raitt, R., 7, 211  
 Ramsey, W. H., 25  
 Rankine, W. J. M., 352  
 Rayleigh, Lord (J. W. Strutt), 407, 418  
 Read, H. H., 345  
 Reich, F., 155  
 Revelle, R., 29  
 Rice, D. A., 70, 73, 121, 234, 257, 262, 263,  
     267–270, 273, 275, 276, 291, 297, 299,  
     310  
 Richarz, F., 155  
 Rieckmann, E., 94  
 Ringwood, A. E., 403  
 Ritsema, A. R., 439, 440  
 Rittmann, A., 25, 431

- Robertson, Fl., 6  
 Rooymans, C. J. M., 407  
 Ros, H. C. M., 354  
 Rose, J. C., 123  
 Rudzki, M. P., 156, 157, 186
- Salonen, E., 172, 186  
 Sauramo, M. R., 359, 366  
 Sax, H. G. J., 354  
 Schairer, J. F., 407  
 Schiøtz, O. E., 129, 130, 146  
 Sederholm, J. J., 442  
 Shepard, F. P., 314, 352  
 Shor, 210  
 Shurbet, G. L., 221  
 Sitter, W. de, 56, 57, 230  
 Slichter, L. B., 210  
 Smoluchowski, M., 319  
 Snellius, W., 226  
 Snoo, G. de, 375  
 Sollins, A. D., 69, 70, 279, 297  
 Somigliana, C., 74, 297  
 Sonder, R. A., 442  
 Spencer-Jones, H., 56, 58, 230  
 Spicer, H. Cecil, 407  
 Sterneck, R., 98  
 Stokes, G. G., 141, 150, 228, 240, 258, 297  
 Swallow, 211
- Taber, S., 389  
 Takeuti, H., 22  
 Tanni, L., 73, 96, 122, 164, 172, 178, 186,  
     203, 220, 241, 243, 245, 246, 270, 281,  
     282, 284–287, 292, 293, 297  
 Tatel, H. E., 205, 210, 221  
 Texeira, C., 375  
 Tisserand, F., 56  
 Tsuboi, C., 268  
 Tuve, M. A., 205, 210, 221
- Umbgrove, J. H. F., 372, 375  
 Uotila, U. A., 78, 79, 83, 230, 247, 270, 298
- Vening Meinesz, F. A., 96, 97, 100, 115–118,  
     122, 138, 140–142, 146, 164, 168, 169,  
     173, 174, 186, 197, 198, 217, 219, 220,  
     240, 242, 243, 245, 249, 252, 258, 277,  
     278, 281, 288, 297, 302, 303, 310
- Veronnet, 173  
 Verwey, E. J. W., 407  
 Vestine, E. H., 25–27  
 Voigt, W., 22  
 Volet, C., 94  
 Vos. van Steenwijk, J. A. de, 70, 73, 262,  
     297
- Walbeck, 230  
 Wavre, 173  
 Wegener, A., 433  
 Whitten, C. A., 233, 235, 291, 297, 304,  
     310
- Wideland, Bror, 178, 186, 203, 221, 232,  
     274, 275, 298
- Wiechert, E., 297  
 Wilson, J. T., 6  
 Wolf, H., 292, 298  
 Woppard, George P., 97, 121, 122, 123,  
     171, 186, 196, 208, 210, 211, 221, 242,  
     298
- Worden, Sam, 109  
 Worzel, J., 117, 205, 206, 219, 220, 242, 298
- Young, Thomas, 153
- Zagrebin, D. V., 281  
 Zahradnicek, J., 155  
 Zhongolovich, I. V., 270, 271

## SUBJECT INDEX

- Achievements of isostasy, 198–217  
Adjustment of triangulation, meaning of, 224  
Air Force Cambridge Research Center, 234, 243, 294  
Airy-Heiskanen isostatic system, 135  
normal thickness of earth's crust, 137  
principles of, 135  
thickness, under mountains, 137  
under oceans, 137  
with  $T = 30$  km, used in gravimetric method, 245, 246  
Airy-Heiskanen reduction, 166–168  
computation tables, 167  
effect on, of station height, 167, 168  
of thickness of earth's crust, 166  
formulas, 137, 166  
principles, 135  
reduction tables and maps, 167  
Airy hypothesis, 7  
Alpine arc, 342, 344  
Alpine orogenesis, 344  
Andaman Islands, 372  
Anegada Strait, 385  
Ångermanland, 366  
Anguilla, 385  
Antillean arc, 355  
Arc measurement, in Lapland, 227  
in Peru, 227  
Arc measuring methods, 225–227  
of Eratosthenes, 225, 226  
limitations of, 238, 239  
principle of, 225  
significance of initial point, 224  
significance of reference ellipsoid used, 224  
Asiatic parts of geosyncline, 436  
Astronomic-geodetic deflections of the vertical (*see* Deflections of the vertical)
- Asymmetry of thickened crust, 327  
Atwood's machine, 84  
Bali, 375–377, 383  
Baltic Geodetic Commission, 233  
Banda arc, 438  
Banda Basins, 438, 439  
Banda Sea, 371  
*Barrot, dôme du*, 354  
Basaltic melt, 435  
Basins, deep, in island-arc areas, origin, 436–440  
Bataafsche Petroleum Company, 178  
Beata Ridge, 386  
Belts of negative gravity anomalies, in Indonesia, 371ff.  
near Japan, 386  
north of Haiti, 376  
Bending of crust, elastic, 320, 321  
Bonin-Marianas arc, 386, 387  
Borneo, rivers, 371  
Bothnia, Gulf of, 366  
Bouguer gravity anomalies, 155, 188–201  
Hawaiian area, 200, 201  
limitations of, 198–201  
in mountains, 188–197  
in Randsenken, 199, 200  
at sea, 197, 198  
Bouguer reduction, 150–155  
computation method, 152, 153  
effect of infinite plate, 153  
expanded, 155  
formula for, 155  
horizontal effect of, 195, 199  
terrain correction, 152, 154  
Buckling of crust, plastic, 341, 372–374  
Buckling limit, elastic, of crust, 318, 319  
Bulk modulus  $k$ , 13, 14

- Bulletin Géodésique, 213  
 Buru, 372
- Calibration lines, 111, 120  
 California crust, 6  
 Canada, 311, 312  
 Celebes, 372, 377, 385  
 Celebes Sea, 371, 438  
 Celestial methods, moon camera, 235  
     occultation, 235  
     solar eclipse, 235  
 Central and South America, relative movement in, 386  
 Ceram, 372-374, 382  
 Christmas Island, 377  
 Coincidence apparatus, 99  
 Coincidence time, 99  
 Compression in crust, gravity anomaly for, 315  
 Compressive stress, sign of, 316  
 Constituent quantities, 16  
 Continent, "ur," 431-433  
 Continental borders coinciding with shear pattern, 451  
 Continental coasts, similarity of, 433, 434  
 Continental crust, 7, 8  
     consolidation of, before oceanic crust, 433, 434  
 Continental shields, thickness of, 432  
 Continents, elevation of, 432  
     migration of, 433  
 Control of small-scale maps, 306-308  
 Control point systems, 222-224  
     local, 223, 224  
     national, 223, 224  
 Convection, half-turn, 408  
     harmonic distribution of, 409, 413  
 Jeffreys's quantity  $\lambda$  dominating, 49, 411, 418, 422  
     stationary, 408  
         stresses during, 412, 419, 420  
 thermal, in entire earth, 421-423, 430-432  
     in plane layer, 407ff.  
     in spherical shell, 412ff.  
     third and later stages of, 435  
 Convection currents, breaking through transition layer, 406, 407, 439  
     descending, mass concentration above, 430
- Convection currents, in earth, trigger effect, 408, 431, 433, 438  
 mantle, 12, 397-442  
     distribution of, 436  
     incomplete systems of, 436  
 Cooling of earth, 404  
 Core of earth, 25  
     currents in, 28  
     density in, 25  
     ferromagnesium silicates in, 25  
     formation of, 430, 431  
     great seismic velocity in, 25  
     hydrogen in, atomic form, 25  
     inner (central body), 25  
     nickel-iron, 25  
     undifferentiated solar matter in, 25  
 Crust, in California, 6  
     deformation of, 328  
         loaded broken, 323-325  
         loaded unbroken, 322  
         plastic, classic, 328  
             direction of, 349ff.  
     divided in blocks, 373, 386, 437, 443  
     in Europe, 6  
     faulting in, 352ff.  
 M, continental, 7, 8  
     oceanic, 7, 8  
     of many layers, 319  
     in Missouri, 7  
     in New England, 6  
     oceanic, consolidation of, later than continental, 433, 434  
     origin of, 435  
 plastic downbuckling of, 326ff., 347  
 principal stress in, angle  $\theta$  between faulting and, 352-354, 373, 385  
 relative rotation of, and earth's interior, 437, 443ff.  
 rigid, 12  
     and M crust, coincidence of, in continents, 12  
     thickness of (*see* Thickness of earth's crust)  
 shear in, 352ff.  
 stress components in fault in, normal, 351, 354  
     shear-, 351, 354, 383  
 stress release in, 389ff.  
 sucking down of, 319  
 thickening of, plastic, 326ff., 347  
 uniaxial compression in, 350ff.

- Crustal blocks, readjustment of, 437  
 relative movement of, 373, 386  
 in California, 386  
 tilted, 393
- Crustal deformation (*see Crust*)
- Crustal downbuckling and compression, 55° angle between, 373, 377, 383, 385, 386
- Crustal pattern in Indonesian Archipelago, 373
- Crustal radioactivity, differences in, 407, 435
- Crustal shear pattern, 443, 447ff.  
 adapted to North Atlantic seafloor topography, 448, 449, 451
- Crustal subsiding, acceleration of, 339
- Crustal "wrench" faulting, in California, 386  
 in Indonesia, 373–374, 377–379, 381, 383
- Crystallization of olivine, 435
- Cuba, 386
- Curaçao, 386
- Currents, core, 28  
 electric mode of, 28  
 magnetic mode of, 28
- Day, variations in length of, 29
- Deflections of the vertical, 250–277  
 astronomic-geodetic, 240, 250–257  
 equations, 251, 252, 254  
 Laplace, 251  
 factor  $F$ , 255  
 reduction of astronomic data, 256, 257  
 relationship with dimensions of earth and initial point, 238, 239  
 topographic and isostatic reduction, 252, 256  
 Hayford zones for, 254  
 equations, 251, 252, 299  
 classic, 239  
 modern, 299  
 expressed in gravity anomalies, 69–71  
*gravimetric* (*see Gravimetric deflections of the vertical*)  
 illustration of, 250  
 origin of, 237
- Deformation, of crust (*see Crust*)  
 = strain, 15ff.
- Density, in earth, 10, 25  
 in mantle, 9–11, 403ff.
- Density-transition layer in mantle, 403ff.
- Depth of sea outside geosyncline, maximum, 9
- Deviation masses (earth minus spheroidal earth), 59ff.
- Dimensions, of earth, Bessel, 230  
 Clarke, 229, 230  
 Eratosthenes, 225  
 Hayford, 230, 231  
 Heiskanen, 230, 231  
 Jeffreys, 230, 231  
 Krassowski, 229, 230, 232  
 Ledersteger, 230–232  
 most used, 230  
 U.S. Army Map Service, 230, 232
- of reference ellipsoid, significance of astronomic observations, 299  
 significance of deflections of the vertical, 299, 302
- Displacement vector, 15
- Distance geoid spheroid ( $N_0$ ) expressed in spherical harmonics, 62
- Downbuckled belts, topography in, 374
- Downbuckling, crustal, 326ff., 347  
 catastrophic phase of, 341ff.  
 and crustal thickening, table, 334  
 plastic, in anomaly belt, 372–374  
 in Indonesia in upper Miocene, 372
- Downbuckling deductions, approximate character of, 336
- Downbuckling experiments, Kuenen's, 341
- Earth, mean density of, 155, 156
- Earth dimensions, effect of geoid undulations on, 236, 237
- Earth spheroid, = equipotential surface of spheroidal earth, 45, 46  
 flattening of, 45  
 gravity on, 49, 50  
 radius vector of, 46, 47, 49, 50
- Earthquake area, deep, tilted fault planes in, 438, 440
- Earthquake face, in California, 386  
 in Indonesia, 378, 380, 439, 440
- Earthquake foci, deep and intermediate, 439, 440
- Elastic creep, 23, 24
- Elastic flow creep, 24

- Elastic limit, of crust, 327
  - = strength, 12, 18, 20, 436
  - of subcrustal layer, 326
- Elastic-limit criterions, Huber-Hencky-von Mises, 20
  - maximum-shear, 20
- Elastic part of plastic strain deviator  $D_{de}$ , 20
- Elastic reaction to loading or unloading, 359, 360, 366
- Elastic strain, energy of, in crust, 451
  - relaxation, 357ff.
- Elastically bending crust, moment in, 321
  - shear force in, 321
- Electronic methods, Decca, Shoran, Hiran, 233
- Ellipsoid, earth, normal gravity = gravity on, 52, 53
  - radius vector of, 52, 53
- Ellipsoidal earth, exterior field of, 54, 55
- Ellipticity, mechanical, 44
  - flattening derived from, 57, 58
- Eötvös effect, 158
- Equilibrium, phase, 403ff.
  - (*See also* Isostatic equilibrium)
- Equilibrium earth spheroid, difference, and earth ellipsoid, 59
  - radius vector and gravity of, 58, 443
- Equipotential surface, 33
- Error of representation, 271–273
  - size of area represented by one observation, 272, 273
- Escarments, straight, in Pacific Ocean, 389
- Europe, crust, 6
- Existing gravity material, 241–242
  - in continents, 241–242
  - at sea, 241, 242
  
- Fennoscandia, 357, 363, 365
  - land uplift in, 212–215
    - before end of glacial period, 212
    - in future, 215
    - now, 212
- Ferromagnesium silicates in core, 25
- Finland, high-precision leveling in, 365
  - land uplift in, 213
- Flattening, of crustal shells, change in direction, 437, 443ff.
  - decrease in, 437
- Flattening, derived from mechanical ellipticity, 57, 58
- Flores Deep, 371
- Flow, in Newtonian fluids, 19
  - plastic, pseudo-viscous, 19, 20, 23, 24
- Flow reaction, subcrustal pseudo-viscous to loading and unloading, 361ff.
- Fracturing and faulting, 20
- Free-air anomalies, effect of station height on, 247, 248
- Free-air reduction, 148–150
  - effect of curvature of earth on, 149–150
  - elevation correction, 149
  - formula for, 148
- Friction, internal, angle of, 353, 354
  
- Galileo's tilted plane, 84
- Geocentric coordinates, 34
- Geodesy, basic hypothesis of, 72
  - ellipsoidal era, 228
  - geoidal era, 228
  - geometrical, 234
  - historical development of, 224–228
  - physical (*see* Physical geodesy)
  - spherical era, 228
- Geodetic coordinates, conversion from one system to another, 299–304
  - accuracy of, 300, 301
  - formulas for, 299, 302–304
- Geodetic datum, initial point of, 224, 299
- Geodetic systems, 222–235
  - differences between, 233
  - European, 234
  - Indian, 234
  - local, 223
    - meaning of, 223–224
    - national, 223
    - North American, 234
    - Russian, 234
    - significance of initial point, 233
    - world, 299–304
- Geographic coordinates, astronomic-geodetic, 223, 224, 250, 251, 305
  - astronomic-gravimetric, 299, 305
- Geoid, 33, 223, 239, 279, 294
  - accuracy of, 286–288
  - Bomford, 291, 292
  - circle-ring method, 279, 280
  - Columbus, Ohio, 289
  - computation formulas, 279–281

- Geoid, computation formulas, astronomic-  
geodetic, 257–279, 293  
gravimetric, 293  
effect of, 300  
for Europe, 286, 289  
Hirvonen, 241, 282  
Indian, 290  
practical procedure, 279–285  
Rice, 291  
shape of, 279, 294  
slope of, 286  
square method, 281  
Stokes' coefficient, 279, 281, 285  
sample of, 285  
Stokes' function, 258, 280  
Stokes' theorem for, 65  
tables, Lambert and Darling, 279  
    Sollins, 279  
Tanni, 241, 282–287  
    comparison with Bomford, 293  
undulations of (*see* Undulations of  
geoid)  
Zhongolovich, 270, 271
- Geomagnetic secular field, 25–27  
    westward velocity of, 28
- Geomagnetism, 12, 25–29
- Geosyncline, later history of, 343ff.  
    Mediterranean, 436  
    oceanic, 345  
    sea depth outside, maximum, 9  
    Thetys, 436
- Geosyncline belts, two major, formation  
of, 436
- Geosyncline formation, 327ff., 435ff.  
    mountain, rising of, 343
- Ghost flights to tie base stations, 121
- Gimbal arrangement, 114, 117
- Graben, breadth of, 392  
    gravity anomalies over, 389, 394, 395  
    gravity over, 394, 395  
    later history of, 395  
    upbending of crust beside, 394
- Graben escarpments, height of, 394
- Graben faults, dip of, 390  
    formation of second, 390
- Graben formation, 389ff.
- Grand Canyon, 321
- Granite hypothesis of Read, 345
- Gravimeters, 101–115  
    astatic-balance, 108  
    balance, 84, 104
- Gravimeters, dynamic, 101  
Frost, 109  
gas-pressure, 84, 101, 103  
Gulf, 105, 106  
Hartley, 104  
LaCoste-Romberg, 109  
Magnolia, 109  
Nørgaard, 107  
North American, 109  
stable, 104  
static, 101  
tidal, 120  
underwater, 113  
unstable, 107  
Worden, 109, 113
- Gravimetric deflections of the vertical,  
257–279  
absolute, 239  
accuracy of, 273–277  
average values, 290  
circle method, 262  
circle-ring method, 266–268, 281  
computation of, 262–266  
    in Argentina, 275  
    in Finland, 263–267, 273, 274  
    in Sweden, 275  
    in U.S. Army Map Service, 275, 276  
    in U.S. Coast and Geodetic Survey,  
        263, 276
- computation formulas, 258, 261  
derivation from the geoid contour  
    curves, 290
- effect on, of area beyond  $3^\circ$ , 273  
    of area beyond  $20^\circ$ , 273  
    of nearest neighborhood, 264–266, 274
- functions  $E$  and  $G$ , 272
- Kasansky's circle rings, 267
- local, 268–270
- Rice circle rings, 262
- square method, 261, 262
- stereographic projection, advantage of,  
    259, 260
- three-gradient method, 262
- use of spherical harmonics, 270
- Vening Meinesz coefficients, 258
- Vening Meinesz formulas, 258
- Gravimetric method, 242  
    best fitting isostatic system, 245
- Bouguer method, limitations of, 198–  
    200
- existing gravity material, 241–242

- Gravimetric method, needed gravity material, 240–241  
 significance in, of free-air anomalies, 243  
 of gravimeters, 242  
 underwater, 242  
 of inversion method, 243  
 of isostatic method, 243  
 of oil companies, 242  
 of Vening Meinesz pendulum apparatus, 242
- Gravitational constant, 155, 156
- Gravity, normal, 52, 53  
 units of (gal, milligal, microgal), 120
- Gravity anomalies, 187–219  
 Airy-Heiskanen, 188–201  
 Alps, 192–195  
 map, 195  
 profile across, 195  
*Randsenken* of, 199, 200  
 over Banda Basin, 439  
 Bouguer (*see* Bouguer gravity anomalies)  
 in Burma and Indonesia, 372  
 Canada, 189, 190  
 comparison between, 188–201  
 East Africa, 191, 192  
 expressed in spherical harmonics, 62  
 Fennoscandia, 214  
 free-air, 188–201  
 over graben, 389, 394, 395  
 Hawaiian area, 200, 201  
 India, 190, 191  
 Indonesian Archipelago, 371ff.  
 Pratt-Hayford, 188–201  
 reduction of (*see* Reduction)  
 at sea, 197, 198  
 reduction of, 158  
 United States, 187–189  
 profile in, 196  
 Vening Meinesz, 217–219
- Gravity anomaly for compression in crust, 315
- Gravity base stations, 86  
 international, 85  
 national, 85, 86  
 tie between, 121  
 world, 84, 85, 120  
 of first order, 120
- Gravity formulas, 74–80  
 Bowie, 78  
 computation of, 76–78
- Gravity formulas, Heiskanen, 78, 79  
 Helmert, 78, 79  
 international, 74–75  
 with longitude term, 79, 80  
 without longitude term, 78, 79  
 Uotila, 80
- Gravity measurements, 84  
 absolute, 84, 85  
 field, 85  
 relative, 84
- Gravity profile, over Bali Strait, 335, 376  
 over Benkulen, 378, 379  
 over Padang, 378, 379  
 over Surigao Strait, 381  
 over West Java, 375, 376
- Green's theorem, 156
- Grenada, 386
- Gulf pendulum, 100
- Gulf Research and Development Company, 100, 114, 242
- Gulf underwater gravimeter, 113–115
- Gunung Api, 371
- Haalek's gas-pressure gravimeter, 103
- Haiti, 374, 384, 385  
 belt north of, 376
- Halmahera, 371, 372, 385
- Hartmann's lines, 350
- Heavier phase, percentage of, 9, 405ff.
- High Atlas, 343
- History of the earth, early, 430, 435ff.
- Hooke's law, 18
- Houston Technical Laboratories, 109, 111, 112
- Huber-Hencky criterion, 20, 351, 354, 355
- Hydrogen in atomic form in core, 25
- Hydrostatic compressive stress pressure, 13
- “Ideelle störende Schicht” of Helmert, 156
- Indian Ocean, 436
- Indonesian arc, 355ff.
- Indonesian Archipelago, 313ff., 439  
 gravity anomalies in, 372  
 belts of, 371ff.
- Inner core (central body), solid state of nickel-iron in, 25
- Instability in mantle, 403, 407, 433
- Interface, at about 5000 km depth, 25

- Interface, M, 6, 7, 12  
depth of, 345
- Interface mantle core, density increase in, 25
- International Association of Geodesy, 167, 246
- International Bureau of Weights and Measures, 94
- International Geodetic Association (Madrid 1924), 52
- International Geophysical Year, 120, 242
- International Gravity Center, 176, 178
- International gravity formula, 74, 75
- International Union of Geodesy and Geophysics, 120, 167, 292
- Internationale Erdmessung, 228
- Island arcs, large islands on, 384
- Isostasy, 124–144  
achievements of, 198–217  
idea of, 124–146  
assumptions, Airy's, 126, 128, 129  
Pratt's, 126, 127  
conception of, Leonardo da Vinci's, 125, 126  
definition of, 124, 125  
explanation of, Boscovich's, 126  
historical development of, 124–146  
ocean minus continent, 218  
volcanic-island areas, 217
- Isostatic assumptions, other, 142–144  
Cizancourt's "undation" hypothesis, 144  
Daly's hypothesis, 143, 144  
Heiskanen's intermediate, 143  
Putnam's method, 142
- Isostatic compensation, local, 124  
regional, 124
- Isostatic equilibrium, depths of compensation, 124  
"dough" hypothesis, 132, 141  
floating theory, 135, 141, 209  
Hayford's assumption, 133, 134  
readjustment of, 22, 357ff., 369  
in terms of equal mass, 132–134  
in terms of equal pressure, 132–134
- Isostatic experiments of nature, 212–215
- Isostatic Institute of IAG, 167, 176–178, 214, 215, 282  
isostatic reduction maps, 167–169, 176–181
- Isostatic Institute of IAG, isostatic reduction tables, 167–169, 176–181
- Isostatic reduction, 148, 158–170  
in electronic computers, 183, 184  
meaning of, 148  
methods of, cartographic, 176–178  
comparison with rigorous method, 179–180  
circular-ring, 175, 176  
mass-line, 181–184  
recent, 175–184  
reduction maps, 177, 178
- Isostatic systems, main, 131–142  
(*See also* Pratt-Hayford isostatic system)
- Japan Trench, 386
- Java, 354, 377  
rivers of, 371
- Java Sea, 371
- Java Trench, 371
- Jeffreys's quantity  $\lambda$ , 411, 418, 422  
dominating convection, 49, 411, 418, 419
- Kai Islands, 372–374, 382
- Krakatoa, 383
- Kurile Islands, 386
- Labrador, 311, 312
- Land uplift, in Fennoscandia, 212–215  
in Finland, 213
- Laplace equation, 35, 36, 251
- Laplace points, 251
- Leveling, high-precision, in Finland, 365  
results of, 365
- Lineamenttektoniker*, 442
- Loading or unloading, reactions to, elastic, 359, 360, 366  
subcrustal plastic-flow, 361ff., 367  
transition-layer, 360, 367, 405, 406
- Lombok, 377, 383
- Lunar bodily tide, 25
- M discontinuity, 6, 7, 12, 205–211  
depth of, 205–211
- Europe, 208
- Gutenberg assumption, 205–207

- M discontinuity, Hess' assumption, 205, 209  
 North America, 208  
 oceans, 208  
 South Africa, 208
- M interface (*see Interface*)
- Mantle, consisting of olivine, 12  
 density in, 9–11, 403ff.  
 density-transition layer in, 403ff.  
 instability in, 403, 407, 433  
 temperature equations for, 405  
 transition layer in, 12, 403ff.  
 origin of, 404
- Mantle convection currents, 12, 397–442  
 correlation with topography, 432, 433  
 distribution of, 436  
 incomplete systems, 436  
 smaller, 434–436
- Mapping and Charting Research Laboratory of OSU, 181, 247, 289, 294
- Marigraphs, 365
- Martinique, 355, 385
- Mechanical ellipticity, 44, 57, 58
- Mediterranean Basins, 439
- Mediterranean geosyncline, 436
- Mendocino escarpment, 389, 390
- Midocean ridges, 434, 436
- Migration, of continents, 433  
 polar, 437, 442ff.
- Mineralogical and Geological Institute, Utrecht, 365
- Missouri crust, 7
- Mitteleuropäische Gradmessung, 228
- Mittelgebirge*, formation of, 344  
 roots of, 344
- Model earth, 243, 244  
 geopotential surface, 244  
 spheropotential surface, 244
- Mohr's circle, 350, 352–354
- Molucca Sea, 371, 372, 377, 382, 385, 386
- Moon, second, 431
- Moon effects, 431
- Morotai Basin, 371
- Mountain formation, geosyncline, rising of, 343
- Mountain-range disappearance, by erosion, 343  
 by melting mountain root, 344, 432
- Mountain root spreading under foreland, 344
- Mountain-root theory, 128, 129
- $N_0$ , geoid-spheroid distance expressed in spherical harmonics, 62
- National Research Laboratories, Ottawa, Canada, 94
- Neap tide, 119
- Netherlands Geodetic Commission, 176
- New England crust, 6
- New Guinea, 385
- Nicobar Islands, 372
- Normal gravity = gravity on earth ellipsoid, 52, 53
- North American system, initial point of, 234
- Oceanic crust, 7, 8
- Oceanic geosynclines, 345
- Oceanic ridges, low, 345  
 no disappearance of, 345
- Ohio State University, The, 181, 243, 247, 289, 294
- Olivine, mantle consisting of, 12  
 orthorhombic and spinel phases, 403  
 transition heat for, 403, 404
- Orogenesis, Alpine, 344
- Orogenic cycle, regressions in first period, 407
- Orogeny, world-wide and regional, 437
- Overriding, of Indian Ocean crust, 378, 379  
 of Pacific Ocean crust, 381, 382
- Pacific Ocean, straight escarpments in, 389
- Palao Trench, 371, 385
- Panama, Isthmus of, 386
- Pendulum, 84  
 amplitude of, 87  
 center of gravity, 93  
 elongation angle of, 87  
 fictitious, 96  
 forced, 95  
 free, 95  
 inverted, Holweck-Lejay, 101  
 length of, 90, 92  
 mathematical, 87  
 minimum, 100  
 moment of inertia, 92  
 oscillation time, 88  
 period of, 87  
 phase angle of, 87  
 physical, 90–92  
 reversing, 84, 93, 94

- Pendulum, swinging center, 92  
     swinging time, 90
- Pendulum apparatus, 98  
     Holweck-Lejay, 101, 102  
     modern, 98  
     Sterneck's, 98  
     Vening Meinesz, 115–118  
         path of light rays, 116  
         principle of, 96, 115, 116
- Pendulum equation, 87
- Pendulum observations, 84, 87  
     coincidence time of, 99  
     corrections, arc, 89, 94, 97  
         barometric, 94  
         clock-rate, 94  
         flexure, 94–96  
         temperature, 94, 96  
     theory of, 87–93
- Permanent strain, 18
- Phase equilibrium, 403ff.
- Philippine Islands, 314, 355, 373, 374, 381, 384
- Philippine Trench, 371, 372, 381
- Physical geodesy, 235–250  
     mathematical basis of, 240  
     physical basis of, 237
- Physikalisch-Technische Bundesanstalt, Brunswick, Germany, 94
- Planetary phenomenon, 443
- Plastic crustal deformation, direction of, 349ff.
- Plastic flow, pseudo-viscous, 19, 20, 23, 24
- Plastic strain, 24
- Plastic-strain deviator  $D_d$ , elastic part of, 20  
     pseudo-viscous part of, 20
- Plumb line, 236
- Poisson's constant, 18, 19, 21, 22, 314, 317, 350  
      $m$ , 18, 21, 22  
     for Newtonian fluids, 19
- Poisson's theorem, 35
- Polar migrations, 437, 443ff.
- Postglacial phenomena, 357ff., 405
- Postglacial rising of Ångermanland, elastic part of, 366  
     plastic-flow part of, 366, 367  
     transition-layer part of, 367
- Postglacial unloading, supposition of harmonic distribution of, 362, 364
- Potential  $W$ , 33, 34  
     second-order derivatives of, 35  
     discontinuities of, 36
- Pratt-Hayford isostatic system, 131  
     Bowie's interpretation, 132  
     depth of compensation, 131  
     main principle of, 131
- Pratt-Hayford reduction, 159–166  
     computation formulas, 160  
     computation tables, 163, 164  
     effect on, of depth of compensation, 160, 163  
     of earth's curvature, 162  
     factors  $E_t$ ,  $E_c$ ,  $E_r$ , 163  
     fundamental formula, 159  
     Hayford zones and compartments, 161  
     modification of, Bullard, 164  
         Heiskanen, 143
- Pressure = hydrostatic compressive stress, 13
- Profile, gravity (*see* Gravity profile)
- Pseudo-viscosity modulus  $N$ , 19, 22, 23, 368  
     deduction, 368
- Puerto Rico, 374, 384
- Puerto Rico Trench, 374
- Pyrenees, 342
- Radioactive effect of sial concentration, 438
- Radioactivity, crustal, differences in, 407, 435
- Readjustment of isostatic equilibrium, 22, 357ff., 369
- Reduction, of base lines from geoid to ellipsoid, 308, 309  
     of gravity anomalies, 147–186  
         Airy-Heiskanen, 245  
         Bowie, or indirect effect, 172–175  
         Bouguer, 147  
         de Graaff Hunter, 243–245  
         Faye or free-air, 150  
         free-air, 147, 244  
         geological correction, 170–172  
         Helmert condensation, 147, 243  
         isostatic geological, 170–172  
         nonisostatic, 147–159  
         Pratt-Hayford (*see* Pratt-Hayford reduction)  
         Rudzki inversion, 147, 243, 245

- Reduction, of gravity anomalies, at sea,  
    158  
    terrain correction, 147  
    Vening Meinesz, 168–170  
isostatic (*see* Isostatic reduction)  
Vening Meinesz (*see* Vening Meinesz  
    reduction)  
Reference ellipsoid, 223, 230  
Reference surfaces, ellipsoid of revolution,  
    222  
    geoid, 222  
    plane, 222  
    sphere, 222  
Regressions in first period of orogenic  
    cycle, 407  
Remote control, 114  
Rhone Valley, upper, 321  
Rigid crust (*see* Crust)  
Rising of tectonic arc, 439  
    above rising mantle currents, 439  
Root-formation theory, 211  
Rotation, earth, irregularities in, 25, 28,  
    29  
    relative, of crust and interior of earth,  
        437, 443ff.  
    need for moment of forces, 453  
    stresses in crust by, 446  
        inability of crust to endure, 447  
Rotti, 377  
Ryukyu arc, 386
- Saint Lucia, 355  
Saint Vincent, 385  
San Andreas fault, 386  
Scandinavia, 311, 312  
Sea depth outside geosynclines, maximum,  
    9  
Seismic velocities in earth, 11  
Seismic work at sea, 7  
Shear modulus  $\mu$ , 17, 21, 22, 25  
Shorelines, old, 365  
Sial concentration, radioactive effect of,  
    438  
Solar matter in core, undifferentiated, 25  
Spherical harmonics, 36–39, 423ff., 430ff.  
    associated = sectorial or tesseral, 38  
    developing of function in, 41, 42  
    external gravity field of, 47, 48, 51  
    external gravity potential of, 42ff.  
    Legendre (zonal), 37
- Spherical harmonics, topography developed in, 423ff.  
    waves in, 425ff., 430ff.  
Spheroid, earth (*see* Earth spheroid)  
Spheroidal earth, external gravity field of,  
    47, 48, 51  
    external gravity potential of, 42ff.  
Spring tide, 119  
Stokes' formula, 228  
Stokes' functions, table, 81  
Stokes' theorem, 65  
    applicability of, 72, 73  
    for exterior equipotential surfaces, 64,  
        65, 70–73, 81  
    for geoid, 65  
Strain in mixed rocks in la Vanoise, 19  
Strain affinor = deformation affinor, 15  
Strain deviator = deformation deviator  
     $D_d$ , 15, 16, 20  
Strain tensor = deformation tensor, 16  
Strength = elastic limit, 12, 18, 20, 436  
Stress deviator  $S_d$ , 17  
Stress release in crust, 389ff.  
Stress-strain relations, 12ff.  
Stress tensor  $S$ , 16  
Stresses during stationary convection,  
    412, 419, 420  
Subsiding, crustal, acceleration of, 339  
Subsiding basin above subsiding mantle  
    current, 439  
Sumatra, 314, 354, 355, 371, 373, 374, 377,  
    378, 381, 384  
    island ridge west of, 354  
    rivers of, 371  
Sumba, 372, 373, 377  
Sumbawa, 377  
Sunda Strait, 377, 383, 385  
Supercontrol points, 304–306  
Survey of India, 129, 290, 291
- Taland Islands, 372  
Tanimbar Islands, 372, 374, 377  
Temperature equations for mantle, 405  
Temperature gradients, in continents and  
    oceans, 403, 407ff.  
    horizontal, 433, 438, 440  
Terrain corrections, 152, 154–155  
    list of, 154  
    sign, 152, 154  
Thetys geosyncline, 436

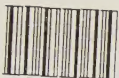
- Thickening of crust, plastic, 326ff., 347  
 Thickness of earth's crust, 201–205  
   East Alps, 203, 205  
   Ferghana Basin, 203, 205  
   under mountains, 204–205  
   Northeast Italy, 203, 205  
   Norway, 203  
   under oceans, 204–208  
     dependent only on temperature, 13,  
       434  
   South Africa, 203, 205  
   Sweden, 203, 205  
   West Carpathians, 203, 205
- Tidal effect, 118–120  
 Tidal force, 118  
 Tidal friction, 437  
 Tide gauges, 365  
 Timor, 372, 374, 375, 377, 382  
 Tobago, 374, 386  
 Tonga Trench, 387  
 Topography, correlation of mantle currents and, 432, 433  
   developed in spherical harmonics, 423ff.  
   of earth, first-order term, 430, 431
- Transition heat, for olivine, 403, 404  
   stabilizing effect of, 403, 407
- Transition layer, current breaking through,  
   406, 407, 439  
   in mantle, 12, 403ff.  
   origin of, 404
- Transition-layer reaction to loading or unloading, 360, 367, 405, 406
- Triangulation, 228  
   development of, 226–228  
   principle of, 226
- Triaxial ellipsoid, Russian, 80
- Trigger effect for convection currents in earth, 408, 431, 433, 438
- Trinidad, 374, 385, 386
- Undifferentiated solar matter in core, 25
- Undulations of geoid, astronomic-geodetic,  
   291–294  
   gravimetric, 279–290  
   origin of, 237–238
- Uniaxial compression in crust, 350ff.
- U.S. Army Map Service, 230, 233, 276,  
   290–292, 305
- U.S. Coast and Geodetic Survey, 131, 142,  
   175, 176, 233, 245, 243, 291
- Upper Rhone Valley, 421  
 Ur continent, breaking up of, 431–433
- Variometer, 84  
 Varves, 365  
 Vening Meinesz formulas, 240  
 Vening Meinesz reduction, 168–172  
   bending of crust, 139  
   computation tables, 169  
   fundamental tables, 168  
   of gravity anomalies, 168–170  
   principles of, 138  
   two-dimensional tables, 169, 170
- Vening Meinesz regional isostatic system,  
   137–142  
   continental margins, 215–217  
   local and regional theories, difference  
     between, 138  
   principles of, 138–141  
   regionality of, 138  
   volcanic islands, 215–217
- Viscosity modulus  $\eta$ , pseudo-viscosity  
   modulus  $\eta$ , 19, 22, 23
- Volcanic arc, Celebes-Sangihe Islands,  
   382  
   Indonesia, 382  
   straighter than tectonic arc, 386  
   Sunda Islands, 383
- Volcanic row, Ternate-Batjan, 382
- Volcanic and tectonic belts, distance between, 383–384
- Volcanoes, on concave side of tectonic arc,  
   384  
   interruption, north of Timor, 382  
   Java, 383  
   Sumatra, 382, 383
- Volet's machine, 84
- von Mises criterion, 20, 351, 354, 355
- Wavelength, constant crustal downbuckling of, 334–335  
   elastic, of crust, 319
- Waves in spherical harmonic development of topography, 425ff., 430ff.
- Weber Deep, 371
- Wegener's theory, 433
- Westward velocity of secular geomagnetic field, 28

- Worden gravimeter, 109, 113  
accuracy of, 109, 111  
calibration of, 111  
exterior view, 113  
principle of, 109  
range of, 109  
spring system of, 111  
temperature compensation of, 110, 111  
World geodetic system, 299–310
- World geodetic system, conversion of existing geodetic systems to, 309  
World-wide Gravity Project, 178
- Young's modulus,  $E$ , 18, 22, 317
- Zero-length spring, 109, 110





551.16 H47E



a39001



007035861b

551.16  
H47e

65-1              23-1  
66-111            74-111  
67-1 |  
68-1 |  
71-111 |  
72-1 |

